Review 4-81

# AEROMEDICAL REVIEW

## USAF RADIOFREQUENCY RADIATION BIOEFFECTS RESEARCH PROGRAM--A REVIEW

Editor: John C. Mitchell, B.S. (USAFSAM/RZP)

December 1981

DTIC
ELECTF
MAY 1 2 1982
S       D

D

USAF SCHOOL OF AEROSPACE MEDICINE
Aerospace Medical Division (AFSC)
Brooks Air Force Base, Texas 78235

ADA114344

DTIC FILE COPY

82  05-12  011

# NOTICES

This review was submitted by personnel of the Radiation Physics Branch, Radiation Sciences Division, USAF School of Aerospace Medicine, Aerospace Medical Division, AFSC, Brooks Air Force Base, Texas, under job order 7757-01-85.

When U.S. Government drawings, specifications, or other data are used for any purpose other than a definitely related Government procurement operation, the Government thereby incurs no responsibility nor any obligation whatsoever; and the fact that the Government may have formulated, furnished, or in any way supplied the said drawings, specifications, or other data is not to be regarded by implication or otherwise, as in any manner licensing the holder or any other person or corporation, or conveying any rights or permission to manufacture, use, or sell any patented invention that may in any way be related thereto.

This report has been reviewed by the Office of Public Affairs (PA) and is releasable to the National Technical Information Service (NTIS). At NTIS, it will be available to the general public, including foreign nations.

This technical report has been reviewed and is approved for publication.

JOHN C. MITCHELL, B.S.
Chief, Radiation Physics Branch

JOHN E. PICKERING, M.S.
Chief, Radiation Sciences Division

ROY L. DEHART
Colonel, USAF, MC
Commander

| REPORT DOCUMENTATION PAGE | | READ INSTRUCTIONS<br>BEFORE COMPLETING FORM |
|---|---|---|
| 1. REPORT NUMBER<br>Aeromedical Review 4-81 | 2. GOVT ACCESSION NO. | 3. RECIPIENT'S CATALOG NUMBER |
| 4. TITLE (and Subtitle)<br>USAF RADIOFREQUENCY RADIATION BIOEFFECTS<br>RESEARCH PROGRAM - A REVIEW | | 5. TYPE OF REPORT & PERIOD COVERED<br>Interim Report<br>22-24 June 1981 |
| | | 6. PERFORMING ORG. REPORT NUMBER<br>SAM-TR-81-30 |
| 7. AUTHOR(s)<br>John C. Mitchell<br>USAFSAM/RZP<br>Editor | | 8. CONTRACT OR GRANT NUMBER(s) |
| 9. PERFORMING ORGANIZATION NAME AND ADDRESS<br>USAF School of Aerospace Medicine (RZP)<br>Aerospace Medical Division (AFSC)<br>Brooks Air Force Base, Texas 78235 | | 10. PROGRAM ELEMENT, PROJECT, TASK<br>AREA & WORK UNIT NUMBERS<br>62202F<br>7757-01-85 |
| 11. CONTROLLING OFFICE NAME AND ADDRESS<br>USAF School of Aerospace Medicine (RZP)<br>Aerospace Medical Division (AFSC)<br>Brooks Air Force Base, Texas 78235 | | 12. REPORT DATE<br>December 1981 |
| | | 13. NUMBER OF PAGES<br>439 |
| 14. MONITORING AGENCY NAME & ADDRESS(if different from Controlling Office) | | 15. SECURITY CLASS. (of this report)<br>Unclassified |
| | | 15a. DECLASSIFICATION/DOWNGRADING<br>SCHEDULE |

16. DISTRIBUTION STATEMENT (of this Report)

Approved for public release; distribution unlimited.

17. DISTRIBUTION STATEMENT (of the abstract entered in Block 20, if different from Report)

18. SUPPLEMENTARY NOTES

19. KEY WORDS (Continue on reverse side if necessary and identify by block number)

Radiofrequency radiation
Radiation protection

20. ABSTRACT (Continue on reverse side if necessary and identify by block number)

These papers were presented during a comprehensive Air Force radio-
frequency-radiation-bioeffects research program review. This first-
of-a-kind meeting brought together all investigators, contractor
as well as in-house, currently supported by Air Force funding, to
present technical summaries of their work and to interact and
exchange information with their peers. During the 2½-day con-
ference, research in a number of key areas was described. This

DD FORM 1473 JAN 73    EDITION OF 1 NOV 65 IS OBSOLETE

20. ABSTRACT (Continued)

demonstrates the breadth and overall integration of objectives of the Air Force program in this vital area.

PREFACE

THE U.S. AIR FORCE RADIOFREQUENCY RADIATION
BIOEFFECTS PROGRAM

John C. Mitchell

Chief, Radiation Physics Branch
Radiation Sciences Division
USAF School of Aerospace Medicine

The U.S. Air Force operates many radiofrequency radiation (RFR) emitters, and the potential hazard of personnel exposures has been well recognized for years. In the midfifties the Air Force had an active role in the triservice program to assess the biological effects of RFR and to establish appropriate safety guidelines. The 10-mW/cm$^2$ standard was set on the basis of such research. In recent years a more comprehensive national research program has significantly advanced the understanding of the interactions of RFR fields and biological systems. The Air Force program remains an important part of the national program, while focusing on service-specific problems.

The major objectives of the program are to (1) determine the effects of pulsed RFR exposures, (2) assess the effects of long-term low-level RFR exposures, (3) characterize the fundamental mechanisms of RFR interactions, (4) advance dosimetric methodologies in accordance with empirical requirements, (5) develop and provide RFR guidelines for the timely revision of Air Force Occupational Safety and Health (AFOSH) Standard 161-9, (6) improve the technical information used in preparing environmental impact statements, and (7) assess RFR exposures in Air Force workplaces.

The purpose of this 2½-day conference is to (1) bring together for the first time persons intimately involved in the Air Force program, (2) present individual research efforts, and (3) allow open discussions among the attendees. The proceedings of this conference are published as a USAFSAM Aeromedical Review.

1

BLANK PAGE

# CONTENTS

CONTENTS (Continued)

# THEORETICAL AND EXPERIMENTAL DOSIMETRY

Carl H. Durney
Electrical Engineering Department
University of Utah
Salt Lake City, UT  84112

5

# INTRODUCTION

This paper is a brief review of work done under the project "Comparison of Theoretical and Experimental Absorption of Radio-Frequency Power" that began in 1973. The basic objectives of the project at that time were the calculation and measurement of internal power deposition in models of humans and other animals irradiated by electromagnetic (EM) fields; i.e., theoretical and experimental dosimetry. The significant interest in possible health hazards caused by the ever-increasing use of radio-frequency (RF) electromagnetic equipment and the resulting increased exposure of both occupational workers and the general public to RF radiation (RFR) that existed when the project began has perhaps even increased over the years of the project.

Dosimetry is an essential element of the research related to RF biological effects and hazards because biological effects are related to the _internal_ fields in the body, which are _not_ the same as the incident fields of the radiation. Determination of the internal fields, either by calculation or by measurement, is often very difficult. Generally speaking, the internal fields are a function of the incident fields, the size and shape of the object, the electrical properties of the object, and the frequency of the incident fields. Thus for a given incident radiation field, the internal fields in an object of a given size and shape may be quite different from the internal fields in a different object.

When this project began, the basic dosimetry work found in the literature consisted primarily of the analysis of planar and spherical

6

models. Effects such as changes in power absorption with polarization, which are now well known, were not well understood at that time. The work in this project has been a systematic attack on the dosimetry problem. It began with a long-wavelength approximate analysis of the internal power absorption in prolate spheroidal models of humans and other animals. This analysis provided the first calculated description of polarization effects, but the results were limited to low frequencies, up to about 30 MHz for models of man. The work then progressed to extend the frequency range of these initial calculations, to develop improved models, and to refine the calculations. Effort during the first few years was devoted primarily to the analysis of planewave irradiation. As knowledge of planewave dosimetry developed, the work was extended to include the more complicated near-field calculations. The work has also included heat-response calculations and pulsed-field absorption calculations.

## TECHNICAL APPROACH

Since the basic framework of classical electromagnetics is Maxwell's equations, dosimetry consists primarily of solving Maxwell's equations for the specific models and irradiation conditions being considered. However, because these equations are very difficult to solve, a variety of special techniques have generally been used by workers in the field to solve them for limited ranges of parameters. A combination of various techniques and a number of different models have been used to develop a reasonably comprehensive picture of dosimetry.

7

This section briefly describes the techniques used in this project, first for planewaves and then for near fields.

## Methods for Planewave Dosimetry

Long-Wavelength Approximation--For frequencies at which the length of the irradiated object is approximately two-tenths or less of a free-space wavelength, calculations of the specific absorption rate (SAR) have been made by an approximation based on the first-order term of a power series expansion in k of the electric and magnetic fields, where k is the free-space propagation constant [1]. This is called a perturbation method because it is based on the fact that the resulting fields are only a small change from the static fields. The field equations resulting from the approximation are easier to solve than Maxwell's equations because they require only solutions to Laplace's equation instead of a solution to wave equations. The approximation is valid for man-sized models up to about 30 MHz. Long-wavelength analyses have been carried out for both prolate spheroidal and ellipsoidal models. These analyses have been very useful because they provide an easy way to calculate the SAR at low frequencies for any size spheroid, because they provide important insight into the qualitative nature of SAR character-istics, and because they provide a good check at lower frequencies for other analysis techniques.

Extended Boundary Condition Method (EBCM)--The extended boundary condition method (which is a method developed by Waterman [2], consisting of a matrix formulation based on an integral equation), has proven to be very useful for calculations of the SAR in prolate spheroidal models of

humans and other animals [3]. It makes use of a spherical harmonic expansion of the incident and scattered EM fields. A system of linear equations relating the unknown expansion coefficients of the scattered field to the known coefficients of the incident field is obtained from the boundary conditions and solved by matrix inversion. For man-sized models, the EBCM can be used to obtain SAR data up to about 70 MHz for E polarization.

Cylindrical Models--The use of cylindrical models has been found to be very useful for calculating average SARs in the range of frequencies from about 400 MHz to 7 GHz, where other methods cannot ordinarily be used. In this range, numerical techniques cannot be used because the wavelength is short enough that the matrices are extremely large and difficult to invert. Yet, the frequency is still low enough that the geometrical optics approximation described in the next subsection is not valid. Fortunately, it has been found that cylindrical models provide useful information in this frequency range [4]. The techniques used for calculation of the SARs in cylindrical models are standard electromagnetic techniques based on classical electromagnetic equations. Although the solution is well known and straightforward, the technique is limited at the high end of the frequency range by difficulties in calculating the higher order Bessel functions of large complex argument that occur in this range. Cylindrical models cannot be used to calculate the SARs for K polarization because the models are infinitely long, but they have provided much useful information for E polarization and H polarization.

Geometrical Optics Approximation--In the frequency range for which the wavelength is much smaller than the size of the irradiated object,

9

the incident electromagnetic wave may be approximated by rays (called the geometrical optics approximation) and the SAR calculated on the basis of planewave absorption in each differential surface area [5]. The lower frequency limit of this approximation is determined by requiring 20 percent correspondence with the Mie solution for spherical models with the same minimum radius of curvature. The SAR calculated by the geometrical optics method has been shown to give nearly the same value for a truncated cylinder as for a spheroid, with these values very close to the value calculated by the cylindrical approximation [6]. The geometrical optics approximation has been very valuable because it has allowed calculation of the SARs in spheroidal models in the frequency range for which calculations for cylindrical models fail. This has allowed extension of the SAR calculations to the high-frequency range of the spectrum.

Empirical Formula--An empirical formula based on the characteristic behavior of the SAR for E polarization has been developed by obtaining the least-squares best fit of the formula to all the available calculated data for prolate spheroidal models of humans and other animals [7]. The result is a simple formula that can be used to calculate the SAR for E polarization as a function of frequency for prolate spheroidal models ranging in size from rats to humans. The equation is simple enough to be used with a hand calculator, and the accuracy is a few percent.

Heat-Response Calculations--Approximate methods based on the overall heat balance equation for the human body have been used to calculate the effect of increased heat load due to RF irradiation [8].

10

The criterion for setting the upper level of heat stress tolerance was chosen to be a rectal temperature of 39.2°C. Calculations were made to determine what incident planewave power density would produce a rectal temperature of 39.2°C in the irradiated subject during an exposure time of 60 minutes, as a function of ambient temperature and humidity.

Semiempirical Ground-Plane Calculations--A semiempirical formula based on the power absorbed in a series RLC circuit was used to obtain the best least-squares fit to the numerical results of the SAR in a man model on a ground plane [9]. After the parameters in the equation were determined by this curve fitting, the equation was used to represent a man standing on a ground plane but separated from it by a small gap, such as would be provided by shoes, and irradiated by an EM planewave. This technique allowed approximate calculations for a situation that would be very difficult to analyze by classical methods, yet is very important because it represents a realistic exposure condition.

Layered Cylindrical Models--The analysis of cylindrical models was extended to layered cylindrical models, with the layers representing the effects of inhomogeneities in the human body such as those produced by combinations of muscle and fat [10]. The analysis is a straightforward extension of the classical method used for homogeneous cylindrical models.

Surface Integral Equation (SIE) Method--We have adapted a method ce 'ed the surface integral equation (SIE) method [11, 12] for calculating SARs in capped cylinder models of humans and other animals [13]. The SIE is a formulation of the electromagnetic field equations in terms of integrals of induced currents on the surface of the body. The moment

11

method is used to solve the integral equations. The SIE method works better than the EBCM for large length-to-width absorber ratios because the EBCM depends heavily on spherical harmonic expansions, while the SIE method does not. Calculations by the SIE method have extended SAR data up to 400 MHz for models of man, whereas the EBCM is limited to about 80 MHz for such models. The SIE calculations are particularly valuable because they can be used for K-polarization calculations. Because of the nature of the SIE equations, it is easier to use a truncated cylinder with spherical end caps as a model than spheroids or other models.

Experimental Methods—Measurements to verify theoretical calculations were made in prolate spheroidal saline phantoms at frequencies below resonance by S. J. Allen and his colleagues at Brooks Air Force Base [14, 15].

## Methods for Near-Field Dosimetry

Planewave dosimetry was developed first because mathematically it is much simpler than near-field dosimetry. However, near-field dosimetry is important because many exposure conditions involve near fields. The extensive knowledge about planewave dosimetry formed a sound basis for the extension to near-field dosimetry. It would have been very difficult indeed to attempt near-field analyses without having the basic information provided by the simpler planewave analyses upon which to build. This subsection describes techniques that have been applied to the analysis of near-field power absorption.

EBCM and Long-Wavelength Analysis With Simple Sources—The work in near-field theoretical dosimetry began with simple models and simple

sources, just as all complicated theoretical analyses begin with the simplest possible configurations. Both the long-wavelength approximation and the EBCM were used to analyze the SARs in prolate spheroidal models of humans and other animals irradiated by short dipoles and small-loop antennas [16, 17]. Prolate spheroidal models were used because the average SAR calculated for planewave irradiation of these models gives results that agree very well with those obtained from more realistic models, and because they are the simplest mathematically. Likewise, the simplest small antennas were used as sources because the mathematics are simpler for them than for more realistic models. Insight gained from these analyses were later used to develop more complicated realistic analyses.

Aperture-Field Representation of Sources--To work towards the analysis of realistic near-field sources, the radiation fields of electrically small apertures were first considered. The fields in a small aperture might represent exposure conditions such as those produced by leakage fields in RF sources like microwave ovens and small holes in waveguides. The method of analysis consists of replacing the electric and magnetic fields incident on one side of a small aperture by an equivalent configuration of electric and magnetic dipoles that describe the defracted fields on the other side of the aperture. The EBCM was used to calculate the SAR produced by these sources.

Since the small-aperture field analysis is limited in the sources that it can represent, the methods were extended to the analysis of SARs produced by fields in electrically large apertures, which can be used to represent more realistic exposure conditions, such as those produced by

13

large reflector antennas. The method of solution is to expand the incident fields in vector spherical harmonics about an origin suitably located in the aperture plane. This expansion is then shifted to the origin of the prolate spheroid model by means of an addition theorem for rigid translations of the vector spherical harmonics. Such a shift in a coordinate system is necessary so that analytic continuation of the incident and the induced field expansions can be made with respect to a single coordinate system centered at the origin of the spheroid. With this new field expansion, the EBCM is employed to calculate the fields inside the spheroid [18].

A technique was later developed for expanding the spherical harmonics about the origin of the spheroid without requiring the addition theorem. This method turns out to be more useful for calculating the absorption in spheroidal models close to the source, while the method described above is better for calculating the scattered fields farther away from the source.

Block Model and Moment Method--In order to calculate SAR distributions, and in particular to study the SAR in a model of a fetus in a sitting woman, we have used a block model and the moment method, a technique used by several others. Our computer program is adapted from a program written by Livesay and Chen for planewave irradiation [19]. We modified the program to include the calculation of internal fields and SAR distribution due to near-field exposures. We first calculated the SARs in a standing model of man irradiated by a short electric dipole to test the program and get initial near-field SAR data. From the data, we were able to show that the _average_ near-field SAR in a

prolate spheroidal model of man is very close to that in a block model [20]. This is important information because it justifies the use of the simple spheroidal model for average near-field SAR calculations. We then constructed a sitting model of a woman and wrote the program to calculate the SARs in that model.

Subdivision of Mathematical Cells--The SAR distribution in a block model cannot be calculated with very good accuracy because the number of mathematical cells in the model must be limited at present to less than 200. This means that the inhomogeneities in the human body can be represented only to a very limited extent. It is not possible, for example, to represent the structure of an arm in terms of bone, muscle, and fat or to represent the size, shape, and composition of a typical internal organ with a model of only 200 mathematical cells. In the present inhomogeneous models of man, the mathematical cells are each assigned a permittivity that represents an average permittivity of a particular region of the body represented by the cell. Since it does not seem possible to increase the number of mathematical cells to the point where an adequate representation of the body could be obtained, we have begun to investigate an approximation that will allow one specific region of the body, for example an internal organ, to be represented by a large number of small mathematical cells, while the remainder of the body is represented by larger mathematical cells. This would allow a significantly greater resolution in the SAR distribution in a given small subvolume of the body, while other regions of the body in which as much accuracy is not required would be represented by much coarser mathematical cells. The method is based on the tensor Green's-function

15

integral equation as follows:

$$\underline{E}_1(\underline{r}) = \int_V \underline{G}(\underline{r},\underline{r}') \cdot \underline{E}_1(\underline{r}')dV' + \underline{E}_i(\underline{r}) \qquad (1)$$

Equation 1 shows the integral equation where $\underline{E}_1$ represents the field in a block model with coarse mathematical cells, $\underline{r}$ is the field point, $\underline{r}'$ is the source point, $\underline{G}$ is the Green's function, and $\underline{E}_i$ is the incident field. V represents the total volume of the block model. This equation is first solved with coarse cells and the solution $\underline{E}_1$ obtained. Then the integral equation is rewritten as shown in Eq. 2.

$$\underline{E}_\ell(\underline{r}) = \int_{V_1} \underline{G}(\underline{r},\underline{r}') \cdot \underline{E}_1(\underline{r}')dV' + \int_{V_\ell} \underline{G}(\underline{r},\underline{r}') \cdot \underline{E}_\ell(\underline{r}')dV' + \underline{E}_i(\underline{r})$$

$$(2)$$

Equation 2 is the integral equation for the same block model, but now with one or more of the original cells subdivided into smaller cells. $V_\ell$ represents the volume consisting of the subdivided cells, and $V_1$ represents the remaining volume of the original model. The approximation is that the $\underline{E}_1$ obtained from the solution of Eq. 1 before the subdivision of the cells is now considered to be a known quantity in all the cells in volume $V_1$ in Eq. 2. This reduces the number of unknowns in Eq. 2 to $\underline{E}_\ell$, the field in the subdivided cells, which would allow solution of Eq. 2 with as many as 100-200 mathematical cells consisting of the smaller cells resulting from subdivision. This means that if the method works, it would allow calculation of the SAR in a given organ, for example, with that organ divided into as many as 100-200 mathematical cells, thus providing much greater resolution than could ordinarily

16

be obtained. The validity of the approximation that $\underline{E}_1$ is the same in the undivided cells both before and after subdivision remains to be established. The approximation would be expected to be good for remote undivided cells because the Green's function decreases rapidly with distance, but the real question is how good the approximation is for undivided cells adjacent to the subdivided cells. Some results of preliminary investigations of this method are given in the section RESULTS AND PROGRESS.

Calculation of SARs from Measured Fields--An important remaining need in dosimetry is to be able to measure the field existing in a given region and from those measured field values calculate the SAR that would be produced by an object placed in those fields. Although this could be done by measuring amplitude and phase of the vector fields at each point corresponding to the center of a mathematical cell in the block model of man, the number of measurements required would be prohibitive and impractical, especially the measurement of phase. To determine whether a practical method for measuring fields and calculating expected SARs can be developed, we are collaborating with Dr. Art Ludwig of General Research Corporation, Santa Barbara, California, through a subcontract to this project to develop a method for representing measured fields by a spherical harmonic expansion, with statistical methods for minimizing the effects of measurement noise. This expansion would then be used with the EBCM to calculate SARs in spheroidal models, and later with the moment method to calculate SARs in block models. The techniques for expanding fields in spherical harmonics that were described above for aperture-field methods will be an important asset in this study.

17

The first step in the investigation will be to develop a composite computer program for expanding the measured fields in spherical harmonics and calculating the SAR in spheroids by the EBCM. The SAR will then be calculated from the composite program and compared with the SAR calculated by previous methods directly from the known dipole fields, without noise. This will allow an evaluation of the validity of the field expansions and the effects of noise. We will then proceed to investigate the number of field measurements required to get adequate accuracy in the calculation of the SAR. We will attempt to establish the correlation between the error bounds on the SAR and the number of measurements. In particular we will attempt to determine whether reasonably accurate SARs can be calculated from measurements of the incident field amplitude only, without measuring the phase of the incident fields. This is important to know because measurement of the phase on the incident field is very difficult. After the program is developed for spheroids, it will be extended to the calculation of SARs in block models irradiated by near fields.

Pulsed-Field Methods--To investigate whether the SARs produced by pulsed fields are significantly different in nature from those produced by CW incident fields, we have developed two approaches. The first is the analysis of SARs produced by pulsed fields incident on spheroids that are small compared to wavelengths in the main frequency spectrum of the pulsed fields. In this approximation, the long-wavelength analysis is used to calculate the internal fields in the spheroid. Calculations have been made for a small spheroid irradiated by the fields of a pulsed

18

phased array of short dipole antennas. To allow investigation of the effect of the rise time of the pulse, a more realistic pulse form than the traditional step-function pulse is used. The representation of the current pulse on the antenna is shown in Fig. 1, and the mathematical expression is given in Eq. 3.

$$i(t) = \left[\tanh \alpha(t + \gamma + \tau/2) - \tanh \alpha(t + \gamma - \tau/2)\right] \cos \left(\omega[t + \gamma] + \delta\right)$$

(3)

where $\alpha$ is a factor representing the rise time, the parameter $\gamma$ shifts the pulse to the right or left in time, $\tau$ is the length of the pulse, and $\delta$ is a phase factor. Some results of this analysis are given in the next section.

The second approach is the calculation of internal fields produced by a pulsed planewave incident on a lossy inhomogeneous dielectric half space. Since a Laplace transform analysis would be difficult for an inhomogeneous dielectric and for the pulsed waveform shown in Fig. 1, we have developed a numerical analysis based on computer solution of two coupled integral equations in the time domain. The coupled integral equations are given in Eqs. 4 and 5.

$$j_p(z,t) = \sum_{i=1}^{3} \frac{\varepsilon_r \left(\varepsilon_{oi} - \varepsilon_{\infty i}\right)}{\tau_i} E(z,t) - \frac{\varepsilon_r \left(\varepsilon_{oi} - \varepsilon_{\infty i}\right)}{\tau_i^2} \int_o^t e^{-(t-\hat{t})/\tau_i} E(z,\hat{t})d\hat{t}$$

(4)

19

$\alpha = 2.0 \times 10^9$/second

$f = 500$ MHz

$\tau = 6.0$ nanoseconds

$\delta = \gamma = 0$
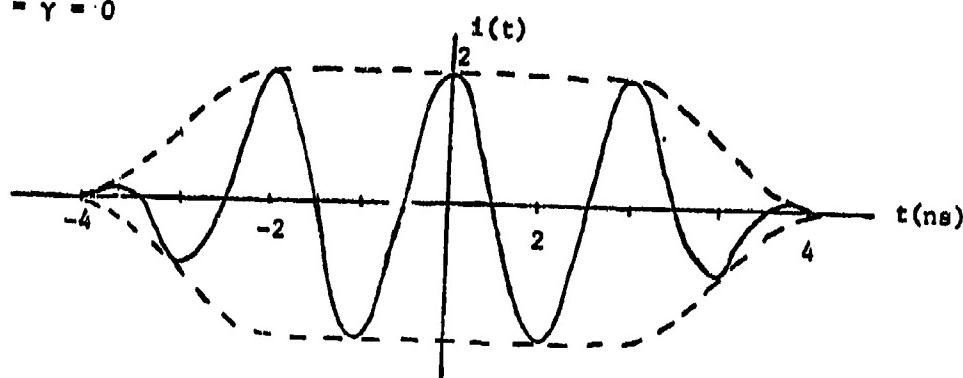


Fig. 1. Current pulse of Eq. 3.

$$E(z,t) = \frac{1}{2}\sqrt{\frac{\mu_0}{\epsilon_0}}\left[\int_{z_0^-}^{z} u\left(t + \frac{z - \hat{z}}{c}\right)j_p\left(\hat{z},t + \frac{z - \hat{z}}{c}\right)d\hat{z}\right.$$

$$- \int_{z_0^+}^{z} u\left(t - \frac{z - \hat{z}}{c}\right)j_p\left(\hat{z},t - \frac{z - \hat{z}}{c}\right)d\hat{z}$$

$$+ \int_{z_0^-}^{z} u\left(t + \frac{z - \hat{z}}{c}\right)j_s\left(\hat{z},t + \frac{z - \hat{z}}{c}\right)d\hat{z}$$

$$- \int_{z_0^+}^{z} u\left(t - \frac{z - \hat{z}}{c}\right)j_s\left(z,t - \frac{z - \hat{z}}{c}\right)d\hat{z} + ca^+(z - ct,0)$$

$$\left. - ca^-(z + ct,0)\right] \tag{5}$$

where the steady-state permittivity is given by the Debye equation

$$\epsilon(\omega) = \sum \epsilon_{\infty i} + \frac{\epsilon_{oi} - \epsilon_{\infty i}}{1 + j\omega\tau_i} \tag{6}$$

In these equations, $a^+$ and $a^-$ represent initial electric and magnetic field values, $j_s$ is source current, $j_p$ is polarization current, and $u$ is a step function. These equations are derived in reference [18].

Experimental Methods--SARs have been measured in scaled saline spheroidal phantoms irradiated by the near fields of short electric monopoles above ground planes, simulating spheroids irradiated by short electric dipoles [21]. Since the actual fields of the dipoles are not

21

the same as the calculated fields of an ideal short electric dipole, specific comparisons between calculated and measured values of SARs are not meaningful. However, the measured and calculated values have shown good qualitative agreement as described in the next section.

## RESULTS AND PROGRESS

Since most of the results of this project are contained in the three editions of the Radiofrequency Radiation Dosimetry Handbook that have been published, a brief summary of each of these editions of the handbook is given in this section, along with some additional results.

### Planewave Dosimetry

Radiofrequency Radiation Dosimetry Handbook (First Edition)--The first edition of the handbook was published in September 1976 [22]. It contains planewave dosimetric data for spheroidal and ellipsoidal models of humans and other animals. The frequency range of the data was 10 kHz-1.5 GHz. The dosimetric data showed polarization effects clearly, but contained little on resonance effects because the calculations were made by the long-wavelength approximation and the EBCM.

Radiofrequency Radiation Dosimetry Handbook (Second Edition)--In May 1978, the second edition of the handbook was published [8]. In this edition the frequency range of the dosimetric data was extended to 10 MHz-100 GHz. This edition of the handbook has been widely circulated and used by many researchers throughout the world interested in dosimetry and electromagnetic radiation hazards. Data in the handbook was used, along with other data, by the ANSI C95.4 Committee on Safety

22

Levels and/or Tolerances With Respect to Personnel in revising its safety standard. Handbook data was also used by the National Institute of Occupational Safety and Health in developing safety standards. Similar organizations in foreign countries have likewise used the data. Improved methods of calculation included the EBCM, the use of cylindrical models, and the geometrical optics methods, as described in the previous section of this paper. The handbook includes derivation of the empirical formula for calculating the SAR in spheroidal models, and the semiempirical formula for calculating the SAR in models on ground planes. Heat-response calculations are included, along with rather extensive metabolic-rate and other biological data. Tables of permittivities of tissues compiled from the literature are given. The handbook also includes a summary of the articles in the literature on dosimetry. Comparisons are made between published values of theoretical and experimental SARs.

Figure 2 is an illustration of how a combination of techniques has been used to obtain the average SAR data as a function of frequency. As explained earlier, it has been necessary to use a combination of techniques because of the difficulty of solving Maxwell's equations in any frequency range. As indicated in Fig. 2, numerical techniques have been used up to frequencies of about 600 MHz. Beyond this frequency, numerical techniques are impractical because they require excessive amounts of computer storage. The long-wavelength approximation has been very useful up to about 30 MHz for man-sized models. From about 400 MHz to 7 GHz cylindrical models have been used. Above 7 GHz the geometrical optics technique has been employed.

23
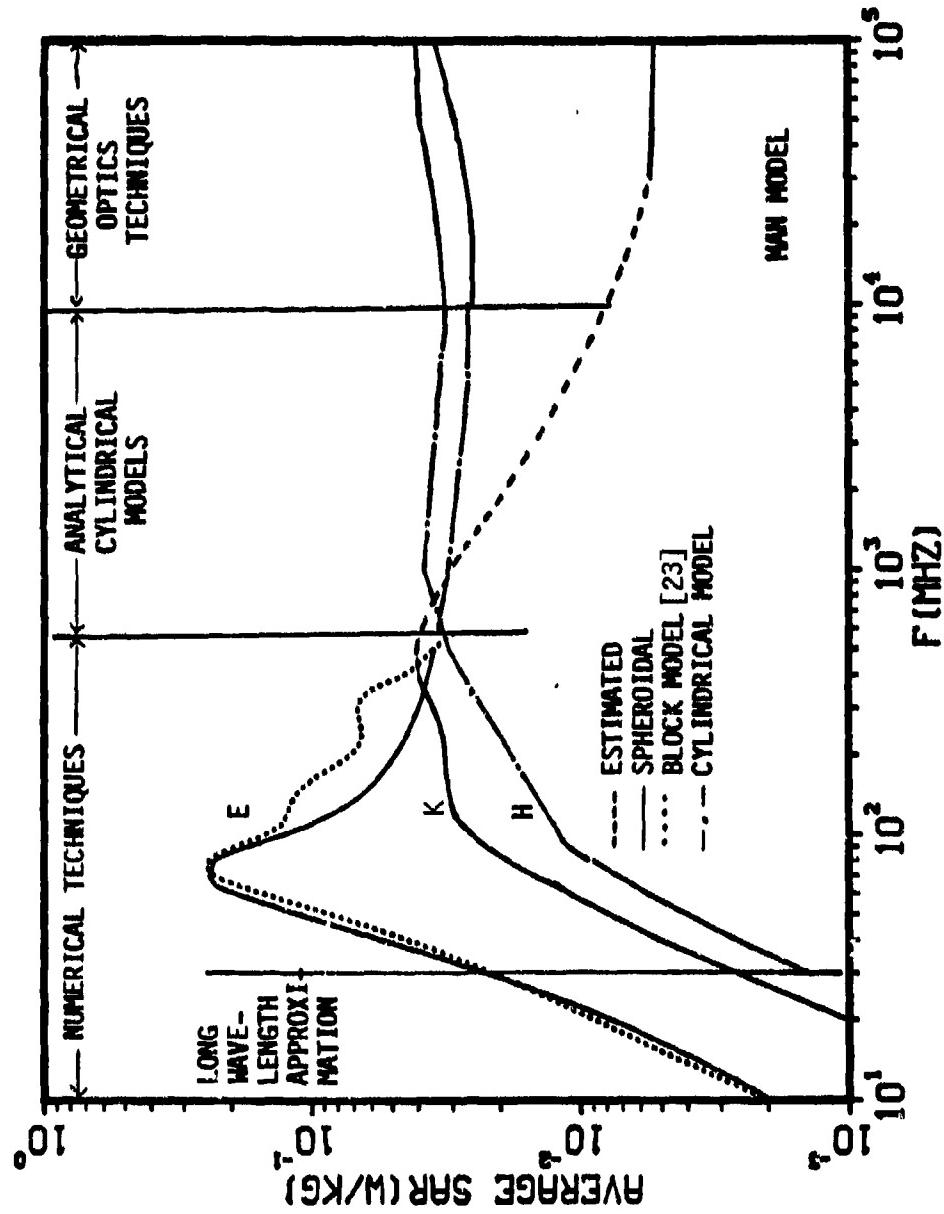
Fig. 2. Average SAR for models of an average man irradiated by an EM planewave of 1 mW/cm² power density. E, K, and H designate polarizations in which the incident electric field vector, propagation vector, and magnetic field vector, respectively, are parallel to the long axis of the body. The various methods used to make the calculations are shown.

24

Figure 3 illustrates the value of the dosimetric data in the handbook to the researcher. Without this kind of dosimetric data, it would not be possible to extrapolate observed biological effects induced in animals by electromagnetic radiation to those expected in man. For example, it is clear from Fig. 3 that if both a man and a rat were irradiated by a 650 MHz-planewave, the average SAR in the rat would be more than an order of magnitude greater than that in the man. Hence, if a biological effect were observed in a rat with a given incident power density, it would be expected that a similar biological effect in man would occur at much higher incident power density. Another important difference would be that the local SAR in the rat would be quite different from that in the man. In the man, the heating would tend to be more superficial than in the rat, since the size of the man is much larger compared to a wavelength than the rat. The second edition of the handbook describes an approximate method for adjusting frequencies and power levels of radiation in animals to correspond to similar irradiation conditions in man.

Figure 4 shows the ground-plane information contained in the handbook. The curves show that the effect of the ground plane is to shift the curve to the left and that a gap between the absorber and the ground plane gives an intermediate effect between irradiation in free space and irradiation on the ground plane. This information is very valuable because most exposures are of people involved in some relation to the ground plane.

Figure 5 shows a comparison between calculated data and experimental data obtained by Gandhi and Hagmann [24]. It can be seen that the

25
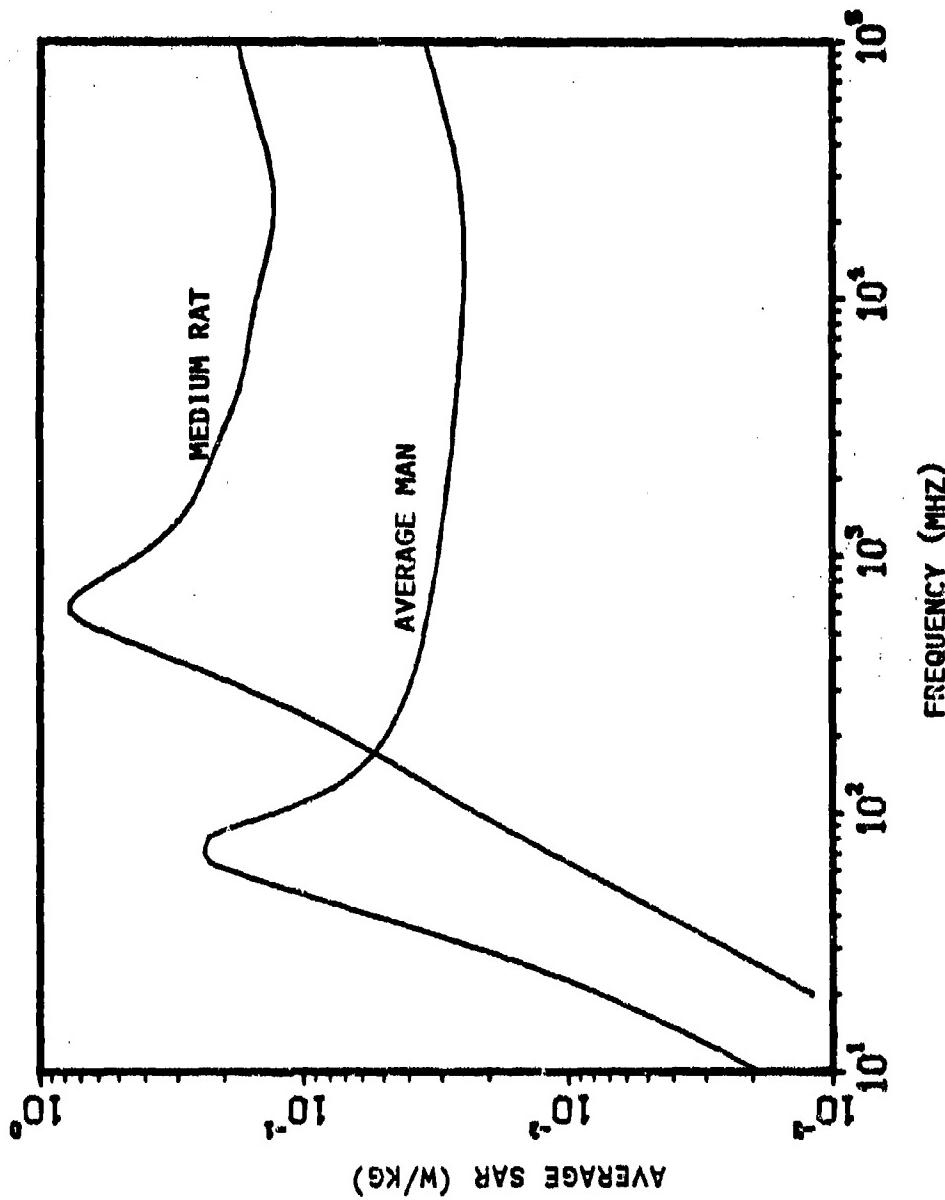
Fig. 3. Average SAR for prolate spheroidal models of an average man and a medium rat for E polarization, for an incident planewave power density of 1 mW/cm².

26
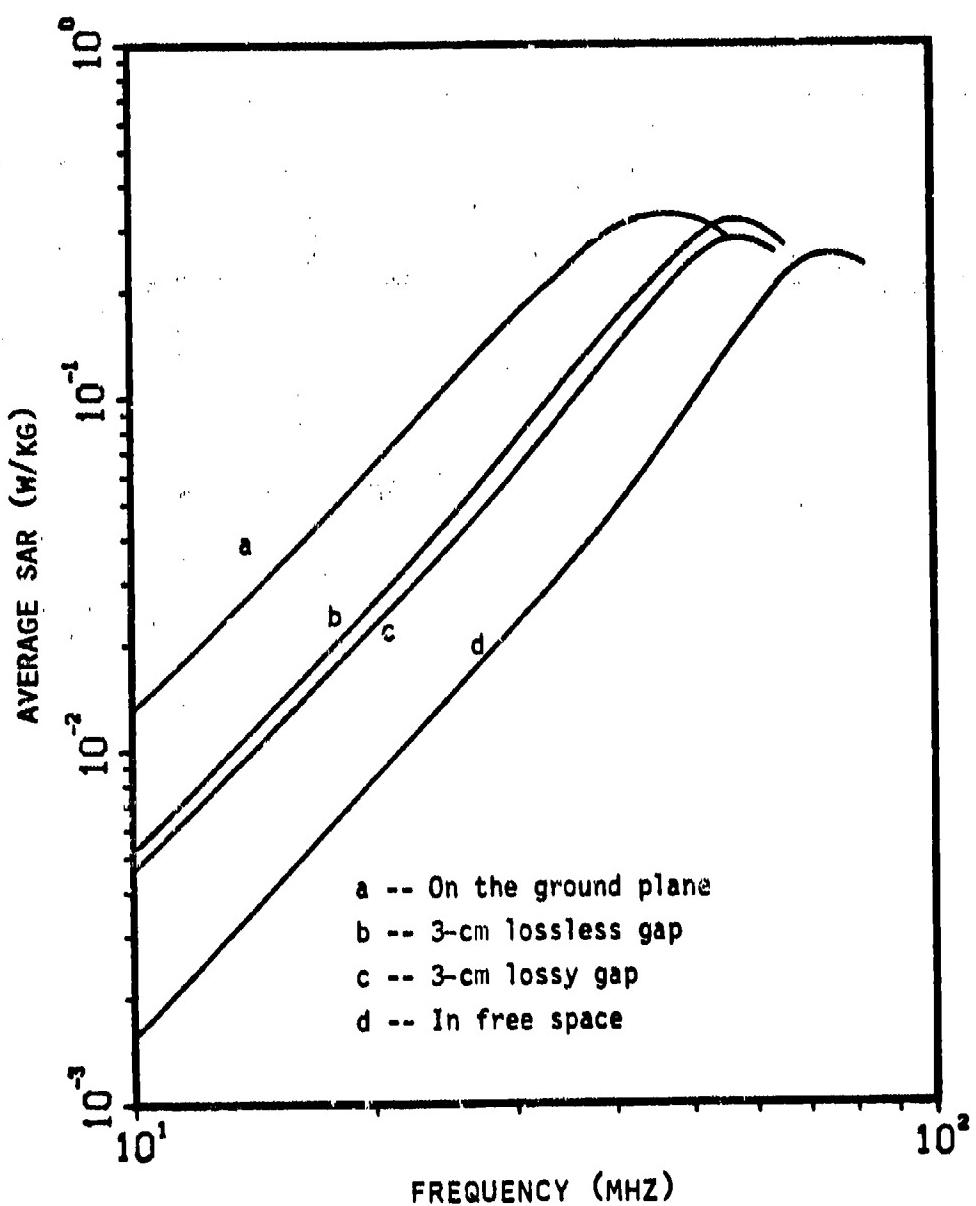
Fig. 4. Average SAR for an average man separated from a perfect
ground plane by a gap of 3 cm, both with and without
loss.     Curves for the man standing on the ground
plane and in free space are shown for comparison.

27
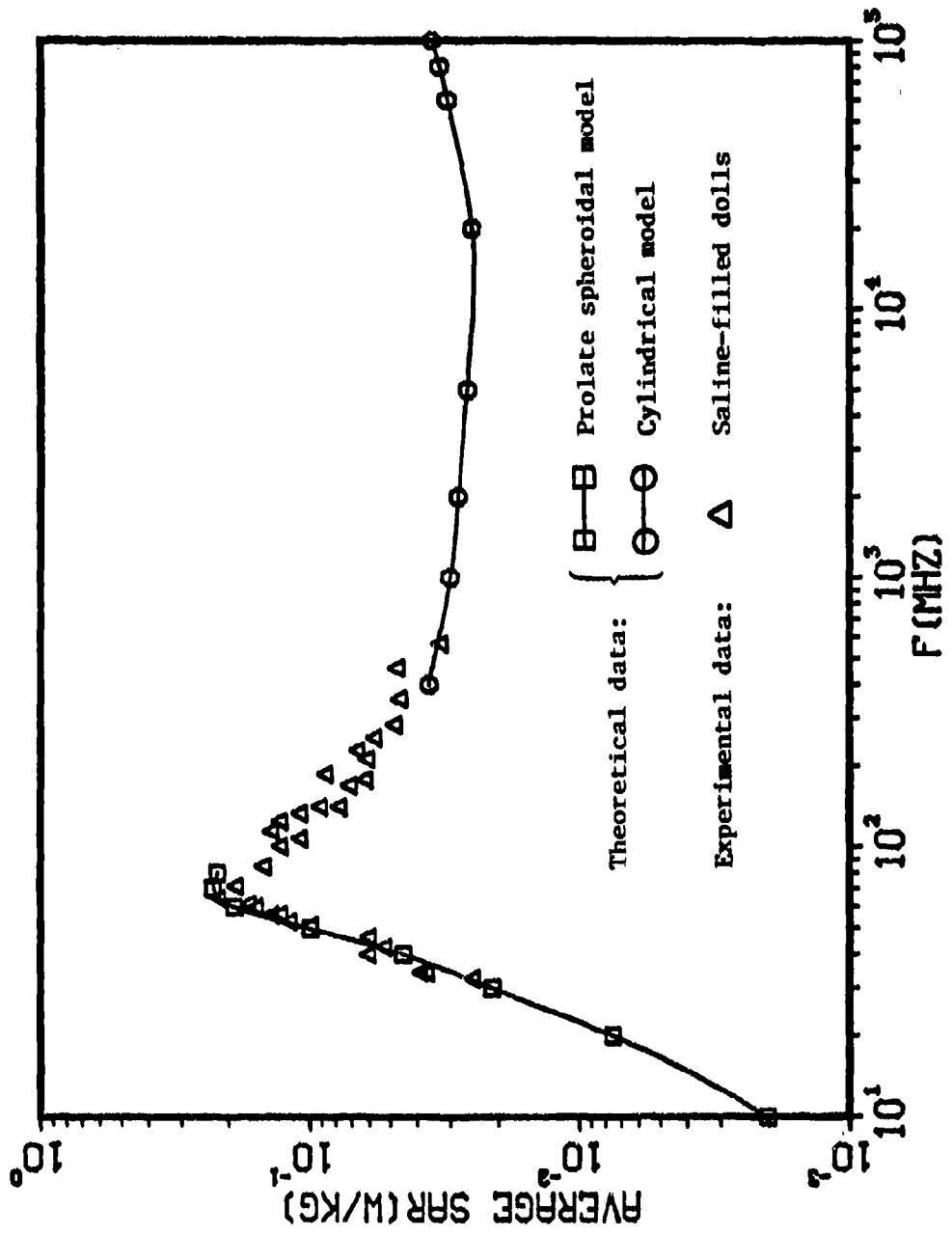
Fig. 5.  Calculated and measured values of the average SAR for models of an average man, E polarization.  Incident power density is 1 mW/cm².

agreement of the data is quite good. Although all experimental data do not agree that well with calculated data, the theoretical calculations and experimental results are generally in good agreement.

The rather extensive compilation of permittivity values for tissue from the literature that is given in the handbook has also proven to be very useful to researchers. Tables of other biological data and qualitative explanations of electromagnetics are other important features of this edition of the handbook.

Radiofrequency Radiation Dosimetry Handbook (Third Edition)--The third edition of the RFR Dosimetry Handbook was published in August 1980 [25]. In this edition, the tables in the second edition were updated with the recent information from the literature. Although the main emphasis of the third edition is on near-field dosimetry, the third edition also contains planewave dosimetric data for layered cylindrical models, SARs for circularly and elliptically polarized planewaves, and improved K-polarization calculations. Figure 6 shows the data for the layered model compared with data for homogeneous models. As the data indicate, the layering effect is only important for frequencies above about 400 MHz. Explanations for effect of the layers are given in the handbook. The improved K-polarization calculations for the rat agree well with recently obtained experimental values [26]. In the second edition, the values for K polarization above the range where the long-wavelength approximation was valid were primarily estimated values because the cylindrical model is not valid for K polarization. The estimated values were based on some early experimental results given in the literature, which apparently were too low.
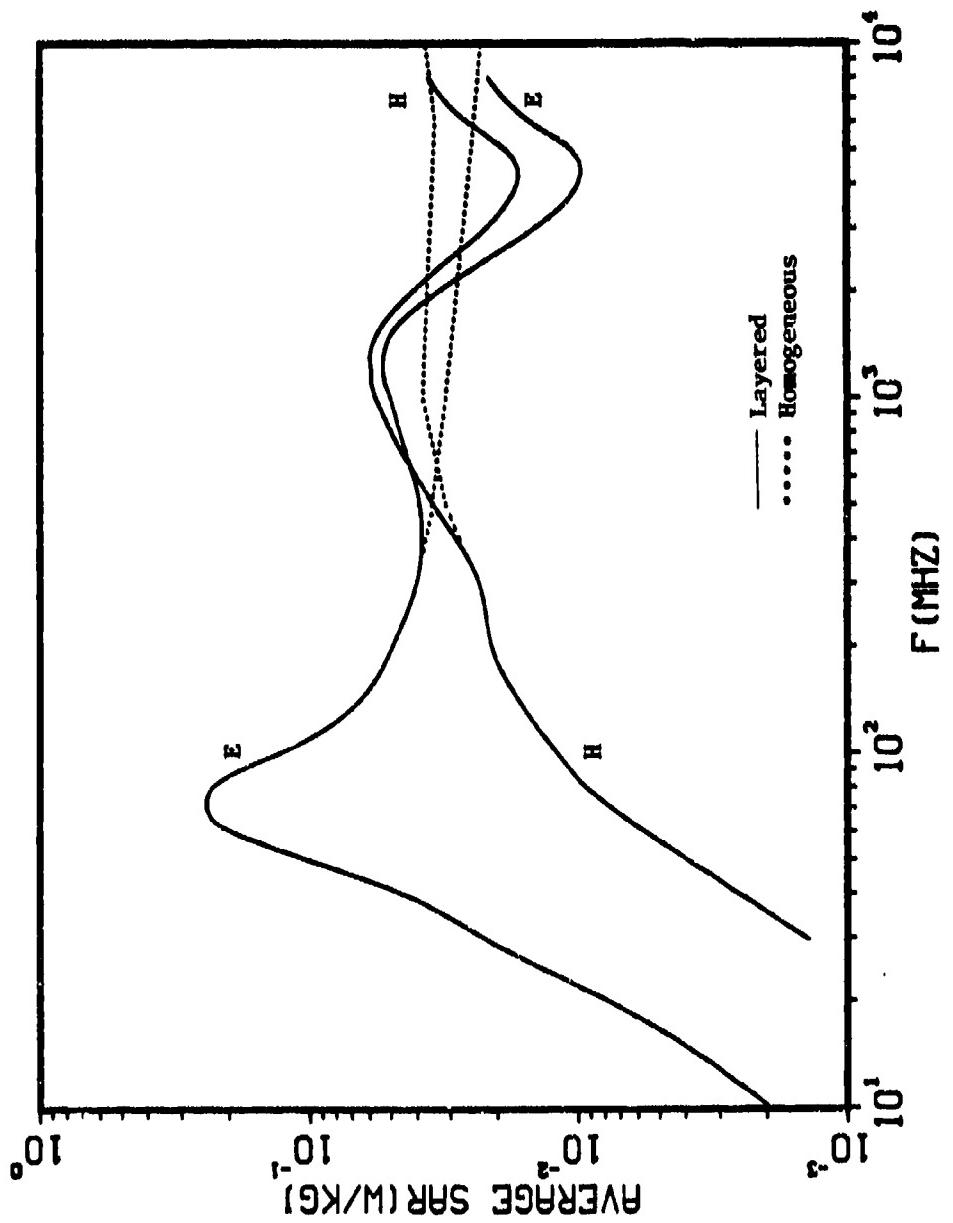
Fig. 6. Calculated average SAR in homogeneous and multilayered models of an average man for an incident power density of 1 mW/cm² for two polarizations.

Radiofrequency Radiation Dosimetry Handbook (Third Edition)--The main emphasis of the third edition of the handbook is near-field dosimetry. However, since near-field dosimetry is much more complicated than planewave dosimetry, the dosimetric data in the third edition is quite different in nature from that in the first two editions. The main reason for the difference is that near-field SARs cannot be normalized to an incident power density as planewave SARs can be. Consequently, each set of near-field dosimetric data must be related to the source that produced the near fields, and it is not possible to generalize the dosimetric data. Thus, researchers desiring dosimetric information about their experiments would need a set of data for each particular near-field source, which of course is not practical. For these reasons, the near-field data in the third edition is given only for some typical idealized near-field sources, namely, short electric dipoles and small-loop antennas. The purpose of the data is to show the characteristics of near-field SARs and to provide insight and understanding about near-field absorption. The insight and understanding from these and other near-field data have been used to formulate two qualitative principles that can be used to predict relative values of near-field SARs. The derivation and applications of these principles are described in the third edition of the handbook. An example of the dosimetric near-field data and the understanding provided by the qualitative principles is shown in Fig. 7, which displays the average SAR produced in a spheroidal model of an average man irradiated by a short electric dipole at 200 MHz as a function of the distance between the dipole and the spheroid.

31
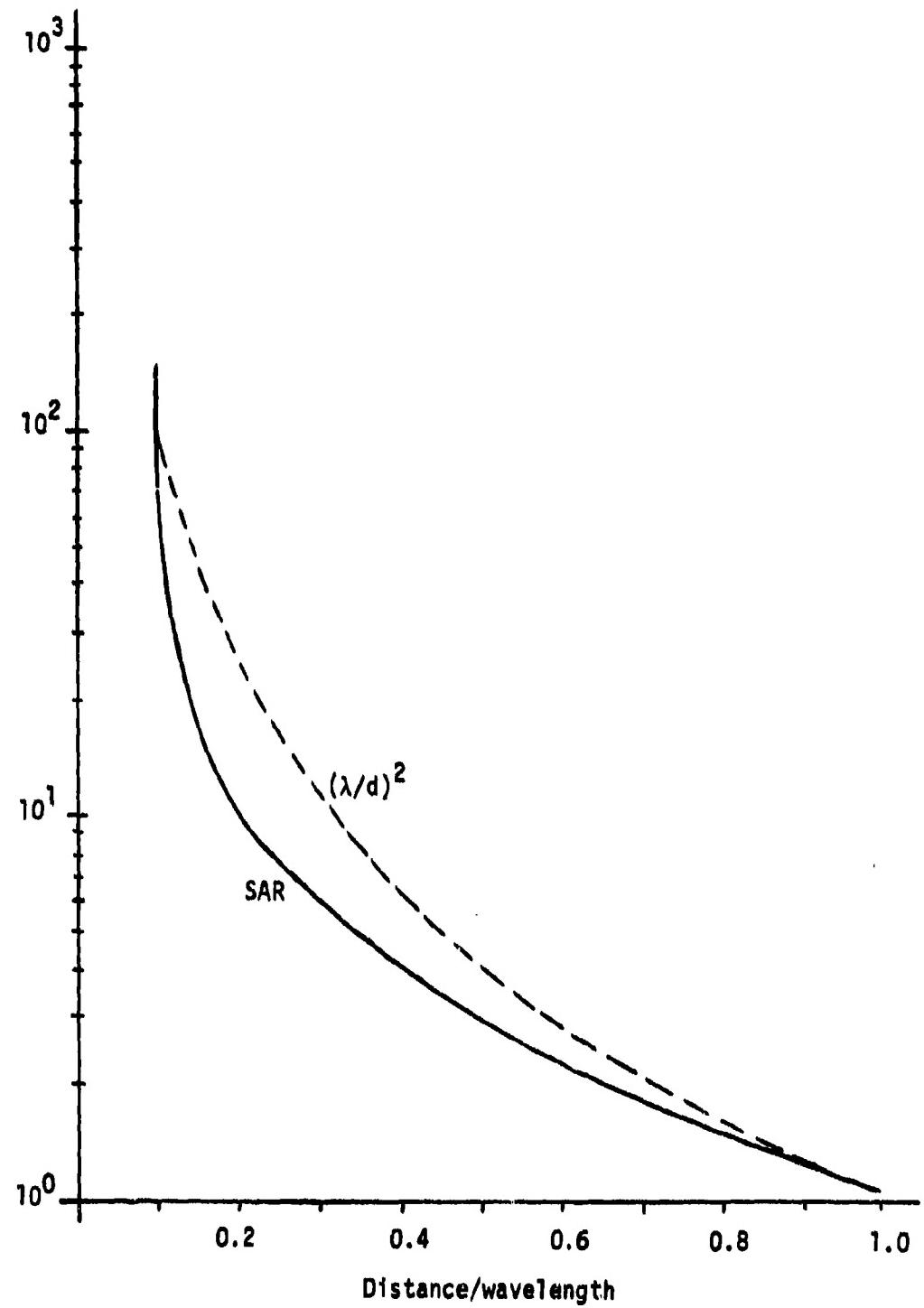
Fig. 7. Calculated values of normalized SAR and $(\lambda/d)^2$ for a spheroidal model of an average man irradiated by a short electric dipole for E polarization at 200 MHz; d is the distance between the dipole and the spheroid and $\lambda$ is the wavelength of irradiation.

32

Note that the SAR does not increase as fast as the inverse distance squared, as might be expected from the 1/r variation of the far fields, which would correspond to a $1/r^2$ variation in the incident power density of the far fields. One might expect that in the near fields, the increase in the SAR would be greater than it would be in the far fields, since the near fields vary faster than 1/r. The reason that the SAR does not increase as fast as inverse distance squared is explained below in terms of the incident near-field variation. Similar behavior has been found in measurements of the average SAR in spheroidal models [21].

A brief summary of the qualitative principles derived in the third edition of the handbook is given next as a basis to explain the SAR characteristics in Fig. 7. At the lower frequencies, the internal electric fields can be thought of as being generated by the incident $\underline{E}$ and $\underline{H}$ separately. That is,

$$\underline{E}_{in} = \underline{E}_e + \underline{E}_h \tag{3}$$

where

$\underline{E}_e$ is the internal electric field caused by $\underline{E}_{inc}$, the incident $\underline{E}$ field.

$\underline{E}_h$ is the internal electric field caused by $\underline{H}_{inc}$, the incident $\underline{H}$ field.

$\underline{E}_{in}$ is the total internal electric field in the body.

33

At the lower frequencies, $\underline{E}_e$ and $\underline{E}_h$ can be calculated separately from $\underline{E}_{inc}$ and $\underline{H}_{inc}$, and added to obtain $\underline{E}_{in}$, as given in Eq. 3. This is not true at higher frequencies, where $\underline{E}_e$ and $\underline{E}_h$ cannot be separately attributed to $\underline{E}_{inc}$ and $\underline{H}_{inc}$, respectively, since E and H are coupled together by Maxwell's equations. However, the general concepts based on Eq. 3 do seem to have some validity at higher frequencies, sometimes even up to resonance.

The following two principles can be used to predict the relative values of $\underline{E}_{in}$:

    1. $\underline{E}_e$ is <u>stronger</u> when $\underline{E}_{inc}$ is mostly <u>parallel</u> to the boundaries of the object, and <u>weaker</u> when $\underline{E}_{inc}$ is mostly <u>perpendicular</u> to the boundaries of the object.

    2. $\underline{E}_h$ is <u>stronger</u> when $\underline{H}_{inc}$ intercepts a <u>larger</u> cross section of the object and <u>weaker</u> when $\underline{H}_{inc}$ intercepts a <u>smaller</u> cross section of the object.

Figure 8 shows some examples of qualitative evaluations of internal fields based on these principles. For simplicity, only simple objects are used for illustration, but the principles apply to more complicated shapes like the human body.

Figure 9 illustrates the qualitative explanation of the difference in average SAR shown in Fig. 2 for the three polarizations. For frequencies below resonance, the average SAR for E polarization is the greatest because both $\underline{E}_e$ and $\underline{E}_h$ are strong. The SAR for H polarization is lowest because both $\underline{E}_e$ and $\underline{E}_h$ are weak. The average for K polarization lies between that for E polarization and that for H polarization
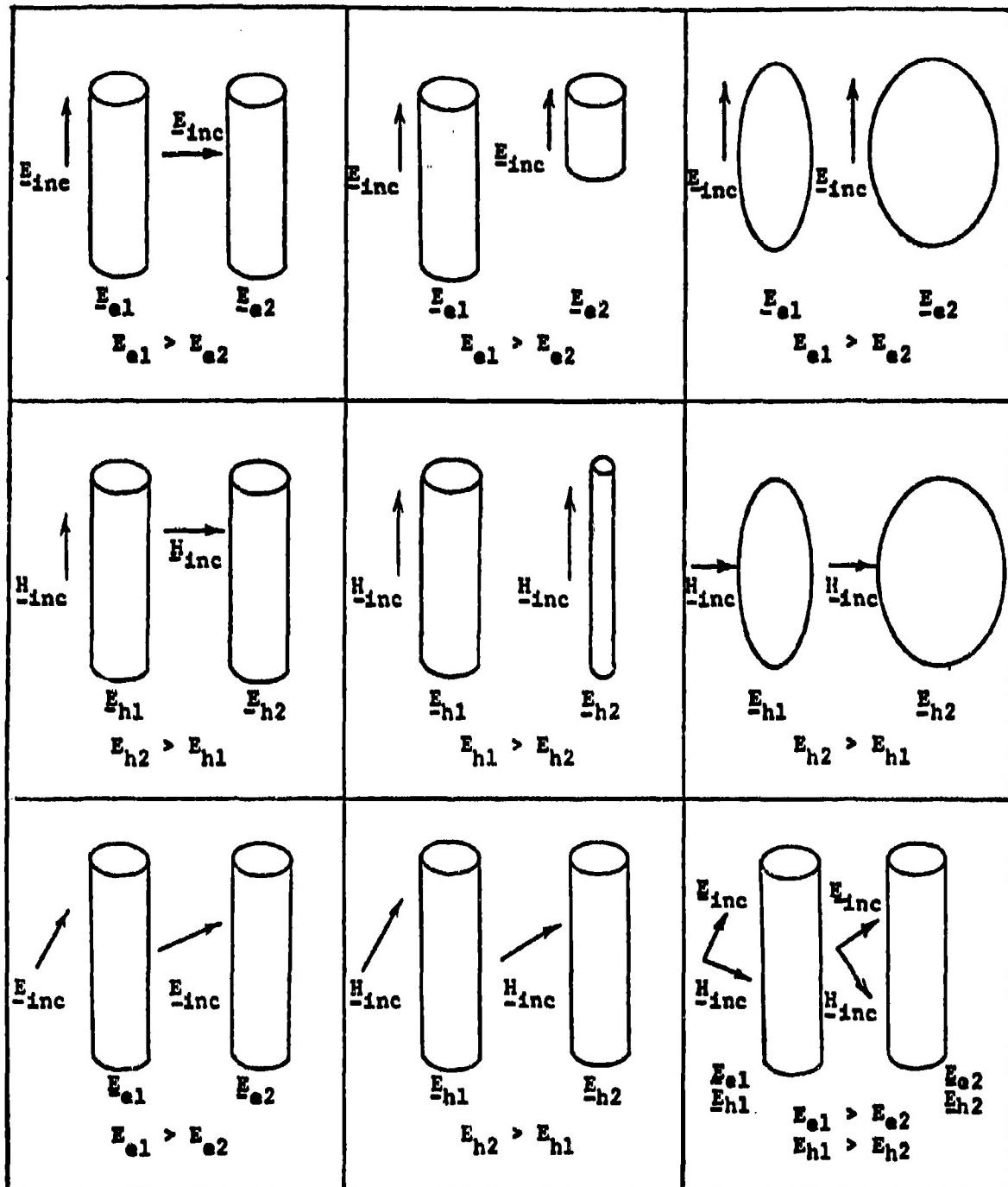
Fig. 8.  Qualitative evaluation of the internal fields based on quali-
tative principles;     $E_e$ is the internal electric field
generated by $E_{inc}$, the incident E field, and $E_h$ is the
internal electric field generated by $H_{inc}$, the incident H field.
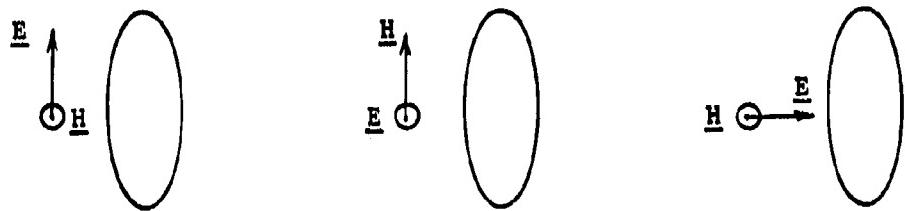
Fig. 9.    Qualitative explanation of the differences
           in average SAR shown in Fig. 2 for the
           three polarizations in spheroidal models.
           ⊙ means the vector is normal to the paper.

36

because $\underline{E}_e$ is weak, but $\underline{B}_h$ is strong. Thus the two qualitative principles very nicely explain why the SAR is a strong function of the polarization. Other similar qualitative explanations can be used to predict whether the average SAR will be large or small for a given set of conditions.

Similarly, the qualitative principles can be used to explain near-field absorption characteristics. Figure 10 shows the same information as Fig. 7, along with information about the electric field. Note that $|E|^2$ is less than $(\lambda/d)^2$, but follows along nearly parallel with it. The change in $|E|^2$ does not explain why the average SAR increases more slowly than $(\lambda/d)^2$ until it rises suddenly between $\lambda/d = 0.2$ and 0.3 and then rapidly increases above $(\lambda/d)^2$ for $\lambda/d$ less than 0.2. The explanation is found in the change of the orientation of the $\underline{E}$ field with respect to the spheroid, as described by $\alpha$, the angle between $\underline{E}$ and the major axis of the spheroid. Note that $\alpha$ is increasing from $\lambda/d = 1$ to about 0.25, where it suddenly begins to decrease. As $\alpha$ is increasing, E is changing from mostly parallel to more perpendicular to the spheroid. According to the first qualitative principle, this means that $\underline{E}_e$ is becoming weaker as $\alpha$ increases. Thus $\underline{E}_e$ is getting weaker from about $\lambda/d = 1$ to about 0.25, and then becomes stronger as $\alpha$ decreases again. This factor causes the average SAR to begin to rise rapidly as $\alpha$ decreases. This is an example of how the qualitative principles can be used to explain near-field absorption characteristics, as well as planewave absorption characteristics.

Aperture-Field Representation of Sources--As described in the previous section, TECHNICAL APPROACH, the formulation for the calculation of SARs in prolate spheroids irradiated by the fields of electrically small apertures and the fields of electrically large apertures has

37
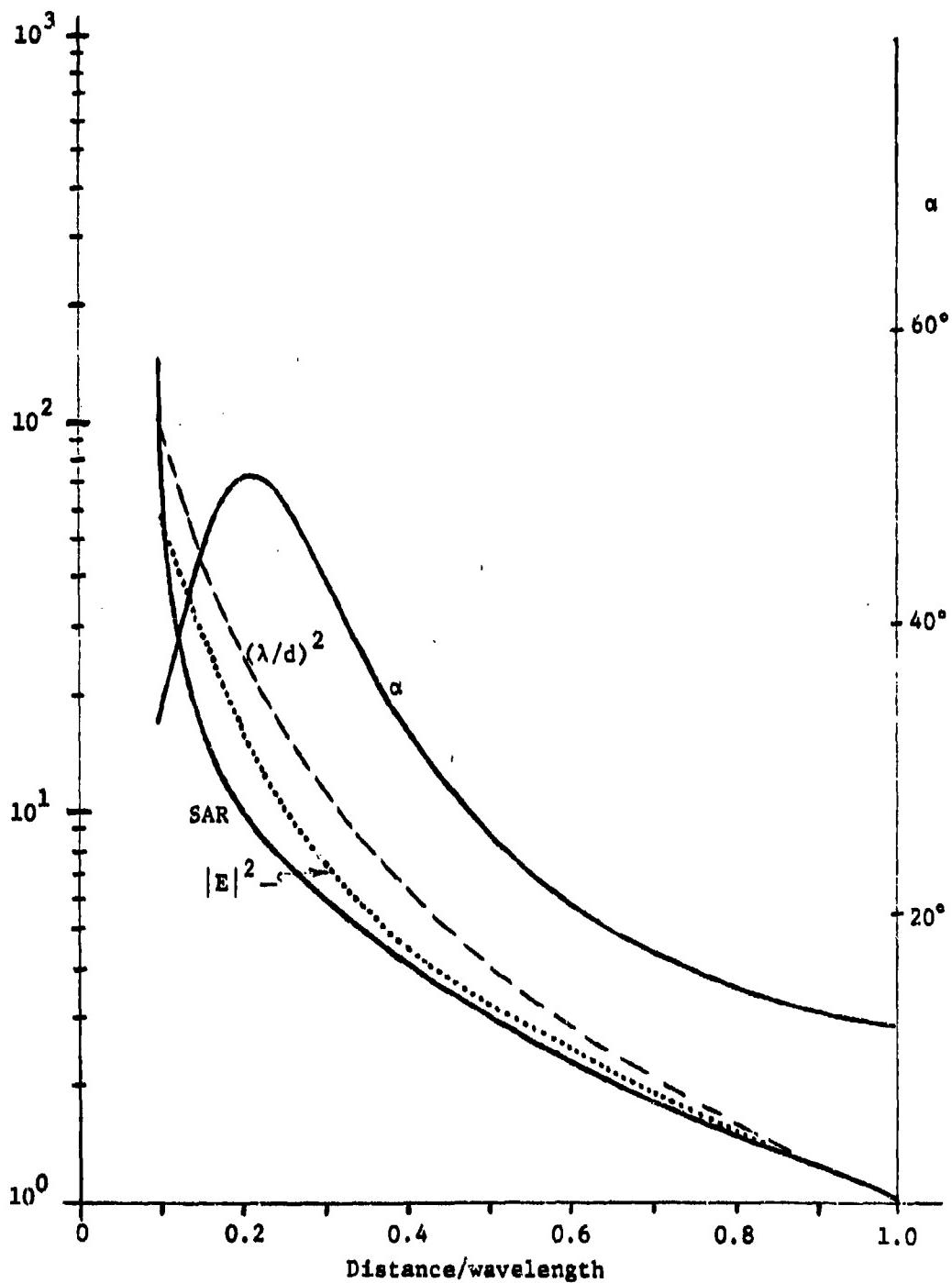
Fig. 10. Calculated values of normalized SAR, normalized $|E|^2$, and angle between $\underline{E}$ and the spheroid's major axis for a spheroidal model of an average man irradiated by a short electric dipole for E polarization at 200 MHz; d is the distance between the dipole and the spheroid, $\lambda$ is the wavelength of the radiation, and $\alpha$ is the angle between $\underline{E}$ and the spheroid's major axis.

been completed. Data have been generated for average SARs in prolate spheroidal models of man irradiated by typical small-aperture fields [18]. The data show that in the near zone a magnetic dipole induces greater absorption in the model than does an electric dipole. The general absorption characteristics of the data are consistent with the qualitative explanations of near-field absorption described in the subsection. One interesting application of the electrically small aperture analysis might be the case where some industrial machines have an equivalent electric dipole parallel to the operator, which causes maximum absorption. In order to protect the generator, a conducting shield is often placed between the operator and the aperture. However, the eddy currents induced on the conducting shield would introduce an equivalent magnetic dipole. Since the small-aperture analysis shows that magnetic dipoles cause more absorption than electric dipoles, the conducting shield may not provide much protection for the operator.

At this time, only preliminary data have been obtained from the large-aperture analysis. Checks on the validity of the data have been made, and present efforts are being directed towards studying more realistic exposure conditions, including reflector antennas of diameters larger than 10 wavelengths, which are characterized by a focused radiation pattern and, hence, have an extended near zone.

Subdivision of Mathematical Cells--In order to study the validity of the approximation involved in the subdivision of mathematical cells (see the section TECHNICAL APPROACH), we have made calculations for a simple block model of a cube of tissue. The cube was first divided into

27 cells, each having sides 10 cm long. Figure 11 shows the local SAR values in the center of each cell due to an incident planewave at 27.12 MHz.

Figure 12 shows the SAR distribution in a cubical tissue-block model for which a cell at the very center of the cube has been subdivided into eight cells. Comparison of the SAR data given in Figs. 11 and 12 shows that partitioning of a cell at the center of the cube does not perturb the SAR values in the neighboring cells. The only change occurs in the value of the SAR in the partitioned cell. In this case the value of the SAR in the center of the cube has changed by ten percent and the average SAR in the cube has remained unchanged.

Figure 13 shows the SAR distributions in a cubical tissue-block model for which a cell on one surface of the cube (a cell at the center of the first layer in the x-y plane) has been subdivided into eight cells. In this case it can be seen that the values of the SAR in the undivided cells have not changed from the values given in Fig. 11.

Figure 14 shows the SAR distributions in a cubical tissue-block model for which a cell at a corner of the cube has been subdivided into eight smaller cells. In this case, the value of the SAR in the neighboring cells was changed by up to 60 percent (compare these values with those given in Fig. 11). The SAR value at the corner, i.e., in the subdivided region, has increased, approaching a value 49 percent greater than the estimated value using one cell; but the change in the average SAR in the cube is only four percent. These data indicate that internal cells (those without a corner interfacing with air) can be subdivided without seriously changing the field values in neighboring cells, but

z = 25 cm

| .039 | .022 | .039 |
|------|------|------|
| .047 | .031 | .047 |
| .039 | .02: | .039 |

Back layer

z = 15 cm

| .022 | .011 | .022 |
|------|------|------|
| .031 | .018 | .031 |
| .022 | .011 | .022 |

Middle layer

z = 5 cm

| .039 | .022 | .039 |
|------|------|------|
| .048 | .031 | .048 |
| .039 | .022 | .039 |

Front layer
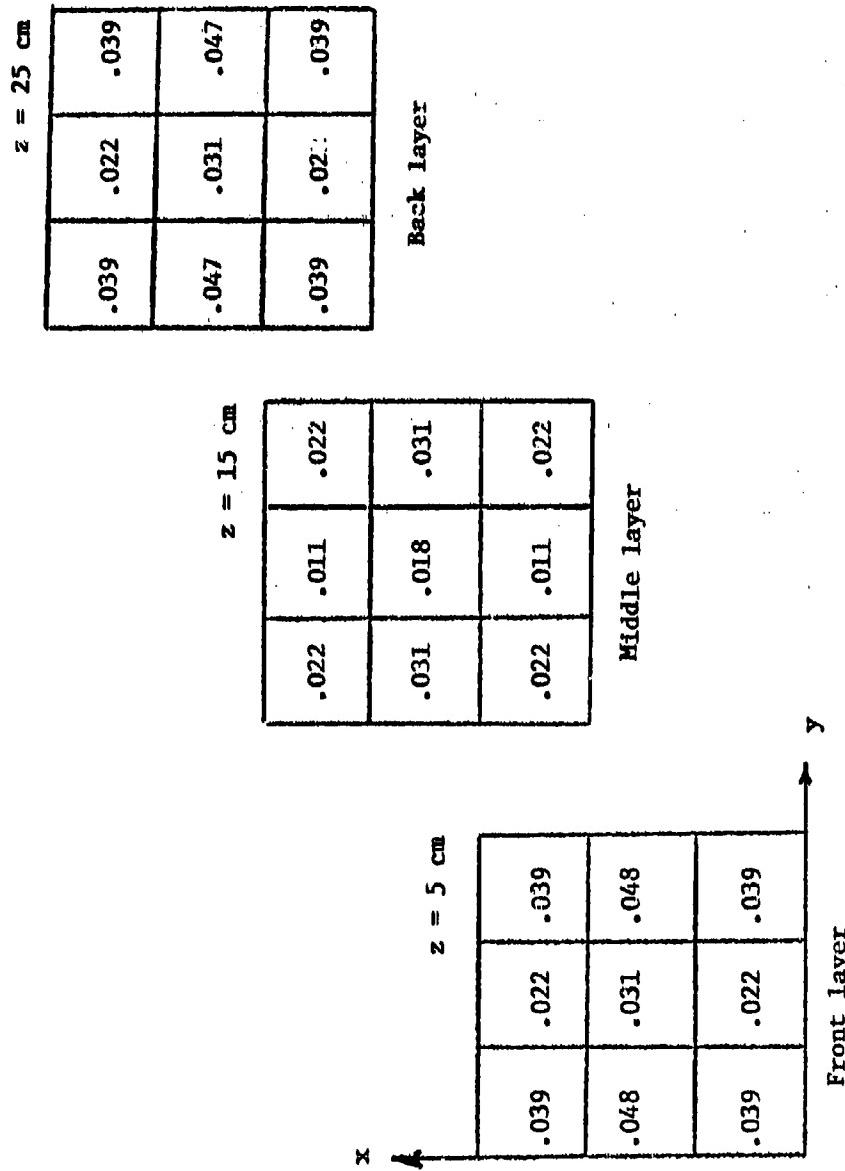
Fig. 11. SAR ($\mu$W/kg) distribution in a cubical tissue-block model (30 x 30 x 30 cm$^3$) irradiated by an incident EM plane wave at 27.12 MHz. $E^i \parallel \hat{x}$, $H^i \parallel \hat{y}$, $|E^i| = 1$ V/m, $\sigma = 0.42$ S/m, and $\epsilon'/\epsilon_o = 76$. The average SAR is $3.103 \times 10^{-5}$ mW/kg.
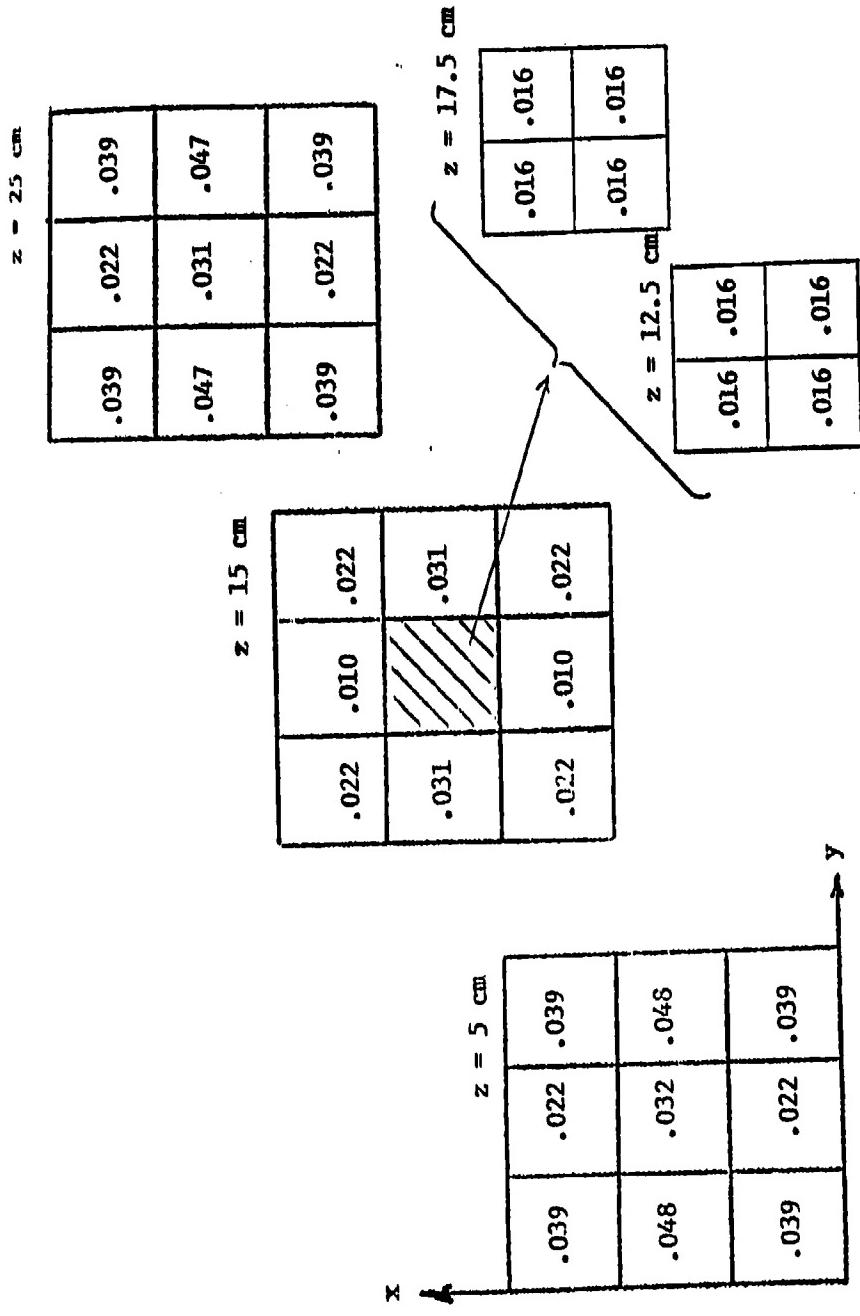
Fig. 12. SAR (μW/kg) distributions in a cubical tissue-block model (30 x 30 x 30 cm³) irradiated by an incident EM plane wave at 27.12 MHz. $\underline{E}^i \| \hat{x}$, $\underline{H}^i \| \hat{y}$, $|\underline{E}^i| = 1$ V/m, $\sigma = 0.42$ S/m, $\epsilon'/\epsilon_0 = 76$. The average SAR is $3.102 \times 10^{-5}$ mW/kg.

42
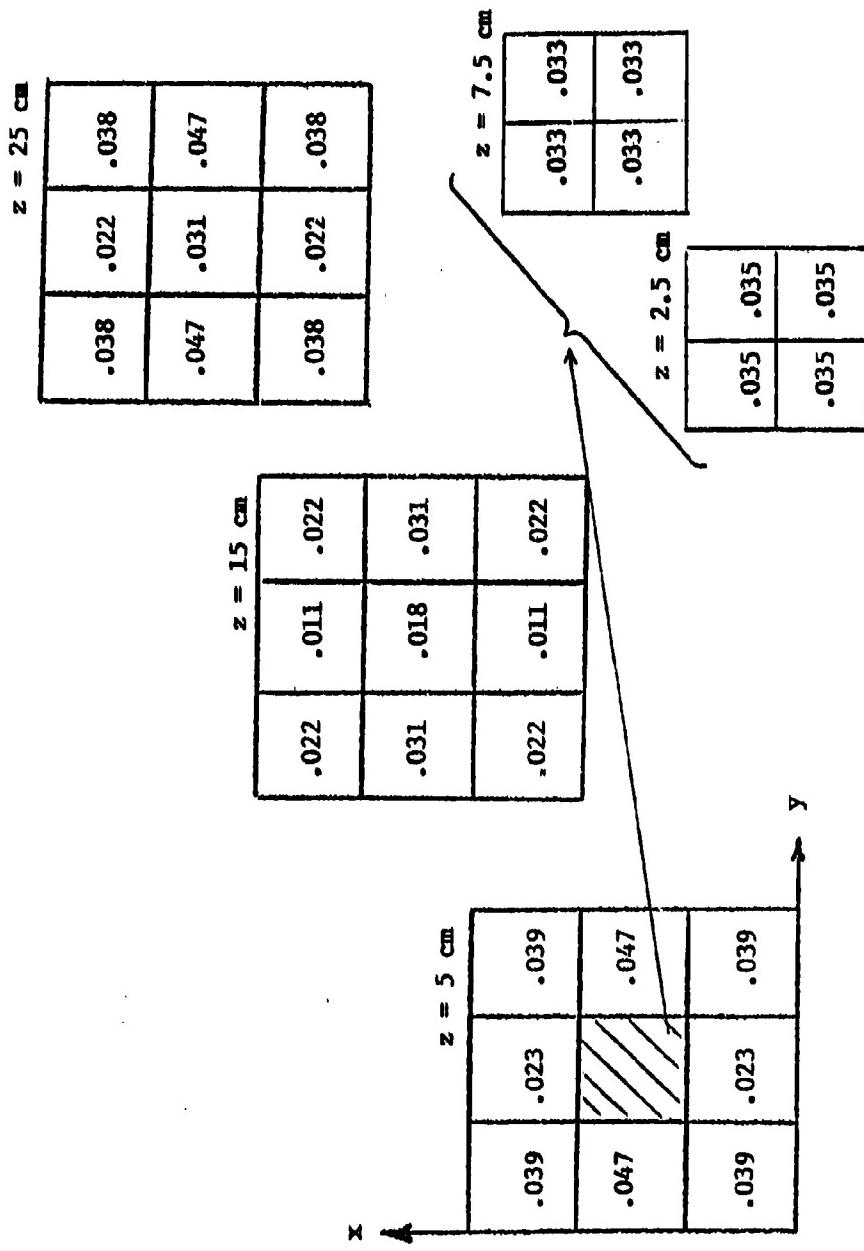
Fig. 13. SAR ($\mu$W/kg) distributions in a cubical tissue-block model ($30 \times 30 \times 30$ cm$^3$) irradiated by an incident EM plane wave at 27.12 MHz. $\mathbf{E}^i \parallel \hat{\mathbf{x}}$, $\mathbf{H}^i \parallel \hat{\mathbf{y}}$, $|\mathbf{E}^i| = 1$ V/m, $\sigma = 0.42$ S/m, $\epsilon'/\epsilon_o = 76$. The average SAR is $3.105 \times 10^{-5}$ mW/kg.

43

z = 25 cm

| .038 | .022 | .038 |
|------|------|------|
| .045 | .030 | .043 |
| .038 | .021 | .038 |

z = 7.5 cm

| .059 | .074 |
|------|------|
| .017 | .040 |

z = 2.5 cm

| .074 | .090 |
|------|------|
| .039 | .069 |

z = 15 cm

| .022 | .021 |
|------|------|
| .030 | .018 | .029 |
| .022 | .011 | .024 |

z = 5 cm

| .038 | .021 | .049 |
|------|------|------|
| .044 | .029 | .077 |
| .038 | .023 | |

x

y
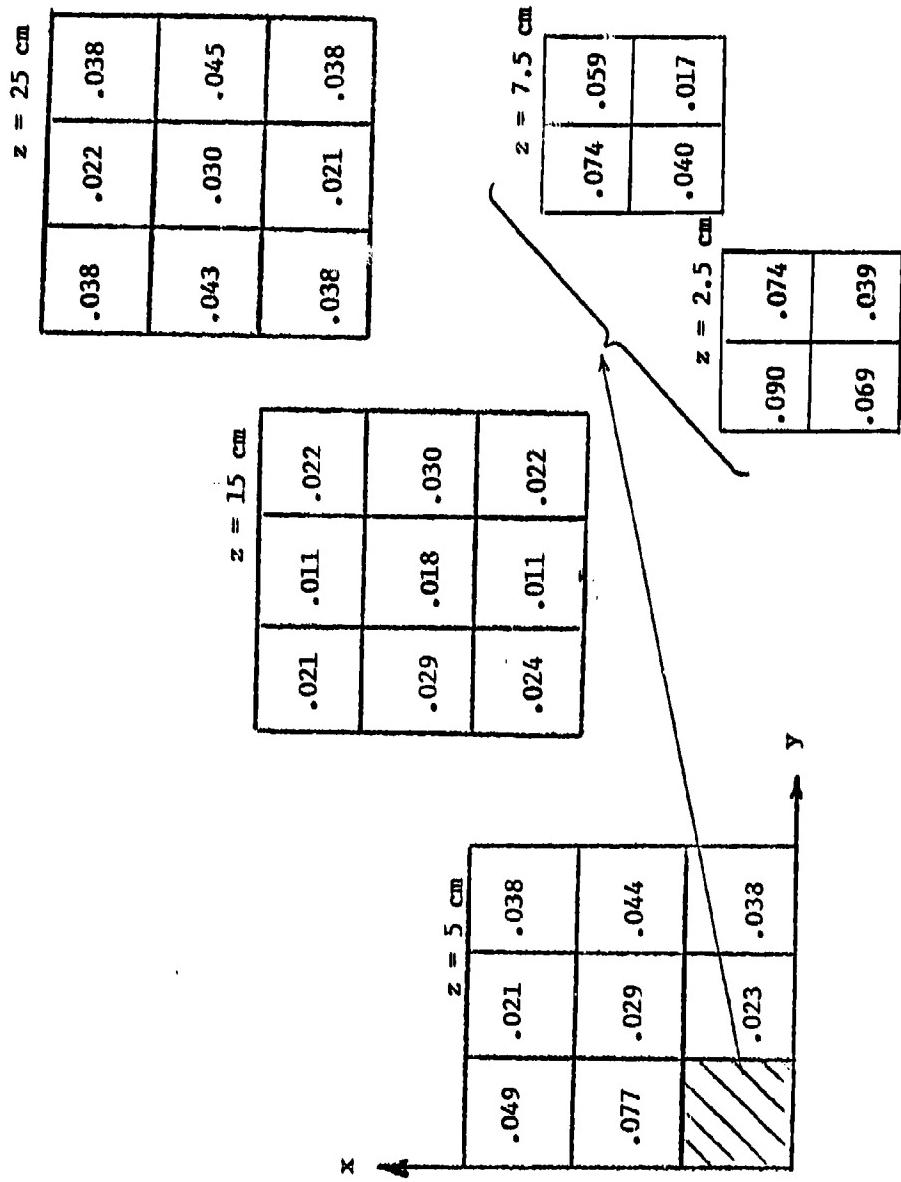
Fig. 14.  SAR ($\mu$W/kg) distributions in a cubical tissue-block model ($30 \times 30 \times 30 \text{ cm}^3$) irradiated by an incident EM plane wave at 27.12 MHz. $E^i \| \hat{x}$, $H^i \| \hat{y}$, $|E^i| = 1 \text{ V/m}$, $\sigma = 0.42 \text{ S/m}$, $\epsilon'/\epsilon_o = 76$. The average SAR is $3.237 \times 10^{-7} \text{ mW/kg}$.

that subdivision of corner cells causes large changes in the calculated values of the fields in neighboring cells. Apparently this occurs because of rapid spatial variation of the fields in the corner cells. When these corner cells are subdivided, the smaller cells give a more accurate calculation of the fields that would actually exist near the corners, which changes the calculated values in neighboring cells. This effect raises questions about the convergence of the moment-method solution and the general accuracy of the SAR distributions calculated by the moment method.

Calculation of SARs from Measured Fields--Present efforts are directed toward developing the composite program for expanding measured fields in terms of spherical harmonics and from this expansion calculating the SARs in spheroidal models using the EBCM. The developments resulting from the aperture-field analyses will be very useful in formulating this composite program.

Pulsed-Field SARs in Small Spheroids--Using the approximate long-wavelength analysis described in the previous section, calculations have been made for the instantaneous power absorption at some point in a small spheroid irradiated by two phased, pulsed electric dipole antennas. The relative values of instantaneous SAR as a function of time for several different pulses, ranging from a slow pulse to a fast pulse, are shown in Fig. 15. It is clear from Fig. 15, a and b, that the instantaneous SAR for a relatively slow-rising pulse is not significantly different from the SAR that would be produced by a continuous wave. However, as shown in Fig. 15, c and d, for sharply rising pulses, the instantaneous SAR near the turn-on and turn-off points of the pulse can be significantly higher than the steady-state SAR. These transient peaks, though

45
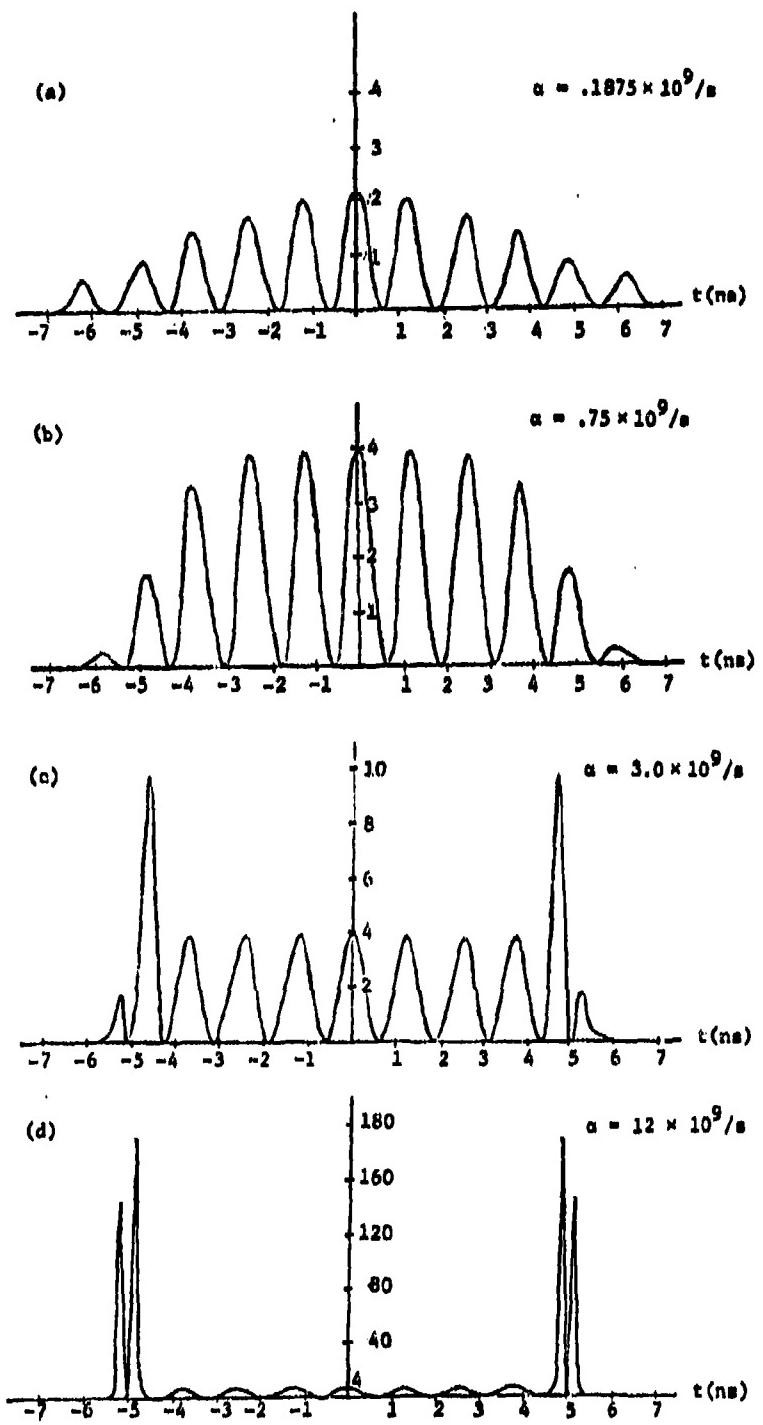
Fig. 15. Relative instantaneous SARs for several values of α.

very high, are also of very short duration. Consequently, the average SAR for a pulse would be affected very little by these sharp transient peaks. Whether these sharp transients are of significant importance in biological effects is a question that still remains to be answered.

Experimental Work--Measurements of averaged SAR have been made in prolate spheroidal models of monkeys and man exposed to the near fields of short electric monopoles on a ground plane simulating electric dipoles. Some results of these measurements are shown in Fig. 16, with the measured incident fields given in Fig. 17. Although the measured results could not be compared with calculated results because the actual fields of the antenna are not the same as the idealized fields of the short dipole, the qualitative characteristics of the measured results compare very well with the calculated results for ideal antennas. The qualitative principles described above can be used to explain the differences in the absorption for the monkey and man models and why the absorption is lower than the $(\lambda/d)^2$ curve [25].

During this past year, a new electromagnetic radiation chamber has been constructed at the University of Utah with funds provided by this project. Inside-wall dimensions are 18' x 22' x 11'. The inside of the chamber is completely lined with galvanized sheet metal having soldered joints. Eighteen-inch Eccosorb pyramids are glued to the ceiling and placed on the floor. Twenty-six-inch Eccosorb pyramids are fastened to the walls with Velcro, allowing them to be removed and rotated. Two nylon zippered curtains are provided to make three compartments, each of

47
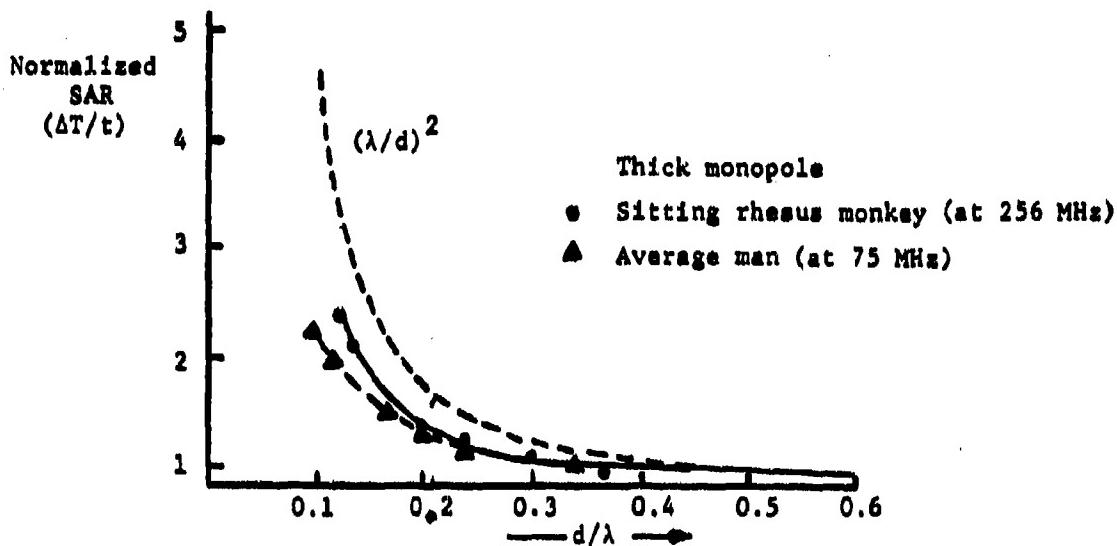
Fig. 16. Measured relative SARs in scaled saline spheroidal
models versus distance. The SAR values for
the different models are normalized with respect to
their planewave value. ΔT is the temperature rise
in the saline solution after exposure for time t.
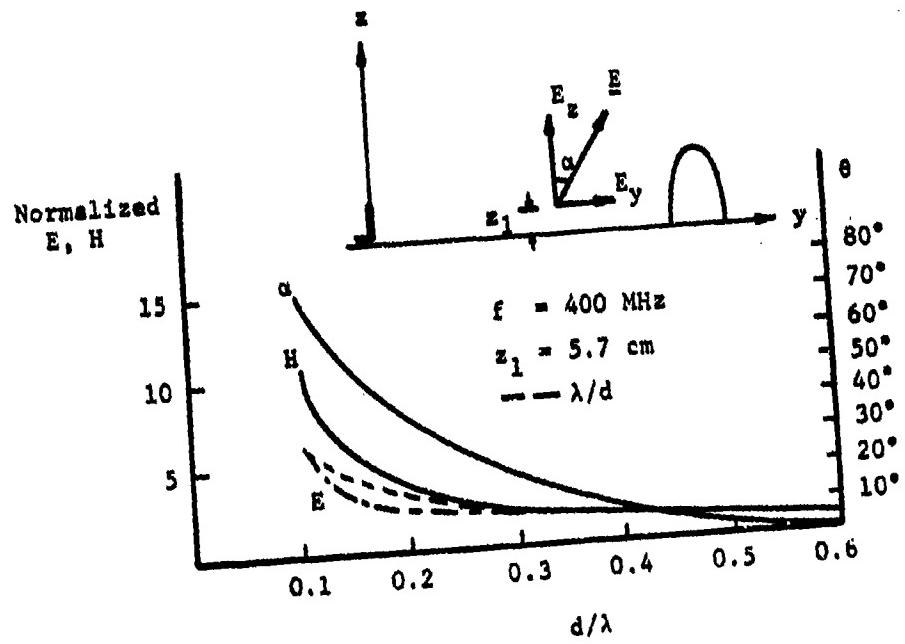
Fig. 17. Measured relative fields versus distance for the thick monopole on a ground plane. The values of E and H are normalized with respect to their values at $d/\lambda = 0.6$.

49

which can be independently air conditioned.  The new chamber will be a significant factor in the experimental work that is planned for this project, since it will allow many kinds of good dosimetric measurements to be made.

## SUMMARY AND CONCLUSIONS

Significant progress has been made in planewave dosimetry.  Two editions of the RFR Dosimetry Handbook have been published containing extensive planewave dosimetric data that have proven to be useful to researchers the world over and used in formulation of a number of safety standards.

Likewise, significant progress has been made in near-field dosimetry, which is a much more difficult area than planewave dosimetry.  The third edition of the Radiofrequency Radiation Dosimetry Handbook contains first-generation near-field dosimetric data.  However, since the near-field SARs cannot be normalized to an incident power density, as planewave SARs can be, it is much more difficult to generalize near-field dosimetric data.  Each set of near-field dosimetric data must be specific to the source that produces the near fields.  Consequently, a handbook of useful dosimetric data for near fields is not possible, as it was for planewave SARs.  However, typical near-field data are given in the third edition of the handbook, and qualitative principles are given that allow one to determine relative near-field SARs from the characteristics of the incident fields.

Useful information has been obtained from the pulsed-field irradiation of small spheroids, indicating that there is a significantly different transient SAR that occurs near the turn-on and turn-off points of

the pulsed fields. However, since this transient does not occur unless the pulse turns on very fast, it is not yet clear how important such transients will be in biological effects.

SARs in prolate spheroid models irradiated by the fields of both electrically small and large apertures can be calculated.

A method for calculating high-resolution SARs by subdividing mathematical cells has been proposed and is being investigated.

Present work on the project is directed towards solution of the following important remaining problems in EM dosimetry:

1. How to calculate SARs from measured field values.

2. How to calculate SAR distributions with better resolution, particularly in a specified organ or region.

3. How to calculate the effects of mutual impedance on internal fields.

4. Are the SARs caused by pulsed fields significantly different from those produced by CW fields?

5. The need for more extensive verification of near-field SAR calculations by experimental measurements.

With the extensive background and information developed in previous work on this project, it is expected that meaningful results will be obtained in each of these areas in future work on the project. This information, along with that from the literature and previous work, should result in a very comprehensive picture of electromagnetic dosimetry, both theoretical and experimental.

51

REFERENCES

1. Durney, C.H., et al. Long-wavelength analysis of planewave irradiation of a prolate spheroid model of man. IEEE Trans Microwave Theory Tech MTT-23(2):246-253 (1975).

2. Waterman, P.C. Symmetry, unitarity, and geometry in electromagnetic scattering. Phys Rev 3:825-839 (1971).

3. Barber, P.W. Resonance electromagnetic absorption by nonspherical dielectric objects. IEEE Trans Microwave Theory Tech MTT-25(5): 373-381 (1977).

4. Massoudi, H., et al. Geometrical optics and exact solutions for internal fields and SARs in a cylindrical model of man as irradiated by an electromagnetic planewave. Radio Sci 14(6S):35-42 (1979).

5. Rowlandson, G.I., and Barber, P.W. RF-energy absorption by biological models: calculations based on geometrical optics, p. 50. In Abstracts of scientific papers. URSI International Symposium on the Biological Effects of Electromagnetic Waves, Airlie, Virginia, October 30-November 4, 1977.

6. Massoudi, H., et al. Geometrical optics and exact solutions for internal fields and SARs in a cylindrical model of man as irradiated by an electromagnetic planewave, p. 49. In Abstracts of scientific papers. URSI International Symposium on the Biological Effects of Electromagnetic Waves, Airlie, Virginia, October 30-November 4, 1977.

7. Durney, C.H., et al. An empirical formula for broad-band SAR calculations of prolate spheroidal models of humans and animals. IEEE Trans Microwave Theory Tech MTT-27(8):758-763 (1979).

8. Durney, C.H., et al. Radiofrequency Radiation Dosimetry Handbook (Second Edition). SAM-TR-78-22, May 1978.

9. Iskander, M.F., et al. Approximate calculations of SAR for plane wave irradiation of man model near a ground plane. Proceedings of the 1979 Symposium on Electromagnetic Fields in Biological Systems, International Microwave Power Institute, 1979.

10. Massoudi, H., et al. Electromagnetic absorption in multilayered cylindrical models of man. IEEE Trans Microwave Theory Tech MTT-27(10):825-830 (1979).

11. Wu, Te-Kao. Electromagnetic fields and power deposition in body-of-revolution models of man. IEEE Trans Microwave Theory Tech MTT 27(3):279-283 (1979).

12. Harrington, R.F., and Mautz, J.R. Green's function for surfaces of revolution. Radio Sci 7(5):603-611 (1972).

13. Massoudi, H., et al. Specific absorption rate in a capped cylindrical model of man and animals irradiated by an axially incident electromagnetic planewave. Submitted to IEEE Trans Biomed Eng.

14. Allen, S.J. Measurements of power absorption by human phantoms immersed in radio-frequency fields. Ann N Y Acad Sci 247:494-498 (1975).

15. Allen, S.J., et al. Comparison of theoretical and experimental absorption of radiofrequency power. SAM-TR-75-52, December 1975.

16. Massoudi, H., et al. Long-wavelength analysis of near-field irradiation of prolate spheroidal models of man and animals. Electron Lett 16(3):99-100 (1980).

17. Iskander, M.F., et al. Irradiation of prolate spheroidal models of humans in the near field of a short electric dipole. IEEE Trans Microwave Theory Tech MTT-28(7):801-807 (1980).

18. Durney, C.H., et al. Comparison of theoretical and experimental absorption of radiofrequency power. Final Report USAFSAM Contract F33615-79-C-0614, April 30, 1981.

19. Livesay, D.E., and Chen, K.M. Electromagnetic fields induced inside arbitrarily shaped biological bodies. IEEE Trans Microwave Theory Tech MTT-22(12):1273-1280 (1974).

20. Massoudi, H., et al. Comparison of the absorption characteristics of a block and a prolate spheroidal model of man exposed to near fields of a short electric dipole. Proceedings of the IEEE, in press 1981.

21. Iskander, M.F., et al. Measurements of the RF power absorption in spheroidal human and animal phantoms exposed to the near field of a dipole source. IEEE Trans Biomed Eng BME-28(3):258-264 (1981).

22. Durney, C.H., et al. Radiofrequency Radiation Dosimetry Handbook. SAM-TR-76-35, September 1976.

23. Hagmann, M.J., et al. Numerical calculation of electromagnetic energy deposition for a realistic model of man. IEEE Trans Microwave Theory Tech MTT-27(9):804-809 (1979).

24. Gandhi, O.P., and Hagmann, M.J. Some recent results on deposition of electromagnetic energy in animals and models of man, p. 51. In Abstracts of scientific papers. URSI International Symposium on the Biological Effects of Electromagnetic Waves, Airlie, Virginia, October 30-November 4, 1977.

25. Durney, C.H., et al. Radiofrequency Radiation Dosimetry Handbook (Third Edition). SAM-TR-80-32, August 1980.

26. D'Andrea, J.A. Electrical Engineering Department, University of Utah, Private Communication, December 1979.

## PUBLICATIONS AND PRESENTATIONS RESULTING
## FROM AIR-FORCE FUNDED EFFORTS

### Publications

1. Durney, C. H., Johnson, C. C., and Massoudi, H. Long-wavelength analysis of planewave irradiation of a prolate spheroid model of man. IEEE Trans Microwave Theory Tech MTT-23(2):246-253 (1975).

2. Johnson, C. C., Durney, C. H., and Massoudi, H. Electromagnetic power absorption in anisotropic tissue media. IEEE Trans Microwave Theory Tech MTT-23(6):529-532 (1975).

3. Johnson, C. C., Durney, C. H., and Massoudi, H. Long-wavelength electromagnetic power absorption in prolate spheroidal models of man and animals. IEEE Trans Microwave Theory Tech MTT-23(9):739-747 (1975).

4. Johnson, C. C., Durney, C. H., Barber, P. W., Allen, S. J., and Mitchell, J. C. Radiofrequency Radiation Dosimetry Handbook. Report SAM-TR-76-35, published by the USAF School of Aerospace Medicine, Brooks Air Force Base, Texas, September 1976.

5. Massoudi, H., Durney, C. H., Johnson, C. C., and Allen, S. J. Theoretical calculations of power absorbed by monkey and human prolate spheroidal phantoms in an irradiation chamber. Biological Effects of Electromagnetic Waves. HEW Publication (FDA)77-8011(2)135-157, December 1976.

6. Allen, S. J., Hurt, S. D., Krupp, J. H., Ratliff, J. A., Durney, C. H., and Johnson, C. C. Measurement of radio frequency power absorption in monkeys, monkey phantoms, and human phantoms exposed to 10-50 MHz fields. Biological Effects of Electromagnetic Waves, HEW Publication (FDA)77-8011(2) 83-95, December 1976.

7. Massoudi, H., Durney, C. H., and Johnson, C. C. Long-wavelength electromagnetic power absorption in ellipsoidal models of man and animals. IEEE Trans Microwave Theory Tech MTT-25(1):47-52 (1977).

8. Massoudi, H., Durney, C. H., and Johnson, C. C. Long-wavelength analysis of plane wave irradiation of an ellipsoidal model of man. IEEE Trans Microwave Theory Tech MTT-25(1):41-46 (1977).

9. Johnson, C. C., Durney, C. H., Barber, P. W., Massoudi, H., Allen, S. J., and Mitchell, J. C. Descriptive summary: Radio Frequency Radiation Dosimetry Handbook. Radio Sci 12(6S):57-59 (1977).

10. Massoudi, H., Durney, C. H., and Johnson, C. C. Comparison of the average specific absorption rate in the ellipsoidal conductor and dielectric models of humans and monkeys at radio frequencies. Radio Sci II(6S):65-72 (1977).

11. Barber, P. W. Resonance electromagnetic absorption by nonspherical dielectric objects. IEEE Trans Microwave Theory Tech MTT-25(5):373-381 (1977).

12. Barber, P. W. Electromagnetic power deposition in prolate spheroid models of man and animals at resonance. IEEE Trans Biomed Eng BME-24(6):513-521 (1977).

13. Durney, C. H., Johnson, C. C., Barber, P. W., Massoudi, H., and Iskander, M. F. Radiofrequency Radiation Dosimetry Handbook (Second Edition). Report SAM-TR-78-22, published by USAF School of Aerospace Medicine, Brooks Air Force Base, Texas, May 1978.

14. Durney, C. H., Iskander, M. F., Massoudi, H., and Johnson, C. C. An empirical formula for broad-band SAR calculations of prolate spheroidal models of humans and animals. IEEE Trans Microwave Theory Tech MTT-27(8):758-763 (1979).

15. Massoudi, H., Durney, C. H., and Johnson, C. C. Geometrical optics and exact solutions for internal fields and SARs in a cylindrical model of man irradiated by an electromagnetic plane wave. Radio Sci 14:(6S):35-42(1979).

16. Iskander, M. F., Durney, C. H., Massoudi, H., and Johnson, C. C. Approximate calculations of SAR for plane wave irradiation of man model near a ground plane. Proceedings of the 1979 Symposium on Electromagnetic Fields in Biological Systems, International Microwave Power Institute, 1979.

17. Durney, C. H., Johnson, C. C., Barber, P. W., Massoudi, H., and Iskander, M. F. Radiofrequency Radiation Dosimetry Handbook: Second Edition. Radio Sci 14(6S):5-7 (1979).

18. Massoudi, H., Durney, C. H., Barber, P. W., and Iskander, M. F. Electromagnetic absorption in multilayered cylindrical models of man. IEEE Trans Microwave Theory Tech MTT-527(10):825-830 (1979).

19. Durney, C. H. Electromagnetic dosimetry for models of humans and animals: a review of theoretical and numerical techniques (invited paper). Proceedings of the IEEE 68:33-40, January 1980.

20. Iskander, M. F., Barber, P. W., Durney, C. H., and Massoudi, H. Irradiation of prolate spheroidal models of humans in the near field of a short electric dipole. IEEE Trans Microwave Theory Tech MTT-28(7):801-807 (1980).

21. Massoudi, H., Durney, C. H., and Iskander, M. F.  Long-wavelength analysis of near-field irradiation of prolate spheroidal models of man and animals.  Electron Lett 16(3):99-100 (1980).

22. Durney, C. H., Iskander, M. F., Massoudi, H., Allen, S. J., and Mitchell, J. C.  Radiofrequency Radiation Dosimetry Handbook (Third Edition).Report SAM-TR-80-32, published by USAF School of Aerospace Medicine, Brooks Air Force Base, Texas, August 1980.

23. Iskander, M. F., Massoudi, H., Durney, C. H., and Allen, S. J.  Measurements of the RF power absorption in spheroidal human and animal phantoms exposed to the near field of a dipole source.  IEEE Trans Biomed Eng BME-28(3):258-264 (1981).

24. Lakhtakia, A., Iskander, M. F., Durney, C. H., and Massoudi, H.  Near-field absorption in prolate spheroidal models of humans exposed to a small loop antenna of arbitrary orientation.  IEEE Trans Microwave Theory Tech MTT-29(6):588-594 (1981).

25. Massoudi, H., Durney, C. H., and Iskander, M. F.  Comparison of the absorption characteristics of a block and a prolate spheroidal model of man exposed to near fields of a short electric dipole.  Proceedings of IEEE, in press,1981.

## Abstracts

1. Durney, C. H., Johnson, C. C., and Massoudi, H.  Long-wavelength analysis of plane wave  electromagnetic power absorption by a pro-late spheroid tissue body.  Annual Meeting of USNC/URSI, Boulder, Colorado, October 14-17,1974.

2. Allen, S. J., Hurt, W. D., Krupp, J. H., Ratliff, J. A., Durney, C. H., and Johnson, C. C.  Measurement of radio frequency power absorption in monkeys, monkey phantoms, and human phantoms exposed to 10-50 MHz fields.  Annual Meeting of USNC/URSI, Boulder, Colorado, October 20-23,1975.

3. Massoudi, H., Durney, C. H., Johnson, C. C., and Allen, S. J.  Theoretical calculations of power absorbed by monkey and human spheroidal and ellipsoidal phantoms in an irradiation chamber.  Annual Meeting of USNC/URSI, Boulder, Colorado, October 20-23, 1975.

4. Massoudi, H., Durney, C. H., and Johnson, C. C.  Comparison of the average specific absorbed power in the ellipsoidal conductor and dielectric models of humans and monkeys at radio frequencies.  Annual Meeting of USNC/URSI, Amherst, Massachusetts, October 11-15, 1976.

5.  Johnson, C. C., Durney, C. H., Barber, P. W., Massoudi, H., and Allen, S. J. Radiofrequency Radiation Dosimetry Handbook. Annual Meeting of USNC/URSI, Amherst, Massachusetts, October 11-15, 1976.

6.  Durney, C. H., Johnson, C. C., Barber, P. W., Massoudi, H., and Iskander, M. F. Radiofrequency Radiation Dosimetry Handbook: Description of the Second Edition. URSI International Symposium on the Biological Effects of Electromagnetic Waves, Airlie, Virginia, October 30-November 4, 1977.

7.  Massoudi, H., Durney, C. H., and Johnson, C. C. Geometrical optics and exact solutions for internal fields and SARs in a cylindrical model of man as irradiated by an electromagnetic planewave. URSI International Symposium on the Biological Effects of Electromagnetic Waves, Airlie, Virginia, October 30-November 4, 1977.

8.  Iskander, M. F., Durney, C. H., Barber, P. W., and Massoudi, H. A technique for calculating absorption of radio frequency energy in models of man at and above the resonant frequency. URSI International Symposium on the Biological Effects of Electromagnetic Waves, Airlie, Virginia, October 30-November 4, 1977.

9.  Rowlandson, G. I., and Barber, P. W. RF-energy absorption by biological models: calculations based on geometrical optics, p. 50. URSI International Symposium on the Biological Effects of Electromagnetic Waves, Airlie, Virginia, October 30-November 4, 1977.

10. Allen, S. J., Durney, C. H., and Johnson, C. C. Implications of the Radiofrequency Radiation Dosimetry Handbook (Second Edition). 1978 Symposium on Electromagnetic Fields in Biological Systems, Ottawa, Canada, June 27-30, 1978.

11. Durney, C. H., Iskander, M. F., Massoudi, H., and Johnson C. C. An empirical formula for calculating the SAR of prolate spheroidal models of humans and animals irradiated by plane wave. 1978 Symposium on Electromagnetic Fields in Biological Systems, Ottawa, Canada, June 27-30, 1978.

12. Iskander, M. F., Durney, C. H., Massoudi, H., and Johnson, C. C. Approximate analysis of plane wave irradiation of man near a ground plane. 1978 Symposium on Electromagnetic Fields in Biological Systems, Ottawa, Canada, June 27-30, 1978.

13. Iskander, M. F., Barber, P. W., Durney, C. H., and Massoudi, H. Near-field irradiation of prolate spheroidal models of humans and animals. Open Symposium on Biological Effects of Electromagnetic Waves, 19th General Assembly of URSI, Helsinki, Finland, August 1-8, 1978.

14. Iskander, M. F., Massoudi, H., Durney, C. H., and Allen, S. J. Measurements of RF power absorption in human and animal phantoms exposed to near-field radiation. URSI National Radio Science Meeting and Bioelectromagnetics Symposium, Seattle, Washington, June 18-22,1979.

15. Han, C. K., Iskander, M. F., Durney, C. H., and Massoudi, H. Near-field irradiation of cylindrical models of humans and animals. URSI National Radio Science Meeting and Bioelectromagnetics Symposium, Seattle, Washington, June 18-22, 1979.

16. Massoudi, H., Durney, C. H., Barber, P. W., and Iskander, M. F. Electromagnetic absorption in multilayered cylindrical models of man. URSI National Radio Science Meeting and Bioelectromagnetics Symposium, Seattle, Washington, June 18-22,1979.

17. Tell, R. A., Mantiply, E. D., Durney, C. H., and Massoudi, H. Electric and magnetic field intensities and associated induced body currents in man in close proximity to a 50-kW AM standard broadcast station. URSI National Radio Science Meeting and Electromagnetics Symposium, Seattle, Washington, June 18-22,1979.

18. Massoudi, H., Durney, C. H., Barber, P. W., and Iskander, M. F. Specific absorption rate in a capped cylindrical model of man and animals irradiated by an axially incident electromagnetic plane wave. Second Annual Meeting of the Bioelectromagnetics Society, San Antonio, Texas, September 14-18,1980.

19. Durney, C. H., Massoudi, H., and Iskander, M. F. Analysis of SARs in small spheroids produced by irradiation from an elemental model of a pulsed, phased-array antenna. Second Annual Meeting of the Bioelectromagnetics Society, San Antonio, Texas, September 14-18, 1980.

20. Massoudi, H., Durney, C. H., and Iskander, M. F. Long-wavelength analysis of electromagnetic absorption in prolate spheroidal models of man and animals irradiated by a small loop antenna. Second Annual meeting of the Bioelectromagnetics Society, San Antonio, Texas, September 14-18, 1980.

21. Lakhtakia, A., Iskander, M. F., Durney, C. H., and Massoudi, H. Near-field absorption in prolate spheroidal models of humans exposed to a small-loop antenna of arbitrary orientation. Second Annual Meeting of the Bioelectromagnetics Society, San Antonio, Texas, September 14-18, 1980.

22. Lakhtakia, A., Iskander, M. F., Durney, C. H., and Massoudi, H. Near-field absorption due to aperture fields. Second Annual Meeting of the Bioelectromagnetics Society, San Antonio, Texas, September 14-18, 1980.

59

23. Durney, C. H., Iskander, M. F., and Massoudi, H. Qualitative explanations of near-field SAR characteristics based on experimental and theoretical observations. Second Annual Meeting of the Bioelectromagnetics Society, San Antonio, Texas, September 14-18, 1980.

24. Lakhtakia, A., Iskander, M. F., Durney, C. H., and Massoudi, H. Scattering and absorption of lossy dielectric objects irradiated by the near fields of an aperture source. International IEEE/AP-S Symposium National Radio Science Meeting, Los Angeles, California, June 16-19, 1981.

## Presentations

1. Durney, C. H., and Johnson C. C. Radiofrequency power absorption in humans. American Industrial Hygiene Conference, New Orleans, Louisiana, May 22-27, 1977.

2. Durney, C. H. Radiofrequency radiation dosimetry: a review of theoretical methods and experimental results. NATO RSG-2 Radiofrequency Radiation Workshop, Farnborough, United Kingdom, April 6-8, 1981.

# CHRONIC MICROWAVE EXPOSURE OF LARGE ANIMAL POPULATION:
## QUANTITATIVE APPROACH

A.W. Guy, C.K. Chou, and R.B. Johnson

Bioelectromagnetics Research Laboratory
Department of Rehabilitation Medicine
University of Washington School of Medicine
Seattle, WA 98195

## 1.0   INTRODUCTION

Much of the past work on the chronic exposure of test animals involved the use of anechoic chambers, metal capacitor plates, or resonant cavities in exposing a large group of subjects. When using these methods, the energy coupled to each animal is a function of the group size, group orientation, and orientation of each animal within the group, as well as the presence and orientation of water and food dispensers. In such cases, extrapolation of the biological results from animals to humans is virtually impossible.

Although the problem of absorbed energy variation with orientation of the animals can be partially eliminated by restricting the size of the exposed groups to a single restrained animal, it is impossible to expose an animal over a long period of time in a restrained position. In addition, the cost of resources and time required for even simple experiments involving chronic exposures of animal populations in the large anechoic chambers now in use would be prohibitive.

In this study, we have chosen to use a system described by Guy and Chou (1975) and Guy et al. (1979) for exposing a population of animals to a single source while independently maintaining relatively constant and quantifiable EM power coupling to each animal. Systems such as these

61

operating at 918 MHz and 2450 MHz have been used successfully in our laboratory since 1975 for physiological and behavioral studies (Moe et al., 1975; Johnson et al., 1977; Lovely et al., 1977, 1978). Since the major goal of this study is to simulate the chronic exposure of man to 450-MHz RF radiation, with an incident power density of 1 mW/cm$^2$, the 2450-MHz system was selected so that a small laboratory test animal such as the rat would be approximately the same electrical size (compared to a wavelength) as a human. The initial consideration was to produce the same average specific absorption rate (SAR) in test animals as predicted for man exposed to the 1-mW/cm$^2$ 450-MHz RF fields. It was estimated, based on previous experience with the exposure system, that an average power density level of 500 $\mu$W/cm$^2$ for animal exposure would be equivalent to human exposure at the lower frequency.

The system, consisting of a number of independent waveguides for providing each animal with an individual exposure cell, provides a relatively inexpensive and convenient method for exposing a sizable number of animals to RF energy from a single source while independently maintaining relatively constant and quantifiable coupling of the energy to each animal. The individual waveguides allow the animals to be continuously exposed while unrestrained and living under normal laboratory conditions with access to food and water. Each exposure cell consists of a cylindrical waveguide that is excited by circularly polarized guided waves that provide relatively constant and easily quantifiable coupling of the fields to each animal regardless of their position, posture, or movement. Food and water are provided to the animals with negligible perturbation of the fields. The theory of operation, the construction details of a single waveguide cell, and the details of the complete system consisting of 100 experimental waveguides and 100 control waveguides that will allow the RF and sham exposure of 200 animals are explained below.

## 2.0   TECHNICAL APPROACH

### 2.1   Theory

The operation of a single exposure waveguide is described by the sketch shown in Figure 1-a. The main body of the 20-cm-diameter exposure

62

waveguide is constructed of wire screen to provide ventilation and visibility of the subject. At the left side of the tube, there is attached a transducer consisting of a smaller diameter waveguide fabricated from the outer shell of standard 3 1/8" (approximately 8 cm) diameter EIA coaxial transmission line. At the left end of the smaller diameter waveguide, there are two orthogonal excitation probes of proper length and distance from the shorter end of the waveguide so that each is matched to a 50-ohm coaxial feedline when the opposite end of the small-diameter section is terminated in the characteristic impedance of the $TE_{11}$ mode excited by the probe. When energy is fed to the vertical probe, it will excite a propagating $TE_{11}$ mode in the small-diameter guide. A short distance down the guide from the excitation probe, there is a circular polarizer consisting of four stubs that convert the linearly polarized $TE_{11}$ mode to the circularly polarized $TE_{11}$ mode. The circularly polarized mode in the smaller diameter guide, in turn, is matched to the larger diameter waveguide by means of four additional tuning stubs, while the latter is terminated in the characteristic impedance of the propagating modes. From size and dosimetry considerations three propagating modes, $TE_{11}$, $TM_{11}$, and $TE_{31}$ modes, can be excited at the aperture of the small waveguide. The electrical field configuration of the three modes is shown at the top of Figure 1-a. Since the first two of the three modes have electrical field distributions that most closely match those of the exciting aperture, they represent most of the propagating energy in the waveguide. Thus the length of the large-diameter waveguide is chosen such that these two propagating modes will reach the termination in the large waveguide in the same phase relation that exists at the feed end. This phase relationship requires that the length of the guide, L, be equal to an integer, n, multiplied by the reciprocal of the difference between the reciprocals of the wavelengths of the two important modes, $TE_{11}$ and $TM_{11}$.

The termination at the end of the waveguide consists of a transducer similar to the transmitting transducer but without the circular polarizing stubs. Energy of the propagating modes in the large guide is coupled to the smaller diameter waveguide termination through the four impedance

63

matching stubs where it finally couples to probes that are connected to 50-ohm loads.

The fields in the large waveguide will not be uniform and will vary as a function of both transverse and longitudinal position due to interference between the different propagating modes. Tests have shown, however, that the average SAR in the tissues of an exposed subject will remain relatively constant over a period of time. When the exposure waveguide is empty, energy coupled to the transmitting transducer on the left side of the system will be transmitted through the large-waveguide portion of the system in the form of circularly polarized TE and TM modes with very little insertion loss, approximately 10%, and very little reflection to the source (VSWR less than 1.5).

If an electrical short were placed in the center of the cylindrical waveguide during excitation, the right-hand circularly polarized travelling waves would be completely reflected but would still rotate in a clockwise direction with respect to the Z axis (left to right) or rotate in the counter-clockwise direction with respect to the -Z axis. Therefore, reflected waves travelling in the -Z direction would be circularly polarized in the left-hand sense and would couple directly to the smaller diameter waveguide. The coupling would be virtually complete since the total path length from the aperture to reflector and back to aperture again is such that the fields of the important $TE_{11}$ and $TM_{11}$ modes would be in phase over the aperture of the smaller guide. The reflected left-hand circularly polarized $TE_{11}$ wave in the transmitting transducer would then reverse and pass the circular polarizing stubs, which in turn would convert the circularly polarized reflected $TE_{11}$ mode in the small guide to a linear polarized $TE_{11}$ mode, where the polarization is in space quadrature with the original $TE_{11}$ mode excited by the input probe. Therefore, all of the reflected energy would couple directly to the $P_{RL}$ terminal with no reflected energy coupled to the $P_{in}$ feed terminal. This provides good isolation between reflections occurring in the large-diameter waveguide and the source energizing the small transmitting transducer. If the short were imperfect, for example, a circular metal disk not quite filling the waveguide, some of the energy would be transmitted beyond the obstacle. In

64

this case, however, the waves would still be predominantly right-hand circularly polarized and the transmitted components would propagate to the end of the large waveguide, arriving such that the transverse electric fields would be in phase at the aperture, thereby coupling to the small-diameter 2450-MHz circular waveguide where the energy would be absorbed in the terminated probes that are oriented in space quadrature.

When an animal is placed in the chamber as shown in Figure 1-b and is exposed to the traveling waves by feeding energy into the terminal $(P_{in})$, some energy $(P_A)$ will be absorbed by the animal, some $(P_W)$ will be absorbed by the walls of the chamber, some will be reflected in the form of both right-hand $(P_{RR})$ and left-hand $(P_{RL})$ circularly polarized waves that couple back to the probes on the feed section for the 2450-MHz circular waveguide, and some $(P_{TA}$ and $P_{TB})$ will be absorbed at the termination terminals. The reflected-component $P_{RR}$ can be measured at the reflecting arm of the bidirectional coupler placed between the source and the input probe as $CP_{RR}$, where C is the coupling coefficient of the bidirectional coupler. The reflected-component $P_{RL}$ can be measured directly at the other terminal of the feed transducer. The power level of the incident energy launching the right-hand circularly polarized waves can be measured at the incident wave terminal of the bidirectional coupler as $CP_{IN}$. The power level of energy transmitted beyond the animal can be measured at the terminals $P_{TA}$ and $P_{TB}$, of the terminator transducer. The sum of power levels of energy absorbed by the animal, $P_A$ and the waveguide, $P_W$, can be obtained from the expression in Figure 1-b in terms of the known components of energy transmitted to the various terminals of the transducers and the directional couplers. Twin-well calorimetry, described in the dosimetry section of this paper, is required to determine the amount of the total system energy loss in the animal, $P_A$, and the amount in the waveguide, $P_W$.

Since the wavelengths of the $TM_{11}$ and $TE_{11}$ modes are 18.06 and 13.09 cm, respectively, we find that a large-diameter (20.3 cm) waveguide approximately 95 cm long would satisfy the equation for a good match to the termination transducer for a value of n = 2. The transverse components of the electric fields for the two important propagating modes would be in

65

phase on the axis in the center of the large-diameter waveguide. The maximal deviation from this phase relationship for a distance of 12 cm on each side of the midpoint would be $90^\circ$. A distance of 24 cm centered at the midpoint would correspond to the region where the important propagating modes are reasonably in phase, insuring that a subject would be well exposed to the electric and magnetic field of both modes. Experimental measurements have shown that reflections from the animal placed at the midpoint position would undergo little change from the original direction of rotation or polarization with respect to propagation. Thus, the reflections arrive at the feed transducer chiefly as circularly polarized waves of the opposite direction of rotation and with a phase relationship that couples quite well with $P_{RL}$ terminal of the feed transducer. Energy transmitted beyond the animal remains chiefly in the same sense, as circular polarization coupling to terminals $P_{TA}$ and $P_{TB}$ at the termination transducer. The laboratory measurements discussed in the dosimetry section indicate that the mean value of input VSWR is below 1.7 at the input terminal of the cell when it is loaded with a freely moving rat, and the net mean power coupling to the animal varies from 25 to 90%, depending on its position. The water supply is electrically decoupled from the animal by two concentric quarter wavelength choke sections so that the tip of the water nozzle is extremely high in impedance, virtually preventing conduction currents between it and any contacting object.

## 2.2    Design and Assembly of Complete Exposure System

A large mass-production program for fabricating 100 exposure waveguides and 100 control waveguides as well as a number of spare waveguides was implemented during the first year of the research project.

A complete multiple-animal exposure system consisting of 100 exposure waveguides and 100 control (sham) waveguides was installed in rooms designed for maintaining specific-pathogen-free (SPF) rats. The general configuration of the rooms is shown in Figure 2. The dimensions of each room are approximately 5.49 X 6.10 meters with a center workspace with dimensions of 5.49 X 3.05 meters. Six alcoves, each with dimensions approximately 157 X 114 cm are arranged around the perimeter of the central area, five of which are individually isolated by sliding glass doors. The

66

alcoves are kept at positive pressure with respect to hallways with approximately 18 air changes per hour. The five alcoves were increased in size to 157 X 150 cm so that each could hold 20 waveguides on four horizontal shelves as shown in Figure 3, giving a total waveguide capacity of 200 units for the two rooms. The sixth alcove was partitioned off as a separate room for bloodletting and to serve as a data collection center. The rooms are temperature and humidity controlled to $21\pm1^{\circ}C$ and $50\pm5\%$ R.H. and have cycled room lighting. The alcove identification, A-J, and power distribution system are shown in Figure 2.

## 2.3    Power Generator and Distribution

Each exposure room is equipped with two 2450-MHz pulsed microwave sources, each capable of providing an average output power of 20 watts and a peak power of 5 kW. Generators are controlled by a microprocessor to deliver repetitive pulse trains consisting of fifty 10-microsecond-wide pulses separated by 1.25-millisecond intervals. This is the equivalent of an 800-pulse-per-second source being square-wave modulated at the rate of eight times per second with equal on/off durations of 1/16 second. These modulation characteristics provide an 8-Hz modulation component corresponding to the dominant EEG frequency in the rat (Coenen, 1975). The RF exposure is amplitude modulated based on the reported effects of $Ca^{++}$ efflux increase observed in chick and cat brain by Bawin, Kaczmarek, and Adey (1975) and replicated later by Blackman et al. (1979). Since the Bawin group feels that the effects are most pronounced when the modulation frequencies correspond to the EEG spectrum of the experimental subjects, the modulation frequency was set to 8 Hz, within the EEG spectrum of rats which peaks between 7 to 10 Hz.

The power from one generator in the equipment rack (Fig. 4) is transmitted to three alcoves by means of a 7/8"-diameter foam-filled coaxial cable as shown by the schematic diagram in Fig. 5. The power is equally distributed to each of the three alcoves, A-B-C, in room T131 and, F-G-H, in room T137 via a three-way power splitter and transmitted to the interior of the alcove by means of another section of 7/8" cable. At the back wall of the alcove, the power is fed through SPDT coaxial relay to a

two-way power splitter. Power from each arm of the two-way splitter is fed by sections of 1/2"-diameter foam-filled coaxial cable to two five-way power splitters, where the power is again equally divided (left and right) and transmitted through isolators to the two groups of five active exposure waveguides in each alcove. The distribution system of the second generator in each room is similar to that just described except that the power is initially split in two ways rather than three ways to power the remaining two alcoves, D-E, in room T131 and, I-J, in room T137. The power to any particular alcove can be removed by shunting it to a 20-watt load located at the SPDT coaxial relay which is activated by switches located on the control panel at the equipment rack containing the signal sources and the microprocessor. A red light above the door to an alcove indicates when the waveguides within are activated. The average attenuation for RF power transmitted through the transmission lines, power splitters, coaxial relay, and isolator to the waveguide exposure cell is approximately 2.7 dB. Thus, for typical operating conditions with an output power of 8.4 watts from the source, the power delivered to each of the 10 exposure cells in the alcove would be .15 watt, which would produce an average power density of 500 $\mu W/cm^2$ and a peak power density of 125 $mW/cm^2$ in each exposure cell. The actual incident average power density, however, may be set at any level from 0 to 1.2 $mW/cm^2$ as determined by the output of the power generator. The maximum average power density of 1.2 $mW/cm^2$ would allow peak power densities as high as 300 $mW/cm^2$ to be produced in each exposure cell with the selected modulation parameters. The forward and reflected power at each generator output terminal is measured through a directional coupler and digital power meters interfaced to the microprocessor. Also, the input, the reflected, and the transmitted power associated with one exposure cell per room are monitored to obtain a continuous on-line recording of the average absorption loss of the waveguide/rat assembly, from which the average SAR can be calculated from the known waveguide power loss and weight of the rat.

2.4    Calibration of Power Distribution System

A number of measurements were made to determine the relationship between the output power from the signal generator and the power delivered

68

to each exposure cell, and the total transmission loss in dB to each exposure cell. The mean and standard deviation of the power delivered to each cell was also calculated for each alcove cluster (groups of cells fed by a particular signal generator). The output power of a calibrated CW source of known frequency was measured with a calibrated directional coupler and power meters and compared to the power delivered to each exposure cell as measured with a calibrated directional coupler and power meter. Typical values, shown in Table 1, are based on the chosen operating level for the chronic study as determined by the dosimetry measurements as discussed in the next section. During the course of the measurements, it was found that there was considerable variation of power delivered to groups of cells in different alcoves fed by the same generator. The problem was traced to the power splitters which were extremely sensitive to any slight impedance differences as seen at the output cables to the different alcoves. This caused significant variations of power delivered to the different output arms of the power splitter. The problem was eliminated through the use of coaxial tuners connected to each output arm of the power splitters delivering power to each alcove. The tuners were adjusted slightly to compensate for the imbalances in impedance. During calibration a CW signal source was set to the proper frequency, using a conventional electronic counter. During actual pulse operation, however, the pulse generator frequencies are set to the correct frequency periodically by means of a HP 5345A frequency counter designed for measuring pulsed signals. Each room contains a total of nine power meters, two each for the incident and reflected power at each generator and five for the incident, reflected, and transmitted power at the multiple terminals of the respective exposure cells designated for determining the average SAR in the experimental animal. During the duration of the chronic study, the monitoring system is connected each day to a different exposure cell so that every cell is monitored for 21 hours every 50 days over the course of the experiment.

3.0 DOSIMETRY

The dosimetry studies were directed toward establishing an input power level for each waveguide to best simulate, with rats, the exposure of

69

man to 450- MHz, 1-mW/cm$^2$ RFR. In order to determine the conditions necessary for simulating such exposures, it was necessary to quantify the relationship between the input power and the average and distributed SAR in the body of an exposed rat living in the exposure cell. It was also necessary to determine the relationship between 450-MHz, 1-mW/cm$^2$ radiation to the average and distributed SAR in an exposed man.

A microprocessor-controlled twin-well calorimetry system was developed for measurement of the average SAR in the bodies of the exposed rats. Through the exposure of scale models of man filled with a liquid synthetic tissue, it was possible to measure average SAR; and through the exposure of similar models filled with synthetic gel, it was possible to measure SAR distribution patterns thermographically as described by Guy et al. (1976, 1978). The 1/5 scale models were exposed to 2450-MHz radiation in an anechoic chamber to simulate the exposure of full-scale man to 450 MHz.

Though several methods were employed, twin-well calorimetry was found to be the most effective and accurate means for measuring the SAR in rats exposed in the waveguide exposure chambers. Figure 1-a illustrates an exposure waveguide (containing a rat) and the five power measurements needed to establish the sum of the absorbed power $(P_A)$ in the rat and the power lost in the waveguide system $(P_W)$. The twin-well calorimetry was used to measure $P_A$ and $P_W$.

Twin-well calorimetry is one of the techniques that has been used for many years for measuring average SAR in laboratory animals exposed to RFR. It was originally developed by Phillips et al.(1975). Two different size calorimeters were used in the dosimetry study. One consisted of wells with internal dimensions of 20.3 cm long by 6.74 cm diameter, used for 100-650-g rats; and one consisted of wells with internal dimensions 25.4 cm long by 9.8 cm diameter, used for 650-800-g rats.

70

Two twin-well calorimeters are connected in series to a constant temperature circulator (Fig. 6). The temperature of the circulating water is kept at 30.5°C. One of the twin-well calorimeters is used to stabilize the temperature of two rat carcasses of similar body weight. The other twin-well calorimeter was used to measure the microwave energy absorbed by the exposed-rat carcass. The voltage output of the thermocouple array in the calorimeter is sampled by a Fluke 8005A voltmeter as a function of time and integrated by a Z-80 based microcomputer coupled to the voltmeter by means of an IEEE interface. The measured energy delivered to the exposure system was derived from the five power meters monitoring the incident (approximately 300 watts), reflected, and transmitter powers. The net power delivered to the system was integrated by the microcomputer over the exposure period (15-20 seconds typical). Software used with the microcomputer allows automatic computation of the average SAR for the exposed-rat carcass, first assuming that the power loss in the waveguide is negligible. By comparing the data on average SAR measured for the rat obtained from the twin-well calorimeter and that obtained using the five power meters, assuming negligible waveguide loss, one can calculate the actual power loss ($P_w$) in the system so that the average SAR of the rat may be quantified based on the measurements of the five power meters used to monitor a particular exposure chamber during the long-term study. The correction factor for power or system loss can then be taken into account, based on the body weight of the rat. After a brief exposure (less than 30 seconds) of a rat, the exposed and sham-exposed animals are placed in the twin-well calorimeter. All data and SAR computations from a series of twin-well calorimeter measurements are stored on a five-inch floppy disk for subsequent display on a terminal or printer output.

## 4.0 RESULTS

### 4.1 Average SAR Measurements in Rats

Measurements were made using liquid phantoms simulating a rat, as well as actual rat carcasses. Subjects with a range of 100-650 grams in mass, exposed to the 2450-MHz circularly polarized fields in the exposure

waveguide, were used for the studies. Only the results for the actual rats are reported here.

Pairs of rats of similar body mass were euthanized and placed in the stabilizing calorimeter at a temperature of 30.5°C for at least seven hours. The rats were then placed in exposure and control waveguides and, after exposure, were immediately placed in the calorimeter. The average SARs were then determined for a large number of rats exposed at the center and off center of the waveguide, with the results shown in Figures 7 and 8. The calculated average SARs from the twin-well calorimeter measurements are denoted by the dashed lines for the entire system, and those obtained by the power-meter measurements are denoted by the solid lines. The data points were used to calculate experimental curves based on a least-squares fit.

The smaller animals experienced a higher than average SAR, higher than that received by the larger animals, which was similar to that observed in liquid phantoms. Also, the power-meter measurements show proportionally higher system loss when exposing a small body mass. Note that the calculated average SAR in the exposed animal in the middle of the cage (Figure 7) varies from 3.5 W/kg per watt input for a 100-g rat to 0.7 W/kg per watt input for a 800-g rat. Similar plots of SAR data are shown (Figure 8) for the rats exposed at the side of the waveguide where coupling is less, corresponding to 2.32 W/kg per watt input for a 100-g rat and 0.76 W/kg per watt input for an 800-g rat. Figure 9 illustrates the average SAR per watt input as a function of age and body mass for the exposed rat.

## 4.2     SAR Distribution in Rats

Based on previous rat SAR distribution measurements made by Guy et al. (1979), Figure 10 illustrates the SAR distributions showing areas of constant SAR normalized for 1-watt input for a 324-g rat cadaver exposed in two positions along the axis of the waveguide: (a) anterior, with maximal SAR of 4.39 W/kg, an average SAR of 2.47 W/kg, and a whole-body power loss of 0.8 watt; and (b) posterior, with a maximal SAR of 6.08 W/kg, an average SAR of 2.34 W/kg, and a whole-body power loss of 0.76

watt. Since the measurements reported in the above reference assumed zero
system loss, the average SAR in whole-body power loss value should be
multiplied by a 0.88 correction factor to account for the calculated
waveguide loss obtained from Fig. 8. It should be noted that the SAR
distributions do not require the correction factor since they were measured
directly by a thermograph camera.

## 4.3   SAR in Man Exposed to Plane Waves

Since it was desired to simulate the exposure of a full-scale man to
450 MHz, it was necessary to select a suitable dielectric constant for the
synthetic tissue to match the scaling criteria. Comparisons between the
full-scale dielectric constants and the scale-model synthetic tissue
dielectric constants are shown in Table 2. Note that the only change
between the full-scale and the scale-model dielectric properties is that
the electrical conductivity of the latter is increased by the scale factor
(inverse of the reduction factor from the full-scale man to the scale-model
man). The dielectric properties for the scale-model tissues were measured
under controlled temperature conditions of $20^{\circ}C$. The properties were
obtained by using transmission line methods described by Guy et al.
(1976, 1978). In addition to the scaled liquid muscle, a scaled liquid
tissue with the properties of a homogeneous mixture composed of 2/3 muscle
and 1/3 fat and bone representative of the human body as described in the
Radiofrequency Radiation Dosimetry Handbook, Second Edition (Durney et al.,
1978), was used.

### 4.3.1   Average SAR in Man Models

For the scale-model average SAR measurements, the liquid synthetic
tissue was poured in 1/5.54-scaled hollow Styrofoam models of adult men
(full-scale length, 174 cm) and children (full-scale length, 88 cm). Each
model was exposed in the anechoic chamber to 2450-MHz radiation fields of
750-mW/cm$^2$ incident power density (140 cm from a standard gain horn) for
about 20-50 seconds. After exposure, the average temperature rise in the
model was measured by a thermocouple. The heat loss in the Styrofoam was
negligible during the several minutes needed for making the measurements.

The results of the measurements are listed in Table 3. Every number represents the average of 2-3 measurements. The largest variation was less than 10%. The average SAR measured for the composite tissue model is slightly higher or equal to that measured for the muscle model for all positions. The measured average SAR for the child was much higher than that for the adult (i.e., 187 mW/kg vs. 52 mW/kg), which is expected since the frequency is closer to the resonant frequency for the child.

### 4.3.2 Thermographic Measurement of SAR Distribution in Man Models

In addition to the measurements of the average SAR, thermographic measurements were made of the SAR distributions in similar phantom scale models of man consisting of the gelled synthetic muscle tissue with scaled conductivity. Thermographs were taken in the same manner as was described previously (Guy et al., 1976).

Figures 11 and 12 illustrate the thermographic data for the 5.54-scale man model exposed to radiation from the side and front respectively. The figures contain intensity scans (brightness proportional to SAR), profile scans (vertical deflection proportional to SAR), and single scans taken before and after exposure (vertical separation proportional to SAR). Data is shown for scans using a standard lens and close-up scans using a narrow-angle lens.

## 5.0 CONCLUSIONS

### 5.1 Comparison of Results with Other Work

The average SAR and SAR-distribution data for the exposure of man to 442 MHz is compared to data obtained previously by the authors and other investigators in Tables 4 and 5. One may note from Table 4 that measured values of average SAR using phantom scale models of man, consisting of dolls or figurines exposed to all polarizations, is somewhat greater than values calculated theoretically using the prolate spheroidal models of man or computer models consisting of a finite number of blocks. The average values of SAR based on the prolate spheroidal model of man varies from 16

74

to 34 mW/kg depending upon polarization. These values are consistent with the average SAR reported for the computer block model (Gandhi et al., 1979). Our measurements of the average SARs for the 3- to 4-year-old child model (half the weight of the man model) is also significantly (2-3 times) higher than that predicted by theory using the prolate spheroid model. Though Table 4 indicates that the average SAR decreases with the increasing tissue conductivity, the changes are insufficient to account for the measured discrepancy between theoretical and measured results. In fact, Gandhi's measured results, with dolls and human figurines (Gandhi et al., 1977, 1979), are consistent with our most recent measurements. We therefore must conclude that the shape of the model must play an important role in determining the average SAR during exposure, as pointed out by Gandhi, who stated that dolls were not proportioned properly to represent the average human. Since there are considerable differences between actual and average body shapes, we could expect similiar variations in the real world.

## 5.2    Selection of Exposure Levels

Based on the worst-case interpretation of the data presented in Table 4 to simulate the exposure of an adult male to 450 MHz based on average SAR, it would require animal exposure conditions that would produce an average SAR of about 68 mW/kg in the animal. In addition to the average SAR, we would need to be concerned with comparison of hot spots in the exposed humans and laboratory animals. Table 5 compares the maximum SAR measured at various points for simulated human exposure to 442-MHz, 1-mW/cm$^2$ RFR. Note that the theoretical values reported in the literature for 500 MHz for the computer block model (Chen and Guru, 1977) are considerably less than those measured by our group with thermography (Guy et al., 1976). Since the maximum values measured by Chen and Guru are barely above the average SAR values reported by the Utah group, we feel that there must be some error or that the different geometries for the models have a large effect on the calculated results. One may note from the thermographic measurements that the maximum SAR values could be as high as 192 mW/kg or four times the average SAR, in the head and 1020 mW/kg, or 15 times higher than the average, in the wrist or the perineum. Our most

recent measurements seem to compare favorably with those made by Guy et al. (1976) at 442 MHz. During the planning stages of the first experimental use of the exposure system, various options were studied, each based on a useful scientific consideration, in simulating chronic human exposure to RFR. These options are outlined in Table 6. The first option is consistent with an original intent to simulate exposure of man to 450-MHz, 1-mW/cm$^2$ RFR. The second option would simulate an exposure regime where the worst-case conditions corresponding to the maximum allowed average SAR, 400 mW/kg, specified in the newly proposed ANSI C95.4 Radiation Protection Guide (RFPG) would exist at some period in time but would not be exceeded. The third option would utilize an exposure level set for an average SAR, as averaged over the lifetime of the animal, equal to the maximum 400 mW/kg allowed by the newly proposed ANSI C95.4 RFPG. This exposure level is obtained by taking an average over all ages of the average SAR for a given input power as shown in Figure 9. One may note in option one that the decrease in average SAR from 270 mW/kg for the young 200-g rat to 68 mW/kg for the 800-g adult rat qualitatively spans a wide range similiar to that of human exposures shown on Table 4. After careful consideration of all three options, it was decided the exercise of option two would provide the best scientific data since it best simulated the exposure of humans to the maximum exposure levels allowed by the proposed ANSI C95 RFPG. Thus an input power level to each exposure alcove cluster was set so that the average input power averaged over time and all exposure waveguides for the entire group was 144 mW.

REFERENCES

Bawin, S.M., L.K. Kaczmarek, and W.R. Adey (1975). Effects of modulated VHF fields on the central nervous system. Ann. N.Y. Acad. Sci. 247:74-81.

Blackman, C.F., J.A. Elder, C.M. Weil, S.G. Benane, D.C. Eichinger, and D.E. House (1979). Induction of Ca ++ efflux from brain tissue by radio-frequency radiation: Effects of modulation frequency and field strength. Radio Sci. 14(6S):93-98.

Chen, K.M., and B.S. Guru (1977). Focal hyperthermia as induced by RF radiation of simulacra with embedded tumors and as induced by EM fields in a model of human body. Radio Sci. 12(6S):27-37.

Coenen, A.M.L. (1975). Frequency analysis of rat hippocampal electrical activity. Physiol. Behav. 14:391-394.

Durney, C.H., et al. (1978). Radiofrequency Radiation Dosimetry Handbook, 2nd Ed., Rop. SAM-TR-78-22, USAF School of Aerospace Medicine, Brooks Air Force Base, Tex.

Gandhi, O.P., M.J. Hagmann, and J.A. D'Andrea (1979). Part-body and multibody effects on absorption of radio-frequency electromagnetic energy by animals and by models of man. Radio Sci. 14(6S):23-30.

Gandhi, O.P., E.L. Hunt, and J.A. D'Andrea (1977). Deposition of electromagnetic energy in animals and in models of man with and without grounding and reflector effects. Radio Sci. 13(6S):39-47.

Guy, A.W., and C.K. Chou (1975). System for quantitative chronic exposure of a population of rodents to UHF fields. In Biological Effects of Electromagnetic Waves, Selected Papers, USNC/URSI Annual Meeting (Boulder, Colo., Oct. 20-23, 1975, C.C. Johnson and M.L. Shore, Eds. HEW Publication (FDA) 77-8011, Washington, D.C. 20402: U.S. Gov. Printing Office, Vol. 1, pp. 389-422.

Guy, A.W., M.D. Webb, and C.C. Sorensen (1976). Determination of power absorption in man exposed to high frequency electromagnetic fields by thermographic measurements on scale models. IEEE Trans. BioMed. Eng. BME-23(5):361-371.

Guy, A.W., M.D. Webb, A.F. Emery, and C.K. Chou (1978). Measurement of Power Distribution at Resonant and Non-Resonant Frequencies in Experimental Animals and Models, University of Washington Bioelectromagnetics Research Laboratory, Scientific Report 11, Final Report Contract No. F 41609-76-C-0032, March 1978, for USAF School of Aerospace Medicine.

Guy, A.W., J. Wallace, and J.A. McDougall (1979). Circularly polarized 2450-MHz waveguide system for chronic exposure of small animals to microwaves. Radio Sci. 14(6S):63-74.

Johnson, R.B., S. Mizumori, D.E. Myers, A.W. Guy, and R.H. Lovely (1977). Effect of pre- and post-natal exposures to 918 MHz microwaves on development and behavior in rats. Abstracts, 1977 USNC/URSI Int. Symp. Biol. Effects Electromagnetic Waves (Oct. 30-Nov. 4, 1977, Airlie, Va), p. 70.

Lovely. R.H., D.E. Myers, and A.W. Guy (1977). Irradiation of rats by 918-MHz microwaves at 2.5 mW/cm$^2$: Delineating the dose-response relationship. Radio Sci. 12(6S):139-146.

Lovely, R.H., S. Mizumori, R.B. Johnson, and A.W. Guy (1978). Irradiation of rats by 918-MHz microwaves at 5 mW/cm$^2$: Delineating the dose-response relationship II. Abstracts, 1978 IMPI/URSI Symp. Electromagnetic Fields Biol. Syst. (Aug. 1-8, 1978, Helsinki, Finland), p. 83.

Moe, L.E., R.H. Lovely, D.E. Myers, and A.W. Guy (1975). Physiological and behavioral effects of chronic low-level microwave radiation in rats. Biological Effects of Electromagnetic Waves, Selected papers, USCN/URSI Annual Meeting (Boulder, Colo., Oct. 20-23, 1975), C.C. Johnson and M.L. Shore, Eds. HEW Publication (FDA) 77-8011, Washington, D.C. 20402: U.S. Gov. Printing Office, Vol. I, pp. 248-255.

Phillips, R.D., E.L. Hunt, and N.W. King (1975). Field measurements, absorbed dose and biologic dosimetry of microwaves. Ann. N.Y. Acad. Sci. 247:499-509.

# PUBLICATIONS AND PRESENTATIONS RESULTING FROM STUDY

Publications:

1. Guy, A.W., C.K. Chou, R.B. Johnson, and L.L. Kunz. Study of effects of long-term low-level RF exposure on rats: A plan . Proc. of IEEE, Vol. 68, No. 1, Jan. 1980.

Presentations:

1. A.W. Guy, C.K. Chou and R.B. Johnson. Instrumentation and dosimetry for multiple-animal 2450-MHz chronic exposure system. Second Annual Meeting, The Bioelectromagnetics Society, Sept. 14-18, 1980, San Antonio, Texas.

2. R.B. Johnson, C.K. Chou, A.W. Guy and L.L. Kunz. Long-term low-level radio frequency exposure of rats: An on-going study. Second Annual Meeting, The Bioelectromagnetics Society, Sept. 14-18, 1980, San Antonio, Texas.

3. J.H. Krupp. Chronic low-level RFR exposure studies. NATO A/C 243 Panel VIII Research Study Group 2, Radiofrequency Radiation Workshop, Farnborough, U.K., April 6-8, 1981.

4. R.B. Johnson, L. Kunz, C.K. Chou, and A.W. Guy. Long-term low-level exposure of rats to pulsed radiofrequency, PART I. Third Annual Meeting, The Bioelectromagnetics Society, Aug. 10-12, 1981, Washington, D.C.

5. L. Kunz, A.W. Guy, C.K. Chou, and R.B. Johnson. Pathobiological evaluation of rats exposed to long-term low-level pulsed radiofrequency radiation, PART II. Third Annual Meeting, The Bioelectromagnetics Society, Aug. 10-12, 1981, Washington, D.C.

## Table 1
### POWER DISTRIBUTION CHARACTERISTICS ALCOVE CLUSTER A-B-C
### DELIVERED POWER = 7.70 WATTS (DIR. COUPLER READ = 8.423 mW)

| CIRCUIT NO. | SERIAL NO. | DIR. COUPLER OUTPUT (mW) | INPUT POWER (mW) | ATTENUATION (dB) |
|---|---|---|---|---|
| **ALCOVE A** | | | | |
| AL1 | 1 | 1.62 | 141 | 2.58 |
| AL2 | 7 | 1.83 | 160 | 2.05 |
| AL3 | 9 | 1.66 | 145 | 2.46 |
| AL4 | 6 | 1.70 | 148 | 2.38 |
| AL5 | 3 | 1.65 | 144 | 2.49 |
| AR1 | 2 | 1.69 | 147 | 2.41 |
| AR2 | 5 | 1.75 | 153 | 2.24 |
| AR3 | 10 | 1.79 | 156 | 2.15 |
| AR4 | 8 | 1.77 | 154 | 2.21 |
| AR5 | 4 | 1.68 | 146 | 2.44 |
| MEAN INPUT POWER/S.D. = 149.7/5.93 | | | | |
| | | | | |
| **ALCOVE B** | | | | |
| BL1 | 11 | 1.70 | 148 | 2.38 |
| BL2 | 17 | 1.73 | 151 | 2.29 |
| BL3 | 19 | 1.62 | 141 | 2.58 |
| BL4 | 16 | 1.64 | 143 | 2.52 |
| BL5 | 13 | 1.66 | 145 | 2.46 |
| BR1 | 12 | 1.66 | 145 | 2.46 |
| BR2 | 15 | 1.68 | 146 | 2.44 |
| BR3 | 20 | 1.63 | 142 | 2.55 |
| BR4 | 18 | 1.46 | 127 | 3.03 |
| BR5 | 14 | 1.66 | 145 | 2.46 |
| MEAN INPUT POWER/S.D. = 143.7/6.30 | | | | |
| | | | | |
| **ALCOVE C** | | | | |
| CL1 | 21 | 1.56 | 136 | 2.74 |
| CL2 | 27 | 1.57 | 137 | 2.71 |
| CL3 | 29 | 1.56 | 136 | 2.74 |
| CL4 | 26 | 1.62 | 141 | 2.58 |
| CL5 | 23 | 1.60 | 139 | 2.64 |
| CR1 | 22 | 1.68 | 146 | 2.44 |
| CR2 | 25 | 1.53 | 133 | 2.83 |
| CR3 | 30 | 1.54 | 134 | 2.80 |
| CR4 | 28 | 1.61 | 140 | 2.61 |
| CR5 | 24 | 1.61 | 140 | 2.61 |
| MEAN INPUT POWER/S.D. = 139/4.0 | | | | |

ALCOVE CLUSTER MEAN INPUT POWER/S.D. = 144.0/6.97

Table 2

Characteristics of Scaled Synthetic Tissues
For Simulating 442-MHz Exposure at 2450-MHz

| Full Scale Dielectric Constant (T=37°) | Scaled Synthetic Tissue | Composition % Total Weight | | | | | | Scaled Dielectric Constant* T=20°C | Specific Heat (kcal/kg·°C) | Density (g/cm³) |
|---|---|---|---|---|---|---|---|---|---|---|
| | | $H_2O$ | Ethylene Glycol | $NH_4Cl$ | NaCl | PEP | TX150 | | | |
| '=53 =1.18 | Muscle (gel) | 82 | | | 4.2 | 5.8 | 8.0 | '=53.3 = 6.4 | .86 | 1.000 |
| '=53 =1.18 | Muscle (liquid) | 53.9 | 40.6 | 5.5 | | | | '=50.2 = 6.4 | .87 | 1.074 |
| '=33 = .88 | MIXTURE 2/3 Muscle 1/3 Fat (liquid) | 29 | 65.2 | 5.8 | | | | '=33.1 = 4.8 | .71 | 1.099 |

*Scale Factor = 5.54

81

Table 3

Measured Average SAR in Scaled Man Models[1]

| Position | | Adult Muscle Model | Child Muscle Model | Adult Mixed Model |
|---|---|---|---|---|
| **Standing** | | | | |
| Facing horn | (EHK) | 49.63 | 163.73 | 59.27 |
| Back to horn | (-EHK) | 52.87 | 174.91 | 56.89 |
| Side to horn | (EKH) | 41.34 | 187.17 | 46.33 |
| **Lying on Back** | | | | |
| Head to horn | (KHE) | 49.25 | 94.76 | 50.37 |
| Feet to horn | (-KHE) | 50.12 | 94.63 | 48.22 |
| Side to horn | (HKE) | 41.18 | 60.89 | 41.64 |
| **Lying on Side** | | | | |
| Facing horn | (HEK) | 49.24 | 108.21 | 54.01 |
| Head to horn | (KEH) | 52.90 | 158.14 | 54.08 |
| Feet to horn | (-KEH) | 62.94 | 165.39 | 61.20 |

[1]Unit in mW/kg per 1 mW/cm$^2$

Scale factor, 5.54

Adult height, 174 cm

Child height, 88 cm

Operating frequency, 2450 MHz

Simulated frequency, 442 MHz

Table 4
Theoretical and Experimental Compilation of Data
on Average SAR for Human Exposure to Frequencies
Near or Equal to 450 MHz at 1 mW/cm

| Investi-gator and Freq. (MHz) | Model | * | (S/m) ** | SAR mW/kg Polarization of Exposure | | | | | | | |
|---|---|---|---|---|---|---|---|---|---|---|---|
| | | | | EKH | EHK | HEK | HKE | KEH | KHE | -KEH | -KHE |
| Durney et al (1978) | Prolate Sphere. Avg Man | 36 | 0.82 | 34 | 34 | 30 | 30 | 16 | 16 | 16 | 16 |
| 450 MHz | Skinny Man | 36 | 0.82 | 49 | 49 | 36 | 36 | 22 | 22 | 22 | 22 |
| (Theo-retical) | 5-year Child | 36 | 0.82 | 62 | 62 | 42 | 42 | 31 | 31 | 31 | 31 |
| | 1-year Child | 36 | 0.82 | 94 | 94 | 43 | 43 | 52 | 52 | 52 | 52 |
| | Infant | 36 | 0.82 | 125 | 125 | | | | | | |
| Gandhi (1977) 462.3 MHz (Mea-sured) | Human Figur-ine Saline | Unknown Saline | Unknown Saline | 45 | | 44 | | 63 | | | |
| Gandhi (1979) 462.3 MHz (Theo-retical) | Compu-ter Avg Man | 36 | 0.82 | | 35 | | | | | | |
| (Mea-sured) | Human Figure Saline | Unknown Saline | Unknown Saline | | | | | | | 56 | 57 |
| Guy et al (1977) 442 MHz (Mea-sured) | Human Doll | 58.9 | 1.68 | 40.7 | 46.1 | 48.7 | 48.8 | 68.6 | 42.7 | 36.8 | 38.8 |
| Current project | Human Doll | 50.2 | 1.18 | 41.4 | 49.6 | 49.2 | 41.2 | 62.9 | 49.9 | 52.9 | 49.2 |
| | Adult | 33.1 | 0.89 | 46.4 | 59.3 | 54.0 | 41.6 | 61.2 | 48.2 | 54.1 | 50.4 |
| 442 MHz (Mea-sured) | 3-4-yr Child | 50.2 | 1.18 | 187 | 164 | 108 | 61 | 165 | 94 | 158 | 95 |

* Assumed full-scale dielectric constant
** Assumed full-scale conductivity

Table 5
Theoretical and Experimental
Compilation of Maximum SAR for Human Exposure
to Frequencies Near or Equal to 450 MHz at 1 mW/cm

| Investi-gator and Freq. | Model | * | (S/m) ** | Maximum SAR (mW/kg) | | | | | | | |
|---|---|---|---|---|---|---|---|---|---|---|---|
| | | | | Polarization of Exposure & Location of Maximum | | | | | | | |
| | | | | EKH | EHK | HEK | HKE | KEH | KHE | -KEH | -KHE |
| Chen & Guru (1977) 500 MHz (Theo-retical) | Compu-ter | 32.5 | 1.49 | | 21.7 head 49.0 neck 2.8 hand | | | | | | |
| Guy et al (1977) 442 MHz (Mea-sured) | Human Fig-urine | 54.1 | 1.43 | 109 head 308 neck 675 hand | 38.8 head 153 neck 112 hand 367 arm | 101 head 321 hand | 188 head 291 foot | 131 head 1020 peri-neum 560 wrist | 200 head 231 peri-neum 329 foot | 150 head 545 neck 964 wrist | 210 head 148 ankle |
| Current project 442 MHz | Human Fig-urine | 50.2 | 1.18 | 133 head 232 neck 610 arm | 43 head 210 neck 281 arm | 120 head 120 neck 519 arm | 350 head 145 arm 202 foot | 77 head 139 neck 848 peri-neum | 61 head 93 neck 197 foot | 207 head 319 neck 827 arm | 291 hand 486 neck 119 ankle |

* Assumed full-scale dielectric constant
** Assumed full-scale conductivity

## TABLE 6
### Circular Waveguide Exposure Parameters for Simulation of Chronic Exposure of Man to RFR

| OPTION 1 | OPTION 2 | OPTION 3 |
|---|---|---|
| 450-MHz 1-mW/cm RFR From child to adult (based on 68 mW/kg for adult) | Equivalent to no more than allowed by ANSI RPG at any time during lifetime (max 400 mW/kg during childhood) | Equivalent to maximum allowed by ANSI RPG 400 mW/kg averaged over entire lifetime |
| Waveguide input = 0.097 W Average power density = 324 μW/cm Average SAR 200-g rat = 270 mW/kg Average SAR 800-g rat = 68 mW/kg Predicted range of hot-spot magnitude in 330-g rat 517-1090 mW/kg | Waveguide input = 0.144 W Average power density = 480 μW/cm Average SAR 200-g rat = 400 mW/kg Average SAR 800-g rat = 101 mW/kg Predicted range of hot-spot magnitude in 330-g rat 632-1330 mW/kg | Waveguide input = 0.39 W Average power density = 1300 μW/cm Average SAR 200-g rat = 1080 mW/kg Average SAR 800-g rat =273 mW/kg Predicted range of hot-spot magnitude in 330-g rat 1710-3600 mW/kg |

85
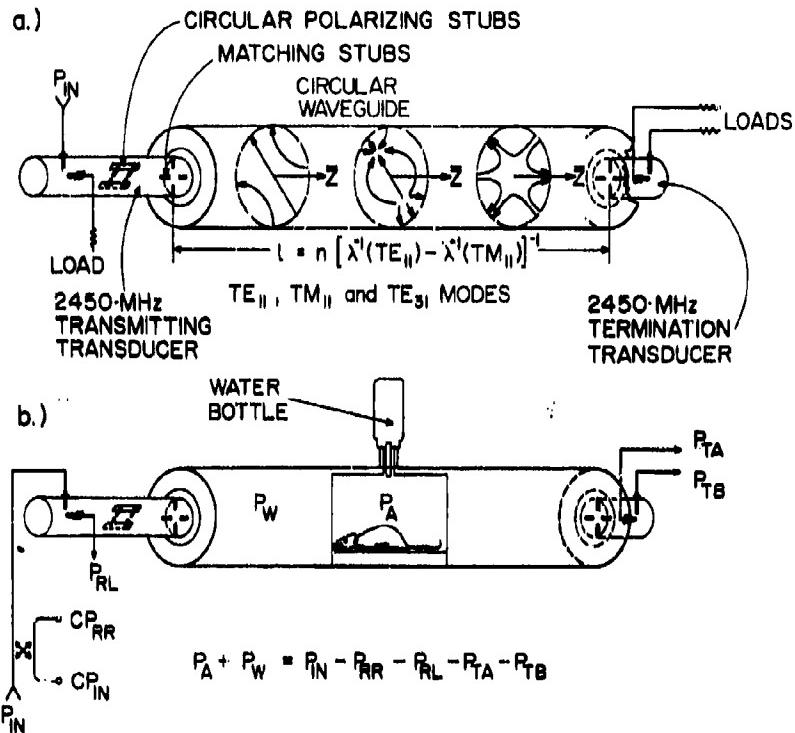
Fig. 1. Sketch illustrating operation of
2450-MHz exposure chamber;
a) empty, b) with animal.
(After Guy et al., 1979)
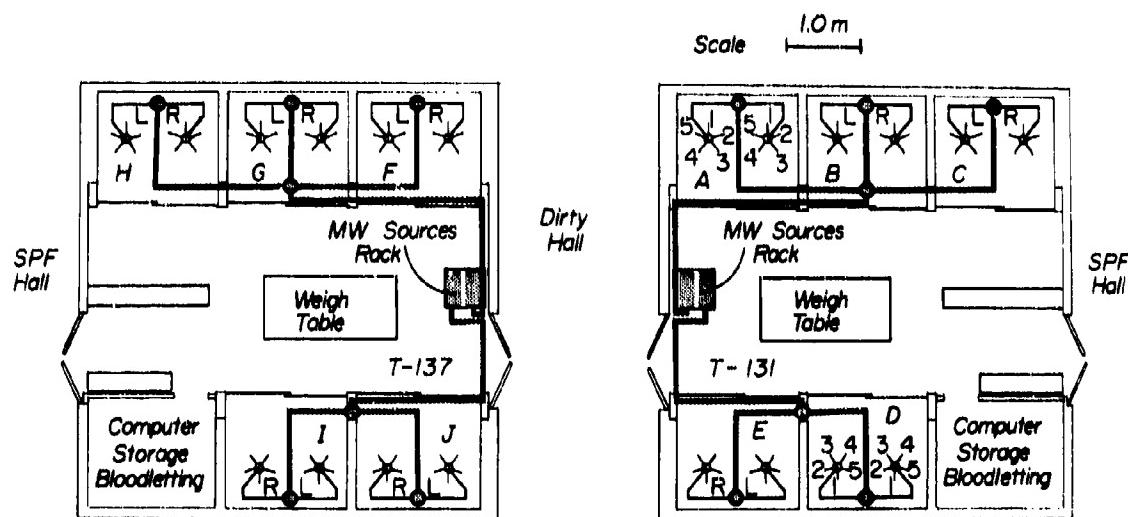


Fig. 2. Top view of exposure rooms with associated
exposure cell identification system.

86
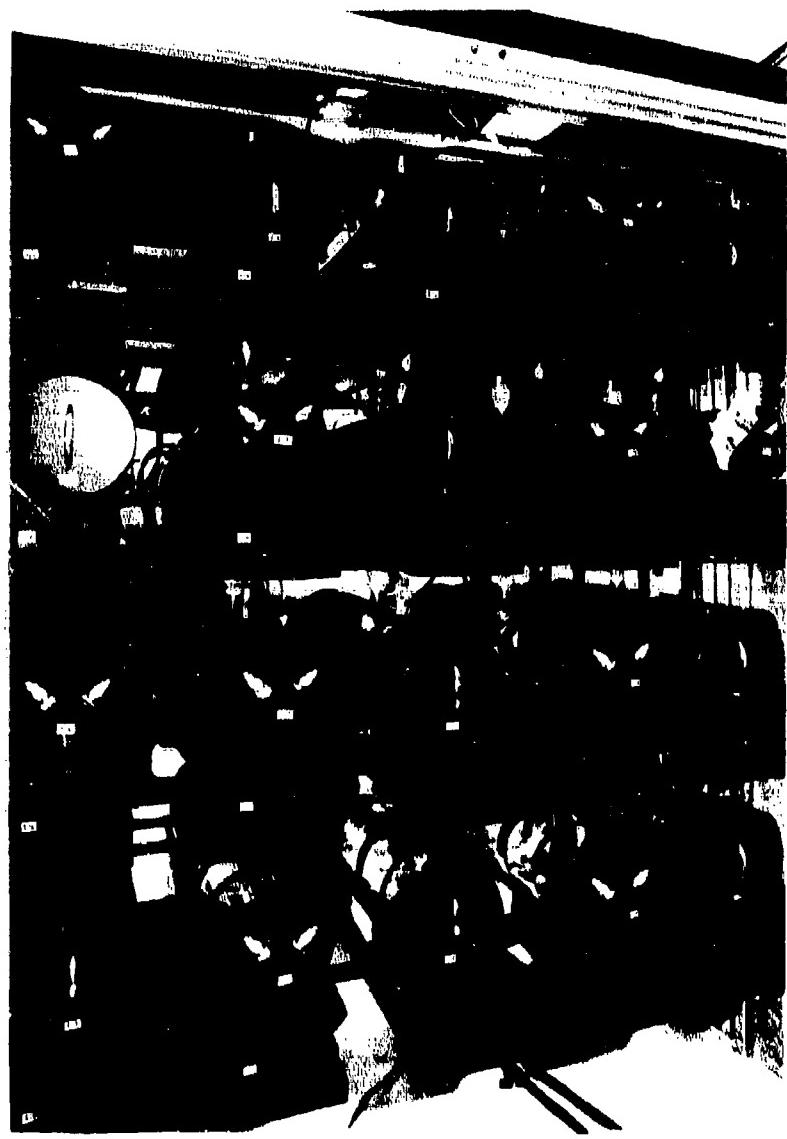
Fig. 3. Photograph of an alcove (glass doors removed)
complete under radiating conditions.
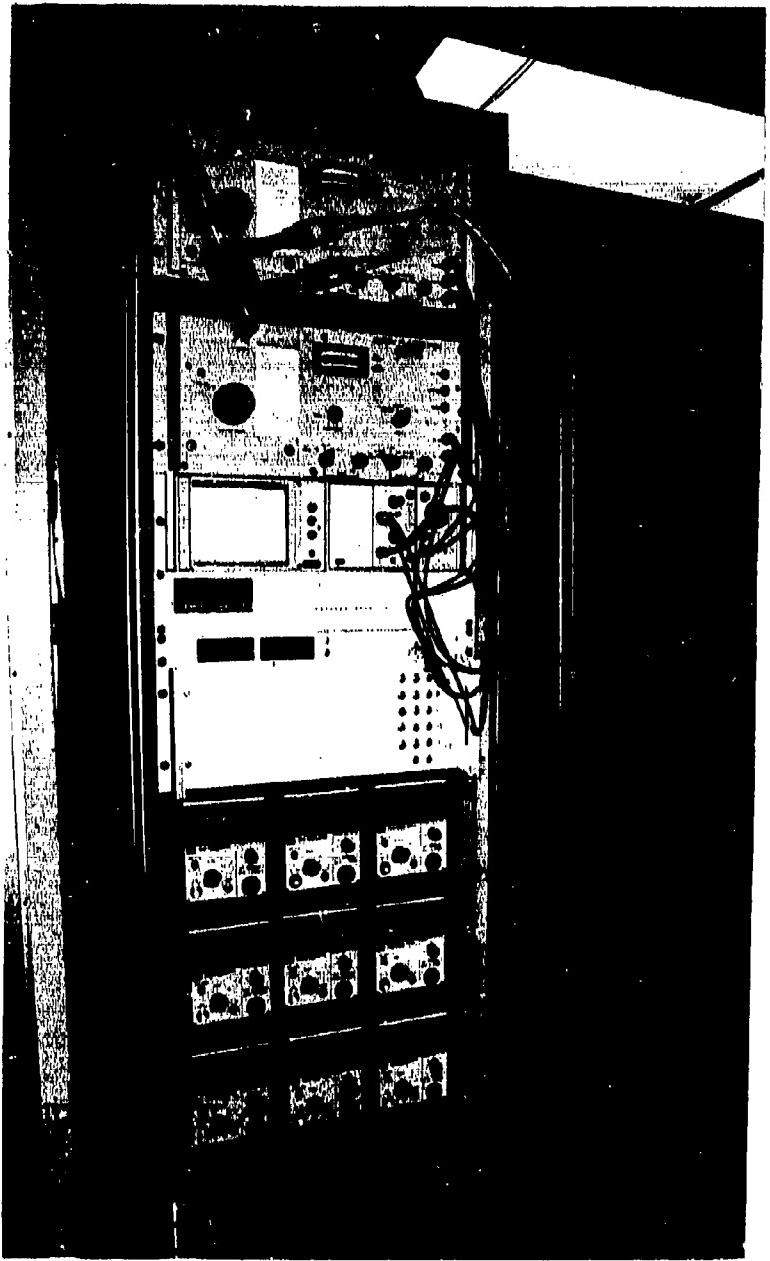
Fig. 4 . Equipment rack, (from top) two power generators, oscilloscope, temperature and humidity meter, power indicators, power meters, and emergency power supply.

88
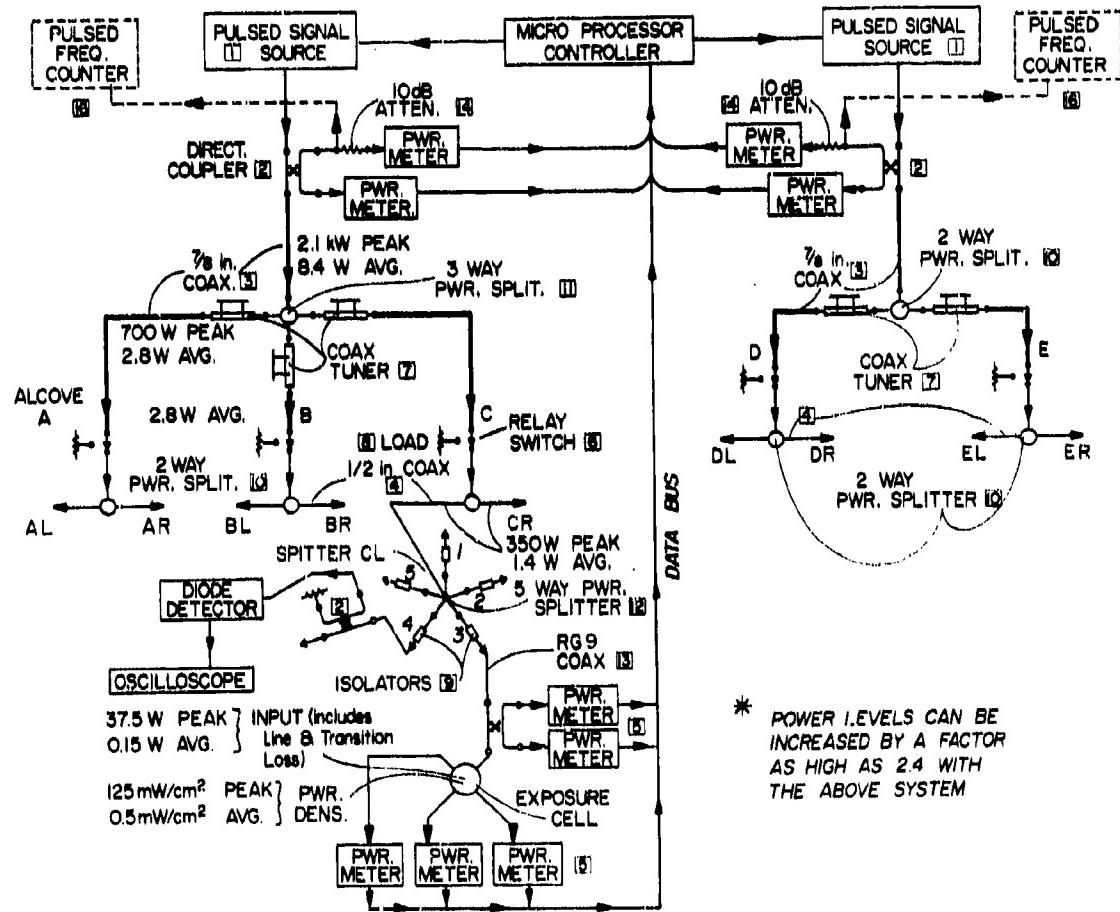
Fig. 5. Diagram of the power distribution system in room T-131.

# CALORIMETRY SYSTEM
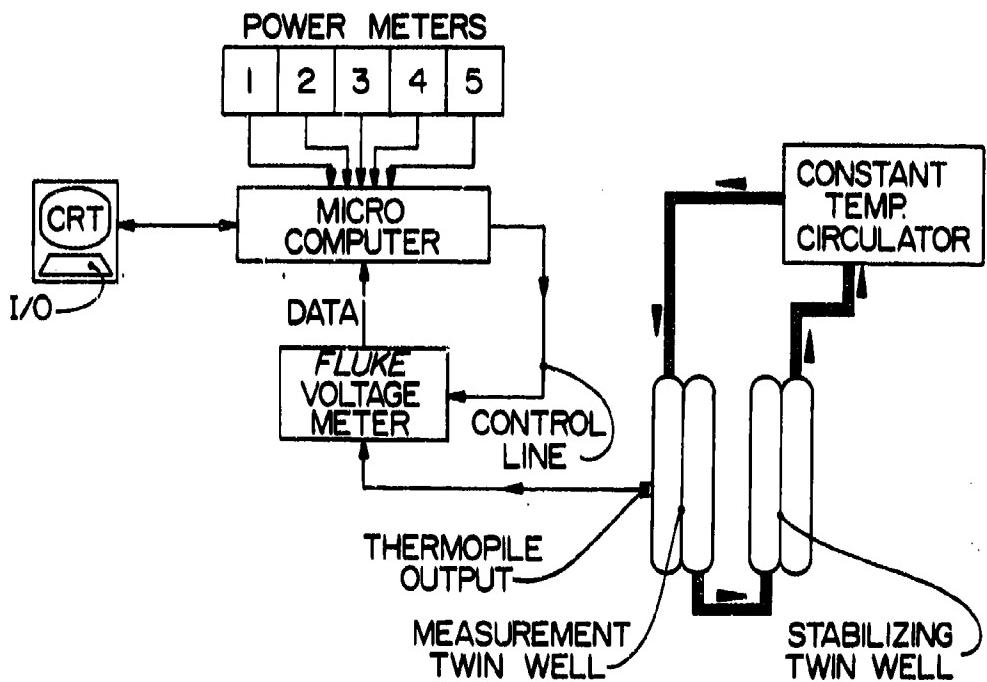


Fig. 6. Diagram of the twin-well calorimetry system.
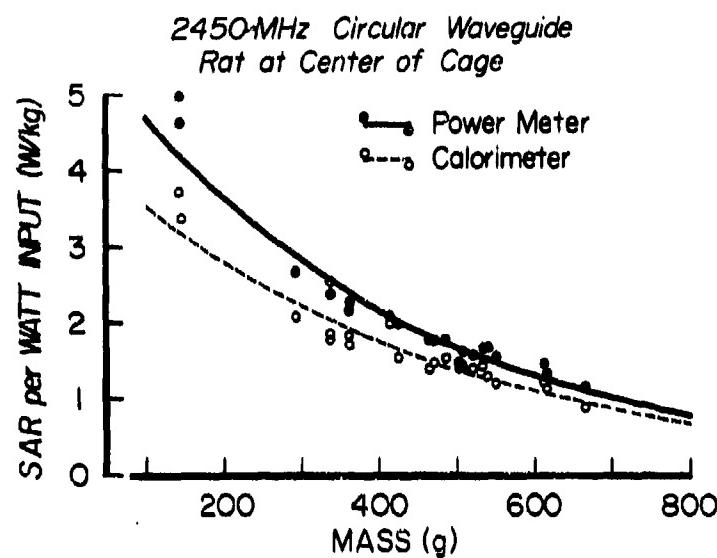
Fig. 7. Comparison of average SAR in rats of various mass exposed in the center of plastic cage in the 2450-MHz circular waveguide.
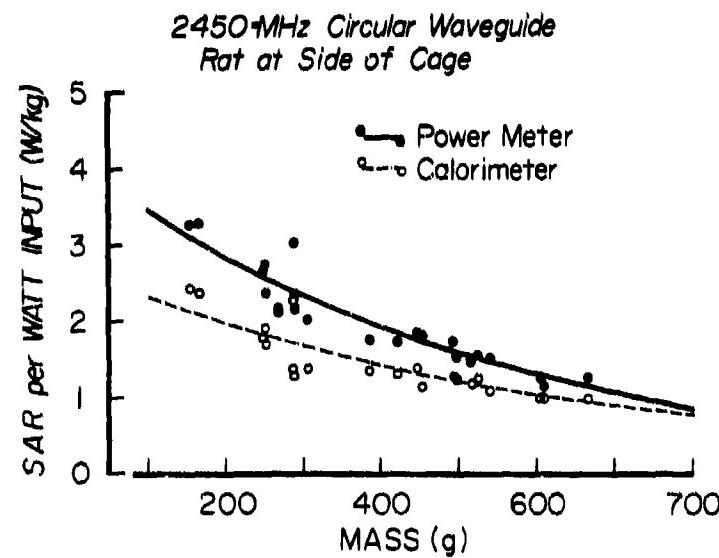


Fig. 8. Comparison of average SAR in rats of various mass exposed at the side of the plastic cage in the 2450-MHz circular waveguide.

91

Average SAR per Watt Input
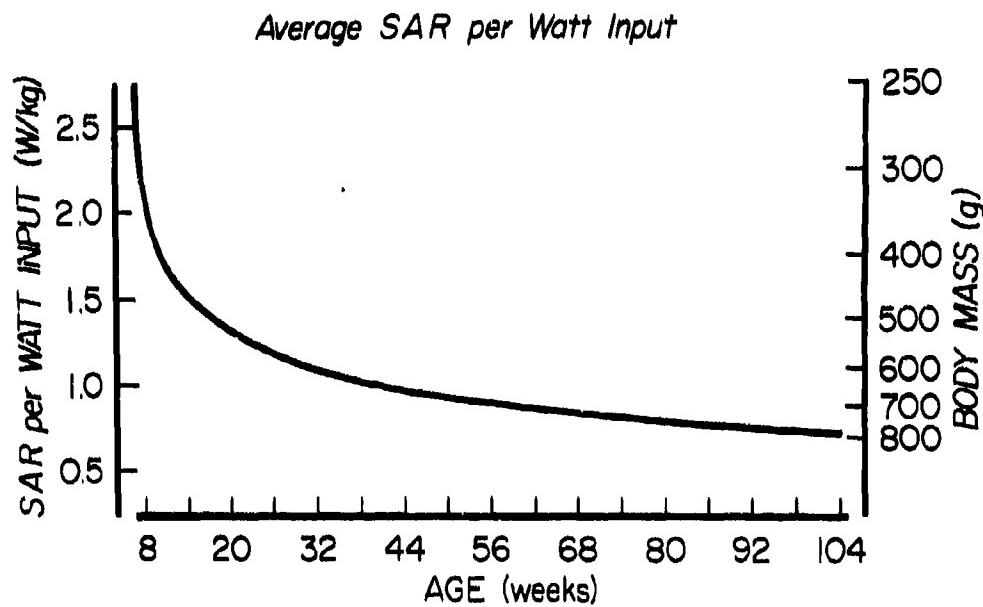
Fig. 9  Average SAR in rats exposed to 2450 MHz
in the circular waveguide at different
ages and body mass.

SAR IN EXPOSED RAT WITH 1.0-WATT INPUT

PEAK 4.39 W/kg
AVG. 2.47 W/kg
WHOLE-BODY PWR. LOSS 0.800 W
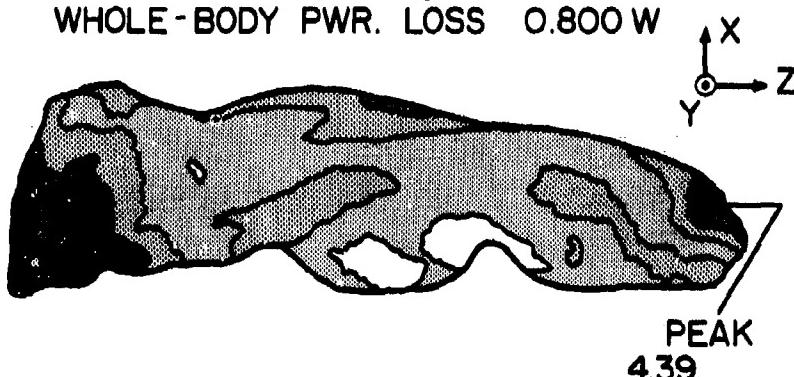


PEAK
4.39

a.) ANTERIOR EXPOSURE

O to l    l to 2    2 to3    3 to4    4 to5

Key: SAR (W/kg)

SAR IN EXPOSED RAT WITH 1.0-WATT INPUT

PEAK 6.08 W/kg
AVG. 2.34 W/kg
WHOLE-BODY PWR. LOSS 0.760W



PEAK
6.08

b.) POSTERIOR EXPOSURE

O to l·   l to 2    2 to3    3 to4    4 to5    5 to 6    6 to7
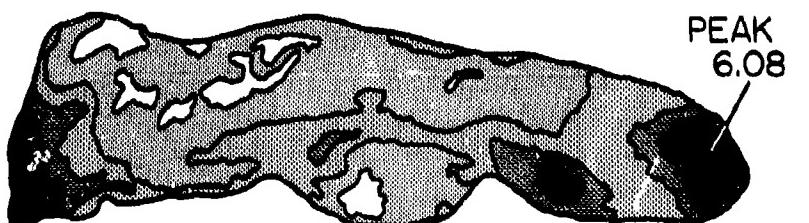
Key: SAR (W/kg)

Fig. 10. Computer-processed thermographic recording
of SAR in cadaver of a 324-g rat exposed
along axis of the waveguide chamber.
(after Guy et al.,1979).

70 kg MAN  h = 1.74m  sf = 5.54
$P_{inc}$ = 1.0 mW/cm² f = 442 MHz
THERM 15080-32
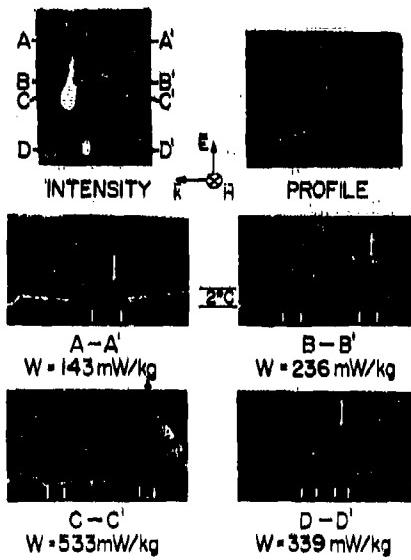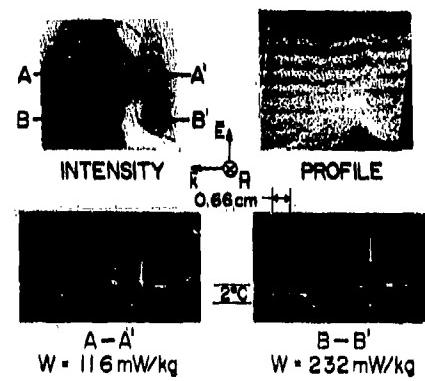
INTENSITY    PROFILE

A-A'
W = 143 mW/kg

B-B'
W = 236 mW/kg

C-C'
W = 533 mW/kg

D-D'
W = 339 mW/kg

70 kg MAN  h = 1.74m  sf = 5.54
$P_{inc}$ = 1.0 mW/cm² f = 442 MHz
THERM 14380-11

INTENSITY    PROFILE

0.66 cm

A-A'
W = 116 mW/kg

B-B'
W = 232 mW/kg

70 kg MAN  h = 1.74m  sf = 5.54
$P_{inc}$ = 1.0 mW/cm² f = 442 MHz
THERM 14480-20

INTENSITY

0.66 cm

A-A'
W = 55 mW/kg

B-B'
W = 130 mW/kg

70 kg MAN  h = 1.74m  sf = 5.54
$P_{inc}$ = 1.0 mW/cm² f = 442 MHz
THERM 14280-02

INTENSITY

0.66 cm

A-A'
W = 113 mW/kg

B-B'
W = 56 mW/kg

C-C'
W = 59 mW/kg
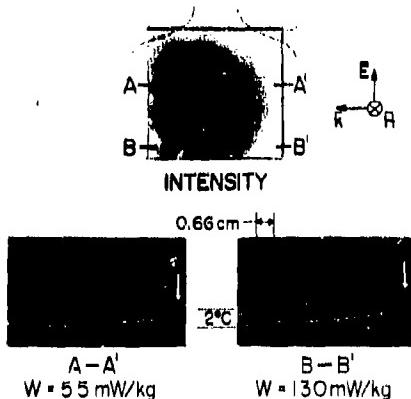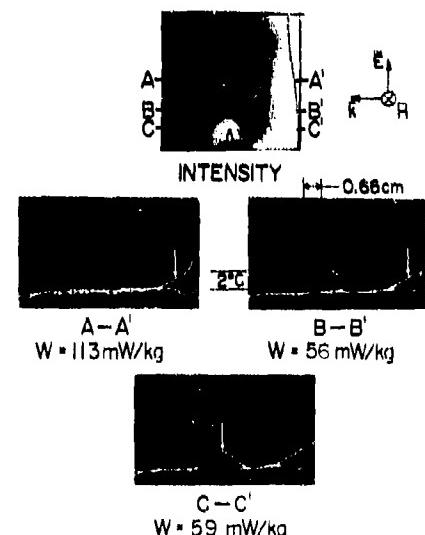
Fig. 11. Thermograms and calculated SARs for
model man exposed to EKH polarization
electromagnetic radiation.

70-kg MAN  h = 1.74 m  sf = 5.54
$P_{inc}$ = 1.0 mW/cm² f = 442 MHz
THERM 10780-01
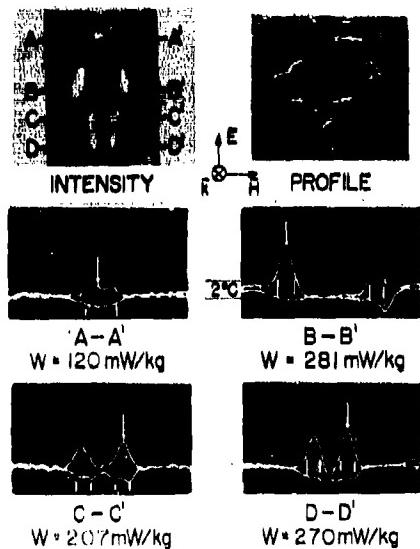
70-kg MAN  h = 1.74 m  sf = 5.54
$P_{inc}$ = 1.0 mW/cm² f = 442 MHz
THERM 14380-10

INTENSITY      PROFILE

INTENSITY      PROFILE

0.66cm

A–A'
W = 120 mW/kg

B–B'
W = 281 mW/kg

A–A'
W = 43 mW/kg

B–B'
W = 210 mW/kg

C–C'
W = 207 mW/kg

D–D'
W = 270 mW/kg

70-kg MAN  h = 1.74 m  sf = 5.54
$P_{inc}$ = 1.0 mW/cm² f = 442 MHz
THERM 14280-01

70 kg MAN  h = 1.74 m  sf = 5.54
$P_{inc}$ = 1.0 mW/cm² f = 442 MHz
THERM 14480-19

0.66cm

INTENSITY

0.66cm

A–A'
W = 31 mW/kg

INTENSITY

0.66cm

A–A'
W = 25 mW/kg

B–B'
W = 31 mW/kg
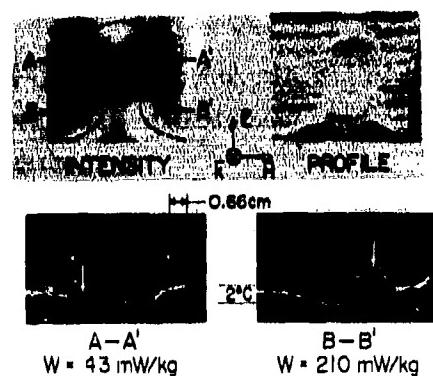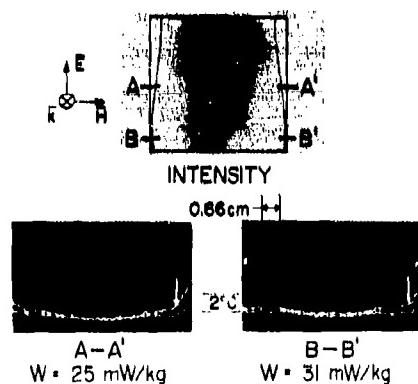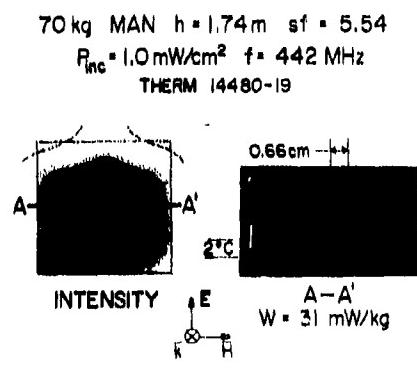
Fig. 12. Thermograms and calculated SARs for model
man exposed to EHK-polarization electro-
magnetic radiation.

# A CIRCULAR PARALLEL-PLATE RADIATION FACILITY FOR CHRONICALLY EXPOSING LARGE RODENT POPULATIONS TO 435-MHZ ENVIRONMENTS

J. C. TOLER

BIOMEDICAL RESEARCH DIVISION

GEORGIA INSTITUTE OF TECHNOLOGY

ATLANTA, GA  30332

## I.  INTRODUCTION

Over the past several years, an extensive public and scientific interest has evolved concerning the possibility that long-term exposure of biological systems to low-level radiofrequency radiation may adversely affect the vital processes of organisms. The basis for this concern is a consequence of the postulated existence [1] of

- an interaction between natural electromagnetic environments and the regulation of vital processes, and

- the role of endogenous electromagnetic fields in the coordination of physiological processes.

The Biomedical Research Division at Georgia Tech, under sponsorship of USAFSAM/RZP, has undertaken research efforts over the past two years for the purpose of providing a technically valid and cost-effective 420- to 450-MHz radiofrequency radiation facility suitable for long-term bioeffects studies involving large rodent populations. Design specifications stipulated that, for radiated animals, the facility had to provide both pulsed- and continuous-wave fields and a power density variable up to 10 mW/cm$^2$. Control animals had to be housed in an identical, colocated, but nonenergized facility. Suitably designed cages capable of individually housing 200 radiation and control rats had to be provided, and a transmitter system for the facility was required.

96

## II. TECHNICAL APPROACH

During the initial research efforts, several commonly used and new radiation facility concepts were analyzed to determine their adequacy for long-term bioeffects studies involving large rodent populations exposed to 420- to 450-MHz fields. These concepts included the

- Circular waveguide radiation concept,
- Free-space radiation concept,
- Compact range radiation concept,
- Circular, parallel-plate radiation concept, and
- Reverberation chamber radiation concept.

Primary technical considerations during the analysis of these concepts were exposure-field configuration, access to the animals for assay and observation, dosimetry, floor space requirements, and cost. The circular, parallel-plate concept was determined to be the most technically and economically feasible, and a detailed design for this concept was developed. In the development of this design, it was noted that the available literature provided no indication that parallel metal plates had been considered for chronic exposure of large rodent populations. Yet, these plates can have energy coupled to them in such a way that electromagnetic fields travel outward to animal cages positioned along the plate periphery. When the plates and energy-coupling device are designed to provide circular symmetry, the exposure field will exhibit symmetry and all animals will be exposed to fields with the same amplitude. A simplified circular, parallel-plate radiator is shown in Figure 1.

The field configuration developed by circular, parallel plates is a function of spacing between the plates. For example, if the plate spacing is less than one-half wavelength, only the dominant TEM mode will propagate. For this mode, the electric and magnetic field vectors are transverse to the direction of propagation which, in the circular, parallel plates, is radially outward. Therefore, the electric field vector is perpendicular to the parallel plates, and the exposure field is vertically polarized. This is undesirable since the long dimension of the animals is horizontal, and maximum energy is coupled when the electric field vector and animal long dimension are in the same direction. The vertical polarization is

97

Plan View

Feed Antenna          Circular Parallel Plates

Cage

Section AA

Cage
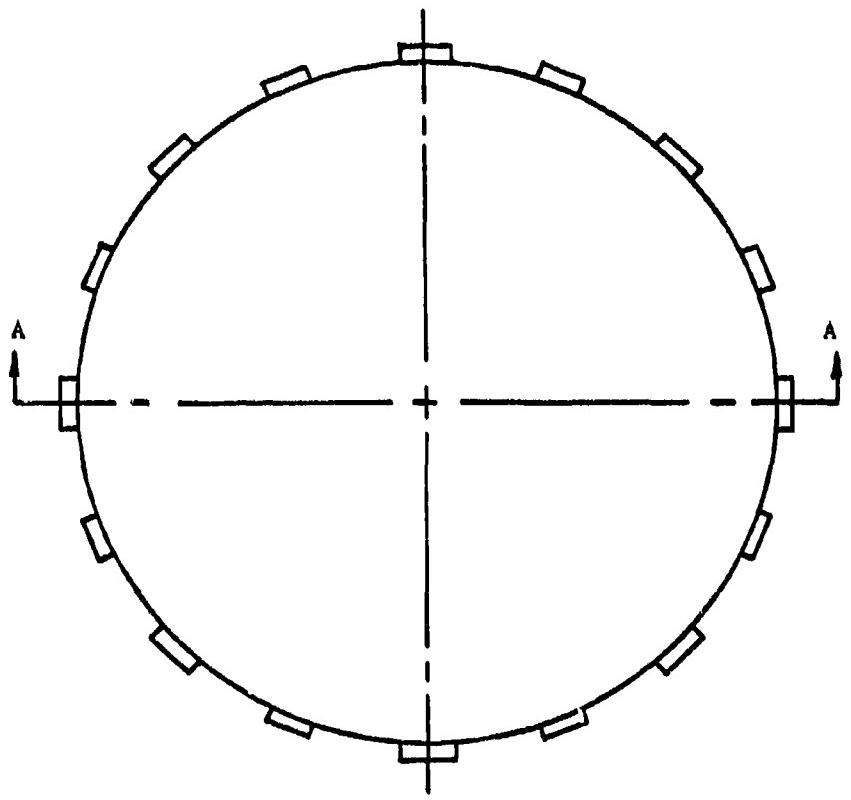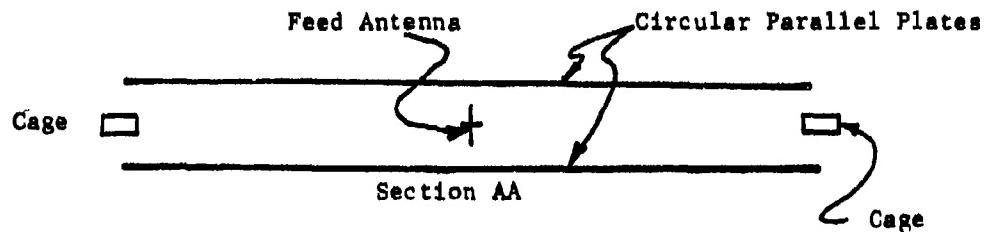
Figure 1.   Schematic illustration of circular   parallel-plate
            radiation facility.

98

changed if the spacing between the plates is greater than one wavelength. In this case, the TE and TM modes will propagate and the electric field vector will be parallel to the plates. By maintaining the plate spacing greater than one-half wavelength but less than one wavelength, only the lowest order TE mode can propagate.

The design for a circular, parallel-plate facility used a frequency of 435 MHz (midpoint in the 420- to 450-MHz range) and assumed that n rat cages were to be arrayed around the plate periphery. The plate diameter and center-to-center cage spacing were designated D and S, respectively. Also, it was assumed that, at 435 MHz (wavelength = 27.14 inches), an intercage spacing of approximately two-thirds wavelength would not introduce exposure field scattering sufficient to affect dosimetry. Using these assumptions, the diameter of a pair of parallel plates capable of exposing 100 rats was calculated. The calculation indicated that a 48-foot diameter would be necessary. Obviously, this diameter was not practical; however, the radiation concept is maintained for an arrangement in which several identical pairs of plates are stacked as shown in Figure 2. In this case, the plate diameter is reduced without decreasing the number of exposure animals.

Another major part of the design development involved the antenna to couple or feed energy to the circular, parallel plates. Slotted cylinder antennas were considered since they provide a horizontally polarized field with nearly constant amplitude in the azimuth plane. Performance of this antenna can be intuitively understood by referring to Figure 3 [2]. The antenna is first considered to be a slot in a flat metal sheet. This slot is center-fed with a coaxial cable, and current directions are indicated by the arrows. The metal sheet may then be formed into a U-shape and finally into a cylinder, with the coaxial feed located inside the cylinder. If the impedance around the cylinder circumference is sufficiently low, current will flow in horizontal loops around the cylinder. Under these conditions, a vertical slotted cylinder will radiate a horizontally polarized field. The amplitude of this field in the horizontal plane is dependent on the cylinder diameter. In general, the radiated field tends to be greater on the cylinder side

Plan View

Cage ☐     + Feed     ☐ Cage

Cage ☐     + Feed     ☐ Cage

Cage ☐     + Feed     ☐ Cage

Cage ☐     + Feed     ☐ Cage

4-High Stack of Parallel Plates
Section AA
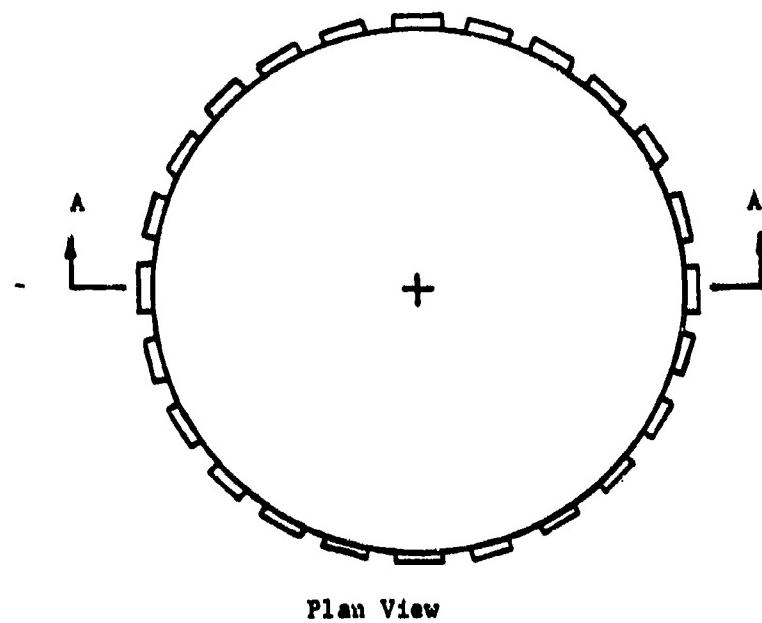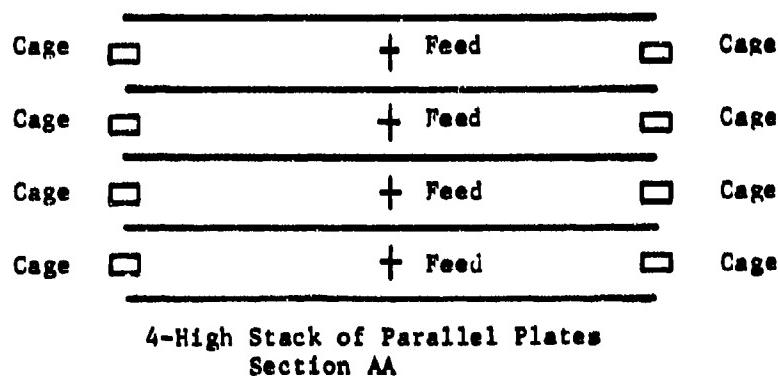
Figure 2.    Illustration of a stack of four circular parallel plates for chronic exposure of 100 rats.

100
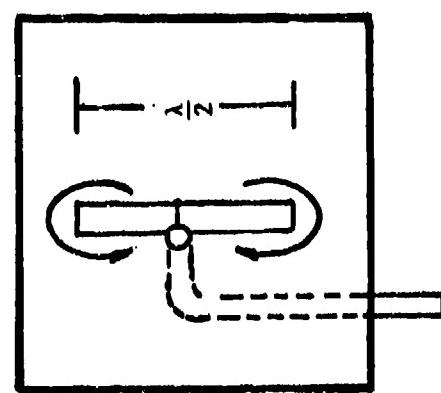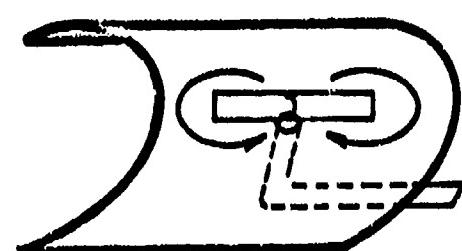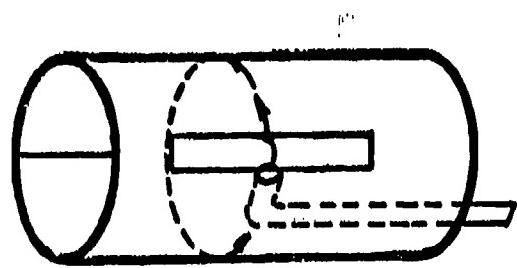
Figure 3. Formation of a slotted-cylinder antenna (see Reference 2).

where the slot is located; however, if the cylinder diameter is a
sufficiently small part of a wavelength, i.e., approximately $0.1\lambda$, the
radiated field in the horizontal plane becomes essentially uniform.  If
the cylinder diameter is increased to the point of becoming a significant
part of a wavelength, the field in the region of the shadow cast by the
cylinder becomes small.  Generally, as the cylinder diameter becomes
large, the horizontal field approximates a cardioid [3].  To complete
the antenna design, features such as bandwidth, resonant frequency,
input impedances, etc. were considered in terms of the capacitive effect
of slot length and width and the inductive effect of cylinder diameter.

III.   RESULTS/PROGRESS

A circular parallel-plate radiation facility complying with the
above-described design is currently under construction. Major features
of the facility are evident in Figure 4. The plate diameter is 12 feet
since this permits 100 rats to be accommodated when four sets of plates
are stacked one above the other. A 1.5-foot plate separation distance
is provided such that this distance will be greater than one-half wavelength
but less than one wavelength. An 18-inch center-to-center cage spacing
will be maintained, and the cages will be positioned on Styrofoam blocks
at the plate edges. Microwave-absorbing material will be used on the
facility walls to reduce signal reflections to tolerable levels. The
transmitter system will be located in the transmitter room, and cables
to connect the antennas will be routed overhead. The slotted-cylinder
antenna will be positioned at the center of the plates and will have the
following dimensions:

- Cylinder outside diameter: 4 inches
- Cylinder wall thickness: 0.125 inches

A single slot will be 14 inches long and 0.0624 inches wide, cut along
the axial dimension of the cylinder at the location of each set of plates.

In addition to areas for the circular parallel plates and transmitter,
the facility includes an assay room, computer room, wash room, storage
room, and buffer area. The assay room will provide space where biological
endpoints can be monitored. Typically, these endpoints will require an
electronic balance interfaced with the computer; transducers for measuring
blood pressure, heart rate, and blood volume; devices for collecting
blood samples; etc. A small computer capable of managing data from 200
animals will be located in the computer room. This computer will also
be used for data analysis, field monitoring, energizing the emergency
notification system, etc. The wash room will house the cage washer, and
the storage room will be used for food, litter, spare cages, etc.

103
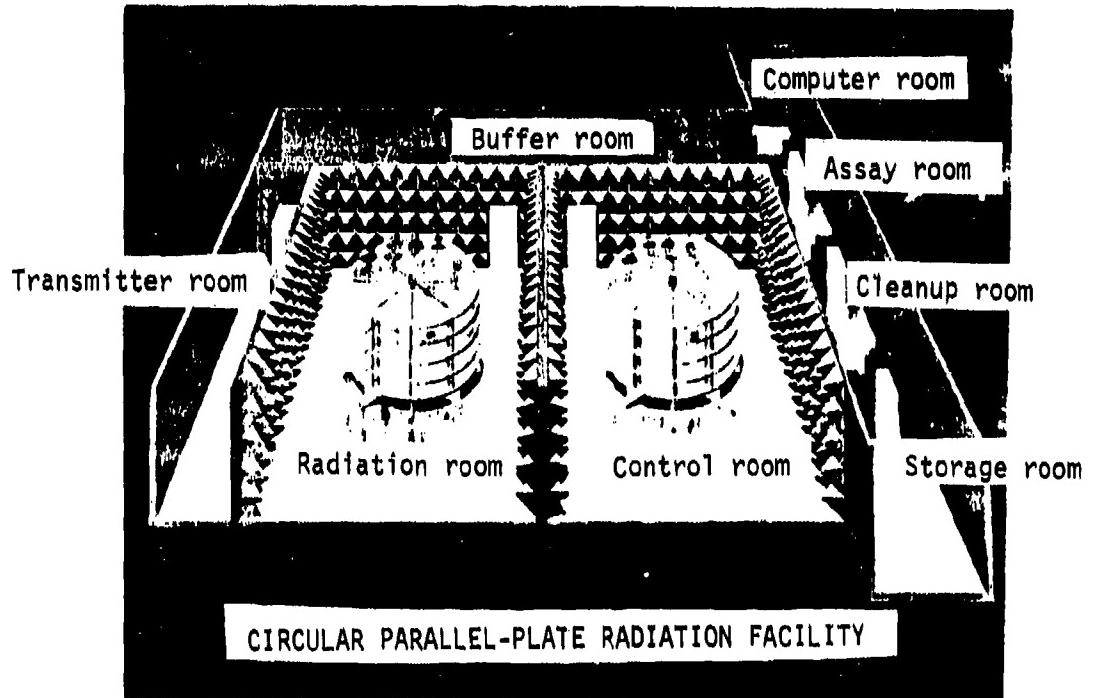
Figure 4. Circular parallel-plate facility currently under construction.

# IV. SUMMARY AND CONCLUSIONS

Research efforts have resulted in the design of a technically valid and cost-effective radiation facility for chronically exposing large rodent populations to pulsed- and continuous-wave fields in the frequency range of 420 to 450 MHz. The facility is simple in design since it consists of aluminum sheets, a support base, and an aluminum tube. Additionally, it is highly versatile in that

- variations in the circular-plate diameter make possible the exposure of either more or less rodents,

- variations in the plate separation distance changes the operational frequency, and

- changes in cable interconnections make it possible to couple the transmitter output signal to any combination of antennas; therefore, the facility can be used as a low-level exposure device for a large population of rodents or a high-level exposure device for a reduced number of rodents.

## V. REFERENCES

1. A.S. Presman. Electromagnetic Fields and Life, Plenum Press, New York/London, 1970.

2. J.D. Draus. Antennas, McGraw-Hill, New York, 1950.

3. G. Sinclair. "The Patterns of a Slotted Cylinder Antenna," Proc. of the IRE, Dec. 1948, pp. 1487-1492.

## VI. Resulting Publications and Presentations

- J. Toler, R. Seaman, R. Johnson, and F. Cain. "Feasibility Study To Determine Design and Construction Criteria for a 420-450-MHz Chronic RFR Exposure Facility for Rats," Georgia Tech Final Report on Subcontract No. SCEEE-ARB/78-3, July 1979.

- J. Toler, D. Freedman, and R. Johnson. "Prototype Circular Parallel-Plate Facility for Chronically Exposing Large Rodent Populations to 420-450-MHz Radiofrequency Radiation", Georgia Tech Final Report on Subcontract No. SCEEE-ARB/79-20, January 1980.

- J. Toler, R. Schaefer, and D. Freedman. "Construction and Evaluation of a Circular Parallel-Plate Facility for Long-Term, Low-Level Bioeffects Studies," Georgia Tech Final Report on Subcontract No. SCEEE-ARB/80-34, in preparation.

- J. Toler. "Design and Evaluation of a Facility for Chronically Exposing Large Animal Populations to a 420-450-MHz Environment," Digest of AF Review of Basic Research in Environmental Protection, Toxicology, and Electromagnetic Radiation Effects, San Antonio, Tex., January 1980.

- J. Toler. "A Circular Parallel-Plate Radiofrequency Facility for Chronically Exposing Large Rodent Populations to 435-MHz Environments" To be Published in Aeromedical Review.

- J. Toler and V. Popovic. "The Cannulated Rat as an Unrestrained, Unanesthetized Animal Model for Bioeffects Studies." To be submitted to BEMS Jour., in preparation.

- J. Toler, B. Jenkins, and J. Schaefer. "A New Radiation Facility Concept for Chronic Exposure of Large Rodent Populations." To be presented at the 3rd Annual Meeting of the Bioelectromagnetics Society, Washington, D.C., Aug. 10-12, 1981.

# BIOEFFECTS OF LONG-TERM, LOW-LEVEL RADIOFREQUENCY RADIATION EXPOSURE ON RATS: THE FIRST NINE MONTHS

L.L. Kunz, R.B. Johnson, C.K. Chou, and A.W. Guy

Bioelectromagnetics Research Laboratory
Department of Rehabilitation Medicine
University of Washington, Seattle, WA  98195

## I. INTRODUCTION

The effort entitled "Effects of Long-Term, Low-Level Radiofrequency Radiation Exposure on Rats" has involved two phases. Phase I was supported under contract F33615-78-C-0631, from September 22, 1978, to May 31, 1980, and was devoted to preparation for the main study. Phase II of the project is supported under contract F33615-80-C-0612 and provides for the evaluation of a life-time exposure of 98 rats to radiofrequency fields and 98 sham-exposed rats.

Although there are more than 5,000 published articles in the literature pertaining to the biological effects of electromagnetic radiation, the question of whether long-term, low-level radiofrequency radiation (RFR) is hazardous to health remains open. Under the initial contract, an experiment was designed to (1) answer the question of whether long-term, low-level modulated RFR exposure affects the general health of rats, and (2) extrapolate any information learned to humans so as to make inferences regarding safe exposure levels for humans. This paper reports the status of biological evaluation following the initial 9 months of exposure.

## II. RESULTS/PROGRESS

The serum chemistry data from the interim bleedings have been preliminarily assessed and are presented in this document. Open-field

109

assessment data is provided covering the first 8 months of the study. Histological summaries are also presented for those animals that have spontaneously or otherwise died during the first 10 months.

Of the sixteen animals that have died during the course of the study, over half have died during or subsequent to a bleeding session. In addition, the number of animals that require extraordinary measures to obtain blood appears to be rising with each bleeding session. These observations have led to the presumption that it may be time to reduce the frequency of bleeding from once every 6 weeks to once every 12 weeks. Though this reduction could begin immediately with the elimination of the bleeding session scheduled for the end of June, there are important scientific grounds for postponing such a reduction in bleeding frequency until after the September session. This would allow for the maintenance of the 6-week collection period for one complete year and provide data taken at the same time as the interim sacrifice of animals and the immunology profile. It would also provide for collection of additional corticosterone samples that are needed for analysis.

## Urinalysis

The newly designed stainless steel screens for the urine collection cups were completed and utilized during the April - May collection period. The screen significantly reduces the amount of food- dust contamination in the urine samples. The lessened contamination allows for more accurate evaluation of the urine

samples, especially the specific gravity.  Based on the urinalysis
results of the last collection, five rats are suspected of suffering
from various stages of chronic nephropathy:

A06 - exposed - possible early stage, bodyweight changes and food and
water consumption do not appear abnormal at this time.

B10 - exposed - possible early stage, excessive water consumption
noted for the past  2  months.

F07 - exposed - possible early stage, bodyweight changes and food
consumptions do not appear abnormal at this time.

G13 - control - chronic nephropathy, excessive water consumption noted
for the past 2  months.

I13 - control - possible early stage, bodyweight changes and food and
water consumptions do not appear abnormal at this
time.

The improved quality of the collected urine samples will increase
the value of monitoring the experimental animals during the remainder
of the project.

Blood Chemistry Evaluations

A.  Data Entry and Reduction

111

The backlog of raw data values from previous bleeding sessions to be entered into the computer-maintained database has been eliminated. All available blood chemistry, hematology, and protein electrophoresis data have now been hand-entered. Preliminary descriptive statistical analyses are completed on all blood chemistry, and sample summary printouts are included from the most recent bleeding session for the parameters GLUCOSE, BUN and CALCIUM as Attachments 1, 2, and 3.

Inspection of these and other summaries has revealed occasional anomalies in the database that have now been traced to erroneous data having been fed initially into the database in the form of raw chemistry values or basic dilution factors. The program currently in use for the hand-entry of chemistry data into the computer system provides no internal error-checking facility. Error checking was not included in the program because, at the time, insufficient normal data was available from within this laboratory for this particular strain of rat and for the chemistry-processing procedures employed. This data is essential to establish the warning and limit values on which error- trapping algorithms may be based.

Tens of thousands of data values now have been tabulated, and a clear picture of the mean and standard deviation associated with each parameter has emerged. Highest priority, therefore, has been assigned to modifying the data entry program before the next bleeding session in June, to include stringent error- trapping

routines. This will prevent the costly double-entry system of data checking that was contemplated initially. It will also prevent the present practice of multiple passes over the raw data summaries by visual inspection to detect possible entry errors. It is felt that preventing initial entry of erroneous data into the database is preferable to detecting it after the fact.

Although the reliability of the data currently in the database and used for the attached summaries is subjectively judged to be above the 99% level of confidence, until all anomalous entries have been removed, all current data summaries will be marked PRELIMINARY to avoid later confusion.

The small degree of uncertainty in the current database affects the estimates of mean and standard deviation; therefore, any tentative conclusions based on small mean differences between exposed and sham-exposed conditions must be tempered. It is expected that all errors of data entry will be removed in time for data presentation at the August BEMS meeting and for inclusion into the 5th quarterly progress report in September.

In addition, final adjustments have not, as yet, been made to correct for the minor nonlinear drift, peculiar to each chemistry parameter directly associated with the dilution process. This will be accomplished from analysis of the effects of the dilution process on the pooled control serum samples.

113

A comparison of the diluted and undiluted pooled control serum is presented in Table 1. From this it can be observed that the obtained mean glucose values for this pooled serum appears to be extraordinarily high (200-220 mg/dl) as compared with the experimental subjects of the study (140-150 mg/dl). These values are also higher than "standard" values presented in the literature and those obtained previously in this laboratory on other strains of rats. The values for standard literature citations for rat glucose levels range from 70-200 mg/dl, with the median value approximately 130 mg/dl. A review of the literature and serum-handling techniques has suggested plausible explanations for these differences:

1. The level of arousal of the animal immediately prior to bleeding affects the release of epinephrine that in turn stimulates glycogen breakdown and raises the actual level of blood glucose.

2. The length of time following the actual removal of blood from the animal and its preparation through spinning and pipetting off the red cells and whether the samples were maintained refrigerated or on ice decreases assayed levels.

3. Time of day and whether the animals were fasted or on ad lib diet prior to sampling affects assayed levels.

The actual procedures used to obtain the blood samples which produced the above-mentioned parameter estimate discrepancy

114

suggest a simple direct correlation between the procedure
and ultimate values assayed.

1. The procedures used to obtain our pooled serum sample
would tend to maximize the final assayed values of the parameter
GLUCOSE.

a. The animals were anesthetized and samples drawn
via intracardiac puncture. Other animals to be bled were
housed in the same room as the bleeding.

b. Samples were immediately placed into tubes and
spun in a refrigerated centrigue following clotting, and the
serum was withdrawn upon completion and frozen.

2. The procedures used in the current study would have
tended to minimize arousal. The blood was prepared generally
within an hour of sampling but was not refrigerated. These
factors would tend to lower the assayed glucose levels compared
to the control serum.

3. Earlier work done in our laboratory often centered
around obtaining corticosterone samples. Therefore, particular
emphasis was placed on obtaining samples from completely non-
aroused animals. However, blood chemistry samples often remained
unrefrigerated and unprepared for several hours before analysis.
These procedures would tend to lower the assayed levels of glucose
even further, compared to the present control serum.

4. Standard laboratory practice, it would be assumed, would fall between the procedural extremes exemplified by those outlined under 1 and 3, thereby leading to glucose-level estimates that also fall between these extremes--as was found to be the case.

Before final conclusions can be drawn on this matter and ultimate correction of the raw data for dilution effects made, we will conduct a small study in tandem with the June bleeding. We will prepare new pooled samples from animals not participating in this study. They will be sampled under parametric conditions of arousal/nonarousal and fasted/ad lib, using various preparation delays before assay of the samples.

B. Blood Chemistry Parameters Analysis

The data from the seven bleedings covering the initial base-line values and six subsequent 6-week intervals are presented in Figures 1 through 5 for five representative chemistry parameters: glucose, BUN, $K^+$, $Na^+$, and $T_4$. The bar graphs represent mean values and standard deviations for exposed and sham-exposed conditions based on the combined values of all animals in each condition.

It is clear from these preliminary analyses that no gross clinical abnormalities are discernible due to the experimental conditions imposed.

These data are, as discussed above, for the most part internally reliable and validated externally by the following:

1.  Mean values for any parameter do not vary consistently from bleeding sessions that involved dilution of the samples (sessions 1, 2, 4, and 6) to sessions in which nondiluted samples were assayed (sessions 3, 5, and 7).

2.  Mean values obtained for the 25 parameters are within the range of standard literature citations for that particular parameter.

Tables 2 and 3 present a more detailed summary of all parameters from the two bleeding sessions conducted this quarter.

## Corticosterone Analysis

There have been suggestions that corticosterone might either be dropped as an endpoint or limited to samples taken during the interim sacrifice. These concerns are based on the perceived increase in the death rate due to problems associated with the frequency of bleeding. If the sampling sessions are rescheduled on a 12-week basis, the data obtained from each session would become relatively more valuable. The inclusion of corticosterone taps an inordinate amount of serum to obtain a single endpoint. Sessions in which corticosterone is obtained require dilution of the remaining sample in order to assay the remaining 25 blood chemistry endpoints. This dilution causes loss of data integrity as previously discussed.

117

Before such a preemptive decision should be made to drop the corticosterone assay, a complete analysis of the corticosterone data thus far obtained should be made. This has been completed and an abbreviated presentation included in the following paragraphs. Preliminary conclusions based on a limited availability of data should always be made with the highest priority placed on maintaining a perspective with regards to the magnitude of any effect and the scale to which it ought to be compared. This has been attempted in the presentation of the corticosterone data and accompanying discussion.

Corticosterone is released from the adrenal glands in response to ACTH hormone released from the pituitary gland as a direct result of perceived physical or psychological stress. Corticosterone functions as a mobilizing agent for processes associated with the need for "fight or flight" in possibly sustained situations. The level of plasma corticosterone has traditionally been taken as a direct measure of the magnitude of the stress- producing factors associated with an experimental environment or specific treatment.

Assayed levels of plasma corticosterone will range on a continuum from a low of near 0 ng/ml to as high as 1,000 ng/ml. The factors that affect the instantaneous corticosterone level in the rat are varied. These levels follow a sinusoidal pattern throughout each circadian period,with the trough occurring in the early morning hours (if the animal is maintained on a natural day/night cycle) and reaching a peak about 12 hours later. In addition, the overall level of this circadian pattern will rise as a result of other factors.

118

Females have chronically higher circadian levels than males. Individual housing conditions generally are accepted as leading to higher levels as opposed to group housing. General levels of ambient temperature, noise, and environmental lighting will raise the circadian pattern.

Superimposed on this circadian background, specific effects of acute treatments can be readily discerned. The simple removal of an animal from its cage will, for example, cause a marked rise in assayed plasma corticosterone beginning approximately 3 minutes later. Even if the stimulus of handling is removed immediately, this rise will require 30-60 minutes to subside. In addition, the magnitude of this stimulated rise is itself a function of the time of application with respect to the circadian pattern.

The wide natural variance of corticosterone levels and its extreme sensitivity should be recognized, with comparison of samples limited only to those obtained under nearly identical circumstances (except for the treatment of interest.) With this in mind, parlance was standardized with a general dichotomy established between "basal" and "stress" levels of corticosterone, delineated on the basis of so-called resting, or quiescent, levels and levels obtained at intervals following a standard stressor such as etherization. Use of this terminology has, however, caused problems similar to those found in the metabolism literature with the definition and use of the terms "resting metabolism," "minimal metabolism," "lowest observed metabolism," and "mean metabolic output." The subjective and objective

119

assessment of the environmental and behavioral conditions necessary to meet "basal" requirements are at best difficult to standardize. Therefore, the simple fact that assayed corticosterone is higher in one study than another cannot imply anything about the presumed levels of stress in the environment, out of context of the respective control populations.

In the specific context of this experiment we have, as part of our general daily logistics, a sampling problem that precludes obtaining "true" basal or resting levels of corticosterone. The 200 samples are obtained over a 4-day span during a 4-hour period each day that extends from midmorning through noon. During this time period the circadian level of corticosterone is on the rise. The temporary housing environment in which the animals are maintained while "protected" is not "quiet." Further, the time from prior handling to bleeding cannot be kept to a constant for all animals. However, every effort is made while retrieving the animal from this common environment to maintain uniform and nonagitated conditions. The accepted practice of obtaining the blood sample within 3 minutes of retrieving the animal is employed.

Therefore, given the constraints imposed by the SPF environment and housing conditions, the levels of corticosterone obtained from this population might best be characterized as coming from animals that are in various stages ranging from resting (not "basal" or "quiescent") to semiactive and will be marked by a high degree of variance.

120

However, despite these many qualifications to the data here presented, the values so far obtained are in the range that, with respect to the literature, they are    considered within the bounds of basal or resting levels.

Corticosterone data has been analyzed for all samples taken at the 6-, 18 ,and 30-week postexposure periods. In addition, samples from a common pooled control serum have been submitted with each analysis for independent quality control comparisons on the assay technique.

The basic data have been presented in bar-graph form in Figure 6 as the mean plus/minus the standard error. This graphing format is employed as it does not make any assumptions about the levels of the mean values between the 12-week sampling intervals. A scale was purposely chosen that visually tempers the mean differences between groups.

In addition, two presentations are tentatively offered. The left-hand graph includes all data values obtained for the subjects in each condition. The right-hand graph depicts a subset of the data that was presumed, at least initially, to provide a truer representation of the data. During any particular bleeding session extraordinary measures were required to obtain the required blood volume from certain animals. This may have entailed repeated anesthetization, multiple entries into the orbital sinus, resuscitation, or suturing torn eyelids. Based on these subjective assessments of what "obviously" must have been traumatic, a list was

121

independently compiled of these animals and their data was eliminated from the initial analysis. It is this subset that is presented in the right-hand presentation.

It is now clear that the data cannot reliably be edited by this method. While the elimination of data based on these behavioral observations does in general lead to a lowering of the overall corticosterone levels by discarding extremely high and presumably "stressed" animals, it does so on a totally unreliable basis. Some of the lowest assayed values obtained were samples from "obviously" stressed animals, and some of the highest values actually obtained were not eliminated by these observations. In one instance this technique actually raised the mean value slightly. Therefore, until some alternative method can be found, the left-hand presentation that includes all data values will be employed as the preferred method of data presentation.

Inspection of Figure 6, therefore, suggests that while differences exist between conditions, no dramatic effects are active since neither group has consistently higher values than the other.

The control serum data is presented graphically in Figure 7. A truncated scale was used justifiably since these measures are based on repeated analysis of a common serum pool with uniform characteristics. This pooled serum was obtained following termination of group housed animals and exsanguination within the 3-minute time limit guideline. These data indicate that corticosterone values can be very

122

accurately determined by the procedures employed (within 1-2 units of measure), given that the samples do not exhibit the variance associated with an actual study. On this expanded scale, there is some suggestion that the overall analysis of the second (or 18-week) samples were significantly lower than the first or third sample.

If the experimental values and the control values are placed into perspective (as in Figure 8) using an expanded scale reflective of the actual data range observed, any minor differences become less obvious and considerably less meaningful. This figure contains on the left margin an indication of the actual range of values obtained during this study, and on the right margin those values that would, in the literature, be classified within the "normal" ranges of basal and stress levels.

In Figure 9 a different graph technique is applied to the data of Figure 6. This graphing format implies that a continuous physiological process is active and makes assumptions about the intervening periods between sampling sessions. Presentation in this format raises the speculation that while the basal level of corticosterone is slowly rising in the sham-exposed population, it is at least static in the exposed population.

It might have been expected that both groups would, in time, show a rise in basal levels in accordance with what has come to be known as the "isolation stress syndrome." Basically, this is the observation that in chronic individually housed rats, basal corticosterone levels

123

rise gradually with the length of isolation. It had been assumed from our previous work that this phenomenon did not occur when using this type of waveguide maintenance and daily handling schedule.

However, the current study has confined these rats in this individual environment for 9 months. This is much longer than any previously known study in which corticosterone was an active endpoint. A process that may not have been apparent during a relatively short 3-month study now may be distinguishable.

Admittedly, the latter form of graphic presentation implies a function that may not, in fact, exist. However, the possibility that such an effect might be substantiated with additional sampling, forces the continued inclusion of corticosterone value as an endpoint for at least the next two sampling periods to see if the initial trend persists or is merely a random fluctuation of minimal data availability.

## Histopathology

Complete examination of tissues collected from all experimental rats that have died has been made. No significant microwave-induced lesions have been found in any of the spontaneous and anesthetic-induced deaths during the first 9 months of exposure.   Table 4

124

summarizes the cause of death in the experimental animals that have died, and Table 5 summarizes all of the histopathological lesions present in both the control and exposed animals.

Anesthetic-related complications have resulted in the deaths of three exposed and four control rats, for a total of seven rats. Two exposed and two control rats have died of renal failure as a result of chronic nephropathy. Chronic nephropathy is a common degenerative condition in the rat whose lesions are so characteristic that those working with rats readily recognize it. The mild or early lesion is comprised of dilated collecting tubules that contain protein casts with or without infiltrating interstitial lymphocytes. The tubular epithelium is flattened and often exfoliates into the ectatic lumens. The developing lesions result in a wedge-shaped area of atrophy, fibrosis, and reactive cell infiltration which gives the kidney the gross appearance of a pitted surface. Chronic nephropathy increases in severity with age and obesity in most rat strains, and these renal lesions are accentuated by high protein diets.

One control rat died of complications secondary to the development of atrial thrombosis, and one control rat died following puncturing of the nasal sinus during bleeding which led to the inhalation of blood and asphyxiation. Three control rats have died with lesions that, when considered alone, are not sufficient to provide a definitive cause of death at this time. Additional studies on these three rats are being done.

Immunology

Preliminary results of the rat immunological experiments have been informative. The mitogen assay techniques, following only minor changes in cell and reagent concentration, produce acceptable results. The "T" and "B" cell enumeration, since it must be performed on the same day as the other tests, will be more easily and accurately performed using direct immunofluorescence. Tests for plaque-forming cells (PFC) can involve the use of two different antigens: DNP, to induct antibody production by "B" cells without the presence of "T" cells ("T" independent antigen); and sheep red blood cells (SRBC), which induce antibody production by "B" cells in the presence of "T" cells ("T" dependent antigen).

When the animals are tested during the interim sacrifice, the spleens will be removed and a suspension of spleen cells will be used to test (on the same day) for "T" and "B" cell numbers, response to mitogen stimulation; enumeration of complement receptor positive (CR+) cells and FC receptor cells and plaque-forming cells. In order to test for plaque-forming cells, the antigens must be injected 7 days prior to sacrifice. The full effect (if any) of prior introduction of antigen on the "normal" responses of cells to the other tests is under study. Preliminary tests have indicated that both the DNP and SRBC antigens injected into the same animal produce a significantly higher response than either antigen introduces alone, and the responses cannot be distinguished even when the doses are varied. The SRBC antigen response indicates involvement of two lymphocytic

126

cell types (which can be further enumerated in the mitogen and "T" and "B" cell assays) rather than only one cell type as found in the DNP assay.

The SRBC antigen response requires a functioning reticuloendothelial cell (RE cell) system and therefore serves as a method of screening for normal functioning of this system. The use of colloidal carbon clearance and an isotopically labeled liquid emulsion were considered as a specific method of RE cell evaluation; however, they were discounted, and the indirect screening of the RE cell system by the SRBC antigen response will be employed. The colloidal carbon impairs the functioning of the RE cells affecting the SRBC plaque assay, and the isotopically labeled liquid emulsion test creates handling problems during the interim sacrifice necropsies and may affect the mitogen responses conducted on the same animals.

## Open-field Behavioral Assessments

The data from four open-field activity assessments covering the first 6 months of exposure has now been reduced and a summary is presented in Table 6. It can be seen that no significant differences exist between the exposed or sham-exposed conditions on either measure of horizontal or vertical activity.

The value of open-field assessments is to gauge the reaction of a population to a novel environment and the levels of fear or apprehension it may arouse. The increased variance in the data

127

following the first session is taken to be indicative of the bipolar response of the animals following repeated exposure to a non-novel environment, indicative of either bored (inactive) acceptance or active exploration.

This measure might be decreased in frequency to retain some degree of novelty. Alternatively, the open-field environment itself could actively be made novel with each test session through inclusion of novel objects or Plexiglas barriers that can be rearranged. Possibly, a combination of reduced frequency of measurement and introduction of environmental stimuli should be employed.

## III. SUMMARY AND CONCLUSIONS

The primary objective of this project is to maintain a colony of microwave-exposed rats in a disease-free state from infancy through adolescence and maturity to reach old age. The successful progress of this endeavor encompasses in-depth preparation beginning nearly three years ago with an initial 3-month period to conduct the groundwork of research prior to submission of the work proposal. The first 18-month phase of the contract was spent in acquiring and integrating all the various engineering hardware required to complete the exposure facility, training laboratory personnel, perfecting chemistry techniques, and debugging the daily procedure. Nearly one year ago the weanling SPF rats arrived from the supplier to begin their 30-month participation in this project.

The first 11 months of the current phase of the project can be considered a success; the animals have been maintained in a specific pathogen-free state, and the collection of baseline data from the selected biological parameters has complied with quality control standards.

All efforts to date have merely brought us to the most critical, remaining portion of the project. It is during the later phases of these animals' maturity that the neoplastic and age-associated lesions and metabolic changes will be documented in an effort to detect any differences between the exposed and control populations with respect to age of onset, frequency of occurrence, and severity.

The preliminary data available at this time fails to reveal any gross clinically significant differences between these populations. Subtle differences that may be gleaned from the data may disappear or be accentuated as additional data is obtained, refined, and statistically analyzed.

CHRONIC RFR BIOEFFECTS　　　　　　　　　　CHEMISTRY RUN :　　**** 7 ****
BLOOD CHEMISTRY - DESCRIPTIVE STATISTICS　　TEST PARAMETER:　　(1)  GLUCOSE

PREPARED BY : JOHNSON　　DATE: 6/17/81　　　　PREP COMMENT :　　PRELIMINARY

#### **** ALCOVE SUMMARY ****

| ALC | GRP | DED | QNS | MIS | NBD | DATA | MIN | MAX | SUMX | SUM SQ | MEAN | SD | SE | CV |
|-----|-----|-----|-----|-----|-----|------|-----|-----|------|--------|------|-----|-----|-----|
| A | E | 0 | 0 | 0 | 0 | 10 | 126.0 | 200.0 | 1449.0 | 214775 | 144.9 | 21.9 | 6.9 | 15.1 |
|   | S | 0 | 0 | 0 | 0 | 10 | 125.0 | 176.0 | 1504.0 | 228640 | 150.4 | 15.6 | 4.9 | 10.4 |
| B | E | 0 | 0 | 0 | 0 | 10 | 119.0 | 171.0 | 1367.0 | 188911 | 136.7 | 14.3 | 4.5 | 10.5 |
|   | S | 1 | 0 | 0 | 1 | 8 | 128.0 | 158.0 | 1119.0 | 157211 | 139.9 | 9.3 | 3.3 | 6.6 |
| C | E | 1 | 0 | 0 | 0 | 9 | 127.0 | 148.0 | 1232.0 | 169054 | 136.9 | 6.7 | 2.2 | 4.9 |
|   | S | 0 | 0 | 0 | 0 | 10 | 126.0 | 163.0 | 1398.5 | 196403 | 139.9 | 9.1 | 2.9 | 6.5 |
| D | E | 0 | 1 | 0 | 3 | 6 | 99.0 | 157.0 | 828.0 | 116494 | 138.0 | 19.3 | 7.9 | 14.0 |
|   | S | 0 | 1 | 1 | 0 | 8 | 123.0 | 201.0 | 1200.0 | 185996 | 150.0 | 27.4 | 9.7 | 18.3 |
| E | E | 1 | 0 | 0 | 0 | 9 | 118.0 | 150.0 | 1157.0 | 149813 | 128.6 | 10.9 | 3.6 | 8.5 |
|   | S | 1 | 0 | 0 | 0 | 9 | 131.0 | 231.0 | 1384.0 | 221056 | 153.8 | 30.2 | 10.1 | 19.7 |
| F | E | 1 | 0 | 0 | 0 | 9 | 104.0 | 163.0 | 1148.0 | 148892 | 127.6 | 16.5 | 5.5 | 13.0 |
|   | S | 1 | 0 | 0 | 0 | 9 | 116.0 | 151.0 | 1208.5 | 163029 | 134.3 | 9.2 | 3.1 | 6.8 |
| G | E | 0 | 0 | 0 | 0 | 10 | 112.0 | 289.0 | 1511.0 | 250309 | 151.1 | 46.9 | 14.8 | 31.0 |
|   | S | 2 | 0 | 0 | 0 | 8 | 99.0 | 151.0 | 1084.0 | 149404 | 135.5 | 17.8 | 6.3 | 13.1 |
| H | E | 0 | 0 | 0 | 0 | 10 | 111.0 | 188.0 | 1364.0 | 191356 | 136.4 | 23.0 | 7.3 | 16.9 |
|   | S | 1 | 0 | 0 | 0 | 9 | 117.0 | 136.0 | 1159.0 | 149509 | 128.8 | 5.3 | 1.8 | 4.1 |
| I | E | 1 | 0 | 0 | 0 | 9 | 135.0 | 160.0 | 1316.5 | 193198 | 146.3 | 8.3 | 2.8 | 5.7 |
|   | S | 0 | 0 | 1 | 0 | 9 | 113.0 | 153.0 | 1268.0 | 180096 | 140.9 | 12.7 | 4.2 | 9.0 |
| J | E | 0 | 1 | 0 | 0 | 9 | 129.0 | 166.0 | 1264.5 | 178674 | 140.5 | 10.6 | 3.5 | 7.5 |
|   | S | 2 | 0 | 0 | 0 | 8 | 130.0 | 300.0 | 1278.0 | 227222 | 159.8 | 53.7 | 19.0 | 33.6 |

#### **** ROOM SUMMARY ****

| GRP | DED | QNS | MIS | NBD | DATA | MIN | MAX | SUMX | SUM SQ | MEAN | SD | SE | CV |
|-----|-----|-----|-----|-----|------|-----|-----|------|--------|------|-----|-----|-----|
| E | 2 | 1 | 0 | 3 | 44 | 99.0 | 200.0 | 6033.0 | 839047 | 137.1 | 16.4 | 2.5 | 12.0 |
| S | 2 | 1 | 1 | 1 | 45 | 123.0 | 231.0 | 6605.5 | 989306 | 146.8 | 20.9 | 3.1 | 14.3 |
| E | 2 | 1 | 0 | 0 | 47 | 104.0 | 289.0 | 6604.0 | 962430 | 140.5 | 27.1 | 4.0 | 19.3 |
| S | 6 | 0 | 1 | 0 | 43 | 99.0 | 300.0 | 5997.5 | 869260 | 139.5 | 27.6 | 4.2 | 19.8 |

#### **** GRAND SUMMARY ****

| GRP | DED | QNS | MIS | NBD | DATA | MIN | MAX | SUMX | SUM SQ | MEAN | SD | SE | CV |
|-----|-----|-----|-----|-----|------|-----|-----|------|--------|------|-----|-----|-----|
| E | 4 | 2 | 0 | 3 | 91 | 99.0 | 289.0 | 12637.0 | 1801480 | 138.9 | 22.6 | 2.4 | 16.3 |
| S | 8 | 1 | 2 | 1 | 88 | 99.0 | 300.0 | 12603.0 | 1858570 | 143.2 | 24.7 | 2.6 | 17.2 |

PREPARED BY : JOHNSON     DATE: 6/17/81          PREP COMMENT :     PRELIMINARY

#### **** ALCOVE SUMMARY ****

| ALC | GRP | DED | QNS | MIS | NBD | DATA | MIN | MAX | SUMX | SUM SQ | MEAN | SD | SE | CV |
|-----|-----|-----|-----|-----|-----|------|------|------|-------|--------|------|-----|-----|------|
| A | E | 0 | 0 | 0 | 0 | 10 | 16.0 | 25.0 | 184.0 | 3448 | 18.4 | 2.5 | 0.8 | 13.6 |
|   | S | 0 | 0 | 0 | 0 | 10 | 17.0 | 22.0 | 193.0 | 3747 | 19.3 | 1.5 | 0.5 | 7.7 |
| B | E | 0 | 0 | 0 | 0 | 10 | 16.0 | 24.0 | 194.0 | 3818 | 19.4 | 2.3 | 0.7 | 12.0 |
|   | S | 1 | 0 | 0 | 1 | 8 | 17.0 | 23.0 | 157.0 | 3119 | 19.6 | 2.2 | 0.8 | 11.1 |
| C | E | 1 | 0 | 0 | 0 | 9 | 18.0 | 21.0 | 177.0 | 3487 | 19.7 | 0.8 | 0.3 | 4.2 |
|   | S | 0 | 0 | 0 | 0 | 10 | 18.0 | 21.0 | 194.0 | 3776 | 19.4 | 1.1 | 0.4 | 5.7 |
| D | E | 0 | 1 | 0 | 3 | 6 | 19.5 | 24.0 | 124.5 | 2597 | 20.8 | 1.5 | 0.6 | 7.3 |
|   | S | 0 | 1 | 1 | 0 | 8 | 18.0 | 22.0 | 165.0 | 3419 | 20.6 | 1.4 | 0.5 | 6.8 |
| E | E | 1 | 0 | 0 | 0 | 9 | 18.0 | 23.0 | 175.0 | 3423 | 19.4 | 1.5 | 0.5 | 7.7 |
|   | S | 1 | 0 | 0 | 0 | 9 | 18.0 | 21.0 | 174.0 | 3378 | 19.3 | 1.2 | 0.4 | 6.5 |
| F | E | 1 | 0 | 0 | 0 | 9 | 16.0 | 20.0 | 163.0 | 2967 | 18.1 | 1.3 | 0.4 | 7.1 |
|   | S | 1 | 0 | 0 | 0 | 9 | 18.0 | 23.0 | 174.0 | 3388 | 19.3 | 1.6 | 0.5 | 8.4 |
| G | E | 0 | 0 | 0 | 0 | 10 | 16.0 | 22.0 | 190.0 | 3636 | 19.0 | 1.6 | 0.5 | 8.5 |
|   | S | 2 | 0 | 0 | 0 | 8 | 17.0 | 40.0 | 175.0 | 4217 | 21.9 | 7.0 | 2.5 | 31.9 |
| H | E | 0 | 0 | 0 | 0 | 10 | 17.0 | 21.0 | 192.0 | 3704 | 19.2 | 1.3 | 0.4 | 6.9 |
|   | S | 1 | 0 | 0 | 0 | 9 | 18.0 | 24.0 | 178.5 | 3563 | 19.8 | 1.6 | 0.5 | 8.1 |
| I | E | 1 | 0 | 0 | 0 | 9 | 16.5 | 27.0 | 186.5 | 3954 | 20.7 | 3.2 | 1.1 | 15.2 |
|   | S | 0 | 0 | 1 | 0 | 9 | 18.0 | 22.0 | 181.0 | 3653 | 20.1 | 1.2 | 0.4 | 6.0 |
| J | E | 0 | 1 | 0 | 0 | 9 | 18.0 | 21.0 | 169.5 | 3202 | 18.8 | 1.1 | 0.4 | 5.6 |
|   | S | 2 | 0 | 0 | 0 | 8 | 18.0 | 22.0 | 160.0 | 3220 | 20.0 | 1.6 | 0.6 | 7.9 |

#### **** ROOM SUMMARY ****

| GRP | DED | QNS | MIS | NBD | DATA | MIN | MAX | SUMX | SUM SQ | MEAN | SD | SE | CV |
|-----|-----|-----|-----|-----|------|------|------|-------|--------|------|-----|-----|------|
| E | 2 | 1 | 0 | 3 | 44 | 16.0 | 25.0 | 854.5 | 16773 | 19.4 | 2.0 | 0.3 | 10.4 |
| S | 2 | 1 | 1 | 1 | 45 | 17.0 | 23.0 | 883.0 | 17439 | 19.6 | 1.6 | 0.2 | 8.1 |
| E | 2 | 1 | 0 | 0 | 47 | 16.0 | 27.0 | 901.0 | 17464 | 19.2 | 2.0 | 0.3 | 10.5 |
| S | 6 | 0 | 1 | 0 | 43 | 17.0 | 40.0 | 868.5 | 18041 | 20.2 | 3.4 | 0.5 | 16.9 |

#### **** GRAND SUMMARY ****

| GRP | DED | QNS | MIS | NBD | DATA | MIN | MAX | SUMX | SUM SQ | MEAN | SD | SE | CV |
|-----|-----|-----|-----|-----|------|------|------|--------|--------|------|-----|-----|------|
| E | 4 | 2 | 0 | 3 | 91 | 16.0 | 27.0 | 1755.5 | 34237 | 19.3 | 2.0 | 0.2 | 10.5 |
| S | 8 | 1 | 2 | 1 | 88 | 17.0 | 40.0 | 1751.5 | 35480 | 19.9 | 2.7 | 0.3 | 13.3 |

CHRONIC RFR BIOEFFECTS          CHEMISTRY RUN :    **** 7 ****
BLOOD CHEMISTRY - DESCRIPTIVE STATISTICS     TEST PARAMETER:    (14) CALCIUM

PREPARED BY  : JOHNSON     DATE: 6/17/81        PREP COMMENT  :    PRELIMINARY

#### **** ALCOVE SUMMARY ****

| ALC | GRP | DED | QNS | MIS | NBD | DATA | MIN | MAX | SUMX | SUM SQ | MEAN | SD | SE | CV |
|-----|-----|-----|-----|-----|-----|------|-----|-----|------|--------|------|-----|-----|-----|
| A | E | 0 | 0 | 0 | 0 | 10 | 9.90 | 10.70 | 101.6 | 1033 | 10.16 | 0.25 | 0.08 | 2.4 |
|   | S | 0 | 0 | 0 | 0 | 10 | 9.75 | 10.60 | 102.9 | 1058 | 10.29 | 0.26 | 0.08 | 2.5 |
| B | E | 0 | 0 | 0 | 0 | 10 | 9.90 | 10.50 | 101.6 | 1033 | 10.16 | 0.20 | 0.06 | 2.0 |
|   | S | 1 | 0 | 0 | 1 | 8 | 9.90 | 10.40 | 81.8 | 837 | 10.23 | 0.16 | 0.06 | 1.5 |
| C | E | 1 | 0 | 0 | 0 | 9 | 9.70 | 10.50 | 90.8 | 917 | 10.09 | 0.26 | 0.09 | 2.6 |
|   | S | 0 | 0 | 0 | 0 | 10 | 9.80 | 10.50 | 100.4 | 1008 | 10.04 | 0.21 | 0.07 | 2.1 |
| D | E | 0 | 1 | 0 | 3 | 6 | 10.10 | 10.60 | 62.0 | 641 | 10.33 | 0.18 | 0.07 | 1.7 |
|   | S | 0 | 1 | 1 | 0 | 8 | 10.00 | 10.80 | 82.5 | 851 | 10.31 | 0.24 | 0.08 | 2.3 |
| E | E | 1 | 0 | 0 | 0 | 9 | 9.30 | 10.40 | 87.7 | 855 | 9.74 | 0.30 | 0.10 | 3.1 |
|   | S | 1 | 0 | 0 | 0 | 9 | 9.30 | 10.60 | 88.7 | 875 | 9.86 | 0.36 | 0.12 | 3.7 |
| F | E | 1 | 0 | 0 | 0 | 9 | 9.40 | 10.50 | 90.4 | 909 | 10.04 | 0.32 | 0.11 | 3.2 |
|   | S | 1 | 0 | 0 | 0 | 9 | 9.45 | 10.20 | 88.8 | 876 | 9.86 | 0.28 | 0.09 | 2.8 |
| G | E | 0 | 0 | 0 | 0 | 10 | 9.80 | 11.20 | 101.7 | 1036 | 10.17 | 0.40 | 0.13 | 3.9 |
|   | S | 2 | 0 | 0 | 0 | 8 | 9.60 | 10.60 | 80.8 | 817 | 10.10 | 0.27 | 0.10 | 2.7 |
| H | E | 0 | 0 | 0 | 0 | 10 | 9.80 | 11.10 | 102.6 | 1053 | 10.26 | 0.35 | 0.11 | 3.4 |
|   | S | 1 | 0 | 0 | 0 | 9 | 9.80 | 10.20 | 90.5 | 910 | 10.06 | 0.17 | 0.06 | 1.7 |
| I | E | 1 | 0 | 0 | 0 | 9 | 9.80 | 10.80 | 91.2 | 925 | 10.13 | 0.34 | 0.11 | 3.3 |
|   | S | 0 | 0 | 1 | 0 | 9 | 9.60 | 10.40 | 90.7 | 915 | 10.08 | 0.23 | 0.08 | 2.3 |
| J | E | 0 | 1 | 0 | 0 | 9 | 9.40 | 10.40 | 90.1 | 902 | 10.01 | 0.31 | 0.10 | 3.1 |
|   | S | 2 | 0 | 0 | 0 | 8 | 9.90 | 11.20 | 82.8 | 858 | 10.35 | 0.40 | 0.14 | 3.9 |

#### **** ROOM SUMMARY ****

| GRP | DED | QNS | MIS | NBD | DATA | MIN | MAX | SUMX | SUM SQ | MEAN | SD | SE | CV |
|-----|-----|-----|-----|-----|------|-----|-----|------|--------|------|-----|-----|-----|
| E | 2 | 1 | 0 | 3 | 44 | 9.30 | 10.70 | 443.7 | 4478 | 10.08 | 0.31 | 0.05 | 3.0 |
| S | 2 | 1 | 1 | 1 | 45 | 9.30 | 10.80 | 456.3 | 4630 | 10.14 | 0.31 | 0.05 | 3.0 |
| E | 2 | 1 | 0 | 0 | 47 | 9.40 | 11.20 | 475.9 | 4825 | 10.13 | 0.36 | 0.05 | 3.5 |
| S | 6 | 0 | 1 | 0 | 43 | 9.45 | 11.20 | 433.6 | 4376 | 10.08 | 0.32 | 0.05 | 3.2 |

#### **** GRAND SUMMARY ****

| GRP | DED | QNS | MIS | NBD | DATA | MIN | MAX | SUMX | SUM SQ | MEAN | SD | SE | CV |
|-----|-----|-----|-----|-----|------|-----|-----|------|--------|------|-----|-----|-----|
| E | 4 | 2 | 0 | 3 | 91 | 9.30 | 11.20 | 919.6 | 9303 | 10.11 | 0.34 | 0.04 | 3.3 |
| S | 8 | 1 | 2 | 1 | 88 | 9.30 | 11.20 | 889.8 | 9006 | 10.11 | 0.31 | 0.03 | 3.1 |

132

NTROL COMPARISON
GLUCOSE

| | | lution | Min. | Max. | Mean | $S_E$ | CV |
|---|---|---|---|---|---|---|---|
| | | 1:1 | 214 | 240 | 220.5 | 1.4 | 2.9 |
| | ... | --- | 212 | 222 | 215.5 | .5 | 1.1 |
| o | DC | 1:1 | 208 | 222 | 215.6 | .8 | 1.7 |
| | UDC | --- | 214 | 218 | 216.3 | .3 | .6 |
| 5 | DC | 2:1 | 208 | 219 | 213.2 | .5 | 1.1 |
| | UDC | --- | 191 | 229 | 209.8 | 1.5 | 3.0 |
| 4 | DC | 2:1 | 202 | 219 | 209.3 | .7 | 1.6 |
| | UDC | --- | 204 | 210 | 207.9 | .4 | 1.0 |
| 3 | DC | 2:1 | 190 | 214 | 209.4 | 1.1 | 2.4 |
| | UDC | --- | 204 | 218 | 209.6 | .7 | 1.5 |
| 2 | DC | 1:1 | 206 | 212 | 208.7 | .4 | .7 |
| | UDC | --- | 206 | 210 | 207.9 | .2 | .5 |
| 1 | DC | 1:2 | 204 | 219 | 214.1 | 1.2 | 2.2 |
| | UDC | --- | 206 | 213 | 209.9 | .4 | .9 |

133

Table 2. BLOOD CHEMISTRY PARAMETER SUMMARY - PRELIMINARY
BLEEDING SESSION #6, March 30 - April 2, 1981

| PARAMETER | EXPOSED | | SHAM | |
|---|---|---|---|---|
| | MEAN | $S_D$ | MEAN | $S_D$ |
| Glucose | 144.4 | 13.5 | 150.0 | 18.7 |
| BUN | 19.4 | 1.8 | 19.7 | 3.2 |
| Creatinine | 0.58 | 0.24 | 0.57 | 0.23 |
| $Na^+$ | 144.2 | 6.1 | 143.6 | 3.3 |
| $K^+$ | 4.90 | 0.35 | 4.95 | 0.40 |
| $Cl^-$ | 95.6 | 13.5 | 98.3 | 8.2 |
| $CO_2$ | 23.4 | 5.0 | 23.9 | 3.4 |
| Uric Acid | 0.95 | 0.23 | 1.06 | 0.63 |
| T. Bilirubin | 0.13 | 0.05 | 0.15 | 0.04 |
| D. Bilirubin | 0.04 | 0.07 | 0.03 | 0.06 |
| Electrolyte Bal. | 7.62 | 11.78 | 5.88 | 7.46 |
| Ionized Calcium | 5.87 | 0.58 | 5.78 | 0.28 |
| $T_4$ | 4.70 | 0.85 | 4.70 | 0.67 |
| Calcium | 9.98 | 0.40 | 10.03 | 0.25 |
| Phosphorus | 5.35 | 0.42 | 5.30 | 0.40 |
| Alk. Phosphatase | 212.9 | 43.1 | 205.8 | 31.7 |
| LDH | 329.9 | 148.7 | 319.3 | 145.1 |
| SGOT | 106.5 | 77.2 | 94.5 | 29.0 |
| SGPT | 57.5 | 76.0 | 57.8 | 78.3 |
| Cholesterol | 80.0 | 22.3 | 78.9 | 16.1 |
| Triglycerides | 113.8 | 45.0 | 113.3 | 34.7 |
| Total Protein | 6.1 | 0.3 | 6.2 | 0.3 |
| Albumin | 3.47 | 17.0 | 3.47 | 0.15 |
| Globulin | 2.67 | 0.25 | 2.71 | 0.21 |
| A/G Ratio | 2.36 | 1.77 | 2.03 | 0.78 |

Table 3.   BLOOD CHEMISTRY PARAMETER SUMMARY - PRELIMINARY
           BLEEDING SESSION #7, May 13 - 15, 1981

| PARAMETER | EXPOSED MEAN | $S_D$ | SHAM MEAN | $S_D$ |
|---|---|---|---|---|
| Glucose | 138.9 | 22.6 | 142.7 | 25.3 |
| BUN | 19.3 | 2.0 | 19.8 | 2.7 |
| Creatinine | 0.56 | 0.11 | 0.56 | 0.10 |
| $Na^+$ | 143.3 | 15.3 | 144.3 | 5.5 |
| $K^+$ | 5.44 | 14.4 | 4.89 | 0.33 |
| $Cl^-$ | 99.1 | 11.2 | 99.9 | 5.0 |
| $CO_2$ | 26.3 | 8.8 | 25.5 | 3.1 |
| Uric Acid | 1.32 | 2.68 | 1.03 | 0.54 |
| T. Bilirubin | 0.11 | 0.08 | 0.09 | 0.03 |
| D. Bilirubin | 0.03 | 0.05 | 0.03 | 0.05 |
| Electrolyte Bal. | 7.42 | 4.66 | 7.46 | 2.78 |
| Ionized Calcium | 5.10 | 0.69 | 5.03 | 0.59 |
| $T_4$ | NA | NA | NA | NA |
| Calcium | 10.11 | 0.34 | 10.07 | 0.45 |
| Phosphorus | 5.19 | 0.42 | 5.07 | 0.48 |
| Alk. Phosphatase | 196.9 | 37.6 | 197.4 | 34.9 |
| LDH | 308.9 | 152.6 | 296.7 | 132.6 |
| SGOT | 96.8 | 34.6 | 97.0 | 45.3 |
| SGPT | 57.7 | 26.5 | 58.5 | 32.2 |
| Cholesterol | 89.1 | 25.8 | 86.8 | 20.9 |
| Triglycerides | 117.7 | 52.1 | 119.7 | 42.0 |
| Total Protein | 6.1 | 0.2 | 6.1 | 0.3 |
| Albumin | 3.16 | 0.16 | 3.17 | 0.20 |
| Globulin | 2.98 | 0.19 | 2.93 | 0.19 |
| A/G Ratio | 1.25 | 0.60 | 1.24 | 0.52 |

Table 4.   CAUSES OF ANIMAL DEATHS

| Cause of Death | Exposed | Animals Control | Total |
|---|---|---|---|
| (1) Anesthetic Death | (3) C14,E1,H16 | (4) F18,J9,G9,D17 | 7 |
| (2) Renal Failure | (2) 17,F5 | (2) G8,B3 | 4 |
| (3) Undetermined | | (3) H20,E9,I18 | 3 |
| (4) Atrial Thrombosis | | (1) J12 | 1 |
| (5) Asphyxia secondary to blood inhalation | | (1) B13 | 1 |

Table 5.    SUMMARY OF HISTOPATHOLOGICAL LESIONS.

| Organ and Lesions | Animals Exposed | Control | Total |
|---|---|---|---|
| **Lung:** | | | |
| Acute blood inhalation-marked | | (1)-B13 | 1 |
| Acute hypostatic congestion-marked | | (1)-I18 | 1 |
| Acute hypostatic congestion-moderate | (1)-H16 | | 1 |
| Pulmonary congestion and edema-moderate | (1)-C14 | (3)-F18, E9,D17 | 4 |
| Pulmonary congestion and edema-mild | (1)-17 | | 1 |
| Pulmonary congestion and edema-marked | | (3)-J9,H20, J12 | 3 |
| Acute multifocal pulmonary petectal hemorrage-mild | (2)-G9,E9 | | 2 |
| Acute multifocal pulmonary petectal hemorrage-minimal | (1)-H16 | | 1 |
| Pulmonary arteriolar tunica media hyperplasia-moderate | | (1)-E9 | 1 |
| Pulmonary arteriolar tunica media hyperplasia-marked | | (1)-J12 | 1 |
| **Deep lacrimal gland:** | | | |
| Lacrimal gland megalocytosis-minimal | (2)-C4,J9 | | 2 |
| Lacrimal gland megalocytosis-mild | (2)-E1,F5 | (1)-G9 | 3 |
| Lacrimal gland megalocytosis-marked | | (3)-G8,H20, J12 | 3 |
| Lacrimal gland megalocytosis-moderate | (1)-H16 | (1)-E9 | 2 |
| Subacute nonsuppurative lacrimal gland adenitis-moderate | (1)-H16 | | 1 |
| **Prostate:** | | | |
| Chronic multifocal nonsuppurative prostatitis-moderate | (1)-C14 | | 1 |
| Chronic multifocal nonsuppurative prostatitis-mild | | (2)-B13,D17 | 2 |
| Prostatic intraluminal mineralization-moderate | | (2)-B13,D17 | 2 |
| Prostatic intraluminal mineralization-minimal | (1)-H16 | | 1 |
| **Pancreas:** | | | |
| Focal pancreatic ductal fibrosis-minimal | (1)-E1 | (1)-J12 | 2 |
| **Parathyroids:** | | | |
| Parathyroid hyperplasia-marked | | (1)-G9 | 1 |
| Parathyroid hyperplasia-moderate | (1)-17 | | 1 |
| Parathyroid hyperplasia-minimal | | (1)-D17 | 1 |

Table 5. (Continued)

Trachea:
| | | | |
|---|---|---|---|
| Tracheal submucosal glandular ectasia-minimal | (1)-H16 | (1)-G8 | 2 |
| Tracheobronchial lymphnode hemorrhage-mild | (1)-I7 | | 1 |

Heart:
| | | | |
|---|---|---|---|
| Chronic cardiomyopathy-minimal | | (3)-G8,B3, J12 | 3 |
| Chronic cardiomyopathy-moderate | (2)-I7,F5 | | 2 |
| Atrial mural nonsuppurative thrombosis-marked | | (1)-J12 | 1 |

Kidney:
| | | | |
|---|---|---|---|
| Chronic nephropathy-mild | | (2)-J12,I18 | 2 |
| Chronic nephropathy-marked | (2)-I7,F5 | (2)-G8,B3 | 4 |
| Chronic nephropathy-minimal | (1)-H16 | (4)-G9,E9, B13,D17 | 5 |
| Unilateral embryonal nephroma | | (1)-H20 | 1 |

Urinary Bladder:
| | | | |
|---|---|---|---|
| Urinary bladder squamous metaplasia-marked | | (1)-G8 | 1 |

Stomach:
| | | | |
|---|---|---|---|
| Subacute gastritis-moderate | | (1)-J12 | 1 |
| Subacute gastritis-mild | | (1)-E9 | 1 |
| Gastric glandular ectasia-minimal | | (1)-B3 | 1 |
| Gastric mucosal mineralization-mild | (1)-F5 | | 1 |
| Gastric squamous mucosal hyperkeratosis-moderate | | (2)-E9,J12 | 2 |
| Gastric mucosal fibrinoid arteritis-moderate | | (1)-J12 | 1 |

Aorta:
| | | | |
|---|---|---|---|
| Aorta tunica media mineralization-mild | (1)-I7 | | 1 |

Harderian Gland:
| | | | |
|---|---|---|---|
| Focal cystic ductal ectasia-marked | (1)-H16 | | 1 |
| Harderian gland hyperpigmentation (porphyrin)-moderate | (1)-I7 | | 1 |
| Harderian gland hyperpigmentation (porphyrin)-minimal | | (2)-H20,D17 | 2 |
| Harderian gland hyperpigmentation (porphyrin)-mild | | (1)-B13 | 1 |

Cervical Lymph Node:
| | | | |
|---|---|---|---|
| Lymph node plasma cell hyperplasia-moderate | (1)-I7 | | 1 |
| Acute lymph node hemorrhage-marked | | (2)-J9,J12 | 2 |
| Lymph node lymphoid hyperplasia-marked | | (1)-H20 | 1 |
| Lymph node lymphoid hyperplasia-mild | | (1)-G9 | 1 |
| Lymph node lymphoid hyperplasia-moderate | | (1)-I18 | 1 |

138

Table 5. (Continued)

Spleen:
| | | | |
|---|---|---|---|
| Splenic hemosiderosis-moderate | | (1)-H20 | 1 |
| Splenic hemosiderosis-mild | | (2)-B13,D17 | 2 |

Eye:
| | | | |
|---|---|---|---|
| Acute intraocular hemorrhage-mild | (1)-F5 | | 1 |

Liver:
| | | | |
|---|---|---|---|
| Hepatic congestion-moderate | (1)-H16 | (1)-E9 | 2 |

Thymus:
| | | | |
|---|---|---|---|
| Acute thymic petechial hemorrhages-<br>  minimal | | (1)-E9 | 1 |

Thyroid:
| | | | |
|---|---|---|---|
| Thyroid atrophy-moderate | (1)-H16 | (1)-D17 | 2 |

## Table 6.   ACTIVITY MONITOR DATA

| | HORIZONTAL | | | | VERTICAL | | | |
| | Exposed | | Sham | | Exposed | | Sham | |
| | $\overline{X}$ | $S_E$ | $\overline{X}$ | SE | $\overline{X}$ | $S_E$ | $\overline{X}$ | $S_E$ |
|---|---|---|---|---|---|---|---|---|
| 1 | 141 | 5.6 | 150 | 6.4 | 11 | 1.2 | 11 | 0.6 |
| 2 | 269 | 38.2 | 263 | 39.3 | 11 | 3.3 | 12 | 3.4 |
| 3 | 206 | 35.5 | 207 | 38.1 | 11 | 2.7 | 9 | 2.6 |
| 4 | 189 | 37.8 | 197 | 36.3 | 13 | 3.6 | 11 | 2.7 |

**GLUCOSE**
**(preliminary)**

Figure    1



**BUN**
**(preliminary)**

Figure    2

141

Na+
(preliminary)



Figure 3

K+
(preliminary)



Figure 4

T₄
(preliminary)



Figure 5

142

All Sampled Data

Excluding data
Subjectively Assessed as
"Stressed" during Bleeding



Figure 6

CONTROL SERUM
COMPARISON



Figure 7

143
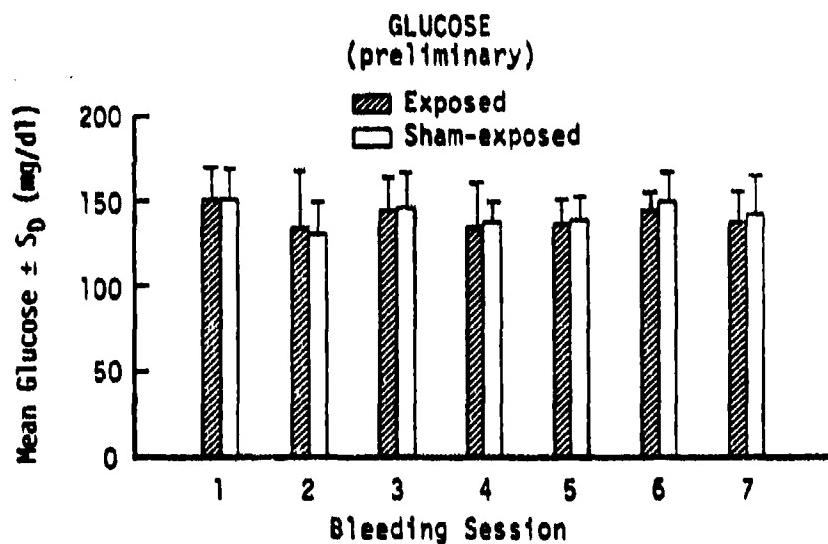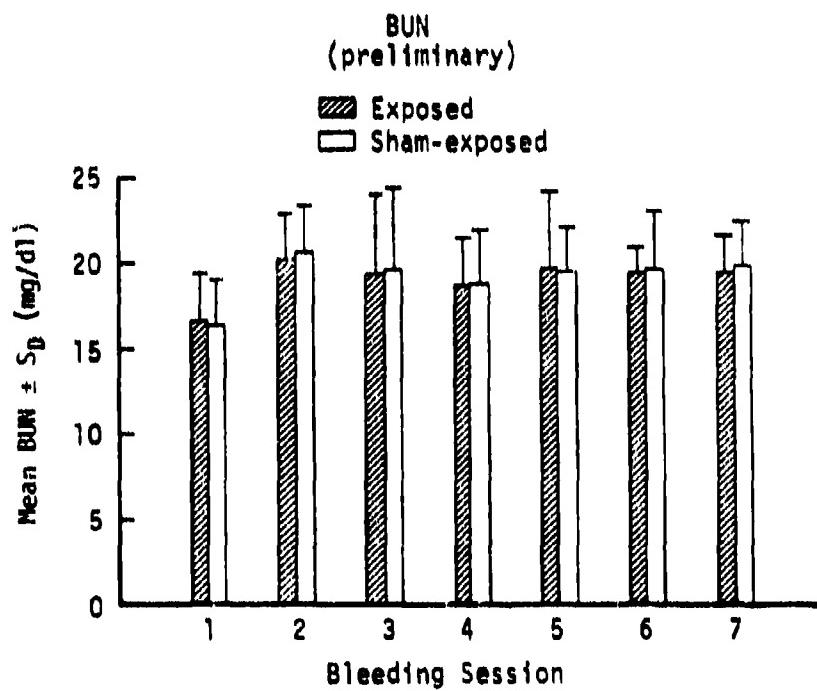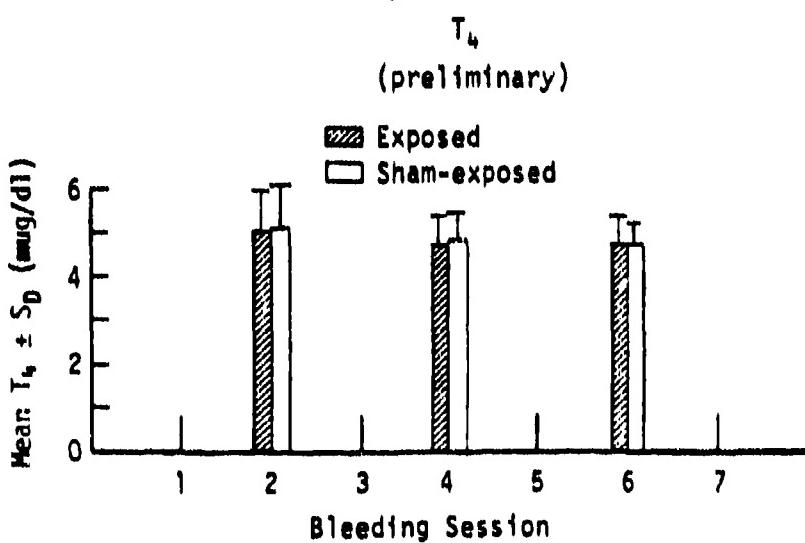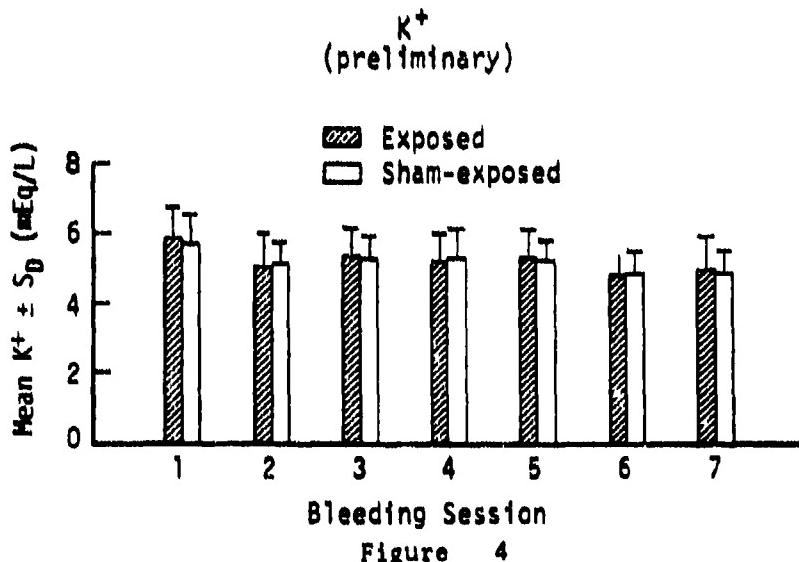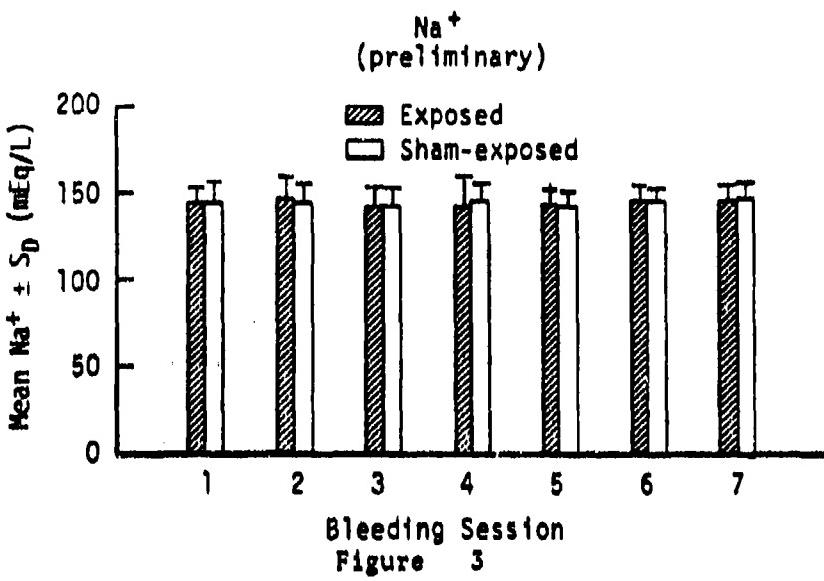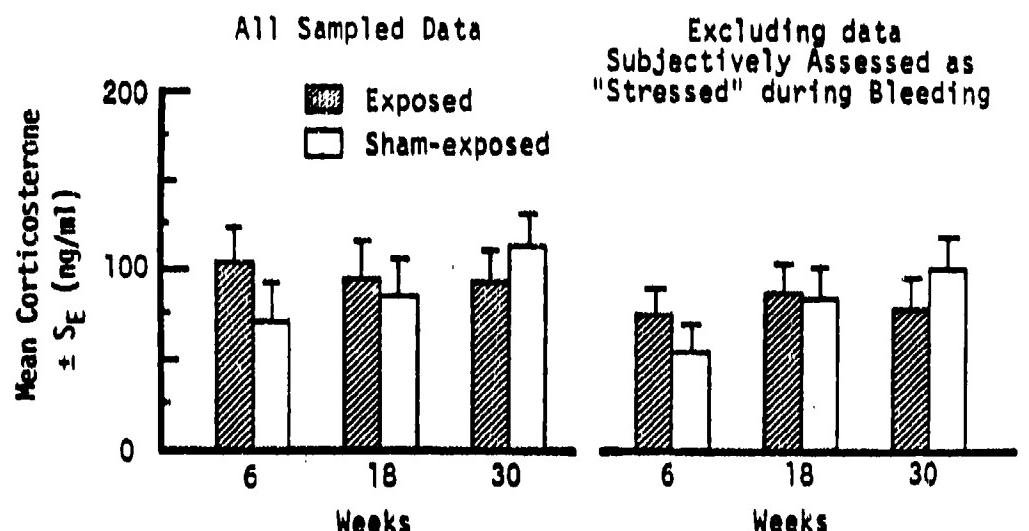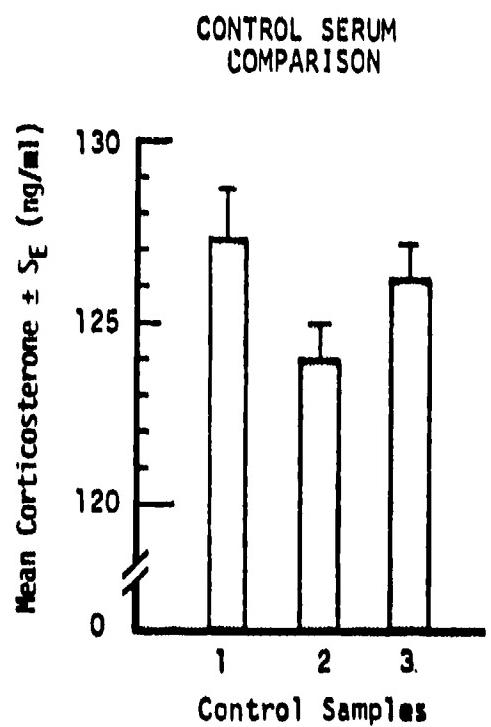
# CORTICOSTERONE in PERSPECTIVE



Figure 8



Figure 9

144
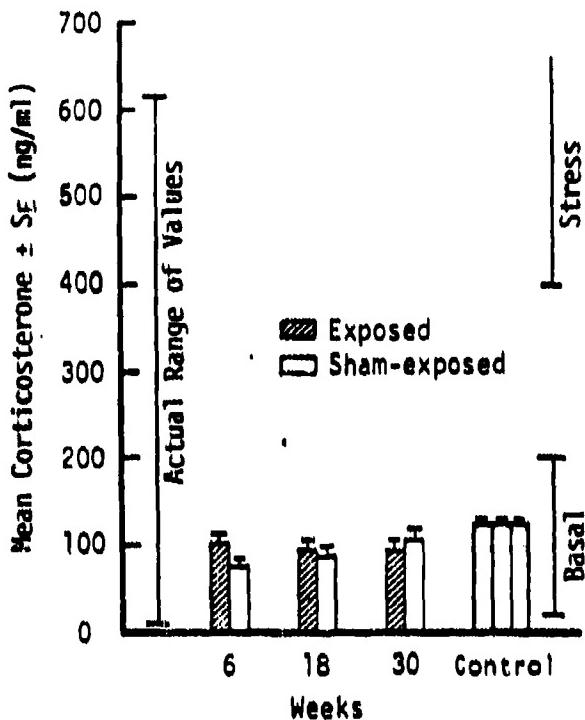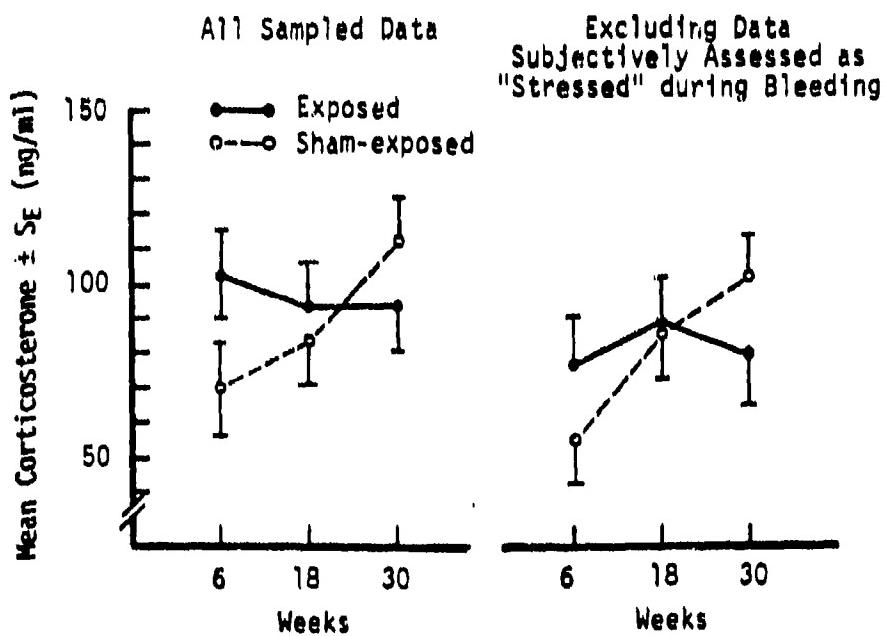
# MICROWAVES AND THERMOREGULATION

Eleanor R. Adair
John B. Pierce Foundation Laboratory
New Haven, CT 06519
AFOSR Grant #77-3420

## I.   INTRODUCTION:

Warm-blooded organisms, called endotherms, are able to maintain a stable internal body temperature in the face of rather wide fluctuations in the temperature or their environment. This is accomplished by fine adjustments in appropriate autonomic response systems, through which the body gains or loses heat, acting in concert with behavioral responses that provide a hospitable microclimate whenever possible. The particular autonomic response that may be operative at a given time is dictated primarily by the environmental temperature: thus, animals shiver in the cold and pant or sweat in the heat, but not the reverse.

Using the standard heat balance equation and methods of partitional calorimetry (Hardy and Stolwijk, 1966), it is possible to quantify the steady-state contribution of each autonomic response system to the total thermoregulatory response across a selected range of environmental temperatures. The result is a thermoregulatory profile for the species in question. Figure 1 shows an example of such a profile for the squirrel monkey, Saimiri sciureus (Stitt and Hardy, 1971), the experimental animal we use to investigate the effects of microwave exposure on thermoregulatory function. In cold environments, up to an ambient temperature ($T_a$) of $26.5^\circ$C, thermoregulation is accomplished by adjustments in metabolic heat production (M). In general, the lower the $T_a$, the higher the M, with the response systems for heat loss remaining at constant low levels. At $T_a = 26.5^\circ$C, designated the lower critical temperature (LCT), resting heat production is minimal and fine control of the body temperature is taken over by the peripheral vasomotor system (Lynch and Adair, 1978; Lynch, Adair, and Adams, 1980). Peripheral vessels in first the tail and then the extremities vasodilate, bringing warm blood from the body core to the surface, greatly increasing conductance (K). Peripheral vasodilation is complete and thermoregulatory sweating is initiated at $T_a = 36^\circ$C, designated the upper critical temperature (UCT). In the squirrel monkey, however, heat loss through evaporation is limited, and since M tends to increase in warm environments, the animal may quickly become hyperthermic at $T_a \geq 39^\circ$C.

It is clear from inspection of Fig. 1 that if the animal is exposed to a microwave field, the particular response system that may be altered by absorbed thermalizing energy will be directly related to the particular $T_a$ at which the exposure is made. In a series of studies conducted over the past three years, we have examined individual response systems to quantify the effects on thermoregulatory function of both brief and prolonged whole-body exposure to 2450-MHz CW microwaves. We have consistently found that the monkeys regulate their internal body temperature with precision, even when the energy absorbed is nearly equivalent to their resting metabolic heat production. We have also

145

found that the microwave power density that will just initiate a change in thermoregulatory responses can be quite low: thus 4-6 mW/cm$^2$ (SAR = 1.0 W/kg) will reduce the elevated heat production of monkeys in the cold (Adair, 1980; Adair, 1981); 6-8 mW/cm$^2$ (SAR = 1.1 W/kg) will initiate criterion vasodilation in the tail veins of monkeys in a 26°C environment, a $T_a$ just below the LCT (Adair and Adams, 1980a); and the same intensity will reliably stimulate squirrel monkeys to lower the chamber air temperature behaviorally (Adair and Adams, 1980b).
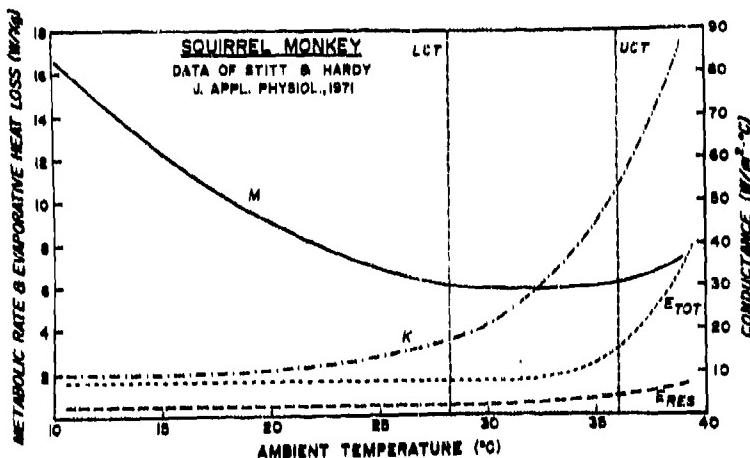


Figure 1.  Thermoregulatory profile of restrained squirrel monkey (Saimiri sciureus) across a range of environmental temperatures from 10 to 39°C.  M = metabolic heat production (W/kg); K = conductance (W/m$^2$·°C); E$_{tot}$ = total evaporative heat loss (W/kg); LCT = lower critical temperature; UCT = upper critical temperature.  The region between LCT and UCT is called the thermoneutral zone.  Data adapted from Stitt and Hardy, J. Appl. Physiol. 31: 48-54 (1971).

In this paper we turn our attention to the effects of microwave exposure on the primary heat-loss response of squirrel monkeys in warm environments, sweating from the palms and soles (Nadel and Stitt, 1970).  Our experiments were designed to determine the minimal power density of brief exposures to 2450-MHz CW microwaves that will reliably initiate thermoregulatory sweating from the foot of monkeys restrained at $T_a$'s just below the UCT. We also wished to determine the efficiency of the sweating response in regulating the body temperature during microwave exposures in warm environments. Since sweating in this species has an emotional as well as thermoregulatory component, it is essential to assess changes in metabolic rate that may accompany experimentally induced changes in sweating.  This has been done in the experiments to be described.

II.   TECHNICAL APPROACH:

The subjects were four adult male squirrel monkeys.  During the experiments the monkeys were chair restrained singly in the far field of a 15-dB standard gain horn antenna inside a 6' x 6' x 8' electromagnetically anechoic chamber

(see Figure 2). Air from a closely regulated source ($\pm$ 0.5$^\circ$C) circulated
through a 1' x 1' x 2' Styrofoam box enclosing the monkey, thereby creating an
environment of constant temperature for the assessment of autonomic thermoregu-
latory responses. A Lucite window in the box ceiling admitted light, and a
second window in the box wall allowed constant video surveillance of the animal.
All experiments were conducted in the presence of a 73-dB SPL masking noise.
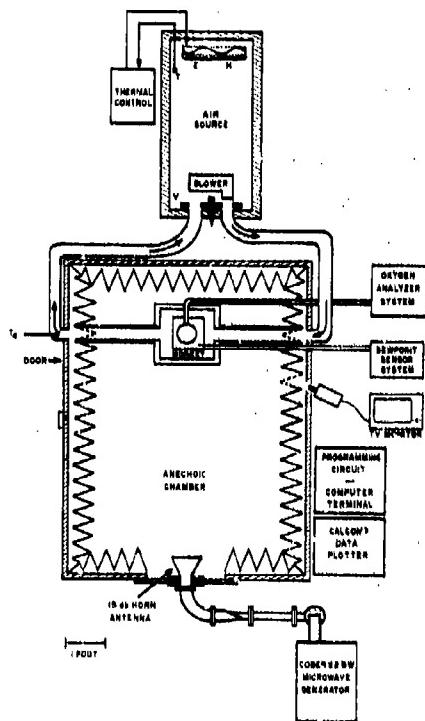


Figure 2. Schematic diagram (as viewed from above) of anechoic chamber, micro-
wave generator and transmission system, oxygen analyzer, dewpoint
sensor, and system for air temperature control. Valves (V) permit
source air to circulate through Styrofoam box in which monkey sits.
Source air temperature, sensed by thermistor (T), is controlled by
heat exchanger (E) and coil heaters (H).

Rectal temperature and four representative skin temperatures (abdomen,
tail, leg, and foot) were monitored continuously using 36-gauge copper-constantan
thermocouples carefully shielded and held out of alignment with the E-vector. A
Plexiglas hood over the monkey's head collected the expired air which was drawn
outside the chamber through Teflon tubing. Oxygen deficit was measured down-
stream by a Beckman F-3 paramagnetic oxygen analyzer which sampled the passing
airsteam at 0.3 L/min. Metabolic heat production was calculated from oxygen
consumption assuming a constant R.Q. of 0.83.

147

Thermoregulatory sweating from the foot was measured by a dewpoint sensing device controlled by a Peltier module, recently developed at the Pierce Laboratory. The monkey wore an L-shaped Plexiglas boot with the sole of the foot resting on a nylon mesh support. Chamber air was drawn through the boot and thence outside the chamber where the dewpoint temperature ($T_{dp}$) was measured and recorded continuously. From $t_{dp}$, the vapor pressure of water in the sampled air was calculated using Antoine's equation (Wood, 1970). The water evaporated from the sole, or sweating rate ($M_w$), was then calculated from a modified gas equation:

$$\dot{M}_w = \frac{(M.W.) \; (\Delta P_{H_2O}) \; AF}{R.T_a} \quad \text{g/min}$$

where: M.W. = molecular weight of water

$\Delta P_{H_2O}$ = the difference in water vapor pressure in air before and after evaporation of foot sweat

AF = air flow (L/min)

R = gas constant 62.396

$T_a$ = the air temperature in $^{\circ}K$.

Continuous microwaves of a single-frequency 2450 ($\pm$ 25) MHz were generated by a Cober 62.5W source and fed to the antenna via standard waveguide components. Field measurements at the animal's location (Adair and Adams, 1980b) revealed a maximum nonuniformity of 8% with the restraining chair absent, and an additional 5% with chair present. Insignificant changes occurred with the introduction of the Plexiglas hood and hose connections for measurement of oxygen consumption, fine thermocouples for measurement of body temperatures, or the Plexiglas boot with tube connections for measurement of thermoregulatory sweating.

A rough assessment of whole-body energy absorption over the power density range 5-40 mW/cm$^2$ has been based upon temperature increments produced at 4 depths in 3 sizes of saline-filled cyclindrical Styrofoam models by 10-min microwave exposures. (See Adair and Adams, 1980b, for details.) The mean temperature rise in the liquid above an equilibrated 35$^{\circ}$C, ranging from 0.1$^{\circ}$C at 5 mW/cm$^2$ to 0.6$^{\circ}$C at 40 mW/cm$^2$, yielded a calculated specific absorption rate (SAR) for a 1.1-liter model that ranged from 0.8 W/kg to 5.8 W/kg (see Figure 6). These dosimetric determinations have recently been confirmed in experiments to measure steady-state adjustments in metabolic heat production (Adair, 1980; Adair and Adams, in preparation).

The experimental procedure was designed to determine the power density of 10-minute microwave exposures that will reliably initiate thermoregulatory sweating in monkeys restrained in $T_a$'s just below that at which sweating normally occurs. After a minimal 90-minute equilibration period (see Figure 3) for stabilization of all measured parameters, the animal was exposed to 10-minute periods of 2450-MHz CW microwaves of increasing power density (e.g., 2.5, 4, 6, 8, 10 mW/cm$^2$). These exposures were separated by sufficient time for reequilibration of the animal's responses. Each animal was tested several times at $T_a$'s ranging from 32$^{\circ}$ to 35$^{\circ}$C.

## III. RESULTS:

Figure 3 presents a representative experimental session on one monkey conducted at a $T_a$ of $35^\circ C$. After a 30-minute calibration period to determine instrument baselines ($O_2$ meter, dewpoint sensor), the animal was introduced into the chamber and instrumented. During the 100-minute equilibration period, vaso-dilation of the extremities occurred, evidenced by an abrupt rise in foot skin temperature. Mean skin temperature stabilized at $\sim 3^\circ C$ above $T_a$, indicating complete peripheral vasodilation. Internal body temperature was regulated by a reduction of heat production to the resting level. Minimal, pulsatile sweating from the foot was evident. The monkey then underwent 10-minute microwave expo-sures of increasing power density (in this case 2.5, 4, 6, 8, and 20 mW/cm$^2$) to determine the power density at which a reliable increase in thermoregulatory sweating occurred. Figure 3 shows a reliable, regulated rise in the dewpoint temperature of foot capsule air at 6 mW/cm$^2$ and above. (Although a rise in $T_{dp}$ is also evident at 4 mW/cm$^2$, it is somewhat erratic and also accompanied by a correlated increase in M.) The sweating responses to 8 and 20 mW/cm$^2$ were even more rapid and dramatic, although the response to the highest power density failed to prevent a significant rise in internal body temperature ($T_{re}$).
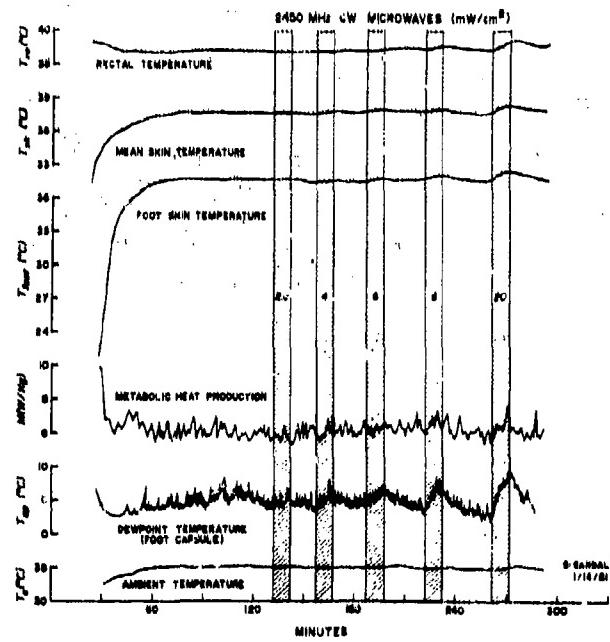


Figure 3. Representative experiment on one monkey equilibrated to an ambient temperature ($T_a$) of $35^\circ C$ to determine effects on metabolic heat pro-duction (M) and on dewpoint temperature of foot-capsule air ($T_{dp}$) of 10-minute exposures to 2450-MHz CW microwaves of increasing power density. Also shown are rectal ($T_{re}$), weighted mean skin ($T_{sk}$), and foot skin ($T_{foot}$) temperatures.

The power density required to initiate thermoregulatory sweating from the foot was directly related to the environmental temperature in which the monkey was restrained. Figure 4 summarizes the data from 30 experiments on four animals at discrete ambient temperatures that range downward from $36^\circ$C, the temperature at which sweating in a sedentary monkey may occur spontaneously. The plotted points appear to describe two functions that are roughly linear with power density or SAR: two monkeys (open symbols) showing minimal sweating and relative insensitivity to microwaves and two monkeys (closed symbols) showing generous sweating and greater sensitivity to microwaves. We have classified the former as "inefficient sweaters" and the latter as "efficient sweaters," although their ability to regulate internal body temperature during microwave exposure in warm environments appeared to be about equal. Efficient sweaters tended to have a somewhat higher level of resting heat production than inefficient sweaters. In any case, for all animals, at a $T_a$ just below the UCT, thermoregulatory sweating was reliably initiated by a 10-minute microwave exposure at a power density of 6-8 mW/cm$^2$ (SAR $\approx$1.1 W/kg). This represents roughly 20 percent of the resting metabolic heat production of the squirrel monkey (Stitt and Hardy, 1971; Lynch, 1976) and is comparable to microwave thresholds we have determined for other thermoregulatory responses (see Figure 6).
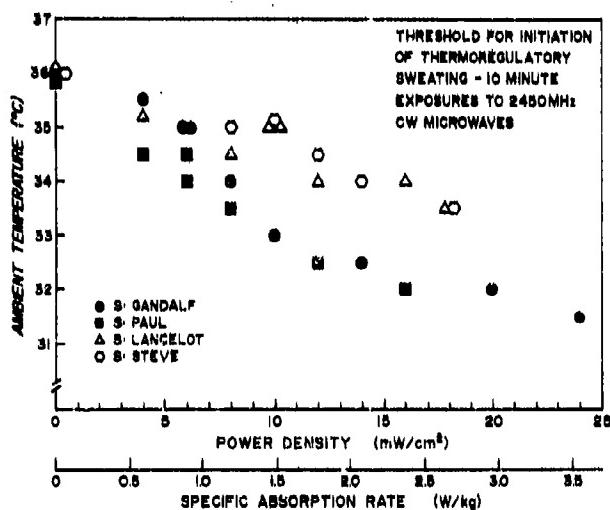


Figure 4. Threshold function for initiation of thermoregulatory sweating from the foot of squirrel monkeys by 10-minute whole-body exposures to 2450-MHz CW microwaves. Each data point represents the least microwave power density, or absorbed microwave energy, required to induce criterion increase in sweating rate at the ambient temperature indicated. Open symbols ( $\triangle$ $\bigcirc$ ) indicate "inefficient sweaters"; closed symbols ( $\bullet$ $\blacksquare$ ) indicate "efficient sweaters."

150

The magnitude of the change in sweating rate at a given $T_a$ was directly related to the intensity of the microwave field. Clearly evident in Figure 3, this finding is quantified for one monkey in Figure 5. At each $T_a$ (ranging from 35.5°C to 32°C), each plotted point represents the change in sweating rate measured from t=0 to t=10 min of each 10-minute microwave exposure plotted against the power density of that exposure. The points for any given $T_a$ are best described by a straight line, the slope of which varies in regular fashion with $T_a$. Thus, at any $T_a$ at or below 35.5°C, the higher the power density the greater the increase in sweating rate of the monkey under microwave exposure, but this increase becomes less and less in cooler and cooler environments, i.e., as the skin temperature falls. Indeed, there is a strong suggestion that if $T_a$ were to fall much below 32°C, sweating could not be initiated by microwave exposure, no matter how high the intensity.
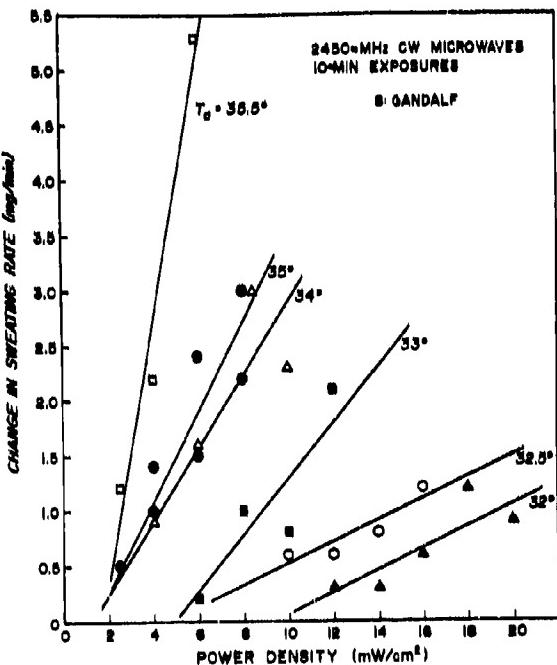


Figure 5. Change in foot sweating rate from baseline level produced by 10-minute microwave exposures of different power densities. The parameter is the ambient temperature ($T_a$) at which the experiment was conducted. Data from one monkey, an "efficient sweater."

The relationships displayed in Figure 5 are qualitatively similar to human data reported by Nadel, Bullard, and Stolwijk (1971). The local sweat rate of exercising humans increases linearly as body core temperature rises during exercise in a given $T_a$. But a higher core temperature is necessary to initiate sweating as skin temperature falls, and the rate of increase in sweating during exercise is lower and lower in cooler and cooler environments. This suggests that in the squirrel monkey the rate of thermoregulatory sweating initiated by microwave exposure depends not only upon the ambient (skin) temperature, but

151

also upon the temperature of the body core as it is directly increase by absorbed microwave energy.

Figure 6 summarizes experimentally determined microwave thresholds (5-10-min exposures) for the alteration of four types of thermoregulatory responses in terms of both power density and specific absorption rate. A power density of 6-8 mW/cm² will reliably stimulate squirrel monkeys to lower the chamber air temperature behaviorally (Adair and Adams, 1980b). The same intensity will initiate criterion vasodilation of the tail veins in monkeys restrained in a 26°C environment, a $T_a$ just below the LCT. A slightly lower power density (4-6 mW/cm²) will reliably lower the metabolic heat production of monkeys restrained in 15° and 20°C environments (Adair, 1980), while a power density of 6-8 mW/cm² will initiate thermoregulatory sweating from the foot of monkeys restrained in a 35°C environment, a $T_a$ just below the UCT (present report). The whole-body energy absorption in all cases represents 15-20% of the resting metabolic heat production of the squirrel monkey (Stitt and Hardy, 1971; Fuller, Sulzman, and Moore-Ede, 1979; Lynch, 1976). The remarkable similarity of these thresholds suggests strongly that the same configuration of deep-body thermosensitive sites is being stimulated by absorbed microwaves (during whole-body exposure) to provide the neural impetus for response change. Further, the entire thermoregulatory armament, autonomic response systems for heat production and heat loss as well as thermoregulatory behavior, that functions over a wide range of environmental temperatures (Figure 1), appears equally sensitive in coping with exogenous deep-body heating.
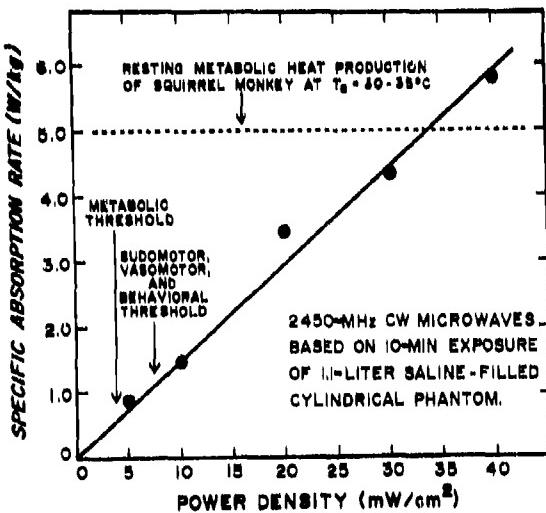


Figure 6.  Specific absorption rate (W/kg) as a function of power density mW/cm²) calculated on the basis of mean temperature increments produced in a 1.1-liter saline-filled cylindrical model by 10-min exposures to 2450-MHz CW microwaves. Model was equilibrated to an ambient temperature ($T_a$) of 35°C. Dashed line at 5 W/kg indicates average resting metabolic heat production of squirrel monkey in thermoneutral zone. Arrows indicate microwave thresholds for alteration of thermoregulatory behavior, initiation of tail vaso-dilation, reduction of metabolic heat production in the cold, and initiation of thermoregulatory sweating in warm environments.

Over the last 100 years, a variety of experimental procedures in many species has produced a great body of evidence pinpointing the medial preoptic area of the hypothalamus (PO/AH) as the major CNS thermosensitive site that controls behavioral as well as autonomic thermoregulatory responses. For this reason, this region of the brainstem is often referred to as the "central thermostat." Our own researches with the squirrel monkey (see for example, Adair, Casby, and Stolwijk, 1970; Adair, 1974; Adair and Rawson, 1974) have consistently shown that a highly localized PO/AH temperature change of the order of $0.2-0.3^{\circ}C$, produced by an implanted thermode device, is sufficient to trigger an immediate and appropriate change in thermoregulatory responses. We have recently determined that a temperature rise of this magnitude in the PO/AH area of the squirrel monkey brain accompanies a 10-minute microwave exposure at a power density of $6-8$ mW/cm$^2$.

We have developed an implantable nonmetallic reentrant tube system that can be used as an orifice for inserting a VITEK (Bowman, 1976) probe to measure local brain tissue temperature. Closed tubes, machined from nylon or Teflon rod, have an inside diameter of 1.1 mm and a wall thickness of 0.005". An inner rod system holds the tube securely for accurate placement during stereotaxic surgery and is then removed from the preparation. Nylon screws and dental acrylic tie the implant to the skull.

Two animals (acute preparations) have been implanted with several of these tubes in both the PO/AH and the midbrain reticular formation (MB). Postsurgically, the anaesthetized animals were placed in the restraining chair inside the anechoic chamber and exposed to a variety of microwave power densities. Pertinent data appear in Figure 7 which shows the temperature increase in the PO/AH or the MB measured with the VITEK probe (inserted in the implanted tubes) as a function of the power density of 10-minute exposures to 2450-MHz CW microwaves. Also indicated in the figure is the local PO/AH tissue temperature rise (produced via thermode) that is usually necessary to initiate changes in thermoregulatory responses. The data provide strong evidence that a power density of $6-8$ mW/cm$^2$ produces a PO/AH temperature rise of $0.2-0.3^{\circ}C$ in a squirrel monkey restrained in our exposure chamber. The data confirm earlier measurements we had made of temperature increases under controlled microwave exposures in tissue-equivalent spheres (Guy, 1971) using the procedures of Burr and Krupp (1980). Theoretical analyses (Kritikos and Schwan, 1979) have also suggested that internal hotspots of this magnitude could occur in the brain under our experimental conditions. Thus, we must conclude that whatever temperature changes may occur elsewhere in the body during whole-body microwave exposure, the local tissue temperature rise in the "central thermostat" of the brainstem is probably sufficient to trigger changes in thermoregulatory effector responses at a threshold power density of $6-8$ mW/cm$^2$.

IV. SUMMARY AND CONCLUSIONS:

Low intensity microwave fields have been shown to influence the normal responses, both autonomic and behavioral, that function to regulate the body temperature. Using the squirrel monkey as an animal model, we have determined the minimal incident energy (in mW/cm$^2$) derived from 2450-MHz CW microwaves that is necessary to lower metabolic heat production in the cold, alter peripheral vasomotor tonus in thermoneutral environments, initiate thermoregulatory sweating
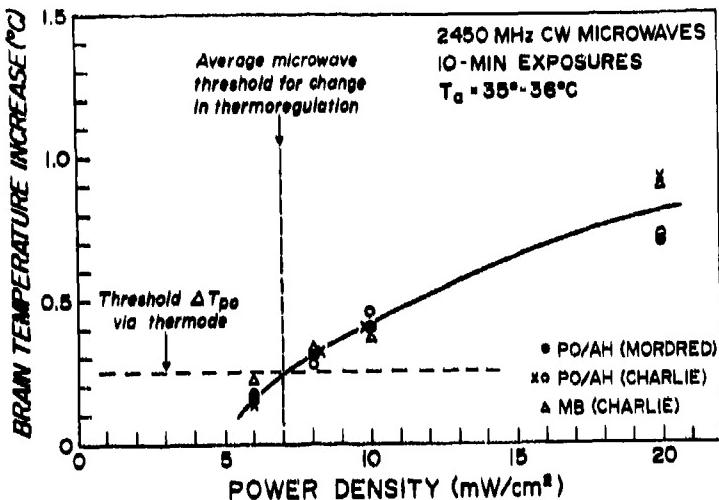
Figure 7.   Measurements of temperature increases in the medial preoptic area
(PO/AH) and midbrain reticular formation (MB) using the VITEK probe
inserted in stereotaxically implanted nylon or Teflon reentrant tubes.
Anaesthetized monkeys underwent 10-minute whole-body exposures to
2450-MHz CW microwaves at different power densities.  Animals equili-
brated to 35-36°C environment had internal body temperature within
normal range (39.0-40.0°C).

in the heat, and stimulate a behaving animal to select a cooler environment.
The threshold power densities in all cases are remarkably similar, suggesting a
common thermal basis for the response changes.  The whole-body SAR (in W/kg) at
threshold represents 15-20% of the resting metabolic heat production of the
squirrel monkey.  Experiments on anaesthetized animals have determined that the
local tissue temperature rise in the "central thermostat" of the brainstem at a
threshold power density of 6-8 mW/cm$^2$ is probably sufficient to trigger the
observed changes in thermoregulatory effector responses.  Follow-on efforts will
involve the confirmation of these results, using a chronic implant preparation
that will allow both the measurement and control of local brainstem tissue
temperature in awake, behaving squirrel monkeys as they are exposed to low
intensity microwave fields.

Our ultimate goal is to evaluate the impact of microwave exposure on the
human thermoregulatory system with reference to current maximum permissible
exposure standards.  This must necessarily involve careful power and frequency
extrapolations as well as considerations of body heat balance in man vs the
animal model.  It would appear that, with the possible exception of exposure to
moderate microwave intensities in warm environments, the squirrel monkey model
will be extremely useful in this regard.  Our most important single finding  to
date is that, no matter in what environment the organism finds itself, it detects
and responds immediately to low intensity microwave fields as it does to other
environmental thermal stimuli.  The net result is that internal body temperature
is regulated with precision at the normal level.

154

## V. REFERENCES:

Adair, E. R. Displacements of rectal temperature modify behavioral thermo-regulation. Physiol. Behav. 7: 21-26 (1971).

Adair, E. R. Metabolic adjustments during whole-body 2450 MHz CW microwave exposure. Bioelectromagnetics 1: 209 (1980).

Adair, E. R. Adjustments in metabolic heat production during whole-body 2450 MHz CW microwave exposure. Fed. Proc. 40: 421 (1981).

Adair, E. R., and Adams, B. W. Microwaves induce peripheral vasodilation in squirrel monkey. Science 207: 1381-1383 (1980a).

Adair, E. R., and Adams, B. W. Microwaves modify thermoregulatory behavior in squirrel monkey. Bioelectromagnetics 1: 1-20 (1980b).

Adair, E. R., Casby, J. U., and Stolwijk, J. A. J. Behavioral temperature regulation in the squirrel monkey: Changes induced by shifts in hypo-thalamic temperature. J. Comp. Physiol. Psychol. 72: 17-27 (1970).

Adair, E. R., and Rawson, R. O. Autonomic and behavioral temperature regula-tion: Unilateral vs bilateral preoptic thermal stimulation. Pflügers Arch. 352: 91-103 (1974).

Bowman, R. R. A probe for measuring temperature in radio-frequency-heated material. IEEE Trans. Microwave Theory Tech. MMT-24: 43-45 (1976).

Burr, J. G., and Krupp, J. H. Real-time measurement of RFR energy distribution in the Macaca mulatta head. Bioelectromagnetics 1: 21-34 (1980).

Fuller, C. A., Sulzman, F. M., and Moore-Ede, M. C. Variations of heat production cannot account for the circadian rhythm of body temperature in the squirrel monkey. Fed. Proc. 38: 1053 (1979).

Guy, A. W. Analysis of electromagnetic fields induced in biological tissues by thermographic studies on equivalent phantom models. IEEE Trans. Microwave Theory Tech. MTT-19: 205-214 (1971).

Hardy, J. D., and Stolwijk, J. A. J. Partitional calorimetric studies of man during exposures to thermal transients. J. Appl. Physiol. 21: 1799-1806 (1966).

Kritikos, H. N., and Schwan, H. P. Potential temperature rise induced by electro-magnetic field in brain tissues. IEEE Trans. Biomed. Engr. BME-26: 29-33 (1979).

Lynch, W. C. Autonomic responses to changes in preoptic and ambient temperature in Saimiri sciureus. The Physiologist 19: 279 (1976).

Lynch, W. C., and Adair, E. R. Ambient and hypothalamic temperatures alter vasomotor thresholds in squirrel monkey (Saimiri sciureus). In Y. Houdas and J. D. Guieu (Eds.) New Trends in Thermal Physiology, Paris: Masson, 1978, pp. 130-132.

155

Lynch, W. C., Adair, E. R., and Adams, B. W. Vasomotor thresholds in the squirrel monkey: effects of central and peripheral temperature. *J. Appl. Physiol.*: *Respirat. Environ. Exercise Physiol.* 48: 89-96 (1980).

Nadel, E. R., Bullard, R. W., and Stolwijk, J. A. J. The importance of skin temperature in the regulation of sweating. *J. Appl. Physiol.* 31: 80-87 (1971).

Nadel, E. R., and Stitt, J. T. Control of sweating in the squirrel monkey. *Physiologist* 13: 267 (1970).

Stitt, J. T., and Hardy, J. D. Thermoregulation in the squirrel monkey *(Saimiri sciureus)*. *J. Appl. Physiol.* 31: 48-54 (1971).

Wood, L. A. The use of dewpoint temperature in humidity calculations. *J. Res. Natl. Bur. Stand.* 74C: 117-122 (1970).

VI. **PUBLICATIONS AND PRESENTATIONS RESULTING FROM AF-FUNDED EFFORTS:**

A. **Publications**

Adair, E. R. Microwaves influence behavioral thermoregulation. *Bull. Psychonomic Soc.* 12: 251 (1978).

Adair, E. R. Microwaves alter thermoregulatory behavior. *Fed. Proc.* 38: 1295 (1979).

Adair, E. R., and Adams, B. W. Microwaves modify thermoregulatory behavior in squirrel monkey. *Bioelectromagnetics* 1: 1-20 (1980).

Adair E. R., and Adams, B. W. Microwaves modify thermoregulatory behavior but exposure duration matters little. *Bull. Psychonomic Soc.* 14: 244-245 (1979).

Adair, E. R., and Adams, B. W. Microwaves induce peripheral vasodilation in squirrel monkey. *Science* 207: 1381-1383 (1980).

Adair, E. R. Metabolic adjustments during whole-body 2450 MHz CW microwave exposure. *Bioelectromagnetics* 1: 209 (1980).

Adair, E. R. Microwave modification of thermoregulatory behavior: Effects of exposure duration. *International Symposium on Electromagnetic Waves and Biology*, June 30 - July 4, 1980, Jouy en Josas, France, pp. 183-187.

Adair, E. R., and Adams, B. W. Behavioral thermoregulation: Absence of adaptation to prolonged microwave exposure. *Bull. Psychonomic Soc.* 16: 164 (1980).

Adair, E. R. Adjustments in metabolic heat production during whole-body 2450 MHz CW microwave exposure. *Fed. Proc.* 40: 421 (1981).

Adair, E. R., and Adams, B. W. Adjustments in metabolic heat production by squirrel monkeys exposed to 2450 MHz microwaves. (In preparation)

B. Presentations at Scientific Meetings

| | |
|---|---|
| 9 November 1978 | "Microwaves influence behavioral thermoregulation"<br>Psychonomic Society, San Antonio, Tex. |
| 9 April 1979 | "Microwaves alter thermoregulatory behavior"<br>FASEB, Dallas, Tex. |
| 18 June 1979 | "Microwave modification of thermoregulatory behavior:<br>Threshold and suprathreshold effects"<br>Bioelectromagnetics Society, Seattle, Wash. |
| 10 September 1979 | "Microwave modification of thermoregulatory behavior:<br>Threshold and suprathreshold effects"<br>International Congress of Biometeorology, Shefayim, Israel. |
| 9 November 1979 | "Microwaves modify thermoregulatory behavior but exposure<br>duration matters little"<br>Psychonomic Society, Phoenix, Ariz. |
| 2 July 1980 | "Microwave modification of thermoregulatory behavior: Effects<br>of exposure duration"<br>International Symposium on Electromagnetic Waves and Biology,<br>Jouy en Josas, France. |
| 16 September 1980 | "Metabolic adjustments during whole-body 2450 MHz CW micro-<br>wave exposure"<br>Bioelectromagnetics Society, San Antonio, Tex. |
| 14 November 1980 | "Behavioral thermoregulation: Absence of adaptation to<br>prolonged microwave exposure"<br>Psychonomic Society, St. Louis, Mo. |
| 14 April 1981 | "Adjustments in metabolic heat production during whole-body<br>2450 MHz CW microwave exposure"<br>FASEB, Atlanta, Ga. |

C. Seminars (colloquia)

| | |
|---|---|
| 8 November 1978 | School of Aerospace Medicine, Brooks AFB, Tex. |
| 22 January 1979 | John B. Pierce Foundation Laboratory, New Haven, Conn. |
| 21 February 1979 | Walter Reed Army Institute of Research, Washington, D.C. |
| 19 March 1979 | Wellesley College, Wellesley, Maine. |
| 19 April 1979 | VA Medical Center, Kansas City, Mo. |
| 19 November 1979 | Armed Forces Radiobiology Research Institute, Bethesda, Md. |
| 18 January 1980 | Environmental Protection Agency, HERL, Research Triangle<br>Park, N.C. |

26 February 1981    Mt. Holyoke College, So. Hadley, Maine.

15 April 1981       Naval Medical Research Institute, Bethesda, Md.

# A MODIFIED WAVEGUIDE EXPOSURE FACILITY FOR EXAMINING EFFECTS OF MICROWAVES ON IMMUNOCOMPETENT AND HEMATOPOIETIC CELLS[1,2]

Shin-Tsu Lu

Norbert J. Roberts, Jr.

Sol M. Michaelson

University of Rochester School of Medicine

Rochester, New York

[2]Correspondence:  Dr. N.J. Roberts, Jr; Infectious Diseases Unit; Department of Medicine; University of Rochester School of Medicine; Rochester, NY 14642

## INTRODUCTION

Radiofrequency and microwave radiation is ubiquitous, potentially affecting all individuals to some degree, many to a greater degree. Studies by several investigators have raised the possibility that the immunocompetent cells of humans are particularly susceptible to microwaves (2,8,9). Many animal systems have been studied as well, but the species, frequencies, power intensities, durations, environmental conditions, and other factors have been so varied that extrapolation to humans would be exceedingly difficult, even if appropriate. The reported human studies in particular have been admittedly "poorly reproducible and non-quantitative" (2).

It is the purpose of this project to expose human leukocytes to microwaves _in vitro_ to determine whether cell functions are affected; if effects are observed, to determine whether they might be beneficial or detrimental to the host; and to examine the relationship of temperature variation to observed effects. Moderate changes in temperature may be associated with marked changes in immune function (5). This report describes the components and dosimetry of a waveguide exposure system modified for such studies.

## TECHNICAL APPROACH

### 1.  Facility.

Figure 1 shows the block diagram of the waveguide exposure facility for exposure of cell cultures to microwaves. The components are identified in Table I. It should be noted that the agitator is located external to the incubator and is attached by a shaft to the movable Plexiglas shelf upon which the waveguides rest. The frequency used in the present studies was 2.45 GHz, continuous waves. The power source components can

160

provide amplitude and pulse modulation over carrier frequencies of
2-4 GHz. The dimensions, and spatial relations of the dual vials to the
waveguides (WR 430), are shown in Figure 2. For initial studies, a stub
tuner was used; the tuner was subsequently removed because it was ineffective
at low power application (less than 0.5 watt). Two types of microwave
application were investigated: shorted waveguide exposure (Results,
sections 1-4) and transmitted waveguide exposure (Results, sections 5-
8). The shorted waveguide exposure was achieved by replacing the waveguide-
coaxial adapter and coaxial termination (Hewlett-Packard 908A), as
shown in Figure 2, by a WR 430 end plate. Determinations of specific
absorption rate (SAR) in the waveguide exposure systems were performed
at 23°C ambient temperature. Temperature measurements during microwave
exposures were determined using Vitek Electrothermia monitors exclusively.

2. Techniques for determination of averaged SAR.

Steady-state determination of averaged SAR (Method A). The In
vitro SAR can be determined by the following equations, according to Ali
et al (1):

$$SAR = C \cdot \Delta Tss \cdot k \qquad (eq\ 1)$$

where C is the specific heat in cal/°C/g, $\Delta Tss$ is the new steady-
state temperature increment from the initial steady-state without microwaves,
and k is the cooling constant. The relationship between $\Delta Tss$ and k
during microwave exposure is

$$Ln\ (\Delta Tss - \Delta T) = Ln\ \Delta Tss - k \cdot t \qquad (eq\ 2)$$

where $\Delta T$ is the temperature increment from initial steady-state
without microwaves at a given time of exposure, t. After reaching a new
steady-state induced by microwave exposure, the relationship between
$\Delta Tss$ and k is

161

$$\text{Ln } \Delta T = \text{Ln } \Delta Tss - k \cdot (t - \mathcal{T}) \qquad \text{(eq 3)}$$

where $\mathcal{T}$ is the duration of a constant microwave exposure until a
steady-state temperature is achieved and microwave exposure is terminated.
Equations 2 and 3 can be used to obtain $\Delta Tss$ and k by a logarithmic
plot. Values of $\Delta Tss$ and k can then be used to determine SAR as indicated
in equation 1. The specific heat of the culture medium used in these
studies (medium 199) is 0.97 cal/°C/g, by the method of thermal dilution
in a vacuum bottle.

Non-steady-state determination of the SAR profile (Method B). The
SAR determination by a non-steady-state heating analysis is based on

$$\text{SAR} = C \cdot A \qquad \text{(eq 4)}$$

where A is the rate of energy absorption in the absence of losses.
As indicated by Johnson (4), the rate of energy absorption, A, and the
temperature increment, $\Delta T$, assume the following relationship:

$$\lim_{t \to 0} d/dt \, (\Delta T) = A \qquad \text{(eq 5)}$$

The SAR can be determined according to equation 4 if A can be
accurately determined by equation 5. The criteria used are minimal
temperature increment, to avoid the influences of thermal gradients and
losses on accuracy of determinations, and the initial linear rate of
heating, used to avoid the influence of $\Delta T$ changing with time.

Determination of average SAR by thermal insulation (Method C).
Averaged SAR in the culture can be determined by the heating rate if a
constant microwave exposure is given, the conversion of absorbed microwave
energy to heat is complete, and the system is without loss. As an
alternative procedure, low-density foamed polystyrene was used for
thermal insulation, to reduce thermal losses in order to obtain a linear

162

heating rate. Inhomogeneity of absorption was minimized by agitation of the culture medium. Therefore, the temperature increment from a steady-state, $\Delta T$, of the culture medium was a linear function of the microwave absorption rate; i.e.,

$$\Delta T = A \cdot t \qquad \text{(eq 6)}$$

The method of least-squares fit was used to obtain k and $\Delta Tss$ in equations 2 and 3, while the sample was agitated to obtain a uniform temperature distribution. The A in equation 5 was determined graphically from the temperature tracing recorded on a linear recorder with a deflection of one inch per 0.1°C.

## RESULTS/PROGRESS

1. Steady-state determination of averaged SAR (shorted waveguide).

Typical temperature tracings using 4 different forward powers are shown in Figure 3. A near steady-state temperature was achieved at the end of 60 minutes of exposure. Averaged SAR was determined according to equation 1. $\Delta Tss$ and k, derived from equations 2 and 3, showed a deviation from linearity, usually occurring around 20 minutes for either heating or cooling analysis. The deviation from linearity could be attributed in part to digitalized data at 0.1°C intervals. Changes in the environment are also to be expected. The differences between SAR determinations by heating and cooling were 0.58, 0.97, 1.19, and 1.47% in these examples.

The replication of SAR determination by heating and cooling was not a general rule. To obtain such replication, we had to maintain constant heat exchange between the exposed sample and the environment. More than 20% difference could occur if caution was not exercised to maintain a

163

constant heat exchange. For example, a relatively large cooling constant could be obtained by circulating air through the waveguide.

Two observations indicate that heating analysis is superior to cooling analysis in the present facility: (1) deviation from linearity occurred consistently earlier in the cooling curve than in the heating curve; and (2) a slower and larger deviation was noted in the cooling constant determined by cooling analysis than in the cooling constant determined by heating analysis. The cooling constant was $0.0776 \pm 0.093$ (S.D., n=19) from cooling analysis and $0.0838 \pm 0.0087$ (S.D., n=20) from heating analysis. (One of the cooling curves was useless because the deviation from linearity occurred in less than 10 minutes.) The difficulties of cooling analysis were apparently attributable to the Styrofoam spacer, which alters the heat exchange due to its insulation characteristics. In a relatively short period of time, the contribution of Styrofoam was neglible, since the temperature of Styrofoam did not deviate substantially from the initial temperature.

SAR was then determined by Method A. A 60-minute exposure period and 40-minute cooling period were standardly used in the determination of SAR. Analysis of the heating curve was used for reasons stated above; the data are shown in Table II and Figure 4 (open circles). The correlation between SAR and forward power was highly significant (correlation coefficient = 0.95). The regression coefficient was 4.24 mW/ml per watt forward power, or 4.56 mW/ml per mW forward power at sampling efficiency of -20.4 dB.

2. <u>Averaged SAR determination by instrumentation (shorted waveguide).</u>

The purpose of these experiments was to determine the SAR from the power readings sampled by the bidirectional coupler. The SAR determined by instrument reading (closed circles in Figure 4) is a compound function

164

of the forward power ($P_f$) and reflected power ($P_r$). The data shown (Figure 4) are from four series of determinations with a change in tuning. The formula $[P_r \cdot (P_f - P_r)/(P_f + P_r) \ / \ \text{volume}]$ provides a simple and accurate estimate of SAR in the present facility.

3. <u>Relationship between steady-state temperature increment and SAR (shorted waveguide).</u>

Figure 5 shows the relationship between steady-state temperature increment and SAR using 20 data points (see Table II). The regression coefficient was 0.2161 °C/mW/ml; the correlation coefficient was 0.98.

4. <u>Prediction of steady-state temperature increment by the cooling constant (shorted waveguide).</u>

From equation 1, we obtain

$$\Delta Tss = 0.0147 \cdot SAR/k$$

The cooling constant has a dimension $min^{-1}$, the SAR a dimension mW/ml. The constant 0.0147 is a conversion factor for the units used. The 95% confidence limit of the cooling constant was 0.0655 to 0.1021 $min^{-1}$. Therefore, the steady-state temperature increment was in the range of 0.2243 to 0.1440 °C/mW/ml. Experimental data were within this range. The range of cooling constants also predicted that the heating would be 98% to more than 99% complete by one hour of exposure.

5. <u>Dosimetry using a muscle phantom (transmitted waveguide).</u>

For these and subsequent studies, a WR 430 waveguide-to-coaxial adapter and coaxial termination were substituted for the end plate.

The muscle phantom was prepared according to the formula provided by Guy (3). Two cut vials of 1.2-cm diameter and 1.6-cm height were used for these determinations. These vials were filled with muscle phantom without air bubbles. A 5x6 grid (30 points) was used. (Points

165

of measurement are indicated in Figure 6). Landmarks for these 30 points were the center of the vial, and 0.5 cm to the front (proximal to power source), 0.5 cm to the back (distal), 0.5 cm to the right, and 0.5 cm to the left from the center of the vial. A 0.3-cm incremental spacing from the bottom of the vial was used to determine 6 points of measurement for each of the 5 vertical columns. A 6-second exposure time was used for each determination, with triplicate measurements. Method B was used to determine the SAR profile. The temperature tracing was usually linear with time, except at the highest SARs. In the latter cases, a linear portion of the first 1.5-3.5 seconds of exposure was used to avoid the initial overshoot of the power-generating equipment, and the rate of heating was used to calculate SAR. A forward power of 0.55 watt was used throughout these determinations.

The averaged SAR was $58.7 \pm 46.2$ (S.D., n=30), and $63.4 \pm 45.4$ (n=29) in the right vial in two series of determinations, and $76.1 \pm 63.9$ (n=30) in the left vial. The ratio of the SAR at each point to the averaged SAR in the given vial ranged from 0.12 to 3.94 for the right vial and 0.24 to 3.39 for the left vial. These ratios were plotted in planes (Figure 7). A geometric resonance was apparent. Maximal absorption occurred approximately in the center of each vial.

The correlation between points in the duplicate series of determinations using the right vial was highly significant (correlation coefficient = 0.7471, P <0.001). (Replication of each exact location for measurement was difficult, preventing identical determinations from the two sets. Averaged SAR values did approximate each other).

6. <u>Effect of agitation on temperatures in the culture medium</u>
   <u>(transmitted waveguide).</u>

166

Two points were selected according to the SAR distribution determined previously. These points were the highest SAR (300 mW/ml) and lowest SAR (9 mW/ml), with an averaged SAR of 76 mW/ml within the vial. Figure 8 indicates the temperature tracing for these points with or without agitation. (Agitation is provided by an Eberback Shaker located external to the incubator and attached to the movable platform upon which the waveguides rest within the incubator.) Comparison of these tracings without agitation revealed a thermal gradient, with heat transfer from the high SAR to the low SAR point. The thermal gradient was reduced and maintained at approximately 0.1°C with agitation. With agitation, the change in rate of heating became insignificant after 10 seconds of exposure. At a lower absorption rate, the temperature inhomogeneity is probably insignificant.

7. <u>Determination of averaged SAR by heating analysis (transmitted waveguide).</u>

<u>Heating analysis with low-density Styrofoam for thermal insulation.</u> Method C was used in these determinations. For a representative value of the averaged SAR, a point within the vial was selected for measurement when heat loss was negligible. Criteria used to select that point were: (1) the heating curve for the last 15 seconds of the 20-second exposure was linear; (2) the temperature increment during the exposure did not exceed 0.2°C; and (3) after termination of exposure, the temperature changes in the first 5 seconds did not exceed 0.01°C. A forward power of 0.55 watt was used. The averaged SAR thus determined was $34.1 \pm 2.86$ (S.D., n=4) in the right vial and $31.3 \pm 3.16$ mW/ml (S.D., n=4) in the left vial.

<u>Steady-state study.</u> Method A was used. The cooling constant, k $(-0.0838 \text{ min}^{-1})$, was determined previously. The time required to reach a

167

steady-state temperature can be determined from this constant, k; 99% of steady-state temperature increment can be achieved in 55 minutes of exposure. The $\Delta Tss$ was determined in culture medium with agitation after 60 minutes of continuous exposure. The initial 15 to 20 minutes of the heating curve was used. The temperature increment ( $\Delta T$) of every 30-second period was digitalized for calculation of k and $\Delta Tss$. Forward power was set at 0.55 watt. Results indicated that the right vial absorbed at 27.4 $\pm$ 4.4 (S.D., n=4) and the left vial at 28.8 $\pm$ 0.67 mW/ml (S.D., n=4).

8. Exposure of human leukocyte cultures (transmitted waveguide).

Cultures were incubated for four hours to bring the culture temperatures into exact equilibrium with the incubator environment( 37°C). Two-hour microwave exposures were used. The absorption rates were calculated from results in the preceding section. For each absorption rate, steady-state temperature increments between microwave and sham-exposed cultures were very close to the predicted values. The differences were 0.07°C at 4 mW/ml, 0.06°C at 1 mW/ml, and 0.01°C at 0.5 mW/ml (Table III).

## SUMMARY AND CONCLUSIONS

A comprehensive approach in calibration of a dual-vial waveguide exposure facility is presented. The principles and techniques used for calibration are readily available in the literature. Results indicated that averaged absorption rates within culture vials could be predicted easily using a measurement of the forward power. The differences between the two vials were negligible. Furthermore, the steady-state temperature increment could be predicted precisely from the averaged absorption rate. The steady-state temperature increment could therefore be a

useful parameter for monitoring the performance of the exposure facility, in addition to measurements of the forward and reflected power.

The in vitro exposure of sufficient volumes (4 ml) for multiple biological studies can be achieved in the present exposure facility. However, inhomogeneity and significant resonance absorption were noted in the dual-vial waveguide exposure facility. A 30-point measurement of SAR distribution revealed that the SAR at any of the measured points could range between 0.12- and 3.94-fold of the averaged SAR within the given vial. However, such variable SARs did not create significant thermal gradients within the vials when external agitation was applied.

The difference between the maximum and minimum SAR within a culture vial was 28-fold. However, the difference in thermal environment between these points was negligibly small; furthermore, studies with much lower averaged SAR are planned. A study of biological parameter-temperature relationships, in microwave-exposed and sham-exposed leukocyte cultures using the present facility, can provide an assessment of the importance of inhomogeneous SAR for a biological system without substantial compromise by thermal mechanisms.

The use of a dual-vial exposure facility allows concomitant determinations of the effects of microwaves on cells in the resting and stimulated states. This is important, since differences may be apparent only with exposure of cells in one or the other state. Specifically pertinent to studies of microwave effects are prior observations regarding hyperthermia (38.5 versus 37°C) and human leukocyte functions. Enhanced recognition (mitogen- or antigen-induced lymphocyte transformation responses) and response (mitogen- or antigen-induced production of immune mediators)

169

were noted at the elevated temperature without substantial concomitant effects on unstimulated DNA synthesis or mediator production (6,7).

Incident power density is probably the only reasonable measurement for judging environmental contamination and determining personnel protection guidelines. Extrapolation from in vitro experiments to an in vivo biological effect can be achieved by converting the SAR in waveguide-exposed biological material to an equivalent incident power density in vivo. Efforts to calibrate the present facility were designed to make such conversion possible.

# REFERENCES

1. Ali, J.W., C.F. Blackman, M.L. Fromme, and S.W. Bernance. 1977. Measurement of microwave radiation absorbed by biological systems. I. Analysis of heating and cooling data. Radio Sci. 12:1-8.

2. Czerski, P. 1975. Microwave effects on the blood-forming system with particular reference to the lymphocyte. Ann. N.Y. Acad. Sci. 247:232-242.

3. Guy, A.W. 1971. Analyses of electromagnetic fields induced in biological tissues by thermographic studies on equivalent phantom models. IEEE Trans. MTT 19:205-214.

4. Johnson, C.C. 1975. Recommendations for specifying electromagnetic wave irradiation conditions in biological research. J. Microwave Power 10:249-250.

5. Roberts, N.J., Jr. 1979. Temperature and host defense. Microbiol. Rev. 43:241-259.

6. Roberts, N.J., Jr., and K. Sandberg. 1979. Hyperthermia and human leukocyte functions. II. Enhanced production of and response to leukocyte migration inhibition factor (LIF). J. Immunol. 122:1990-1993.

7. Roberts, N.J., Jr., and R.T. Steigbigel. 1977. Hyperthermia and human leukocyte functions: Effects on response of lymphocytes to mitogen and antigen and bactericidal capacity of monocytes and neutrophils. Infect. Immun. 18:673-679.

8. Stodolnick-Barańska, W. 1967. Lymphoblastoid transformation of lymphocytes in vitro after microwave irradiation. Nature 214:102-103.

9. Stodolnik-Barańska, W. 1974. The effects of microwaves on human lymphocyte cultures. In Biologic Effects and Health Hazards of Microwave Radiation. Czerski, P., K. Ostrowski, M.L. Shore, Ch. Silverman, M.J. Suess, and B. Waldeskog (eds.). Polish Medical Publishers, Warsaw. pp. 189-195.

Table I

## COMPONENTS OF WAVEGUIDE EXPOSURE FACILITY

Power Source:

1. Hewlett-Packard Signal Generator, HP8616A

2. Krohn-Hite Function Generator, 5500 AR

3. Hughes Amplifier, 1177-01

Delivery:

1. Andrew Superflexible Heliax 1/4-in. coaxial cable

2. Harris Isolator, PRD 12211C

3. Weinschel Stub Tuner, DS 109

4. Omega Waveguide, WR 430

5. Hewlett-Packard Coaxial Termination, 908A

Power Measurement:

1. Narda Bidirectional Coupler, 3022

2. Sage Lab. Switch, STN 2180A Type 1P2T

3. Hewlett Packard Power Sensor, 8478B

4. Hewlett Packard Power Meter, 4328

Temperature Measurement:

1. Vitek 101 Electrothermia Probe and Monitor

2. YSI 520 Tissue Implantable Probe

3. Markson Bridge, T-16458

Other:

1. National Water-Jacketed Incubator, 7241, Modified

2. Eberbach Shaker, Variable Speed, 5850

Table II

## CALORIMETRIC DETERMINATION OF SAR USING HEATING ANALYSIS

| Forward Power (W) | $\Delta T_{ss}(°C)$[a] | $k$ (min$^{-1}$)[b] | SAR (mW/ml)[c] |
|---|---|---|---|
| 0.22 | 2.28 | -0.0617 | 9.54 |
| 0.33 | 3.04 | -0.0928 | 15.96 |
| 0.45 | 3.47 | -0.0710 | 16.70 |
| 0.55 | 4.91 | -0.0794 | 26.49 |
| 0.55 | 4.53 | -0.0961 | 29.57 |
| 0.67 | 4.79 | -0.0751 | 24.45 |
| 0.67 | 4.57 | -0.0921 | 28.59 |
| 0.77 | 6.98 | -0.0763 | 35.68 |
| 0.78 | 6.44 | -0.0866 | 37.89 |
| 0.78 | 5.63 | -0.0824 | 31.48 |
| 0.79 | 5.10 | -0.0864 | 29.92 |
| 0.89 | 7.24 | -0.0798 | 39.22 |
| 0.89 | 6.40 | -0.0841 | 36.54 |
| 1.00 | 6.60 | -0.0783 | 35.12 |
| 1.01 | 7.03 | -0.0882 | 42.10 |
| 1.01 | 7.43 | -0.0942 | 47.54 |
| 1.10 | 6.40 | -0.0902 | 39.20 |
| 1.13 | 8.10 | -0.0896 | 49.26 |
| 1.18 | 9.24 | -0.0809 | 50.78 |
| 1.28 | 9.39 | <u>-0.0909</u> | 57.95 |
| | | -0.0838 | |
| | | ±0.0087 (mean ± S.D.) | |

[a] $\Delta T_{ss}$ = steady-state temperature increment;   [b] $k$ = cooling constant;

[c] SAR: specific absorption rate

173

Table III

TEMPERATURE INCREMENTS IN MICROWAVE-EXPOSED HUMAN LEUKOCYTE CULTURES

| Absorption rate (mW/ml) | N | Microwave-exposed (°C) | Sham-exposed (°C) | Difference (°C) | Predicted temperature increment (°C) |
|---|---|---|---|---|---|
| 4 | 8 | 1.21 + 0.17* | 0.42 + 0.15 | 0.79 + 0.13 | 0.86 |
| 1 | 5 | 0.66 + 0.05 | 0.38 + 0.13 | 0.28 + 0.11 | 0.22 |
| 0.5 | 6 | 0.47 + 0.12 | 0.35 + 0.12 | 0.12 + 0.04 | 0.11 |

* Mean + S.D.; N=number of observations

174
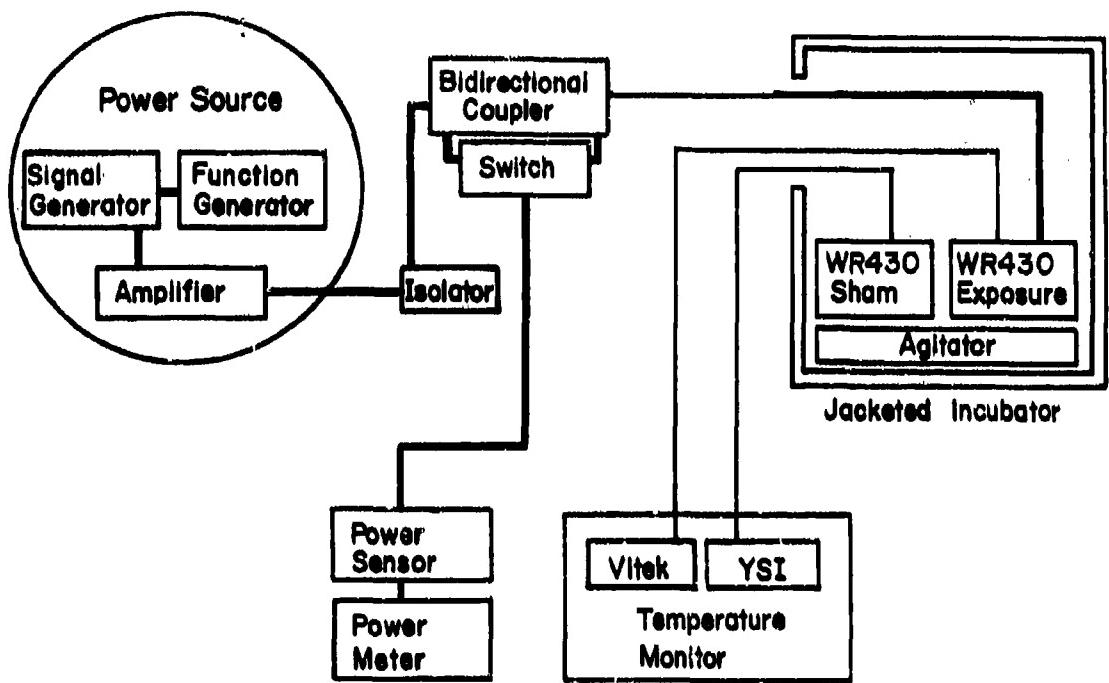
Figure 1.   Microwave exposure system.
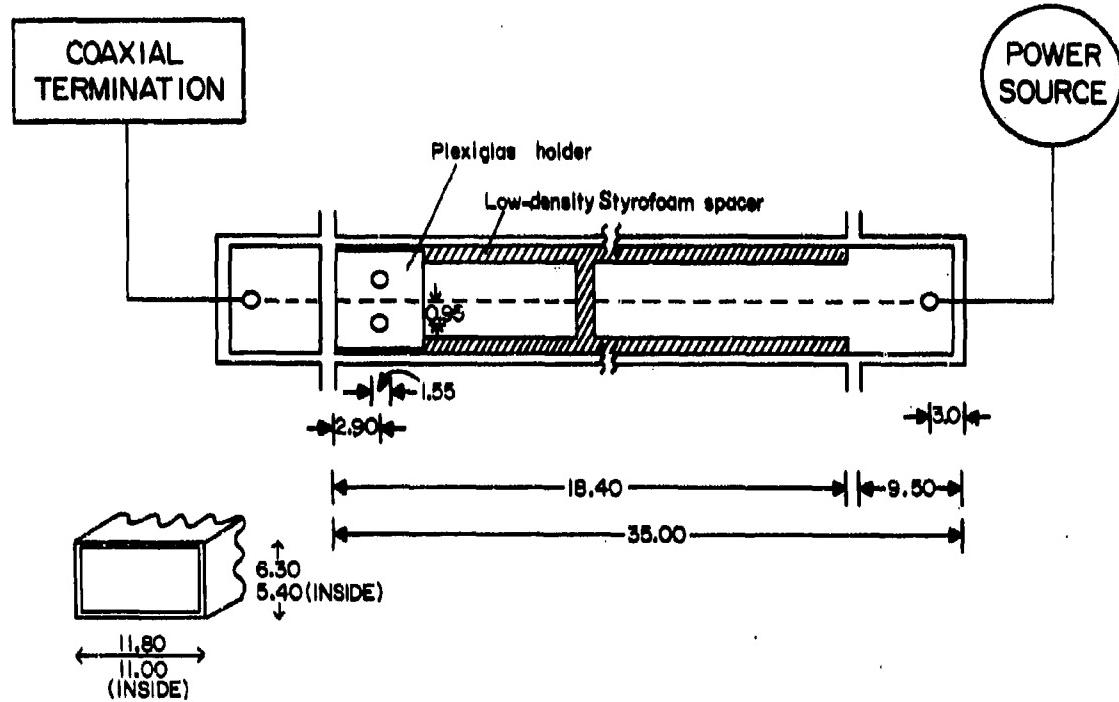
Figure 2. Waveguide exposure chamber. (Dimensions are in cm.)
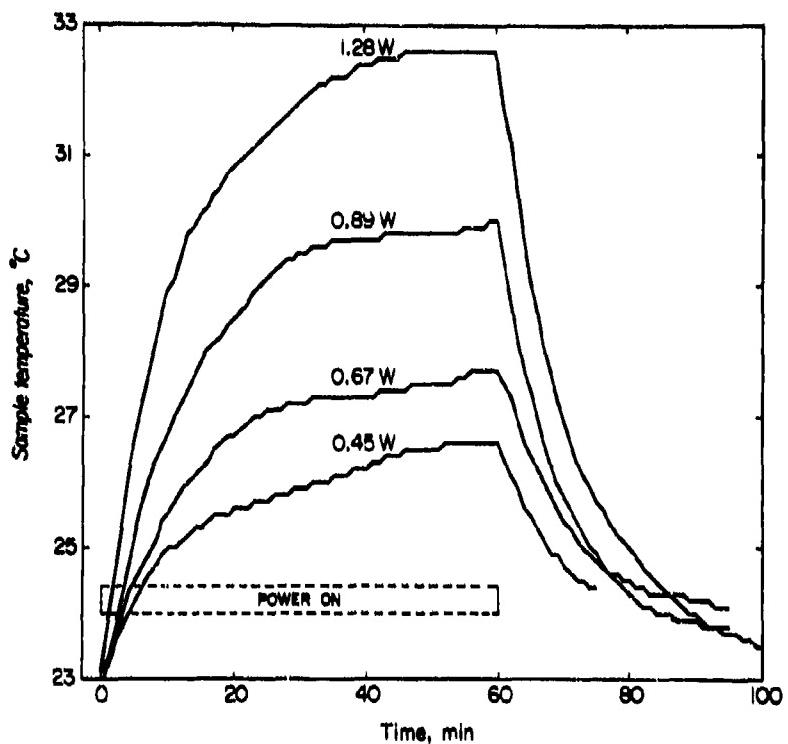
Figure 3. Temperature tracings at different forward powers ($T_{air} = 24°C$).
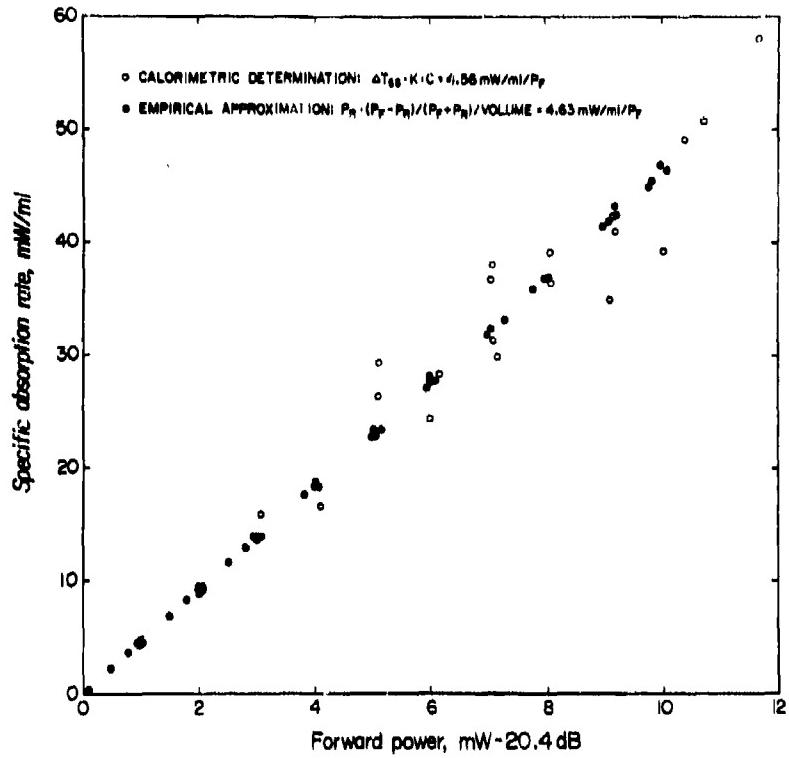
Figure 4. Calibration of waveguide exposure facility with end plate $(T_{air}=24^\circ C)$.

178
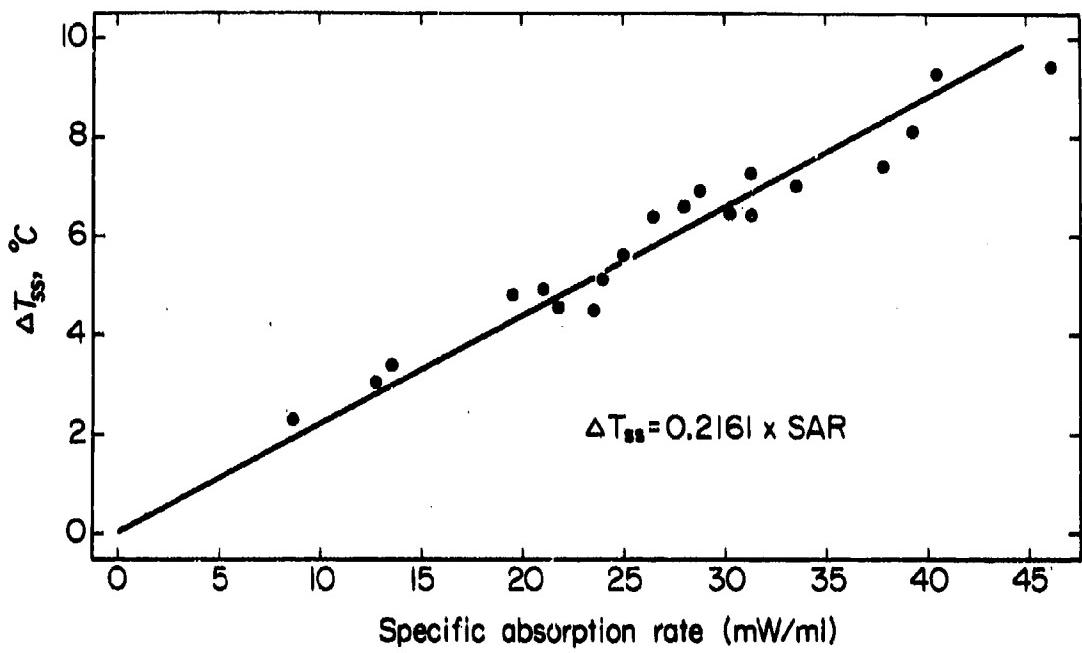
Figure 5. Steady-state temperature increment in waveguide exposure facility ($T_{air} = 24°C$).
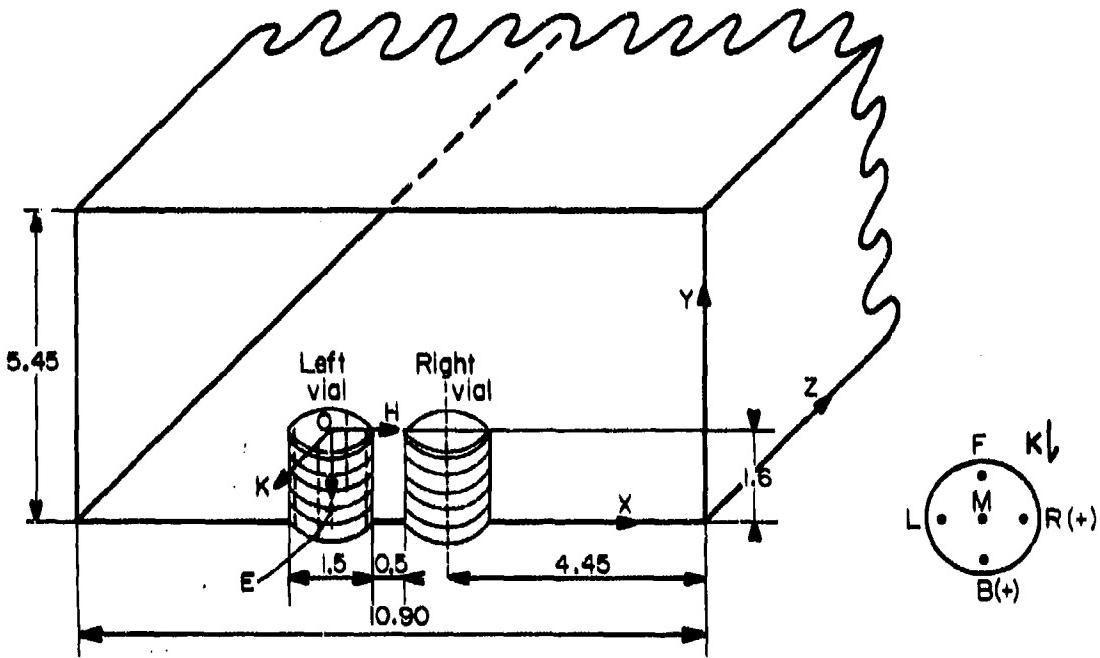
Figure 6. Locations within culture vial used for determination of SAR
profile. (Dimensions are in 1 cm.)
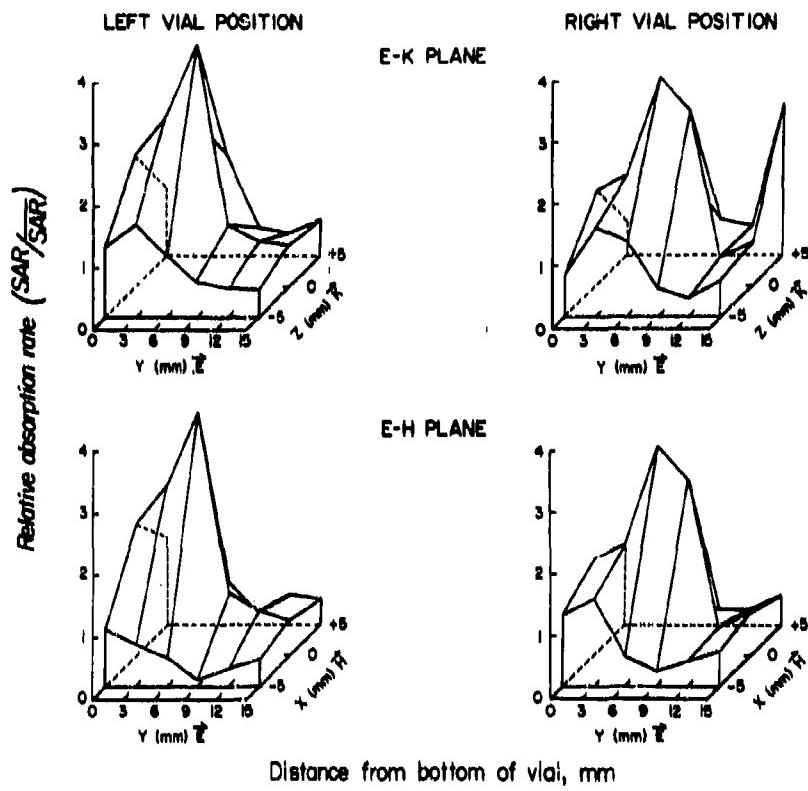
Figure 7. SAR profile in muscle phantom. Forward power=0.55W. N=30.
Left vial average SAR $\pm$ S.D.=76 $\pm$ 64 mW/ml. Right vial average
SAR $\pm$ S.D.=59 $\pm$ 46 mW/ml.
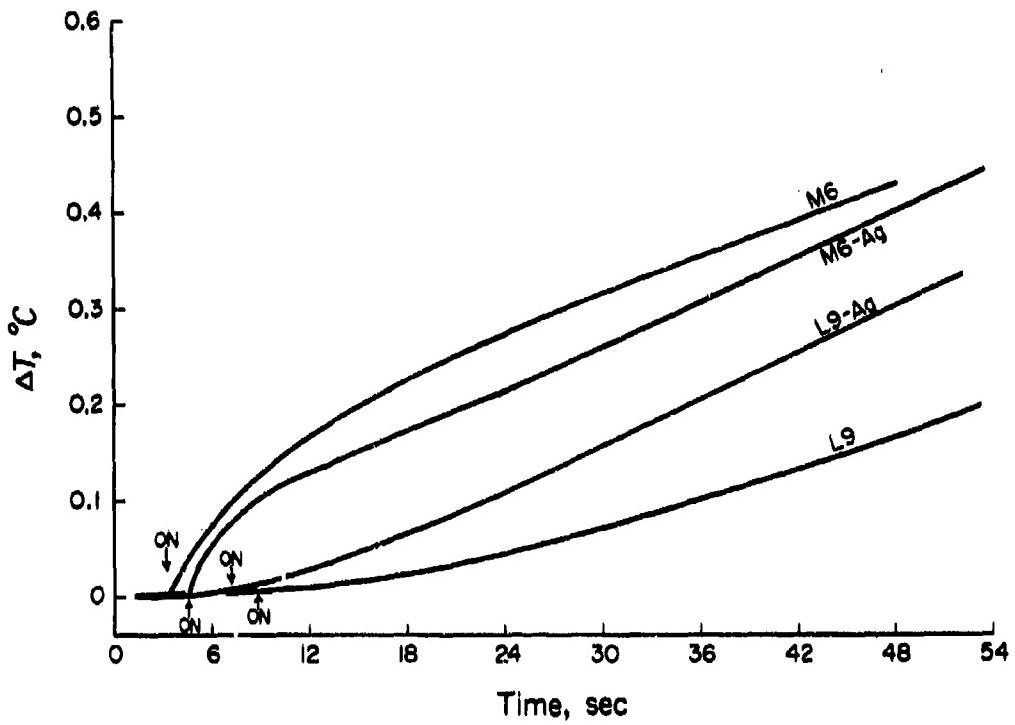
Figure 8. Effect of agitation on temperature tracings of exposed sample. L9 is the point of lowest SAR and M6 is the point of highest SAR (see Figure 7). Ag indicates that agitation was applied.

Figure 9.   Determination of average SAR (summary).

# EFFECTS OF RFR ON EXCISION-TYPE
# DNA REPAIR IN VIVO

R.F. Brown, S.V. Marshall, and C.W. Hughes
Depts. of Life Sci.(RFB), Elec. Engr.(SVM), and Psychology(CWH)
University of Missouri-Rolla
Rolla, MO 65401

# I. INTRODUCTION

A limited number of investigations of RFR bioeffects have focused on chromosomal damage and repair, genetic responses, and related parameters. Exposure of mice to 2.45 GHz (CW) has been reported to have no discernible effects on either the frequency of sister chromatid exchanges in bone marrow [1] or the incidence of chromosome aberrations in lymphocytes [2]. In addition, lymphocytes cultured from 2.45-GHz irradiated mice have shown no evidence of RFR-induced DNA repair. These findings, together with similar negative data from bacterial systems [3,4], suggest that the RFR frequencies tested have no direct effects on DNA that may be genetically expressed. They do not, however, rule out genetic responses resulting from RFR inhibition of some enzymatic mechanism, a mechanism such as DNA repair, for example. Indeed, some enzymatic processes have been reported to be partially inhibited by RFR. These include DNA replication in cultured cells irradiated at 1.0 GHz [5] and hydrolysis of creatine phosphate in rat brain exposed to 591-MHz RFR [6].

This study was conducted to determine if exposure of mice to RFR at 400 MHz (CW) would partially inhibit excision repair of lesions induced by treatment of the animals with streptozocin (STZ), a mutagenic/carcinogenic agent known to damage DNA in the rodent liver [7]. The rationale for this investigation was that somatic cells of personnel exposed to RFR might be subjected to chromosome damage by known mutagenic hazards present in the environment if RFR should affect one or more DNA repair mechanisms. The physiologic importance of repair is underscored by the high incidence of cancers in individuals with inherited deficiencies in various DNA repair processes [8].

185

Assay of excision repair involved density- and isotopic-labeling of DNA in the intact animal followed by isolation of liver nuclei and isopycnic centrifugation to separate repair and semiconservative replication. The amount of STZ given to the mice increased DNA repair activity in the liver to about 8-fold above the baseline level. We report here that the levels of repair maintained by animals treated with STZ and then exposed to 400-MHz RFR at incident power densities of 1.6 mW/cm$^2$ and 16 mW/cm$^2$ - or  SAR levels of 0.41 W/kg and 4.1 W/kg, respectively, for E polarization - were the same as that in the liver of animals that were sham irradiated after the STZ treatment.

## II.  TECHNICAL APPROACH

### Mice

Female strain CD-1 mice were purchased from Charles River Laboratories. The animals were group housed with free access to food and water. Weights of the mice used during the course of this investigation ranged from 22 to 29 g. Animals used in each replicate experiment were matched in weight (within ± 10%) and age.

### RFR Exposure System

The RFR facility used in this investigation, patterned after the system designed by Allen et al. [9], included a Narda Model 8801 transverse electro-magnetic mode (TEM) chamber with CW power supplied by an Epsco Model EP250C source. A mock exposure chamber constructed to match the interior of the TEM chamber was used for sham irradiation. For each experiment, six animals were positioned parallel to the E-field in each chamber, three on either side of the center conductor. Room air was forced through the two chambers at a flow rate of about 26 m/min. Temperature of the airflow was maintained at 30.5 ±

$0.2^O$ C except where stated otherwise. The RFR facility is diagramed sche-
matically in Fig. 1, and a photographic view of the TEM and sham chambers is
given in Fig. 2. Effects of RF and sham irradiation on core temperature were
tested with the Vitek Model 101 Electrothermia Monitor.

## Dosimetry

Whole-body average SAR values were calculated from power meter recordings
of forward, reflected, and transmitted power as described in the Radiofrequency
Radiation Dosimetry Handbook, 3rd ed. [10]. Subjects for these measurements
included live mice in specially constructed Plexiglas restraining cages [11],
mouse cadavers placed either in the Plexiglas restrainers or on Styrofoam
sheets, and 2.5-cm x 7.6-cm prolate spheroid models prepared to simulate the
dielectric properties of muscle [12]. SAR measurements were performed over a
range of 200 to 475 MHz.

The SAR values calculated from power meter readings for mouse cadavers
positioned on Styrofoam were compared with SAR values obtained for the same
subjects by Dewar-flask calorimetry, performed essentially as outlined in the
Radiofrequency Radiation Dosimetry Handbook, 3rd ed. [10]. A dry cadaver
equilibrated to room temperature was placed in a complementary-shaped cavity
of a Styrofoam block, positioned parallel to the E-field, and irradiated
10 min at 400 MHz with an incident power level of 46 mW/cm$^2$. The cadaver was
then immediately transferred to a Dewar flask of known heat capacity con-
taining 35 ml of water ($1.0^O$ C below ambient). The sealed flask was peri-
odically shaken until thermal equilibrium was attained. Temperatures were
monitored with the Vitek 101 probe.

Absolute power density in the TEM chamber was measured with a Narda 8623
probe. Relative power densities at positions occupied by the test animals
were determined with a General Microwave RAHAM probe.

## Quantitation of Excision Repair

It was necessary in this study to intravenously administer labeled precursors concomitant with 400-MHz irradiation of the test animals. In preparation for this, mice were placed in Plexiglas restrainers and a lateral tail vein was cannulated with Teflon tubing (no metal needles left in place) as described elsewhere [11]. The cannulae were connected with a syringe pump set to deliver 0.2 ml/h, and the animals then positioned parallel to the E-field in the TEM and the sham chambers, six animals per chamber.

The assay involved infusion of three solutions given in immediate succession. First, $10^{-2}$ BrdU was administered to the mice for 2 h to density-label replicating DNA. Then a solution of $10^{-2}$ M BrdU plus [$^3$H]TdR (100 µCi/ml) was infused for 4.5 h. Finally, $10^{-2}$ BrdU was given for 1 h. To induce excision repair, STZ dissolved in 0.15 M NaCl-0.015 M NaCitrate (pH 4.2) was injected iv at a dosage of 90 mg/kg 10 min after commencing infusion of the BrdU-[$^3$H]TdR solution. RFR exposure was initiated 15 min after the STZ injection and was continued for the remaining 4 h of the BrdU-[$^3$H]TdR infusion. At the end of the third and final infusion, the animals were sacrificed by air injection, livers were removed, and crude nuclei were isolated. The infusion protocol is represented on Fig. 3.

Nuclei were lysed by mixing with an alkaline detergent solution. The resultant lysate was sheared by passage through a 23-gauge needle and then mixed with NaI-0.1 N NaOH to a final density of 1.550 g/ml and a volume of 21.5 ml. Centrifugation was for 48 h at 34,000 RPM and 20° C in the Beckman 42.1 fixed-angle rotor.

The peak of $^3$H-DNA formed by excision repair was recovered from the developed gradients by visible marker/syringe withdrawal procedure to be

described in detail elsewhere [13]. Briefly, the recovery technique involved piercing the side of the gradient tube with an 18-gauge needle attached to a 5-ml syringe at a point identified by a visible density marker to aspirate a single 4.8-ml volume containing the excision repair product. An aliquot of this volume was mixed with cold trichloroacetic acid and the precipitate collected on a filter. The filter was dried and placed in 5 ml of toluene-PPO liquid scintillation solution for determination of acid-insoluble radioactivity. DNA was precipitated with TCA from a second aliquot and measured colorimetrically by reaction with diphenylamine.

During the initial phases of the study, some of the developed gradients were fractionated by collection of 23 fractions from the bottom of the tube. Each fraction was analyzed for acid-insoluble radioactivity and diphenylamine-positive material.

## Statistical Analysis of Results

A $t$-test for independent groups [15] was utilized to compare the mean of the levels of DNA repair in RFR-exposed animals with the corresponding mean of the sham animals of each experiment. Individual values that differed from the group mean by $\geq 2x$(s.e.m.) were excluded from the calculation of the group mean. A one-way analysis of variance [15] was used to assess replication differences. The Scheffe' post hoc mean comparison [15] was performed where appropriate.

## III. RESULTS

Measurements were made of absolute and relative power densities in the empty TEM chamber. Relative power densities were uniform, within 0.8 dB, over a frequency range of 200 MHz to 475 MHz for all six positions occupied by the test animals.

Colonic temperatures of the mice, as recorded with the Vitek 101 probe, were not greatly altered by 400-MHz RFR at the power densities used. Groups of four animals each were restrained and colonic temperatures recorded with the animals initially positioned outside the exposure chambers. Differences of $1.5^o$ C and higher were noted between the four animals of the same treatment group, both immediately before and during the RFR and sham exposures. The mean colonic temperature for each of three RF irradiated groups increased ($\leq 0.2^o$ C) upon exposure to 400 MHz at 16 mW/cm$^2$, while the corresponding means of the sham groups did not. Despite this trend, the differences were not significant.

Several tests were also performed to determine how the animal's core temperature would respond to variation of the temperature of the air ventilating the TEM and sham chambers. Mean colonic temperatures remained relatively constant with ventilation temperature maintained at $30.5^o$ C. With most of the animals tested, decreasing the temperature of the air flow to $29.5^o$ C resulted in a slight drop in colonic temperature (about $0.1^o$ to $0.4^o$ C), although the drop did not prove to be significant. Nevertheless, we inferred from our data that a $1.0^o$ C difference in air flowing through the TEM and sham chambers would compensate for a slight RF heating effect. Thus, during RFR exposures at 16 mW/cm$^2$, the air temperature of the TEM chamber was adjusted to $29.5^o$ C as shown in Fig. 3. There was no indication of any elevation of core temperature at 400-MHz exposures at 1.6 mW/cm$^2$. For exposures at that power density, air temperature was maintained at $30.5^o$ C.

The means of the whole-body SAR values calculated from power meter readings obtained during the ten repair experiments for mice exposed to 400 MHz

were 4.1 W/kg and 0.41 W/kg for 16 mW/cm$^2$ and 1.6 mW/cm$^2$ incident power levels, respectively. Normalized to 1 mW/cm$^2$, the mean SAR was 0.25 W/kg/mW/cm$^2$ for mice in the Plexiglas restraining cages. SAR values were also determined for mouse cadavers. Results obtained over a frequency range of 200 MHz to 400 MHz with cadavers positioned in the Plexiglas restrainers or on Styrofoam sheets are shown in Fig. 4. The SAR values for the cadavers in the Plexiglas restrainer were 1.34-fold higher than the values obtained for the same cadavers on Styrofoam. The empty restrainers exhibited no detectable RF absorption over a range of 200 to 475 MHz. Thus, the Plexiglas restrainers appeared to 'focus' the RFR, resulting in increased RF absorption by the test subjects.

Dewar calorimetry was used as an alternate method of determining SAR. The mean of the SAR values determined calorimetrically for five cadavers was 0.18 W/kg/mW/cm$^2$ (Fig. 4) versus a mean of 0.20 W/kg/mW/cm$^2$ calculated for the same subjects from power meter readings.

Fig. 4 also includes SAR values calculated from power meter readings for prolate spheroid models of a large mouse. The solid line in Fig. 4 was redrawn from a portion of the curve depicting SAR values of the large-mouse model presented in the Radiofrequency Radiation Dosimetry Handbook, 2nd ed. [12]. Clearly, the SAR values obtained in this investigation for the prolate spheroid models agree with the Handbook values for similar subjects.

Dose-response experiments were performed to determine the levels of repair induced in the mouse liver by iv injection of various dosages of STZ. Excision repair activity increased as a function of STZ dosage as shown in Fig. 5. A comparison of repair levels induced by increasing dosages of STZ, as determined by fractionation and syringe withdrawal techniques, is presented in

191

Table I. Very similar values were, as shown, obtained by the two different procedures, indicating that the visible marker/syringe withdrawal procedure is a reliable method of routinely measuring in vivo excision repair. The highest dosage of STZ tested, 90 mg/kg, increased excision repair activity in the mouse liver to about 6-8-fold above baseline.

Effects of RFR or sham exposure on repair of liver DNA damage induced by STZ, 90 mg/kg, are summarized in Fig. 6 and Table II. In none of the ten RFR/repair experiments was a significant RFR-sham difference found, either at the 0.41 W/kg or the 4.1-W/kg power absorption level. Significant replication differences were found for the replications of the 0.41-W/kg RFR treatment [$F_{(4,25)}$=4.64, p=0.006] and its corresponding sham-exposure treatment [$F_{(4,25)}$= 5.31, p=0.003]. These replication differences may reflect a slight change in [$^3$H]TdR specific activity or some other similar factor. In any case, it is important to note that within each experiment the mean repair synthesis values obtained for the RF- and sham-irradiated animals were essentially the same.

## IV.  SUMMARY AND CONCLUSIONS

The SAR values for the mice used in this investigation, as calculated from power meter readings of forward, reflected, and transmitted power, were about twice the theoretical values [12]. The accuracy of these SAR values is directly supported by the Dewar calorimetry results and indirectly supported by the similarity between the SAR data determined here for prolate spheroid models and the values reported for the same size and type of models exposed to the    same RF parameters [12]. The differences between the SAR values of the mouse and the prolate spheroid model may reflect geometric differences as discussed elsewhere [9,15]. Additional measurements at frequencies above 500 MHz would be required to determine if the twofold difference between the

192

SAR values of the mouse and the prolate spheroid model are unique to the frequency range tested in this project.

The premise of this investigation was that RFR might inhibit one or more enzymes involved in DNA repair, as has been reported for other enzyme systems [6]. We found, however, that exposure of mice to 400 MHz CW at incident power densities of 1.6 and 16 mW/cm$^2$ did not alter the level of excision repair of damaged hepatic DNA induced by treatment of the animals with STZ. We may, with caution, infer from these results that humans exposed to RFR, at frequencies and power densities similar to those used here, are not subject to greater-than-normal risk of chromosome damage by some of the mutagenic hazards present in the environment. This inference is based, in part, on evidence that absorption of 400-MHz radiation by ellipsoidal human models is about half that of prolate spheroid models of mice, with both subjects oriented in the E-field [12]. This assumes, of course, that risk is a function of RF power absorption. Also, a large number of endonucleases appear to be involved in recognition and removal of lesions induced by the various types of mutagens. [17]. Hence, the results obtained here are, perhaps, applicable only to those mutagenic agents which induce lesions similar to those resulting from the STZ treatment.

## V. REFERENCES

1. McRee, D.I., and G. MacNichols, "Incidence of sister chromatid exchange in bone marrow cells of the mouse following microwave exposure." Radiat. Res. 85: 340-48, 1981.

2. Huang, A.T., M.E. Engle, J.A. Elder, J.B. Kinn, and T.R. Ward, "The effect of microwave radiation (2450 MHz) on the morphology and chromosomes of lymphocytes." Radio Sci. 12: 87-96, 1977.

3. Blackman, C.F., M.C. Surles, and S.G. Benane, "The effect of microwave exposure on bacteria: mutation induction," pp. 406-413. In Biological Effects of Electromagnetic Waves, Vol. 1 (C. Johnson and M. Shore, eds.), HEW Pub. (FDA) 77-8010, 1977.

4.  Dutta, S.K., M.A. Hossain, H.S. Ho, and C.F. Blackman, "Effects of 8.6 GHz pulsed electromagnetic radiation on an Escherichia coli repair-deficient mutant," pp. 76-95. In Proceedings of 1978 Symposium on Electromagnetic Fields in Biological Systems (S.S. Stuchly, ed.), 1978.

5.  Chang, G.K., A.T. Huang, and W.T. Joines, "Inhibition of DNA synthesis and enhancement of the uptake and action of methotrexate by low-power-density microwave radiation in L1210 leukemia cells." Cancer Res. 40: 1002-1005, 1980.

6.  Sanders, A.P., D.J. Schaefer, and W.T. Joines, "Microwave effects on energy metabolism of rat brain." Bioelectromagnetics 1: 171-182, 1980.

7.  Petzold, G.L.,and J.A. Swenberg, "Detection of DNA damage induced in vivo following exposure of rats to carcinogens." Cancer Res. 38: 1589-94, 1978.

8.  Setlow, R.B., "Repair deficient human disorders and cancer." Nature (London) 271: 713-717, 1978.

9.  Allen, S.J., W.D. Hurt, J.H. Krupp, J.A. Ratliff, C.H. Durney, and C.C. Johnson, "Measurement of radio-frequency power absorption in monkeys, monkey phantoms, and human phantoms exposed to 10-50-MHz fields." USAF School of Aerospace Medicine, Aerospace Medical Division (AFSC), Brooks AFB, TX 78235, Report SAM-TR-76-5.

10. Durney, C.H.,M.F. Iskander, H. Massoudi, S.J. Allen, and J.C. Mitchell, "Radiofrequency Radiation Dosimetry Handbook (3rd edition)." USAF School of Aerospace Medicine, Aerospace Medical Division (AFSC), Brooks AFB, TX 78235, Report SAM-TR-80-32.

11. Brown, R.F., C.W. Hughes, and S.V. Marshall, "A procedure for continuous intravenous infusion of rodents during exposure to microwave radiation." Laboratory Prac. 30: 466, 1981.

12. Durney, C.H., C.C. Johnson, P.W. Barber, H. Massoudi, M.F. Iskander, J.L. Lords, D.K. Ryser, S.J. Allen, and J.C. Mitchell, "Radiofrequency Radiation Dosimetry Handbook (2nd edition)." USAF School of Aerospace Medicine, Aerospace Medical Division (AFSC), Brooks AFB, TX 78235, Report SAM-TR-78-22.

13. Brown, R.F., "Simplified isopycnic analysis of DNA repair in the intact animal." (in preparation)

14. Li, J.C.R., Statistical Inference, Vol. I, Edwards Brothers, Inc., Ann Arbor, Mich., 1964.

15. Massoudi, H., C.H. Durney, and C.C. Johnson, "Long-wavelength electromagnetic power absorption in ellipsoidal models of man and animals." IEEE Trans. on Microwave Theory Tech. MTT-25: 47-52, 1977.

16. Hanawalt, P.C., P.K. Cooper, A.K. Ganesan, and C.A. Smith, "DNA repair in bacteria and mammalian cells." Ann. Rev. Biochem. 48: 783-836, 1979.
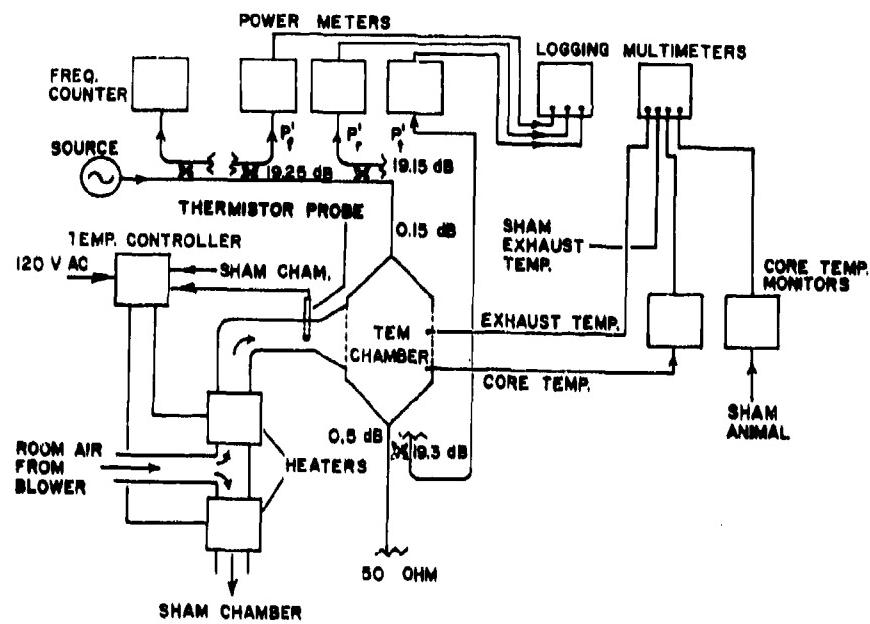
Fig. 1. Schematic diagram of system used for RFR exposure of mice.
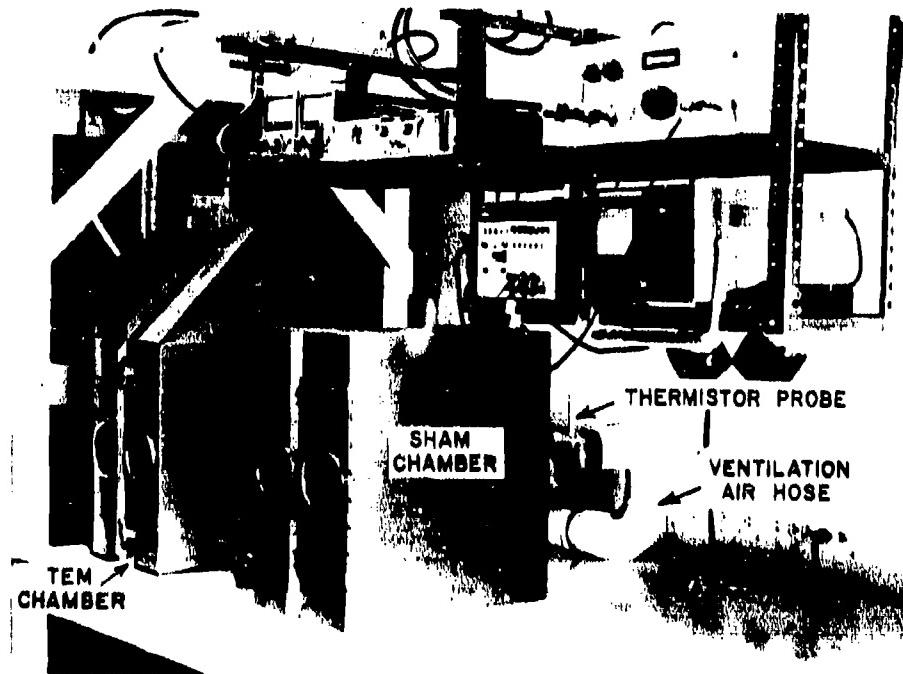


Fig. 2. Photographic view of TEM and sham chambers. Also shown is the hose used to introduce heated air from the back of the chambers. Not shown in the CW source.

195

TIME (h)
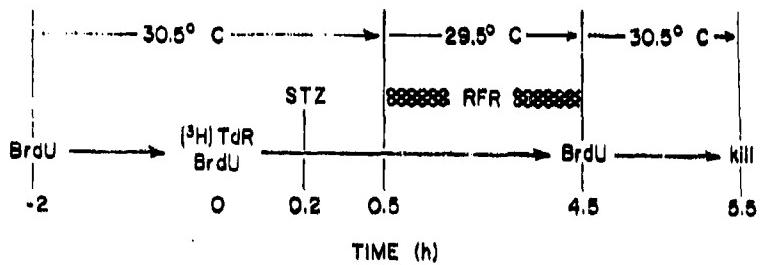
Fig. 3. Protocol for administration of DNA precursors and $RFR_2$ exposure of mice. During the 4-h exposure to 400 MHz at 16 mW/cm$^2$, air temperature in the TEM chamber was reduced to 29.5$^D$ C, as shown here. Air temp was maintained at 30.5$^O$ C for animals irradiated at 1.6 mW/cm$^2$ or sham exposed.



FREQUENCY, MHz
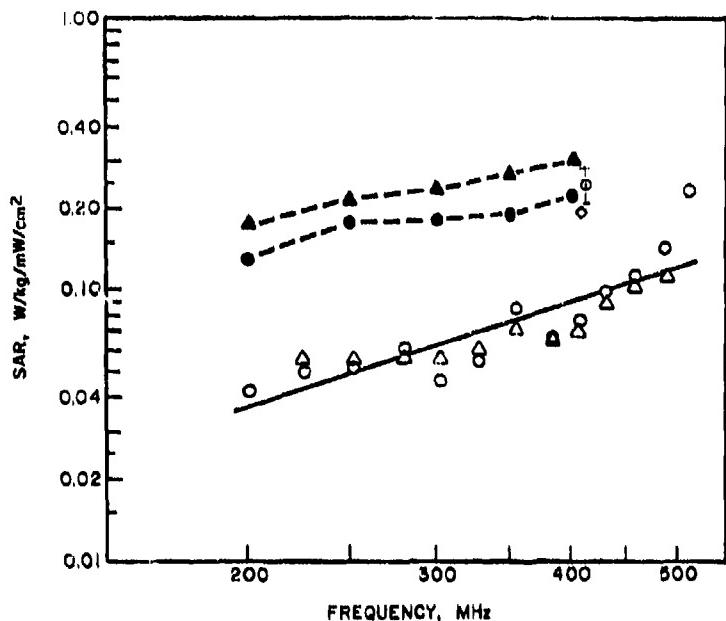
Fig. 4. Summary of SAR values determined for mice and models of mice. (◉) Mean ± s.d. of SAR values calculated from power meter readings for the restrained live mice used in the ten RFR/excision repair experiments performed at 400 MHz. SAR values calculated from power meter readings for four mouse cadavers positioned (▲) in the Plexiglas restrainers or (●) on Styrofoam sheets and irradiated over a range of 200 to 400 MHz. (K' Mean of SAR values determined by Dewar calorimetry for five cadavers irradiated separately at 400 MHz. (O,△) SAR determined from meter readings for two separate preparations of 2.5-cm x 7.6-cm prolate spheroid models of large mice. The solid line was redrawn from values presented by Durney et al. [12] for similar subjects in E-polarization.

196
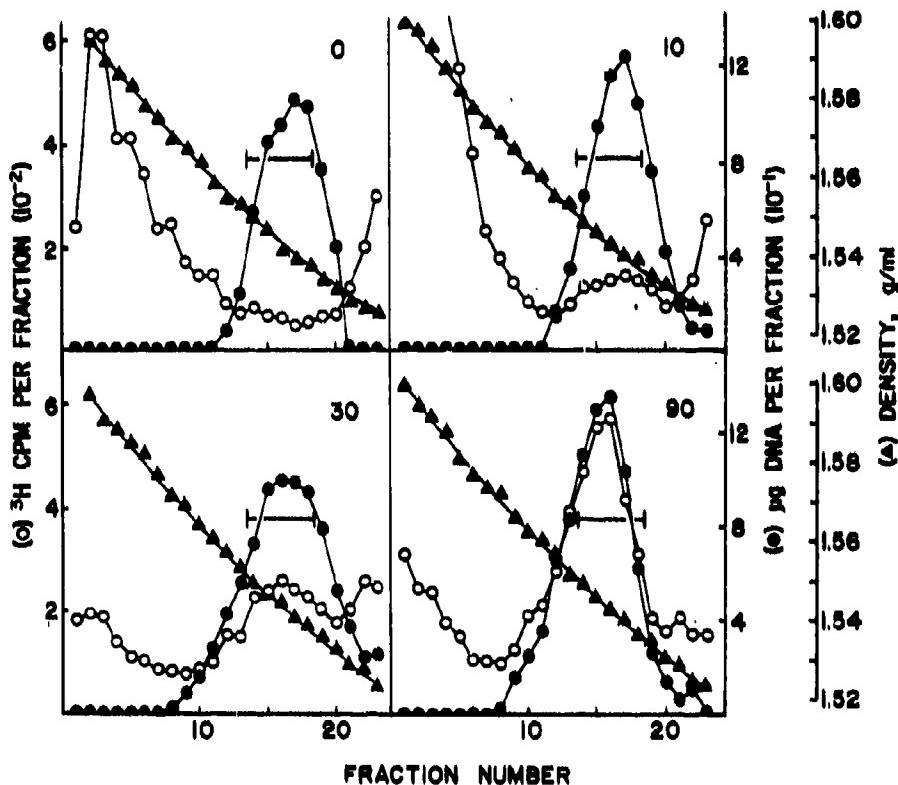
Fig. 5. Density gradient profiles of excision repair of STZ-induced damage of liver DNA in the intact animal. STZ was dissolved in SSC and given iv to mice at dosages of 0 (control animal; given vehicle only), 10, 30, or 90 mg/kg. Labeling with BrdU and [3H]TdR was as described in TECHNICAL APPROACH. Liver nuclei prepared from each animal were lysed and equal amounts placed on two NaI gradients. After centrifugation, 23 fractions were collected from one gradient and assayed (results shown above). The bracketed portion was removed with a syringe from the second gradient and assayed (results presented in Table 6). Numbers in upper right of each panel indicate STZ dosage (mg/kg).
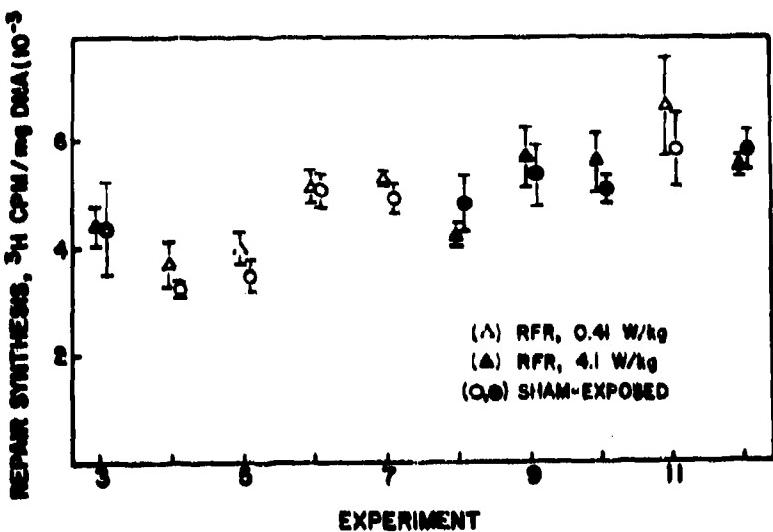
Fig. 6. Comparison of repair synthesis in RFR- and sham-exposed mice. Points represent treatment-group mean values, and vertical bars are standard error of the mean

TABLE I. EXCISION REPAIR OF LIVER DNA DAMAGE INDUCED BY VARIOUS DOSAGES OF STZ: COMPARISON OF SYRINGE RECOVERY AND FRACTIONATION RECOVERY RESULTS.

Syringe withdrawal was used to remove the band of parental density DNA from one set of developed gradients. Values obtained by the fractionation technique represent mean specific activity for fractions 14 to 18 of a second, companion set of density gradients.

| Experiment | STZ dose (mg/kg) | Repair synthesis ($^{3}$H CPM/mg DNA) | |
|---|---|---|---|
| | | Syringe recovery | Fractionation recovery |
| 2 | 0 | 822 | 766 |
| | 30 | 3197 | 3177 |
| | 90 | 5239 | 5301 |
| 3 | 0 | 597 | 655 |
| | 10 | 1124 | 1260 |
| | 30 | 2632 | 2582 |
| | 90 | 4331 | 4492 |

TABLE II.

EFFECTS OF RFR AND SHAM EXPOSURES ON THE LEVEL OF REPAIR OF STZ-INDUCED
DNA DAMAGE IN THE LIVER OF INTACT MICE.

Each value is the mean of results obtained with six RFR-exposed or six
sham-exposed animals. The $\underline{t}$ test comparisons revealed no differences
at the 95% level between the RFR mean and the sham mean within any of the
experiments, either at the 0.41-W/kg or the 4.1-W/kg SAR level. Values in
parentheses are mean weights (g) of the test animals in each group.

| SAR Level W/kg | Expt. No. | Repair Synthesis $^3H$ CPM/mg DNA | |
|---|---|---|---|
| | | RFR Exposed $\bar{x} \pm$ s.e.m. | Sham Exposed $\bar{x} \pm$ s.e.m. |
| 0.41 | 4 | 3678 ± 466 (28.2) | 3173 ± 525 (28.2) |
| | 5 | 3970 ± 329 (26.2) | 3474 ± 326 (26.2) |
| | 6 | 5124 ± 333 (24.3) | 5053 ± 346 (24.8) |
| | 7 | 5269 ± 134 (24.0) | 4935 ± 289 (23.6) |
| | 11 | 6619 ± 1012 (25.9) | 5831 ± 782 (25.7) |
| 4.1 | 3 | 4404[a] ± 370 (28.5) | 4372[a] ± 870 (27.7) |
| | 8 | 4246 ± 221 (22.9) | 4843 ± 571 (23.3) |
| | 9 | 5697 ± 620 (25.2) | 5380 ± 632 (25.0) |
| | 10 | 5623 ± 594 (25.5) | 5104[b] ± 260 (25.8) |
| | 12 | 5512 ± 214 (26.5) | 5841 ± 403 (26.0) |

a - mean of four values only; two samples lost
b - mean of five values; one value excluded (>2xs.e.m.)

## VI. PAPERS AND PRESENTATIONS RESULTING FROM CONTRACT WORK.

Papers (accepted or in revision):

Brown, R., C. Hughes, and S. Marshall, "A Procedure for Continuous Infusion of Rodents During Exposure to Microwave Radiation," Laboratory Practice 30: 466, 1981.

Brown R., "A Simplified Isopycnic Procedure for Measurement of Excision Repair of Hepatic DNA In Vivo" (submitted to Mutation Research; returned for revision; revised manuscript prepared).

Presentations (presented or scheduled):

Brown, R., Simplified Isopycnic Analysis on Excision Repair of DNA In Vivo, Environmental Mutagen Society, 12th Annual Meeting, San Diego, Calif., March 6, 1981.

Marshall, S.V., R.F. Brown, C.W. Hughes, and R.L. Thompson, "Experimental Determination of Whole-Body Average Specific Absorption Rate (SAR) of Mice Exposed to 200-400 MHz CW." Scheduled for presentation at 3rd Annual Meeting of Bioelectromagnetics Society, Washington, DC, August 10-12, 1981.

Brown, R., S.V. Marshall, and C.W. Hughes, "Effect of RFR (400 MHz CW) on Repair of STZ-induced Damage of Liver DNA In Vivo." Scheduled for presentation at 3rd Annual Meeting of Bioelectromagnetics Society, Washington, DC, August 10-12, 1981.

Marshall, S., R. Brown, C. Hughes, and P. Marshall, "An Environmentally Controlled Exposure System for Irradiation of Mice at Frequencies Below 400 MHz," (accepted for publication in Proceedings of 1981 IEEE International Symposium on Electromagnetic Compatibility, Boulder, Colo., 18-20, 1981.

Manuscripts in Preparation:

Marshall, S.V., R.F. Brown, C.W. Hughes, and R.L. Thompson, "Measurement of Whole-Body Average Specific Absorption Rate (SAR) in Mice Exposed to 200 to 475 MHz, CW" (to be submitted to Bioelectromagnetics).

Brown, R., S.V. Marshall, and C.W. Hughes, "Effects of 400 MHz (CW) on Repair of Streptozocin-Induced DNA Damage in the Liver of the Intact Animal" (to be submitted to Bioelectromagnetics).

Project Title:
GENETIC EFFECTS OF MICROWAVE EXPOSURE
ON MAMMALIAN CELLS IN VITRO


Project Grant No. F33615-80-C-0607

Manuscript Title:
RFR EFFECTS ON DNA REPAIR MECHANISMS
IN MAMMALIAN CELLS

Martin L. Meltz and Kathleen A. Walker
Division of Radiation Oncology
Department of Radiology
University of Texas Health Science Center
at San Antonio
7703 Floyd Curl Drive
San Antonio, Texas 78284

# I.   Introduction

Theoretical considerations have been proposed (1) which suggest that radiofrequency radiation (RFR) of specific frequencies may be absorbed in small regions of DNA molecules, thereby causing at least momentary perturbations of the DNA molecules.  If this were to be the case, it would suggest the possibility that those metabolic processes in living cells which directly involve DNA might be altered in the presence of a radiofrequency field.

The very fact that energy is being absorbed by a molecule, giving it added motion, is a basic mechanism by which heating takes place.  In this study, the experiments were performed under conditions where (a) the power level employed was sufficiently low so as not to cause a detectable increase in the temperature of the medium during the period of RFR exposure; (b) the temperature of incubation was maintained at 37° C; (c) there was sufficient medium over the cells being exposed so that any heat being deposited in the cells could readily transfer to the surrounding medium; and (d) cells were not allowed to attach to a "hot spot" in the center of the square tissue culture vessel used.

Three metabolic processes in proliferating mammalian cells which directly involve DNA are DNA synthesis, RNA synthesis, and DNA repair synthesis after UV, X-irradiation, or chemical damage of DNA.  Because of their importance to cell survival and the correct passing on of genetic information to daughter cells, DNA synthesis and repair are considered the most important.  Our initial investigations, which are described herein, examine whether or not there are any RFR-induced alterations at selected frequencies and low power levels in the extent of radioactivity incorporated into preexisting cell DNA molecules by the DNA repair process after the DNA is damaged by a selected dose of ultraviolet (UV) light.  The frequencies investigated are 350 MHz and 1.2 GHz; continuous-wave (C.W.) exposure was performed with the former, and C.W. and pulsed-wave (P.W.) exposures were performed with the latter.  The cells which were used in this investigation are normal human diploid MRC-5 fibroblasts which are maintained in vitro in plastic tissue culture flasks.

The DNA repair synthesis process is comprised of a sequence of steps which occur after UV light produces thymine dimers in the DNA of exposed cells.  These steps include:

1)   Recognition of the altered (damaged) bases;
2)   Nicking of the DNA strand (to cause a break in the DNA strand) close to the thymine dimer;
3)   Excision of a length of DNA (about 100 nucleotides long) including the thymine dimer;
4)   Repair synthesis of the excised region using the complementary undamaged strand as template; and
5)   Rejoining of the end of the repaired region to the preexisting DNA end by action of a ligase.

The experimental technique selected for measuring the repair synthesis is one which is designed for detecting repair in

proliferating cells. It is called repair replication and will detect perturbations which might occur in any of the first four steps listed above. The technique involves incubating cells with a DNA precursor, 5-bromodeoxyuridine (5-BrUdR), which if incorporated into a strand of DNA by normal semiconservative DNA synthesis results in an increase in the density of the DNA strand containing it. This in turn allows for the separation of newly synthesized DNA from preexisting DNA after the DNA is isolated from the cells and subjected to alkaline cesium chloride-cesium sulfate density gradient centrifugation.

If the incubation described above is performed with radioactive $^3$H-thymidine ($^3$H-TdR) also present, some of the latter precursor will be used by the cell when it synthesizes its DNA (in place of some of the more abundant 5-BrUdR molecules). The $^3$H-TdR will not affect the density shift, but the newly synthesized DNA will now also be radiolabeled.

If the preexisting DNA in the cells is damaged prior to the incubation with the $^3$H-TdR/5-BrUdR mixture, not only will these molecules be incorporated by normal DNA synthesis, but by repair synthesis as well. In the latter case, however, the amount incorporated per molecule of DNA will be very small (a percentage of each 100-nucleotide-long sequence repaired, depending on the thymine content), and therefore it will not result in a density shift in the much longer DNA molecule that was originally UV damaged. Any radioactivity associated with this nondensity shifted preexisting DNA would be repair-replication-labeled DNA; the amount of radioactivity incorporated would be both UV-dose dependent and repair-labeling-time dependent.

## II. Technical Approach
### A. Exposure Facilities

The exposures in this project were performed at the Radiation Sciences Division, U.S. Air Force School of Aerospace Medicine, San Antonio, Texas.* The 1.2-GHz irradiations were performed in an anechoic chamber. The incubation dishes with the UV-irradiated cells were placed in a specially constructed Plexiglas waterbath (to maintain the incubation temperature at 37° C), with the horn directed downward at the dish. A Cober Electronics, Inc. High Power Microwave Generator (Model No. 1831) was employed. The pulse-wave exposures were performed at 5000 pulses per second, 10 μsec pulse width, with a 0.05 duty factor. For a 1-mW/cm$^2$ average power level, the peak power was 20 mW/cm$^2$; for a 10-mW/cm$^2$ average power level, the peak power was 200 mW/cm$^2$. Dishes with the control cells (non-microwave-exposed) were incubated in a waterbath similar to the exposed cells in the anechoic chamber; the latter was removed from the area of the horn and was surrounded by Eccosorb. Vitek temperature probes were pla d into the medium through holes in the covers of the RFR-exposed and control dishes to allow continuous monitoring of the medium temperature during the repair labeling period. The

*We wish to express our appreciation to Mr. Stewart Allen and his research group for performance of the RFR exposures.

temperature in the medium remained at 37° ± 0.5° C in all of these experiments. The 350-MHz irradiations were performed in a Transverse Electric Mode (TEM) Transmission Cell (NARDA Model No. 8801). A chamber of similar dimensions was constructed for control incubations. Both chambers were fitted with small fans to maximize air circulation within the chambers; the latter were placed inside a larger anechoic chamber serving as a 37° C warm room. An MCL RF Power Generator (Model No. 15022) was employed for the continuous-wave exposures. Vitek probes were used for temperature monitoring as described above. Medium temperatures in the dishes remained at 37° ± 0.5° C in the warm-room air; waterbaths were not necessary to maintain the temperature.

## B. Biological Procedures
### 1) Cell Line

The MRC normal human diploid fibroblast cell line used in these investigations is an "aging" cell line; it was obtained from the American Type Culture Collection (ATCC) and is kept frozen under liquid nitrogen (in sterile ampoules) until experiments are to be performed. Cells are used only at relatively early passage numbers (prior to passage 35). The cells (once thawed) are maintained in the biohazard tissue culture laboratories of the Dept. of Radiology (UTHSCSA) in Basal Minimal Essential Medium (BME) with Hanks Salts; HEPES at 25 mM is added to maintain the pH in an air atmosphere. The concentration of fetal calf serum is 10%; antibiotics are added. On the day preceding a radiofrequency exposure, the required numbers of cells in proliferative growth are transported in T-75 flasks to the 37° C incubator at USAFSAM; that same day the cells in all of the T-75 flasks are trypsinized to prepare a suspension of single cells, and these are distributed in appropriate cell numbers into large square 24-cm x 24-cm sterile dishes (with cover) (NUNC; Southland Cryogenics, Carrollton, Tex.) for exposure on the following day. The numbers of cells seeded are such as to have proliferating cells (nonconfluent cells) in the dishes at the time of UV exposure. A Plexiglas circle is used to prevent cells from attaching at an RFR "hot spot" in the center of the dish.

### 2) Repair Replication Protocol

The standard procedure employed (2) is as follows: One hr prior to UV irradiation, the attachment medium is removed from a dish, and fresh warm medium containing $1 \times 10^{-6}$M 5-fluorodeoxyuridine (FUdR) (to inhibit endogenous thymidine synthesis) and $5 \times 10^{-6}$M 5-BrUdR is added to each dish. After 1 hr of incubation at 37° C in the 37° incubator, this prelabeling medium is aspirated, and the attached cells are washed twice with warm phosphate-buffered saline (PBS) to remove UV-absorbing serum proteins. The cells are immediately UV irradiated in a specially built irradiation chamber (dose rate 1.4 $J/m^2$/sec) (3), and fresh warm repair-replication-labeling medium is added to the dish immediately after UV exposure. This medium contains $1 \times 10^{-6}$M FUdR, $5 \times 10^{-6}$M 5-BrUdR, 12 μCi/ml $^3$H-TdR (53-59 Ci/mM), and 5 mM hydroxyurea (HU). The latter is added to inhibit incorporation by normal semiconservative DNA synthesis. A second dish is similarly UV irradiated and labeling medium added for incubation

as the non-microwave-exposed control. The two dishes are then
incubated for either 1, 2, or 3 hr in or outside of the
radiofrequency field. At the end of this incubation, the labeling
medium is aspirated from the dishes, the attached cells are washed
with warm BME without serum, and fresh medium with $1 \times 10^{-6}$M FUdR
and $5 \times 10^{-6}$M 5-BrUdR is added for a final 1-hr incubation in the
37° C incubator. The cells are then washed with cold salt
solution, scraped free into suspension, pelleted in a tube by
centrifugation, and quick-frozen by immersion of the tube in
ethanol-dry ice. The subsequent steps (2) include a) isolation of
the DNA using an RNase digestion, pronase digestion, chloroform-
isoamyl alcohol extraction procedure; b) dialysis of the DNA
solution to remove aqueous soluble digestion products; c) alkali
cesium chloride-cesium sulphate density gradient centrifugation
(40,000 rpm at room temperature for a minimum of 36 hr); d)
collection of approximately equal volume fractions from the
centrifuge tube with continuous recording of optical density at
254 nm to locate the tubes containing the bulk preexisting DNA;
e) spotting of small aliquots (20 µl) from each fraction on filters
and counting to determine the location of the radioactivity in the
gradient; f) pooling of the gradient fractions containing the bulk
DNA, and recentrifuging as above; g) fractionating these second
gradients as described above, again recording optical density and
determining the cpm in each fraction; h) again pooling the bulk
preexisting DNA (the optical density peak); i) diluting the pooled
material with water, and pelleting the DNA by high-speed
centrifugation; j) resuspending the DNA in a small volume of
low-salt solution; k) determining the DNA concentration (µg/ml) by
a spectrofluorimetric technique and the radioactivity concentration
by adding a small volume to a liquid scintillation counting system
(dpm/ml); and l) calculating the specific activity of the repair-
replicated DNA in dpm/µg.

        3) Temperature-Effect Studies

           These studies were performed using the repair-
replication-labeling protocol described above, except that the
temperature of incubation during the repair-labeling period
immediately following the UV exposure was at 39° C or 42.5° C.
This increased temperature was also maintained during the
subsequent 1-hr chase incubation. These incubations were
performed in a FORMA incubator.


## III. Results
### Preliminary Studies

                Repair Radioactivity Incorporation in MRC-5
                Cell DNA after Increasing UV Exposure

    As shown in Figure 1, the extent of repair radioactivity
incorporated during a 3-hr repair-labeling interval after
increasing UV exposures increases with increasing dose. The
protocol used in this experiment is that described above, except
that $^3$H-5-BrUdR (10 µCi/ml, $5 \times 10^{-6}$M BrUdR) was used in place
of the $^3$H-TdR/5-BrUdR mixture. A significant amount of
radioactivity is incorporated after a UV exposure of 21 J/m$^2$.

Effect of Increased Temperature During the
Repair-Labeling Interval on the Rate of DNA
Repair

This experiment, summarized graphically in Figure 2, was performed as described above after an 8-sec UV exposure (11.2 $J/m^2$) except that round 100-mm petri dishes and $^3H$-5-BrUdR were used. Increasing the temperature during the repair incubation interval from 37° C to 39° C did not affect the incorporated repair radioactivity during the 8 hr of incubation post UV exposure. At 42.5° C, there was an obvious reduction in the amount of incorporated repair radioactivity beyond 5 hr. This could be reflecting hyperthermic killing of the mammalian cells.

The temperature study was repeated using the square exposure dish and the $^3H$-TdR/5-BrUdR repair-labeling mixture for a 39° C incubation as compared to a 37° C incubation after a UV exposure of 21 $J/m^2$ (Figure 3). Again, no effect of 39° C on incorporated repair radioactivity was seen. Since a plateau of incorporated radioactivity after this UV exposure dose (21 $J/m^2$) was observed at 3 hr, this was chosen as the maximum incubation time for further studies.

## Control Studies

Two types of "control" experiments were performed prior to exposing cells to radiofrequency radiation.

A. The first allowed for a determination of the background level of incorporated radioactivity in preexisting DNA (without exposing the cells to UV irradiation), during a 3-hr incubation period at 37° C, with the microwave generator on vs. off. The cells were not exposed to microwaves. The background values were consistently similar; e.g., for 3-hr incubations with the 350-MHz generator on vs. off, they were 83 dpm/μg and 59 dpm/μg; for 1.2 GHz with the generator on vs. off, they were 89 dpm/μg and 80 dpm/μg, respectively.

B. The second allowed for a comparison of the rate/extent of incorporation of repair radioactivity into preexisting DNA after one dose of UV irradiation, during 1- and/or 3-hr incubation periods at 37° C, in the microwave irradiation chamber with the microwave generator on vs. off. The cells were not exposed to microwaves. The values obtained in these experiments were consistently similar at both time points; e.g., for 3-hr incubations with the 350-MHz generator on vs. off, they were 638 vs. 598 dpm/μg; with the 1.2-GHz generator on vs. off, they were 578 vs. 580 dpm/μg.

## Experimental Studies

A. One type of experiment addressed itself to whether or not radiofrequency exposure at each frequency and wave pattern could itself induce DNA repair synthesis (without any prior UV irradiation). When cells were incubated for 3 hr at 37° ± 0.5° C in radiofrequency fields of 350 MHz, C.W., and 1.2 GHz, C.W. and P.W., at an average power level of 10 mW/$cm^2$, no measureable DNA repair synthesis (over non-microwave-exposed control) was detected (e.g., 72 dpm/μg (with 350 MHz C.W.) vs. 76 dpm/μg (no RFR); 48 dpm/μg (with 1.2 GHz P.W.) vs. 68 dpm/μg (no RFR)).

B. The major question posed in this study has been whether or not the DNA repair process is affected if cells are incubated for 1, 2, and 3 hr post UV exposure at 37° ± 0.5° C in continuous- or pulse-wave radiofrequency fields at power levels of 1 or 10 mW/cm$^2$ (average for P.W.).

The results for 1.2-GHz radiation, both during continuous- (Figure 4) or pulsed-wave exposure (Figure 5) at 1 or 10 mW/cm$^2$, is that DNA repair synthesis is <u>not</u> affected in a significantly measurable way. The same statement can be made for 350-MHz C.W. radiation (Figure 6) at 1 mW/cm$^2$. While for the 350-MHz C.W. exposure at 10 mW/cm$^2$ the incorporated repair radioactivity values at each time point are each higher for exposed than for control values, indicating an increased incorporation "trend", the maximum difference is only 25% of control. The significance of this increase would require further study over longer repair times or at a higher power level. We are therefore not yet prepared to conclude, considering the overall variability in our experiments, that there is any affect on DNA repair at 350 MHz C.W. at a 10-mW/cm$^2$ power level.

## IV. Summary and Conclusions

The results of these investigations have to this point not revealed any perturbation of the DNA repair process by 350-MHz C.W. or 1.2-GHz C.W. and P.W. radiofrequency exposures, at power levels of 1 or 10 mW/cm$^2$, when the normal diploid human fibroblast cells are UV irradiated and allowed to carry on DNA repair at 37° C.

These studies are continuing; the radiofrequency exposures will be extended to include 800 MHz C.W. and P.W. Further, the series of experiments will be repeated at the three selected frequencies with the repair-labeling incubation being performed at 39° C. Preliminary experiments in this project indicated that over the 3-hr repair interval, this temperature did not affect the extent of repair radioactivity incorporated (compared to 37° C), while a still higher temperature of incubation (42.5° C) did. The 39° C temperature will thus provide an initial "stress" to the repair process, which may or may not prove synergistic with radiofrequency exposures of up to 10 mW/cm$^2$.

In addition, the studies will be expanded to look for cytogenetic effects under these carefully controlled exposure and incubation conditions; our initial approach will be to look for induction of sister chromatid exchange (SCE) in mammalian cells exposed as described above.

REFERENCES
1.  Prohofsky, E., 1981, "Microwave Absorption by Nucleic
    Acids." (these proceedings)
2.  Meltz, M. L., 1976, "DNA Repair in Baboon Alveolar
    Macrophages:  A System for Assessing Biohazardous Materials."
    Environmental Res. 11:359-366.
3.  Staier, H., and Cleaver, J. E., 1969, "Exposure Chamber for
    Quantitative Ultraviolet Photobiology."
    Lab. Pract. 18:1295.

INCORPORATED REPAIR
RADIOACTIVITY
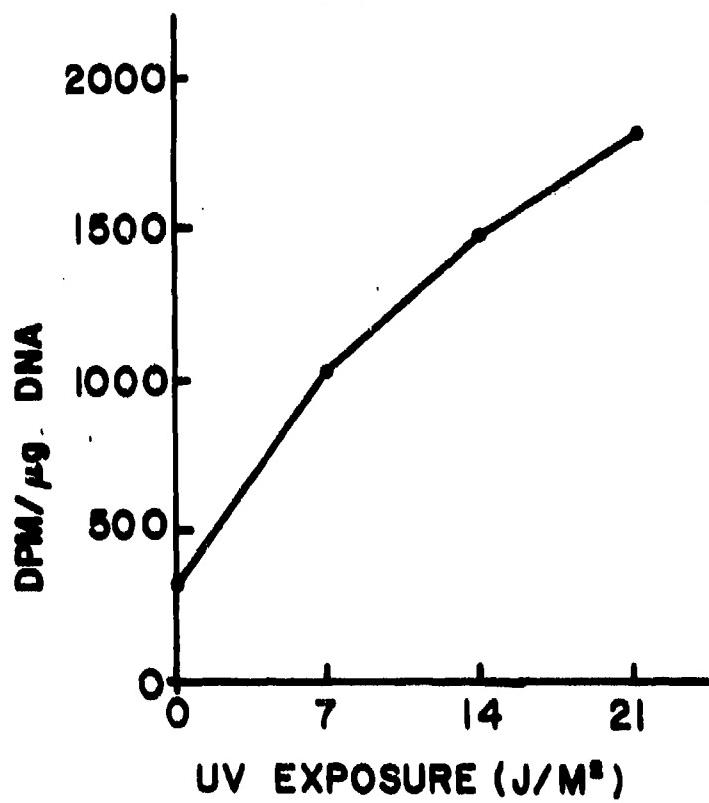
FIGURE 1

FIGURE 2

FIGURE 3

211

FIGURE 4

212

1.2 GHz P.W.

FIGURE 5

213

FIGURE 6

214
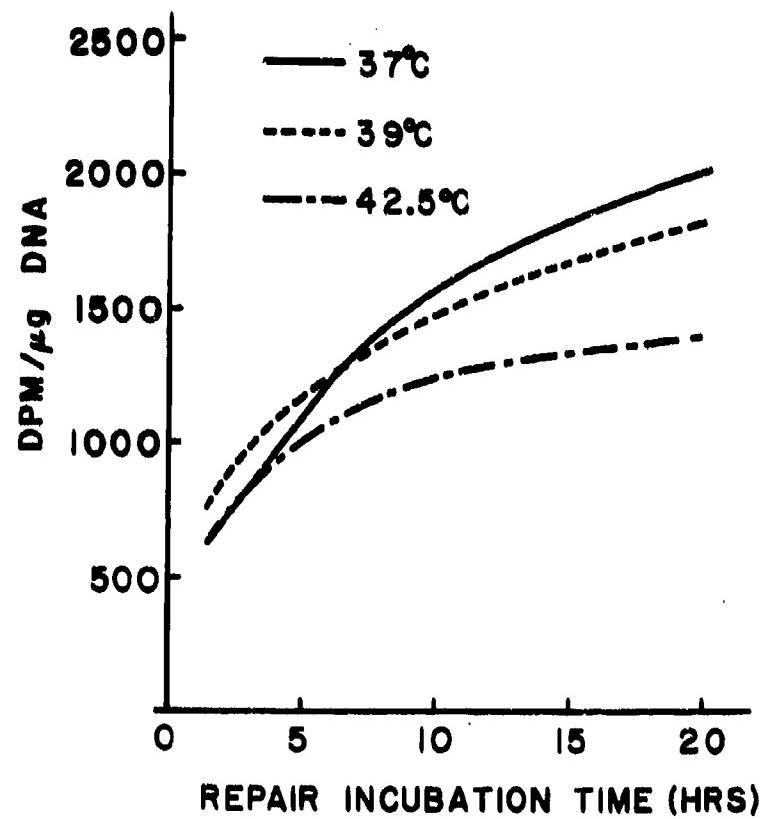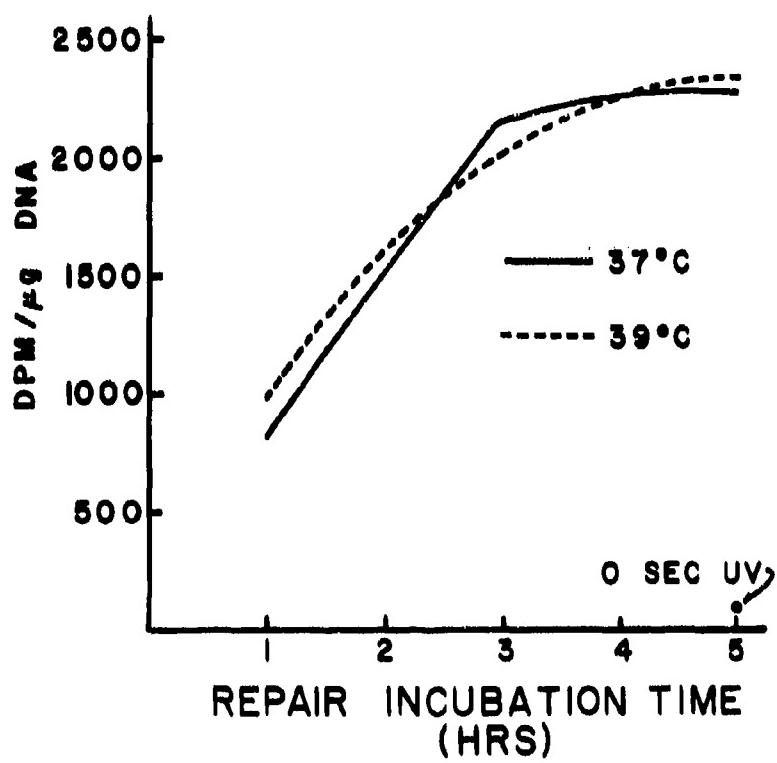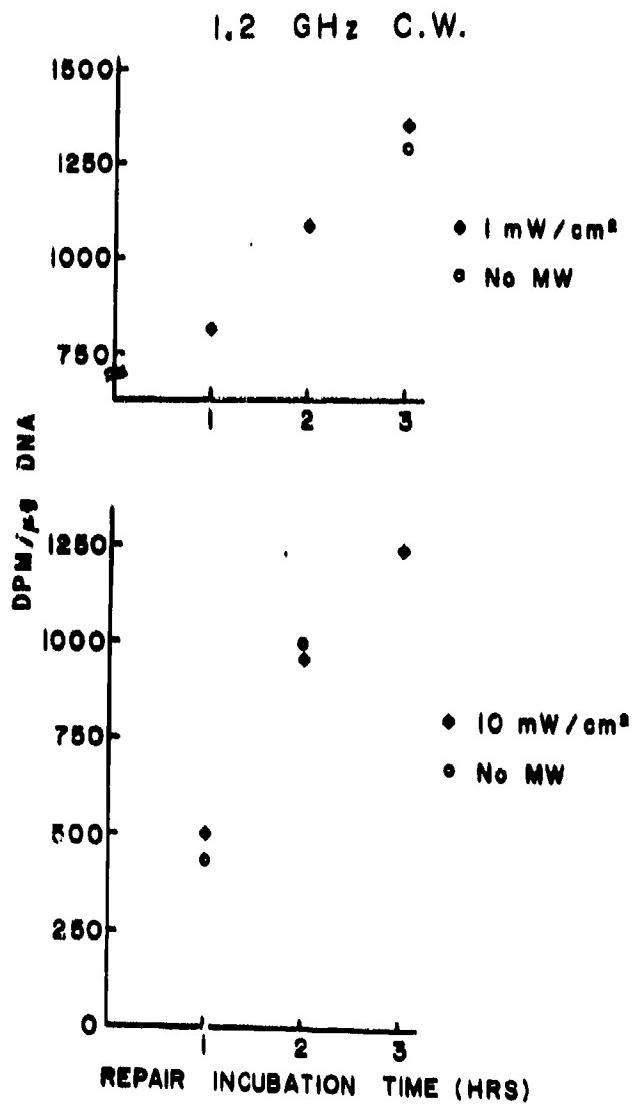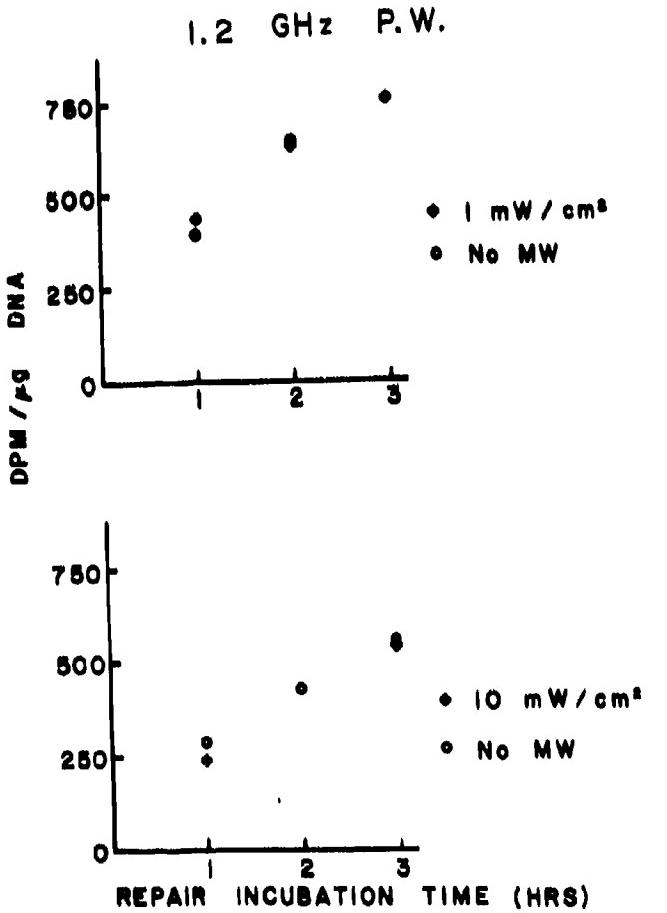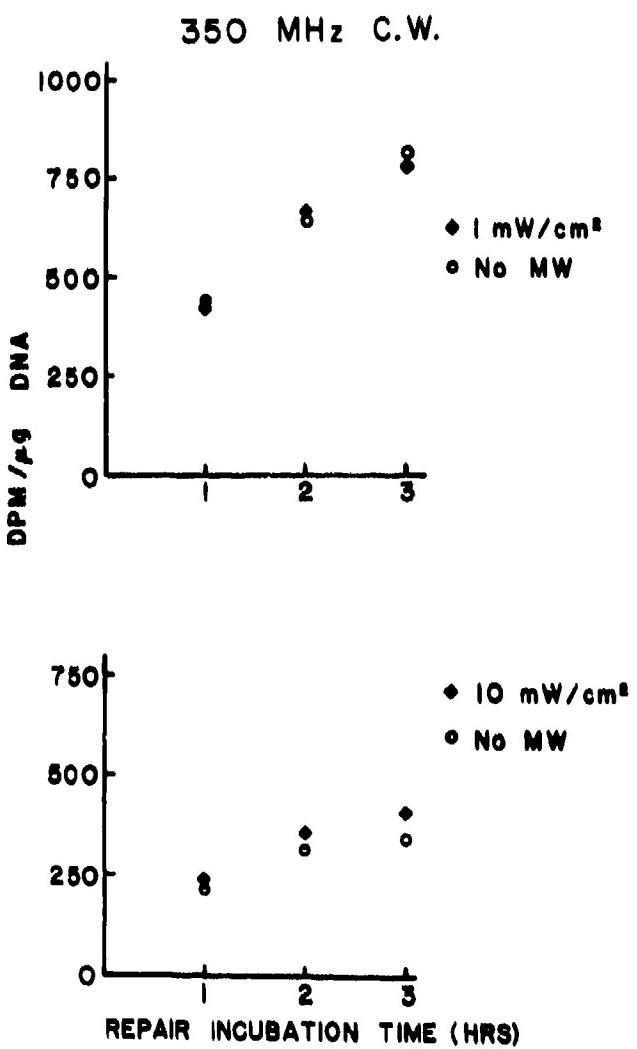
# EFFECTS OF RADIOFREQUENCY RADIATIONS
## ON BIOLOGICAL MEMBRANES

Robert M. Dowben, M.D., and Rosaria B. Haugland, Ph.D.
Baylor University Medical Center Dept. Pathology
Dallas, TX 75246

INTRODUCTION: Early reports, especially from Eastern European researchers, indicate that nonionizing radiations, such as those generated by alternating electrical and/or magnetic fields, particularly high-energy pulsed electromagnetic radiation, may be deleterious to biological systems (1,2,3). These reports have not been confirmed by European and American investigators, who have generally found that there is no measurable effect of microwaves on growth, body weight, and general health of the experimental animal.

Nonionizing radiations have been reported to cause insomnia, restlessness, vertigo, and at high doses even seizures (4). Microwave-exposure-related behavior modifications have been recently confirmed (5,6). In total-body irradiation these functional changes in the nervous system could be due to a direct action of radiofrequency radiations (RFR) on the nervous tissue or to a secondary effect due to changes in metabolism and function of other eventual target organs.

This project focuses on the effects of chronic total-body microwave irradiation at the power of 10 mW/cm$^2$ on cell membranes. Cell membrane function is seminal to the function of excitable tissues such as the nervous system and muscle; it is heavily implicated in carcinogenesis; it is involved in hormonal storage and secretion and in many other cell functions. Thus many of the gross effects of nonionizing radiations could possibly be explained by primary effects on cell membranes.

In collaboration with the Radiation Sciences Division of the USAF School of Aerospace Medicine at Brooks Air Force Base, Texas, we undertook a series of experiments to investigate the effect of "chronic" all-body irradiation with continuous or pulsed microwaves at the power of 10 mW/cm$^2$ on membranes of three major body systems: brain, skeletal muscle, and liver. Function of the membranes was probed by monitoring their major enzymatic or binding activity, and changes in structure were investigated by the use of the fluorescent probes 12-(9-anthroyloxy)-stearic acid (12-AS) and diphenylhexatriene (DPH).

METHODS: Adult male rats (Sprague-Dawley) weighing 250 ± 5g were used in this study. The irradiations were performed for one hour daily for 9 consecutive work days in the first four experiments and prolonged to 16 continuous days in the last two. The irradiation of the rats, held in Plexiglas and Styrofoam containers, with their long axis in the plane of the E field vectors, was performed in an environmentally controlled anechoic chamber maintained at 23 ± 1°C and 50-70% relative humidity. The transmitters used were Cober Electronics,

Inc., Model 1362 for 1.2 GHz frequency and Model 2852 for 2.05 and 2.8 GHz.
The 1.2-GHz exposures were continuous wave or pulsed at 1000 PPS (pulses per
second), 100 $\mu$sec pulse width. The 2.05- and 2.8-GHz exposures were pulsed
mode only, 5000 PPS, 20 $\mu$sec pulse width, and 350 PPS, 2 $\mu$sec pulse width. The
average power density for all exposures was 10 mW/cm$^2$, as measured with a Narda
Model 8316B monitor with Model 8321 isotropic probes. Hewlett-Packard Model
436 A power meters were used to continuously monitor transmitter outputs.
Rectal temperature of all the animals was continuously monitored during experi-
mentation, using Vitek Model 101 non-RFR-interfering temperature probes or
Yellow Springs Instruments, Inc. Model 46 TVC telethermometer with Model 402
thermistor probes.

Sham-exposed and temperature controls were run in parallel. The thermal
controls were placed for 1 hour/day in a Blue M Electric Company Model VP-
100AT-1 controlled temperature and humidity chamber, and their rectal tempera-
ture raised to obtain an equivalent pattern and elevation as the irradiated
rats'. According to the "Radiofrequency Radiation Dosimetry Handbook" (7,8),
under our experimental conditions the specific absorption rate at 1.2, 2.05,
and 2.8 GHz is approximately 2.0-3.0 W/kg for an average power density of
10 mW/cm$^2$.

The rats were sacrificed by decapitation within two hours from the last irradia-
tion. In the first four experiments two rats per group were transported to
Baylor University Medical Center in Dallas and sacrified within a few days to
investigate the possibility that eventual microwave effects are of short
duration and reversible. In later experiments all the animals were sacrificed
at Brooks Air Force Base and membranes prepared on the site and transported to
Baylor, with the remaining tissues, frozen in liquid nitrogen.

BIOCHEMICAL PROCEDURES: Immediately after sacrifice the liver was perfused
through the mesenteric vein with cold saline, and plasma membranes were prepared
and purified according to the procedure described by Lesko et al (9). The liver
plasma membranes were assayed for Na$^+$, K$^+$ATPase, an enzyme involved in maintain-
ing membrane potential, electrolyte balance, conductivity, and active transport,
and for Mg$^{2+}$ATPase. The function of this enzyme is still obscure; it might be
involved in hormone binding or transport (10). Sarcoplasmic reticulum (SR) was
prepared from leg muscles as described by Martonosi and Halpin (11). These
membranes were assayed for Ca$^{2+}$ATPase, which is responsible for accumulating
calcium and releasing it for the myofibrils at the onset of muscle contraction.
This enzyme might also be involved in energy production by regulating the Ca$^{2+}$
concentration necessary for the activation of creatine kinase and phosphorylase
b kinase. ATPase activity was assayed at 36$^0$C by a spectrophotometric method in
which the oxidation of NADH is monitored (12). The activity of Na$^+$K$^+$ATPase was
calculated as the amount of ATP hydrolysis which is inhibited by 0.1mM ovabain.
The activity of Ca$^+$ATPase of SR was corrected for the very small basal Mg$^{2+}$ATPase
activity measured in absence of calcium.

Brain synaptosomes were prepared from a crude mitochondrial fraction isolated
from brain homogenate by differential centrifugations (12). Part of the crude
fraction was used for the determination of acetylcholine muscarinic receptors.
The rest was fractionated on a discontinuous Ficoll-500 gradient. The concen-
tration of muscarinic receptors was determined by the procedure of Yamamura
and Synder (14) in which a fixed aliquot of membranes (100 $\mu$g protein) were incu-
bated for one hour at room temperature, in the presence of increasing concentra-
tions of quinuclidylbenzylate (QNB). The mixtures were then filtered through

216

Whatman GF/f filters, the filters rinsed with buffer and treated with 2% sodium dodecylsulfate (SDS) before counting in a standard scintillation fluid. The binding site concentration and affinity of the drug for the receptors were evaluated from a Scatchard plot, after correcting for nonspecific binding. Nonspecific binding was measured by adding atropine or cold QNB (a gift from Dr. W. E. Scott of Hoffman-LaRoche) to the incubation mixture. Acetylcholinesterase activity was measured as in Ellman et al (15).

The protein pattern of all the membranes in study was routinely analyzed by slab SDS-polyacrylaminde gel electrophoresis performed according to Ames (16). Protein was assayed by the Lowry's system after dissolving the membranes in SDS.

FLUORESCENCE STUDIES: Fluorescence spectroscopy studies to investigate properties of the structure of membranes consist in allowing a small fluorescent compound to diffuse into the membrane or to bind covalently to specific constituents. Changes in basic fluorescence parameters such as fluorescence intensity, excitation and/or emission spectra, fluorescence lifetime, or polarization anisotrophy provide information on the microenvironment of the membrane in which the probe is located. Microviscosity, lateral diffusion, localized pH, and transmembrane or surface potential can be measured by this method (17). In fluorescence polarization measurements restriction of freedom of rotation by an increase in viscosity of the environment results in a higher value for the fluorescence polarization p (18,19).

Fluorescence experiments were performed at pH 7.5 and room temperature. In most experiments membrane protein was 100 $\mu$g/ml and the florescent probe 12-AS or DPH 1 mM, maintaining the molar ration 12-AS/lipids of the order of 1/200 (12). Incorporation curves of the probe together with emission and excitation spectra were obtained on a Farrand Mark I spectrofluorimeter. Polarization was measured with a photon-counting apparatus built in our laboratory. The excitation wavelength was 260 nm, and the emission was determined by two 400-nm cutoff filters. Polarization of the fluorescence was calculated according to the formula

$$p = \frac{(I_{||} - I_{||}^S) - (I_{\perp} - I_{\perp}^S)}{(I_{||} - I_{||}^S) + (I_{\perp} - I_{\perp}^S)}$$

which corrects for membrane scattering ($I^S$) in absence of the probe.

RESULTS: The average elevation in rectal temperature in the irradiated and temperature control rats was $1.5 \pm 0.6^\circ C$. Except for the first two days of experimentation, no difference in increase in body weight was detected among the experimental groups.

As Table 1 shows, acetylcholinesterase activity in crude mitchondrial fraction and purified brain synaptosomes was unaffected by microwave irradiation or temperature elevation. Also the number of muscarinic receptors or their affinity for QNB (Table II) appeared unchanged. These results indicate that alteration in synaptic function is probably not implicated in the microwave-related behavior modifications reported in the literature.

217

No significant differences were found in either the Na$^+$, K$^+$ATPase (Table III) or the basal Mg$^{2+}$ATPase activities (Table IV) of liver plasma membranes from the various experimental groups. Preliminary results from rats irradiated for 16 days with very narrow pulses did not show differences except in the Mg$^{2+}$ATPase activity of the thermal control group.

The Ca$^{2+}$ATPase activity of SR (Table V), the major enzyme responsible for regulating the free calcium concentration in skeletal muscle, was not significantly altered by total-body microwave exposure. Preliminary results from rats irradiated for 16 days indicated, however, that the activity of this enzyme might be increased by periodic elevation in body temperature.

SDS-Gel electrophoresis of membrane proteins did not show any alteration in pattern among the experimental groups.

We used 12-(9-anthroyloxy)-stearic acid (12-AS) and diphenylhexatriene (DPH) as selective probes to investigate the hydrophobic microenvironment of membranes to detect eventual changes in structure due to microwave irradiation.

In Table VI we report the fluorescence polarization value (p) of 12-AS in synaptosomes, liver plasma membranes (LPM), and sarcoplasmic reticulum (SR). No differences in p value, and consequently in membrane fluidity, was found in the irradiated group when compared with shams and thermal controls. The latter group exhibited a lower p value for SR, indicating that temperature changes affect the fluidity of these membranes. In preliminary experiments, however, with membranes from rats irradiated for 16 days, no significant differences in p value were found among the experimental groups, using either the fluorescent probe 12-AS or DPH (Table VIII). As expected, considerable differences in p value and, as a consequence, in membrane fluidity were found among the different types of membrane.

SUMMARY AND CONCLUSIONS: Brain synaptosomes, liver plasma membranes (LPM), and sarcoplasmic reticulum (SR) of skeletal muscle were prepared from rats exposed for 9 consecutive work days, 1 hour/day, to all-body microwave irradiation at a power level of 10 mW/cm$^2$. Either continuous or pulsed waves were used. Membranes from sham-irradiated and temperature control animals were prepared in parallel.

For all the experimental groups no significant difference was found in acetylcholinesterase activity of synaptosomal membranes nor in their concentration of muscarinic receptors nor in their binding affinity for quinuclidinylbenzylate.

Na$^+$K$^+$ATPase and Mg$^{2+}$ATPase of LPM and Ca$^{2+}$ATPase of SR were also unaffected by the irradiation.

Using 12-(9-anthroyloxy)-stearic acid and diphenylhexatriene (DPH) as fluorescent probes of the hydrophobic environment of the membranes, we found that the rate of incorporation of the probe, excitation and emission spectra, and fluorescence polarization (p) were practically identical in all experimental groups.

With the reservation that the results presented here for the rats irradiated for 16 days are still in preliminary phase, it is concluded that under the experimental conditions investigated, all-body microwave irradiation at a power level of 10 mW/cm$^2$ does not cause any functional or structural alteration in the cell membranes studied.

PUBLICATIONS AND PRESENTATIONS RESULTING FROM USAF CONTRACT #F33615-80-C-0602:

1. Haugland, R.B., Lin, G.T-I, Burgum, J.C., and Dowben, R.M.: Comparative study of various cellular membranes using fluorescent probes - Presented as poster at the Biophysical Society Meeting 1981, manuscript in preparation.

2. Haugland, R.B., Burgun, J.C., Hardy, K.A., and Dowben, R.M.: Effect of all-body microwave irradiation on rat cell membranes. Submitted to Radiat Res, 1981.

3. Haugland, R.B., Dowben, R.M., and Hardy, K.A.: Effect of all-body microwave irradiation on rat cell membranes. To be presented as poster at BEMS Meeting, August 1981.

REFERENCES

1. Czerski, P., Ostrowski, K., Shore, M.L., Silverman, Ch., Suess, M.J., and Waldesberg, B., Eds, 1974. Biological effects and health hazards of microwave radiation. Polish Med Publ, Warsaw.

2. Johnson, C.C., and Shore, M.I., Eds, 1976. Biological effects of electro-magnetic waves. U.S. Printing Office, Washington, D.C.

3. Baranski, J., and Czerski, P.: Biological effects of microwaves. Strousburg, Pa.: Hutchinson and Ross, Inc. (1976).

4. Michaelson, S.M.: Microwaves and radiofrequency radiation. Copenhagen: World Health Org Rep ICP/CEP 803, 1977.

5. Stern, S.: Neurobehav Toxicol 2, 49-58, 1980.

6. Cabe, P.A., and McRee, D.I.: Neurobehav Toxicol 2, 291-296, 1980.

7. Radiofrequency Radiation Dosimetry Handbook, Second Ed, Feb 1978, Report SAM-TR-78-22, USAF-AFSC.

8. Radiofrequency Radiation Dosimetry Handbook, Third Ed, Aug 1980, Report SAM-TR-80-32, USAF-AFSC.

9. Lesko, M., Dolon, M., Marinetti, G.V., and Hare, J.D.: Biochem Biophys Acta 311, 173-179, 1973.

10. Rubin, M.W., Swislocki, N.I., and Sonenberg, M.: Arch Biochem Biophys 157, 243-251, 1973.

11. Martonosi, A., and Halpin, R.A.: Arch Biochem Biophys 144, 66-71, 1971.

12. Barnett, R.E.: Biochem 9, 4644, 4648, 1970.

13. Morgan, I.G., Wolfe, L.S., Mandel, P., and Gambos, G.: Biochem Biophys Acta 241, 737-751, 1971.

14. Yamamura, H.W., and Synder, S.H.: Proc Natl Acad Sci USA 71, 1725-1729, 1974.

15. Ellman, G.L., Courtney, K.D., Andres, V., Featherstone, R.M.: Biochem Pharmacol 7, 88-95, 1961.

16. Ferro-Luzzi Ames, G.: J Biol Chem 249, 634-644, 1974.

17. Azzi, A.: Quarterly Rev Biophys 8, 237-316, 1975.

18. Thulborn, K.R., and Sawyer, W.H.: Biochem Biophys Acta 511, 125-140, 1978.

19. Yguerabide,J., and Stryer, L.: Proc Natl Acad Sci USA 68, 1217-1221, 1971.

Table I: Acetylcholinesterase Activities in Crude Mitochondrial Fraction and in Synaptosomes from Rat Brains. (Activities are expressed in nanomoles of acetylthiocholine hydrolysed per minute per mg protein.)

| Experiment | Group* | Irradiation | | | Acetylcholinesterase | |
| --- | --- | --- | --- | --- | --- | --- |
| | | Frequency (GHz) | Mode | Width | CMF | Synaptosomes |
| 1 | I | 1.20 | CW | — | 129 ± 7 | 25.0 ± 2.4 |
| | S | | | | 120 ± 11 | 23.2 ± 2.5 |
| | CC | | | | 130 ± 11 | 24.1 ± 2.7 |
| 2 | TC | 2.05 | 5000 pps | 20 μsec | 131 ± 11 | 17.4 ± 2.8 |
| | I | | | | 138 ± 10 | 17.2 ± 2.8 |
| | S | | | | 125 ± 8 | 16.8 ± 2.9 |
| | CC | | | | 129 ± 8 | 21.2 ± 3.0 |

*I: Irradiated; S: Sham-irradiated; TC: Temperature control;

CC: Cage control.

**pps: Pulses per second

221

Table II: ACH Muscarinic Receptors in Crude Mitochondrial Fractions from Rat
Brains. (Receptor concentrations and affinities are expressed in
picomoles QNB bound per mg protein and in molar.)

| Experiment | Group* | Irradiation | | | ACH Musc. Receptors | |
| | | Frequency | Mode | Width | No. Recept. (pmol./mg prot) | Affinity (M) |
|---|---|---|---|---|---|---|
| 1 | TC | 1.20 | CW | – | $2.10 \pm 0.23$ | $(0.92 \pm 0.12)10^{-10}$ |
| | I | | | – | $2.01 \pm 0.19$ | $(0.82 \pm 0.12)10^{-10}$ |
| | S | | | – | $2.12 \pm 0.24$ | $(0.87 \pm 0.11)10^{-10}$ |
| 2 | TC | 2.05 | 5000 pps | 20 μsec | $2.27 \pm 0.14$ | $(1.10 \pm 0.18)10^{-10}$ |
| | I | | | | $2.46 \pm 0.15$ | $(1.49 \pm 0.47)10^{-10}$ |
| | S | | | | $2.30 \pm 0.20$ | $(1.27 \pm 0.19)10^{-10}$ |

* TC: Temperature control; I: Irradiated; S: Sham-irradiated.

Table III: Na$^+$K$^+$ATPase Activity of Liver Plasma Membrane

(measured in presence of 0.1 mM ouabain

and expressed as μmoles ADP/mg·min).

| Experiment | Day | Irradiation | | | Group | | | |
| --- | --- | --- | --- | --- | --- | --- | --- | --- |
| | | Frequency (GHz) | Mode (pps) | Width (μsec) | TC | I | S | CC |
| 1 | 9 | 1.20 | CW | — | .32±.06 | .42±.12 | .37±.08 | .42±.03 |
| 2 | 9 | 1.20 | CW | — | .43±.08 | .22±.09 | — | — |
| 3 | 9 | 1.20 | 1000 | 100 | .25±.03 | .14±.08 | .24±.04 | — |
| 4 | 9 | 1.20 | 1000 | 100 | .22±.07 | .14±.06 | .20±.04 | — |
| 5 | 9 | 2.05 | 5000 | 20 | .25±.05 | .31±.05 | .15±.07 | — |
| 6 | 9 | 2.05 | 5000 | 20 | .43±.09 | .42±.07 | .44±.07 | .35±.05 |
| 7 | 15 | 2.80 | 350 | 2 | .33±.06 | .32±.01 | .26±.14 | — |

## Table IV: Mg$^{2+}$ATPase Activity of Liver Plasma Membranes

### (expressed as μmoles ADP/mg·min).

| Experiment | Day | Irradiation | | | Group | | | |
| --- | --- | --- | --- | --- | --- | --- | --- | --- |
| | | Frequency (GHz) | Mode (pps) | Width (usec) | TC | I | S | CC |
| 1 | 9 | 1.20 | CW | - | 1.37±.12 | 1.33±.17 | 1.90±.23 | - |
| 2 | 9 | 1.20 | CW | - | 1.42±.14 | 1.25±.20 | - | - |
| 3 | 9 | 1.20 | 1000 | 100 | 1.16±.16 | 1.01±.09 | 1.28±.12 | - |
| 4 | 9 | 1.20 | 1000 | 100 | 1.42±.17 | 1.23±.13 | 1.74±.24 | - |
| 5 | 9 | 2.05 | 5000 | 20 | 1.37±.18 | 1.16±.14 | 1.35±.20 | - |
| 6 | 9 | 2.05 | 5000 | 20 | 2.00±.21 | 1.24±.18 | 1.98±.09 | 1.30±.25 |
| 7 | 15 | 2.80 | 350 | 2 | 1.71±.19 | 1.33±.013 | 1.39±.06 | - |

224

Table V: $Ca^{2+}$ATPase Activity of SR (expressed as μmoles ADP/mg min).

| Experiment | Day | Irradiation | | | Group | | | |
| | | Frequency (GHz) | Mode (pps) | Width (μsec) | TC | I | S | CC |
|---|---|---|---|---|---|---|---|---|
| 1 | 9 | 1.20 | CW | - | 4.59±.18 | 3.80±.23 | 5.59±.37 | - |
| 2 | 9 | 1.20 | CW | - | 4.31±.14 | 3.36±.14 | 4.66±.18 | - |
| 3 | 9 | 1.20 | 1000 | 100 | 4.53±.13 | 4.23±.28 | 5.80±.27 | - |
| 4 | 9 | 2.05 | 5000 | 20 | - | 3.12±.17 | 2.98±.13 | 2.43±.31 |
| 5 | 9 | 2.05 | 5000 | 20 | 3.70±.25 | 2.60±.29 | 3.70±.18 | - |
| 6 | 16 | 2.80 | 350 | 2 | 3.80±.20 | 2.57±.21 | 2.47±.03 | - |
| 7 | 16 | 2.80 | 350 | 2 | 4.87±.78 | 3.65±.47 | 3.82±.24 | - |

Table VI: 12-AS Fluorescence Polarization Values in Membranes from Microwave-Exposed Rats (10 mW/cm$^2$ · 1 hour/day · 9 days)

| Membranes | Irradiation | | | Polarization (p) | | | |
| | Frequency (GHz) | Mode (pps) | Pulse Width (μsec) | Group | | | |
| | | | | TC | I | S | CC |
|---|---|---|---|---|---|---|---|
| Synaptosomes | 1.20 | CW | - | .135±.006 | .143±.006 | .140±.008 | - |
| | 2.05 | 5000 | 20 | .130±.004 | .136±.005 | .135±.005 | .140±.006 |
| LPM | 2.05 | 5000 | 20 | .143±.004 | .139±.007 | .132±.007 | - |
| | 2.05 | 5000 | 20 | .139±.004 | .125±.006 | .126±.010 | .135±.010 |
| SR | 1.20 | CW | - | .122±.003 | .114±.002 | .121±.004 | - |
| | 1.20 | 1000 | 100 | .107±.002 | .114±.009 | .111±.005 | - |
| | 2.05 | 5000 | 20 | .105±.002 | .115±.004 | .110±.002 | - |
| | 2.05 | 5000 | 20 | - | .115±.003 | .119±.003 | - |

Table VII: Fluorescence Polarization (21°C) of DPH and

12-AS in SR and LPM from Microwave Exposed

Rats (2.8 GHz, 350 pps, 1 hr/day · 15 days)

**DPH**

Polarization (p)

| Membranes | Exp. Date | TC | Group I | S |
|---|---|---|---|---|
| SR | 4/7 | .212±.009 | .218±.005 | .222±.007 |
|  | 5/21 | .192±.010 | .198±.009 | .216±.012 |
| LPM | 5/21 | .280±.009 | .267±.014 | .296±.006 |

**12-AS**

| | | | | |
|---|---|---|---|---|
| SR | 4/7 | .126±.017 | .139±.006 | .124±.023 |
|  | 5/21 | .123±.005 | .117±.009 | .110±.004 |
| LPM | 4/7 | .142±.006 | .148±.007 | .149±.008 |
|  | 5/21 | .170±.002 | .157±.010 | .162±.007 |

# RADIOFREQUENCY RADIATION EFFECTS ON EXCITABLE TISSUES

Interim Technical Report
Project A-2974
June 1981

Under

Contract F33615-81-K-0618

By

R. L. Seaman

228

# RADIOFREQUENCY RADIATION EFFECTS ON EXCITABLE TISSUES

Ronald L. Seaman

Biomedical Research Division

Engineering Experiment Station

Georgia Institute of Technology

Atlanta, Georgia

## I. INTRODUCTION

There has been interest in the effects of radiofrequency radiation (RFR) on biological systems for quite some time. In many cases, research on the biological effects of RFR has focused on excitable tissues, nerve and muscle. The normal functioning of excitable tissues involves changing electric fields and ionic currents which can be altered by applied static and slowly changing electromagnetic fields. It is conceivable that high frequency oscillating fields, such as those associated with RFR, could also interact with these tissues.

Several preparations of excised nerve and muscle tissues have previously been used to show that RFR can affect excitable cells. The RFR-induced changes include shifts in firing rates of cardiac and neural pacemakers, modification of membrane electrical properties, and alteration of ion fluxes. However, since some experiments have shown no RFR effect, the RFR influence on nerve and muscle has remained controversial. While many of the observed effects seem to be the result of RFR heating, others do not, so the mechanisms for effects have not yet been completely specified.

The program described here uses aggregates of cultured heart cells to study the RFR effects on a living-model excitable membrane. Aggregates are cultured in the laboratory of Dr. Robert L. DeHaan at Emory University. This program is a collaborative investigation by the Biomedical Research Division of the Georgia Tech Engineering Experiment Station and the Department of Anatomy of the Emory University School of Medicine.

229

The overall objective of this program is to investigate the effects of pulsed- and continuous-wave RFR at 2450 MHz on the electrical properties of beating heart-cell aggregates. The specific research objectives can be summarized as the following:

1    development of an exposure system to provide well-characterized dosimetry for cellular-level RFR exposure,

2.   investigation of possible alterations of spontaneous beating rhythm and of action potential characteristics during RFR exposure of aggregates, and

3.   investigation of possible alterations in specific slow- and fast-channel ion currents during RFR exposure.


## II.    TECHNICAL APPROACH

### A.    RFR Exposure System

The system used to expose cardiac-cell aggregates to RFR consists of RF-generating equipment connected to a special coaxial exposure device. An in-line bidirectional coupler is used to sample power transmitted to and power reflected from the exposure device. The exposure device (Figure 1) uses the fringing field of an open-ended 1/4-inch semirigid coaxial cable to couple to bathing medium in a 35-mm plastic dish. The cable's open end is flush with the surface of a heating plate used to maintain temperature of the preparation. Using this device, RFR is coupled to beating aggregates under normal culture conditions in the medium. The exposure device rests on a microscope stage so that aggregates can be observed for electrode placement or video imaging, even during RFR exposure. No coupling of the RF fields to the microelectrodes used in this study has been observed.

The RF field intensity distribution in the medium in the culture dish has been characterized by measurements of electric fields and temperature changes. Electric fields were probed with small monopole and dipole antennas inserted into the medium. Temperature rises at onset of RFR were sensed with very small thermistors and converted to specific absorption rates (SARs) in mW/g. Figure 2 shows SAR as a function of distance from the bottom of the culture dish. Values of SAR have been
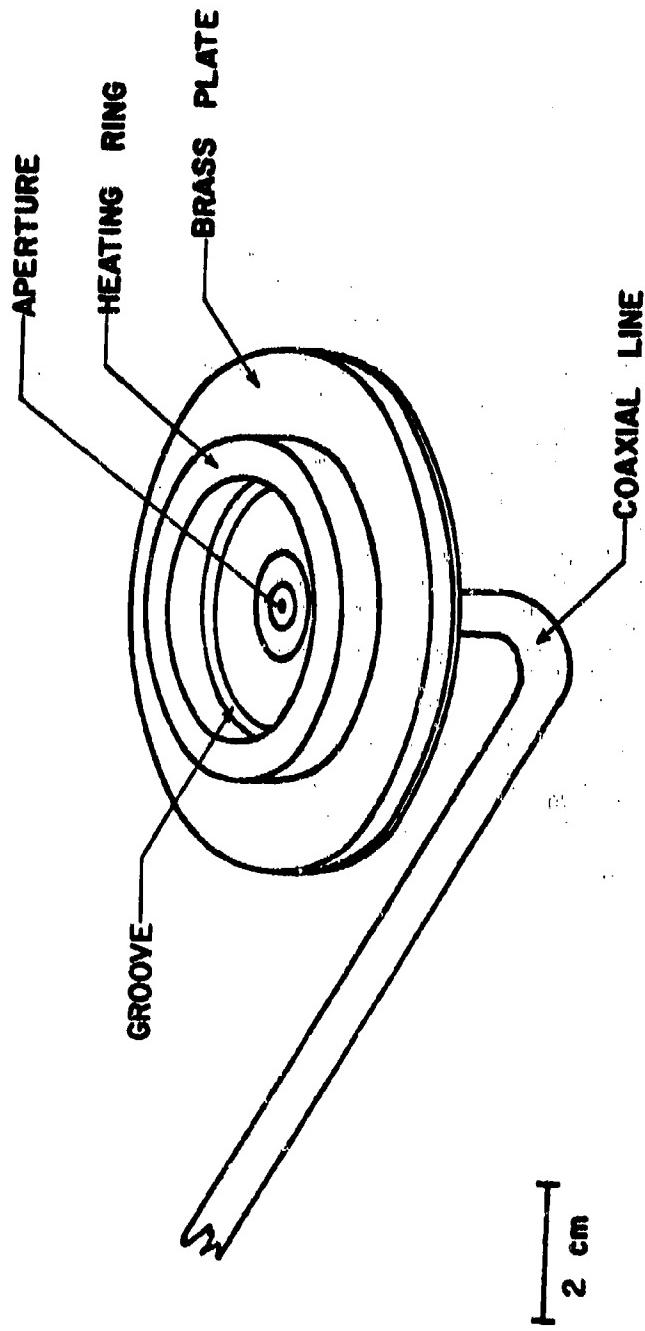
Figure 1. Isometric projection of c  xial exposure device showing 1/4-inch semirigid coaxial cable, brass heating plate and ring, and coaxial aperture. The bottom rim of a 35-mm culture dish fits into the small groove for mechanical stability and direct contact of dish and aperture.

231
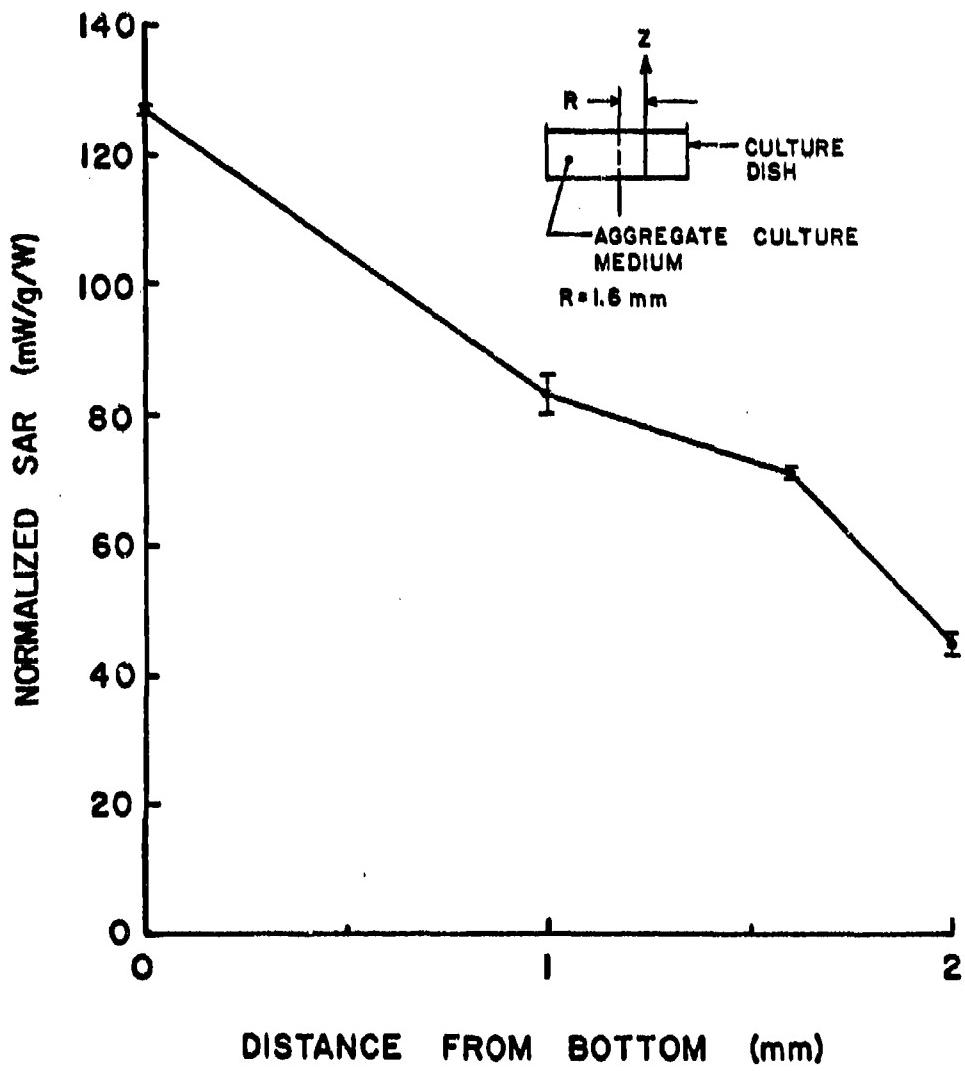
Figure 2. Plot of specific absorption rate (SAR) in mW/g as a function of distance from the bottom of the culture dish. SAR is normalized to the net RF input power to the exposure device. All measurements are for points located a distance of 1.6 mm from a projection of the coaxial cable's axis which is also the center of the dish.

normalized to the net input power to the exposure device. Thus, for a given aggregate position and net input power, SAR at an aggregate can be accurately calculated. For extracellular electrode recording, aggregates are positioned 1 mm above the dish bottom to avoid steep field gradients seen in antenna measurements.

Exposure durations in early experiments ranged from 21 seconds to 5.3 minutes. Exposure duration in later experiments has been set at 190 seconds as described below. Applied RFR at 2450 MHz is in the form of one of the following: continuous wave (CW), no modulation; pulsed (PW), 10.9-μs pulses at 10,000 pps; "modulated" with a 16-Hz square wave; or "gated" at a 1.7-Hz or slower square wave.

### B. Heart-Cell Aggregates

In 1972, the spheroidal heart-cell aggregate was introduced as a tissue culture model for studies of the electrical properties of the heart-cell membrane [1,2]. The advantages that these aggregates offer over more traditional cardiac preparations include the following:

1. All cells within an aggregate are closely coupled by low-resistance junctions, so each aggregate approximates an isopotential system for both spontaneous and imposed signals [3,4].

2. Because of these properties, the aggregate action potential approximates a true nonpropagated membrane potential, whose electrical field builds and collapses with each beat.

3. Aggregates can be prepared for any desired embryonic age and in any size within a 30-300-μm-diameter range, from a few cells to several thousand cells beating in a coordinated fashion.

4. Aggregates exhibiting spontaneous rhythmic beating can be maintained in healthy condition for many days in culture.

For the investigations described here, measurements were made on spheroidal aggregates of cells derived from embryos of white Leghorn chickens by procedures standard in Dr. DeHaan's laboratory. After incubation for 7 days at 37.5°C, embryos were harvested in amniotic fluid and decapitated. Hearts were dissected free, trimmed of extraneous tissue, and the ventricles were dissociated with trypsin. Aggregates were prepared by placing an inoculum of $5 \times 10^5$ or $8 \times 10^5$ cells in 3 ml

of 818A culture medium. Cells were allowed to aggregate during flask gyration at 62 rpm and 37.5°C with an atmosphere containing 5% $CO_2$, 10% oxygen, and 85% nitrogen. Aggregates were used after either 48 or 72 hours of gyration. For experiments, aggregates were placed into a plastic dish containing either 818A or a balanced salt solution, and the volume brought to 4 ml. The plastic dish was placed under a microscope on the RFR exposure device where temperature, pH, gaseous atmosphere, and evaporation were controlled.

### C. Recording Methods

Three different methods have been used to record aggregate activity: intracellular electrodes, extracellular electrodes, and video imaging. Intracellular electrodes, pulled from glass capillary tubing to a fine tip and filled with 3M KCl, were used to penetrate aggregates to obtain a transmembrane potential. Beat rate and action potential parameters were measured using this technique.

To obtain long-term recording of beat rate, extracellular electrodes and video imaging were used. Extracellular electrodes were pulled from glass tubing to a tip with an outer diameter of 100 to 200 μm. These electrodes were filled with bathing medium and were used to hold the aggregate by means of a small negative pressure applied to the electrode. Video imaging involved obtaining a TV image of a beating aggregate by placing a camera at one of the microscope's ocular objectives. A photodetector placed over the edge of the aggregate's TV image provided a voltage signal indicative of beat occurrence. Most beat-rate data were gathered with the extracellular-electrode technique.

### D. Data Collection and Analysis

Cellular potentials obtained from intracellular electrode experiments were recorded on magnetic tape and later replayed onto a storage oscilloscope display at different sweep speeds. Measurements were made on a photograph of the display and converted to appropriate voltage and time values by using the display calibrations. Representative action potentials under various RFR exposure conditions were chosen for analysis.

Exposures during the longer experiments using video imaging and extracellular electrodes were timed by means of a digital circuit.

234

Radiofrequency radiation exposure or sham exposure (no-RFR control) was applied during 190-second periods separated by similar periods of no exposure. The exposure and no-exposure periods consisted of two parts indicated by the timing circuit. The half-period interval just before an exposure was designated PRE; the interval just after an exposure, POST. The POST interval was followed by a POSTPOST interval which was usually the PRE interval for the next exposure. The exposure period itself was divided into the intervals BEG (for beginning) and END.

Interbeat intervals (IBIs) from video and extracellular-electrode experiments were analyzed by using either the recorded photodetector output or a recorded pulse which had been triggered by the extracellular electrode signal. The recorded signal was replayed into the Schmitt-trigger level detectors of a DEC PDP-11/40 computer system at Emory University. Computer programs sorted IBIs into 5-millisecond bins [5] and computed several statistical parameters for each experimental interval. Mean IBI and coefficient of variation (CV = standard deviation/mean, in %) were later plotted. By using the Georgia Tech CDC CYBER 70/74 computer, mean IBI and CV values were averaged for each exposure condition within an experiment in attempts to eliminate the influence of occasional IBI variations not related to microwave exposure. To remove the effect of variations from exposure to exposure and experiment to experiment, mean IBI and CV values for a particular exposure were normalized to PRE-interval values by dividing all five values (PRE through POSTPOST) by the PRE-interval value for that exposure.

III. RESULTS/PROGRESS

The open-ended coaxial exposure device has been used to expose heart-cell aggregates to several RFR SAR levels and modulations. Of the several parameters studied in experiments with intracellular electrodes, beat rate and action potential upstroke velocity showed the largest changes with RFR exposure. Trends in these data showed apparent increases in the variability of both parameters under exposure to CW and PW RFR. Subsequent experiments using video and extracellular-electrode techniques were designed to study further the variability in beat rate by gathering IBI data over longer periods.

235

Mean IBI and CV data have been obtained from aggregates in several experiments using extracellular electrodes. In Figure 3, one aggregate's mean IBI is shown for 3 sham exposures and 3 exposures to CW RFR at 12.2 mW/g. The averaged mean IBI decreased by less than 1% over 6 minutes without RFR, as seen in the plot of normalized IBI for sham exposure. In this experiment, as in most others, the averaged mean IBI did not change during the RFR exposure at this SAR level. As shown in Figure 4 for another experiment, the mean IBI averaged across 3 sham exposures again showed a small decrease. There was a larger decrease of 1-1.5% in this averaged parameter during exposure to CW RFR at 42.6 mW/g. The decrease was similar for all 3 exposures in this experiment. Similar decreases in mean IBI were observed for 40-mW/g exposures in other experiments. This differs from IBI changes seen during exposures at SAR less than about 15 mW/g. These changes were variable from exposure to exposure, as exemplified by data in Figure 3. Data analyses of mean IBI and IBI variations (CV) now in progress average data from the same RFR conditions from different experiments. The influence of experimental factors not related to RFR will be reduced by this procedure so that possible small RFR influences which may have been obscured by events in one experiment will become more obvious.

Since IBI is known to decrease with increased temperature, the smaller IBIs seen for SAR greater than about 40 mW/g were consistent with the effect expected from RF heating. The preparation temperature was regulated to $37 \pm 0.4°C$ as measured with a YSI thermistor outside the RF field. Temperature within the RF-field-coupled region was warmer than this during exposure. Changes in IBI parameters are currently being correlated with induced temperature increases. Comparison with the known response of IBI to temperature will provide information on the thermal basis for changes during exposure.

## IV. SUMMARY AND CONCLUSIONS

The cardiac-cell aggregate is an extremely useful model of living excitable tissue for studying RFR effects. Experiments with these aggregates
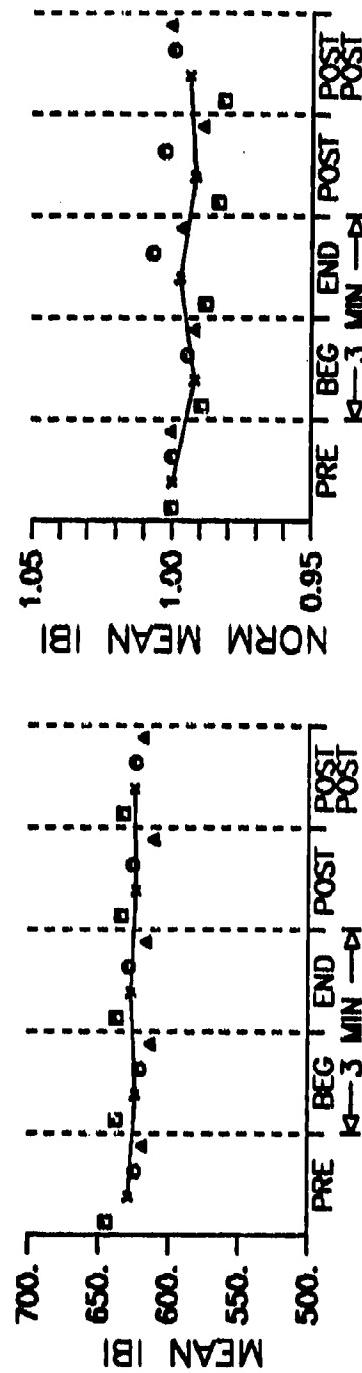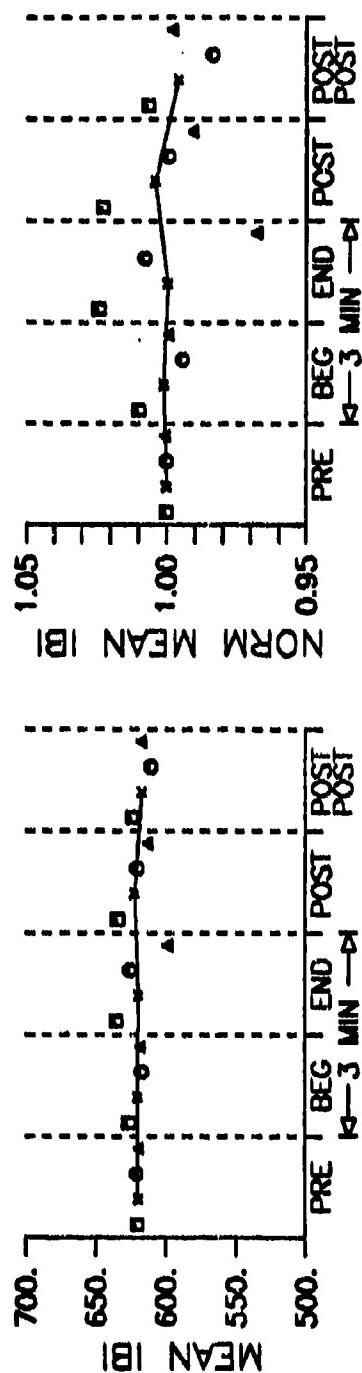
Figure 3. Mean and normalized mean interbeat intervals (IBIs) for sham exposures and exposures to 12.2-mW/g CW RFR in one experiment. The three exposures for each condition are indicated by different symbols. Bulk temperature = 37°C. Mean IBI is in milliseconds.

237
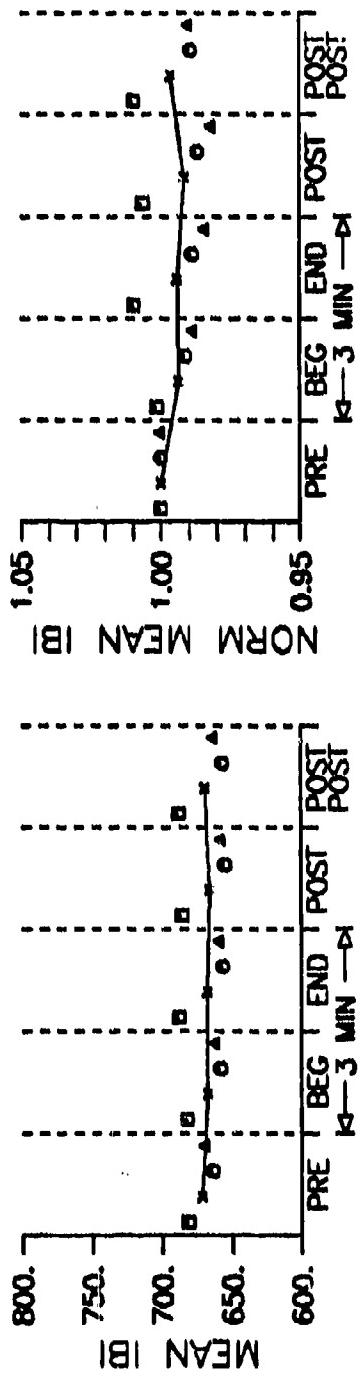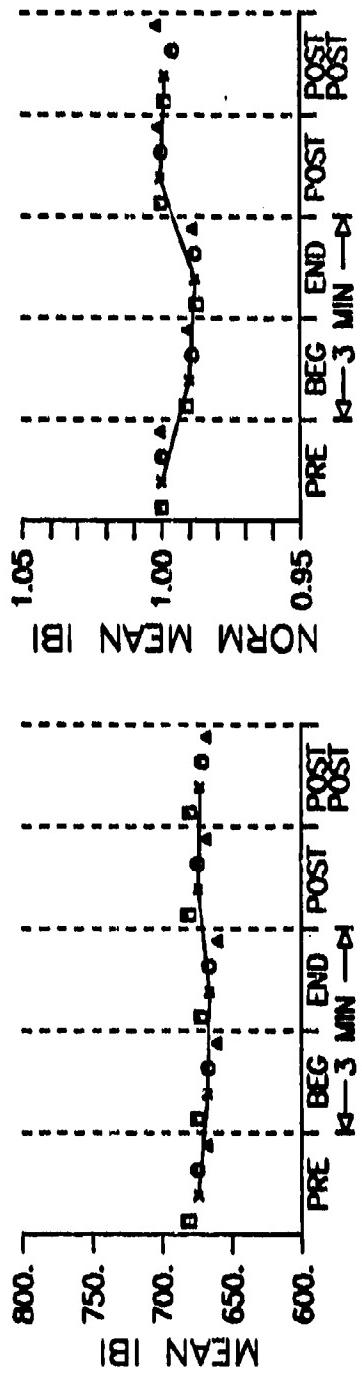
Figure 4. Mean and normalized mean interbeat intervals (IBIs) for sham exposures and exposures to 42.6-mW/g CW RFR in one experiment. The three exposures for each condition are indicated by different symbols. Bulk temperature = 37°C. Mean IBI is in milliseconds.

238

are providing information on RFR levels effective in interacting with
excitable membranes. This information is not only directly applicable
to cardiac cells but also to other excitable cells since the well-studied
aggregate membrane has representative excitable properties.

With the known RFR levels provided by the open-ended coaxial exposure
device, RFR effects can be related to SAR in an accurate and repeatable
manner. So far, experimental results have shown that aggregate mean
beat rate is changed by average SARs of 40 mW/g and above in a way consistent
with RFR heating. For 15 mW/g and below, this effect has not been seen
in data analyzed to date. Levels between 15 and 40 mW/g will require
further investigation to define a minimum effective SAR for this RF-
induced IBI decrease. Effects other than those consistent with RF heating
have neither been confirmed or refuted by data analyzed to date. The
variability in beat rate may also change with RFR exposure, and data are
being analyzed to study this possibility. Further study of the heart-cell
aggregate will be very useful in delineating RFR levels and modulations
which cause changes in excitable tissues.

After effective RFR levels are specified in terms of SAR for the
aggregate, these can be translated into RFR fields which might influence
the hearts of exposed personnel. For example, we can use the Radiofrequency
Radiation Handbook [6] to find that the 42.6 mW/g effective in changing
mean IBI by 1% corresponds to an incident plane-wave field of about
2,000 mW/cm$^2$ at 2450 MHz for an adult human. This very intense field
would probably not be encountered without manifestation of other, perhaps
more detrimental, physiological changes. Of course, a given induced RF
field may not cause the identical effect on heart rate that was seen in
aggregate beat rate since the intact, innervated heart is carefully
regulated. However, RFR effects on aggregate membranes can be used to
predict RFR membrane effects, some of which may not be immediately expressed
in the activity of the intact heart and nervous system.

# V. REFERENCES

1. T. F. McDonald, H. G. Sachs, and R. L. DeHaan, "Development of Sensitivity to Tetrodotoxin in Beating Chick Embryo Hearts, Single Cells, and Aggregates," *Science* 176:1248-1250, 1972.

2. H. G. Sachs and R. L. DeHaan, "Embryonic Myocardial Cell Aggregates: Volume and Pulsation Rate," *Dev. Biol.* 30:233-240, 1973.

3. R. L. DeHaan and H. A. Fozzard, "Membrane Response to Current Pulses in Spheroidal Aggregates of Embryonic Heart Cells," *J. Gen. Physiol.* 65: 207-222, 1975.

4. L. J. DeFelice and R. L. DeHaan, "Membrane Noise and Intercellular Communication," *Proc. IEEE* 65:796-799, 1977.

5. J. R. Clay and R. L. DeHaan, "Fluctuations in Interbeat Interval in Rhythmic Heart-Cell Clusters," *Biophys. J.* 28:377-389, 1979.

6. C. H. Durney et al., "Radiofrequency Radiation Dosimetry Handbook (Second Edition)," Report SAM-TR-78-22, USAF School of Aerospace Medicine, Brooks AFB, Texas, 1978.

## VI.   PUBLICATIONS AND PRESENTATIONS RESULTING FROM AF-FUNDED EFFORTS

1.  E. C. Burdette, R. L. Seaman, and R. L. DeHaan, "Investigation of Radiofrequency Radiation Effects on Excitable Tissues," Review of Air-Force-Sponsored Basic Research in Environmental Protection, Toxicology, and Electromagnetic Radiation Bioeffects, 15-17 January 1980, San Antonio, Texas.

2.  R. L. Seaman, E. C. Burdette, and R. L. DeHaan, "Alteration of Action Potential Parameters in Embryonic Heart Cell Aggregates by Radiofrequency Radiation," Review of Air-Force-Sponsored Basic Research in Environmental Protection, Toxicology, and Electromagnetic Radiation Bioeffects, 15-17 January 1980, San Antonio, Texas   (presented by R. L. DeHaan).

3.  E. C. Burdette, R. L. Seaman, and R. L. DeHaan, "Investigation of Radiofrequency Radiation Effects on Excitable Tissues," Annual Technical Report No. 1, Contract F49620-79-C-0055, Project A-2335, April  1980.

4.  E. C. Burdette, R. L. Seaman, and R. L. DeHaan, "Open-Ended Coaxial Exposure System for Small Biological Preparations," Bioelectromagnetics Society Second Annual Meeting, 14-18 September 1980, San Antonio, Texas.

5.  R. L. Seaman, E. C. Burdette, and R. L. DeHaan, "RF Radiation Alteration of Cardiac-Cell Aggregate Electrical Parameters," Bioelectromagnetics Society Second Annual Meeting, 14-18 September 1980, San Antonio, Texas.

6.  R. L. Seaman, E. C. Burdette, and R. L. DeHaan, "RF Radiation Effects on Cardiac-Cell Aggregate Beat Rate," Bioelectromagnetics Society Third Annual Meeting, 10-12 August 1981, Washington, D.C. (abstract accepted).

# EFFECTS OF 200 – 2450-MHz MICROWAVES
# ON RAT-BRAIN ENERGY METABOLISM

Aaron P. Sanders, Ph.D.
Division of Radiobiology
Duke University Medical Center
Durham, NC   27710



William T. Joines, Ph.D.
Department of Electrical Engineering
Duke University
Durham, NC   27706

242

# I. INTRODUCTION

Earlier work in our laboratory tested the hypothesis that microwaves induced molecular vibration in divalent metal atoms, or functional protein molecules, in mitochondrial electron transport chains, resulting in inhibition of respiratory chain function and decreased tissue adenosine triphosphate (ATP) and creatine phosphate (CP) concentrations [1]. If this be true, such effect(s) can be measured by continuous fluorimetry monitoring of reduced nicotinamide adenine dinucleotide (NADH), the first entry point to the electron transport chain. NADH excitation (366 ±5 nm) and fluorescence (460 ±5 nm) recording techniques were used to continuously record the relative NADH levels _in situ_ before, during and after microwave exposures. Microwave tissue interaction(s) which inhibit electron transport chain function, or cell functions using ATP, would result in increased NADH and NADH fluorescence.

The measurement of brain NADH fluorescence is complicated by wide variation among animals in the location of blood vessels on the surface of the cerebral cortex. Hemoglobin absorbs both NADH excitation and fluorescence light. Consequently, each animal must serve as its own control. All figures showing NADH fluorescence levels as a function of microwave exposure were optimal curves obtained from a single animal for each exposure type. A minimum of 6 animals were used, for each exposure group, to ascertain microwave effects on NADH fluorescence.

The inhibition of respiratory chain function results in decreased ATP production. However, the CP – CP-kinase + ADP → ATP + creatine interaction, which functions rapidly to sustain tissue ATP, is able to maintain brain ATP at control levels until brain CP is decreased below 60% of control concentrations in normal-cell physiology.

Figure 1 shows the effects of 591-MHz, CW, 13.8-mW/cm$^2$ microwave exposures for 0.5, 1, 2, 3 and 5 min on rat-brain NADH fluorescence, CP, and ATP at 35.6 and 39°C brain temperature, and the effect of hypoxia (2% $O_2$ + 98% $N_2$) on 35.6°C brain [2] (ATP and CP assays were performed by the method of Lowry and Passonneau [3].) No increase in brain temperature was observed over the entire exposure interval.

It should be noted that in the normothermic brain (35.6°C for urethane anesthesia), the 2% $O_2$ hypoxia at 0.5 and 1 min caused CP to decrease 21% and 41%, while normal ATP concentration was retained. This was due to the rapid action of the CP – CP-kinase + ADP → ATP + creatine system which sustains ATP at control levels under normal cell physiological conditions. The microwave exposures caused a significant increase in brain NADH fluorescence and decreases in CP and ATP (39.4 and 25.2% respectively after only 0.5-min exposure) after 0.5, 1, 2, 3, and 5 min. The 25.2% decrease in ATP occurred when CP was 60.4% of control. This level of CP under normal cell physiology would maintain ATP within normal limits. Thus the rapid increase in brain NADH fluorescence and decrease in ATP and CP during microwave exposure supports the concept of nonthermal microwave inhibition of electron transport chain function in its production of ATP.

243
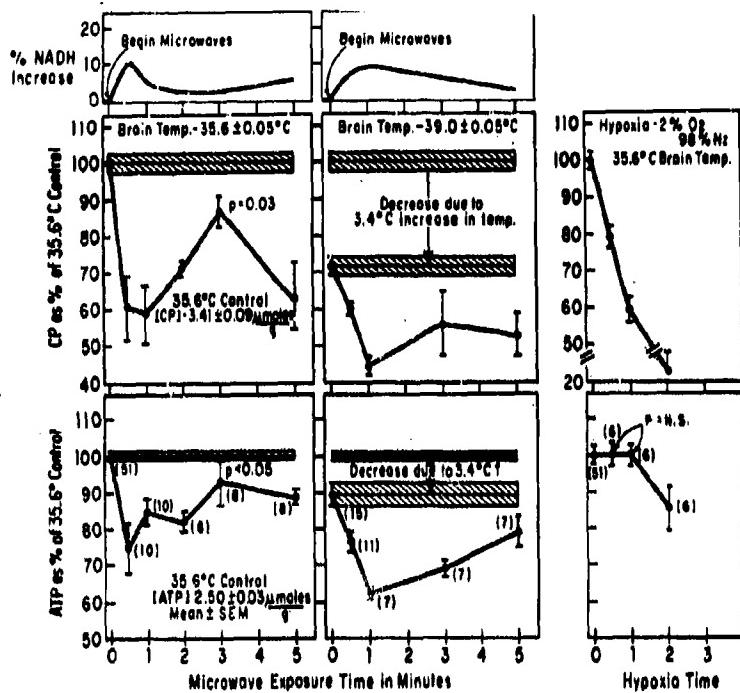
Figure 1. Rat brain ATP and CP normoxic at 35.6 and 39.°C with and without microwave exposure, and hypoxic (2% oxygen) at 35.6°C. Unless shown, P < 0.0.

The idea of direct microwave effects, independent of tissue hyperemia on tissues has been controversial [4-10]. In an effort to ascertain if our results could have been related to localized hyperthermia, rat-brain temperature was increased to 39 ± 0.1°C. Brain ATP and CP were determined on sham exposed and nonthermogenic microwave exposures of the 39°C rat-brain temperature [2]. These data are shown in the middle graphs in Figure 1. Note the decrease in brain ATP and CP due to the 3.4°C increase in temperature. This may be attributed to increased metabolism of the hyperthermic tissue, and inability of mitochondrial ATP production and CP - CP-kinase support of ATP to meet the increased intracellular demand for ATP.

When the 39°C rat brain was exposed to the same microwave exposures as the normothermic brain for 0.5, 1, 3, and 5 min, significant decreases with respect to the sham-exposed 39°C brain were observed in ATP and CP. As in the normothermic brain, ATP and CP were rapidly decreased at 0.5 min. This further supports the concept of direct microwave inhibition of mitochondrial electron transport chain function.

Another problem to be resolved was whether the observed microwave effects were frequency specific or general microwave effects independent of frequency. This paper reports the effects of different frequencies between 200 and 2450 MHz, while maintaining the rat-brain surface power density constant, on NADH fluorescence and on ATP and CP

244

## II.   TECHNICAL APPROACH

### Animal Preparation and Instrumentation

Male Sprague Dawley rats, 175-225 g, were anesthetized with urethane (1250-1350 mg/kg, IP injection). The scalp and muscle at the top and side of the skull were removed from the brain area to be studied. A 5-x 5-mm aperture was made through the skull, leaving the dura intact. Animals exposed to 200- thru 2450-MHz microwaves were positioned in a microstrip irradiation system as follows: the head was held rigid in a Teflon head holder and located directly below a 1.5-cm hole in the upper plate of the microstrip system. This system permitted continuous NADH fluorescence measurements before, during, and after microwave exposures.

The optical head of the 366-nm excitation light source was focused to a 1-2-mm spot on the cerebral cortex of the rat brain. A fiber-optic bundle with plastic tips was positioned approximately 45° to the excitation light beam and at a distance of 1 to 2 cm from the focal spot on the cerebral cortex. The fiber optics were divided approximately 15 cm from the end, and each end attached to a filter-photomultiplier-amplifier assembly. One of these was a 460±5nm half- band-width (HBW) filter system for measuring NADH fluorescence, the other a 549±2nm HBW interference filter system for recording general brain fluorescence. This allowed correcting, if necessary, NADH fluorescence measurements for the effect of changes in hemoblogin concentration in the field on NADH fluorescence, as detailed by Kramer and Pearlstein [11].

An AIL 125A microwave generator was used to produce the 200-through 2450- MHz exposures. This was connected to a circulator (Western Microwaves Model 3J-1997, 35A-2086, or 3JA-2040), a dual direction coupler (NARDA Model 3020A or 3022) (with sensors to the two HP435A power meters for measuring power transmitted to the antenna or microstrip system, and the reflected power), an antenna or microstrip system, and a Termaline Model 8135 Coaxial resistor.

### Calculation and Measurement of Microwave Power Absorbed by Test Animal

For applying microwave energy at frequencies between 200 MHz and 2450 MHz, we have used an air-filled stripline for our own construction, and a waveguide horn antenna previously described [1]. The stripline (also known as microstrip) consists of two parallel planes, the width and spacing of which yield a 50-ohm characteristic impedance at any plane perpendicular to the direction of energy propagation. Most of the energy will propagate in a transverse electromagnetic (TEM) wave between the stripline planes as long as the spacing between planes is less than one-half of the wavelength. Thus a line with 6 cm between planes was used at all frequencies up to 2500 MHz. The problem of generation of higher order modes when a test animal is placed in the line, thus potentially lowering the upper frequency limit of the stripline, will be discussed later in this report.

A diagram of the microstrip system is shown in Figure 2. During a typical exposure with this system, the test animal is placed within the rectangular region indicated. Before the animal is placed in the line, a uniform TEM field (similar to the far-field of an antenna) exists between the conductors spaced 6 cm apart. The width of the uniform field region where the animal will

245
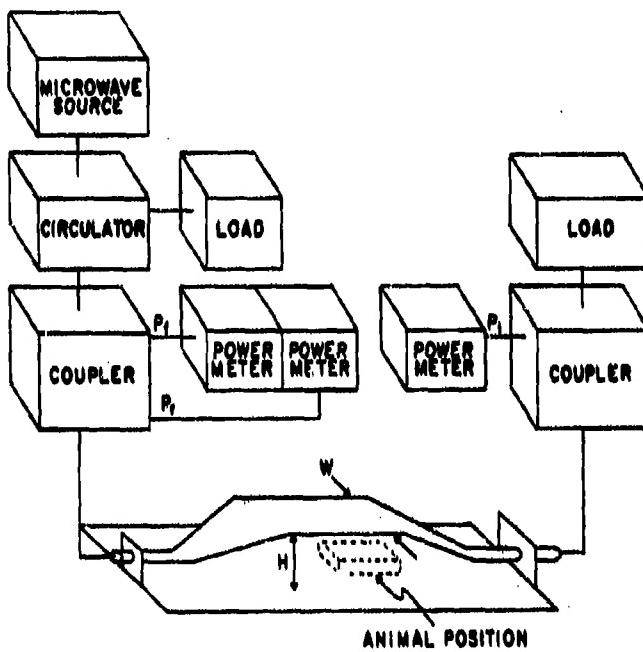
Figure 2. Microstrip transmission line irradiation system. The
conductor of width (w - 29.5 cm) is a sheet of 0.16 cm
aluminum spaced height H = 6.0 cm above an aluminum ground
plane in the region where the animal will be placed. W
and H are adjusted in other regions to maintain a 50-ohm
characteristic impedance throughout.

be placed is about 1.3 x height (H), or 7.8 cm for the line in Figure 2.
Fiber-optic light guides for the time-sharing fluorimeter are located
immediately above a small hole (1.5-cm diam.) cut in the conductor plane
(width - 29.5 cm). The hole causes a small but negligible perturbation
of the field.

## Rat-Brain Dosimetry in Microstrip Line

We used the following method to calculate and measure power absorbed at
a given point within the brain of the test animal. For a long biological
sample in the microstrip line, as for a 320-g rat, the power transmitted
longitudinally through the animal is zero. Hence, from equation (11) of

Joines et al. [12], we find at depth z within the test animal from the surface nearest the source:

$$\frac{P_a(z)}{P_1} = \frac{2}{\delta} (1-|\rho|^2)(1+\Delta w_s) \; e^{-2z/\delta} \frac{mW/g}{mW/cm^2} \tag{1}$$

$$\frac{}{w_s}$$

where $\delta$ is the depth of penetration given by [12].

$$\delta = \frac{2Re\eta}{\sigma|\eta|^2} \tag{2}$$

where $\rho$ is the reflection coefficient given by

$$\rho = \frac{\eta - \eta_0}{\eta + \eta_0} \tag{3}$$

where

$$\eta = \frac{\eta_0}{\sqrt{\varepsilon_r^*}} \tag{4}$$

$\eta_0$ is 377 ohms, $\varepsilon_r^*$ is the relative complex permittivity of the biological tissue, and $\sigma$ is the conductivity of the tissue.

For a 320-g rat facing the source and parallel to the propagation direction, the height and width of the animal are approximated by H = 2.13 cm and $w_s$ = 4 cm. With H = 6 cm, we find $w_s$ = 1.5 cm from equation (4) of [12], or from Figure 3, which is plotted from equation (4) of the reference cited. Thus (3) becomes

$$\frac{P_a(z)}{P_1} = \frac{2.75 \; (1 - |\rho|^2) \; e^{-2z/\delta}}{\delta} \tag{5}$$

For brain tissue, $\delta$ and $|\rho|^2$ vary with frequency [13]. For example, Figure 4 shows $\delta$ = 7.7 cm, $|\rho|^2$ = 0.69 at 200 MHz; $\delta$ = 6 cm, $|\rho|^2$ = 0.61 at 400 MHz; and $\delta$ = 5.1 cm, $|\rho|^2$ = 0.55 at 600 MHz. Using the values and equation (5) we calculated power absorbed at a depth z = 1 cm for three frequencies:

$$\frac{P_a}{P_1} = 0.078 \; \frac{mW/g}{mW/cm^2} \quad \text{at 200 MHz,}$$

$$\frac{P_a}{P_1} = 0.131 \; \frac{mW/g}{mW/cm^2} \quad \text{at 400 MHz,}$$

$$\frac{P_a}{P_1} = 0.150 \; \frac{mW/g}{mW/cm^2} \quad \text{at 600 MHz.}$$
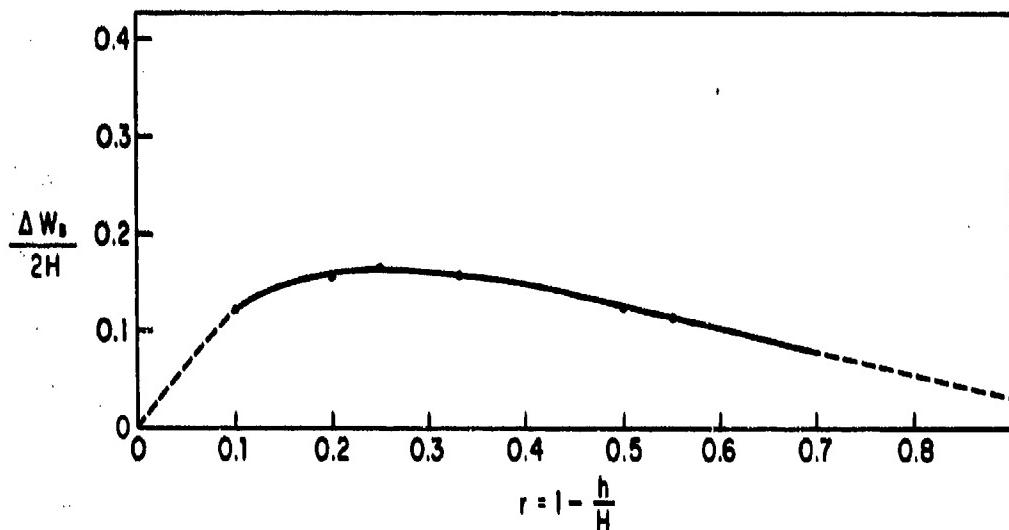
Figure 3. Apparent width increase of a rectangular sample of height
H and width $w_s$ in a uniform field of height H.

Figure 5 shows the values measured at about the same depth within a dead rat, using a Vitek model 101 probe, compared with our calculated values using equation (5).

The density of absorbed power at a site within the rat brain was estimated from the relationship:

$$P_a = K\rho c \Delta T/t \qquad (6)$$

where $P_a$ is the density of absorbed power in W/cc; K is 4.186 joules/cal, $\rho$ is the tissue density in g/cc; c is the specific heat of tissue in cal/g/°C; T is the temperature change in °C; and t is the time in seconds.

From equation (6), if the temperature increase versus time is plotted from a given $P_a$, the initial slope of the curve is $P_a$ divided by $K\rho c$. By recording the temperature increase versus time at successive 1-cm depth of the brain of the animal during a fixed level of irradiation, and using the values of 1.05 g/cc and 0.88/g/°C for the density and specific heat found in brain tissue [14], we derived densities of absorbed power and SAR from the $\Delta T/t$ values recorded.

248
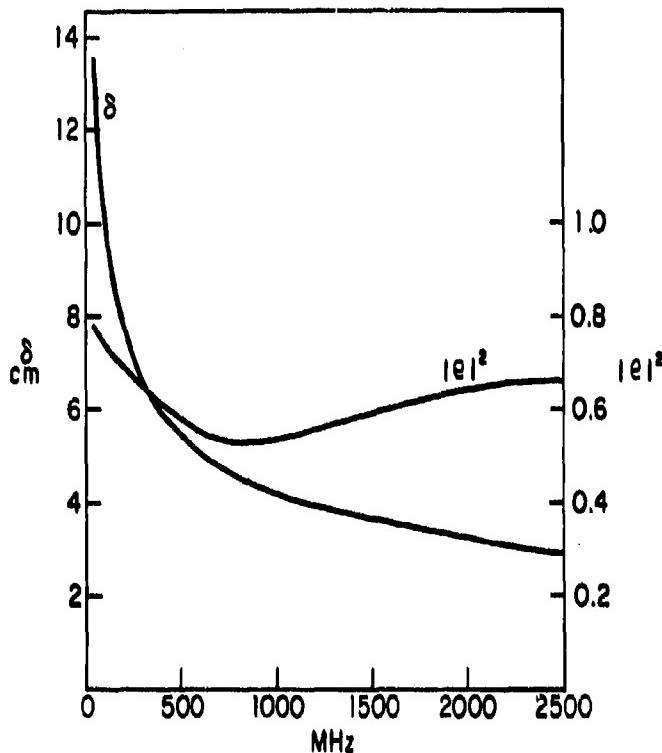
Figure 4. Variation of depth of penetration (δ) and reflection coefficient (ρ) with frequency.

## Discussion and Results and Prediction of Waveguide Modes

The rectangular sample has been assumed to be infinitely long in equation (1). This assumption is valid if the front and back surfaces of the sample are isolated by 20 dB or more of attenuation, which occurs when $L/\delta \geq 2.31$ (as derived in reference [12]), where < is the sample length and δ is penetration depth. For a 320-g rat, L is about 20 cm, and $L/\delta$ exceeds 2.31 at all frequencies above about 100 MHz.

Equation (1), which is plotted as the solid curve in Figure 5, does not take into account resonance effects due to animal size and shape. However, the measured SAR, or $P_a/P_i$, exhibits a resonance peak at 600 MHz. In fact, up to about 800 MHz, the measured SAR follows the pattern of SAR versus frequency obtained for the free-field exposure of a prolate spheroid model of a medium-sized rat (320 g). The difference is that our measured results are shifted downward in frequency so that the resonance peak occurs at 600 MHz instead of about 750 MHz, as given by the RF Dosimetry Handbook [15]. Since in our

situation the animal is on a ground plane, the downward shift of frequency is expected.
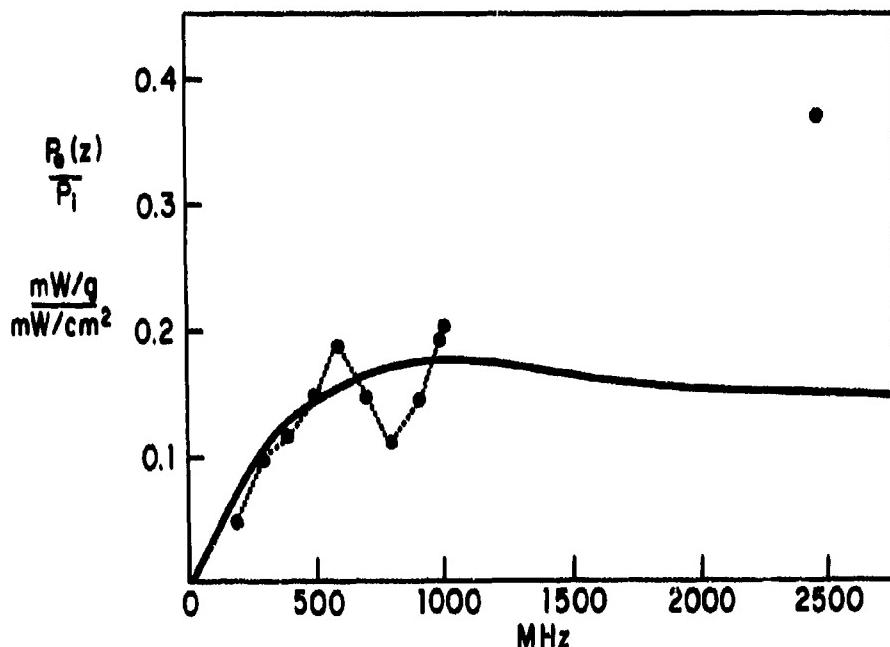


Figure 5. $P_a(z)\ P_i$ vs. frequency at z = 1 cm in rat brain

———————— calculated          ————————— measured

Above 800 MHz the measured SAR in Figure 5 is not predictable by our calculations or by the RF Dosimetry Handbook. At frequencies above 800 MHz we concluded that higher-order modes (higher than TEM) or waveguide modes exist within the line when the test animal is present. The lowest order waveguide mode that can exist in the microstrip is when the height H in Figure 1 is electrically equal to one-half wave length. With no animal in the line, frequency, velocity and wave length are related by:

$$f = \frac{\nu_0}{\lambda} = \frac{3 \times 10^{10}}{\lambda} \quad cm/sec \tag{7}$$

$$H' = (H - h) + h \sqrt{\varepsilon_r} \tag{8}$$

Hence, the frequency at which $H' = \lambda/2$ is

$$f = \frac{\nu_0}{2H'} = \frac{\nu_0}{2[(H-h)+2h\sqrt{\varepsilon_r^*}]} \tag{9}$$

Taking $\varepsilon_r^* = 49$ for brain tissue, and h = 2.13 cm (as used earlier), we have

$$f' = \frac{3 \times 10^{10}\ cm/sec}{2[(3.87)+(4.26)(7)]} = 800 \quad MHz \tag{10}$$

250

At this frequency and above, therefore, waveguide modes of propagation would be expected to exist within the line, thus complicating SAR determinations.

It is worth emphasizing that waveguide modes between 800 MHz and 2500 MHz can only exist along the approximately 25-cm section of line occupied by the body of the 320-g rat. The fact that the entire body of the rat is within the line and oriented along the direction of propagation serves to introduce waveguide modes at the relatively low frequency of 800 MHz. If only the head of the rat had been protruded into the line, much of the complication in determining SAR above 800 MHz would have been avoided.

The measured specific absorption rates (mW/g/mW/cm ) for the designated frequency are summarized below:

| Frequency (MHz) | Microstrip SAR (mW/g/mW/cm$^2$) | Frequency (MHz) | Microstrip SAR (mW/g/mW/cm$^2$) |
|---|---|---|---|
| 200 | 0.046 | 700 | 0.146 |
| 300 | 0.098 | 800 | 0.110 |
| 400 | 0.110 | 900 | 0.143 |
| 500 | 0.148 | 1000 | 0.189 |
| 591 | 0.185 | 2450 | 0.368 |

## III. RESULTS

The change in NADH fluorescence (as % of preexposure baseline) vs microwave frequency (400 to 600 MHz) is shown in Figure 6. The microwave frequency was varied by 10-MHz increments except in the 560- to 570-MHz and the 590-to 600-MHz intervals where smaller increments were studied, i.e. 560, 562, 564, 566, 591, 593.5, and 596. In addition, 4 animals were studied at 455 MHz. Additional studies of microwave effects on brain NADH fluorescence were made at 200, 300, 360, 380, and 390 MHz for frequencies below 400 MHz, and in 100-MHz intervals from 700 to 2400 MHz, and at 2450 MHz.

Distinct frequencies which caused increases in NADH fluorescence were observed at 200, 360, 380, 390, 400, 410, 430, 455, 460, 530, 540, 550, 560 to 566, 570, and 591 - 596 MHz. Decreases in NADH fluorescence were observed at 330, 500, 700, 800, 900 MHz, 14 mW/cm$^2$, CW exposures. In the 100-MHz-interval studies from 1000 to 2400 MHz and at 2450 MHz, 14 mW/cm$^2$, CW exposures, no changes were observed in NADH fluorescence. In addition, no changes in brain NADH were observed in any animal at the 420, 450, 470, 480, 490, 510, 520, and 600-MHz frequencies. In some animals, but not all, no changes in brain NADH fluorescence were observed at 410, 440, 500, 540, 550, 570, 580, and 590-MHz exposures. Thus the microwave effects of inducing changes in brain NADH fluorescence levels were found to be frequency specific (i.e., photon energy dependent) over the range of 200 to 900 MHz. In the region of 1000 to 2450 MHz – where waveguide modes exist in the rat when the animal is present in the microstrip – no changes in brain NADH fluorescence levels were

observed with the 14 mW/cm², CW exposures. The microwave-induced increase in rat-brain NADH fluorescence cannot be a general property of all microwave interaction with biological systems. It must be considered to be frequency (or photon energy) dependent.
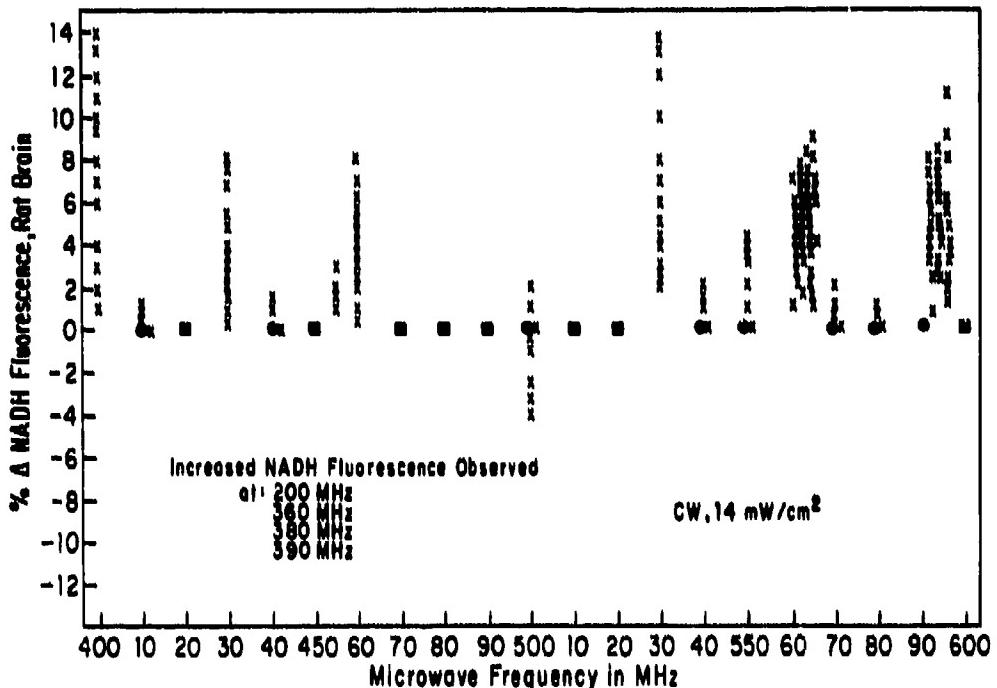


Figure 6.  % ΔNADH fluorescence of rat brain vs microwave frequency (MHz) for 14 mW/cm², CW exposures. Each x represents a different animal at the individual frequency. Most animals were observed at each frequency shown with recovery time permitted between each observation. (Solid circles, the remaining 13 animals showed no change. Solid squares, no change observed in any animal.) At approximately 20 points the ΔNADH was the same % and is shown immediately above or below the point - depending on the space at that frequency.

The changes in rat-brain NADH fluorescence for 20 min and 30 min, 530-MHz, CW, 2.55-W/kg brain SAR, microwave exposures are shown in Figure 7 for 2 different animals. NADH fluorescence rapidly returned to baseline at the end of exposure in both animals.

252
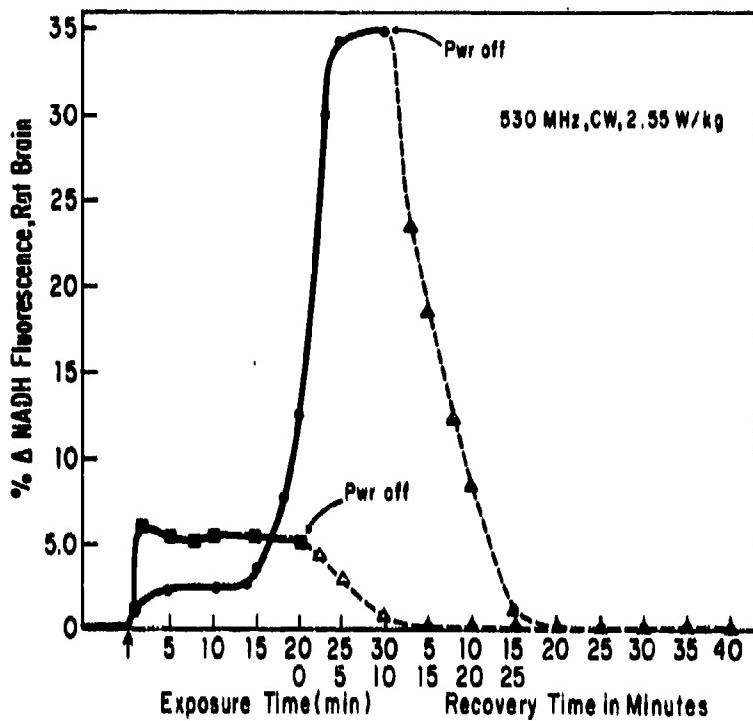
Figure 7. Change in rat-brain NADH fluorescence as a function of exposure
and recovery time; 530-MHz, CW, 2.55-W/kg brain SAR.

The rat which showed the 35% change in brain NADH fluorescence (Figure
7) was allowed to recover for 40 min post exposure. At that time, this
animal was exposed to 530-MHz, CW, 3.82-W/kg brain SAR microwaves for 40
min; brain NADH fluorescence was continuously monitored before, during and
after exposure (Figure 8). The NADH fluorescence increased to 5% through
15 min, increased to 25% from 15 to 28 min, and decreased to 13% from 28
to 40 min when the exposure was stopped. At the end of the exposure the
NADH fluorescence remained the same through 10 min and returned to baseline
at 30 min post exposure; and 45 min post exposure the same animal was
exposed to 530-MHz, CW, 5.10-W/kg brain SAR microwaves. The changes in
NADH fluorescence at this power level are shown in Figure 8. The NADH
fluorescence increased more slowly than for the previous 3.82-W/kg exposure,
reaching 26% at 40 min when the exposure was stopped. After power cut off,
the NADH fluorescence continued to increase to 28% through 5 min, leveled
off at 27% from 5 through 35 min, and slowly dropped to 22% from 35 through
55-min recovery interval. This animal had been under anesthesia for over
4 hr.
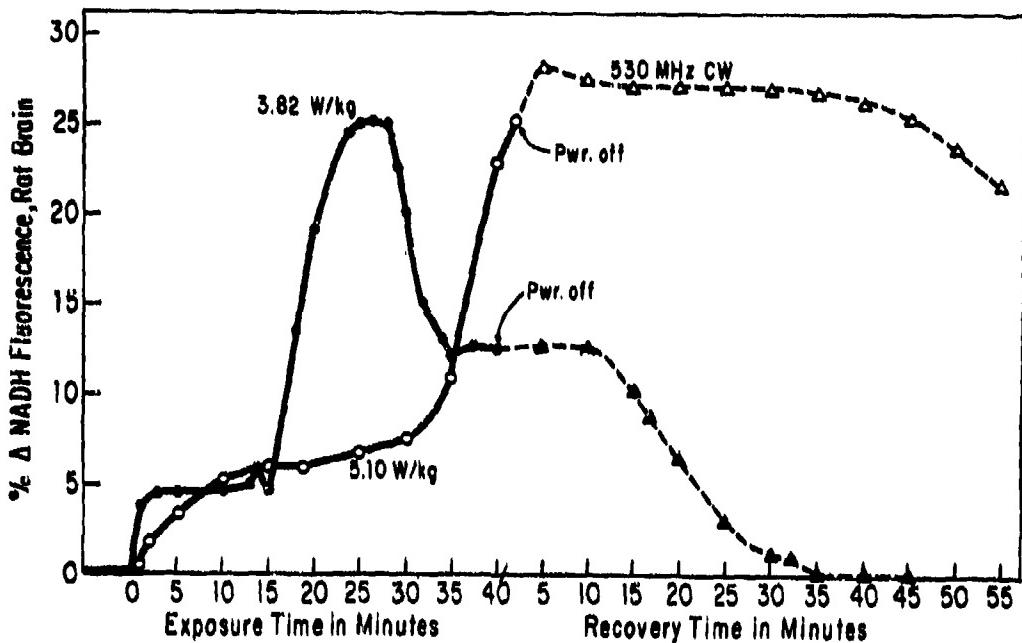
Figure 8. Changes in rat brain NADH fluorescence vs exposure or recovery time; 530-MHz, CW, 3.82-W/kg or 5.10-W/kg brain SAR.

Since there were possible accumulative microwave effects in the brain, a second animal was exposed to 530-MHz, CW, 5.10-W/kg brain SAR for 20 min. The change in brain NADH fluorescence vs time before, during, and after the exposure is shown in Figure 9. The NADH fluorescence increased to 28% from 0 to 8 min, then decreased to 11.5% from 8 to 20 min when the exposure was stopped. The recovery period showed NADH decreasing slowly to 7% through 15 min, remained at 7% through 27 min, and slowly returned to baseline at 40 min where it remained through 60 minutes.

After the 60-min recovery interval, the animal was exposed to 591-MHz, CW, 2.55 W/kg SAR microwaves for 40 min. The change in NADH fluorescence for this exposure is shown as a function of exposure and postexposure times in Figure 10. At the end of the 40-min exposure period the brain NADH fluorescence had increased to 27%. After the exposure, NADH fluorescence increased to 32.5% from 0 to 10 min, held this level through 30 min, and slowly decreased to 17% at 150 min post exposure.

254
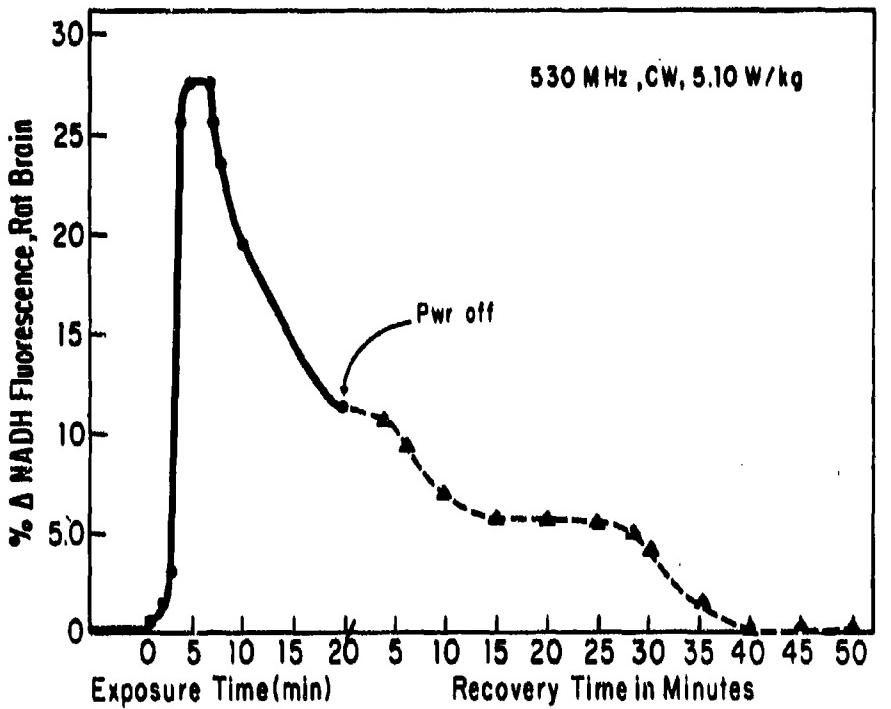
Figure 9.  Change in rat brain NADH fluorescence vs exposure  or recovery
time;     530-MHz, CW, 5.10-W/kg brain SAR.
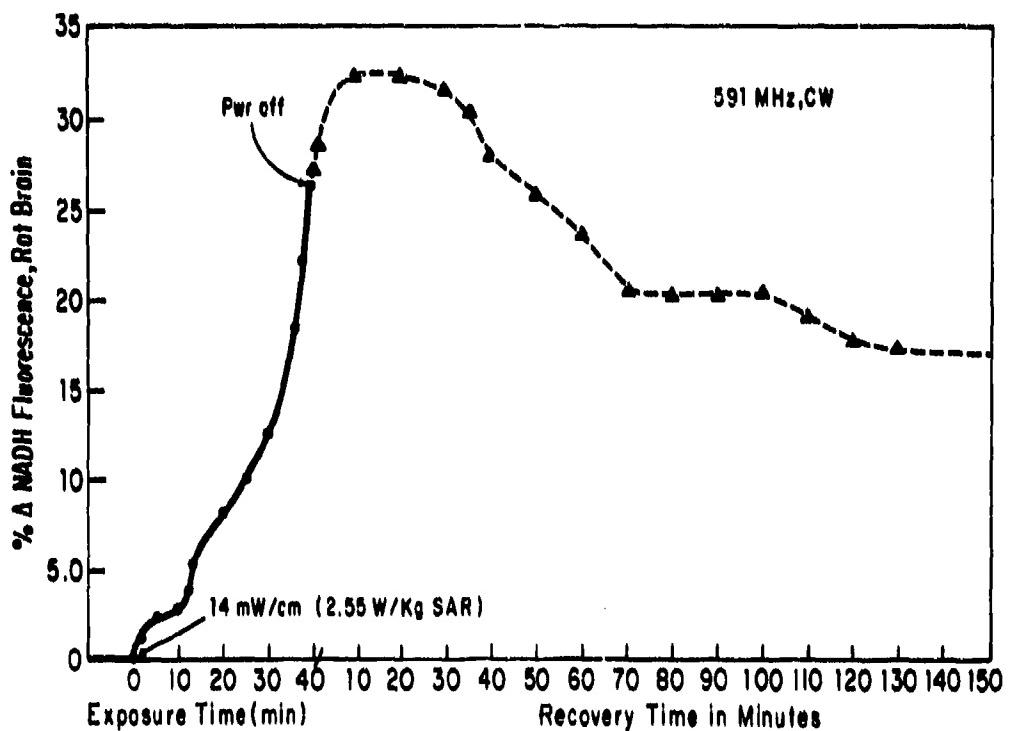
Figure 10. Change in rat brain NADH fluorescence vs exposure or recovery
time; 591 MHz, CW, 2.55 W/kg brain SAR.

The 591-MHz prolonged exposure at 2.55-W/kg brain SAR showed a different NADH fluorescence response than the 530-MHz, 2.55-W/kg exposures. This could have been the result of accumulative effects from the earlier 530-MHz, CW, 5.10-W/kg brain SAR plus the 591-MHz exposure. Additional animals will have to be similarly exposed to ascertain if these changes in NADH fluorescence during and after microwave exposures have similar responses in all animals, or if there are significant differences in the recovery ability among animals.

The change in rat-brain ATP and CP as a function of time of exposure (0.5, 1, 2, 3, 5, 10, 15, and 20 min) is shown in Figure 11 for 591-MHz, CW, 13.8-mW/cm$^2$ (2.5-W/kg brain SAR) microwaves [1]. The decreases in ATP and CP from 5 through 20 min correlate well with the increase in brain NADH fluorescence. The prolonged exposure effect of decreasing ATP through 20 min should be correlated with other functional studies, which require ATP, in the brain to ascertain if major changes are occurring in cell physiology.
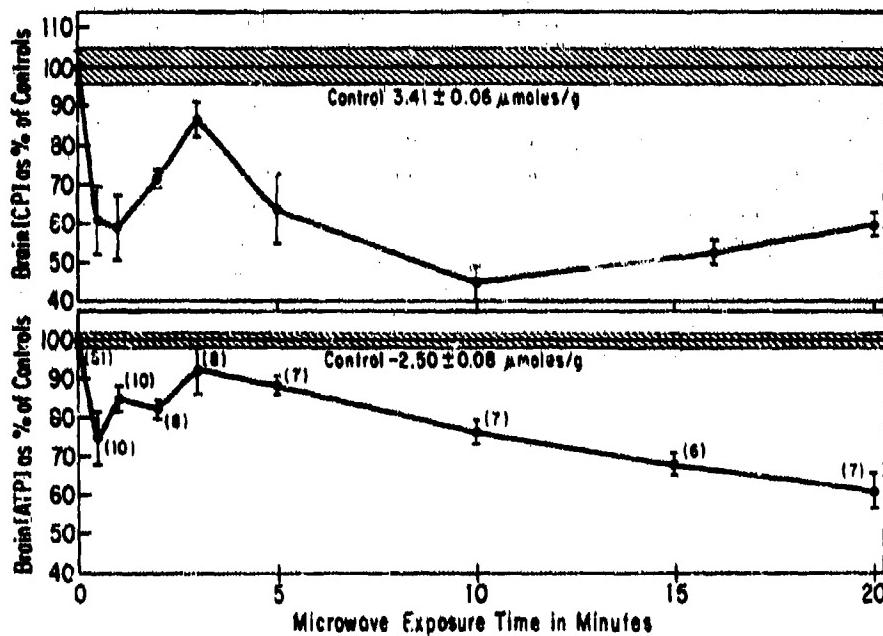


Figure 11.   Change in rat brain ATP and CP vs time of exposure to 591 MHz, CW, 13.8 mW/cm$^2$ microwaves.

The change in rat-brain NADH fluorescence, ATP and CP, is shown as a function of exposure time for 200, 591, or 2450-MHz, CW, 13.8-mW/cm$^2$ microwaves in Figure 12 [2]. The 2450-MHz exposures caused no significant changes in brain NADH fluorescence, ATP, and CP over the 5-min exposure.

257
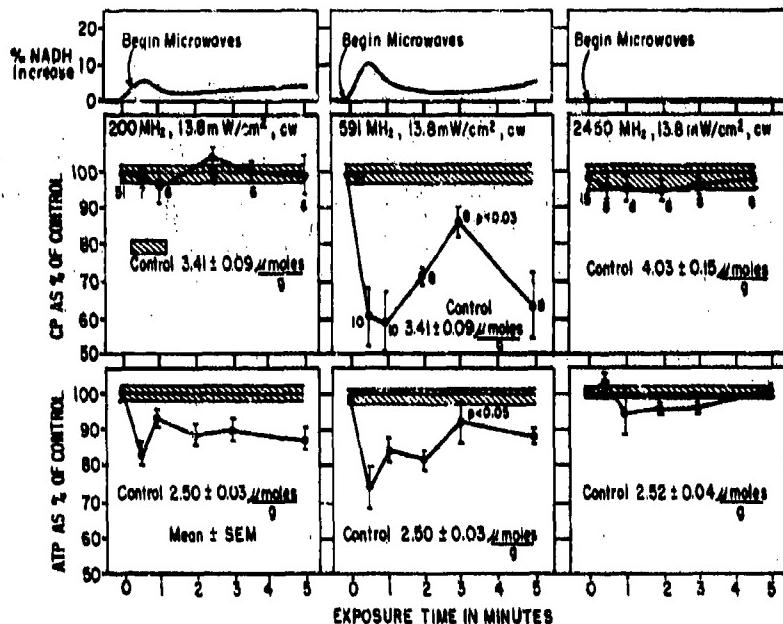
Figure 12. Changes in rat brain NADH fluorescence, ATP, and CP vs exposure time for 200, 591, or 2450 MHz, CW, 13.8 mW/cm$^2$ microwaves.

There is one major difference between the 200 and 591 MHz exposures and their effects on brain ATP and CP. Exposures at both frequencies resulted in significant decreases in ATP at all exposure intervals. The 591 MHz exposures resulted in significant decrease in brain CP, exceeding the % decreases in ATP at each exposure interval. It was noted during the 591 MHz experiments that approximately 1 of 5 exposed brains had normal CP levels with an accompanying greater decrease in brain ATP than usually seen. However, each exposure-interval group had brain CP significantly decreased from control levels when statistically comparing the group with controls by a 2-group comparison Student's t-test. The 200 MHz microwaves caused significant decrease in brain ATP at all exposure intervals, but no exposure group had brain CP statistically different from controls. For all time intervals only one of 31 CP observations for 200 MHz microwaves fell outside the 95% confidence limit for controls.

We hypothesized, on the basis of finding decreased brain ATP but normal CP, that 200 MHz microwaves inhibit the CP + CP-kinase + ADP interactions such that the system is incapable of transferring the high-energy phosphate bond from CP to ADP to yield creatine plus ATP. (Under normal conditions the CP to ADP transferase action (CP-kinase) to yield creatine and ATP, occurs so rapidly that the brain CP can drop as low as 60% of normal and still sustain ATP within normal limits.) The 200- and 591-MHz exposure data support the concept that the microwave exposures at 200 MHz and 591 MHz inhibited mitochondrial electron transport chain function.

258

It is conceivable that if the 200-MHz exposures were increased in power, the decrease in ATP would resemble that seen with 591-MHz microwave exposures. The SARs are 0.046 and 0.185 for 200-and 591-MHz exposures, respectively. For a 13.8-mW/cm$^2$ surface power density, the SAR at 200 MHz was only 21.9% of the 591-MHz SAR, i.e. 0.56 vs 2.55 W/kg. An SAR of 2.55 mW/g at 200 MHz might cause a greater decrease in brain ATP over the exposure intervals. As indicated above, the data at 200 and 591 MHz suggest the possibility that the 2 frequencies may be inducing molecular oscillations at 2 (or more) different points along the transport chain. Lower SAR would be required at the 200 MHz interaction to cause the same degree of inhibition as that observed at 591 MHz.

## IV. SUMMARY AND CONCLUSIONS

The inhibition of rat-brain mitochondrial electron transport chain function by microwaves as shown by increase in NADH fluorescence and decrease in ATP and CP is frequency (thus photon energy) dependent. It is hypothesized that microwaves induced dipole oscillations in critical protein molecules along the respiratory chain, with subsequent inhibition due to rigid stereospecificity requirements of the molecule for the chain to function. The same mechanism would apply to the 200-MHz microwave inhibition of CP-kinase. Similarly, any enzyme-substrate combinations might be affected by microwaves in the same manner. There are multiple enzymes (reductases, dehydrogenases, and transferases) associated with entry points to, along, and at the end of the electron transport chain. It is possible that there are multiple locations (preceding, along, and terminating the chain) where microwave-induced dipole (thus molecular) oscillations could occur. Each such location could have a different natural resonance frequency, threshold SAR, and SAR to produce the maximum effect, the requirements being dependent upon molecular structure and the critical role of the molecule in its specific function at the location of activity, including metal atoms where involved. Thus, there may be multiple frequency-specific sites (enzymes, cofactors, cytochromes, etc) and different threshold SAR values where microwaves could inhibit electron transport chain function. Similarly there may be multiple anabolic and catabolic enzyme reactions throughout the cell which could be microwave inhibited at the proper frequency(ies) and SAR level(s) that may be below thermogenesis. Each enzyme system would have to be studied individually to ascertain such effects. The NADH fluorescence methods for following the function of the electron transport chain only shows that there has been an effect at some point along the chain. It is recognized that there are multiple enzyme focal points along the respiratory chain, of which only one would have to be inhibited to produce the observed effects of increased brain NADH fluorescence and decreased ATP and CP It is essential, however, that the frequencies from 1 to 800 MHz be scanned to determine if there are narrow or broad frequency specific effects on such enzyme(s) function(s).

The data from 1000- to 2450-MHz exposures showing no changes in NADH fluorescence, ATP, and CP suggest that these higher frequencies are incapable of inducing molecular oscillations along the electron transport chain. This is consistent with Pethig's [16] observation that microwave-induced dipole oscillation in protein solutions is observed mainly in the 30 - 300-MHz frequency range - with some microwave-induced protein oscillations being observed at frequencies as high as 900 to 1000 MHz.

All observed decreases in brain [ATP] – and [CP] at 591 MHz – were at power levels that did not cause an increase in the exposed brain temperature (200-MHz, CW, 13.8-mW/cm$^2$, 0.63 W/kg brain SAR, and 591-MHz, CW, 13.8-mW/cm$^2$, 2.55-W/kg brain SAR) as measured by a Vitek 101 temperature probe over 30-min exposure intervals. It is proposed that this is a nonthermal, direct microwave effect at the specific frequencies.

Energy metabolism is a common denominator to all life and is essential to sustaining life in all cells and tissues. Further studies of the effects of microwaves on energy metabolism should include other critical tissues (e.g. heart, liver, and kidney) and the frequency spectrum of 10 to 1000 MHz where microwave-induced protein oscillations have been observed [16].

## V. REFERENCES

1. Sanders, A.P., D.J. Schaefer, and W.T. Joines: Microwave effects on energy metabolism of rat brain. Bioelectromagnetics 1 (2): 171-182, 1980.

2. Sanders, A.P., and W.T. Joines: Microwave (200, 591, and 2450 MHz) effects: cerebral energy metabolism. Final report for EPA contract number 68-02-3233. EPA technical report (in press).

3. Lowry, O.H., and J.V. Passonneau: "A Flexible System of Enzymatic Analysis," Academic Press, New York, 1972.

4. Biological Effects and Health Hazards of Microwave Radiation. Eds. P. Czerski, K. Ostrowski, M.L. Shore, Ch. Silverman, M.J. Suess, and B. Waldeskog; Polish Medical Publishers, Warsaw. (1974), pp 25-28, 67-74, 119-133, 173-177, 261-272, 289-293.

5. Blackman, C.F., S.G. Benane, J.A. Elder, D.E. House, J.A. Lampe, and J.M. Faulk: Induction of calcium ion efflux from brain tissue by radiofrequency radiation: Effect of sample number and modulation frequency on the power-density window. Bioelectromagnetics 1: 35-43, 1980.

6. Baranski, S.: The effect of chronic microwave exposure on the blood forming system in guinea pigs and rabbits. Aerosp. Med 42: 1196-1199, 1971.

7. Adey, W.R.: Introduction: Effects of electromagnetic radiation on the nervous system. Ann. N.Y. Acad. Sci. 247: 15-20, 1975.

8. Bawin, S.M., L.K. Kaczmarek, and W.R. Adey. Effects of modulated VHF fields on the central nervous system. Ibid., 74-81, 1975.

9. Gavalas, R.J., D.O. Walter, J. Hamer, and W.R. Adey: Effect of low-level, low-frequency electric fields on EEG and behavior in Macaca nemestrina. Brain Res. 18: 491-501, 1970.

10. Kaczmarek, L.K.: Cation-binding models for the interaction of membrane with EM fields. Neurosci. Res. Program Bull. 15: 54-60, 1977.

11. Kramer, R.S., and R. Pearlstein: Cerebral cortical microfluorimetry at isosbestic wavelength for correction of vascular artifact. Science 205, 693, 1979.

12. Joines, W.T., G. Dakermandji, R.L. Seaman, and H. Wachtel: Microwave-power absorption by rectangular-shaped conductive dielectric samples in stripline. IEEE Trans. on Microwave Theory and Techniques MTT-24: 536-538, 1976.

13. Foster, K.R., J.L. Shepps, R.D. Stoy, and H.P. Schwan: Dielectric properties of brain tissue between 0.01 and 10 GHz. Phys. Med. Biol. 24: 1177-1187, 1979.

14. Cooper, T.E., and G.J. Trezek: A proven technique for determining the thermal conductivity of tissue. J. Heat Transfer 94: 133-140, 1972.

15. Durney, C.H., C.C. Johnson, P.W. Barber, H. Massoudi, M.F. Iskander, J.L. Lords, D.K. Ryser, S.J. Allen, and J.C. Mitchell: Radiofrequency radiation dosimetry handbook, 2nd edition, <u>Report SAM-TR-78-22</u>, USAF School of Aerospace Medicine, Aerospace Medical Division (AFSC), Brooks AFB, Texas, 1978.

16. Pethig, R.: "Dielectric and electronic properties of biological materials," John Wiley and Sons, New York, 1979.

# VI. PUBLICATIONS AND PRESENTATIONS RESULTING
FROM AF FUNDED EFFORTS

1. Sanders, A.P., M.D. Rafal, and W.T. Joines: Effect of temperature on
   591-MHz, CW exposures on brain energy levels. BEMS Second Annual
   Meeting, September 14-18, 1980, San Antonio, Texas, No. 53

2. Sanders, A.P., M.D. Rafal, and W.T. Joines: Effect of 200-MHz and
   591-MHz Exposures on Rat Brain CP-kinase. Ibid, No. 54.

3. Sanders, A.P., and W.T. Joines: The Effects of 200-to 2450-MHz
   microwaves on rat-brain energy metabolism. USAF RFR Program Review,
   June 22-24, 1980, Brooks AFB, Texas.

Manuscripts in Preparation:

1. Sanders, A.P., and W.T. Joines: Microwave frequency-dependent effects
   on rat-brain energy metabolism. Bioelectromagnetics (to be submitted).

# EFFECTS OF ELECTROMAGNETIC RADIATION ON CALCIUM FUNCTION IN THE BRAIN

Paul Greengard, Ph.D.

Department of Pharmacology, Yale University School of Medicine
New Haven, CT 06510

Contract Number F33615-78-D-0617, Task Number 0044

## I. INTRODUCTION

We have recently undertaken a review of the literature concerning the effects of electromagnetic radiation on calcium function in the brain. The report consisted of two main parts: a review of the effects of radiation on calcium function in the nervous system, and a review of the roles played by calcium in normal neuronal function. We have since proposed to study calcium-dependent protein phosphorylation in brain, an important molecular mechanism through which calcium regulates neuronal function, and the effects of electromagnetic radiation on calcium-dependent protein phosphorylation in the brain.

## II. TECHNICAL APPROACH

In the experimental work which we have reviewed, a variety of experimental facilities, dosimetry, biological procedures, computer support, statistics, and data processing were used by the various investigators. In particular, the studies of calcium efflux in the brain by Drs. Adey and Blackman and their co-workers employed both low-frequency (1-32 Hz) electromagnetic radiation as well as amplitude modulation at frequences of 0.5-35 Hz of a very high radiofrequency carrier (50-450 MHz).

# III. RESULTS/PROGRESS

### A. Effects of Electromagnetic Radiation on Calcium Function in the Brain.

The major area of research that relates to radiation and brain calcium per se is that of Drs. Adey and Blackman and their co-workers. These investigators have studied the effects of radiofrequency radiation on the efflux of radiolabeled calcium from nervous tissue. Exposure of mammalian or avian brain tissue to weak electromagnetic fields causes a decrease in the efflux of calcium from the tissues when the frequency is low (6-16 Hz), but an increase when these same low frequencies are used to modulate a very high radiofrequency carrier (50-450 MHz). The radiation-induced changes in calcium efflux exhibit both a frequency window (the effects not being observed at frequencies lower than 6 Hz or greater than 20 Hz) and a power window which is relatively narrow (the effects being obtained only between 0.1 and 1.0 mW/cm$^2$). For the cat cortex, tissue gradients are of the order of 100 mV/cm, and are thus comparable with the gradients of 20-50 mV/cm associated with the electroencephalogram. Weak direct electrical stimulation of the cortex leads to an increase in labeled calcium efflux.

Despite the large number of studies on calcium efflux, few studies have sought to determine the source of the calcium involved in the observed efflux, the mechanism by which radiation alters calcium efflux, and the functional implications of the radiation-induced changes in calcium efflux. Therefore, while these studies on calcium efflux are potentially interesting, they fail to demonstrate physiologically significant effects of radiation on calcium function in the brain.

### B. Functions of Calcium in the Brain.

Investigators interested in the effects of electromagnetic radiation on calcium function in the brain have concentrated their efforts on radiation-

induced alterations in calcium efflux from brain tissue instead of studying the effects of radiation on a wide variety of neuronal processes in which calcium is known to play an essential role. Many important physiological functions of neurons involve calcium. For example:

(1) External calcium stabilizes excitable membranes

(2) External calcium enters excitable cells, thereby providing some of the current for the action potential

(3) Internal calcium regulates the permeability of neuronal membranes to other cations

(4) The movement of calcium into nerve terminals regulates the synthesis of neurotransmitter in nerve terminals

(5) The movement of calcium into nerve terminals mediates the release of neurotransmitter from nerve terminals.

In recent years, much has been learned about the molecular mechanisms through which calcium acts in the nervous system. In particular, there is increasing evidence to suggest that calcium activation of a type of enzyme, protein kinase, mediates many of the important functions of calcium in neurons.

Future studies on radiation and brain calcium, therefore, should be designed to go beyond both a simple redemonstration of previously observed effects on calcium efflux and a demonstration of effects that are difficult to interpret. In order to determine whether radiation alters calcium function in the brain, for example, one should study the effects of radiation on a series of well-described model systems of calcium action in neurons. Such model systems exist both at the level of the physiological actions of calcium and at the level of the molecular actions of calcium. One such model system is protein phosphorylation.

C.   Proposed Studies on Calcium-Dependent Protein Phosphorylation and

the Effects of Electromagnetic Radiation on Calcium-Dependent Protein Phosphorylation

in the Brain.

Over the past several years, my colleagues and I have obtained much
evidence to support the hypothesis, mentioned above, that many of the effects of
calcium in the nervous system may be mediated by protein phosphorylation.  The
first demonstration of calcium-dependent protein phosphorylation was obtained by
utilizing rat brain synaptosomes  prelabeled with $^{32}P$-phosphate.  Brief exposure
of synaptosomes to depolarizing agents, which are known to increase calcium move-
ment into synaptosomes, increased the incorporation of phosphate into many protein
bands as analyzed by SDS-polyacrylamide gel electrophoresis.  Incubation of synap-
tosomes in calcium-free medium blocked the depolarization-induced changes in pro-
tein phosphorylation.  More recent work has suggested that this calcium-dependent
phosphorylation is the result of the activation by calcium of calcium/calmodulin-
dependent protein kinases.  In contrast to cyclic AMP-dependent and cyclic GMP-
dependent protein kinases, where there appears to be only one catalytic enzyme
for each type of activity, brain apparently contains a minimum of four distinct
calcium/calmodulin-dependent protein kinases which display different substrate
specificities.

Various in vitro studies of brain tissue have identified more than ten
distinct endogenous phosphoproteins that exhibit calcium-dependent phosphorylation.
Support for the contention that at least some of these phosphoproteins are physio-
logically relevant components of neuronal function is provided by studies which
demonstrated that depolarization of intact brain slices increased the phosphoryla-
tion of several specific proteins.  The most prominent phosphoprotein amongst this
group, Synapsin I (MW 80,000), has been purified to homogeneity and extensively
characterized.  Synapsin I is a neuron-specific protein that is concentrated at

267

synapses where it appears to be predominantly associated with neurotransmitter vesicles. Recently, the state of phosphorylation of Synapsin I has been shown to be regulated, in a calcium-dependent manner, by impulse conduction under physiological conditions. In addition to Synapsin I, other endogenous phosphoproteins that exhibit calcium-dependent phosphorylation are presently being investigated.

We propose to study further the many components of the calcium/calmodulin-dependent protein phosphorylation systems of the brain and to determine whether acute or chronic radiofrequency radiation alters some aspect of these protein phosphorylation systems. We propose to determine whether irradiation of laboratory animals alters the total amount, the regional distribution, or the subcellular distribution either of any of the various calcium/calmodulin-dependent protein kinases in brain or of any of the various endogenous substrate proteins for the protein kinases in brain. In addition, we propose to determine whether radiation alters the ability of depolarizing agents to regulate the phosphorylation state of any of the various substrate proteins for calcium/calmodulin-dependent protein kinases in synaptosomes or in brain slices. Furthermore, we propose to study the effects of radiation on neurotransmitter release by determining whether irradiation of animals (a) alters the basal release of neurotransmitter from isolated synaptosomes, (b) alters the ability of depolarizing agents to stimulate the release of neurotransmitter from synaptosomes, or (c) alters the ability of various modulatory compounds to regulate either the basal or the depolarization-stimulated release of neurotransmitter from synaptosomes.

IV: SUMMARY AND CONCLUSIONS:

With well-designed studies, it should be possible to ascertain whether electromagnetic radiation does, indeed, alter neuronal function, whether such

268

alterations in function involve calcium, and, if so, to identify specifically
the molecular processes involved.

# PHYSIOLOGICAL CONSEQUENCES OF RF RADIATION AND CALCIUM

R.D. Myers

University of North Carolina School of Medicine

Chapel Hill, NC   27514

## I. INTRODUCTION

The purpose of this project is to review critically published reports dealing with the possible interaction of radiation sources and the activity of calcium ions in the brain. Calcium is a most important and clearly pivotal cation underlying the functioning of nerve cells in all of their molecular complexity. The applicability to the human situation of exposure to various sources of radiation is, therefore, of paramount importance in relation to possible aberrant activity of calcium ions and the impact of such an effect on the normal operation of the nervous system.

## II. TECHNICAL APPROACH

Pertinent studies are analyzed, evaluated, and/or interpreted in an unbiased effort to ascertain their scientific validity as well as their functional significance to the issue surrounding the possible interaction between calcium and radiation (Myers & Ross, 1981). The neuropharmacology of the $Ca^{++}$ ion has been a topic of wide interest to scientists since the turn of the twentieth century. Numerous original papers based on experimental work on calcium's effect on the brain were published prior to World War II (e.g., review of Myers, 1974a). Since the late 1960's, the study of the neurophysiology of $Ca^{++}$ ions has burgeoned. Investigations into the questions of energy metabolism, body temperature regulation, transmitter release, and even behavior have been undertaken (e.g., review of Myers, 1978).

How each major result could bear upon the $Ca^{++}$ ion-radiation issue has been dealt with in terms of the general biological effects of radiation, with a special emphasis placed upon the central nervous sytem. Thus, we have

considered in some detail the *in vivo* and, in some cases, *in vitro* effects
of different parameters of nonionizing radiation on nerve and sensory tissues.

## A. CALCIUM AND BRAIN FUNCTION

Recent observations strongly suggest that $Ca^{++}$ ions play a unique role
in specific neural control and other functions for which the brain is respon-
sible. One relative comprehensive set of findings accumulated over the last
10 years implicates $Ca^{++}$ ions in the establishment and maintenance of the
steady-state and stable body temperature of 37°C (Myers, 1974b), commonly
referred to as the "temperature set-point."

A brief summary of this evidence is as follows (Myers, 1978; 1981): (1)
A change in the ratio of sodium to calcium ions in the posterior hypothalamus
shifts the set-point temperature up or down as the ratio favors the localized
concentration of $Na^+$ or $Ca^{++}$ ions, respectively; (2) a fever of bacterial
origin, which deflects the set-point temperature upwards, causes an efflux
of Ca++ ions that is presumably due to membrane destabilization and/or unbinding
of $Ca^{++}$ ions specifically within the posterior hypothalamus and perhaps other
parts of the brain; (3) a thermal challenge caused either by peripheral
cooling or heating or by cold or heat applied to hypothalamic thermosensitive
neurons, produces a marked shift in $Ca^{++}$ ion kinetics, including tissue efflux,
depending upon the nature of the stimulus, hot or cold; (4) an exercise-induced
increase in set-point temperature evokes the efflux of $Ca^{++}$ ions from the
hypothalamus; and (5) an antipyretic administered to the febrile animal
inhibits the efflux of $Ca^{++}$ ions as set-point temperature declines to the
normal level.

Other physiological processes which utilize an ionic mechanism involving
calcium include the functions of sleep and arousal as well as emotional

behavior. Considerable support also is building for $Ca^{++}$ ions' role in the diencephalic control of the ingestive process of feeding and the set-point for body weight (Myers, 1978). Overall, energy exchange and thermal input to tissue influence lability of tissue $Ca^{++}$ ions rather remarkably.

## B. RADIATION EFFECTS ON NEURAL SYSTEMS

Insofar as the human is concerned, there are little quantitative data, which are collected with rigidly executed controls, to suggest that a given RF field is a primary cause of a specific set of symptoms. Graves et al. (1979) conclude that ELF and RF effects on tissue can be likened to the "Cheshire Cat Phenomenon" - here today and gone tomorrow, but eventually appearing, given patience, at least transiently. Nearly all experiments, however, in which microwaves or other radiation sources reportedly exert a specific effect on a neural system, can trace their result to a thermal effect, i.e., physiologically significant rise in temperature of the tissue sample.

Considerable debate now exists over the artifactual or real nature of microwaves on auditory and vestibular structures. It is generally agreed upon by most workers in this subarea that RF pulses and other radiation act on these sensory organs by a mechanism which originates as a focal temperature differential. Within the organ of Corti, a localized wave or pressure is set up as the microwave energy is converted to thermal energy (Chou et al., 1980), which in turn produces the perceived sensation. Similarly, a temperature differential in the intralabyrinthine space, following absorbance of the heat generated by microwave radiation, produces caloric stimulation of the vestibular apparatus.

273

The blood-brain barrier is purportedly broken down by microwave and other forms of radiation (Frey et al., 1975). However, other reports do not support this possibility. In fact, it is possible that the data collected originally which show field-induced perturbations of the barrier were misinterpreted (e.g., review of Myers & Ross, 1981). An equally likely explanation put forth recently is that the effects of radiation on the blood-brain barrier are related entirely to the focal increase in the temperature of the brain's parenchyma (Lin, 1980).

Changes reported to occur in the electrical activity of the brain (EEG), CNS transmitters, or in on-going behavior in an operant task following irradiation of the test animal are disappointingly unconvincing. Clearly, if an animal is agitated, aroused, or otherwise incapacitated by a transient but intense hyperthermic episode, EEG activity and/or all other aspects of behavior will be affected in some way. Typically, focal changes in the brain's temperature have not been obtained. However, in several behavioral and EEG studies, the observed effect of a radiation source is traced directly to a localized heating of tissue. Actually, Stern (1980) concludes that the behavioral effect of microwaves depends on no other mechanism than the animal's reaction to heat. Corollaries to this deduction are readily found in the literature on neurotransmitters as well. For example, Merritt et al. (1975) demonstrated that changes in catecholamine level in the brain of the rat depend solely on the power density of the radiation parameter.

III. RESULTS/PROGRESS

The main group of workers to whom the idea of a radiation-calcium interaction is attributed is that of Adey in California. In a series of papers

published in the mid-1970's, Bawin, Adey, and colleagues examined the efflux of $Ca^{++}$ ions from brain tissue as a consequence of UHF or extremely low frequency (ELF) radiation. This work is well summarized (review of Adey, 1979) as follows.

In the newly hatched chick, the brain was excised, placed in a tube containing $^{45}Ca^{++}$ in a Ringers medium without oxygen, and exposed to several fields of varying strength. When the field was amplitude modulated at 147-MHz frequencies at 9, 11, and 16 Hz, a 14% to 18% increase in $Ca^{++}$ efflux from the chick brain occurred. Later, Bawin and Adey reported that at 10- and 56- V/m sine wave electrical fields, the 6- and 16- Hz frequencies produced an in vitro suppression of $^{45}Ca^{++}$ in the chick brain preparation. $Ca^{++}$ ion efflux from gastrocnemius muscle was unaffected by ELF field exposure; moreover, processing the tissue samples at 30°C did not alter the results. Thus, the existence of a 16-Hz "window" was proposed.

Using the same isolated chick brain preparation, the "window" idea was expanded. In different experiments, Adey and co-workers reported that the efflux of $^{45}Ca^{++}$ at 0.1-mW/cm² field intensity was greater than at other intensities ranging from 0.05 to 2.0 mW/cm². As a result, an "amplitude window" was proposed for a weak, 450-MHz field sinusoidally modulated at 16 Hz. In all of these experiments, the data are presented in terms of percent changes. Parametric (t) statistical analyses were done on percentage data, and no actual "raw" data in terms of CPM of $^{45}Ca^{++}$ were presented. In some cases, all tissue samples were discarded by Adey and colleagues when the values of their $^{45}Ca^{++}$ radioactivity exceeded a certain standard deviation level, preselected by the authors, which thus precluded their inclusion in the study.

Two other groups of researchers are known to have attempted to replicate the $Ca^{++}$ ion efflux studies. One has failed to do so (Shelton & Merritt, 1980), but the full report is not yet available. The other group reports that the findings can be replicated. Blackman et al. (1980) used the same excised-tissue incubation preparation, followed the same laboratory procedures, and employed the same parameters of radiation field exposure. Data were "mass normalized" and presented then as "Vt/Vc" ratio (v=variable, t=treated, c=control). Again, absolute data on changes at levels of radioactivity in terms of CPM were not provided to the reader.

Close scrutiny of the results of Blackman et al. (1980) reveals that the statistical differences in efflux were due apparently to the variation (decline) in the ratio values of the control (sham exposed) samples of brain tissue. Graphical plots of the ratio, not actual data, obtained from the table published in the text show that there is a normal, but close, variation around a mean "Vt/Vc" ratio. Figure 1 presents the "exposed" data plotted together as power density at 16 and 9 Hz levels of exposure of chambers containing 4 and 10 tubes of chick brains ($\bar{x}$ = computed mean of the five values in each case). Figure 2 shows the same results for the "sham," nonexposed brains and reveals that at two power densities, 0.55 and 0.83, one or more average "Vt/Vc" values are sharply lower than the mean. It is not known whether such differences among "sham" controls are significant, nor whether there is indeed homogeneity of variance across the "exposed" samples and, hence, no difference. Availability of actual CMP values for all groups would perhaps provide an answer to this vital question and help substantiate the validity of the "replication" studies.
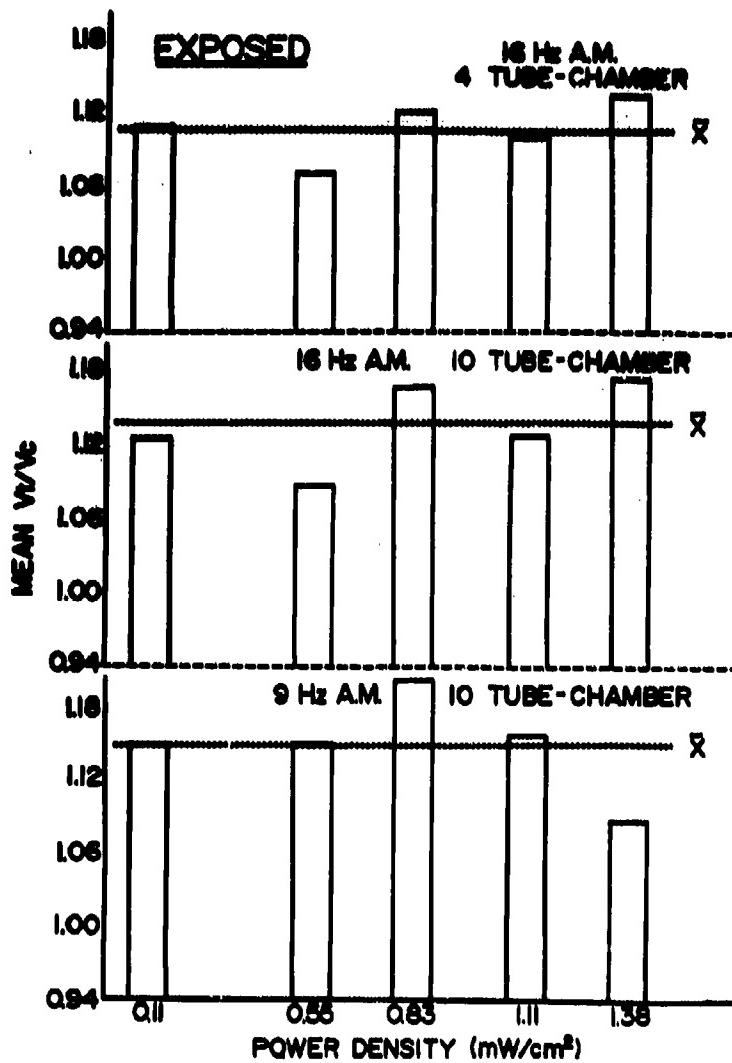
Figure 1. Re-plot of data from Blackman et al. (1980), presented in their Table 1, showing mean Vt/Vc $^{45}Ca^{++}$ efflux from chick brain exposed under the three conditions as denoted. $\overline{X}$ - dotted line is average of 5 values.

277
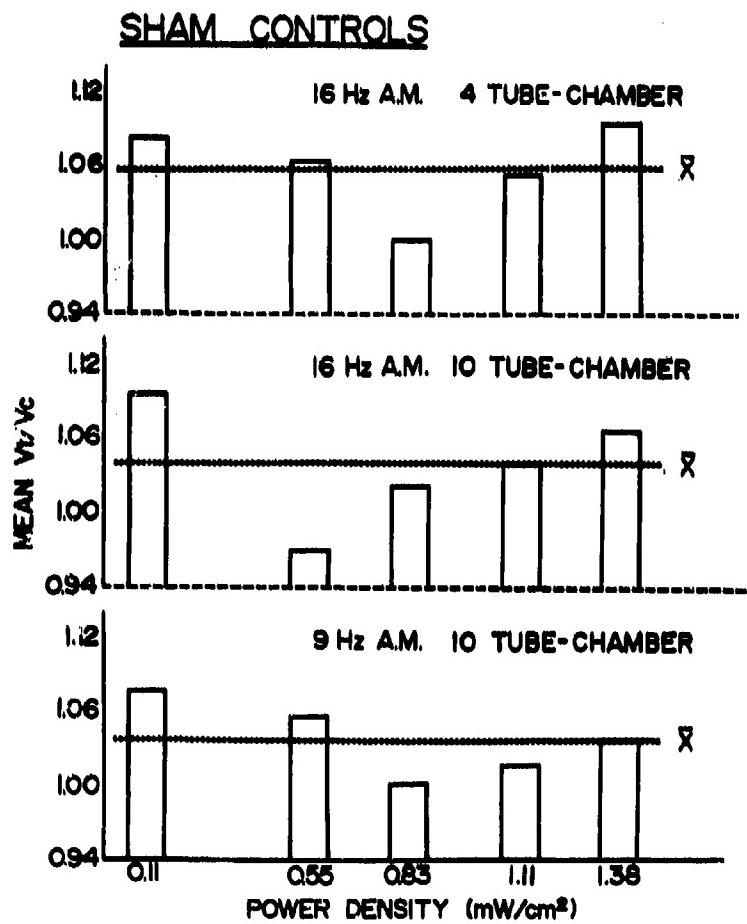
Figure 2. Re-plot of data from Blackman et al. (1980), presented in their Table 1, showing mean Vt/Vc $^{45}Ca^{++}$ efflux from chick brain during sham control under the three conditions as denoted. $\overline{X}$ - dotted line is average of 5 values.

IV. SUMMARY AND CONCLUSIONS

Studies of the physiology of calcium kinetics in living tissue show that the cation is very labile from the standpoint of both membrane and intracellular stores (Ross, 1979). The metabolism, activity, movement, or transport of calcium clearly reflects physiological events in the nervous system (Myers, 1974b). In the case of a temperature perturbation brought about by external heating of the body or by a bacterial challenge, the actual measured deflection in body temperature does not occur until well after calcium efflux ensues (Myers et al., 1976). In fact, calcium activity, unbinding or release, serves to signal either (1) the onset of a temperature change or (2) the occurrence of a thermal challenge in response to which the subsequent compensatory physiological reaction keeps the animal's temperature stable. Therefore, a thermal effect may indeed cause a change in calcium kinetics without the measure of the temperature taken being immediately quantifiable. An important behavioral corollary of this physiological situation is noted in the observation of Adair and Adams (1980): neither skin nor core temperature is necessarily deflected in response to microwave heating simply because the animal's compensatory responses offset the warm thermal challenge.

Clearly there are notable misconceptions about the thermal effect of a radiation stimulus, as illustrated by titles of literally hundreds of articles in this field. Typically they read, "Effect of microwave radiation on ... (a given function)," whereas a more appropriate title might be "Effect of heating on ...," or "Effect of heating by electromagnetic field ...," or "Thermal effects produced by radiation ..." The reason for this statement is that

279

in every section and subdiscipline covered in the review of Myers & Ross (1981), a temperature change has always been implicated in one way or another, and always by one or more groups whenever the crucial experiment was done. In nearly all experiments, there was disappointingly no proper attempt made to quantitate the thermal effects of the radiation source, notwithstanding the fact that in some cases, such as single neuron studies, a measurement of focal temperature was not feasible. For example, because of present technical limitations, one cannot impale a single cell with a thermistor or a thermocouple, even of the miniaturized variety.

Even though a thermal influence may ostensibly be ruled out experimentally by a physical (thermocouple) measure, one, nevertheless, cannot be absolutely certain of the localized thermal effects at the cellular or subcellular level of a radiation source. Surely it would seem too early to invoke an unknown or "magical" physiological quality of a microwave, RF, ELF field, or other source of radiation. In fact, to speculate about membrane properties that are below the level of identification interacting with some unidentified "force" of a radiation field represents an intellectual trip into Alice's Wonderland, at least at this stage in our scientific knowledge.

The road is clearly outlined ahead for what must be done and what technologies must be achieved. In future investigations of radiation effects on the brain's $Ca^{++}$ ion activity, essential considerations would include these points:

(1) The use of in vivo material - a live animal as a test subject is preferable, with the preparation serving as its own control whenever possible. Sophisticated surgical perfusion and other modern techniques now permit this level of experimental strategy.

(2) Tissue with an intact blood supply or which is kept oxygenated is desirable. It is well known, for example, that transmitter, and presumably other neurohumoral activity in the brain of a dead animal, reaches its peak within 10 minutes or less in terms of intracellular extrusion of material into extracellular fluid (Feldberg & Myers, 1966). Thus, field exposure of dead and anoxic tissue, devoid of a circulatory system carrying vital nutrients and disconnected from the rest of the nervous system, is scientifically questionable since the cellular material is not biologically viable.

(3) Sophisticated laboratory techniques must be thoroughly worked out and standardized so as to reduce variability in observation and data collection. Prior to the publication of findings, the pitfalls should be solved. In any case, it is not legitimate scientifically to discard part of one's data, variable or not, just so that statistical criteria requiring homogeneity of variance are met.

(4) The use of accepted statistical practices which are scientifically valid and not subject to biometric debate is essential in this field. In this context, analytical treatment of data should be able to be independently scrutinized or evaluated by other research workers, a situation which is disappointingly uncommon in this field.

(5) Dealing realistically with the question of radiation dosimetry is another item of scientific priority. An empty geometrical design, formula, or calculation cannot be readily extrapolated to a complex biological system, let alone an entire organism. The practical consequences of this realization are that a competent biologist, who understands the physiology of the test organism or tissue, should participate in or consult on the experiments in this field, which are in only one aspect an engineering-physics problem.

(6) A representative set of actual "raw" data must be provided in graphical or tabular form. In the case of $^{45}Ca^{++}$, the real measure of radioactivity in terms of CPM is required, rather than transformed values converted into percentage changes. One of the oldest and most misleading manipulations done by political or business (stock) tacticians, who want to make a fiduciary point in their favor, is to present percentage information rather than absolute numerical values.

(7) The reason that there is great variability in $Ca^{++}$ efflux studies is that in some structures $Ca^{++}$ is retained while in others $Ca^{++}$ unbinds, depending on their own excitation and inhibition mechanisms. Therefore, in one case, there could be a self-cancellation of mutual increase and decrease in ion efflux, and hence no effect. Alternatively, if the brain is moved in a spatial orientation favoring excitation and $Ca^{++}$ ions are unbound, then a resultant efflux would occur, enhancing overall variation in the experimental data. Thus attention to neuroanatomy, i.e., morphological specificity of each vital function, should be a hallmark of CNS-radiation studies.

(8) Control tests with other ions, $Na^+$, $K^+$, $Mg^{++}$, and even $Cl^-$, are essential.

Finally, if a specific neural system is affected biologically by ELF or other radiation fields, the role of temperature as the primary cause has not been unequivocally ruled out in any experiment. If there is an inconsistent effect of radiation on a biological test preparation, then the "Cheshire Cat" is probably smiling invisibly from behind the radiation source. And, if there is no effect of radiation whatsoever, the "Cat" is asleep and the tissue is cool.

## REFERENCES

1. Adair, R. and Adams, B. W. Microwaves modify thermoregulatory behavior
   in squirrel monkey. Bioelectromagnetics 1: 1-20, 1980.

2. Adey, W. R. Neurophysiologic effects of radiofrequency and microwave
   radiation. Bull. N. Y. Acad. Med. 55: 1079-1093, 1979.

3. Blackman, C. F., Benane, S. G., Elder, J. A., House, D. E., Lampe, J.A.,
   and Faulk, J. M. Induction of calcium-ion efflux from brain tissue
   by radiofrequency radiation: Effect of sample number and modulation
   frequency on the power-density window. Bioelectromagnetics 1: 35-43,
   1980.

4. Chow, C.-K., Guy, A. W., Foster, K. R., Galambos, R., and Justesen, D. R.
   Holographic assessment of microwave hearing. Science 209: 1143-1144,
   1980.

5. Feldberg, W., and Myers, R. D. Appearance of 5-hydroxytryptamine and an
   unidentified pharmacologically active lipid acid in effluent from per-
   fused cerebral ventricles. J. Physiol. 184: 837-855, 1966.

6. Frey, A. H., Feld, S. R., and Frey, B. Neural function and behavior: De-
   fining the relationship. Ann. N. Y. Acad. Sci. 247: 433-438, 1975.

7. Graves, H. B., Long, P. D., and Poznaniak, D. Biological effects of 60-
   Hz alternating-current fields: A cheshire cat phenomenon? In: Biolo-
   gical effects of extremely low frequency electromagnetics fields, edited
   by R. D. Phillips, M. F. Gillis, W. T. Kaune,and D. D. Mahlum. Techni-
   cal Information Center, U. S. Department of Energy, pp. 184-197, 1979.

8. Lin, J. C. Mechanisms of microwave-induced blood-brain barrier alterations.
   Scientific Report No. BES-4, Office of Naval Research, pp. 1-23, 1980.

9. Merritt, J. H., Hartzell, R. H, and Frazer, J. W. The effect of 1.6 GHz
   radiation on neurotransmitters in discrete areas of the rat brain. Re-
   port SAM-TR-76-3, USAF School of Aerospace Medicine, pp. 1-11, 1975.

10. Myers, R. D. Handbook of Drug and Chemical Stimulation of the Brain.
    New York: Van Nostrand Reinhold Co., 1974a.

11. Myers, R. D. Ionic concepts of the set-point for body temperature. In:
    Recent Studies of Hypothalamic Function, edited by K. Lederis and K. E.
    Cooper. Basel: Karger, pp. 371-390, 1974b.

REFERENCES (CONT.)

12. Myers, R.D. Hypothalamic mechanisms underlying physiological set-
    points. In: Current Studies of Hypothalamic Function, Vol. 2,
    edited by W. L. Veale and K. Lederis. Basel: Karger, pp. 17-28,
    1978.

13. Myers, R. D. The role of ions in thermoregulation and fever. In:
    Handbook of Experimental Pharmacology, edited by A. S. Milton.
    Berlin: Springer-Verlag, 1981.

14. Myers, R. D., and Ross, D. H. Effects of radiation on brain calcium:
    A review (in preparation, 1981).

15. Myers, R. D., Simpson, C. W., Higgins, D., Nattermann, R. A., Rice,
    J. C., Redgrave, P., and Metcalf, G. Hypothalamic $Na^+$ and $Ca^{++}$
    ions and temperature set-point: New mechanisms of action of a
    central or peripheral thermal challenge and intrahypothalamic 5-HT,
    NE, $PG_1$, and pyrogen. Brain Res. Bull. 1: 302-327, 1976.

16. Ross, D. H., and Cardenas, H. L. Nerve cell calcium as a messenger
    for opiate and endorphin actions. In: Neurochemical Mechanisms of
    Opiates and Endorphins, edited by N. H. Loh and D. H. Ross. New
    York: Raven, pp. 301-336, 1979.

17. Shelton, W. W., and Merritt, J. H. Efflux of $^{45}Ca^{++}$ from rat cortex
    tissue and microwave radiation. Bioelectromagnetics 1: 250, 1980.

18. Stern, S. Behavioral effects of microwaves. Neurobehav. Toxicol. 2:
    49-58, 1980.

# EFFECTS OF RFR EXPOSURE ON CALCIUM BINDING
# TO RAT-BRAIN MEMBRANES

David H. Ross and H. Lee Cardenas
Division of Molecular Pharmacology
Department of Pharmacology
The University of Texas Health Science Center at San Antonio
7703 Floyd Curl Drive
San Antonio, TX 78284

## INTRODUCTION

Recent advances in microwave technology and other forms of nonionizing radiation have increased our awareness that the human nervous system may be sensitive to electric and/or magnetic field strengths. Of particular interest are field strengths originating from radiofrequency radiation, either amplitude or pulse modulated, originating from microwave carriers.

Recent studies (Adey, 1979, 1981) have suggested the central nervous system may be unusually sensitive to nonionizing radiation. Specifically, earlier studies (Bawin and Adey, 1976) have demonstrated $^{45}Ca^{++}$ efflux from cerebral tissues generally decreased after exposure to electric fields of 1-75 Hz with gradients of 5-100 v/m. Blackman et al (1979, 1980) have also reported $^{45}Ca^{++}$ efflux from brain tissue exposed to variable frequency modulation and field strengths.

The importance of calcium in the central nervous system is well established (Triggle, 1971; Ross and Cardenas, 1979). Calcium has been directly implicated in membrane stabilization, enzyme activation, phosphorylation, and neurotransmitter release, to list just a few processes. Therefore, it is understandable that a central control point for many neurotransmitter functions resides in the control of central calcium metabolism.

Previous reports have chosen to observe $^{45}Ca^{++}$ efflux from the brain cortical surface following microwave exposure. Data given in these reports neither defines the locus of this calcium (bound, free, etc.) nor gives any indication of its functional significance. In this report, we use a different exposure system to determine directly $^{45}Ca^{++}$ binding to brain-membrane fractions following in vitro exposure to 2.8-GHz frequency generating a power density of 10 mW/cm$^2$.

## METHODS

### Preparation of Brain-Membrane Fractions

Male Sprague-Dawley rats weighing 120-175 g were sacrificed at 0830-0900 by decapitation. The brains were rapidly removed, rinsed in ice-cold saline, and whole brains minus cerebella were homogenized in 10 volumes of sucrose (0.32 M). Myelin, mitochondria, and synaptosomes were prepared by a slight modification of the procedure of Cotman and Matthews (1971). The initial brain homogenate was centrifuged at 2000 x g for 10 min at 4°C. The resulting pellet (nuclear) was discarded and the supernatant centrifuged at 17,000 x g for 20 min. The resulting pellet (crude synaptosomal) was resuspended in 0.32 M sucrose and layered over a sucrose gradient consisting of

287

0.6, 0.8, 1.0, and 1.2 M sucrose. The gradients were centrifuged at 65,000 x g for 60 min. Gradients were removed and tissue was collected by Pasteur pipette. Myelin was removed at the 0.32-0.6 band, and the 0.6-0.8 band was discarded. Synaptosomes were collected at the 0.8-1.0 and 1.0-1.2 band, while mitochondria were collected as the pellet. Synaptosome fractions were pooled and the myelin, synaptosome, and mitochondria were lysed in 0.5 mM DTE (dithioerythritol) - 20 mM TRIS (pH 8.5 @ 25°C) buffer in ice for 60 min. Membrane fractions were washed twice in TRIS-DTE buffer and then resuspended in buffer at a protein concentration of 1 mg/ml.

In Vitro Exposure of Membrane Fractions to MWR

Membranes isolated at the Division of Molecular Pharmacology, University of Texas Health Science Center, were stored on ice and transported to the Radiation Facility, USAF School of Aerospace Medicine, Brooks Air Force Base. Time from actual isolation to exposure was usually less than 60 min and never longer than 90 min. Membrane fractions stored on ice (4°C) were temperature equilibrated at 22°C for 10 min. Fractions were then placed in exposure chambers and radiated for 10 min with a final average power density of 10 mW/cm$^2$. Temperature was 22°C inside the chamber. Following exposure, membrane fractions were

placed in a Dubnoff metabolic shaker for 10 min at 22°C
for preincubation. Control samples were carried through-
out all steps and were placed under and directly behind
the horn during exposure. Preliminary experiments indi-
cate no appreciable radiation of control tissue at this
exposure position. Preliminary experiments indicated
the temperature in membrane fraction containers (Beckman
vials, 10 ml size) rose 2C°.

## $^{45}Ca^{++}$ Binding to Membrane Fractions

Calcium binding to membrane fractions was performed
as previously reported (Ross and Cardenas, 1977). Membrane
fractions incubated in 20 mM TRIS buffer, pH 7.4, 22°C,
with various concentrations of $^{40}CaCl_2$ (5-500 µM) were ex-
posed to $^{45}Ca^{++}$ for 5 min (0.25 x $10^6$ CPM/assay tube).
Reactions were terminated by Millipore filtration, washed
three times with 5 ml of ice-cold buffer, and filters were
dried and counted by liquid scintillation. The results
are expressed as nanamoles $Ca^{++}$ bound per mg protein.

## RESULTS

The effect of microwave exposure on $^{45}Ca^{++}$ binding
to brain-membrane fractions in vitro was determined for
myelin, mitochondria, and synaptosomes. Results of these
experiments are presented in Figure 1. Ten-minute exposure
to radiation, averaging 10 mW/cm$^2$, produced a slight but

insignificant decrease in $^{45}Ca^{++}$ binding to myelin membranes. Calcium binding to synaptosomal and mitochondrial membranes, however, was significantly reduced compared to control (P < .01).

The binding of calcium to synaptosomal membranes was further studied by varying the calcium concentrations from 5-500 μM and measuring the amount of $^{45}Ca^{++}$ bound to membrane protein. As shown in Figure 2, calcium binds to synaptosomal membranes in a concentration-dependent fashion, which saturates at ≈ 200 μM. Exposure to microwave radiation for 10 min produced a decrease in membrane calcium-binding capacity. This reduced capacity was due principally to a decrease in the number of calcium-binding sites ($B_{max}$) and, to a lesser extent, a change in affinity ($K_D$) of calcium for the membrane sites.

## DISCUSSION

Results of these studies demonstrate that microwave exposure in vitro to brain membranes significantly reduces $^{45}Ca^{++}$ binding capacity to mitochondria and synaptosomal membranes. Further, the loss of binding capacity appears to be due principally to a reduced number of binding sites ($B_{max}$), rather than a significant change in the $K_D$. Since this effect was measured in vitro, the results may be interpreted in one of two ways: Loss of $^{45}Ca^{++}$ binding

290

capacity in vitro may result from an increase in the number of sites occupied by $^{40}Ca$ or may result from sites undergoing a membrane transition to a buried or otherwise inaccessible form.

Calcium binding to membranes has been documented (Ross and Cardenas, 1979) and has been reported to occur through cation-acidic lipid interactions. Whether or not the changes in calcium binding seen here reflect a radiation-induced change in membrane constituents or whether local temperature perturbations were responsible remains open to further in-depth research. Unlike previous reports (Adey, 1979, 1981; Blackman et al, 1979, 1980), the research reported here did not explore any "window" phenomena and has not explored lower power densities of the level which would be achieved in the environment. Also, unlike previous research, our studies have focused on a receptor-type binding assay, which is a common methodology in many laboratories and enables us to measure the exact number of sites and affinity constants. Our studies, in part, may provide future direction for functional aspects of calcium transport since the $K_M$ for voltage-dependent $Ca^{++}$ influx into synaptosomes is 0.25-.5 mM. The upper phase of the binding curve presented in Figure 2 is within this range.

291

## SUMMARY AND CONCLUSIONS

Research presented here has demonstrated a significant effect of microwave radiation <u>in</u> <u>vitro</u> on $^{45}Ca^{++}$ binding to differential brain-membrane fractions. Power densities used here were on the order of 10 mW/cm$^2$. Lower, more environmentally relevant densities and variable frequencies must be explored to achieve an overall view of this single observation. Kinetic analysis, however, suggests that both a low-and high-affinity $Ca^{++}$ binding site may be altered by microwave radiation. This may functionally correspond to $Ca^{++}$ influx and $Ca^{++}$-ATPase activation site, respectively.

# REFERENCES

Adey, W.R.  Bull. N.Y. Acad. Med. 55:1079-1093, 1979.

Adey, W.R.  Physiol. Rev. 61:435-514, 1981.

Bawin, S.M. and Adey, W.R.  Proc. Natl. Acad. Sci. 73:
    1999-2003, 1976.

Blackman, C.F., Elder, J.A., Weil, C.M., Benane, S.G.,
    Eichinger, D.C., and House, D.E.  Radio Sci.
    14:93-98, 1979.

Blackman, C.F., Benane, S.G., Elder, J.A., House, D.E.,
    Lampe, J.A., and Faulk, J.M.  Bioelectromagnetics
    1:35-43, 1980.

Cotman, C.W., and Matthews, D.A.  Biochim. Biophys. Acta
    249:380-394, 1971.

Ross, D.H., and Cardenas, H.L.  Life Sci. 20:1455-1462, 1977.

Ross, D.H., and Cardenas, H.L.  Adv. Biochem. Psychopharm.
    20:301-336, 1979.

Triggle, D.J.  Neurotransmitter Receptor Interactions,
    Academic Press, New York, 1971.
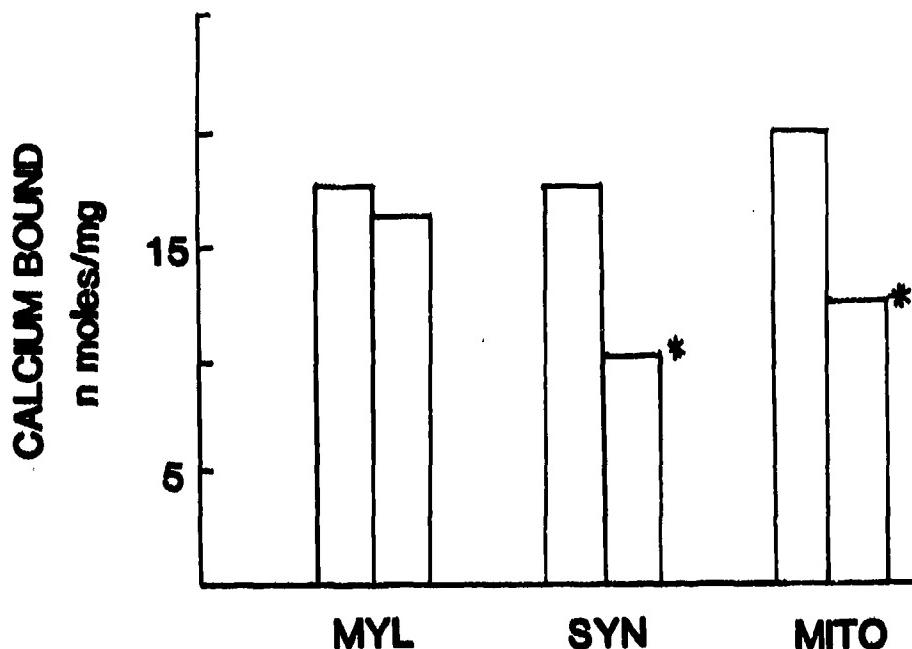
FIGURE 1: [45]Calcium binding to brain membranes was measured _in vitro_ following exposure _in vitro_ to microwave radiation. Each point represents the mean ± SEM of four replicate experiments (four individually prepared batches of tissue). Each experiment was performed in triplicate. Significant decreases in [45]calcium-binding capacity in mitochondrial and synaptosomal membranes were obtained (P < .01).
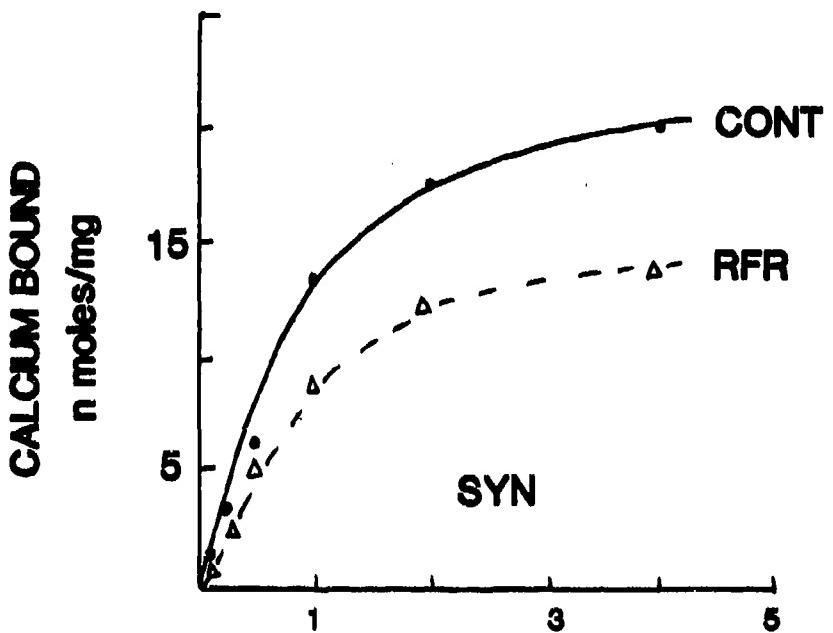
FIGURE 2: [45]Calcium binding to synaptic membranes was determined over a concentration range of 5-500 $\mu M$ [40]CaCl$_2$. Assays were performed as outlined in the METHODS. Each point on the curve represents the mean ± SEM of four replicate experiments (four individually prepared batches of tissue). Each experiment was performed in triplicate. Reduction in [45]calcium-binding capacity was significant at $P < .01$. Differences in B$_{max}$ and K$_D$ for calcium were determined by Scatchard analysis.

# MICROWAVE ABSORPTION BY NUCLEIC ACIDS

E. W. Prohofsky and L. L. Van Zandt

Department of Physics
Purdue University
W. Lafayette, IN 47907

The basic structure of interaction of any oscillatory system with microwave radiation is strongly dependent on the degree to which the oscillatory system is damped. In the case of a strongly damped oscillation, the absorption is relatively weak and forms a broad band in frequency. For very little damping, narrow lines result which are resonant and can have much larger absorption over a final frequency range. In DNA the primary source of damping appears to be free water in the vicinity of the DNA macromolecule.

Most experimental work on DNA has been done on samples in one of two regimes of water content. Work is done on DNA in solution, and these solutions are usually limited to less than 2% DNA by weight. Much work has also been done of fibres and films in which the water is usually limited to the needed water of hydration, and here it ranges to 10 - 50%. Recently Swicord and Davis have reported on microwave absorption by DNA solution[1]. Two groups have reported Brillouin-scattering observations in fibres and films.[2,3]

During the last few years, work has been carried out on the ways in which DNA is packed into chromosomes in eucaryotic cells. The double-helical DNA is wrapped around a histone core, forming a nucleosome. The nucleosomes are packed into thick strands of nucleosomes, and these strands are furthered bunched to form chromosomes. Although there is still some

uncertainty among the workers in this field, the estimates are that in the densest packing the chromatin has approximately 50% water by weight. This amount of water is intermediate between that in solutions and the fibres and films, but closer to the conditions in fibres and films.

## I.  Calculations on Double-Helical DNA in Solution.

We have carried out calculations on how water effects the acoustic modes of the double helix. The helix was treated as a cylinder imbedded in water. Water at the surface of the cylinder was viscously coupled to the compressional-mode motion of the cylinder. The propagation of this motion through the water was determined by a solution of the Navier-Stokes equations for this geometry. The boundary conditions imposed were such that the motion of the water approached zero an infinite distance from the helix. From knowledge of the water behavior, the reaction force on the helix can be determined and a self-consistent solution for helix coupled to water can be found. In Figure 1 the upper line is the logarithmic decrement ($\sim Q^{-1}$) for this coupled system. The line crossed the value 1 at $\simeq$ 200 GHz. The result indicates that this mode is overdamped because of the coupling to the water, and only broad-banded absorption can occur below $\approx$ 200 GHz. We have calculated the absorption at microwave frequencies for this case of fully dissolved DNA. The DNA absorbs roughly 40 times the rate of an equivalent mass of water at 8 GHz; this falls off to -20 times water by 12 GHz. These predictions are in excellent agreement with the absorption reported by Swicord and Davis[1]. Because the damping is so large, the absorbed energy is rapidly distributed to the surrounding water. Very rapid complete thermalization of this absorbed energy is expected.

297

If a 1% solution of DNA the size of chromosome was imbedded in water and was exposed to a milliwatt/cm$^2$ radiation field, one would expect a nanodegree excess temperature in the DNA solution.

## II. Experimental Observations on DNA in Solution

We have carried out measurements on DNA solutions as well. We attempted to measure increased activation of DNA resulting from absorption.

For purposes of this discussion a DNA molecule is viewed as an extended macroion, with negative (phosphate) charges distributed along its length. These charges attract a cloud of counter ions which are loosely bound to the DNA molecule. In addition to the classical Coulomb attraction, which acts to hold the counter ions in the general proximity of the molecule, some of the positive charges may be actually instantaneously bound to a particular phosphate group. This possibility may be pictured quantum mechanically as a series of shallow potential wells, between which positive charges may tunnel (hop) when stimulated by an externally applied electric field.

It is clear that the abundance of electric charge associated with the DNA molecule can contribute to electrical conduction. Similarly, the loosely bound counter-ion cloud can be expected to have an extremely high polarizability: the ions can be redistributed by an applied electric field without being totally removed from the DNA vicinity, giving the molecule (with its immediate surrounding) a large electric dipole moment, and thus leading to a very large contribution of these molecules to the dielectric constant. These processes are expected to occur in reponse to dc or low-frequency electric fields. At high frequencies (above 1 MHz) the ionic responses are expected to be too slow to follow the applied electric fields,

so the arguments set forth above will not apply above a certain critical frequency (referred to as the "dispersion" frequency)..

A measure of the mobility of these counter ions does not measure directly the microwave absorption of the system. It measures those factors which alter the counter-ion mobility, and these are likely to be the excitation level (effective temperature) of the helix and its immediate vicinity. From a biological point of view, enhanced excitation of the helix is the hazardous condition. Microwave absorption which is rapidly thermalized is not likely to present hazards.

## Microwave Effect on DC Conductivity of DNA Solutions

The samples consisted of dilute solutions of calf thymus DNA in water. The sample, contained in a thin glass tube, was placed in a waveguide, as shown in Fig. 2, parallel to the microwave electric field. A dc voltage of 4.5 V was applied to the sample by a battery. The electrodes connecting the sample to the rest of the electric circuit were made of platinum to prevent sample contamination and electrode corrosion. The potential drop across the resistor R was fed directly into a lock-in amplifier. Any variation of the conductivity of the DNA sample as a consequence of the presence of microwaves (modulated with a frequency $\omega_M$) would lead to an incremental ac potential across R oscillating with the same frequency $\omega_M$, which would then be selectively picked up by the lock-in detector.

The microwave power was generated by Hewlett-Packard Microwave Sweeper, Model 8620C. The sweeper allowed us to study the reponse of the sample as a function of frequency in two frequency segments (3.5-7.5 GHz and 7.5-12.0 GHz). As the signal frequency was swept, the lock-in signal was monitored

299

and stored in the memory of an on-line Cromemco Z2 microcomputer via an analog-to-digital converter. The sweep rate was usually 4 seconds per GHz, although other sweep rates were employed when this was deemed advisable. Normally the sweep was repeated 100 times, the signals from all sweeps were averaged, and the averaged signal was plotted as a function of frequency.

We estimate that the conductivity of DNA solutions is affected to less than 1 part in $10^5$ by the incident microwave power of approximately 1 mW. More details of this work can be found in our Air Force Report on this work.[4]

## Microwave Effect on AC Properties

A much better quantity to monitor under microwave irradiation is the low-frequency dielectric constant. The reason is that even in very dilute solutions, almost the entire value of the dielectric constant originates from the presence of the DNA molecules. For example, the dielectric constant of a 0.01% solution (by weight) in water, using salmon sperm DNA of average length 7400 Å, was measured to be 1700 at frequencies below 100 Hz[5]. This is to be compared with the value of 80 for the dielectric constant of the solvent alone. Thus any variation in the dielectric constant of the DNA solution (or any lack of variation) can be ascribed directly to microwave interaction with the macromolecules.

A special cell, shown in Fig. 3, has been constructed for the dielectric measurements of samples which are simultaneously irradiated by microwaves. The sample is enclosed in a lucite chamber with platinum electrodes. The

300

separation between the electrodes is controlled by raising and lowering the upper electrode. This enables us to correct the data for the polarization impedance as suggested by Grant[6]. The microwave radiation is brought to the cell by a waveguide with a tapered section which can be adjusted so that the waveguide height matches the plate separation of the sample holder. For the length of the sample, the platinum electrodes double as the upper and lower walls of the waveguide. Any microwave radiation not absorbed by the sample is then guided to an absorbing termination to avoid unwanted reflections.

In these measurements the cell was filled with 0.01% DNA and was connected to a General Radio 1615-A capacitance bridge while being irradiated with microwaves which are square-wave modulated. The bridge was adjusted to balance during that part of the cycle when the microwaves were off. Any change of impedance of the sample due to microwave interactions with the DNA would then be observed as the bridge became unbalanced at the same frequency as the microwave modulation. The magnitude of the impedance change could be measured by readjusting the bridge to balance when the microwaves are irradiating the sample, and noting the impedance change required.

A sample of the data observed with the capacitance bridge is given in Fig. 4. The lower trace is the output of a detector monitoring the microwave signal. It is high when the microwaves are on and low when they are off. The upper trace is the output from the tuned amplifier and null detector attached to the impedance bridge. The thickness of the trace indicates how well the bridge is balanced. For this data a

301

change of 0.007% in the conductivity or 1% in the dielectric constant would double the trace thickness. From the figure it is evident that there is no difference in the sample impedance between the parts of the cycle when the microwaves are on and off. Our estimated sensitivity was approximately 0.002% in the conductivity and 0.2% in the capacitance. Similar data was taken for microwave frequencies in the range 8 GHz to 12 GHz. The low-frequency impedance measurements were done from 1 kHz to 10 kHz, and various chopping frequencies for the microwaves were tried, consistently indicating no dependence of the impedance upon the micro-wave signal.

The results of our measurements are consistent with the calculations of absorption discussed earlier. The large coupling to water for the solution case insures rapid thermalization. The null result is then ex-pected even though absorption occurs.

## III. Absorption Calculations in the Absence of Damping

We have performed calculations of the microwave absorption by double-helical DNA. For absorption to occur, one requires some geometrical fea-tures which destroy translational invariance and defeat wavevector selec-tion rules. We have made these calculations for finite segments of double helix which can absorb when acoustic waves are resonant in the finite seg-ment. Figure 5 shows the calculated absorption. Only the circles are true absorption levels; as in this case of no damping, the absorption lines are very narrow. The solid lines are an envelope of the absorption peaks for helices which due to somewhat differing lengths or geometrical reasons

302

may absorb at altered frequencies. Note that the absorption for this case can be $10^4 - 10^5$ times the absorption of water.

## IV. Calculations of Damping for Fibres

We have carried out calculations for the coupling of water to DNA appropriate to a more condensed phase of DNA. The geometry had many helices separated by small regions of water. The Navier-Stokes equation for the response of the water was solved for these boundary conditions. The solutions for a compression wave in the helices plus water were found self-consistently. The logarithmic decrement for this arrangement is shown as the lower curve in Fig. 1. Note that the modes are overdamped below ≈ 20 GHz. No well-defined resonant mode should exist below this frequency. This result is in disagreement with the experimental observation of sharp line modes in DNA fibres by Brillouin scattering between 5 and 25 GHz.[2,3]

The reason for the failure of the hydrodynamic predictions is the fact that water molecules cease to behave as water molecules in bulk water in the vicinity of DNA, and this is particularly true for more dense DNA-water mixtures. We are currently using molecular dynamic methods to explore the behavior of water in the vicinity of the double helix. Very definite ordering of the water appears in these calculations. We plan to further evolve this work to the point where one can estimate the absorption and thermalization of microwave energy for DNA in more dense concentrations such as those found in eucaryotic chromatin. More details of our molecular dynamics calculations are in our Air Force Report.[4]

## V. Comments on Possible Nucleosome Absorption

### Absorption

Nucleosmes consist of two loops of DNA wound on a histone core. Such a circular structure can be a resonant structure for a polyion such as the double helix. A full wavelength acoustic wave on the circle will resonate with an oscillating field of the same frequency. For the nucleosome the circumference is approximately 100 base pairs, and the resonant frequency would then be the same as the lowest resonant half-wavelength mode for a finite segment of 50 base pairs. The absorption for the nucleosome would be four times that shown for 51 base pairs in Fig. 5 if the modes were not damped.

Whether such vibrations are damped in concentrated chromatin structures is an open question, as one could not trust results based on hydrodynamic treatment of the water. The amount of water is similar to the amount in fibres or films, and sharp lines are observed in these materials. The resonant frequencies for a compressional wave in a nucleosome is ≈ 50 GHz. That for a bending mode ≈ 3 GHz. The bending mode is more likely to be damped heavily than the compression mode. More detailed description of the modes in DNA and the no-damping absorption can be found in our Report[4] and in published articles.[7,8]

## VI. Vibrational Frequencies of Specific Features of the Double Helix

We have carried out calculations of the vibrational response of the free end of a cut double helix.[9] The low-frequency resonant response is shown in Figs. 6 and 7. Resonance behavior does occur at several points in the microwave frequency range. This response is limited to within ≈ 5 base pairs of the cut end of the helix. The specific coordinate considered

304

is the stretch of the hydrogen bonds which hold the double helix together. The curves shown do not take into account any interaction with surroundings such as water, etc. Considerable damping and broadening can be expected for the case of DNA in solution. Again, the degree of damping for densely packed DNA cannot be estimated at this time but could be very small.

A large degree of excitation of such a mode would likely enhance helix separation originating at a helix terminus. Such excitation could result from absorption.

We believe that the primary significance of this calculation is in the development of the methodology for the study of special features of many types. We also feel it demonstrates that modes associated with special features can have responses at microwave frequencies. Of greater interest from a biological point of view would be special features such as replicating and transcribing forks, separated regions of helix, nicked regions, and regions of excised sections. We have initiated a program of examining the frequency response of a number of such features.

# References

1. Swicord and Davis. Private communication. M. L. Swicord, Ph.D. Thesis, University of Maryland, 1980.

2. G. Maret, R. Oldenbourg, G. Winterling, K. Dransfeld, and A. Rupprecht. Colloid and Polymer Science 257, 1017 (1979).

3. S. A. Lindsay. Private communication.

4. E. W. Prohofsky and L. L. Van Zandt. "Absorption Events of Macromolecules" for USAFSAM, Brooks AFB, Contract S33615-78-D-0617 Order No. 0027, 30 October 1980.

5. S. Takashima. Jour. Phys. Chem. 70, 1372 (1966).

6. E. H. Grant. "The Study of Biological Molecules by Dielectric Methods," Ch. 9, Solid State Biophysics, S. J. Wyard, ed. McGraw-Hill, New York, 1969.

7. W. N. Mei, M. Kohli, E. W. Prohofsky, and L. L. Van Zandt. Biopolymers 20, 833-852 (1981).

8. M. Kohli, W. N. Mei, E. W. Prohofsky, and L. L. Van Zandt. Biopolymers 20, 853-864 (1981).

9. B. F. Putnam, L. L. Van Zandt, E. W. Prohofsky, and W. N. Mei. Biophysical Journal, In Press.
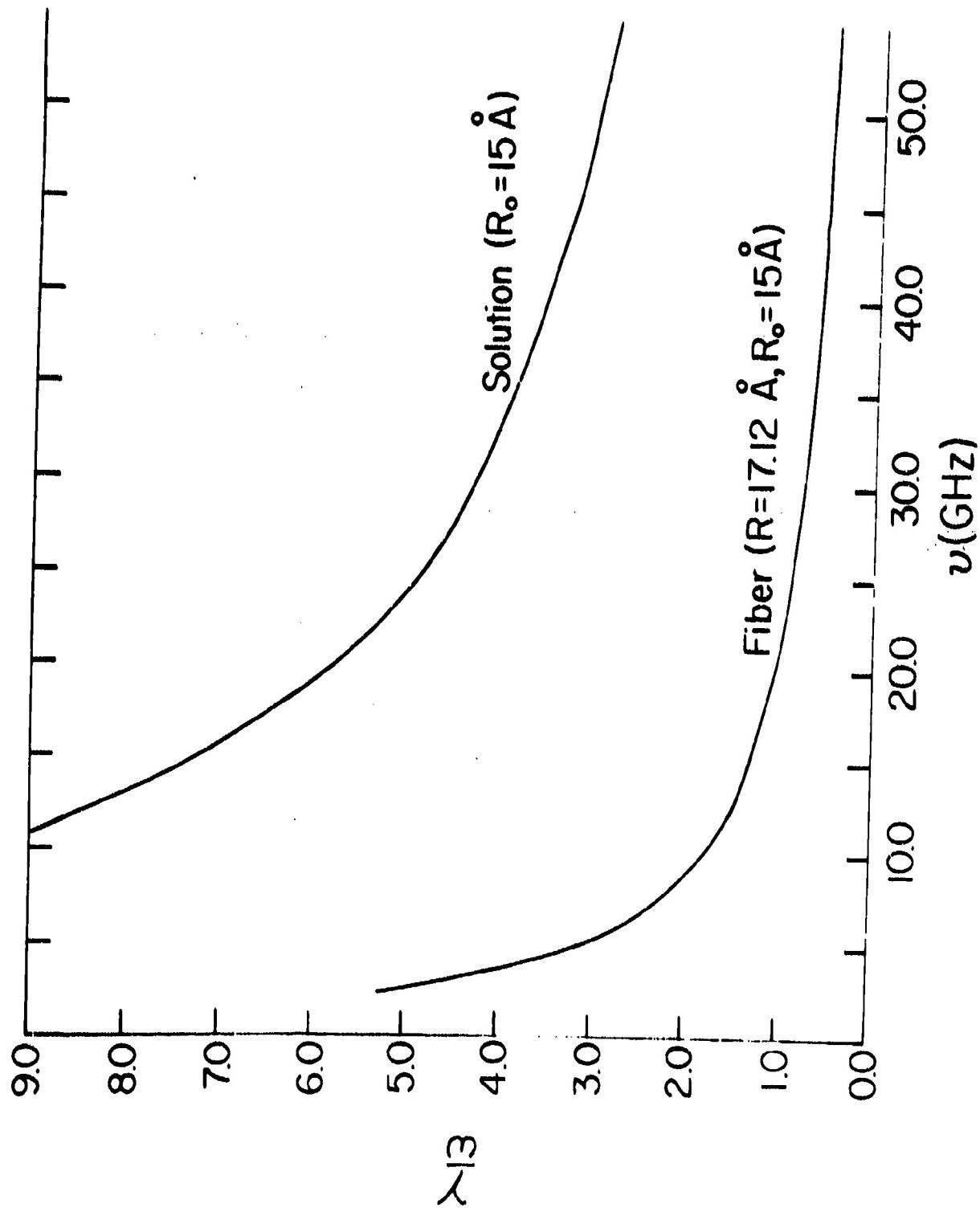
Figure 1. Damping of helix motion by interaction with water. The upper curve is the logarithmic decrement $(1/Q)$ for a single helix in an infinite amount of water. The lower curve is for many helices separated by regions of water such that the mixture is 50% water by weight. The value 1 indicates the onset of critical damping.
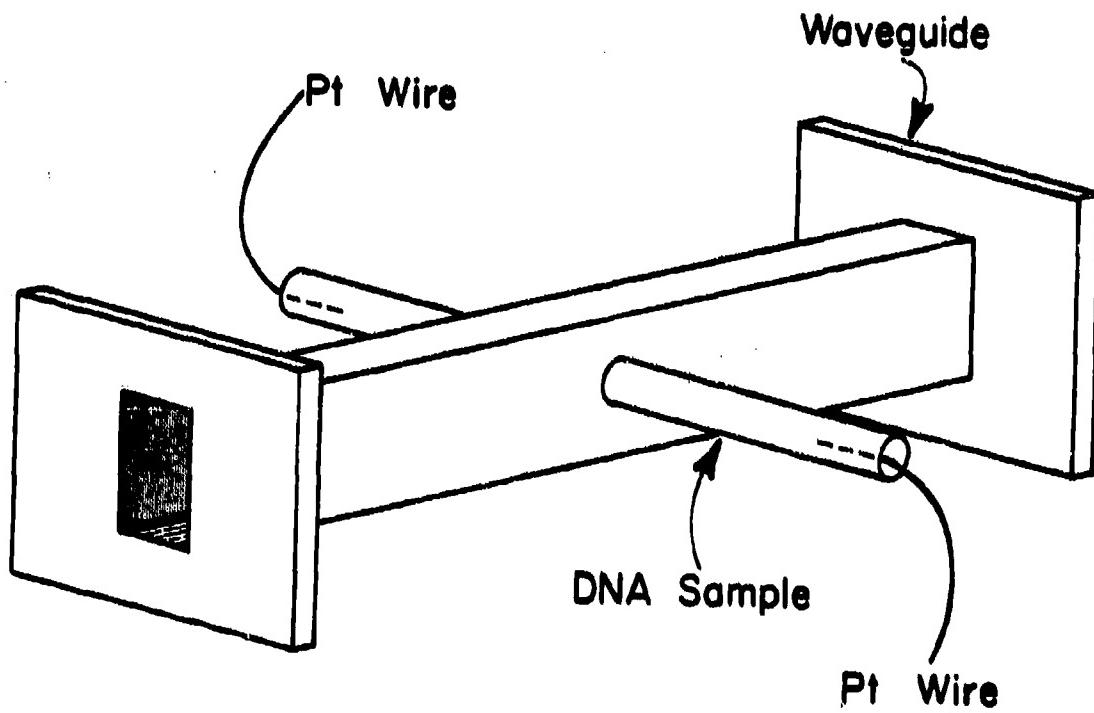
Figure 2. Sample holder to measure conductivity changes.
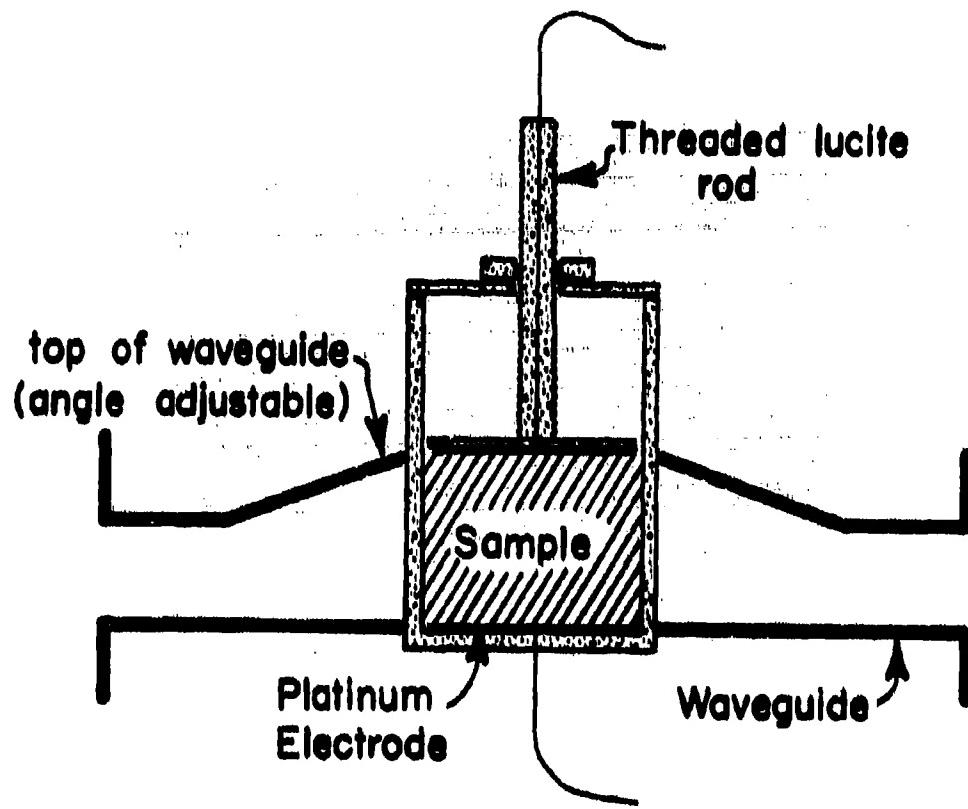
Figure 3.  Sample holder to measure ac properties.
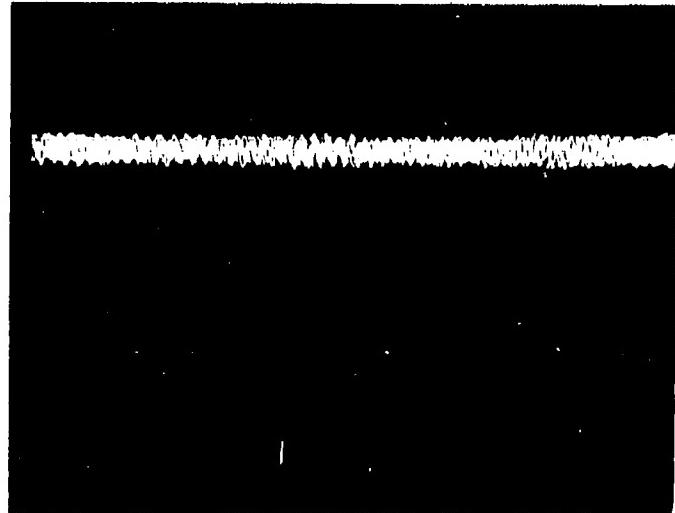
Figure 4.  Upper trace:  The signal from the tuned amplifier and null detector attached to the capacitance bridge.
Lower trace:  A signal proportional to the incident microwave power.
For this data the microwave frequency is 10 GHz, the modulation frequency is 100 Hz, and the frequency of the impedance measurement is 1 kHz.  The sample is a 0.01% solution of calf thymus DNA with an average chain length of 800 base pairs ($\approx$ 3000 Å).
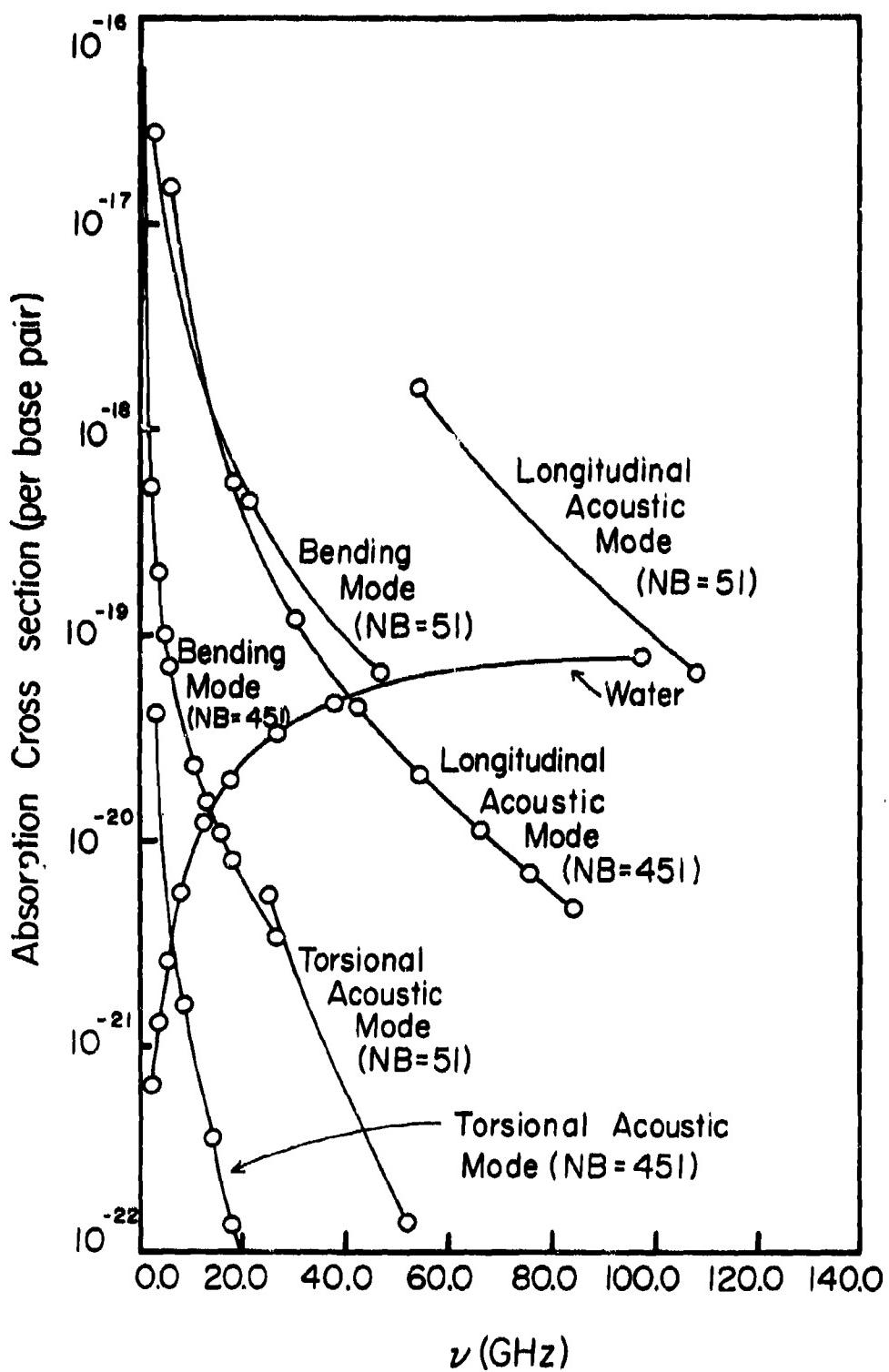
Figure 5. Absorption cross section per base pair versus frequency for the longitudinal acoustic, torsional acoustic, and bending modes for chains having 51 and 451 base pairs, respectively. The absorption cross section for longitudinal acoustic mode is higher than that for water by at least two to three orders of magnitude at microwave frequencies for a chain having 451 base pairs.

311
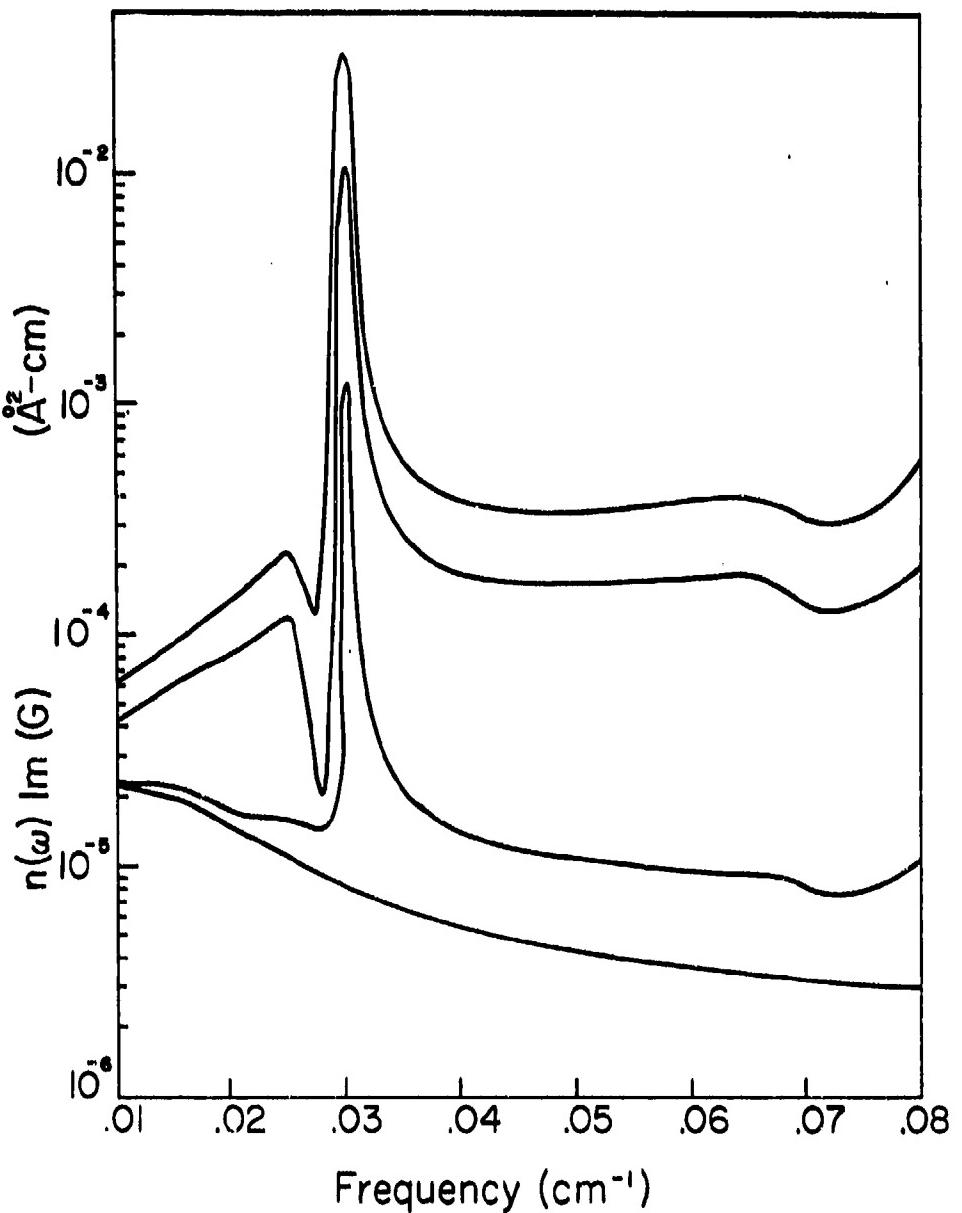
Figure 6. The response of base pairs near a terminus of Poly(dG)·Poly(dC). The lowest curve is for a base pair far from the terminus. The next lowest is the fourth base pair from terminus. The next two curves are the second from end and end base pair. The coordinate is the square of enhanced displacement of the hydrogen bond stretch coordinate of the H-bonds that hold the base pair together. $0.03$ cm$^{-1}$ = $0.9$ GHz, $0.04$ cm$^{-1}$ = $1.2$ GHz.
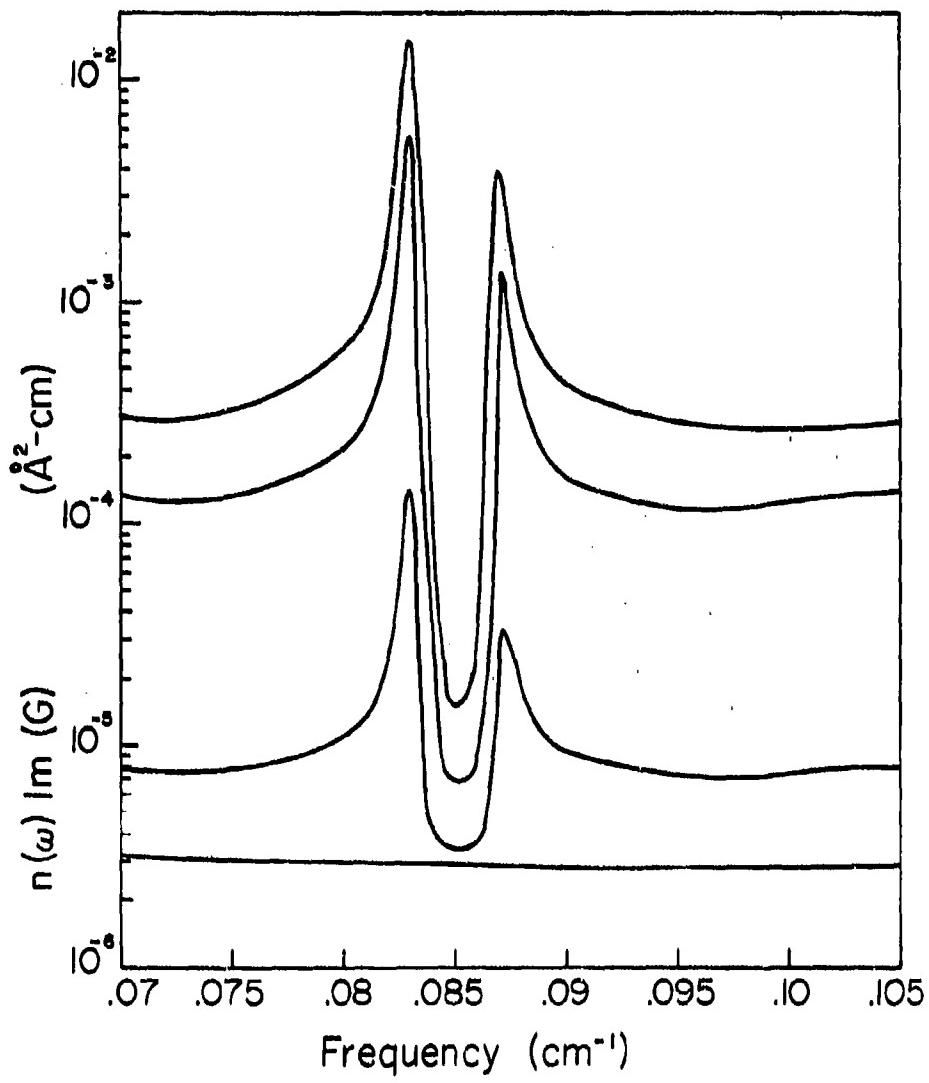
Figure 7. A continuation of Figure 6 to higher frequencies.
0.08 cm$^{-1}$ = 2.4 GHz, 0.09 cm$^{-1}$ = 2.7 GHz.

313

# RFR AND NONLINEAR BIOLOGICAL SYSTEMS

R. Broucke, D. Kondepudi, A. Nazarea, L. Reichl, and J. Speyer
Microwave Studies Group
University of Texas at Austin

I.   INTRODUCTION:  The object of our studies is to determine fundamental nonthermal mechanisms by which microwave radiation might affect biological systems.  Our work focuses on the nonlinear dynamics of biological systems at both the intramolecular and intermolecular levels.  On the intramolecular level, we are studying the way in which energy may be either focused and propagated or randomized because of internal nonlinearities, and we are studying the randomizing effect of microwave radiation on coherent internal dynamics of biological molecules.  On the intermolecular level, we are studying the molecule-solvent interaction for molecules driven at microwave frequencies, the effect of microwaves on the transport of ions through membranes and ligand migration in proteins, and we are studying the effect of external fields on nonlinear chemical pattern formation (a problem of importance to morphogenesis).  Although our approach is to determine microwave effects from an analytical viewpoint, our work is paralleled by an experimental aspect which is the subject of a separate report.

The subsequent sections will elaborate on the following subjects:
Section 2 - a possible $10^{11}$-Hz resonance of the heme plane in hemoglobin and its influence on oxygen binding; Section 3 - the effect of radiation on ionic conductance through biological membranes; Section 4 - the effect of external fields on the critical size of chemical dissipative structures, a subject of importance in morphogenesis; Section 5 - the effect of solvent viscosity on the internal migration of ligands in proteins; Section 6 - the solvent-protein interaction for a microwave-driven protein viewed as a Brownian-motion problem in which inertial effects and solvent structure play an important role;

Section 7 - spectral properties of anharmonic oscillator systems at low and high energies and their possible implications for energy absorption; Section 8 - the onset of chaos in anharmonic oscillator systems at moderately high energies; Section 9 - mathematical properties of anharmonic oscillator systems; Section 10 - conclusions.

II. <u>INFLUENCE OF $10^{11}$-Hz RADIATION ON HEMOGLOBIN</u>: Hemoglobin is a molecule whose structure and, to some extent, dynamics are known in considerable detail. Its vital role in transporting oxygen to tissue in biological systems is well known. Gelin and Karplus[1] have pointed out the critical role that the motion of the heme plane plays in the cooperative interaction of its subunits. Our concern is that microwave radiation can affect heme-plane motion with subsequent impact on oxygen binding and delivery[2].

The heme and its environment has been studied in detail by Kondepudi. To compute the resonance frequency of the heme-plane oscillations, we must know all the interactions that affect the heme. The interaction of the atoms of the heme molecule, and the forces required to move the Fe atom into the plane of the heme, can be obtained from the work of Warshel[4]. For the interaction of the heme with the protein, the x-ray diffraction data of the mean square displacement was used[5]. This data enables us to compute the softness of the globin in the region near the heme. Using this data, and the principles of statistical mechanics, a simple model for the heme-plane oscillations has been developed by Kondepudi. With this model the resonance frequencies of the heme oscillations were computed. It was found that there are two modes that are of interest with frequencies $5.2 \times 10^{11}$ Hz and $5.4 \times 10^{11}$ Hz. Since the computation involves several approximations, only the order of magnitude of these numbers is significant. However, this work has shown the possibility of $10^{11}$-Hz resonance in hemoglobin. If this resonance does exist, an abnormal amount of energy will be transferred from the microwave field to the hemoglobin molecule,

315

and the normal function of the heme plane may be disrupted and the oxygen affinity of hemoglobin changed. This could have an effect on the flow of oxygen to tissues in biological systems.

## III. EFFECT OF RADIATION ON IONIC CONDUCTANCE THROUGH BIOLOGICAL MEMBRANES:

## SOME PREDICTIONS ON THE NOISE SPECTRUM

### a. Scope

The biological (plasma) membrane consists essentially of a phospholipid bilayer in which are embedded different types of constituent protein molecules (e.g., enzymatic or transport proteins) that subserve different functional roles. The structure of such membranes is assumed to be given by the Singer-Nicolson fluid mosaic model[6,7], which corresponds to a polypeptide-doped smectic-A liquid crystalline bilayer.

Nazarea[8] has considered the effects of radiation on transport proteins in lipid bilayers. These channel proteins may be artificially doped into the membrane (gramicidin or alimethicin) or naturally occurring channel complexes (the $Na^+ - K^+$ - ATPase system). We present here a simple theoretical diagnostics of radiative perturbations of the bilayer and channel protein system and study its effect on transmembrane conductance noise. We will write down the normalized ionic conductance noise spectrum and compare the noise spectra of continuous-wave and pulsed-wave radiation.

An experimental scheme for this problem could consist of two chambers separated by an arbitrarily shaped ring holder which supports the membrane bilayer together with the membrane-bound channel proteins of interest. The membrane in the ring holder separates two solutions (of differing ionic concentrations) of ions specific for the membrane-bound channel proteins. The whole system is then voltage clamped. Using this setup, the conductance noise spectrum in the absence of any perturbing field can be measured. This zero-field spectrum is needed for the normalization described in the next sections.

With a suitable radiation source, it should be possible to irradiate the membrane bilayer in the ring holder. For the theoretical discussion given below, we assume that the radiation source is a free-space source propagating transverse to the plane of the bilayer.

b. Theoretical Considerations

Due to the presence of aqueous solvent on both faces of the membrane bilayer, it will be assumed that for small amplitude radiation, the Franck elastic modulus, $K_1$, of the bilayer as well as its shear viscosity, $\eta$, will remain unaffected by the free-space radiation impinging transversely on it.

The assumption is also made that a conformational change in the membrane-bound transport proteins changes the ionic channel properties of these proteins. It is postulated that this change in polypeptide conformation can be brought about by perturbation of the orientational ordering of the phospholipid molecules forming the smectic bilayer in which the polypeptides are embedded. The dynamical parameter that defines this orientational ordering can be identified as the axis of phospholipid rotational averaging in the uniaxial liquid crystal. It is called the D-axis (director axis), $\hat{n}(r,t)$, and its fluctuations $\delta\hat{n}(r,t)$ from a reference steady state obeys a diffusion-type equation in accordance with known hydrodynamic theory as applied to smectic liquid crystals[9,10]. In this theory, the value of the diffusion constant $\gamma = (K_1/\eta)$ equals the ratio between the first-order (Franck) elastic modulus of the bilayer and its shear viscosity.

We assume that the fluctuations $\delta g(r,t)$ in the specific transmembrane conductance have autocorrelation function which is proportional, with parameter $\lambda$, to the autocorrelation of the phospholipid D-axis fluctuations. We can now begin to sketch how the analytical predictions are arrived at. One can consider two types of free-space radiation sources propagating transversely to the plane of the membrane:

317

(A) free-space continuous-wave TE or TEM modes
(B) free-space pulsed-wave TE or TEM modes

On the plane of the membrane (membrane thickness is several nanometers), we assume that the electric field E(t) felt by the membrane depends only on time (the theory is easily extended to space-dependent fields).

Our main assumption is that the perturbing field E(t) couples only to first order to the fluctuations of the phospholipid D-axis. This leads to the dynamical equation:

$$\partial_t \delta \hat{n}(r,t) = \gamma \vec{\Delta}^2 \delta \hat{n}(r,t) + \beta \, Re \, E(t) \, \delta \hat{n}(r,t) \tag{3.1}$$

where $\beta$ is a field-coupling parameter ($\beta$ depends on the type of transport proteins present, the type of phospholipid molecules comprising the bilayer membrane, and in general, is source dependent). We note that this study is restricted by the expected breakdown of (3.1) as a phenomenological description at sufficiently high frequencies. This point will be discussed in more detail in the published report.

A detailed analysis based on (3.1) shows that in the presence of the perturbing field, the power spectrum of the transmembrane ionic conductance noise $G(k,\omega)$, normalized by the conductance noise spectrum, $G_0(k,\omega)$, for the unperturbed membrane is given by

$$\frac{G(k,\omega)}{G_0(k,\omega)} = \lambda \left( \frac{\omega^2 + (\gamma k^2)^2}{\gamma k^2} \right) \left[ \frac{\Gamma(k,\omega)}{\omega^2 + (\Gamma(k,\omega))^2} \right] \tag{3.2}$$

in which $\Gamma(k,\omega) = \gamma k^2 + \beta \, Re \, E(\omega)$, and where k and $\omega$ are wave number and frequency respectively, with $Re \, E(\omega)$ signifying the Fourier transform of $Re \, E(t)$. The above result shows that a radiation source will change the properties of the membrane sufficiently for changes to show in the transmembrane conductance noise spectrum.

318

## c. Discussion

The preceding analysis represents a first attempt at setting up a global theory for the dynamics of transmembrane ionic conductance noise spectra in the presence of a radiation field. It is global in the sense that it relies for its predictions on a universal model (the fluid-mosaic model) of biological plasma membranes. In this first attempt, the influence of magnetic fields is neglected.

We can illustrate the above results by comparing the spectra for the case of continuous-wave and pulsed-wave radiation sources.

(1) <u>Continuous wave</u>: We take the simplest type of free-space TE-or TEM-mode sources with free-space electric field on the plane of the bilayer of the form

$$E(t) = E_0 \exp(i\omega_0 t) \tag{3.3a}$$

For this case the normalized transmembrane conductance noise spectrum will follow the form (3.2) with

$$\Gamma(k,\omega) = \gamma k^2 + \pi E_0 \left\{ \delta(\omega-\omega_0) + \delta(\omega+\omega_0) \right\} \tag{3.3b}$$

(2) <u>Pulsed wave</u>: In the case of a pulsed-wave TE or TEM mode with free-space electric field component on the plane of the bilayer of the form (with width $a_s$)

$$E(t) = \begin{array}{ll} E_0 \exp(i\omega_0 t) & |t| < a_s \\ 0 & |t| > a_s \end{array} \tag{3.4a}$$

Here the ionic conductance noise spectrum will follow (3.2) with

$$\Gamma(k,\omega) = \gamma k^2 + E_0 \left\{ \frac{\sin\left[a_s(\omega-\omega_0)\right]}{(\omega-\omega_0)} + \frac{\sin\left[a_s(\omega+\omega_0)\right]}{(\omega+\omega_0)} \right\} \tag{3.4b}$$

Given the actual cellular milieu in which biological membranes are found, one can expect that membrane conductance changes as reflected in the conductance noise spectrum, will be modulated by a radiation source. Work is in progress to determine the magnitude of the changes which occur in realistic systems.

319

## IV. EFFECTS OF EXTERNAL FIELDS ON THE CRITICAL SIZE OF CHEMICAL DISSIPATIVE STRUCTURES

Reaction-diffusion systems, when far from equilibrium, can form spatial patterns or spatial dissipative structures. In the initial stages of biological morphogenesis, pattern formation and positional information can be viewed as a consequence of far-from-equilibrium diffusion-reaction system[11]. Recently, this model has received some support from the experimental side[12-14].

Nazarea[15] has shown that if the size of a diffusion-reaction system is less than a certain <u>critical size</u>, the formation of a dissipative structure is impossible. This critical size is determined by the diffusion coefficients and the chemical kinetics of the system. The implication of this result in the context of morphogenesis is that, during development, a biological system should reach a minimum size before a chemical-concentration pattern (which acts as the basis for positional information) can form.

Kondepudi[16] and Nazarea[17] have now studied the way in which a static external field (eigher gravitational or electric) can change the critical size of chemical dissipative structures. A completely general expression for the minimum value of the critical size for the onset of a chemical dissipative structure has been obtained by Nazarea[6]. He finds

$$L_c \geq \left[ \rho_0 (2\pi + \rho_0 \Gamma_0) \right] \; E_{11}$$

where $E_{11}$ is the amplitude of the field, $\mu_0$ is the absolute value of the electrophoretic mobility of the fastest drifting reactant in the field, $\Gamma_0$ is the length (in consistent units) of the minimal closed curve, $C_0$, enclosing the spectrum of the operator $\Omega(E_{11})$ on the complex plane,

$$\Omega(E_{11}) = \left[ \underline{F}(\rho^0) - k^2 \underline{D} - k^2_{11} \underline{D}_{11} \;\; + \;\; \frac{4\pi}{\epsilon} \; \underline{N} - i \, k_{11} \, E_{11} \, \underline{M}_{11} \right]$$

and $\rho_0'$ is the maximal value of the resolvent of $\Omega(E_{11})$ on $C_0$. In the expression for $\Omega(E_{11})$, $\epsilon$ is the zero frequency dielectric constant, $F(\underset{\sim}{\nu}^o)$ is the Frechet derivative of the purely reactive flux, the k's and $\underset{\sim}{D}$'s are transverse and longitudinal wave numbers and diffusion matricies respectively, $M_{11}$ is the mobility matrix with elements $\overline{m}_{jj}$, and the linear operator $\underset{\sim}{N}$ has $jk^{th}$ reference steady state and $z_k$ the charge valence q of the $k^{th}$ reactant.

The important point to be noted is that the critical size increases with the field strength. Work is now underway to obtain explicit numerical values for the ratio $L_c/E_{11}$ for reaction diffusion systems of interest in biological systems.

## V. MOLECULAR MIGRATION THROUGH BIOMOLECULES AND PORE PERMEATION

The problem of determining the effect of microwave radiation on the functioning of biological molecules is a difficult one, especially when we realize that little is known about the internal dynamics of these complex entities and their interaction with the medium in which they are embedded, even in the absence of microwave radiation. However, recent experiments by Beece, Eisenstein, and Fraunfelder[18] have shed some light on this problem. They used flash photolysis to study the binding of CO to protoheme and $O_2$ and CO to myglobin in many different solvents. They found that the transition rate over barriers interior to the protein depends upon the solvent viscosity even though there is no solvent present inside the protein! For high-solvent viscosities, they found that the rate constant, k, has an experimental dependence of the form

$$k = \left(\frac{A_1}{\eta} + A_2\right) e^{-H/k_B T} \tag{5.1}$$

rather than a dependence of the form

$$k = \frac{A_1}{\eta} e^{-H/k_B T} \tag{5.2}$$

321

which is the usual form of Kramers' law. (In eqs. 5.1 and 5.2, $A_1$ and $A_2$ are experimental constants, $\eta$ is the solvent viscosity, H is an effective potential barrier height, $K_B$ is Boltzmann's constant, and T is the temperature in degrees Kelvin.) These authors use their results to argue that the barriers internal to the proteins cannot be viewed as static but in fact are dynamic, and furthermore that the internal protein dynamics is strongly affected by changes in the solvent viscosity which communicates information about solvent viscosities to the interior barriers.

The results of the above authors and their interpretation are extremely important for our microwave study. They claim that the internal dynamics of proteins is very sensitive to the properties of the medium in which they are embedded, whereas we view the effect of the medium as a small perturbation on the internal dynamics. Indeed, most mechanical models of large molecules (see the work of Prohofsky[19]), as a first approximation, neglect the medium and attempt to understand the internal dynamics of the molecule as an isolated system. Therefore, we thought it imperative to see if the experimental results of the above authors can be accounted for by a "static" model; i.e., one in which the ligand always sees essentially the same _average_ potential barriers inside the protein, regardless of the solvent the protein is embedded in. We would then account for the observed dependence of internal transition rates on solvent viscosity as a boundary effect.

To solve this problem, Reichl has treated ligand migration as a problem of migration of a Brownian particle (the ligand) in the presence of a multi-barrier potential and a viscosity which is piecewise constant but varies discontinuously (rapidly) in space. The probability density, $P(x,t)$, for finding the Brownian particle at position x at time t is obtained by solving the Smoluchowski equation[20]

$$\theta \, \frac{\partial P(x,t)}{\partial t} = \frac{d}{dx} \left( U'(x)P(x,t) \right) + \frac{d^2 P(x,t)}{dx^2} \qquad (5.3)$$

where $U'(x) \equiv \frac{dU}{dx}$ and

$$\theta = \frac{6\pi R \eta}{K_B T} \qquad (5.4)$$

($\eta$ is the viscosity of the medium in which the Brownian particle is embedded, R is its radius, $K_B$ is Boltzmann's constant, T is the temperature, and $U(x)V(x)/K_B T$ where $v(x)$ is the potential field that the Brownian particle moves in.) Reichl has solved the Smoluchowski equation exactly[21] for the potential fields and viscosities shown in Fig. 1. The exact results show that the rate of transition, K, of the Brownian particle over the internal barrier does have viscosity dependence similar to that found experimentally in proteins, namely

$$k = \frac{A}{\eta_1} + \frac{B}{\eta_2} \qquad (5.5)$$

where $\eta_1 (\eta_2)$ is the interior (exterior) viscosity and A and B are constants that vary depending on the barrier. Thus, we have shown that our view that
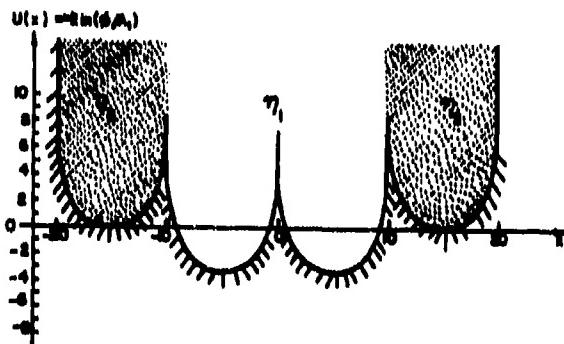


Figure 1. A multiwell potential with spatially varying viscosities. $\eta_1 (\eta_2)$ is the viscosity of the inner (outer) well.

the solvent has only a small effect on the internal dynamics of proteins is consistent with experimental results. It is useful to point out that the mathematical techniques used here to obtain exact solutions to the Smoluchowski equation for diffusion in multibarrier systems, although originally motivated by the ligand migration problem, may also be of great use for the problems of pore permeation and diffusion in multicell systems.

## VI. PROTEIN-SOLVENT INTERACTION

One aspect of the effect of microwave radiation on the behavior of biological molecules concerns the reaction of the surrounding medium on the molecules and the role of the medium in dissipating any energy which may be absorbed by the molecule from an external field. Both translational and rotational motion of a biological molecule can produce shear waves in the surrounding medium. A simple hydrodynamic calculation for a typical protein in water driven at microwave frequencies ($\sim 10^9$/sec) shows that shear waves can penetrate a distance $\sim 10^{-5}$ cm; i.e., a distance roughly equal to the radius of the molecule. The propagation of information about thermal rotational motion of proteins into water has apparently been observed[22]. What is not clear at present is the effect of microwave-driven motions of a protein on the surrounding medium.

In an effort to understand this problem and to determine how the medium reacts back on the protein, Reichl has obtained the noise spectrum and friction on a Brownian particle undergoing translation and rotation in a fluid with internal rotational degrees of freedom. Until now, all theories of Brownian motion have assumed that the fluid surrounding the Brownian particle is composed of point particles. We have considered a fluid with structure and have obtained corrections to the usual Brownian motion theory due to rotational degrees of freedom of the fluid. For a molecule driven at microwave frequencies, inertial effects become important and tend to color the noise felt by the

324

molecule. These inertial connections have also been taken into account in our work.

The results of our work[23,24] are the following: We have obtained explicit expressions for the friction on a translating and rotating Brownian particle in terms of the viscous and rotational transport coefficients of the fluid, the radius of gyration of the fluid particles, and the density of the fluid. We have also obtained explicit expressions for the velocity and angular velocity auto-correlation functions of the fluid and, therefore, the noise correlation functions of the fluid. We find that the correlation function decays as

$$\langle U(t)U(0) \rangle \sim \frac{1}{t^{3/2}}$$

where $U(t)$ is the translational velocity and $t$ is the time, and the angular velocity correlation function decays as

$$\langle \omega(t)\omega(0) \rangle \sim \frac{1}{t^{5/2}}$$

where $\omega(t)$ is the angular velocity. The coefficients of these long tails depend on the viscous and rotational transport coefficients of the fluid. We are presently undertaking work to determine the effect of these long memories on the dielectric functions of a fluid, and thereby their effect on the absorption spectrum of the fluid.

## VII. SPECTRAL PROPERTIES OF ANHARMONIC-OSCILLATOR SYSTEMS

An important aspect of the effects of microwave radiation on biological systems concerns the way in which radiation interacts with biological molecules. Radiation in the microwave region will primarily affect vibrational and rotational states of molecules. Until now, most models of large molecules have viewed the molecule as a chain of coupled harmonic oscillators. We are studying new effects which arise when the nonlinear character of the coupling is taken into account.

325

Two interesting effects occur in nonlinear oscillators, which are not found in linear oscillators. At low energies, they can support soliton propagation. Solitary wave motion is a purely nonlinear phenomenon which allows for rapid and efficient transfer of energy from one part of a nonlinear chain to another. It has been conjectured that this mode of energy propagation plays an important role in the functioning of biological molecules[25,26]. The effects of external fields on soliton propagation is now being studied by Reichl and de Fainchtein[27].

A second interesting effect that occurs in nonlinear oscillators, but not linear oscillators, is the appearance of chaotic motion at higher energies. As the energy of a nonlinear oscillator is increased, the spectrum can change dramatically, and this affects the way energy is absorbed[27]. To illustrate this behavior, let us consider the so-called Henon-Heiles Hamiltonian

$$H = \tfrac{1}{2}(p_1^2 + p_2^2) + \tfrac{1}{2}(x_1^2 + x_2^2) + x_1 x_2^2 - \tfrac{1}{3}x_1^3$$

Without the last two terms, this would describe two uncoupled harmonic oscillators with natural frequency $f = \tfrac{1}{2\pi}$. In Figures 2a and 3a we exhibit the Poincare surface of section for this nonlinear oscillator system for two different energies. (For this system the full phase space, composed of two momentum and two position variables, is four dimensional. Since energy is conserved, the system evolves on a three-dimensional energy surface in this phase space. The Poincare surface of section is a two-dimensional slice of the phase space.) For the low-energy case (Fig. 2a), the system behaves in many respects like a harmonic oscillator system. The power spectrum for low-energy oscillation is given in Figure 2b.

We see that the frequency $f=\frac{1}{2}\pi$ dominates, although there are other frequencies due to the anharmonicities.
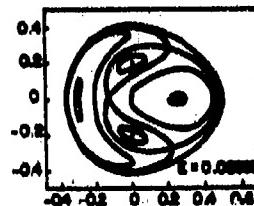


Figure 2a
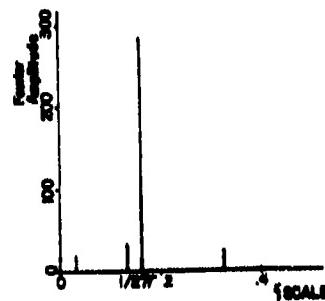


Figure 2b

Figure 2.  a.  The Poincare surface of section for the Henon-Heiles
             Hamiltonian at energy E=0.08333.

         b.  Power spectrum of $x_2(t)$ for energy E=0.08333.

327

If we next consider this same system at high energy (Figures 3a and 3b), we see that the phase space has gone chaotic, indicating rapid spread of energy through the system, and the power spectrum has many components and has broadened about the harmonic frequency $f=\frac{1}{2}\pi$. Thus, the way in which this system will absorb energy has changed qualitatively.

Because the energy of molecules is distributed according to a Boltzmann distribution, some fraction of them will always be in the chaotic regime. There is some indication that the critical energy for onset of chaotic behavior in the absence of an external field occurs near the inflection point of the interparticle potential. It is very likely that an external field will destabilize some molecules not in the chaotic regime, thus destroying coherent mechanical functioning of those molecules. The possible destruction of coherence in an external field is presently being studied by Reichl and de Fainchtein.

## VIII. ANHARMONIC OSCILLATION OF MOLECULAR SYSTEMS

We study a rectilinear chain of particles with mass $m_i$ ($i=0,1,\ldots,N$) connected with nonlinear nearest neighbor potentials $V(x_i)$ depending only on the relative distances $x_i = \xi_i - \xi_{i-1}$ of the particles. The most simple case which is already highly complex and, in fact, nonintegrable, consists of only three particles, $m_0$, $m_1$, $m_2$, with free end-points. The equations of relative motion are

$$\ddot{x}_1 = \left(\frac{1}{m_0} + \frac{1}{m_1}\right) \frac{\partial V(x_1)}{\partial x_1} - \frac{1}{m_1} \frac{\partial V(x_2)}{\partial x_2}$$

$$\ddot{x}_2 = \left(\frac{1}{m_1} + \frac{1}{m_2}\right) \frac{\partial V(x_2)}{\partial x_2} - \frac{1}{m_2} \frac{\partial V(x_1)}{\partial x_1}$$
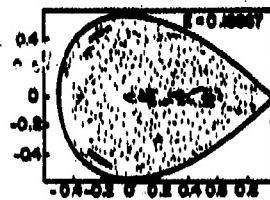
Figure 3a
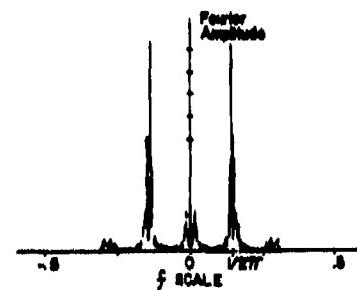


Figure 3b

Figure 3.  a.  The Poincare surface of section for the Henon-Heiles
Hamiltonian at energy E=0.16667.

b.  Power spectrum of $x_2(t)$ for energy E=0.16667.

For the potential V, Broucke has experimented with several of the well-known potentials, such as the Toda, Morse, and Lenard-Jones potentials:

$$V(r) = d \left[ (r - b) + \frac{1}{a} \left( e^{-a(r-b)} - 1 \right) \right] \qquad \text{(Toda)}$$

$$V(r) = d \left[ 1 - e^{-a(r-b)} \right]^2 \qquad \text{(Morse)}$$

$$V(r) = d \left[ 1 - \frac{m}{(m-n)r^n} + \frac{n}{(m-n)r^m} \right] \qquad \text{(Lenard-Jones)}$$

In the numerical studies, we transform the variables $(x_1, x_2)$ to the principal modes of oscillation by the relations

$$2X = x_1 + x_2 \; ; \quad 2Y = x_1 - x_2$$

The two principal modes correspond respectively to $X = 0$ and $Y = 0$. Note that except for a constant factor, the variables $(X, Y, \dot{X}, \dot{Y})$ form a canonical set, which allow us to use the standard surface of section method. In other words, we numerically integrate several solutions, but instead of plotting the complete solution or trajectory, we only plot the point $(X, \dot{X})$ corresponding to the instant $Y = 0$. In this diagram $(X, \dot{X})$, which is the generalization of the phase plots in one-degree-of-freedom systems), the appearance of smooth curves corresponds to regular quasi-periodic motions, while the irregularly distributed points correspond to chaotic motions. Chains of islands indicate the presence of resonances.

The advantage of these $(X, \dot{X})$ diagrams is the fact that they allow us to compare at once all the solutions with a given energy. In particular, they show exactly where we have transitions from regular to chaotic motions. These regions of initial conditions correspond to the particular vibrations of a biological molecule which will be especially sensitive to exterior radiofrequency radiation. The effect of the radiofrequency radiation may be either to stabilize the vibrations or to cause them to break up.

330

Another important feature that is visible on the $(X,\dot{X})$ graph is the appearance of chains of islands. They correspond to stable motions with frequencies p times smaller than the normal mode of vibrations (where p is the number of islands in the chain). They give indications on which subharmonies of the radiofrequency will be most effective in stabilizing the molecule. Our experiments show a prevalence of the case p=3 for all the potentials that were studied. Figure 4 shows an exceptional energy level (E=0.6) in the Morse potential where there are two stable subharmonic frequencies of vibration: p=3 and p=7.

## IX. PROPERTIES OF ANHARMONIC OSCILLATORS

Dynamic systems with irregular, nonperiodic, "chaotic" time evolution are frequently encountered in physics, chemistry, and biology. For example, the motion of three masses connected by a force determined from the Morse potential yields irregular motion for moderate to higher energies. From the Bolzmann distribution, a fraction of the molecules at room temperature will have sufficient energy to induce "chaotic" motion. In addition, microwave radiation could stimulate the transition from regular to chaotic motion, which, from a biological viewpoint, could seriously reduce the coherent function of the molecule. Conservative dynamic systems are first considered because they have a well-studied structure. The dynamic equations can be obtained by extremizing the action integral of Maupertius-Euler-Lagrange-Jacobi. The resulting motions are extremal geodesic paths forming a manifold. If the curvature of the manifold is negative, then the motion is characterized by exponential instability which seems to be a necessary indicator for "chaotic" motion[28].

The local curvature of this manifold is related to the second variation of the action integral about an extremal closed orbit. A sufficiency condition for local optimality of a weak extremum was obtained by Speyer, which corrects
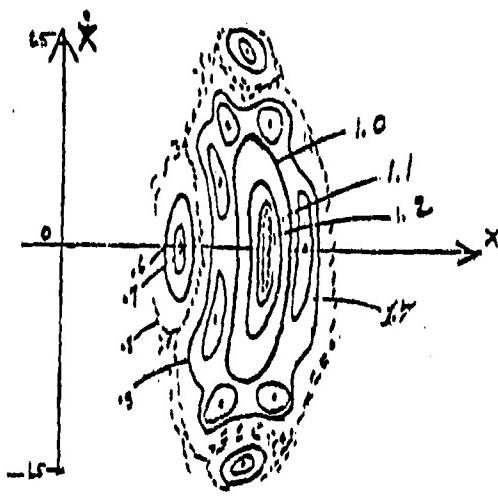
Figure 4.

Figure 4. Poincare surface of section for the Morse potential at energy C=0.6.

and extends earlier work[29]. With a minimal gap, these conditions seem to be also necessary. Heavy use is made of classical mechanics notions with respect to periodic orbits. One result is that the transition matrix associated with the closed orbit over one period has no eigenvalues on the unit circle except two which must always lie at unity. Since this matrix is symplectic, the eigenvalues are evenly spread inside and outside the unit circle, indicating that neighboring paths must have exponential divergent behavior (possible "chaotic" motion).

The idea of maximizing or minimizing the least action integral at constant energy is used to determine adiabatic barriers or wells. A necessary and sufficient condition for the existence of a classically vibrationally adiabatic barrier or well in collinear systems is the existence of a periodic-orbit dividing surface[30]. The second variation is used here to determine if the action is locally a minimum (well) or a maximum (barrier). As the energy increases due to microwave sources, more periodic-orbit dividing surfaces should appear, where at least some are attractive, allowing significantly altered final distribution of products. The above results generalize some of the ideas of Part III of this report to higher dimensional systems.

## X. CONCLUSION

Over the years, many experiments have been performed on animals in a search for microwave effects on living tissue. These experiments are often done with no a priori idea of where effects may be found. The Microwave Studies Group was formed in an effort to approach the problem from the opposite direction. We are attempting to determine, theoretically, where effects might be expected, based on mathematical studies of various types of nonlinear dynamical systems which govern the functioning biological systems. In this way, we hope to pinpoint areas where important effects may be found and experiments should be done. From the practical point of view, the cost of mathematical

feasibility studies is small compared to the cost of "shot in the dark" experiments.

Even though the Microwave Studies Group has been in existence a short time, we have already begun to locate potential trouble spots and areas where more theoretical work is needed. We have isolated an important $10^{11}$-Hz resonance in hemoglobin, which might cause microwaves to interfere with oxygen delivery to tissue. We have shown that external fields can change the ion conductance through membranes, although further work is needed to pinpoint specific effects in the microwave region. We have developed mathematical techniques for studying ligand migration in proteins and pore permeation. These techniques are now being extended to include microwave effects. We have shown that the critical size for the onset of chemical dissipative structures is increased in a constant electric field. This problem is extremely important for morphogenesis, and further studies on the effects of pulsed microwaves on critical size are being started. We have shown that information about microwave-driven motions of proteins can propagate into the solvent to distances of the order of the size of the protein, and we have shown that the noise felt by a microwave-driven protein is colored by inertial effects and details of the structure of the solvent. More work is needed to determine the effect of microwave-driven motions on the protein environment and mechanisms for energy exchange between protein and solvent. We have shown that anharmonic-oscillator systems, similar to those that comprise biological molecules, admit a transition from coherent ordered motion to chaotic motion as energy is increased. We expect this transition to be accompanied by a change in the absorption spectrum of the molecules. It is now widely thought that coherent motions made possible by nonlinearities in the intramolecular interactions play an important role in the functioning of biological molecules. The role of microwave fields in

334

destroying these coherent motions and replacing them by chaotic motions is now being studied.

REFERENCES:

1. B. R. Gelin and M. Karplus, Proc. Natl. Acad, Sci. USA 14 801 (1977).

2. V. A. Kudrjashova et al., Abstr. Symp. Gigtrudai biologitcheskoe deistvie electromagnitnych voln radiotchastat Moskva (1972) p. 4 (Resonance millimeter electromagnetic effects on hemoglobin).

3. D. Kondepudi, "Possible Effects of $10^{11}$ Hz Radiation on the Oxygen Affinity of Hemoglobin" (preprint).

4. A. Warshel, Proc. Natl. Acad. Sci. USA 74 1789 (1977).

5. H. Frauenfelder, private communication.

6. S. J. Singer and G. L. Nicolson, Science 145 720 (1972).

7. G. L. Nicolson, Biochim. Biophys. Acta 457 57 (1976).

8. A. D. Nazarea, "Effect of Radiation on Ionic Transport through Biological Membranes: Some Predictions on the Conductance Noise Spectrum" (in preparation).

9. D. Forster, T. C. Lubersky, P. C. Martin, J. Swift, and P. S. Pershan, Physiol. Rev. Lett. 26 1016 (1972).

10. P. C. Martin, O. Parodi, and P. S. Pershan, Physiol. Rev. A6 2401 (1972).

11. G. Nicolis and I. Prigogine, Self-Organization in Nonequilibrium Systems, Wiley-Interscience, New York, 1977.

12. C. J. P. Grimmelikhuijzen and H. C. Schaller, TIBS Dec. 1979, pp. 264-267.

13. S. A. Kauffman, R. M. Shymko, and K. Traburt, Science 199 259-270 (1978).

14. L. F. Jaffe and R. Nucitelli, Annu. Rev. Biophys. Bioeng. 6 445 (1977).

15. A. D. Nazarea, Proc. Natl. Acad. Sci. USA 11 3751-53 (1974).

16. D. Kondepudi, "Effects of Field-Induced Transport on the Critical Size of a Chemical Dissipative Structure" (submitted to Phys. Lett.).

17. A. D. Nazarea, "Intrinsic Critical Size for Chemical Dissipative
    Structures in an External Electric Field" (in preparation).

18. D. Beece, L. Eisenstein, H. Fraunfelder, et al., Biochemistry (in press).

19. E. N. Prohofsky and L. L. Van Zandt, "Absorption Events of Macromolecules,"
    Final Report, Oct. 1980, for USAF School of Aerospace Medicine.

20. H. A. Kramers, Physica (Amsterdam) 7 284 (1940).

21. L. E. Reichl, "Diffusion in a Multiwell Potential with Spatially Varying
    Viscosity" (submitted to J. Chem. Phys.).

22. K. Hallenga and S. H. Koenig, Biochemistry 15 4255 (1976).

23. L. E. Reichl, "Translational Brownian Motion in a Fluid with Internal
    Degrees of Freedom," Physiol. Rev. (Sept. 1981).

24. L. E. Reichl, "Rotational Brownian Motion in a Fluid with Internal
    Degrees of Freedom," Physiol. Rev. (Sept. 1981).

25. A. S. Davidov, Phys. Stat. Sol. 75 735 (1976); J. Theor. Biol. 66 379
    (1977); Studia Biophysica 62 1 (1977).

26. J. M. Hyman, D. W. McLaughlin, and A. C. Scott, "On Davidov's Alpha-Helix
    Solitons" (to appear in Physica D).

27. L. E. Reichl and R. De Fainchtein, in First Annual Report of the Micro-
    wave Studies Group, University of Texas at Austin, Nov. 1980.

28. V. Arnold, _Mathematical Methods of Classical Mechanics_, Springer-Verlag,
    New York, 1978.

29. J. Speyer and R. Evans, "A Sufficiency Condition for Optimal Periodic
    Processes," Proceedings of the Joint Automatic Control Conference,
    University of Virginia, Charlottesville, Virginia, June 17-19, 1981.

30. E. Pollak, "A Classical Determination of Vibrationally Adiabatic Barriers
    and Wells of a Collinear Potential Energy Surface," Dept. of Chemical
    Physics, Weizmann Institute of Science, Rehovot, Israel, 1980.

12. <u>PUBLICATIONS AND PRESENTATIONS RESULTING FROM A.F. FUNDED EFFORT</u>:

Broucke, R., and W. H. Presler, "Computerized Formal Solutions of Dynamical Systems with Two Degrees of Freedom and An Application to the Contopoulos Potential, Part I: The Exact Resonance Case," Computers and Mathematics with Applications (Sept. 1981).

Broucke, R., and W. H. Presler, "Computerized Formal Solutions of Dynamical Systems with Two Degrees of Freedom and An Application to the Contopoulos Potential, Part II: The Near Resonance Case," Computers and Mathematics with Applications (Sept. 1981).

Kondepudi, D., "Effects of Field-Induced Transport on the Critical Size of a Chemical Dissipative Structure" (submitted to Phys. Lett.).

Kondepudi, D., "Possible Effects of $10^{11}$ Hz Radiation on the Oxygen Affinity of Hemoglobin" (preprint).

Nazarea, A. D., "First Order Macroscopic Dynamics of Chemically Reacting Systems Under the Influence of a Randomly Varying Electric Field" (submitted to J. Chem. Phys. Lett.).

Reichl, L. E., "Diffusion in a Multiwell Potential with Spatially Varying Viscosity" (submitted to J. Chem. Phys.).

Reichl, L. E., "Translational Brownian Motion in a Fluid with Internal Degrees of Freedom," Phys. Rev. (Sept. 1981).

Reichl, L. E., "Rotational Brownian Motion in a Fluid with Internal Degrees of Freedom," Phys. Rev. (Sept. 1981).

Speyer, J., and R. Evans, "A Sufficiency Condition for Optimal Periodic Processes," Proceedings of the Joint Automatic Control Conference, University of Virginia, Charlottesville, Viringia, June 17-19, 1981.

# TRANSIENT FIELDS PRODUCED IN
# HETEROGENEOUS BODIES BY ELECTROMAGNETIC PULSES

Robert J. Krueger

Department of Mathematics

University of Nebraska

Lincoln, NE  68588

I.  <u>INTRODUCTION</u>:  When an electromagnetic field impinges on a medium (such as biological tissue), a field is induced in the medium.  If the incident field is time harmonic, then the induced field is also time harmonic; and so for simple geometries, it is a relatively straightforward matter to mathematically calculate the intensity of the induced field in the tissue.  On the other hand, if the incident field is a pulse, such as a sinusoidally varying field of finite duration, then the structure of the induced field is quite complicated. Of particular concern is the transient field intensity in the tissue and how this compares with the time-harmonic field intensity.

The research reported herein

    1.  presents a method for calculating transient field intensity in one-dimensional tissue models and

    2.  considers several sample problems, comparing transient and time-harmonic field intensity.

II. <u>TECHNICAL APPROACH</u>: In order to determine the structure of induced electromagnetic fields, the problem was modeled mathematically. The assumptions made and the resulting model are given below. In the process of describing the model, the nature of the media and incident fields to be considered will be made clear.

The medium considered in this work is one dimensional and of finite depth L. Thus, it is assumed to vary spatially only in the z direction, extending from z=0 to z=L. The permittivity, $\varepsilon(z)$, and conductivity, $\sigma(z)$, of the medium are piecewise continuous functions as pictured, for example, in Figure 1. By allowing $\varepsilon$ and $\sigma$ to be piecewise continuous, a layered medium can be considered. It is assumed that free space exists outside of the medium so that $\varepsilon(z)=\varepsilon_0$ and $\sigma(z)=0$ for z<0 and z>L. Finally, it is assumed that the medium is nondispersive in that the permittivity and conductivity are independent of the induced field.

An electromagnetic wave propagating along the z-axis normal to the medium has transverse electric field, $E(z,t)$, satisfying

$$E_{zz}-\varepsilon(z)\mu_0 E_{tt}-\sigma(z)\mu_0 E_t=0, \quad -\infty<z<\infty, \quad -\infty<t<\infty \qquad (1)$$

which follows from Maxwell's equations. Here, t denotes time, $\mu_0$ is the constant magnetic permeability, and subscripts denote partial derivatives. It is assumed that the incident electromagnetic pulse, $E^i$, propagates from left to right and first impinges on the medium at time t=0. Thus, the initial condition for equation (1) is

$$E(z,t)=E^i(z-ct) \text{ for } t<0 \qquad (2)$$

where $E^i(z-ct)=0$ for $z-ct\geq0$ and c is the speed of light in free space. The problem considered, then, is that of determining the solution $E(z,t)$ of the system of equations (1) and (2) for $0\leq z\leq L$, t>0 for any given $E^i(z-ct)$, $\varepsilon(z)$, $\sigma(z)$.

339
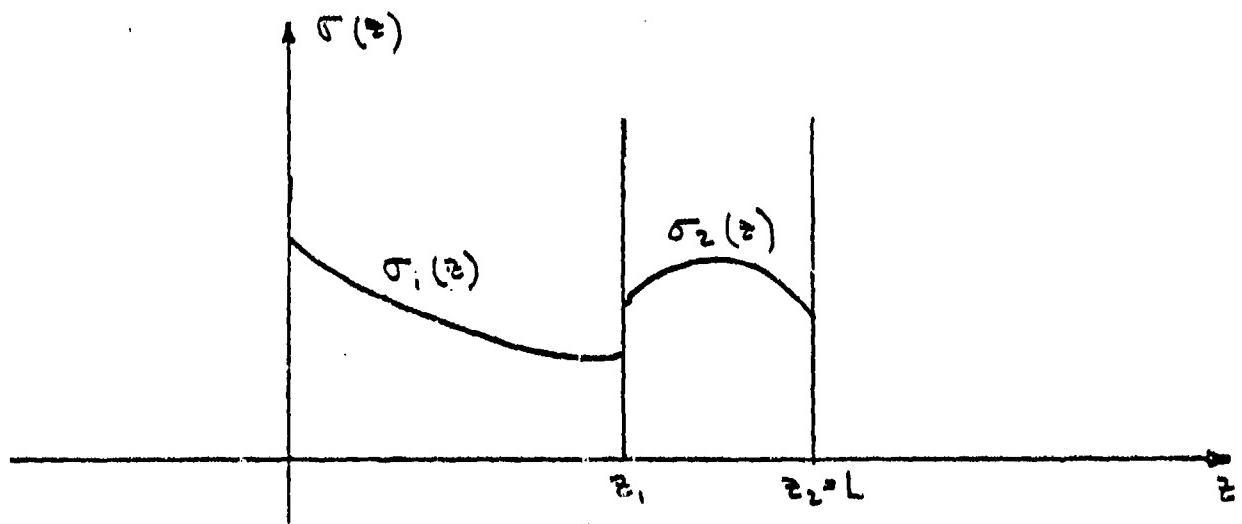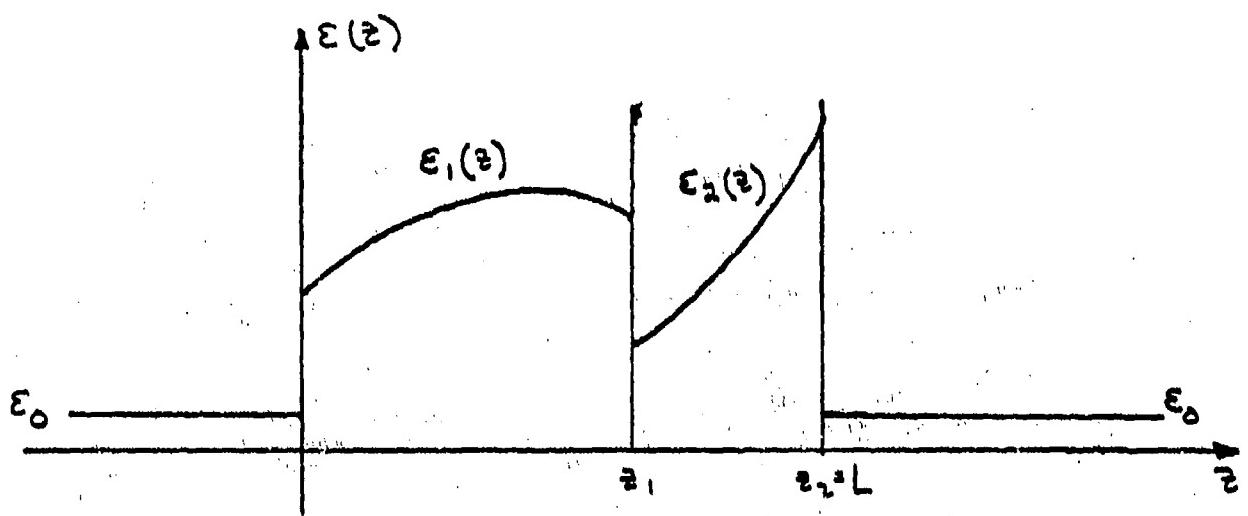
Fig. 1.  Example of permittivity and conductivity profiles for a one-dimensional medium.

340

Although finite differences [1] or integral equation techniques [2] appear to be capable of solving such a problem, it was found that roundoff error and numerical dispersion produced unreliable results for pulses of realistic duration. Therefore a new technique based on scattering operators [3, 4] has been developed. It has been found to produce highly accurate solutions. This technique provides exact analytical representations of the induced fields, with no recourse to low frequency approximations. Details are given in [5, 6, 7].

To numerically implement the scattering operator technique, the HATS (High Accuracy Temporal Solution) computer program was developed. This program allows a user to specify the permittivity and conductivity of the medium as a function of depth and also to specify the incident field. The output is the field at a fixed depth for a certain time interval, or the field at a fixed time throughout the medium.

III. RESULTS: As an example of the results which can be obtained via the HATS program, consider the three-layer medium shown in Figure 2 where it is first assumed that $\sigma(z) \equiv 0$. A 1000-MHz incident field of duration 20 ns impinges on the medium from the left at time $t=0$. Thus, at some time $t<0$ the incident field looks like that shown in Figure 3.

The resulting field inside the medium was generated by the HATS program for the time interval $t=0$ to $t=25$ ns. Figures 4, 5, and 6 show the internal fields as a function of time at three specific locations ($z=.714$ cm, $z=1.067$ cm, $z=2.100$ cm) in the medium. The locations $z=.714$ cm and $z=2.100$ cm were chosen because they represent in some sense the "worst case" behavior in that the transients at these points had the greatest amplitude relative to steady-state (i.e., time harmonic) amplitude of any points in the medium.

341
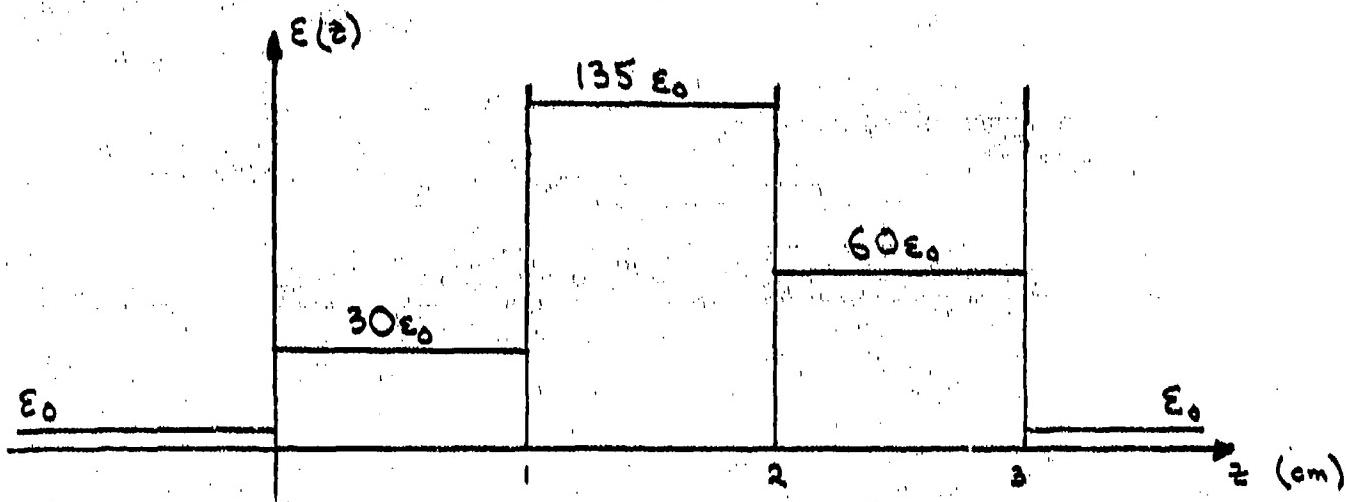
Fig. 2. Permittivity profile for the sample problem.
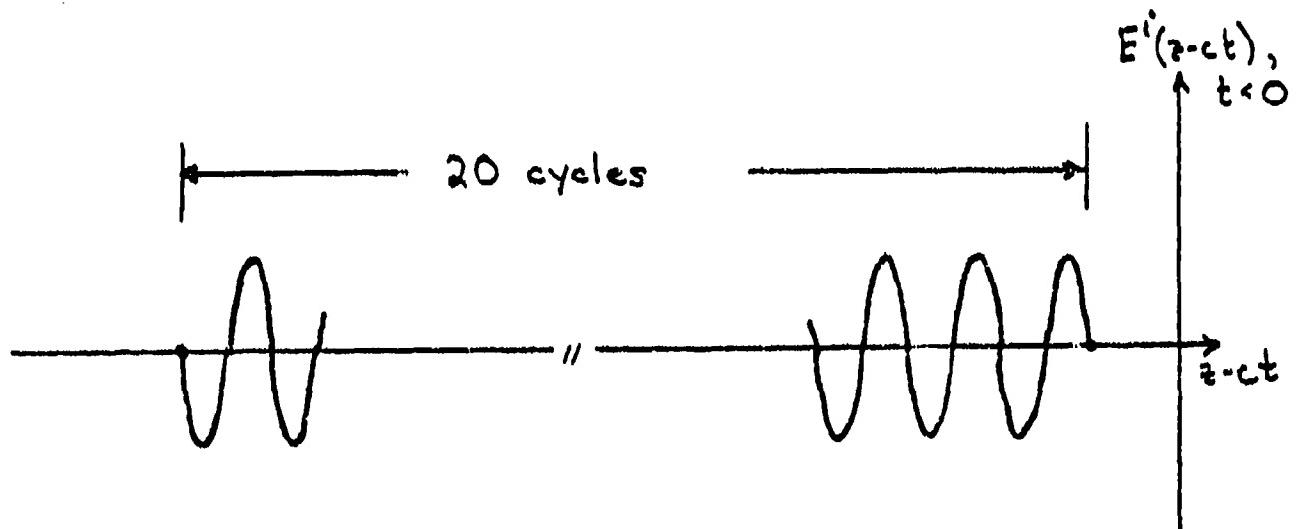


Fig. 3 Incident field for the sample problem. (20-ns pulse, 1000 MHz)

342
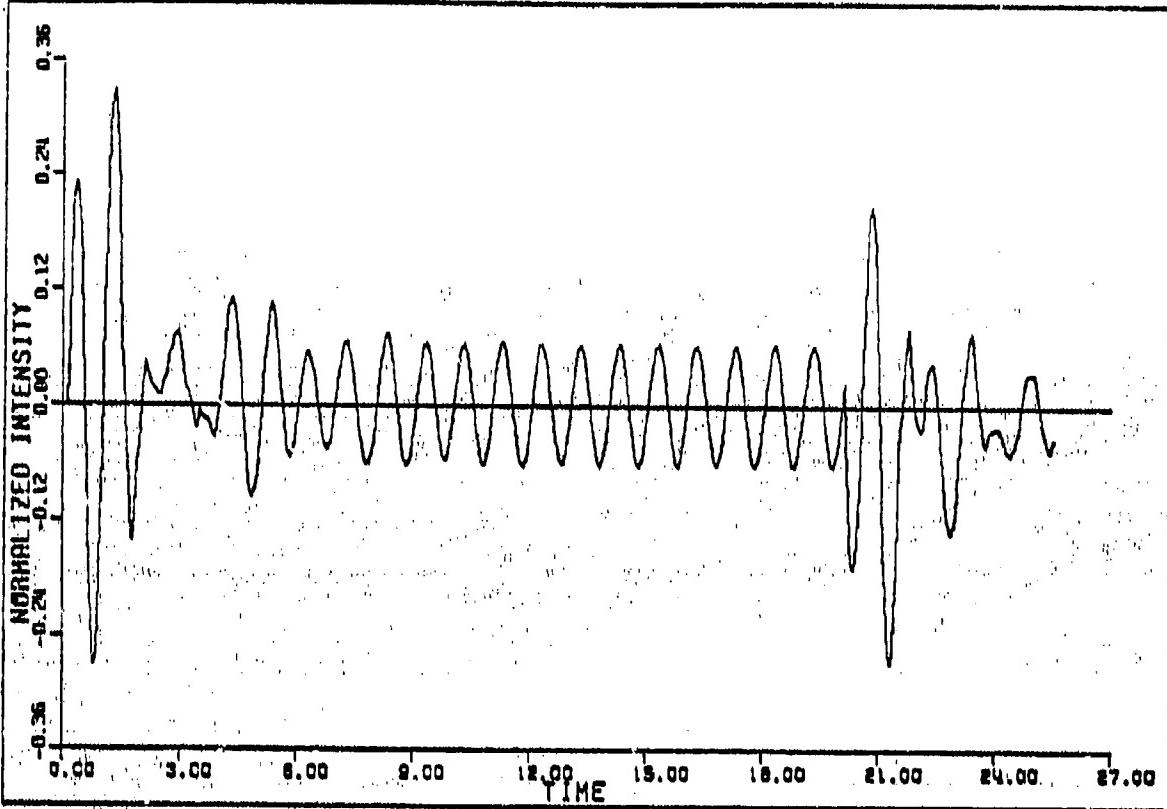
Fig. 4. Internal field (x=0.714 cm) vs. time (ns), zero conductivity.
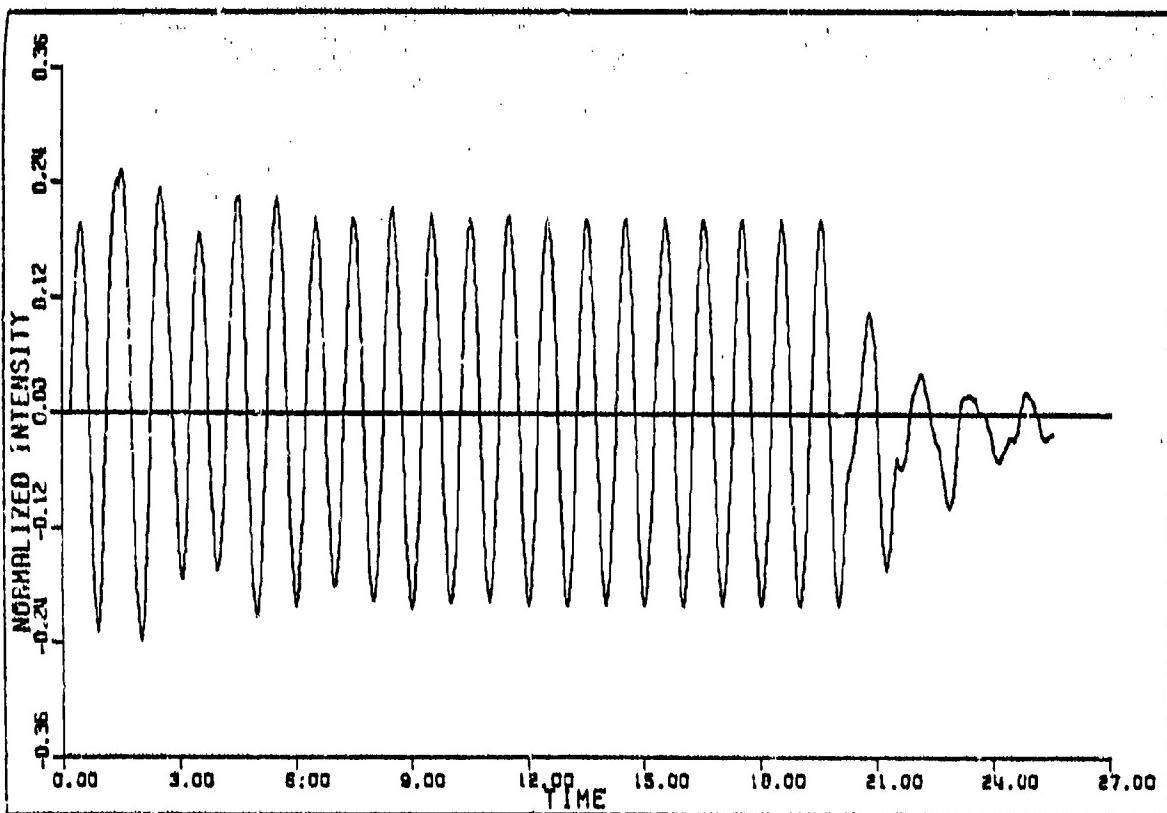


Fig. 5. Internal Field (x=1.06) cm) vs. time (ns), zero conductivity.

343
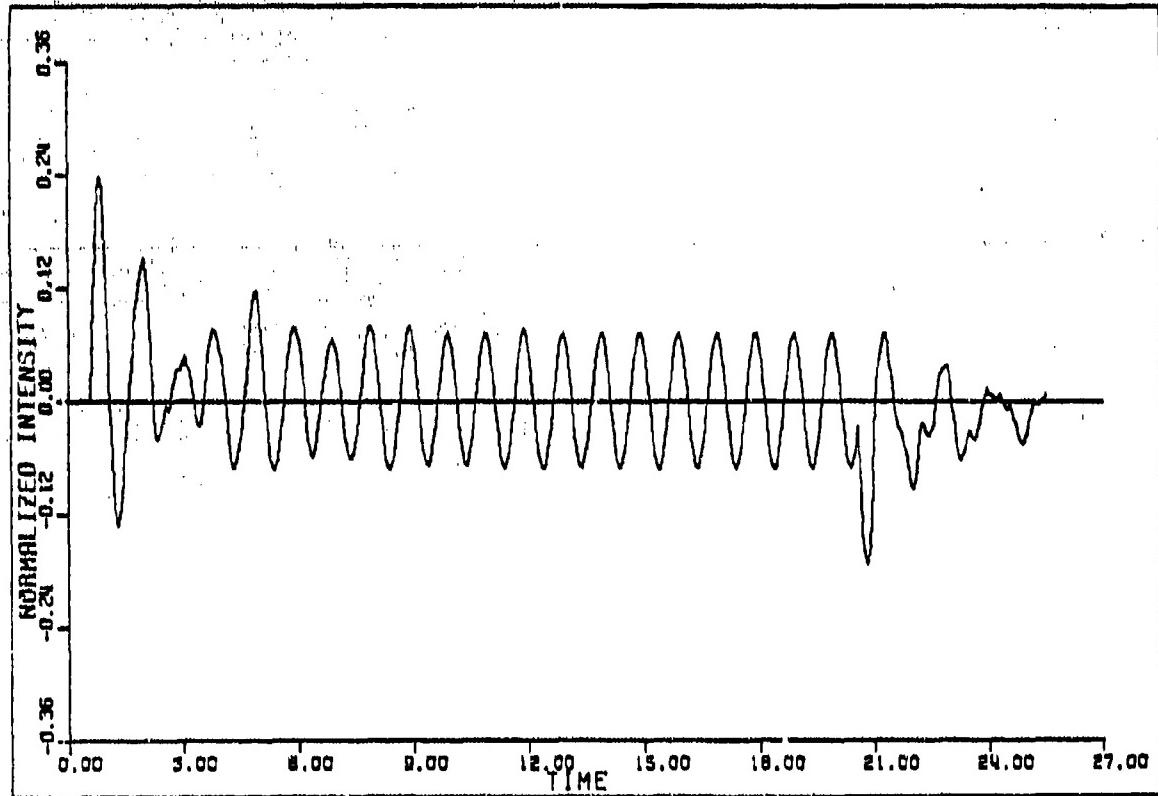
Fig. 6. Internal field (x=2.100 cm) vs. time (ns), zero conductivity.

344

Figure 5 (z=1.067 cm) represents the "best case" behavior in that the ratio of transient amplitude to steady amplitude was the smallest. It was found that at all points in the medium, transient amplitude was greater than steady-state amplitude.

Figure 7 shows a comparison of transient vs. time-harmonic intensities throughout the medium. In Figure 8, the reflected, induced, and transmitted fields are shown at time t=6 ns. (Depth is scaled by a travel time factor in both of these plots.)

Now consider a medium with permittivity profile given in Figure 2 and conductivity profile given in Figure 9. The fields at z=.714 cm, z=1.067 cm, z=2.100 cm, again fairly accurately give "worst" and "best" behavior and are shown in Figures 10, 11, and 12. Again, transient amplitude was everywhere greater than steady amplitude, although the effect of nonzero conductivity is now seen as reducing the ratio of transient to steady amplitude. Figures 13 and 14 are analogous to Figures 7 and 8.

IV. <u>SUMMARY AND CONCLUSIONS</u>: It has been shown that relatively large amplitude transients can occur in a medium when a pulse signal, such as that from a phased array system, impinges on the medium. These transients have amplitude considerably greater than those produced by a time-harmonic signal. Further, the transients will appear periodically if the incident pulse is repeated at periodic intervals. Therefore, the possibility exists that a mediation of biological events can occur in the presence of pulse electro-magnetic radiation even if such mediation does not occur in the presence of a time-harmonic signal. This possibility should be considered when examining safety standards for Air Force personnel.
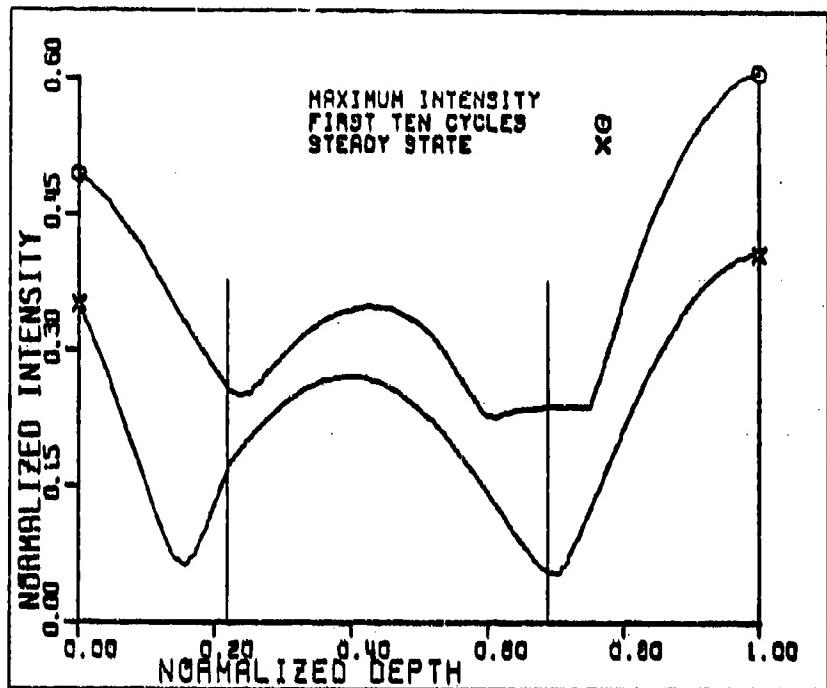
Fig. 7.   Comparison of transient and steady-state intensities in a medium
with zero conductivity.   Incident field is 1000-MHz pulse.
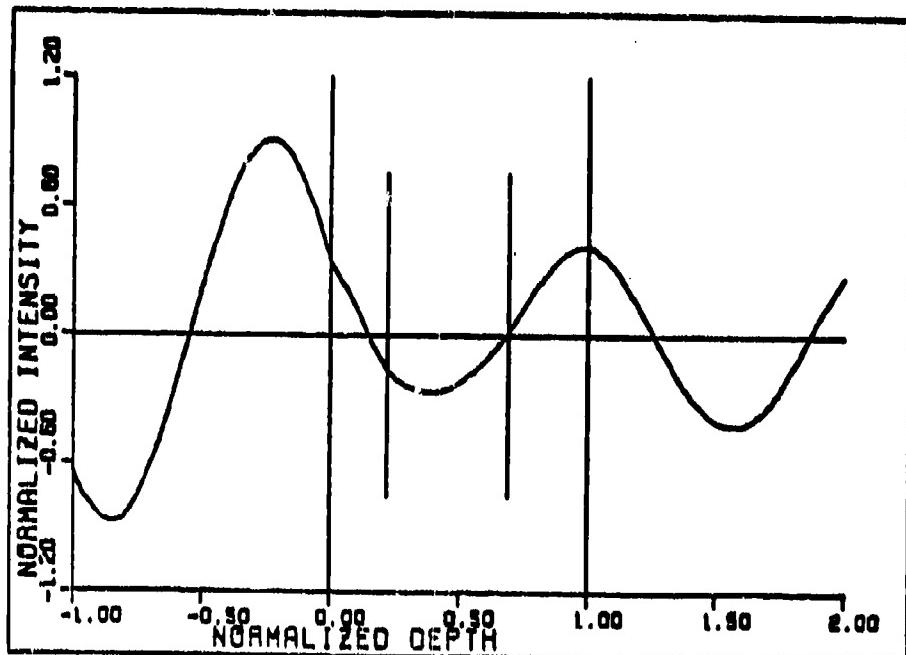


Fig. 8.   Internal, reflected, and transmitted fields for a medium with zero
conductivity, time t = 6 ns.   Incident field is 1000-MHz pulse of
duration 20 ns, impinging on the medium from the left at time t = 0.

346
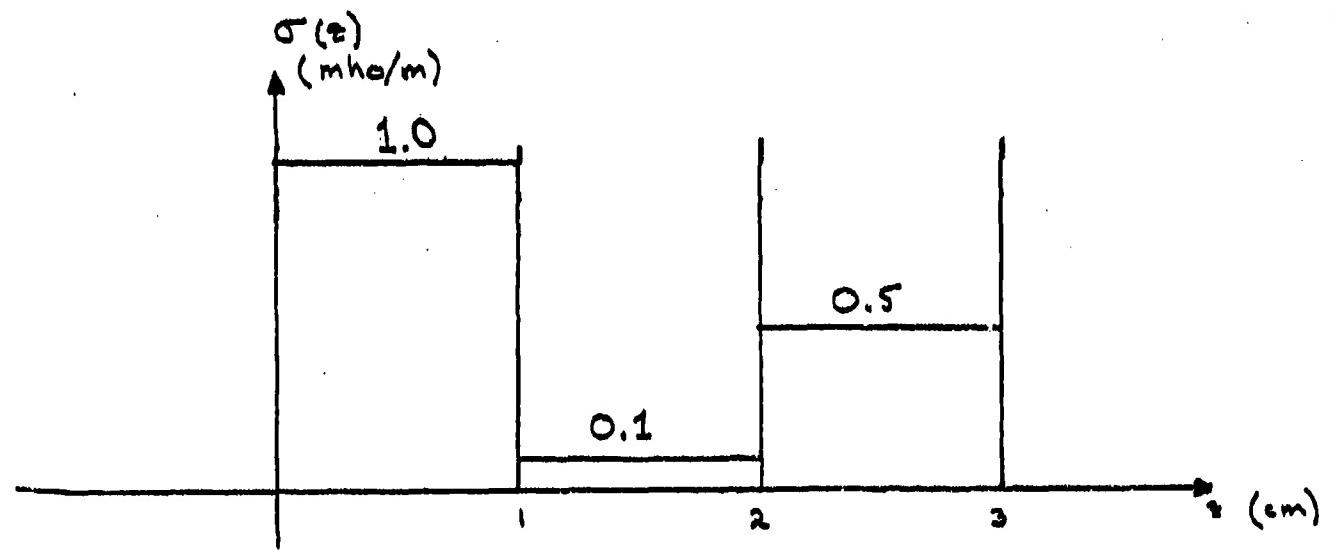
Fig. 9. Conductivity profile for the sample problem.
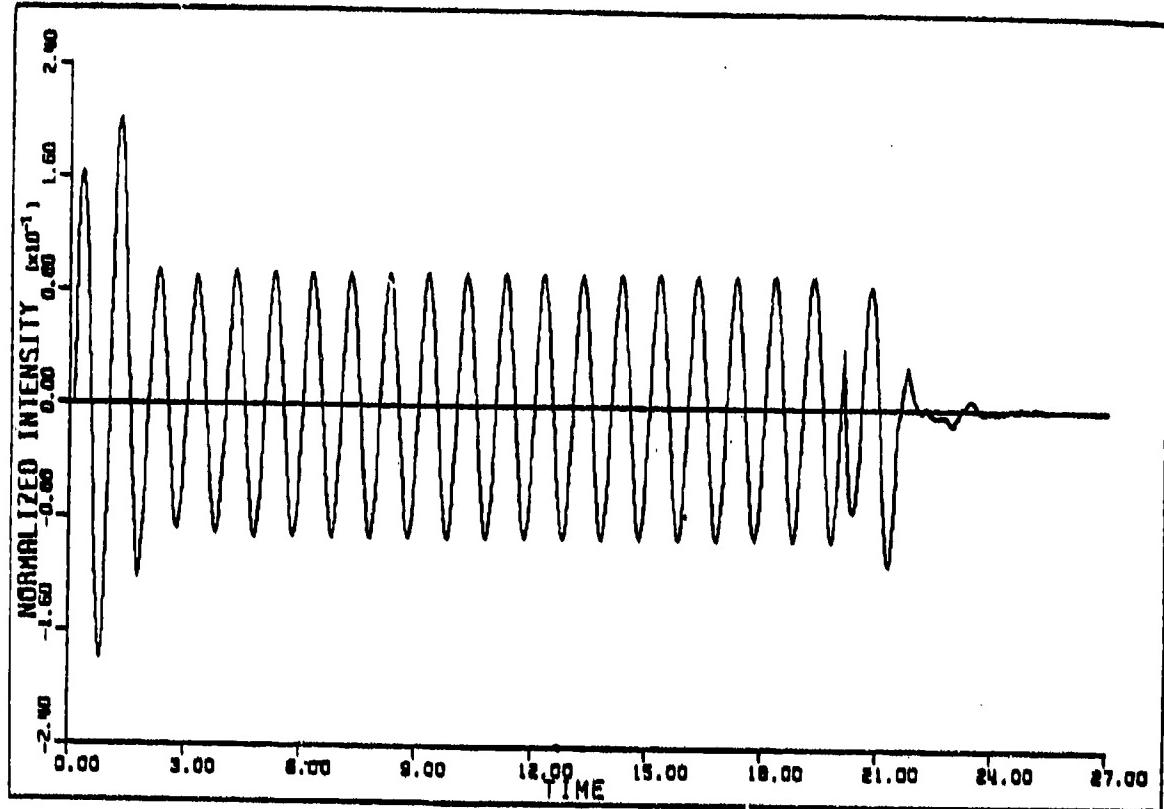
Fig. 10.  Internal field (R=0.714 cm) vs. time (ns), nonzero conductivity.
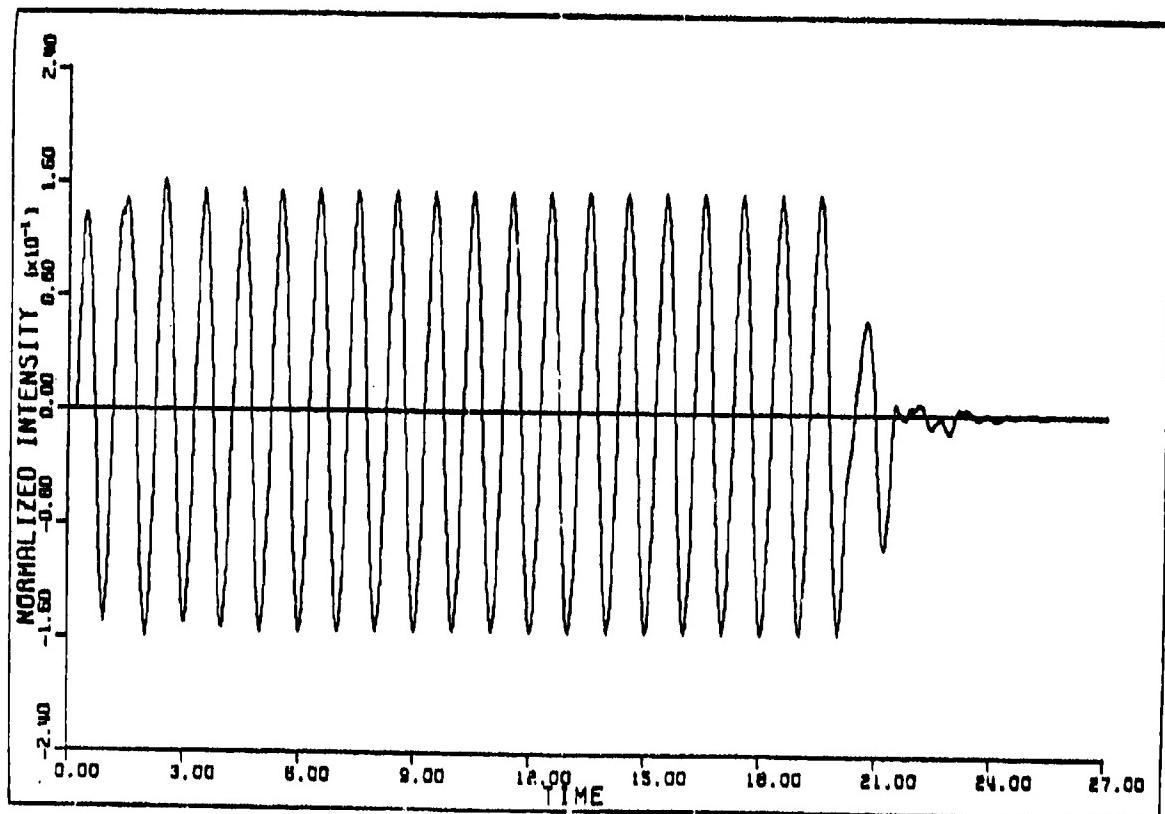


Fig. 11.  Internal field (4=1.067 cm) vs. time (ns), nonzero conductivity.

348
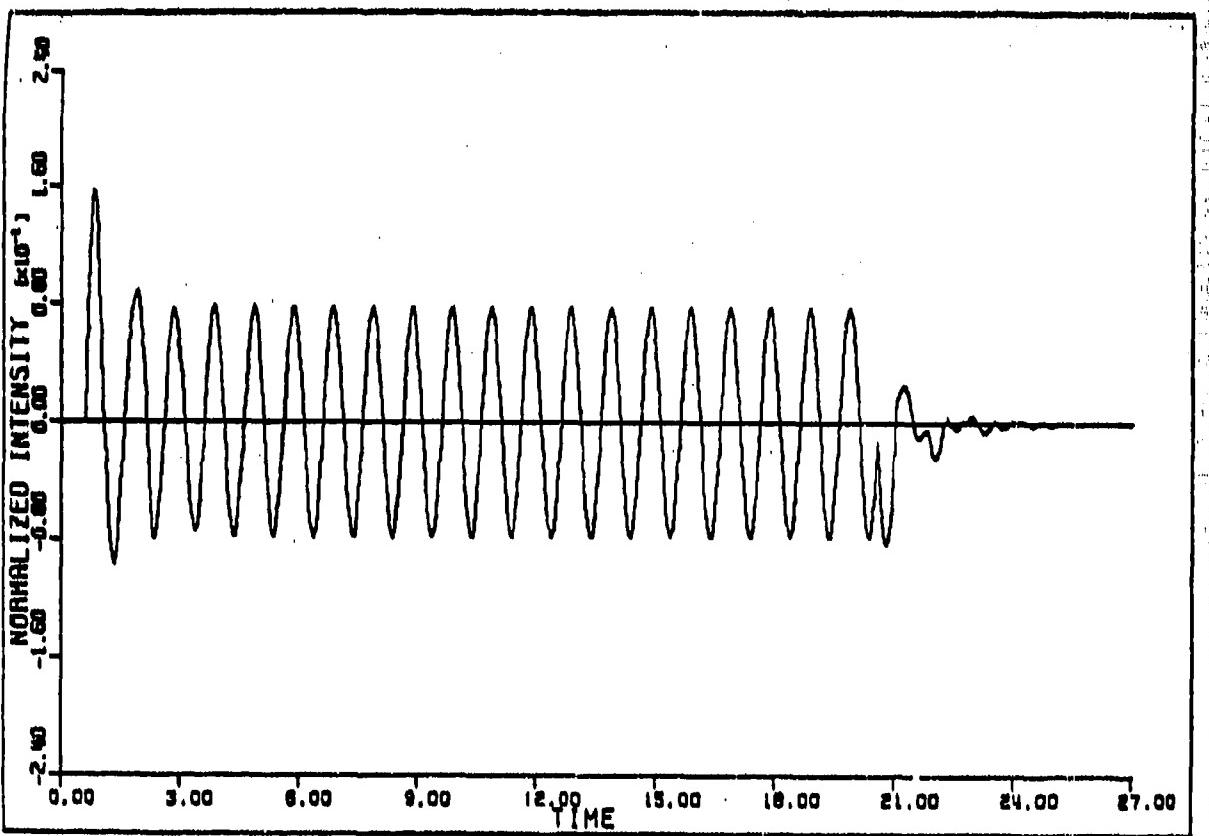
Fig. 12. Internal field (R=2.100 cm) vs. time (ns), nonzero conductivity.

349
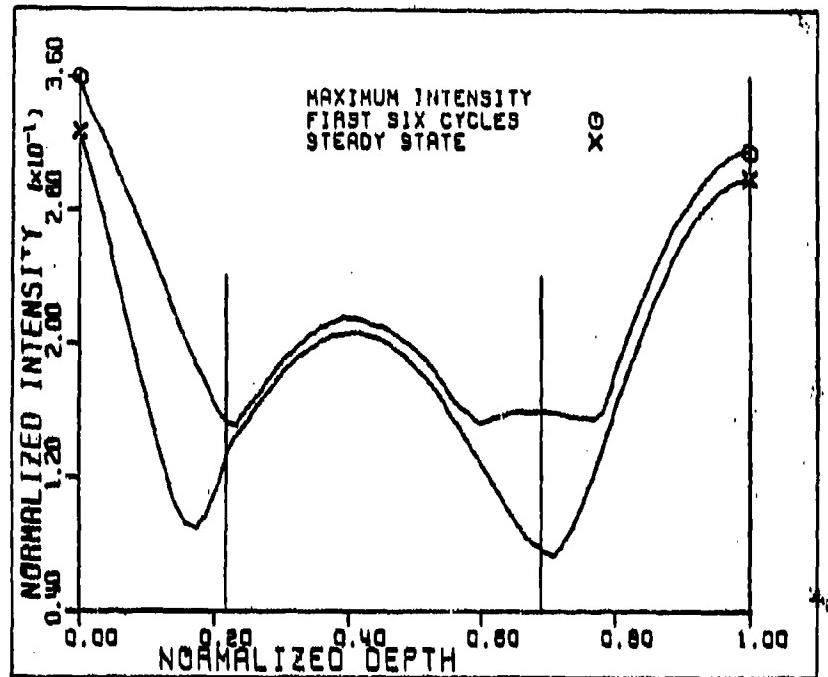
Figure 13. Comparison of transient and steady-state intensities in a medium with nonzero conductivity. Incident field is 1000-MHz pulse.
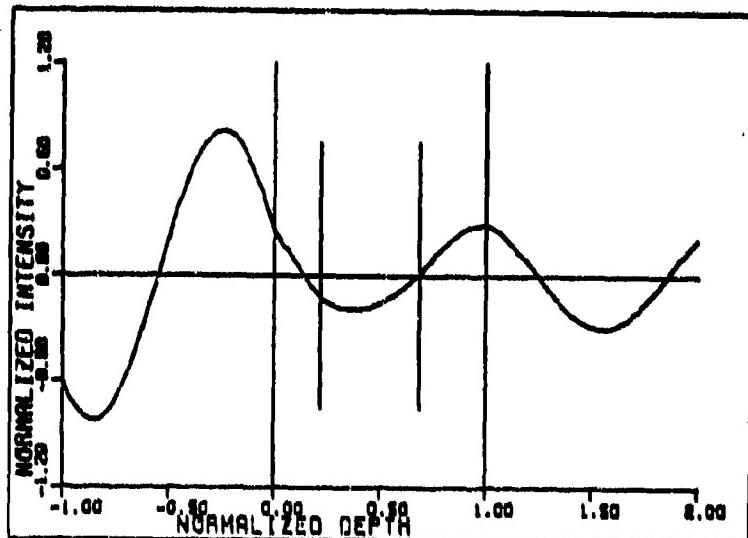


Figure 14. Internal, reflected, and transmitted fields for a medium with non-zero conductivity, time t = 6 ns. Incident field is 1000-MHz pulse of duration 20 ns, impinging on the medium from the left at time t = 0.

While the model used to establish the presence of these transients is a fairly simple one, it is felt that the pattern shown here will extend to more realistic situations. Further work should be directed toward establishing the presence and magnitude of transients for m    e relevant geometries and, in particular, to determine what focusing effects may occur. Additionally, the frequency dependence of the electrical properties of biological tissue should be taken into account.

The research outlined in this report assumes that the electrical properties of the medium are known. A related but more delicate problem is to determine the permittivity and conductivity of heterogeneous tissue in a noninvasive manner by measuring electromagnetic waves scattered from the tissue. This "inverse problem" for reconstructing a medium from scattered fields has been solved in [3, 4]  for the model given by equation (1) above. The implication of this work in the establishment of Air Force safety standards is that through the use of inverse problems it should be possible to non-invasively measure RFR or other damage to biological tissue. For example, reconstructed conductivity and permittivity profiles for healthy and suspected damaged tissue could be compared. Areas of damage would manifest themselves through altered electrical properties. Again, further work is needed to extend the model (1) to a more realistic situation.

V. REFERENCES

[1] W.F. Ames, Numerical Methods for Partial Differential Equations. New York: Academic Press, 1977.

[2] J. Bolomey, C. Durix, and D. Lesselier, "Time domain integral equation approach for inhomogeneous and dispersive slab problems," IEEE Trans. Antennas Propagat., Vol. AP-26, pp. 658-667, 1978.

[3]   R. Krueger, "An inverse problem for a dissipative hyperbolic equation
      with discontinuous coefficients," Quart. Appl. Math., Vol. 34, pp. 129-
      147, 1976.

[4]   R. Krueger, "An inverse problem for an absorbing medium with multiple
      discontinuities," Quart. Appl. Math., Vol. 36, pp.235-253, 1978.

[5]   R. Krueger, "Numerical aspects of a dissipative inverse problem,"
      IEEE Trans. Antennas Propagat., Vol. AP-29, pp. 253-261, 1981.

[6]   R. Krueger, "A scattering operator approach to the numerical solution
      of time-dependent wave equations." In press.

[7]   R. Krueger, "Transient fields produced in heterogeneous bodies by
      electromagnetic pulses," SAM-TR-81-12.        (Laboratory Project
      Scientist in Charge: E. Bell, SAM/BRM).

## VI. PUBLICATIONS AND PRESENTATIONS RESULTING FROM AF-FUNDED EFFORTS:

### Publications

1.   R. Krueger, "Numerical aspects of a dissipative inverse problem,"
     IEEE Trans. Antennas Propagat., Vol. AP-29, pp. 253-261, 1981.

2.   R. Krueger, "A scattering operator approach to the numerical solution
     of time-dependent wave equations." In press.

3.   R. Krueger, "Transient fields produced in heterogeneous bodies
     by electromagnetic pulses," SAM-TR-81-12.        (Laboratory
     Project Scientist in Charge: E. Bell, SAM/BRM)

### Presentations

1.   An example of resolving the nonuniqueness in an inverse scattering
     problem, IEEE/URSI International Symposium, Universite Laval,
     Quebec, Canada, June 4, 1980.  (R. Krueger)

2. The use of scattering operators in the solution of time-dependent wave equations, Ames Laboratory, USDOE, Iowa State University, Ames, IA, Sept. 23, 1980. (R. Krueger)

3. A study of transient fields produced in heterogeneous bodies by electromagnetic pulses, USAFSAM/BRM, Brooks AFB, TX, Oct. 17, 1980. (R. Krueger)

# LIGHT-SCATTERING AND FLUORESCENCE-PROBE STUDIES
## OF MOLECULES SUBJECTED TO 1-5-GHz EM FIELDS

S. E. Webber
Department of Chemistry
University of Texas
Austin, TX 78712

## I. INTRODUCTION

While the observation of behavioral and physiological effects of non-ionizing radiation is well documented,[1] no firm understanding of these biological phenomena at a molecular level is presently available.[2] Our experimental efforts are designed to test theoretical models that bear on the interaction of nonionizing radiation with biological molecules, usually taken to be biopolymers. It has been generally assumed that a kind of "cooperative effect" must pool the interaction of polar subunits of a complex species to yield the overall response of the biological unit. At the present time it is not known if the "polar subunit" is a water molecule in close association with membranes or proteins --the polar amino acids, nucleotides, or saccharides, that comprise the biopolymer main chain in many cases, or side groups such as the base pairs of DNA. One can only guess if nonionizing radiation can serve to modify membrane functionality, protein structure, or even base-pair hydrogen bonding. Since our experimental program is designed to operate in concert with theoretical models which of necessity will be greatly simplified relative to actual biological systems, we feel constrained to search for "model systems" that have some of the features of biological systems, but with a much less complex structure. It is essential to search for experimental observables that are compatible with simultaneous irradiation. Optical spectroscopy meets

this need, and we have decided to focus on the use of elastic light scattering and fluorescence techniques for our initial studies. The former technique can be used to determine the size and shape of macromolecules[3] (angle and concentration dependence of scattering), diffusion constants of macromolecules[4] (using suitable photon correlation techniques), or the onset of turbidity at the critical micelle concentration of a surfactant solution. Fluorescence techniques can be used to assess the local environment of a suitable probe molecule (embedded in a membrane or covalently attached to a biopolymer) or, in the case of some macromolecules, the degree of interaction of pendant chromophores.

One critical consideration in this field is dosimetry.[5] Because of the rather long wavelength of the radiation (millimeter to centimeter range), the physical dimensions of the electrodes and cells containing solutions must be carefully considered. Abrupt changes in the dielectric constant at interfaces (e.g., cell-solution boundaries) can cause local heating at the interface and poor penetration of the incident radiation into the bulk solution. When possible, the electrodes will be immersed in the solution of interest to avoid this problem.

## II. TECHNICAL APPROACH

### (a) Photon-Counting System for Light Scattering and Fluorescence

It is essential to achieve very high precision in measured light-scattering intensity such that small changes can be reliably detected. For this reason we are converting the light detection system of the FICA light-scattering photometer from an analog to a digital system. A schematic representation of this conversion is presented below. The starred items indicate new items that are in the process of being purchased. The (A-B)/C mode on the ORTEC 9320 sampling/control unit has the following meaning: A = photon count during illumination period, B = count during dark period (noise), C = photons collected from source.

355

chopper   sample
          chamber          1-5      microwave
                           GHz      source

Hg lamp                              

          PMT          PMT*
                                     θ

amp-discriminator      amp-discriminator*

        C                  A,B

    (source)          (scattered intensity)

              9315        9520        779*
              counter     controller  interface

average scattered intensity =
(A-B)/C with and without field
as function of θ                          RS-232*

                          HP-85
                          microprocessor
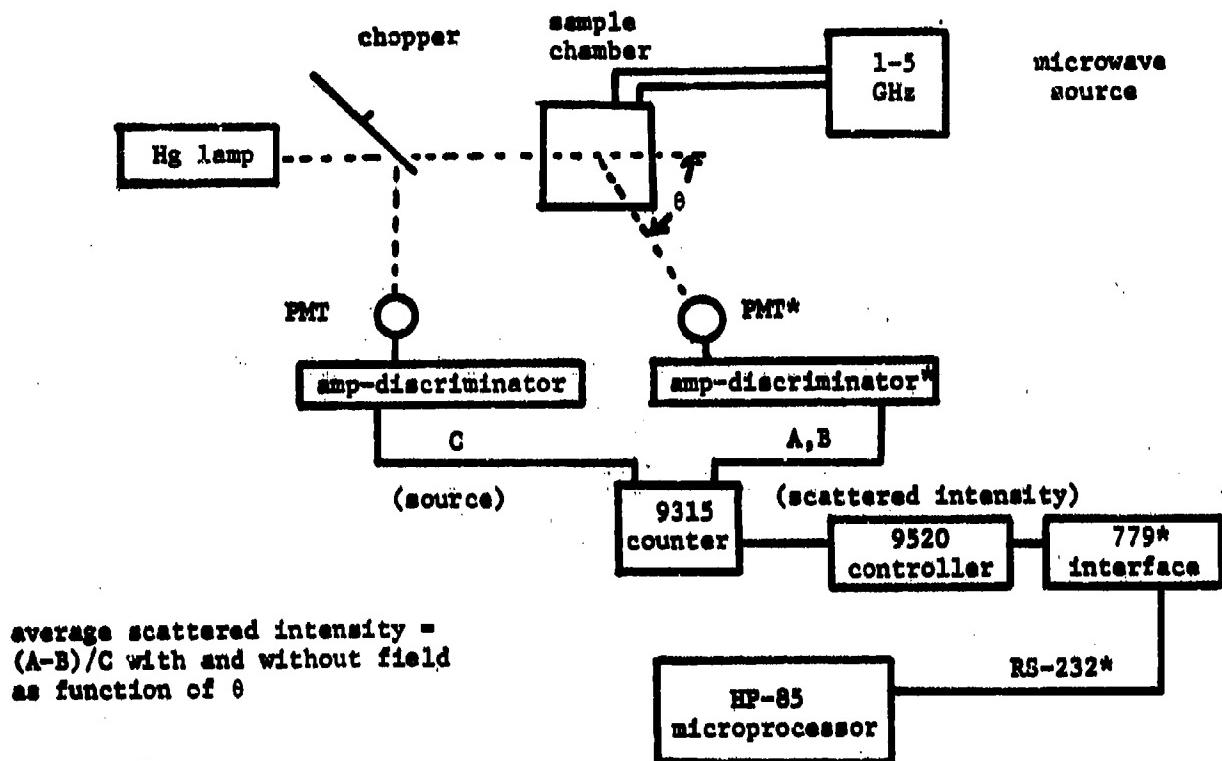
Fig. 1.   Schematic representation of photon-counting system.

Thus any long-term drifts in the illumination source are corrected for,
as well as any drift in the photomultiplier-tube noise level. The counts
collected per period will be averaged, and very accurate differences induced
by the EM field can be determined.

(b)  Cell Design

For light-scattering measurements the most important parameter is
the dissymmetry coefficient,

$$Z_\theta = \left( I(\theta) \right) / \left( I(180 - \theta) \right)$$

where $I(\theta)$ is the intensity of radiation scattered at angle $\theta$ (see Fig. 1).
Within the context of an assumed model, $Z_\theta$ can be used to compute changes
in the molecular dimension of a macromolecule (e.g., $\overline{S^2}$, where $S$ is the
end-to-end distance of a Gaussian chain). In addition, $I(90^\circ)$ is required
to compute the turbidity of a solution  if light scattering is used to
monitor a phase transition such as micelle formation. A partial octagonal

356

cell such as represented in (a) below will be satisfactory for determination
of $Z_{450}$, or fluorescence/light scattering at $90°$. It also has the advantage
of being commercially available in Supersil quartz (Precision Cells Inc.,
Hicksville, New York). A round cross-section cell (b) has the advantage of
accommodating any angle $\theta$ and convenient cross-section area for the
electrodes. Unfortunately commercially available cells of this size are
not available, and it is not known at present if cells of suitable optical
quality can be fabricated in our glassblowing shop. Either cell (a) or
(b) can be used in the SPEX FLUOROLOG for fluorescence measurements. In
order to achieve a uniform EM field inside the electrodes with minimum
leakage, the following equation must be satisfied:

$$d \leq \lambda/10$$

The impedance ($Z_o$) of the parallel plates is given by

$$Z_o = 377(d/W)(1/\sqrt{\varepsilon}) \approx 50\Omega$$

where $50\Omega$ is the impedance of the microwave generator. ($\varepsilon$ is the dielectric
constant of the solution, and the definition of symbols d,W is given in
Fig. 2 below.) Since the wavelength of 1-5-GHz radiation is in the range
30-36 cm, meeting the requirement that $d < \lambda/10$ is not too difficult.
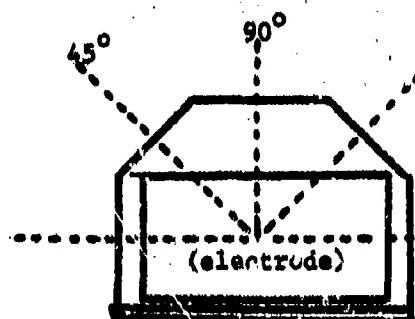


(a) semioctagonal cell          (b) round cell
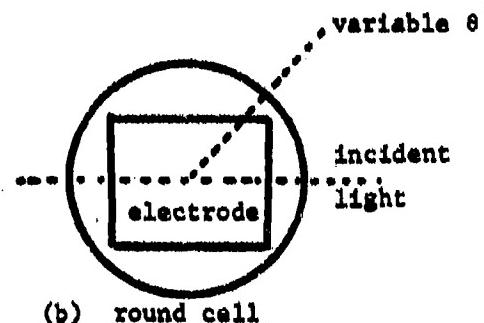
(c) electrode dimensions
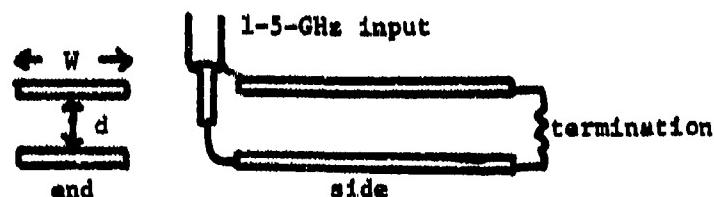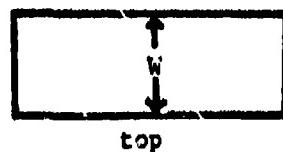
Fig. 2. Cell and electrode configurations.

357

(c) Discussion of Physical Observables and Molecular Systems for Future Studies

**Macromolecular Systems.** Biopolymers are most noted for their highly specific chemical activity which is dictated by a combination of specific reaction sites and molecular geometry. In some cases the molecular geometry is established by crosslinking (typically disulfide bonds) or internal hydrogen bonding. There are two types of synthetic macromolecules that we regard as reasonable models for structural perturbations yet which retain sufficient simplicity for theoretical treatments. These are aryl-methacrylates (general structure like I) and arylglutamates (general structure like II).
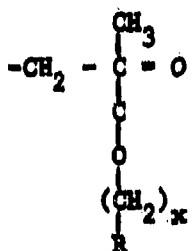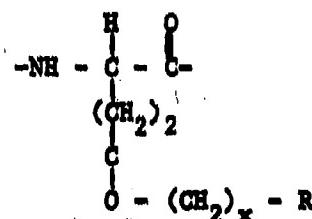
```
         CH3                          H   O
          |                           |   ||
-CH2 - C = O                 -NH - C - C-
          |                           |
          C                          (CH2)2
          |                           |
          O                           C
          |                           |
        (CH2)x                       O - (CH2)x - R
          |
          R

          I                           II
```

The glutamates are well known to form α-helices through internal hydrogen bonds in nonacidic media.[6] If the R groups are planar aromatics, the fluorescence from polymers like I and II shows a low-energy fluorescence feature from the so-called excimer species.[7,8] The formation of an excimer can be represented schematically by the following reaction:



$$^1(R......R)^* \tag{1}$$
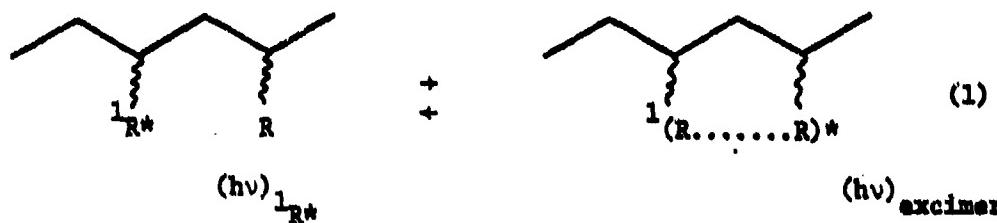
The excimer species, $^1(R...R)^*$, is held together by a significant van der Waals attraction (typical binding energies are on the order of 3000 $cm^{-1}$). It turns out that the tendency for excimer formation is solvent and temperature dependent[9,10] and has been related to the density of the polymer

coil in solution. Thus the structure of a polymer of these two classes may be characterizable from the light scattering and the relative intensity of the monomer and excimer fluorescence. In addition, the temperature and/or solvent dependence of the α-helix to random coil transition of the gluta-mates[11] can be studied as a function of external EM field. Since this transition is a cooperative effect that involves the breaking of internal hydrogen bonds, it is relevant to possible EM-induced DNA damage.

We note that polymers of type I and type II can be dissolved in non-aqueous solvents and their molecular dimensions perturbed by the addition of other nonaqueous solvents. Thus one avoids the strong $H_2O$ absorp-tion of millimeter radiation that plagues aqueous-solution studies. On the other hand, the polarity of these systems is such that if a small amount of water (a few percent) is introduced, it will most likely be adsorbed on the polymer coil. Consequently it is possible that the effect of the EM field on the water hydration can be detected if this hydration has any discernible effect on coil dimensions.

Our proposed experiments may be summarized as follows: light scattering and fluorescence spectra will be obtained for the target macro-molecules I and II in which R is a common aromatic fluorophore (naphthalene, pyrene, or anthracene are suitable). The dependence of $R_g$ (radius of gyration) and the excimer to monomer fluorescence ratio (usually denoted $I_D/I_M$ in the literature) will be determined as a function of solvent com-position and temperature. Our objective is to determine the overall sen-sitivity of $R_g$ and $I_D/I_M$ to these "thermodynamic" parameters for several macromolecular systems. Then the sensitivity of those same two spectro-scopic observables to an external EM field with an energy density of 10 $mW/cm^2$ (or lower) and a frequency in the 1-5 GHz range will be deter-mined. If changes are detected, then the time response can be measured by pulsing the field. As was mentioned in the earlier sections, extensive use of signal averaging is anticipated because small fractional changes in

$R_g$ or $I_D/I_M$ are likely and one must be prepared for meaningful "null" results.

Membrane Systems. Natural and artificial membranes composed of various fractions of phospholipids and the cholesterol have been studied by fluorescence techniques for a number of years. The sensitivity of some fluorescent dye probes to membrane potential has been touted as an excellent probe of excitable membranes,[12] while other studies have determined membrane microviscosity[13] or the exposure of membrane-bound proteins to the aqueous phase.[14] None of these fluorescent characterizations is unambiguous, but certain general observations have been realized that allow the following interpretations: (1) increasing the cholesterol content of a membrane increases the microviscosity, but not necessarily the gel to liquid crystal transition temperature, (2) increasing the microviscosity tends to expose more of a membrane-bound protein to bulk solvent. The study of microviscosity proceeds by means of fluorescence depolarization (which can also be interpreted in terms of the anisotropy of the rotational rates of the fluorophore probe) using the Perrin equation

$$r_0/r = 1 + C(r)(T\tau/\overline{\eta}) \qquad (2)$$

where $r_0$ and $r$ are the anisotropy ratios for the fluorophore in a rigid medium and the fluid medium respectively, $C(r)$ is a factor that is obtained from a calibration procedure (roughly equal to k/V, where k is the Boltzmann constant and V is the molecular volume of the fluorophore), T the temperature, $\overline{\eta}$ the microviscosity, and $\tau$ the lifetime of the fluorophore at temperature T and in the particular medium. The anisotropy ratio is given by

$$r = (I_{\parallel} - I_{\perp})/(I_{\parallel} + 2I_{\perp}) \qquad (3)$$

where $I_{\parallel}$ and $I_{\perp}$ are the intensities of fluorescence parallel and perpendicular to the excitation polarization respectively (often an experimental correction for scattering depolarization is required).

Quenching of a fluorophore in a heterogeneous environment has been analyzed by the expression[15]

$$F_o/(F_o - F(Q)) = \sum_1 \left( (f_i K_{qi}(Q))/(1 + K_{qi}(Q)) \right)^{-1} \qquad (4)$$

in which $F_o$ and $F(Q)$ are the fluorescence intensity in the absence and presence of quencher respectively. In eqn. (4) $f_i$ is the fraction of fluorophores in the ith environment with a quenching rate constant $K_{qi}$. Quite often the physical nature of a quencher can be varied, with a concomitant shift in its position with respect to the membrane-aqueous interface. An example of a quencher series of this type is the quaternary salts of 4-picoline of the type

$$CH_3 - (CH_2)_x - \overset{+}{N}\langle\bigcirc\rangle - CH_3$$

III
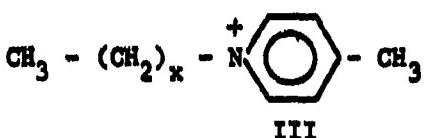
represented by III in which x can vary from 0 to 15.[14] The specific membrane location of the different members of III leads to different degrees of protein-bound fluorophore (tryptophane) quenching, which suggests the extent of protein exposure to the aqueous phase.

The above experiments suggest monitoring the fluorescence properties of membranes with and without an external EM radiation field. Experimentally one need only construct a modified fluorescence cell, along the lines of Fig. 3a. Since membranes are an ordered collection of partially polar molecules, they could well execute a collective response to radiation of this type. Thus one might observe an enhanced fluorescence depolarization, implying a diminished microviscosity. Possibly a change in the fluorescence quenching of a protein fluorophore can be related to a shift of the protein in the membrane. Obviously such experiments must be carried out under carefully thermostated conditions to avoid any "trivial" heating effects. As before, one must anticipate small effects and design experiments to include extensive signal averaging of field-on and field-off intensities.

361

optical excitation

microwave generator

scattering (90°)

(a)
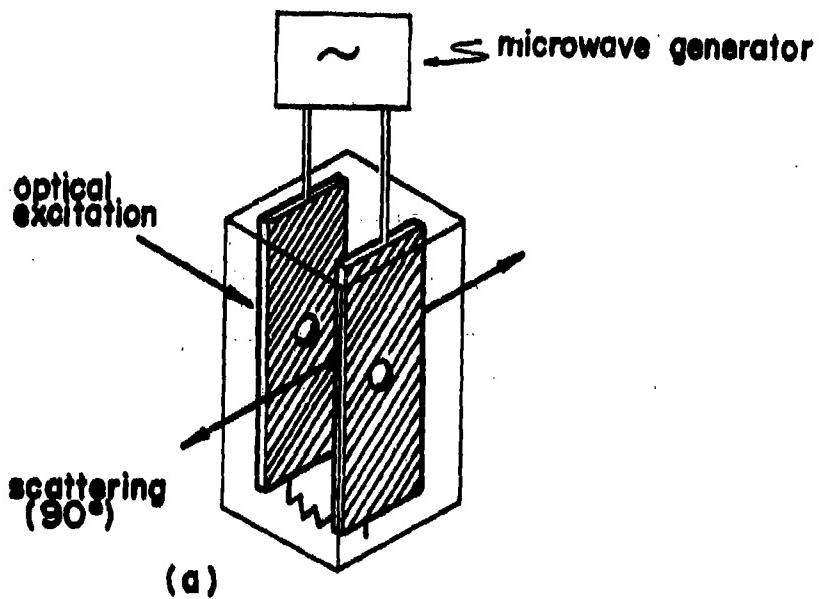
Fig. 3.

III. RESULTS/PROGRESS

Experimental apparatus is just being assembled. Any preliminary re-
sults that are available at the time of the meeting will be presented for
discussion.

IV. SUMMARY AND CONCLUSIONS

The objective of these experiments is to provide a close relation
between physical observables and theoretical models. Fundamental mechanisms
of EM coupling to complex molecules in fluid or ordered states are to be
elucidated. When these mechanisms are understood, then it may be possible
to understand threshholds of potential EM-field biological damage without
having to rely on the extrapolation from test animals to humans. In addi-
tion, one may hope for schemes of prevention or cure without necessitating
total avoidance of EM fields.

## V. REFERENCES

1. A good case in point is the program of the Second Annual Meeting of the Bioelectromagnetics Society (San Antonio, Texas, September 14-18, 1980) in which over 150 pages were presented in this general field.

2. See the panel discussion reported by D.L. Jaggard and J.L. Lords, Proc. IEEE 68, 114 (1980) or the review of Eastern European work by D.I. McRee, ibid, p. 84.

3. B.H. Zimm, J. Chem. Phys. 16, 1099 (1948).

4. See, for example, B.J. Berne and R. Pecona, Dynamic Light Scattering with Applications to Chemistry, Biology and Physics (Wiley-Interscience, London, 1976).

5. See, for example, the discussion by A.W. Guy, Ann. New York Acad. Sci. 1975, 539.

6. See the introductory discussion in Macromolecules: An Introduction to Polymer Science, F.A. Bovey and F.H. Winslow (Academic Press, New York, 1979), Chapter 8.

7. J.B. Birks, Photophysics of Aromatic Molecules (Wiley-Interscience, London, 1970).

8. See the forthcoming review of polymer excimer formation by D.A. Holden and J.E. Guillet in Developments in Polymer Photochemistry, Volume 3 (in press).

9. J.S. Aspler and J.E. Guillet, Macromol. 12, 1082 (1979).

10. E.A. Abuin, E.A. Lissi, L. Gargallo, and D. Radic, Europ. Polym. J. 15, 373 (1979).

11. See F.A. Bovey, Polymer Conformation and Configuration (Academic Press, New York, 1969), p. 110.

12. F.F. Hartline, Science 203, 992 (1979).

13. M. Shinitzky and M. Inbar, Biochim. Biophysica 433, 133 (1976).

14. (a) M. Shinitzky and D. Rivnay, Biochem. <u>16</u>, 982 (1977); (2) U. Cogan, M. Shinitzky, G. Weber, and T. Nishida, Biochem. <u>12</u>, 521 (1973).

15. S.S. Lehrer, Biochem. <u>10</u>, 3254 (1971).

VI. PUBLICATIONS AND PRESENTATIONS RESULTING FROM AF-FUNDED EFFORTS

None.

# BIOLOGICAL EFFECTS OF MILLIMETER WAVE IRRADIATION

Om P. Gandhi
Department of Electrical Engineering
University of Utah
Salt Lake City, UT . 84112

## I.  Introduction

A number of investigators have reported sharp, distinct resonances in the absorption of millimeter wave radio-frequency radiation by various biochemicals and biological preparations [Webb and Booth, 1969, 1971; Stamm et al., 1974; Dardanoni et al., 1976; Lee and Webb, 1977]. Others have reported that exposure to millimeter wave irradiation produces biological effects that exhibit a sharp frequency dependence [Devyatkov et al., 1974; Stamm et al., 1975; Berteaud et al., 1975; Dardanoni et al., 1976, 1979; Grundler et al., 1977; Grundler and Keilmann, 1978]. Reported in this literature are sharp millimeter wave frequency-dependent lethal and mutagenic effects on microorganisms, major effects on metabolic control of growth of cells, effects on oncogenic versus viability properties of cells, protective effects on X-irradiated and cytotoxic-drug-treated animals, etc. It has been suggested that these differences might provide the basis for frequency-specific health hazards and possibilities for new forms of cancer therapy. There also is a great deal of interest in the interaction of millimeter waves with biological media, in order to understand the possible mechanisms of biological effects of RFR.

365

## II. Highlights of Our Previous Work --
## Absorption Spectra of Biological Samples

In order to confirm and pinpoint the resonance frequencies, a solid-state computer-controlled system has been used to make swept-frequency measurements of absorption of biological specimens from 26.5 to 90 GHz [Gandhi et al., 1980; Hagmann and Gandhi, 1981]. A block diagram of the system is shown in Fig. 1. Three similar circuits were used to cover the $K_a$, U, and E bands (26.5-40.0, 40.0-60.0, and 60.0-90.0 GHz, respectively). As the output frequency of the IMPATT oscillators was stepped during each sweep, measurements of the incident, reflected, and transmitted powers were made and stored on magnetic tape. Amplitude and frequency stability of the system were measured at periodic intervals. The extreme variations observed in amplitude were ±0.06 dB (±1.4 percent) in one-hour and ±0.16 dB (±3.8 percent) in 15-hour tests. The frequency shift was typically from 1 to 6 ppm per minute. The dwell time at each of the frequencies was varied from 10 ms to 10 s. A dwell time of 50 ms or larger was found to give identical results, the shorter dwell times being inadequate for the electronic circuits involved in the setup. A dwell time of 50 ms was therefore used for all subsequent measurements. A preselected frequency span was swept by 100 step frequencies. A total of 5 sweeps was typically taken for each of the samples, filling the entire cross section of the waveguide in order to obtain the reflectance and absorbance parameters; the entire procedure taking a time period of less than one minute. In order to allow the measurement of minor differences (as low as 0.1 dB), relative measurements were made by direct comparison of insertion loss and reflectance

of the biological specimens with the aqueous background media in which they were either suspended or dissolved.  A wide range of samples was used, including solutions of DNA and RNA  and suspensions of BHK-21/C13 cells, _Candida albicans_, _C.krusei_, and _Escherichia coli_.  Sharp spectra reported by other workers were not observed.  The strong absorbance of water (13-36 dB/mm) caused the absorbance of all aqueous preparations that we examined to have a waterlike  dependence on frequency.  Reduction of incident power level (to below 1.0 μW), elimination of modulation, and control of temperature to assure cell viability were not found to significantly alter the water-dominated absorbance.

Extensive tests on yeast _C. krusei_ have been conducted using an exceedingly small sampling interval (6 MHz) in a narrow frequency range (41.2-41.794 GHz) in which frequency-specific bioeffects have been reported [Grundler et al., 1977; Grundler and Keilmann, 1978].  Although the frequency interval of 6 MHz should have been adequate to resolve the reported biological spectra, no significant differences were seen in experiments comparing yeast and its nutrient broth for a variety of cell concentrations (up to $2 \times 10^8$/ml), dwell times (50 ms and 5 s), and incident power levels (2, 10, and 60 μW).  Similar experiments have been carried out on BHK-21/C13 cells, using a 35-MHz sampling interval in a frequency range (66-76 GHz) in which strong microwave absorption has been reported [Webb and Booth, 1971].  No significant differences were seen, once again, when the cells were compared with their medium.  The details of these and many other spectral measurements are given in our paper in _Bioelectromagnetics_, Vol. 1, pp. 285-298 (1980).

We have reached the conclusion that interpretations of others

[Webb and Booth, 1969, 1971; Lee and Webb, 1977; Stamm et al., 1974; Dardanoni et al., 1976] concerning spectral resonances of suspensions of cells and solutions of biologically important materials are in error. Such errors might have resulted from the use of unsophisticated micro-wave methodology. For example, Stamm et al. [1974] attributed imbalance in a microwave bridge circuit to differential absorption, when it is more probable that the imbalance was due to phase rather than amplitude differences. Webb et al. [Webb and Booth, 1969, 1971; Lee and Webb, 1977] reported spectra in which the peaks have a fairly uniform spacing, suggesting that they might have resulted from interference in the mea-surement system [Hershberger, 1978].

## Action Spectra

It should be recognized that even though the absorption of milli-meter wave RFR in aqueous biological preparations is dominated by the very high absorbance of water, it may nevertheless be possible to see frequency-specific biological effects. It was consequently decided to study the action spectra of protein synthesis of BHK-21/C13 mammalian cells as a result of irradiation at 0.1-GHz intervals in the 38.0-48.0 and 65.0-75.0 -GHz bands [Partlow et al., 1981; Stensaas et al., 1981; Bush et al., 1981]. The selection of these specific frequency regions was influenced by the previously reported frequency-specific biological effects by Berteaud et al. (69.5-75.5 GHz) and Devyatkov et al. (38.96-51.72 GHz). A block diagram of the irradiation system is shown in Fig. 2. Two similar circuits were used to cover the frequency regions 38.0-48.0 GHz and 65.0-75.0 GHz in U- and E-bands, respectively. OKI kly-strons 40V12 (37-42 GHz), 45V12 (42-48 GHz), and 70V11 A [65.0-75.0 GHz)

were used as power sources because of their superior spectral purity as compared, say, to the IMPATTs used in the setup of Fig. 1. Following a 30-minute warm-up period, power fluctuations were less than a few percent. Frequency shifts considerably less than ±0.025 GHz were observed even after several hours of operation. Monolayer cultures of BHK-21/C13 cells were grown on microwave-transparent polystyrene coverslips, placed directly on the open ends of the U- and E-band waveguides of dimensions 4.8 × 2.4 and 3.1 × 1.55 millimeters, respectively, and irradiated (N = 4) for time durations of 15 minutes at each of the frequencies. The polystyrene coverslip (25-mm diameter; treated for tissue culture) was attached by paraffin to a petri dish with a hole in the bottom in order to allow cooling by pumped culture medium. The temperature of the medium was maintained to within 0.1°C over the entire duration of the microwave exposure. A template was used to mark the under surface of each coverslip so that it could be precisely positioned on the waveguide. The markings were later used to identify the portion of the cell monolayer which had been irradiated. Irradiation was carried out in a walk-in incubator for average power densities of 177 and 292 mW/cm$^2$ at U- and E-bands, respectively. Incorporation of $^3$H-methionine into protein was quantified by measurement of optical densities of autoradiographs in contiguous rectangular regions of width 0.1 mm obtained by a microprocessor-controlled stepping motor. Since microwave power incident on the cells varies along the long dimension of the waveguide aperture as cosine$^2$ from zero at each of the edges to twice the average power density at the center of the waveguide, it was argued

369

that this technique should reveal biological effects which might only be manifested in narrow amplitude domains or "power windows." The results for each of the irradiated frequencies were compared to those for the control cultures sham irradiated as described above, except that no microwave power was supplied from the klystrons.

Observations of protein synthesis in monolayer cultures with 202 closely spaced frequencies in the 38.0-48.0 and 65.0-75.0-GHz bands failed to reveal changes associated with microwave exposure [Bush et al., 1981]. A limited number of experiments to study the incorporation of $^3$H-uridine into RNA for irradiation durations of 1 hour also yielded negative results [Partlow et al., 1981].

## III. Technical Approach

The thrusts of the current Air-Force-funded project are as follows:

1. Mutagenic effects of millimeter wave irradiation.
2. Permittivity measurements for biological tissues.
3. Low-wave-number Raman and Brillouin spectroscopy with and without microwave irradiation.

In the following we will briefly describe the technical approaches for each of the above tasks.

## Mutagenic Effects

The ongoing research is to examine the change in mutation rates of genes of prokaryotic (bacteria and/or bacterio-phage) and eukaryotic (saccharomyces species) organisms by irradiation at closely spaced

frequencies in the 42.0-48.0 and 65.0-75.0-GHz bands to look for frequency-specific biological effects [see e.g., Berteaud et al., 1975; Grundler et al., 1977; Grundler and Keilmann, 1978; Devyatkov et al., 1974]. Toward this end a broadband temperature-controlled irradiation system has been set up [Riasi et al., to be published]. A schematic diagram of this system is shown in Fig. 3. Simultaneous testing at frequencies in the U- and E-bands is possible with the present system. A waveguide switch is used in both circuits to allow accurate measurement of incident powers with thermistors. Near-perfect (larger than 99 percent) coupling of microwave power to the samples allows direct use of the powers so measured as power absorbed by the samples. The sample holders shown in Fig. 4 are rectangular cross-section glass tubes that are mounted to block the opening of the waveguide cut along a plane perpendicular to its narrow wall. Fairly low reflection of the incident microwave power is obtained because of the tapered design of the load provided by the absorbing biological media flowing through these sample holders. Complete absorption of the coupled power is ensured by using a sample thickness of several skin depths and coating the exposed edges of the glass tubing with silver paint to prevent leakage of the microwave energy. A diagram of the thermally insulated housing is given in Fig. 5. The copper base plate of the housing has a temperature set with a proportional temperature controller. Irradiation and control waveguides are fastened to the base plate to minimize their temperature differences. A series of stainless steel tubes connected to the sample flow ciruits are also fastened to the base plate to minimize the temperature differences of the samples. The housing has an aluminum cover and contains Styrofoam insulation to reduce transfer of heat from the base

plate. Copper-constantan thermocouples are used to monitor fluid temperatures at the input and output of each sample holder. A Nichrome heater is fastened to the outside of the glass of each control sample holder to compensate for the observed temperature differences caused by deposition of microwave energy. Compensatory electrical heating is provided in order to control the temperature differences between irradiated and sham-irradiated samples to within ±0.02°C over the course of 30 minutes of exposure periods.

In order to determine the distribution of microwave energy deposition within the sample holders, we have carried out measurements of local heating within an increased-scaled model of the sample holder made for use at X-band. For these experiments, a phantom composition with appropriately scaled dielectric constant and conductivity [Cheung and Koopman, 1976] was used. Figure 6 shows the temperature profile along the central axis of the scaled sample holder. The decrease in energy deposition is approximately exponential as would be expected from theory. In a circulating sample, of course, the various cells would be exposed to the varying SARs in travel through the tube.

The first set of experiments just completed has been on the <u>induction of Lambda phage in lysogenic strains of Escherichia coli</u>. These experiments have been under the direction of Dr. Douglas W. Hill of the Department of Cellular, Viral, and Molecular Biology, University of Utah. Strains of wild-type Lambda phage (papa) and <u>E</u>. <u>coli</u> (TC 600) were obtained from Dr. Costra Georgopoulos. A large number of isolates of lysogens were prepared and characterized with respect to effects of

372

temperature, mitomycin C, and ultraviolet light on frequency of induction. The specific one chosen (y-3) for use showed sensitivity to induction by mitomycin C and ultraviolet but typical wild-type insensitivity to induction at temperatures as high as 39°C.

The experimental design and the conditions of the experiments were as follows. Eighteen-hour log phase cultures of the test lysogen (y-3) were prepared, the organisms harvested by centrifugation and resuspended in fresh growth medium. Immediately prior to use, the organisms were diluted to appropriate cell concentrations, and circulating exposure systems inoculated with measured volumes of these suspensions. Following careful temperature equilibration of both control and experimental test suspensions, they were exposed to microwave irradiation at fixed powers and at the frequencies indicated in Fig. 7 for both the U- and E-bands. The two cell suspensions were removed from the exposure systems, quantitatively diluted and assayed for Lambda phage, employing the appropriate indicator strain of E. coli. Following overnight incubation at 37°C, the plaques were counted and the resulting data converted arithmetically into differences in frequency of induction of irradiated cells and control cells maintained at isothermal conditions.

The data collected from numerous individual experiments are summarized graphically in Fig. 7, a and b. The data are plotted as differences in percentage of induction of irradiated and sham-irradiated, control cells versus frequencies in both the U- and E-bands.

In all of the experiments undertaken so far, the results are consistent with the interpretation that no significant effects at the indicated frequencies or power levels have been observed. It is to be

373

emphasized that these data were collected under very carefully controlled conditions of temperature control, both measurement and continuous recording. At no time during the 30-minute exposure were differences in temperatures at the exit ports allowed to exceed ±0.02°C. Thus at the same temperatures, control and irradiated cells of lysogenic E. coli exhibited no differences in frequencies of induction when exposed to millimeter microwaves.

The same experimental design and procedures are currently in use with temperature sensitive (ts) mutants of Lambda phage. These mutants show characteristics of extreme sensitivity to heat induction. It is anticipated that the study of these classes of lysogens, utilizing the described equipment, will allow experimental verification of the hypothesis that the frequency-specific effects that have been reported in the past have been artifactual due to induced thermal effects.

## Precision Measurements of the Complex
## Permittivities of Biological Tissues

Knowledge of the complex permittivities of the biological tissues is needed at millimeter wavelengths for proper dosimetry and to assess the possibility of any frequency-specific biological effects. We have been studying ways of alleviating the problems with the conventional techniques [Szwarnowski and Sheppard, 1977; Van Loon and Finsy, 1975], namely the need to fabricate precise and fairly thin sample holders which are not readily amenable to biological tissues such as skin, fat, muscle, bone, etc. We have arrived at two approaches that we are currently evaluating for feasibility. These are described in the following:

A.  Measurement of the complex reflection coefficient of an open-
    ended waveguide radiating into a biological preparation.

    The schematic of the proposed arrangement is shown in
Fig. 8.  The method utilizes an open-ended waveguide radiating
into the biological sample through an intermediate layer of
air or a biocompatible moderate-ε medium.  A similar arrange-
ment has previously been used for gaseous plasma diagnostics,
albeit at somewhat lower frequencies.  Even though both open-
ended rectangular and circular waveguides could be used for
the proposed method, the results obtained with the circular
waveguide may be easier to interpret because of a lower self-
reflection [Bailey and Swift, 1968; Croswell et al., 1968] for
such open-ended waveguides.  On the other hand, because of the
compatibility with the rest of the circuit, the rectangular
waveguide may be more advantageous.  It is therefore planned
to evaluate both systems for possible use for millimeter wave
permittivity measurements.  Referring to Fig. 8, an intermedi-
ate layer of air or a biocompatible moderate-ε medium is to be
used to reduce the reflectivity from the sample, thereby
making it possible to detect small differences between differ-
ent biological tissues.  The complex reflection coefficient
(magnitude and phase) would be measured by using the four-
probe method described previously by Caldecott [1973].  A
four-probe reflectometer is capable of measuring not only the
complex reflection coefficient, but also incident power level
and frequency.  If successful, this method could also be used
for measurements on the superficial tissues of intact animals.

B. "Infinite" sample method for the measurement of the complex permittivity.

This method uses a thick "semi-infinite" tissue sample which forms the termination of a waveguide system, alleviating thereby the need to fabricate sample holders of submillimeter thicknesses, especially for the 60-90-GHz band. The method is particularly useful for high-loss materials, since a reasonable length of the waveguide section (few centimeters) would be adequate to simulate an infinite sample. An intermediate section of the waveguide filled with a moderate-$\epsilon$ bicompatible medium would be used as an impedance transformer to reduce the magnitude of the reflectivity from the sample. The previously described four-probe [Caldecott, 1973] reflectometer system may then be used to determine the magnitude and phase of the reflection coefficient. While disadvantageous, because of the requirement to grind the tissue in order to fill the waveguide section, this method is easy to quantify theoretically. This may result in an accurate determination of the needed permittivities. Also, the method could be used to cross-check the values obtained from method A.

## Laser Raman and Brillouin Spectroscopy of Biological Systems

An important area of research in the RFR bioeffects is to determine the mechanisms of interaction between electromagnetic fields and biological media. A promising line of investigation suggested toward this objective is the low-wave-number Raman and Brillouin spectral

376

studies of the biological media. Laser Brillouin spectroscopy [Jacobson and Shen, 1979; Wang et al., 1979] has the advantage of being able to emit (launch) or absorb acoustic phonons in a medium at frequencies on the order of $0.1$-$1.0$ $cm^{-1}$ (3 to 30 GHz). For higher frequency optical phonons ($1.0$-$10.0$ $cm^{-1}$), Raman spectroscopy is more appropriate. The dimensions of the biological membranes and molecules are on the order of several tens to thousands of angstroms and comparable to wavelength of acoustic waves at microwave/millimeter frequencies in the media. It is entirely conceivable, therefore, that Brillouin and Raman spectral studies will provide a new and useful means of studying these media, particularly as regards the mechanisms of interaction at microwave frequencies. Fröhlich [1978] has alluded to the possibility of specific frequencies of a biological system related to the excitability of acoustic/optical phonons in cells. Dimensionally related phonons have also previously been observed in solids and liquids.

Artificial liposomes are a definable model membrane system that is planned for the first experiments for low-wave-number Brillouin and Raman spectroscopy. More complex biological media such as solutions of DNA and RNA, Candida albicans, C. krusei, E. coli, fibroblasts, suspension of BHK21/C13 cells, etc., would subsequently be used to identify any microwave phonon activity. If these experiments are successful, future experiments would then focus on simultaneous irradiation of the biological media by microwaves at the identified frequencies.

## IV. Summary and Conclusions

In summary, the experiments to reveal sharp millimeter wave absorption spectra of biological media have not been successful. The absorbance is dominated by that of water (on the order of 13-36 dB/mm), which is an essential ingredient because of the aqueous nature of the preparations. There is a need to obtain the absolute complex permittivities of the biological tissues for proper dosimetry and to assess the possibility of any frequency-specific biological effects. Experiments have been initiated to obtain the complex permittivities of these tissues in the 26.5-90.0-GHz band.

The action spectra of biological systems have yielded negative results in the systems that we have studied, namely the uptake of $^3$H-methionine into protein of BHK-21/C13 mammalian cells at 202 frequencies and induction of Lambda phage in wild-type E. coli (TC 600) at closely spaced frequencies in the frequency bands 42.0-48.0 and 65.0-75.0 GHz where sharp frequency-specific effects had previously been reported. It is recognized that these studies conducted by biochemical assays are slow and will not give effects that may occur only during irradiation. An entirely new line of investigation has therefore been started to look for mechanisms of frequency-specific effects of irradiation. This is to study the low-wave-number Raman/Brillouin spectra of biological preparations in order to pinpoint the frequencies of microwave phonon activity in these materials. Upon identification of these frequencies, the materials will be irradiated with microwaves in order to look for interaction of electromagnetic fields with these media.
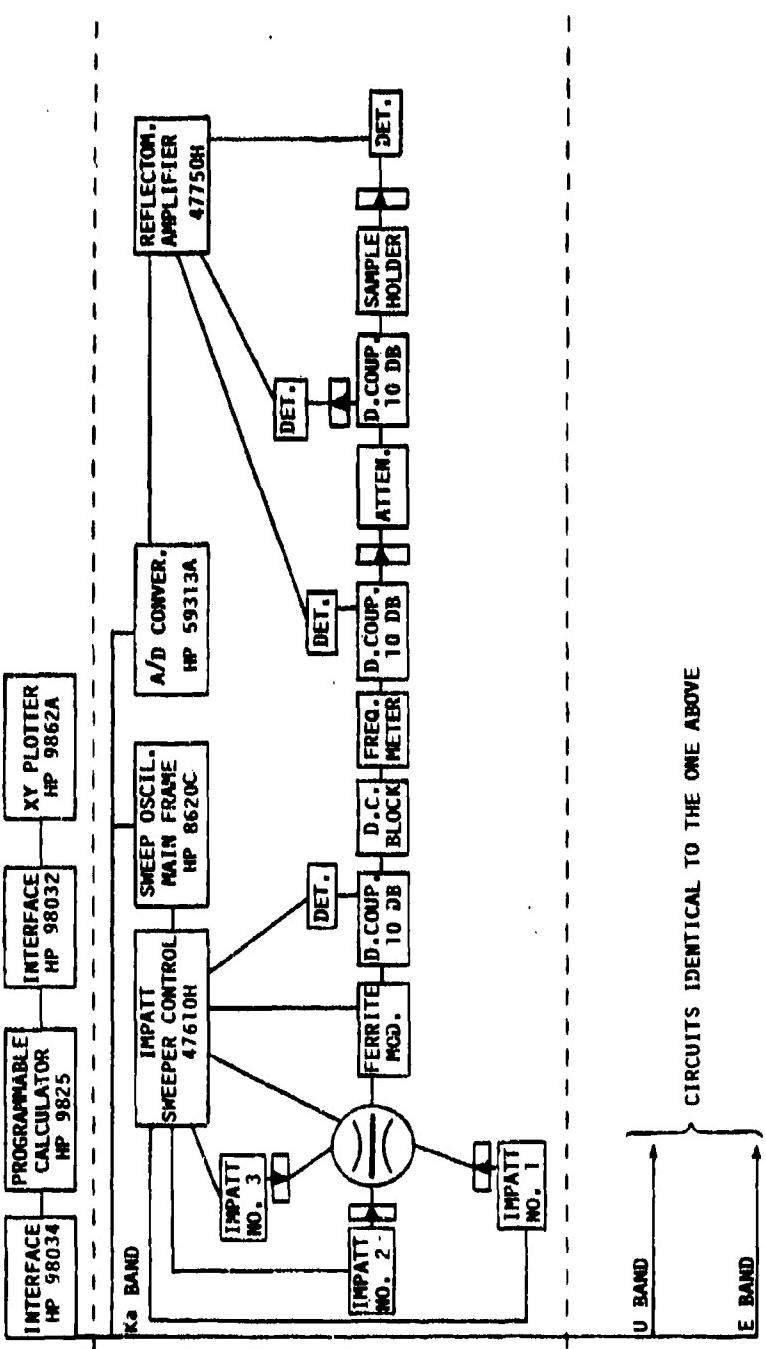
Fig. 1. Block diagram of the measurement system.

379
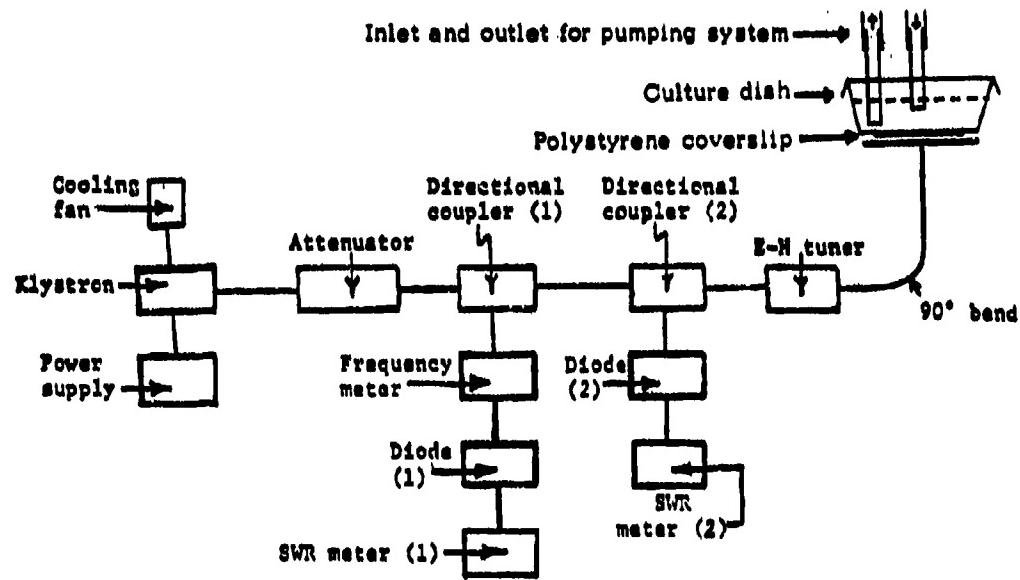
Fig. 2.  Microwave setup  for irradiation of monolayer cultures
of BHK-21/C13 cells grown on polystyrene cover slips.

Fig. 3. Schematic of a broadband U-band/E-band irradiation system.

Thermocouple terminal to uV meter

E-band

U-band
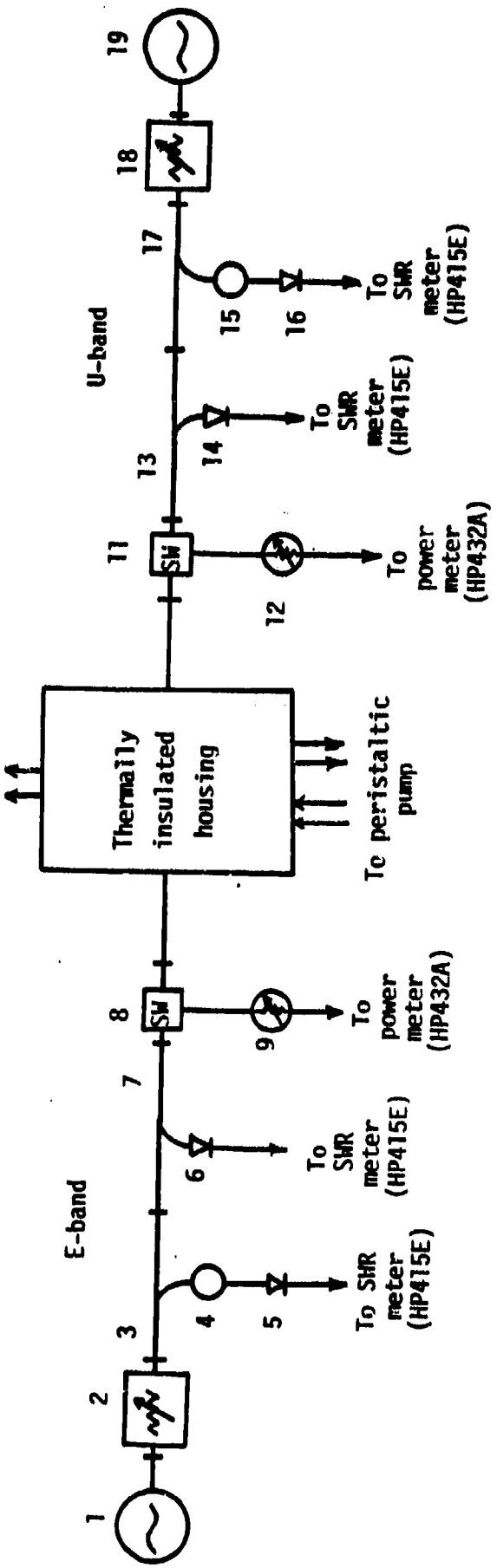
1. Klystron (OKI 70V11A)
2. Precision attenuator (FXR, type M164A)
3 and 7. 10-dB directional coupler (Narda)
4. Frequency meter (Hitachi model S2270)
5 and 6. Diode
8. Waveguide switch (Hughes)
9. Thermistor mount (Hughes model 44895H)

11. Waveguide switch (Hughes)
12. Thermistor mount (Hughes model 44892H)
13 and 17. 10-dB directional coupler (Narda)
14 and 16. Diode
15. Frequency meter (Hitachi model F2210)
18. Precision attenuator (Hitachi model F1513)
19. Klystron (OKI model 45V12 or OKI model 40V12)

381

Fig. 4. Sample holders for control and irradiation channels.

Control waveguide

Irradiation waveguide

Nichrome wire

Glass sample holder

Glass sample holder

382
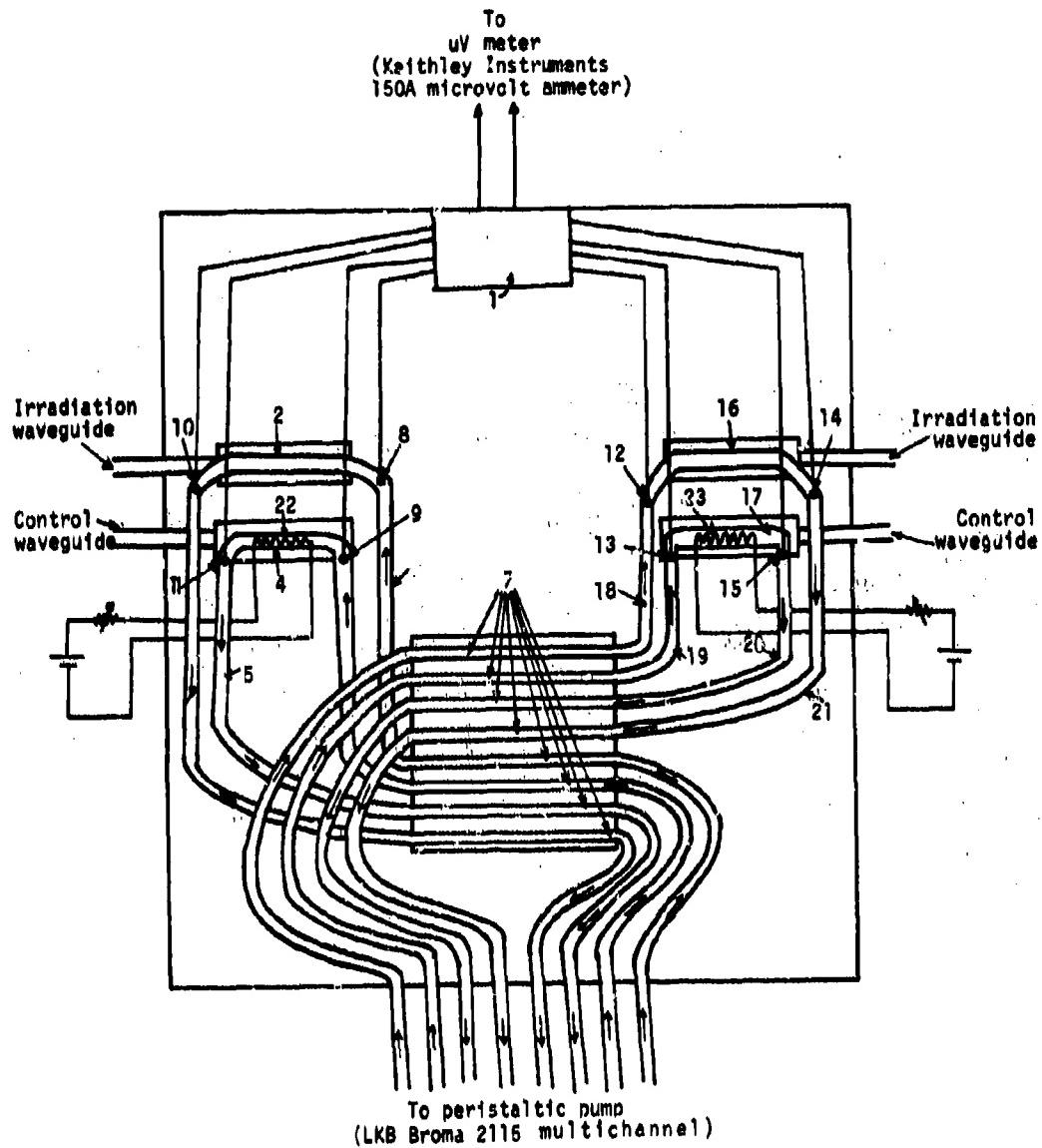
1. Multichannel switch

2 and 16. Sample holder mounted on irradiation waveguide

3, 5, 18, 19, 20, and 21. Rubber tubing (I.D. = 1.3 mm)

4 and 17. Sample holder mounted on control waveguide

7. Metallic tubing mounted on metallic blocks with heat sink paste

8-15. Position of thermocouples

22 and 23. Nichrome wire

Fig. 5.  Diagram of the insulating housing.

383
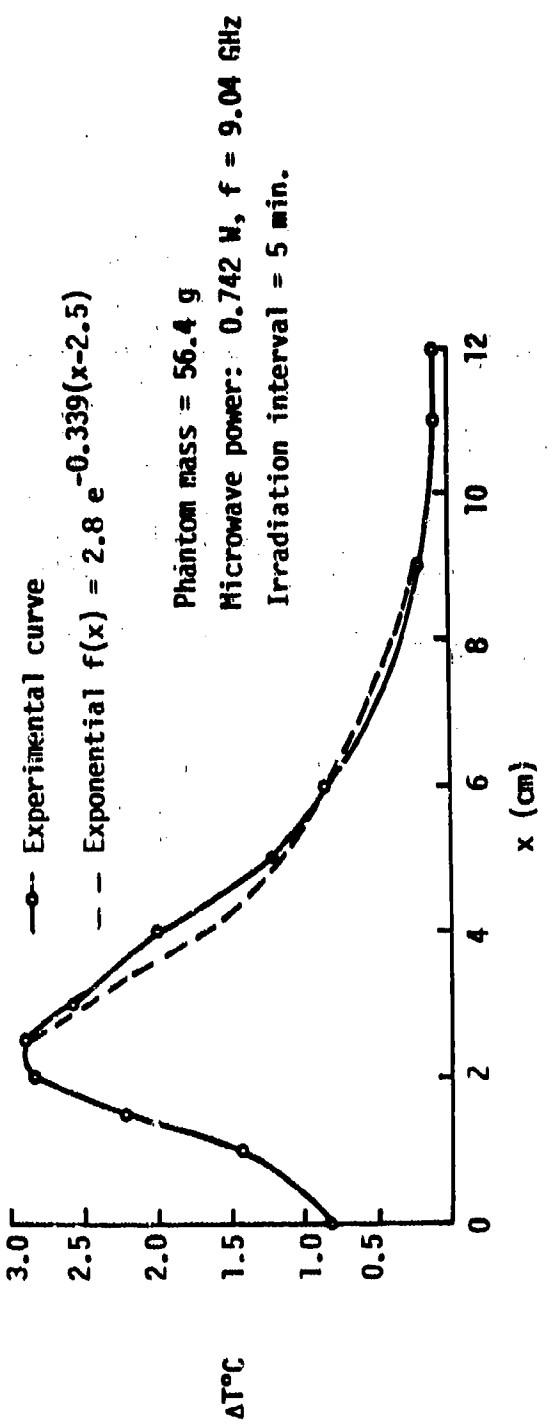
Fig. 6. Variation of heating along the sample holder.

The graph shows:
- Experimental curve
- Exponential $f(x) = 2.8 \, e^{-0.339(x-2.5)}$

Phantom mass = 56.4 g
Microwave power: 0.742 W, f = 9.04 GHz
Irradiation interval = 5 min.

Y-axis: $\Delta T^\circ C$
X-axis: x (cm)
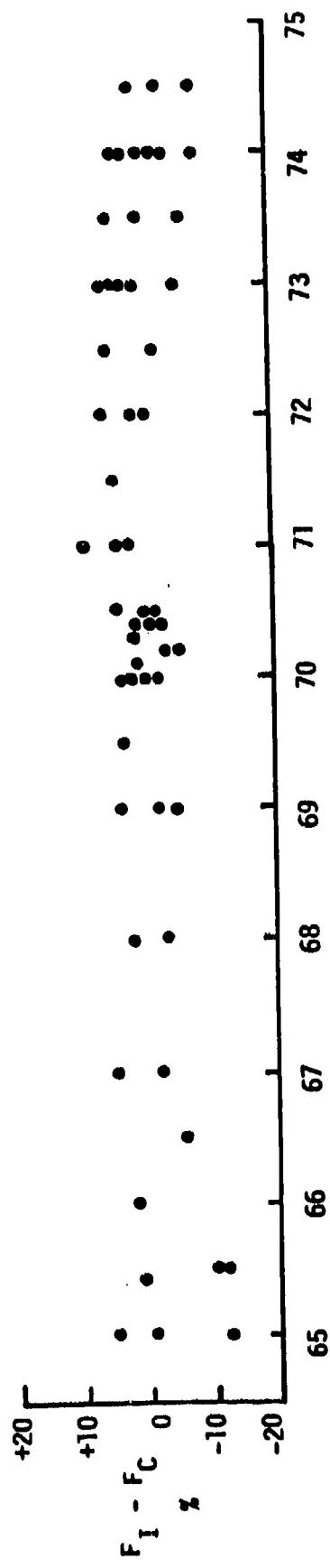
(a) Irradiation frequency (E-band) GHz.
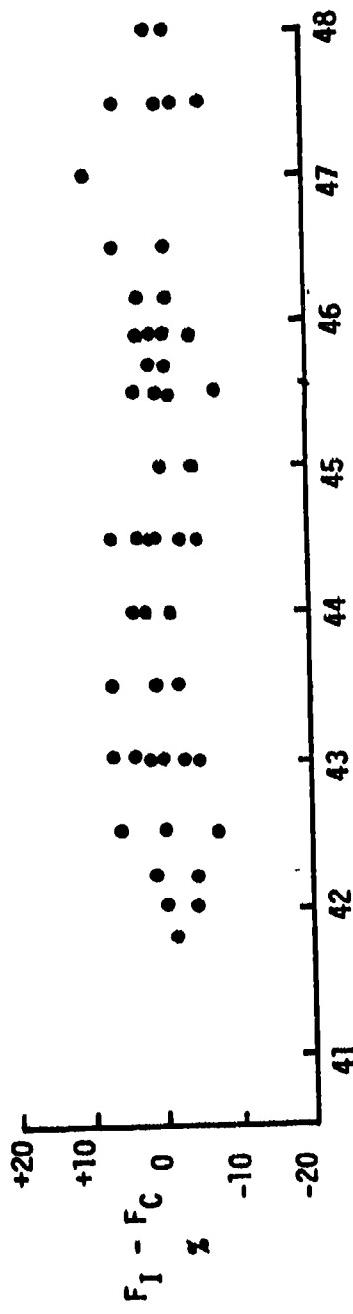
(b) Irradiation frequency (U-band) GHz.

Fig. 7.  Effects of microwave irradiation on induction of Lambda phage.
Difference in the frequency of induction between irradiated
and controls as a percentage of the control samples.
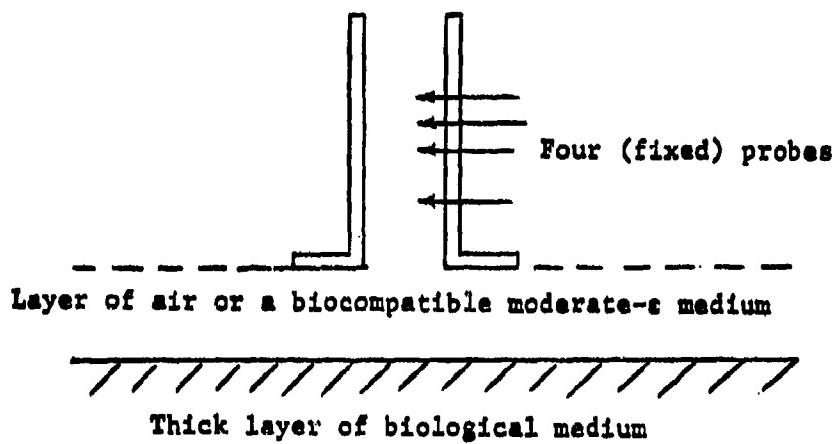
Fig. 8. An arrangement for permittivity measurements at millimeter wavelengths.

## Acknowledgments

## V. References

Bailey MC, Swift CT (1968): Input admittance of a circular waveguide aperture covered by a dielectric slab. IEEE Trans Antennas Propagation AP-16:386-391.

Berteaud AJ, Dardalhon M, Rebeyrotte N, Averbeck D (1975): Action d'un rayonnement électromagnétique à longueur d'onde millimétrique sur la croissance bacterienne. C R Acad Sci (D) 281:843-846.

Bush LG, Hill DW, Riazi A, Stensaas LJ, Partlow LM, Gandhi OP (1981): Effects of millimeter wave radiation on monolayer cell cultures III. A search for frequency-specific athermal biological effects on protein synthesis. Bioelectromagnetics 2:151-159.

Caldecott R (1973): The generalized multiprobe reflectometer and its application to automated transmission line measurements. IEEE Trans Antennas and Propagation AP-21:550-554.

Cheung AY, Koopman DW (1976): Experimental development of simulated biomaterials for dosimetry studies of hazardous microwave irradiation. IEEE Trans Microwave Theory Tech MTT-24:669-673.

Croswell WF, Taylor WC, Swift CT, Cockrell CR (1968): The input admittance of a rectangular waveguide fed aperture under an inhomogeneous plasma: Theory and experiment. IEEE Trans Antennas Propagation AP-16:475-487.

Dardanoni L, Torregrossa V, Tamburello C, Zanforlin L, Spalla M (1976): Biological effects of millimeter waves at spectral singularities. In: "Electromagnetic Compatibility." Third Wroclaw Symposium on Electromagnetic Compatibility. Wroclaw, Poland: Wydawnictwo Politechniki, Wroclawskiej, pp. 308-313.

Dardanoni L, Torregrossa MV, Tamburello C, Zanforlin L (1979): Sensitivity of C.albicans cells to frequency of modulation in the 72-74-GHz band. USNC/URSI Meeting, Seattle, Washington.

Devyatkov ND, et al. (1974): Highlights of the papers presented on millimeter wave biological effects. Soviet Physics--USPEKHI 4:568-579.

Fröhlich H (1978): Coherent electric vibrations in biological systems and the cancer problem. IEEE Trans Microwave Theory Tech MTT-26:613-617.

Gandhi OP, Hagmann MJ, Hill DW, Partlow LM, Bush L (1980): Millimeter wave absorption spectra of biological samples. Bioelectromagnetics 1:285-298.

Grundler W, Keilmann F, Fröhlich H (1977): Resonant growth rate response and yeast cells irradiated by weak microwaves. Phys Lett 62A:463-466.

Grundler W, Keilmann F (1978): Nonthermal effects of millimeter microwaves on yeast growth. Z Naturforsch 33C(1/2):15-22.

Hagmann MJ, Gandhi OP (1981): Substitution method for swept-frequency measurements of dielectric properties at microwave frequencies. IEEE Trans Microwave Theory Tech MTT-29:

Hershberger WD (1978): Microwave transmission through normal and tumor cells. IEEE Trans Microwave Theory Tech MTT-26:618-619.

Jacobson AG, Shen YR (1979): Coherent Brillouin spectroscopy. Appl Phys Lett 34:464-467.

Lee RA, Webb SJ (1977): Possible detection of in vivo viruses by fine-structure millimeter microwave spectroscopy between 68 and 76 GHz. IRCS Med Sci 5:222.

Partlow LM, Bush LG, Stensaas LJ, Hill DW, Riazi A, Gandhi OP (1981): Effects of millimeter wave radiation on monolayer cell cultures I. Design and validation of a novel exposure system. Bioelectromagnetics 2:123-140.

Stamm ME, Warren SL, Rand RW, Wolfson WL, Harris PA, Iwasaki RS, Block JB, Schoenberger JW, Dokken R, Garrett JV, Stoekel TA, Hendricks W, Rutlege CW (1975): Microwave therapy experiments with B-16 murine melanoma. IRCS Med Sci 3:392-393.

Stamm ME, Winters WD, Morton DL, Warren SL (1974): Microwave characteristics of human tumor cells. Oncology 29:294-301.

Stensaas LJ, Partlow LM, Bush LG, Iversen PL, Hill DW, Hagmann MJ, Gandhi OP (1981): Effects of millimeter wave radiation on monolayer cell cultures II. Scanning and transmission electron microscopy. Bioelectromagnetics 2:141-150.

Szwarnowski S, Sheppard RJ (1977): Precision waveguide cells for the measurement of permittivity of lossy liquids at 70 GHz. J Phys 10E:1163-1167.

Van Loon R, Finsy R (1975): The precise microwave measurements of liquids using a multipoint technique and curve-fitting procedure. J Phys 8D:1232-1243.

Wang CH, Lin Y-H, Jones DR (1979): Brillouin scattering and segmental motion of a polymeric liquid, II. Molecular Phys 37:287-298.

Webb SJ, Booth AD (1969): Absorption of microwaves by microorganisms. Nature 222:1199-1200.

Webb SJ, Booth AD (1971): Microwave absorption by normal and tumor cells. Science 174:72-74.

VI. Publications and Presentations Resulting
from Air-Force-Funded Efforts

Riazi A, Hill DW, Hagmann JM, D'Andrea JA, Gandhi OP: A broadband temperature-controlled system for the study of cellular bioeffects of microwaves. Submitted for publication to IEEE Trans Microwave Theory Tech.

Hill DW, Riazi A, Gandhi OP, Hagmann MJ: Effect of U- and E-band milli-meter irradiation on induction of Lambda phage. Paper presented at the Bioelectromagnetics Society Meeting, Washington, D.C., August 10-12, 1981.

Riazi A, Hill DW, Hagmann MJ, D'Andrea JA, Gandhi OP: A broadband temperature-controlled waveguide irradiation system for study of nonthermal bioeffects of microwaves. Paper presented at the Bioelectromagnetics Society Meeting, Washington, D.C., August 10-12, 1981.

# RADIOFREQUENCY RADIATION EFFECTS ON DISPOSTION OF $^{45}Ca^{2+}$ IN THE RAT BRAIN IN VITRO AND IN VIVO

James H. Merritt*, Wesley W. Shelton**,
and Albert F. Chamness*
Radiation Sciences Division
USAF School of Aerospace Medicine
Brooks AFB, Texas 78235

I.    INTRODUCTION: Over the past three years, we have been studying the effect of pulse-modulated radiofrequency radiation (RFR) on the disposition of pre-loaded $^{45}Ca^{2+}$ in the rat brain. The work of Bawin, Adey, and co-workers and Blackman and co-workers on RFR effects on neuronal calcium has been fully reviewed in this symposium (vide supra). These previous investigations had made use of either extremely low frequency (ELF) signals or radiofrequency radiation signals amplitude-modulated at frequencies around 16 Hz.  Since few emitters utilize such amplitude-modulated signals, we have studied effects of RFR pulse-modulated at ELF on $^{45}Ca^{2+}$ movement in mammalian brain. Pulse-modulation is a characteristic of radar signals, and the majority of occupational exposures in the Air Force are to this type of radiation.

II.  TECHNICAL APPROACH:

### Animals

Male Sprague-Dawley rats (150-225g) were used throughout.  The animals were maintained in a vivarium and provided commercial chow and water ad libitum.  On the morning of the experiment, they were transported to the exposure facility in plastic cages lined with fresh litter.

### Microwave exposures

In vitro exposures.  Six individual tissue samples were exposed at one time in a Plexiglas and Styrofoam shaking water bath at 37°C.  This water bath was placed 1 m beneath a standard gain horn.  Radiation was produced by a MCL Model 15022 microwave generator for the 1-GHz exposures and a Cober Model 1831 generator for the 2.45-GHz exposures.  Incident power densities at the sample positions were measured with a Narda Microwave Corp. Broad Band Isotropic RF Monitor (Model 8316B) and Probe (Model 8323).

In vivo exposures.  The rats were placed in Plexiglas and Styrofoam holders. The top, bottom, and end pieces are of Plexiglas, cemented together.  The sides are of Styrofoam and are removable.  The animal is gently squeezed between the two Styrofoam sides so that it is forced to remain with the long axis parallel to the long axis of the holder.  Animals were exposed singly in a climate-controlled anechoic chamber.  The exposure position was 4.5 m in front of the horn antenna.  Radiation was produced by the L-band unit of a Cober Peak Pulse Simulator Transmitter System·(Model 2852) operating at 2.06 GHz.  Pulse width

*USAF School of Aerospace Medicine, Brooks Air Force Base, Texas
**Florida Institute of Technology, Melbourne, Florida

was held constant at 10 ms for all exposures. The specific absorption rate (SAR) was obtained in rat phantoms made of muscle equivalent substance by the calorimetric technique of Allen and Hurt (1). The SAR at this frequency measured by the technique was 0.245 W/kg per mW/cm$^2$.

III. RESULTS: No significant differences were found when tissue loaded in vitro (Table 1), in vivo (Table 2), or loaded and exposed in vivo (Table 3) were exposed to pulse-modulated RFR. Varying the power density failed to define a "power window," and no differences were detected when the carrier frequency was changed. The power densities employed, viz. 0.5, 1, 2, and 15 mW/cm$^2$ were used to define a "power window" for $^{45}Ca^{2+}$ perturbation (4).

TABLE 1.  BRAIN TISSUE, IN VITRO LOADED, EXPOSED
TO PULSE-MODULATED, 1 GHz RFR

| Exp. # | No. of Animals | Average Pwr Density (mW/cm$^2$) | P.W.[a] (msec) | PRF[b] (Hz) | Calcium Efflux Ratio Experimental | Control |
|--------|------|------|------|------|------|------|
| I | 23 | 0.5 | 20 | 16 | 37.3 ± 4.8 | 39.7 ± 5.1 |
| II | 24 | 1.0 | 20 | 16 | 34.4 ± 6.0 | 32.3 ± 6.8 |
| III | 24 | 2.0 | 20 | 16 | 36.7 ± 4.6 | 36.6 ± 4.1 |
| IV | 24 | 15.0 | 20 | 16 | 40.3 ± 5.0 | 39.1 ± 4.6 |
| V | 24 | 1.0 | 20 | 16 | 39.0 ± 4.7 | 39.5 ± 4.0 |
| VI | 24 | 1.0 | 10 | 32 | 39.4 ± 6.8 | 38.5 ± 4.0 |
| VII | 24 | 2.0 | 10 | 32 | 45.2 ± 7.0 | 48.5 ± 8.6 |

[a]P.W. is pulse width.  [b]PRF is pulse repetition frequency.

## TABLE 2. BRAIN TISSUE IN VIVO LOADED, PULSE-MODULATED RFR EXPOSED IN VITRO

| Radiation Conditions | | | $^{45}Ca^{2+}$ Efflux Ratio* $\pm$ S.D. (N) | | P |
|---|---|---|---|---|---|
| Carrier Freq | Mod Freq | Average P.D. | Irradiated | Sham | |
| 1 GHz | 16 Hz | 1 mW/cm$^2$ | 5.70 $\pm$ 1.57 (46) | 6.15 $\pm$ 1.25 (53) | 0.10 |
| 1 GHz | 16 Hz | 10 mW/cm$^2$ | 4.98 $\pm$ 1.44 (22) | 5.04 $\pm$ 1.06 (22) | 0.90 |
| 2.45 GHz | 16 Hz | 1 mW/cm$^2$ | 6.42 $\pm$ 1.63 (22) | 5.70 $\pm$ 1.33 (22) | 0.10 |

## TABLE 3. IN VIVO LOADED, IN VIVO EXPOSED

| Power Density (mW/cm$^2$) | Modulations | | | |
|---|---|---|---|---|
| | CW | 8 Hz | 16 Hz | 32 Hz |
| 0.5 | .737 $\pm$ .169[a] | .817 $\pm$ .132 | .678 $\pm$ .222 | .712 $\pm$ .168 |
| 1.0 | .647 $\pm$ .129 | .762 $\pm$ .174 | .723 $\pm$ .194 | .715 $\pm$ .149 |
| 5.0 | .755 $\pm$ .181 | .737 $\pm$ .141 | .684 $\pm$ .159 | .757 $\pm$ .132 |
| 10.0 | .683 $\pm$ .170 | .700 $\pm$ .149 | .693 $\pm$ .142 | .701 $\pm$ .076 |
| Sham | - - - - - - - - .659 $\pm$ .156 - - - - - - - - - - - - - - - | | | |

Note: N for each combination of power density and modulation was 12, total N = 204.

When these data were subjected to a one-way analysis of variance, there were no significant differences among the 17 combinations. (df = 16, 187; F = 0.8636)

IV. **SUMMARY AND CONCLUSIONS:** In summary, our data does not indicate an effect of pulse-modulated microwave radiation on net efflux of $^{45}Ca^{2+}$ in the rat brain exposed both in vivo and in vitro. The radiation parameters used should have revealed efflux effects that might occur in "windows" for both modulation frequency and incident power density.

Other studies that have shown RFR-induced alterations in calcium efflux have used amplitude-modulated signals (5). The difference between amplitude-modulated and pulse-modulated signals and how they might be recovered by tissue components has been recently discussed (6). Essentially, pulse modulation implies rather abrupt on and off signals in which the percent of time the energy is on is equal to the duty factor (duty factor = number of pulses per second X pulse width in seconds). In amplitude modulation, the signal magnitude spectrum consists of a carrier component with a side band component on each side separated at a distance equal to the modulation frequency.

We conclude that pulse-modulated RFR fields do not affect net calcium efflux in cerebral tissue under the conditions tested, in contrast to the effects induced by amplitude-modulated energy.

V. **REFERENCES:**

1. Allen, S.J., and W. Hurt. Calorimetric measurements of microwave energy absorption by mice after simultaneous exposure of 18 animals. Radio Science 14(6S):1-4, 1979.

2. Cooke, W.J., and J.D. Robinson. Factors influencing calcium movement in rat brain slices. American Journal of Physiology 221:218-225, 1971.

3. Noble, E.P., et al. A simple and rapid method for injecting $H^3$ norepinephrine into the lateral ventricle of the rat. Life Sciences 6:281-291, 1967.

4. Blackman, C.F., et al. Induction of calcium-ion efflux from brain tissue by radiofrequency radiation: Effects of modulation frequency and field strength. Radio Science 14:6S: 93-98, 1979.

5. Adey, W.R. Frequency and power windowing in tissue interactions with weak electromagnetic fields. Proc IEEE 68:119-125, 1980.

6. Shelton, W.W., and J.H. Merritt. In vitro study of microwave effects on calcium efflux in rat brain tissue. Bioelectromagnetics, in press.

# RFR AND MOLECULAR MECHANISMS

Richard A. Albanese, M.D., Earl L. Bell, M.S.,
David K. Cohoon, Ph.D.

United States Air Force School of Aerospace Medicine
Biomathematics Modeling Branch
Brooks AFB, Texas

## I. INTRODUCTION

Epidemiologically significant numbers of Air Force and civilian people are currently being exposed to radiofrequency radiation at intensities which are above background levels. While these exposures do not appear to lead to dramatic overt disease processes, Chinese and Eastern Bloc epidemiological studies point to a variety of medical effects. In order to evaluate reports of biomedical effects and in order to design proper laboratory and epidemiological studies, knowledge of how RFR interacts with tissue structures and systems is imperative. Study of these basic interactions has been and remains our goal, and, to this date, we have emphasized: (a) special dosimetric models, (b) coupled RFR-field and heat-conduction models, (c) reaction-diffusion system models, (d) pulsed-RFR phenomena, and (e) fundamental molecular interactions.

## II. TECHNICAL APPROACH

We have used mathematical models and computer approaches in our attempts to delineate how RFR interacts with tissue structures. However, while our approach has been analytical, it has in every instance been tied to experimental results in several ways. Specifically, all equations used as inputs in our mathematical models and computer calculations have been tested by experiment. Also, all of our numerical results (outputs) have been obtained in order to evaluate or explain already available experimental data, or have been produced in anticipation of experiments to be performed.

Our work with special dosimetric models is motivated by the realization that RFR does not generally deposit energy in tissue in a manner which is constant in space and time. Rather, RFR deposits energy in a manner which varies temporally and spatially, and these variations may impact biological functioning as will be described. Interested in cranial structures, we have worked extensively with a multilayered spherical model of the human or animal head [1]. Maxwell's equations were solved in this spherical structure, assuming a planar incident wave and using series expansions of vector wave functions. To calculate internal fields in nonsymmetric structures, we have explored use of an integral equation approach with an integrand constructed using a tensor Green's function. This approach decomposes the scattering body into an array of three-dimensional cubes within which the field and material properties are considered constant. Because of this local constant field assumption,

calculational accuracy is limited to those cases where field wavelength is long relative to cube dimensions (2).

The basic driving force behind any radiofrequency radiation effect must ultimately be the electromagnetic field itself. In a real tissue, the work done by an electromagnetic field does not all appear as heat, rather chemical-process changes must also occur to some extent through direct field effects on chemical reaction rates (3). However, it is of interest to calculate Joule heating due to impressed fields, since temporally and spatially varying thermal fields can influence a distributed chemical reaction system in addition to any direct effects which may occur. Thus, working with the multilayered sphere model of the head, the electromagnetic field calculated by that model has been used as a Joule heating source term in the heat-conduction equation. Specifically, using eigenfunction expansions, we have solved the equation:

$$\frac{\partial u}{\partial t} = \frac{1}{\rho c} \, div \, (K \, grad \, u) - \frac{bu}{\rho c} + \frac{div \, (\bar{E} \times \bar{H})}{\rho c} \qquad (1)$$

In this equation u is the calculated thermal perturbation given in degrees centigrade. The coefficients $\rho$, c, K, and b are assumed constant in each concentric spherical shell of the model and are, respectively the density, specific heat, thermal conductivity, and blood-flow-cooling terms.

The structure of living cells and tissues is built through chemical reactions. In cells and tissues one finds temporal and spatial order directly linked to time and space patterns in chemical reactions. Viewing cells and tissue as distributed chemical systems, or reaction-diffusion systems, we have studied mathematical models of such systems to explore direct and thermal effects of RFR. Specifically, we have worked with a simple single compartment reaction-diffusion system whose equations are:

$$\dot{x} = h \, (X_e - X) - k(T)x$$

$$\dot{T} = l \, (T_e - T) + (\Delta H) k(T) x + d x + S \qquad (2)$$

In these equations, x is the concentration of reactant within the compartment, while $x_d$ is the concentration (assumed constant) outside. Similarly T is the temperature inside the compartment, while $T_e$ is the constant external temperature. The constants h and $l$ refer to reactant and thermal diffusion properties across the compartment boundary. The term k(T) is the reaction-rate term, and both simple Arrhenius and simple enzyme-kinetic-rate equations have been employed. The term S represents Joule heating by action on the solvent, $dx$ represents heating through specific RFR absorption by the reactant,

and $(\Delta H)k(T)x$ represents heat production or consumption by the chemical reaction itself.

The above described work on electromagnetic and thermal field structures and on reaction-diffusion systems uses only the steady-state solutions to Maxwell's equations of electromagnetism. All research in RFR known to us uses the steady-state picture even when short pulses of radiation are applied to the organisms. Suspecting that there could be relaxation or transient phenomena that would be of interest, we have challenged the steady-state view by reviewing Ref.(4) and calculating transient solutions to Maxwell's equations. This effort has produced intriguing results as will be reported below.

Finally, with a view to understanding the basic interaction of electromagnetic fields with molecules themselves, we have used the theory of stochastic differential equations (5) to study simple molecules imbedded in solvent. Specifically, we have studied the random and field-driven motion of a linear dipolar molecule in solution by using the equations:

$$m\ddot{x}_1 = -r\dot{x}_1 + l(x_2 - x_1) + \mathcal{J}(x) + q_1 E \sin 2\pi f t$$

$$m\ddot{x}_2 = -r\dot{x}_2 - l(x_2 - x_1) + \eta(t) + q_2 E \sin 2\pi f t \qquad (3)$$

In these equations, m is the mass of each of the two atoms in the dipolar molecule; $x_1$ and $x_2$ are the centers of the two atoms; and $q_1$, $q_2$ are the charges carried. The coefficient provides a linear bond characteristic, and $r$ is a viscous damping term. The symbols $\mathcal{J}(t)$ and $\eta(t)$ represent white noise processes which are random solvent forces on the molecule. The sinusoidal terms are of course field effect terms in the long-wavelength approximation.

## III. RESULTS/PROGRESS

The multilayered spherical model of the head is complete for the continuous-wave case (3). Addition of a spherical shell to represent the skull bones resulted in increased deposition of energy within the model brain substance at radiation wavelengths less than the head diameter indicating the role of internal reflections. Greatest energy deposition is in the model center which would approximately correspond to third ventricle and hypothalamic regions of an actual brain.

The electromagnetic fields calculated by the multilayered sphere model were used as the source term in the heat-conduction equation, equation 1 above. Because of thermal diffusion, the passage of time tends to spread the energy absorbed from the electromagnetic field; however, thermal gradients remain even after long time exposures. The blood flow term in equation 1 demonstrated that this has an important effect on thermal distributions. The thermal model without blood-flow term was tested in spherical models of heads and in cadaver heads, and correlation was observed between predicted and observed temperatures

(6,7). In the living monkey head, blood flow was observed both to apparently cool and warm the brain relative to cadaver temperatures (7). These effects could obtain from divergent and convergent flow patterns respectively. The prediction and measurement of thermal gradients in the head induced by RFR is of great interest, for thermal gradients are known to naturally exist in the brain, and the superposition of perturbations could have subtle effects on function particularly in the hypothalamus (8).

Our reaction-diffusion system is a first step toward understanding how energy or thermal deposition could affect a distributed chemical reaction system. Working with the simple set of equations given above (equation 2), we have found these systems capable of exhibiting low frequency modulation resonance effects as well as amplitude resonance effects (9). Thus, a biologically meaningful system has been found to exhibit responses very similar to those reported for cation efflux from irradiated tissue (10).

Our research has shown that it is not sufficient for one to be aware only of the continuous-wave response of material media. Important transients occur due to geometrically determined reflections and due to material dispersion properties. Of greatest interest perhaps is the finding of precursor waves (4,11). The so-called first precursor is associated with frequencies in the X-ray spectrum if the classical calculation is to be trusted (11)!

Lastly, a major goal of our work has been to understand in some detail how individual molecules are perturbed by RFR. Solving equation 3 without RFR, it is found that the bond energy (BE) of the molecule is equal to the kinetic energy of the center of mass (KECM) of the molecule, and that both of these are equal to KT/2 where K is Boltzmann's constant and T is absolute temperature. That is:

$$BE = KECM$$

for all temperatures T in the absence of RFR. Examining electrically neutral molecules (i.e. $q_1 + q_2 = 0$), it is found that:

$$BE > KECM$$

whenever the molecule is in the presence of RFR. Thus it has been found that RFR places a dipole into a state which is otherwise never encountered in the course of changing thermal environments. Since the molecule is assumed to be a linear structure, all excess bond energy is at the field frequency f. The ratio of the excess bond energy to the no-field bond energy at f is the ratio:

$$\frac{(|q_1| + |q_2|)^2 E^2}{8 \gamma KT}$$

Thus, excess energy at f increases as the square of the E field and can be quite large if the medium provides little damping (small). Lastly in the absence of an electromagnetic field, bond stretches, s, have a Gaussian statistical distribution:

$$\frac{1}{\sqrt{\pi KT}} exp\,(-s^2/KT)$$

In the presence of RFR the bond stretch distribution is changed to (12):

$$\frac{1}{\pi.\sqrt{\pi KT}} \int_0^{\pi} exp\left[-(s-P\cos\theta)^2/KT\right] d\theta$$

which is a non-Gaussian distribution with a tendency toward more extreme bond stretching and compression (i.e., a thicker tailed distribution). Therefore, once again we see that the dipole is placed into a physical state by RFR which is not duplicated by normal thermal conditions.


IV. SUMMARY AND CONCLUSIONS.

Basic conclusions from our work to date are as follows:

   A. Unnatural thermal and other energy gradients induced by RFR may have an effect on tissue function through an impact on metabolic activities subserved by reaction-diffusion biochemical systems.
   B. Transient phenomena, including high frequency generation, require further evaluation with regard to bioeffects of pulsed RFR.
   C. Irradiated molecules are not in a physical state duplicated by normal thermal conditions at any temperature.

   Follow-on efforts include more intense theoretical and experimental study of reaction-diffusion systems, a quantum mechanical evaluation of RFR transient phenomena, and statistical physical studies on complex molecules to include nonlinear effects.


V. REFERENCES.

   1. Bell, Earl L., David K. Cohoon, and John W. Penn. "Electromagnetic energy deposition in a concentric spherical model of the human or animal head." USAFSAM-TR-79-6.

   2. Penn, John W., and David K. Cohoon. "Analysis of a Fortran program for computing electric field distributions in heterogeneous penetrable nonmagnetic bodies of arbitrary shape through application of tensor Green's functions." USAFSAM-TR-78-40.

3. Chen, C., R.J. Heinsohn, and L.N. Mulay. "Effect of electrical and magnetic fields on chemical equilibrium." J. Phys. Soc. Japan, Vol 25, No. 2, pp. 319-322, 1968.

4. Sommerfeld, A. "Uber aie Fortpflanzung des Lichtes in dispergierenden Medien." Ann. Phys., Vol 44, No. 10, pp. 127-202, 1914.

5. Wang, M.C., and G.E. Uhlenbeck. "On the theory of Brownian motion, II," in "Selected papers on noise and stochastic processes." Edited by Nelson Wax. Dover Publications, New York, pp. 113-132, 1954.

6. Burr, John G., David K. Cohoon, Earl L. Bell, and John W. Penn. "Thermal response model of a simulated cranial structure exposed to radiofrequency radiation." IEEE Trans. on Biomed. Eng., Vol BME-27, No. 8, pp. 452-460, 1980.

7. Burr, John G., and Jerome H. Krupp. "Real-time measurement of RFR energy distribution in the Macaca mulatta head." Bioelectromagnetics, Vol 1, pp. 21-24, 1980.

8. Werner, J. "Control aspects of human temperature regulation." Automatica, Vol 17, No. 2, pp. 351-362, 1981.

9. Albanese, Richard A., and Earl L. Bell. "Radiofrequency radiation and chemical reaction systems." Bioelectromagnetics, Vol 1, p. 219, 1980.

10. Bawin, S.M., and W.R. Adey. "Sensitivity of calcium binding in cerebral tissue to weak environmental electric fields oscillating at low frequency." Proc. Nat'l. Acad. Sci. U.S.A., Vol 73, No. 6, pp. 1999-2003, 1976.

11. Jackson, J.D. "Classical electrodynamics." John Wiley & Sons, New York, pp. 269-333, 1975.

12. Rice, S.O. "Mathematical analysis of random noise." Edited by Nelson Wax. Dover Publications, New York, pp. 133-294, 1954.

VI. OPEN LITERATURE PAPERS, SAM TECHNICAL REPORTS, ABSTRACTS, AND ORAL PRESENTATIONS

## Papers in Open Literature

1. Krueger, Robert J. "Numerical aspects of a dissipative inverse problem." IEEE Transactions on Antennas and Propagation. (Jan 1981)

2. Krueger, Robert J. "A variant of the tautochrone problem: determining the profile of a nonmonotonic hill." Applied Mathematics and Computation. (Dec 1980)

3. Burr, John G., David K. Cohoon, Earl L. Bell, and John W. Penn. "Thermal response model of a simulated cranial structure exposed to radiofrequency radiation." IEEE Transactions on Biomedical Engineering, Vol. BME-27, No. 8. (Aug 1980)

4. Cohoon, David K. "Reduction of the cost of solving an integral equation arising in electromagnetic scattering through the use of group theory." IEEE Transactions on Antennas and Propagation, Vol. AP-28, No. 1. (Jan 1980)

5. Krueger, Robert J. "An inverse problem for an absorbing medium with multiple discontinuities." Quarterly Applied Mathematics, Vol. 36. (Oct 1978)

## SAM Technical Reports

1. Penn, John W., and Earl L. Bell. "Electrical parameter values of some human tissues in the radiofrequency range." SAM-TR-78-38.

2. Cohoon, David K., and John W. Penn. "Analysis of a Fortran program for computing electric field distributions in heterogeneous penetrable nonmagnetic bodies of arbitrary shape through application of tensor Green's functions. SAM-TR-78-40.

3. Bell, Earl L., David K. Cohoon, and John W. Penn. "Electromagnetic energy deposition in a concentric spherical model of the human or animal head." SAM-TR-79-6.

4. Bell, Earl L., David K. Cohoon, and John W. Penn. "MIE: a Fortran program for computing power deposition in spherical dielectrics through application of Mie theory." SAM-TR-77-11.

5. Albanese, Richard A., and Earl L. Bell. "Radiofrequency radiation and living tissue: theoretical studies." SAM-TR-79-41.

# Abstracts

1. Cohoon, David K., and John W. Penn. "Comparison of translational and spherical symmetry in dielectric structures by analysis of their responses to electromagnetic pulses." Notices of the American Mathematical Society. (1981)

2. Cohoon David K. "Mathematical properties of the Schrodinger operator with some applications." Notices of the American Mathematical Society. (Jan 1981)

3. Cohoon, David K. "Determination of the response of a penetrable body to a Gaussian pulse of electromagnetic radiation." Abstracts of papers presented to the American Mathematical Society, Vol. 1, No. 1. (Jan 1980), p. 154.

4. Cohoon, David K. "Scattering of an electromagnetic pulse by a penetrable body delimited by concentric cylinders." Notices of the American Mathematical Society, Vol. 26, No. 5. (Aug 1979), p. A-488.

5. Cohoon, David K. "Response of penetrable bodies to electromagnetic pulses." Notices of the American Mathematical Society, Vol. 26, No. 4. (Jun 1979), p. A-384.

6. Cohoon, David K. "A model of the thermal response of the head to electromagnetic radiation." Notices of the American Mathematical Society, Vol. 25, No. 5. (Aug 1978).

7. Cohoon, David K. "An analysis of a singular integral equation of electromagnetic radiation." Notices of the American Mathematical Society, Vol. 24, No. 6. (Oct 1977), pp. A-581-582.

8. Cohoon, David K. "A model of thermal response to radiation." Notices of the American Mathematical Society, Vol. 23, No. 5. (Aug 1976), p. A-553.

9. Cohoon, David K. "Numerical solution of boundary value problems." Notices of the American Mathematical Society, Vol. 23, No. 1. (Jan 1976), p. A-213.

## Oral Presentations

1. Cohoon, David K., and John W. Penn. "Comparison of translational spherical symmetry in dielectric structures by analysis of their responses to electromagnetic pulses." 85th Summer Meeting of the American Mathematical Society, Pittsburgh, Pennsylvania. (Aug 1981)

2. Cohoon, David K. "Mathematical properties of the Schrodinger operator with some applications." 87th Annual Meeting of the American Mathematical Society. (Jan 1981)

3. Albanese, Richard A., and Earl L. Bell. "Radiofrequency and chemical reactions." 2nd Annual Meeting of the Bioelectromagnetics Society, San Antonio, Texas. (14-18 Sep 1980)

4. Cohoon, David K. "The response of penetrable bodies to EM pulses." 84th Summer Meeting. Joint Mathematics Meeting sponsored by the American Mathematical Society, Ann Arbor, Michigan. (18-22 Aug 1980)

5. Cohoon, David K. "Thermal response of penetrable bodies to microwave radiation." St. Lawrence University, Canton, New York. (Jul 1980)

6. Cohoon, David K. "Electromagnetic pulse interactions." Texas Seminar on Differential Equations, The University of Texas at Austin. (9 Mar 1980)

7. Cohoon, David K. "The response of penetrable bodies to pulses of microwave." 86th Annual Meeting of the American Mathematical Society, San Antonio, Texas. (3-7 Jan 1980)

8. Cohoon, David K. "Scattering of an electromagnetic pulse by a penetrable body delimited by concentric cylinders." 83rd Summer Meeting of the American Mathematical Society, Duluth, Minn. (21-25 Aug 1979)

9. Albanese, Richard A. "Radiofrequency radiation and living tissue: theoretical studies." Workshop on the Mechanisms of Microwave Biological Effects, University of Maryland. (14-16 May 1979)

10. Albanese, Richard A., and Earl L. Bell. "Radiofrequency radiation and living tissue: theoretical studies." Review of Air Force Sponsored Basic Research in Environmental Protection, Toxicology, and Electromagnetic Radiation Effects, San Antonio, Texas. (15-17 Jan 1979)

403

# EFFECT OF RFR ON ENZYME SYSTEMS

Johnathan L. Kiel, Captain, BSC (VC), USAF
Radiation Sciences Division
USAF School of Aerospace Medicine
Brooks AFB, Texas 78235

I. __INTRODUCTION:__  In evaluating bioeffects resulting from radiofrequency radiation (RFR) exposure, it is important to distinguish between the direct biological effects of such radiation and secondary effects that result from the manipulation of laboratory animals or other biosystems used to detect such effects.  The immune system, for example, is especially sensitive to endogenous glucocorticosteroid release as a consequence of manipulative stress on an animal.  Therefore, primary effects on this system may be masked or counteracted by secondary or physiological effects.

To avoid the observation of such physiological responses manifested by the immune system, an isolated fundamental biochemical component of the system may be examined.  Mixtures of oxidases and peroxidases can duplicate the functions of such a component of immune cells.  Previous investigations have indicated that oxidative enzymes are important in the cytotoxic function of macrophages and natural killer cells (Johnston, 1978; Schleupner and Glasgow, 1978; Nathan et al, 1979; Tracey, 1979).  The direct cytotoxic effect of macrophages on tumor cells in vitro has been mimicked with glucose oxidase immobilized on starch particles (Nathan et al, 1979), indicating that hydrogen peroxide production is a significant macrophage function and that this function can be duplicated by an artificial system.

Lymphocyte function is also intimately involved with oxidative and peroxidative activity.  Peripheral lymphocytes, which are predominantly T cells, contain a cytotoxic peroxidase (Paul, 1979).  Stimulation of thymocytes with a T-cell mitogen, Concanavalin A, has been observed to generate chemiluminescence resulting from peroxide-generating and peroxide-utilizing oxidative metabolism (Wrogemann et al, 1978).  Furthermore, immunization of mice with either soluble or particulate antigen causes an increase in peroxidative activity in the spleen which precedes the generation of specific antibody (Strauss et al, 1977).

The importance of nonphosphorylating oxidative metabolism even extends to the cooperativity of cellular components of the immune system.  If either isolated macrophages or T lymphocytes are first treated with periodate or neuraminidase and galactose oxidase, and recombined with the other cell type, the T cells undergo a strong proliferative response (Greineder and Rosenthal, 1975).  All these observations suggest a central role of oxidative-peroxidative metabolism in the cellular compartment of the immune system which extends beyond activities of granulocytes (McRipley and Sbarra, 1967; Bujak and Root, 1974; Klebanoff et al, 1977; DeChatelet et al, 1978).

The limited number of previous studies in the nonthermal effects of RFR on oxidative enzyme systems have yielded mixed results. For instance, the exposure of suspensions of the membrane-bound enzyme cytochrome oxidase to sinusoidally

modulated 2450-MHz microwave radiation at an SAR of 26 mW/g did not significantly affect its activity during exposure (Allis and Fromme, 1979). The cytochrome oxidase was coupled to a soluble indicator protein system so that spectrophotometric changes could be followed. In contrast, Eley, Mayer, and Pethig (1973) have provided evidence for electron transfer enzymes of mitochondria functioning as organic semiconductors, which can be influenced by a microwave frequency of 9 GHz (Eley and Pethig, 1970; Eley, Mayer, and Pethig, 1972). Studies of horseradish peroxidase in solution have shown that at 25°C an SAR greater than 125 W/cm³ for 20 minutes or above 60 W/cm³ for periods greater than 20 minutes, at a frequency of 2450 MHz, is required to produce irreversible damage to the enzyme (Henderson et al, 1975). Szmigielski (1975) examined the effect of RFR on the superoxide-generating system of rabbit granulocytes in vitro. At 3 GHz with an incident power density of 2 or 5 mW/cm² (the SAR was not given), a significant increase in nitro blue tetrazolium reduction (evidence of NAD(P)H oxidase activity) over controls was observed with exposure times of 30 minutes, but a significant decrease in activity was observed after 60 minutes of exposure. Therefore, oxidative and peroxidative enzymes may vary in their responses to RFR, depending upon their microenvironments and the frequency of RFR.

The complex assemblage of polar molecules of oxidative enzymes in mitochondria or in membranes of leukocytes suggests that a highly structured model system would more closely resemble the in vivo state than aqueous solutions or suspensions of membrane-bound enzymes. This concept is further supported by the requirement for microtubular assembly to yield an active NAD(P)H oxidase in leukocytes (Nakagawara and Minakami, 1979). The immobilized proteins of such compact highly organized structures should have restricted molecular rotation, preventing the dramatic changes in permittivity seen in aqueous protein solutions which result in absorption of energy and heating at low to intermediate frequencies (Schwan, 1977). However, the presence of some bound water and ions should generate small dispersions of permittivity (Grant et al, 1978).

To mimic these biological systems, I designed a model system with which I attempted to meet the following criteria:

(1) The assaying components would not perturb the electromagnetic field.

(2) Enzyme activity would be assayed in the RFR field to reveal reversible changes in activity.

(3) The system would not thermalize readily because of changes in permittivity and friction from molecular rotation.

(4) The system would demonstrate hysteresis, or resistance to change, because of diffusion limitations. This property would allow the system short-term memory of nonuniform activity experienced in the presence of RFR.

(5) The system would be an electron transport chain that would absorb energy based on its geometric properties and macroscopic orientation. The fixed molecules in the system would be aligned in the field based on the orientation of the whole system.

Peroxidases, or hemeproteins in general, contained within crosslinked protein gels are best suited for such a model system. Peroxidase not only

mediates the flow of electrons from electron-donating substrate to electron-accepting substrate, but the protein molecules can also interact with each other to equalize their oxidation states. Therefore, when electron-donating and electron-accepting substrates are added to the gels, a flow of "free" electrons through the redox enzymes should occur. The direction of flow should be influenced by the electric field induced in the gel by exposure to RFR. Therefore, the gel should absorb the most energy during the reduction-oxidation reaction when alternate changes in the protein dipole moments occur.

## II. TECHNICAL APPROACH:

a. **Preparation of crosslinked protein gel.** The enzyme to be crosslinked was prepared by dissolving 10 mg horseradish peroxidase, Type II (170 purpurogallin units/mg) and 600 mg of bovine serum albumin in 8 ml of solution containing 5600, 1400, or 0 units of glucose oxidase (from Aspergillus niger). The solution also contained 0.1 M pH 6.9 phosphate buffer with 0.15 M NaCl. Polymerization was initiated and allowed to proceed at room temperature by adding 110 microliters of 25% glutaraldehyde to the protein solution. The gels used for chemiluminescent assays contained 10 mg luminol (5-amino-2, 3-dihydrophthalazine-1, 4-dione) and no glucose oxidase. The gels were prepared in the form of 4.0-cm X 4.0-cm X 0.5-cm blocks contained within Styrofoam molds, each with a thin transparent polyethylene window in the bottom of the chamber. This inner frame was placed in an outer box of Styrofoam that contained a rubber injection port in its top. The outer dimensions of the box were 6 cm X 6 cm X 4 cm. The boxes used in the chemiluminescent assays were painted black with acrylic paint.

b. **Measurement of Oxidase-Peroxidase Activity.** Initially two techniques were attempted to measure oxidative and peroxidative activity during exposure. The first technique attempted was a colorimetric technique using either p-phenylenediamine hydrochloride (15 mg/ml) in 5.5 mM D-glucose solution, containing 0.1 M pH 7.4 sodium phosphate buffer and 0.15 M NaCl or 0.2 mg/ml 3,4-dihydroxyphenylalanine (L-DOPA) in 0.1 M D-glucose with 0.1 M pH 6.9 sodium phosphate buffer and 0.15 M NaCl. Two milliliters of substrate were injected into each box and onto the surface of each gel. The reaction proceeded for 30 minutes. Then the substrate was poured off and replaced with 0.01 M $NaN_3$ to stop the p-phenylenediamine reaction or 0.1 M $NaN_3$ to stop the L-DOPA reaction. The L-DOPA polymerizes to insoluble melanin and the p-phenylenediamine forms an insoluble chromophore. Activity was measured by removing the gels from the frame and scanning them through the plastic window at the bottom of the gel. A Quick Quant Scanning densitometer (Helena Laboratories) was used at a gain setting of 1 to scan the gels in two perpendicular dimensions. The densities were expressed on an arbitrary scale of 0 to 9.

The chemiluminescent gels were covered with filter paper to disperse substrate evenly over the surfaces. One milliliter of 3% $H_2O_2$ in pH 6.9 0.1 M sodium phosphate buffer with 0.15 M NaCl was used to activate each gel. A 5-cm by 5-cm piece of Tri-X panchromatic film (Kodak) was placed emulsion side up beneath the transparent window within each box. After 30 minutes of exposure, the reaction was stopped with an injection of 1 M $NaN_3$ into the box, and the film was removed for processing. Control strips of film from Kodak were processed with each group of negatives to assure uniformity in processing. The densities of the films were determined by examining them with a photographic densitometer. An 8 by 8 matrix of densities composed of 0.25-cm$^2$ areas was constructed for each film.

406

c. <u>Irradiation and Dosimetry</u>. Gels were exposed in pairs, one box on either side of the center conducting plate in a Narda Model 8801 TEM transmission cell. The cell was placed up on end with the transmitter side on top. The boxes were placed near the center of each side of the plate by mounting each one on a block of Styrofoam. The power was supplied by an MCL transmitter.

Controls consisted of placing activated gels in the same position in the chamber as test gels but without power. Experimental gels were exposed at an incident power level of 10 mW/cm$^2$ at 400 MHz (CW). The surface of each gel was parallel to the E vector of the RFR field. For the purpose of determining SAR, temperature changes in the gel were monitored by Vitek hyperthermia probes previously molded into the gels. Exposures and controls were done at a chamber temperature of 24 $\pm$ 0.6$^{\circ}$C, with the gel temperature varying only by $\pm$ 0.2$^{\circ}$C.

III. <u>RESULTS/PROGRESS</u>: Table 1 is the map of SAR distribution in a 4-cm square gel at 10 mW/cm$^2$. Notice that the center strip of gel has a higher SAR than the side strips. With such a distribution of energy, one would expect a corresponding distribution of activities in the gel if there were an effect of RFR. The mean density of the p-phenylenediamine gels was 5.07 $\pm$ 1.28 ($\pm$ 25% of the mean) for 6 gels with power and 4.65 $\pm$ 1.44 ($\pm$ 31% of the mean) without power for 6 gels. With such variations, there was no apparent significant difference in the means. However, the gels showed topographical differences in activity which were attributed to the tilting of the gels in the Narda chamber. Furthermore, the gels continued to darken after removal from the chamber. The oxidation of substrate was not stopped by NaN$_3$. The L-DOPA gels showed less variation in the mean density and no significant effect of the RFR. The mean density with power for 6 gels $\pm$ the standard deviation was 4.6 $\pm$ 0.46 ($\pm$ 10%), and without power for 6 gels was 4.75 $\pm$ 0.61 ($\pm$13%). These gels were carefully leveled to prevent the effect observed with the p-phenylenediamine gels. The higher concentration of NaN$_3$ also failed to completely stop the auto-oxidation of L-DOPA.

Another problem with colorimetric gels was that substrate, and subsequently the product, was only found in the upper 1 mm of the gel within 30 minutes. A diffusion test with methylene blue showed that it required 2 hours at room temperature to diffuse through a 0.5-cm gel.

The chemiluminescent assay proved more successful as evidenced by uniform bubble production throughout the depth of the gel within 30 minutes. The bubbles are of nitrogen gas from the oxidized luminol. Table 2 shows the mean densities $\pm$ the standard deviation of photographs (chemilumigrams) of chemiluminescent gels (see Figure 1). To date, only 6 chemilumigrams have been produced (gel nos. 1-5 and 11). Even though, as demonstrated in Table 2, there appears to be no significant difference between the mean densities of gels exposed to RFR and shams, there is a tendency for exposed gels to demonstrate a departure from the normal distribution of densities about the mean. This distribution suggests a nonrandom localized compensatory rise and fall of activities within the gel. The change in distribution, as illustrated by Figure 2, a and b, does not correspond well with the SAR distribution. This observation leaves open the question of whether the change in distribution of activity is a genuine effect or an artifact.

IV. <u>SUMMARY AND CONCLUSIONS</u>: Enzyme systems in gel or solid state are probably better models of the <u>in vivo</u> condition than enzyme systems free in solution because of the order and control required in the metabolic pathways of cells.

This statement should be especially applicable to particulate or membrane-associated enzymes of leukocytes and mitochondria.

The wide distribution of peroxidase in mammalian tissues (Neufeld et al, 1958) implies that they are significant in the normal physiological functions of man and animals. Therefore, anything that affects the activities of mammalian peroxidases may adversely affect the health of the organisms that contain them.

Although the localized effect of RFR that is observed appears temporary, the change in activity, if maintained long enough, may affect subsequent slower and irreversible processes to which peroxidative activity is linked. Horseradish peroxidase is an adequate prototype for the chemiluminescent technique, since peroxidases all appear to have the same mechanism of action (Odajima and Yamazaki, 1970).

The observed effect may have resulted from compensatory changes in activity if substrate ($H_2O_2$) is drawn from less active areas to more active areas. The local drop in concentration would cause a further decrease in activity. Also, randomness of crosslinked protein chains may have tended to obscure demarcation between active areas and inactive areas because of less than optimal alignment with the E-field vector. Alignment could perhaps be optimized by polymerization in the RFR field. Finally, there may be an effect on the pathway of degradation of the activated phthalic acid product of luminol, shifting some of the molecules from a nonluminescent to a luminescent pathway or vice versa.

To determine the validity of the observed effect, many more chemilumigrams must be produced and mapped. The corresponding map points of gels must be averaged to eliminate random variations in control or exposed gels. The resulting map of mean densities of controls can then be compared point by point to the map of mean densities of exposed gels. Furthermore, pulsed waves of various frequencies and peak powers should be examined to determine if the nonthermal effect, if any, can be maximized.

The general technique of luminescent solid-state enzymology may be applied in the future to other enzymes and even cells. The NADH-dependent bacterial luciferase system could be used to examine a large number of dehydrogenases through coupled reactions (Stanley, 1978) in RFR fields. The photoprotein aequorin from the jelly fish <u>Aequorea</u> could be used as an indicator of facilitated diffusion or transport of calcium into gel by $Ca^{++}$-$Na^+$ ATPase (Blinks et al, 1978). Therefore, the ATPase activity could be readily measured by bioluminescence during RFR exposure. The effect of RFR on the electron transport system could be monitored in bioluminescent bacteria entrapped in crosslinked protein gel. Finally, the nonphosphorylating oxidative metabolism of activated leukocytes could be measured by the luminescence of cells (Trush et al, 1978) immobilized in or on protein gel.

V. <u>REFERENCES</u>:

a. Allis, J.W., and M.L. Fromme (1979): Activity of membrane-bound enzymes exposed to sinusoidally modulated 2450 MHz microwave radiation. Radio Sci. <u>14</u>, 85-91.

b. Blinks, J.R., P.H. Mattingly, B.R. Jewell, M. Van Leeuwen, G.C. Harrer, and D.G. Allen (1978): Section IV. Aequorin: Practical aspects of the use of aequorin as a calcium indicator: Assay, preparation, microinjection, and interpretation of signals. In Methods of Enzymology, LVll (M.A. DeLuca, ed.), Academic Press, New York, pp. 292-328.

c. Bujak, J.S., and R.K. Root (1974): The role of peroxidase in the bactericidal activity of human blood eosinophils. Blood 43, 727-736.

d. DeChatelet, L.R., R.A. Migler, P.S. Shirley, D.A. Bass, and C.E. McCall (1978): Enzymes of oxidative metabolism in the human eosinophil. Proc. Soc. Exp. Biol. Med. 158, 537-541.

e. Eley, D.D., and R. Pethig (1970): Microwave Hall mobility measurements for bovine plasma albumin. J. Bioenerg. 1, 109-112.

f. Eley, D.D., R.J. Mayer, and R. Pethig (1972): Microwave charge carrier Hall mobility measurements on cytochrome-oxidase prepared from heavy beef heart mitochondria. J. Bioenerg. 13, 271-275.

g. Eley, D.D., R.J. Mayer, and R. Pethig (1973): Microwave Hall mobility measurements on heavy beef heart mitochondria. J. Bioenerg. 4, 187-200.

h. Grant, E.H., R.J. Sheppard, and G.P. South (1978): Dielectric Behavior of Biological Molecules in Solution, Clarendon Press, Oxford, pp. 189-225.

i. Greineder, D.K., and A.S. Rosenthal (1975): The requirement for macrophage-lymphocyte interaction in T lymphocyte proliferation induced by generation of aldehydes on cell membranes. J. Immun. 115, 932-938.

j. Henderson, H.M., K. Hergenroeder, and S.S. Stuchly (1975): Effect of 2450 MHz microwave radiation on horseradish peroxidase. J. Microwave Power 10, 27-35.

k. Johnston, R.B., Jr. (1978): Oxygen metabolism and the microbicidal activity of macrophages. Fed. Proc. 37, 2759-2764.

l. Klebanoff, S.J., D.T. Durack, H. Rosen, and R.A. Clark (1977): Functional studies on human peritoneal eosinophils. Infect. Immun. 17, 167-173.

m. McRipley, R.J., and A.J. Sbarra (1967): Role of the phagocyte in host-parasite interactions. XI. Relationship between stimulated oxidative metabolism and hydrogen peroxide formation, and intracellular killing. J. Bact. 94, 1417-1424.

n. Nakagawara, A., and S. Minakami (1979): Role of cytoskeletal elements in cytochalasin E-induced superoxide production by human polymorphonuclear leukocytes. Biochim. Biophys. Acta 584, 143-148.

o. Nathan, C.F., S.C. Silverstein, L.H. Brukner, and Z.A. Cohn (1979): Extracellular cytolysis by activated macrophages and granulocytes. II. Hydrogen peroxide as a mediator of cytotoxicity. J. Exp. Med. 149, 100-113.

p. Neufeld, H.A., A.N. Levay, F.V. Lucas, A.P. Martin, and E. Stotz (1958): Peroxidase and cytochrome oxidase in rat tissues. J. Biol. Chem. 233, 209-211.

q. Odajima, T., and I. Yamazaki (1970): Myeloperoxidase of the leukocyte of normal blood. I. Reaction of myeloperoxidase with hydrogen peroxide. Biochim. Biophys. Acta 206, 71-77.

r. Paul, B.B. (1979): Human peripheral lymphocytes: Biochemical and antibacterial activities and comparison with polymorphonuclear leukocytes. J. Reticuloendothelial Soc. 25, 49-60.

s. Schleupner, C.J., and L.A. Glasgow (1978): Peritoneal macrophage activation indicated by enhanced chemiluminescence. Infect. Immun. 21, 886-895.

t. Schwan, H.P. (1977): Classical theory of microwave interactions with biological systems. In The Physical Basis of Electromagnetic Interactions with Biological Systems, proceedings of a workshop held at the University of Maryland, 15-17 June 1981. (L.S. Taylor and A.Y. Cheung, eds.) Office of Naval Research and Development Command and Bureau of Radiological Health, FDA, Washington, D.C., pp. 91-112.

u. Stanley, P.E. (1978): Section II. Bacterial luciferase: Quantitation of malate, oxaloacetate, and malate dehydrogenase. In Methods of Enzymology, LV11 (M.A. DeLuca, ed.), Academic Press, New York, pp. 181-188.

v. Strauss, R.R., H. Friedman, L. Mills, and G. Zayon (1977): Relationship between antigenic stimulation and increased splenic peroxidase levels during the immune response. Infect. Immun. 15, 197-203.

w. Szmigielski, S. (1975): Effect of 10 cm (3 GHz) electromagnetic radiation (microwaves) on granulocytes in vitro. Ann. N.Y. Acad. Sci. 247 (Biol. Eff. Nonionizing Rad. Conf.), 1974, 275-281.

x. Tracey, D.E. (1979): The requirement for macrophages in the augmentation of natural killer cell activity. J. Immunol. 123, 840-845.

y. Trush, M.A., M.E. Wilson, and K. Van Dyke (1978): Section VIII. Chemiluminescent Techniques: The generation of chemiluminescence (CL) by phagocytic cells. In Methods of Enzymology, LV11. (M.A. Deluca, ed.) Academic Press, New York, pp. 462-494.

z. Wrogemann, K., M.J. Weideman, T.A. Peskar, H. Staudinger, E.T. Riefshel, and H. Fisher (1978): Chemiluminescence and immune cell activation. Eur. J. Immunol. 8, 749-752.

VI. PUBLICATIONS AND PRESENTATIONS RESULTING FROM AF-FUNDED EFFORTS: "Measurement of Oxidative Enzymic Activity in Radiofrequency Fields" to be presented at the Third Annual Meeting of The Biolectromagnetics Society, Washington, D.C., 10-12 August 1981.

Table 1.  SAR MAP OF CROSSLINKED PROTEIN GEL $(W/kg/mW/cm^2)$

|  | Left | Center | Right |
|---|---|---|---|
|  | .071 | .12 | .071 |
| Center Conducting ← Plate | .075 | .12 | .075 |
|  | .079 | .13 | .079 |

4 cm

Avg = .091 $W/kg/mW/cm^2$ ± .024 for 10 $mW/cm^2$ exposure

SAR = 0.91 W/kg

411

Table 2. DENSITIES OF CHEMILUMIGRAMS EXPOSED AT 400 MHz ($10 \text{ mW/cm}^2$)

| GEL NO. | POWER | MEAN DENSITY ± S.D.* | MAP POINTS |
|---------|-------|----------------------|------------|
| 1 | + | 22.07 ± 7.36 (± 33.3%) | 56 |
| 2 | + | 23.50 ± 9.36 (± 39.8%) | 63 |
| 3 | - | 29.24 ± 6.40 (± 21.9%) | 62 |
| 4 | - | 29.26 ± 6.09 (± 20.8%) | 64 |
| 5 | + | 33.81 ± 10.80 (± 32.0%) | 58 |
| 11 | - | 38.80 ± 5.44 (± 14.0%) | 64 |

*This value is the mean density of the map points of each gel ± the standard deviation.

(a)

(b)

Figure 1.  Positive prints of chemilumigrams of peroxidase–bovine serum albumin gels:  (a) gel sham-exposed for 30 minutes;  (b) gel exposed to RFR at 10 mW/cm$^2$ and 400 MHz (CW).
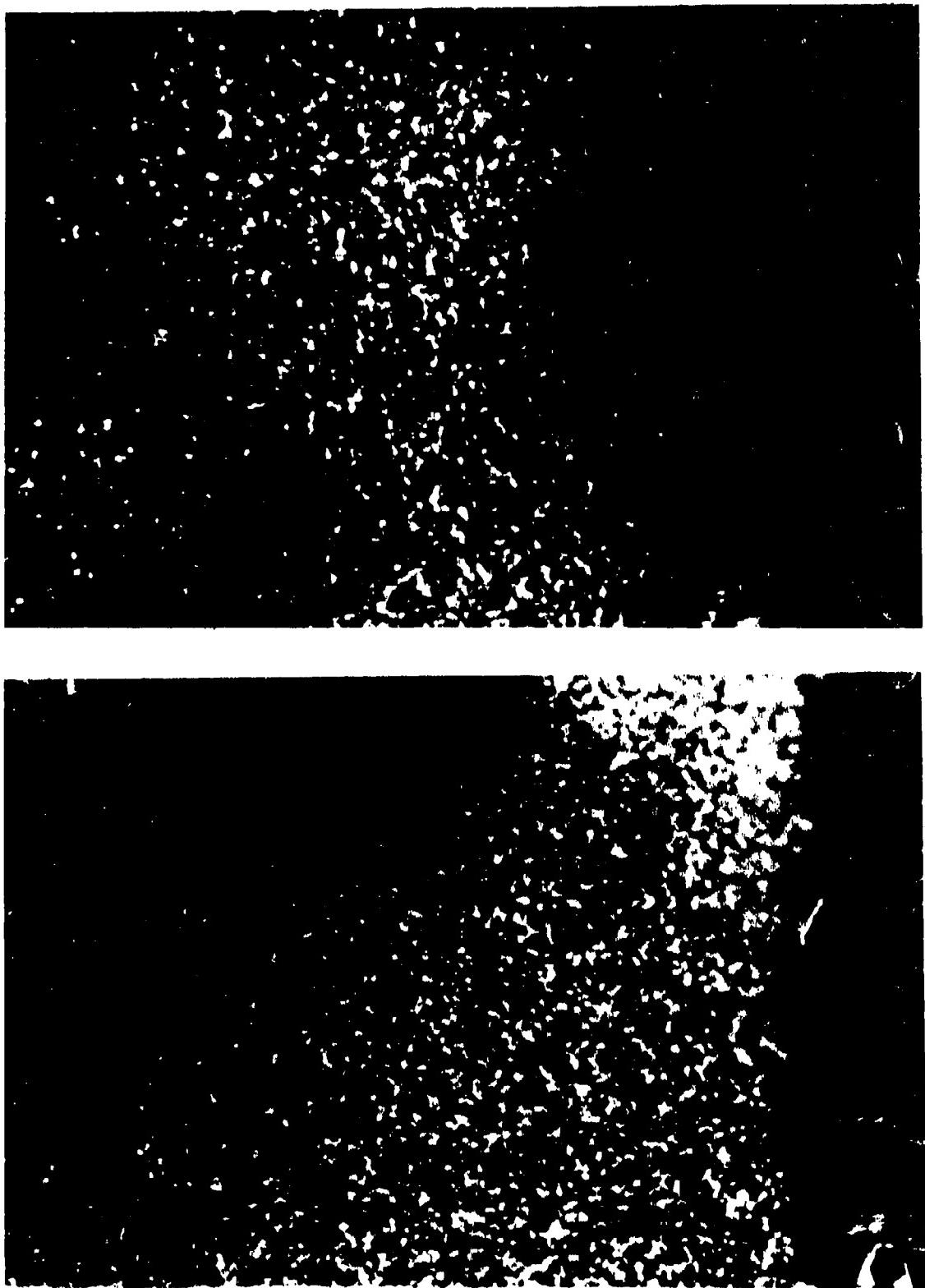
## (a) FILM #3 (NO POWER) 11-6-81

| | | | | | | | |
|----|----|----|----|----|----|----|----|
| 20 | 33 | 30 | 30 | 32 | 32 | 28 | 20 |
| 32 | 37 | 34 | 32 | 34 | 34 | 34 | 30 |
| 23 | 38 | 38 | 37 | 32 | 33 | 32 | 22 |
| 38 | 40 | 40 | 36 | 35 | 26 | 30 | 24 |
| 28 | 38 | 34 | 36 | 34 | 28 | 20 | 14 |
| 24 | 24 | 33 | 30 | 31 | 28 | 18 | 18 |
| 14 | 22 | 30 | 33 | 31 | 26 | 24 | 18 |
| X  | X  | 24 | 30 | 24 | 32 | 25 | 26 |

## (b) FILM #2 (POWER) 11-6-81

| | | | | | | | |
|----|----|----|----|----|----|----|----|
| 16 | 12 | 14 | 26 | 18 | 20 | 10 | 12 |
| 14 | 10 | 10 | 16 | 14 | 15 | 27 | 19 |
| 28 | 16 | 8  | 13 | 24 | 20 | 22 | 18 |
| 16 | 14 | 20 | 26 | 30 | 35 | 30 | 26 |
| 16 | 12 | 18 | 25 | 30 | 30 | 42 | 28 |
| 20 | 22 | 24 | 36 | 32 | 32 | 44 | 24 |
| 14 | 25 | 30 | 36 | 40 | 38 | 45 | 38 |
| 18 | X  | 35 | 28 | 34 | 28 | 22 | 16 |

Figure 2.  Density maps of chemilumigrams of peroxidase-bovine serum albumin gels.  (a), sham gel; (b), experimental gel exposed to 10 mW/cm$^2$ at 400 MHz (CW).  X, obscured areas that were not read.

# RADIOFREQUENCY RADIATION DATA BASE

David N. Erwin, Ph.D.
Radiation Sciences Division
USAF School of Aerospace Medicine
Brooks AFB, Texas 78235

I.  **INTRODUCTION**: The last decade has seen a burgeoning volume of literature in the area of radiofrequency radiation (RFR) bioeffects. More than 6,000 reports have been published, with the majority appearing after 1974. This period has also encompassed a major change in the quality of research done and the detail with which experimental methods are reported. For example, many researchers now report measured values or at least estimates of the specific absorption rate (SAR) as a basis for comparing their results to others.

This tremendous growth in the available data base has made traditional methods of literature review and compilation unwieldly. In addition, there are both older works and modern reports that do not adequately address experimental details, statistical treatment of data, or other factors, which make these reports difficult to interpret. RFR research is a complex, interdisciplinary field and requires a knowledge of both the engineering and biological aspects of experimental design. Thus, a reader new to the field or naive in one or more of the discipines involved may be misled or confused by vague or apparently contradictory reports.

Finally, the traditional literature retrieval sources are necessarily limited in the scope of disciplines covered. For example, those dealing with medical publications will not retrieve literature published in the electronics trade journals.

The effort reported here is an attempt to compile an interpreted and critiqued data base in a form suitable for both publication and computerized retrieval. The emphasis is on critical review of the selected literature, rather than a simple compilation.

II.  **TECHNICAL APPROACH**: Compilations and critiques of the RFR literature are performed under AF Contract F33615-80-C-0608 to SRI International, Menlo Park, Calif. The Air Force monitor is Mr. James Merritt, and SRI personnel include Dr. Lou Heynick, the late Dr. John Krebs, and Dr. Peter Polson (now at NASA's Ames Research Center).

The contractor's tasks include selection of the literature to be reviewed, analysis of the experimental design and results, and an assessment of implications of the findings. The author's abstract is included if available; otherwise, a reviewer's summary is provided. The contractor places each paper in a category, such as epidemiology, modelling, or neurophysiology, and may further break these areas into subcategories. A list of key words and parameters is extracted to be used in the computerized retrieval system.

All analyses are delivered in computer-readable format such that the analyses may be maintained in computer storage as well as published in bound form. In the latter case, the contractor also includes a summary analysis, or "state-of-the-art," in each large category.

The USAF School of Aerospace Medicine has built a network of mainframe and minicomputers to provide a flexible, distributed data automation capability. Although still changing, this system already provides a choice between machines ranging from small word processors to an IBM mainframe; and software options from simple editors to complex database management systems are provided.

Figure 1 illustrates the organization of the network and the types of hardware/software functions available. This system provides the opportunity to combine acquired data, terminal input, computation, and plots or graphs into a report. The RFR literature data base will reside on the VAX 11/780, thus providing its input to such a report-writing scheme.

III. **PROGRESS:** The literature collection, review, and critique by SRI International has passed its one-year milestone. Approximately 150 reports have been reviewed, representing 20 categories of RFR bioeffects research. These reviews have been delivered to USAFSAM/RZP in optically readable (OCR-B) format. The contractor is also preparing a summary report on each of the major categories. The latter will be included in the published reports of this work, but will not reside in the computer data base.

Ms. Beverly Johnson (OAO Corporation) and I have designed and written the computer routines to make this data base functional on the VAX 11/780. The software is in FORTRAN IV running under the VAX/VMS (Digital Equipment Corporation) operating system.

In addition to the internal search, compilation, and reporting routines, the software includes an English-language user interface. The latter is designed to ease the use of the data base by naive computer users. The only prior knowledge required is the ability to log onto the computer and run a program. At that point the user's terminal displays a menu of options to conduct searches by authors, keywords (subject(s), study type, etc.), or other parameters (power density, SAR, year, etc.). The program then assembles sets of citations that match the search parameters. Each set is assigned a number, and the number of citations found is reported. As in other retrieval systems, combinations of keywords can be logically "and"ed or "or"ed to either expand or contract the number of matches.

The reporting options then enable a flexible printout ranging from a single citation (authors, title, and reference) to a full printout of a set of literature. The latter would include the citations, followed by an abstract, the reviewer's comments, and the list of search parameters and keywords.

New entries are easily appended by using standard editors and file manipulation schemes. These processes are not available through the retrieval program, thus preventing accidental compromise of the data base.

The project is now in a stage of limited user access to allow debugging and improvements to the user interface routines. I expect the system to be online by September 1981.
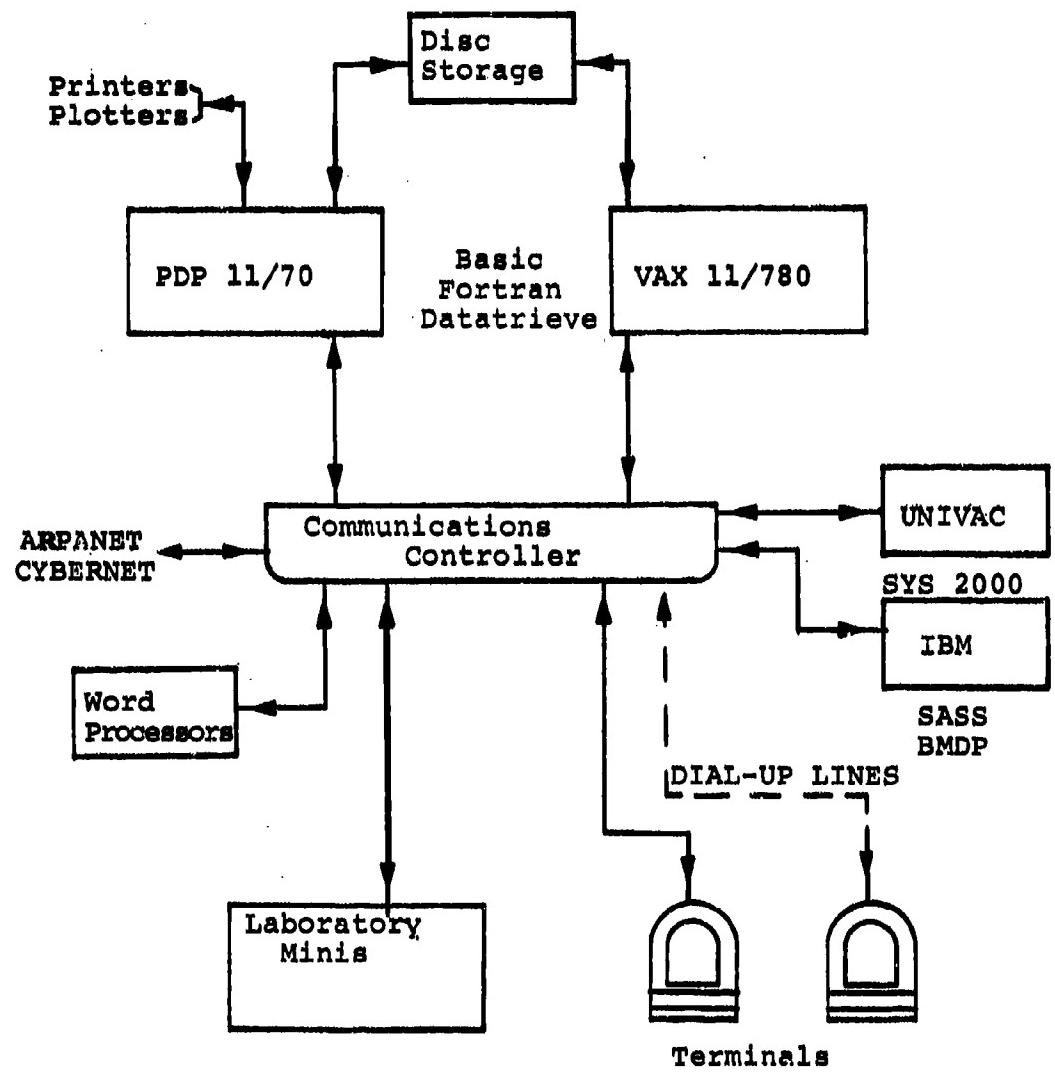
Figure 1.   The USAFSAM Computer Network showing the major
            resources available to all users.

417

IV.    SUMMARY AND CONCLUSIONS:  We have established a minimal RFR literature data base in both written report and computer retrievable format.  No other existing data base provides this breadth of coverage as well as critical review of the literature, to my knowledge.

We expect this system to be an immediate aid in diverse requirements under our Air Force mission:  response to outside inquiries, EIS preparation, safety standard recommendations, preparation of research reports, and the identification and design of new research goals.  Additionally, we expect this system to assist new investigators in their orientation to this complex, multidisciplinary research area.  Future goals include user orientation and expansion/update of the literature covered in the data base.

V.    REFERENCES:  The literature reviews and critiques will be published as SAM Technical Reports, available through the National Technical Information Service or by request to Mr. James Merritt, USAFSAM/RZP, Brooks AFB, TX 78235.

The computer routines will be documented in standard format and filed in the Data Sciences Division, USAFSAM.

VI.    PUBLICATIONS AND PRESENTATIONS RESULTING FROM AF-FUNDED EFFORTS:
SAM-TR(s) - Pending.

# MEASUREMENT OF RFR IN THE
# AIR FORCE WORK PLACE

William D. Hurt
Stewart J. Allen

Radiation Physics Branch
Radiation Sciences Division
USAF School of Aerospace Medicine

I.    INTRODUCTION:  The U.S. Air Force recognizes the requirement to quantify radiofrequency radiation (RFR) exposures in the military work places.  A new program was initiated in 1978 to measure the RFR levels over a broad range of average power densities, including measurements of the peak field intensities. A vehicle was modified and equipped with special instrumentation, and pilot studies were conducted on different types of RFR emitters at several locations throughout the United States.  This paper presents a summary of test results from the RFR survey of (1) a fixed site having three standard radars, (2) a phased-array surveillance radar, and (3) preliminary measurements of the RFR emission on an aircraft flight line from some of the systems on a B-52 aircraft.  The measurements were made by personnel from the Air Force Communications Command, 1839 EIG, Keesler AFB, Miss.

II. TECHNICAL APPROACH:  It was determined that the RFR measurement system should be able to measure the real-time average power densities and peak electric-field intensities over a broad dynamic range—covering frequencies from 0.1 to 10 GHz, average power densities from $nW/cm^2$ to 10 $mW/cm^2$, and peak electric-field intensities up to several thousand volts per meter.  The planned application required that the measurement system be mobile and have sufficient on-board electrical power for the RFR measuring equipment.  The vehicle was equipped with a shielded (screened) enclosure to eliminate direct electromagnetic interference (EMI) with the test instrumentation.  Many standard commercial equipment items, such as chart recorders and desk-top computers, can be seriously disrupted by intense electromagnetic pulses that penetrate the electronic packages.  Adequate EMI shielding is especially important when measurements are to be made in proximity to pulsed radars.

A typical configuration of test equipment is shown in Figure 1.  This example was assembled to measure a 450-MHz phased-array surveillance system. At each test location for the radar, the dipole test antenna was placed on a tripod and elevated approximately 2 m above the ground.  The antenna and tripod were moved horizontally, while orientation was adjusted, until the signal being received was maximized on the field intensity meter (tuned to the radar operating frequency).  Usually this occurs within a horizontal distance of about two wavelengths.  This procedure establishes a worst-case condition due to reflected signals being added to the primary incident signal.

The test antenna was oriented in three orthogonal planes, and a measurement of the radiated signal was made for each antenna orientation.  Peak (rms) and average power density levels less than 0.001 $uW/cm^2$ (1 $nW/cm^2$) were not recorded.

The electric (E) field measurements needed to derive the peak power densities were made with a field intensity meter. The average power density was measured with a power meter and power sensor. The data were processed by a desk-top computer and printed by a thermal line printer. All data were stored on magnetic tape. The analog-to-digital converter provided the interface between the power meter and computer, and sampled the power meter output 100 times per second.

The average power density was obtained by summing the three individual measurements obtained with the test antenna in the three orthogonal orientations. Samples were taken for a 12-second period in each of the three orthogonal planes, at each test location. The resultant electric field is the square root of the sum of the squares of the three orthogonal measurements. Measuring with the dipole antenna in three orthogonal planes is essentially the same as measuring with an isotropic antenna.

The total system was verified before and after the field measurements. This ensured the current operation and accuracy of all test equipment and accessories. Both the field intensity meter and the power meter had internal reference calibrators.

Specific equipment items were changed from survey to survey to accommodate the characteristics of each radar surveyed. For example, horn antennae were used for some system surveys; and in such cases, both vertical and horizontal measurements were made. However, the basic approach was the same: the receiving antennae and instrumentation were selected to measure the peak (rms) electric-field intensity and the real-time averaged power density from each RFR emitter.

III. RESULTS: Fixed Site With Three Emitters. Radiation measurements were made at 44 locations, at distances of about 75 m to about 20 km to quantify potential RFR exposure levels from a typical fixed radar site having three emitters. The three emitters (radar systems) were an L-band search radar, an S-band height-finder radar, and a C-band height-finder radar.

The L-band radar operated at ~1300 MHz with a normal peak power of ~5 MW. It was pulsed at ~240 pulses per second with a 6-microsecond pulse width. The system was located on a 15-m tower, and the directed beam scanned 360° in azimuth at five revolutions per minute.

The S-band radar operated at a frequency of ~2700 MHz with a normal peak power of ~3 MW. It was pulsed at ~330 pulses per second with a pulse width of 2 microseconds. This height-finder radar could be directed to any azimuth on command and scanned a -2° to +32° elevation sector in a 3-second time period using a nodding motion. For these radiation surveys, the radar beam was directed to the exact azimuth of each test location and held there with its normal elevation scan mode in operation. The vertical beam width was less than 1° and the horizontal beam width was ~3°.

The C-band radar operated at a frequency of ~5600 MHz with a normal peak power of ~2 MW. It was pulsed at ~330 pulses per second with a pulse

420

width of ~4 microseconds. This height-finder radar could also be directed to any azimuth on command and scanned a -2° to +32° elevation sector in 3 seconds, using a nodding motion. The vertical beam width was less than 1°, and the horizontal beam width was ~2°.

Measurements on all three radars were made at each of the 44 test locations. Actual measurement periods for each antenna position ranged from 6 to12 seconds, using a sampling rate of about 50-100 per second. More than 65,000 data points were recorded during the RFR survey at this site.

Measurement results from 13 of the 44 locations were selected for presentation in this paper. These results are summarized in Table I. The data on both height finders represent a worst case by a factor of at least 100 since the measurements were made with the height finders specifically directed to each test location. In fact, the maximum time needed to obtain aircraft height data in any azimuth setting is only 30 seconds. Also, in normal operation, the total use of such height finders in a 24-hour period is less than 2 minutes per degree of azimuth. That is, the radar would not be expected to point at any particular azimuth setting for more than 2 minutes in any 24-hour period.

The last column in Table I is the numerical sum of the averaged power densities from each system, thus the worst-case exposure level possible. Note that the real-time peak to average power density ratios range from ~5000:1 to >100,000:1.

Phased Array Surveillance Radar. The phased-array surveillance radar is a relatively large, fixed-base, solid-state, electronically steered radar system. Its primary purpose is to detect, track, and provide early warning of ballistic missiles launched from vehicles at sea. It maintains a long-range wide-area coverage. Also, it tracks objects orbiting the earth. It has multiple-frequency capability over a range of 420 to 450 MHz. Peak power is 580 kW, the maximum duty cycle is 25 percent, and it covers a scan sector of 240°. To carry out its tasks, the pencil beam (~2.2° beam width) formed by the antenna is scanned continuously, forming a solid surveillance net at a minimum elevation angle of 3° and covering the complete 240° (in azimuth) scan sector. The great versatility of the electronically steered beam allows the radar to point or change beam directions at a very rapid rate (within tens of microseconds) to maintain total coverage of the scanned volume.

During this series of radiation measurements, the radar was operated at one frequency (435 MHz) and all of the system power was directed to the surveillance fence at an elevation angle of 3°. This created the maximum exposure levels possible at ground level.

Radiofrequency radiation measurements were made at numerous locations around this radar at distances from 0.1 to 20 km. Representative data are presented in Table II. Unlike the more conventional radar previously discussed, this radar produces exposure levels with real-time peak to average power density ratios from about 30:1 to 200:1.

421

Aircraft Radar.  Flight-line areas where aircraft are parked for equipment calibration and routine maintenance require careful study to assess potential RFR exposures.  Aircraft such as the U.S. Air Force B-52 bomber have many systems that emit RFR.  These include bomb/navigation radar, fire-control radar, communications systems, and electronic counter-measure equipment (ECM).  These systems are periodically energized to check normal operations, perform system calibration and adjustment, and/or to correct minor problems.  Such operations can expose personnel to a wide range of RFR field levels for varying periods of time.  As a part of the integral program to assess potential RFR exposures in the U.S. Air Force workplaces, a series of systems have been surveyed.  Initial tests included three types of aircraft and more than ten types of RFR emitters.  Many of the emitters have multiple modes of operation.  For example, a relatively standard search radar may have numerous specialized tracking modes in addition to its normal function, and ECM equipment can operate at many different frequencies and pulse modulations.  Some of the aircraft systems have complex scanning patterns, adding yet another complication to determining potential or likely RFR exposures.  The actual RFR field levels from these systems are strongly dependent on the mode of operation of the system and the height above the ground that the measurement or exposure takes place.  Table III includes only a few representative RFR field levels recorded during a 2-week survey of aircraft systems.  The information selected for presentation represents some of the worst-case RFR exposures that personnel may encounter under typical flight-line operations.

IV.  SUMMARY AND CONCLUSIONS:  RFR exposures in the military workplace are common.  This paper summarizes the types and levels of exposure likely in the vicinity of fixed radars and on aircraft flight lines.

Fixed-base radar systems generally operate 24 hours per day, 7 days per week.  Thus, persons near such systems are continuously exposed to some level of RFR fields.  Generally the systems are located on high towers  and propagate narrow beams in a scanning motion that restricts personnel exposure to the main beam.  Because of the continuous and repetitive nature of these radar operations, the actual exposure levels, both average and peak, can be quantified quite accurately with the type of instrumentation systems described in this paper.  The data presented in Table I are typical of many standard military radars and the radars used for commercial air traffic control around the world.  Many persons live and work near such systems.

The RFR levels recorded in Table I for the L-band search radar are typical of the continuous exposures received by people within the distances given, since this type of system continues to scan 360° in azimuth. Note that the average power densities are less than 1 $\mu$W/cm$^2$, and the peak power density levels are only tens of mW/cm$^2$.

The height-finder radars frequently change azimuth in an unscheduled manner, so personnel exposures are relatively short (0.5 to 2 minutes).  But when such exposures occur, the average power densities as seen in Table I are tens of $\mu$W/cm$^2$, and the peak power densities are often in the hundreds of mW/cm$^2$.  Also, it is possible to be exposed by the search and height-finder radars simultaneously.  In comparison, the potential radiation exposures from the phased-array radar are considerably lower, especially the peak RFR levels.

RFR exposures around aircraft systems on the flight line are much more difficult to quantify. The number and types of systems, their operational complexity, and the fact that each may be energized at irregular and generally unknown intervals make it nearly impossible to quantify actual exposures. The data presented in Table III illustrate that relatively high RFR exposure levels are certainly possible. In general, safety procedures are adequate to prevent undue radiation exposure, but accidental exposures are much more common in flight-line operations than elsewhere.

A new state-of-the-art mobile shielded laboratory (MSL) is being developed under an AFCC contract as a second-generation system for use in quantifying the RFR exposure levels in the Air Force workplaces. The MSL should be ready to begin RFR measurements in the fall of 1981. RFR levels will be recorded for each of the major emitters on each type of aircraft so that isodose contours can be established to control and document personnel exposures. The same approach is being considered for maintenance shops and fixed-radar installations.

FIGURE 1

# RADIOFREQUENCY RADIATION MEASUREMENT SYSTEM



EMPIRE DEVICES
DIPOLE
DM-205-T3

NARDA MODEL
3000-10
SIGNAL
SPLITTER

E-FIELD
MEASUREMENT

AVERAGE POWER MEASUREMENT

EMPIRE DEVICES
MODEL AT-106-S1
STEP ATTENUATOR

TEKTRONIX
OSCILLOSCOPE
422

VIDEO

SINGER FIELD
INTENSITY
METER
NM-37/57

HP POWER
METER 436A

HP POWER
SENSOR 8484A

HP FOUR-CHANNEL
A/D CONVERTER
59313A

MAGNETIC
TAPE STORAGE

HP COMPUTER
9825A

HP X-Y
PLOTTER
9872A

HP 9866B
THERMAL
LINE PRINTER

424

## TABLE I

### RADIOFREQUENCY RADIATION MEASUREMENTS

| Distance (m) | L-BAND SEARCH RADAR | | | S-BAND HEIGHT FINDER | | | C-BAND HEIGHT FINDER | | | All 3 Systems |
|---|---|---|---|---|---|---|---|---|---|---|
| | Peak(rms) E-Field (V/m) | Peak Pow. Den. (mW/cm²) | Time Avg. Power Density (µW/cm²) | Peak(rms) E-Field (V/m) | Peak Pow. Den. (mW/cm²) | Time Avg. Power Density (µW/cm²) | Peak(rms) E-Field (V/m) | Peak Pow. Den. (mW/cm²) | Time Avg. Power Density (µW/cm²) | Total Avg. Power Density (µW/cm²) |
| 75 | 135 | 4.86 | 0.85 | 428 | 48.6 | 1.4 | 237 | 14.9 | 3.0 | 5.25 |
| 130 | 184 | 9.0 | 0.52 | 403 | 43.1 | 1.7 | 52 | 0.710 | 0.075 | 2.29 |
| 210 | 69 | 1.26 | 0.11 | 582 | 89.9 | 4.1 | 94 | 2.37 | 0.34 | 4.55 |
| 280 | 80 | 1.71 | 0.1 | 239 | 15.2 | 0.8 | 114 | 3.42 | 0.76 | 1.65 |
| 390 | 73 | 1.43 | 0.015 | 816 | 177. | 7.2 | 260 | 17.9 | 1.2 | 8.42 |
| 460 | 202 | 10.8 | 0.1 | 1180 | 369 | 17.2 | 248 | 16.4 | 1.9 | 19.2 |
| 500 | 181 | 8.73 | 0.12 | 1110 | 327 | 10.6 | 874 | 203 | 31.4 | 42.1 |
| 800 | 246 | 16.1 | 0.13 | 854 | 194 | 6.9 | 684 | 124 | 13.1 | 20.1 |
| 900 | 104 | 2.9 | 0.03 | 767 | 156 | 5.0 | 861 | 197 | 20 | 25.0 |
| 3000 | 16 | 0.07 | | 52 | 0.73 | 0.02 | 87 | 2 | 0.2 | 0.2 |
| 4000 | 33 | 0.29 | 0.002 | 106 | 3.0 | 0.07 | 147 | 5.8 | 0.3 | 0.4 |
| 11000 | 26 | 0.18 | 0.001 | 94 | 2.33 | 0.05 | 52 | 0.71 | 0.03 | 0.08 |
| 12000 | 51 | 0.7 | 0.005 | 8 | 0.02 | | 124 | 4.11 | 0.5 | 0.5 |

## TABLE II

### RADIOFREQUENCY RADIATION MEASUREMENTS
### PHASED-ARRAY SURVEILLANCE RADAR

| Distance (m) | Peak E-Field (V/m) | Peak Power Density ($\mu W/cm^2$) | Average Power Density ($\mu W/cm^2$) |
|---|---|---|---|
| 90 | 120 | 3820 | 126 |
| 300 | 17.9 | 85 | 1.55 |
| 1000 | 21.7 | 125 | 2.52 |
| 1800 | 20.0 | 106 | 0.96 |
| 2200 | 8.48 | 19 | 0.13 |
| 2600 | 2.11 | 1.2 | 0.04 |
| 3600 | 2.77 | 2.0 | 0.01 |
| 14500 | 0.55 | 0.08 | <0.001 |
| 15700 | 0.37 | 0.04 | <0.001 |
| 21000 | 0.13 | 0.005 | <0.001 |

## TABLE III

### POTENTIAL RFR EXPOSURE LEVELS FROM
### AIRCRAFT SYSTEMS DURING FLIGHT-LINE OPERATIONS

| System # | Distance (m) | Peak (rms) E-Field (V/m) | Peak Power Density ($mW/cm^2$) | Average Power Density ($\mu W/cm^2$) | Peak to Average Ratio |
|---|---|---|---|---|---|
| 1 | 3<br>14 | 6170<br>1620 | 10,100<br>700 | 730<br>93 | 14,000<br>7,500 |
| 2 | 6<br>18 | 4620<br>1380 | 5,660<br>505 | 13,350<br>1,080 | 420<br>470 |
| 3 | 5<br>15 | 6600<br>3890 | 11,600<br>4,010 | 850<br>180 | 14,000<br>22,000 |
| 4 | 1 | 390 | 40 | 13,900 | 3 |

# EFFECT OF RFR ON THE RODENT FETUS

Kenneth A. Hardy, M.S.
Radiation Sciences Division
USAF School of Aerospace Medicine
Brooks AFB, Texas 78235

I. __INTRODUCTION:__ The increasing roles and numbers of female personnel in the Air Force have made it incumbent that current Air Force occupational safety standards be reviewed further to assure the safety of this vital segment of the Air Force work force. Current safety standards for radiofrequency radiation (RFR) are based on the biologic consequences of exposure to such environments. A few reports have recently appeared in the literature describing effects on the rodent fetus exposed to RFR in utero. Reported effects include tail and extremity abnormalities (a), exencephaly (b), cranioschisis (c), and changes in brain chemistry (d). The Radiation Sciences Division of USAFSAM has launched an investigation into the teratogenic effects of RFR in an effort to gather further data in this area. This report describes the current effort to investigate the effect of low-level RFR at 2450 MHz on the development of the rat fetus in utero.

II. __TECHNICAL APPROACH:__

a. __Exposure System:__ The exposure system used is a circular waveguide system designed and procured from the University of Washington. The basic system has been described in the literature by Guy et al (e). It was designed for the chronic exposure of rodents at 2450 MHz. The USAFSAM system consists of 20 waveguides, 10 RF powered and 10 shams. The waveguides are 20 cm in diameter and 95 cm in length. The transmitter is an Applied Microwaves Model PG5KB pulse-signal source. The pulse width is variable from 0.3 to 50 µsec. The pulse repetition rate is variable from 10 to 25,000 pps. The operating parameters in this study are as follows:

Pulse width: 10 µsec
Pulse repetition rate: 830 pps

The exposure system includes a microprocessor control unit to produce modulated RF outputs, if required. The RF exposures in this study were done without modulation.

b. __Dosimetry:__ The power absorbed by the animal is determined by differential power measurements. The waveguide input power and the orthogonal reflected and transmitted-power components are measured. The power absorbed is the difference between the waveguide input and the sum of the reflected and transmitted powers. Since there is some power absorption in the waveguide itself, the power absorption must be measured both with the animal absent and the animal present. The difference between the two power absorption values is assumed to be the power absorbed by the animal.

Hewlett Packard Model 432B power meters were used in these measurements. Measurements were conducted on all the waveguides. System uniformity was about ± 10%. The empty waveguides were found to absorb about 20% of the input power. Addition of the animal cage, water bottle, and feeder increased this value to about 30%. Introduction of phantoms or animals increased the total power absorption roughly from 70% to 90% of the input power. Power absorption in the animal was found to be a function of weight (or size) and orientation in the cage.

Figure 1 shows the results of the differential power measurements obtained with rat cadavers as a function of weight. Each data point is the average of measurements made over 14 different orientations within the exposure cage. The ordinate is the fraction of the waveguide input power absorbed by the animal. The bars represent the standard deviations of the measurements. The average fraction of the waveguide input power absorbed by the animal appears to vary approximately linearly with weight over the weight range of interest.

Measurements were also made using RF muscle-equivalent-material phantoms molded into the shape of rats. The results are shown in Figure 2. The muscle-equivalent material was found to be somewhat less absorptive (~5% to 10%) than the rat cadavers, but the phantom data tends to corroborate the rat cadaver data in the conclusion of linearity of power absorption versus weight.

Once the average fraction of the waveguide input power absorbed by the animal is established, the specific absorption rate (SAR) can then be computed from the measured waveguide input power and weight of the animal.

To corroborate the SAR values predicted from the differential power measurement data, we undertook a series of calorimetric measurements with rat cadavers and RF muscle-equivalent-material phantoms, using a twin-well calorimeter system (f). The results are shown in Table I. This data effectively confirms the predictions of the differential power data.

In the initial experimental phase of this study an SAR of 0.4 W/kg was chosen to be the exposure level. Figure 3 illustrates the waveguide input power required versus weight to maintain the SAR value of 0.4 W/kg. The average weight of the group of 20 animals is the value used in the determination. The animals are weighed every third or fourth day, and the input power adjusted accordingly.

The power input to the waveguide that most closely represents the average of the overall system is continuously monitored and is used as the reference for the entire system when power adjustments are required. Since the RF power is split between two sections of 5 waveguides via a two-way power splitter, another waveguide input on the other side of the power splitter is also monitored to assure power delivery to both sections. In addition, the power output of the transmitter is continuously monitored by HP Model 432B power monitors. The transmitter power monitor is also connected to a strip-chart recorder for power output constancy and exposure timing purposes.

c. Biological Procedures: The rats used are Sprague-Dawley females obtained from Hilltop Labs. The animals are impregnated at the source and shipped to Brooks AFB the same day. Upon arrival (day 1) the animals are weighed and placed in Plexiglas exposure cages, which are then inserted into the

circular waveguides. The exposure is started immediately after insertion and is continuous, with the exception of about one hour of down time every third or fourth day for weighing, cage cleaning, and instrument checks. The waveguide input power is adjusted accordingly upon reweighing.

In the present series of experiments, the animals are not allowed to come to term. The females are removed from the waveguides and euthanized via halothane or similar gas anesthetic. The uterus is removed and the implantation sites counted. The uterus is placed in warm physiologic saline where the individual sites are opened and all fetuses examined for viability, gross external malformations, and weight. The fetuses are then placed into 3 groups. Fetuses in group 1 are fixed immediately in Bouins fluid for 48 hours, rinsed, and placed in 70% ethyl alcohol. After fixation the fetuses are measured; those with gross abnormalities are photographed and then sectioned at 6 $\mu$m, stained with hematoxylin and eosin and examined by light microscopy. Group 2 contains fetuses with overt skeletal anomalies. If none are present, a random sample of apparently normal fetuses is selected. These fetuses are cleaved and stained with alizarin red by the method of Dawson (g). In group 3 the brain of each fetus is removed for determination of DNA, RNA, protein, and norepinephrine.

III. RESULTS/PROGRESS: To date, two 16-day experimental exposure series have been completed. No gross visual or histological abnormalities have been observed thus far. There also appears to be no significant differences in numbers of offspring between the RF-exposed and sham-exposed groups. Data are still undergoing analysis, and the results are not yet available.

In the next phase of this study, the animals will be allowed to come to term. The pups will be observed for abnormalities and fetal death. Any dead term fetuses will be weighed and examined (gross and histological). The surviving pups will be kept under observation until they reach maturity at approximately 60 days. Experimental runs at higher SAR values are also anticipated.

IV. SUMMARY AND CONCLUSIONS: Reports have appeared in the literature implying potential teratogenic effects from radiofrequency radiation. O'Connor, in an article in IEEE (h), has reviewed this data and concludes that most of these studies involved exposure to radiation at power levels that resulted in frank hyperthermia in the dams. The question remains as to whether chronic, low-level ("nonthermal") RFR exposures, such as those found in USAF operational environments, can produce teratogenic effects. In view of the increasing numbers of female personnel in the Air Force operational scene, the requirement exists to examine the adequacy of current RFR standards. In response to this need, teratogenic studies in rats are currently underway in the Radiation Sciences Division at USAFSAM.

To date, two 16-day exposure series on pregnant female rats have been completed using 2450-MHz RFR at an SAR of 0.4 W/kg. No gross visual or histological abnormalities have been observed thus far. Likewise, no significant population effects between irradiates and shams have been detected. Data are still undergoing analysis, and the results are not yet available. Further experiments at higher SAR values and offspring follow-up studies are anticipated.

## V. REFERENCES:

a. Dietzel, F. Effects of electromagnetic radiation on implantation and intrauterine development of the rat. Ann. N.Y. Acad. Sci. 247: 367-376 (1975).

b. Rugh, R., et al. Are microwaves teratogenic? Biological Effects and Health Hazards of Microwave Radiation: Polish Medical Publishers, Warsaw 1974, pp. 98-107.

c. Berman, E., et al. Observations of mouse fetuses after irradiation with 2.45-GHz microwave. Health Physics 35: 791-801 (1978).

d. Chernovetz, M. A teratological study of the rat: microwave and infrared radiation compared. Radio Science 125: 191-197 (1977).

e. Guy, A., et al. Circularly polarized 2450-MHz waveguides for chronic exposure of rodents. Radio Science 14: 63-74 (1979).

f. Allen, S.J., et al. Calorimetric measurements of microwave energy absorption by mice after simultaneous exposure of 18 animals. Radio Science 14: 6S, 1-4 (1979).

g. Dawson, A.B. A note on the staining of the skeleton of cleaved specimens with alizarin red. Society of Stain Technology 1: 123-124 (1926).

h. O'Connor, M. Mammalian teratogenesis and radiofrequency fields. Proc. IEEE 68: 56-60 (1980).

# TABLE 1

## CALORIMETRIC DETERMINATIONS OF SAR ON THE RZ LTLL CIRCULAR WAVEGUIDE FACILITY
## AT 2450 MHz COMPARED TO SARs PREDICTED BY DIFFERENTIAL POWER DATA

| PHANTOM | MASS | EXPOSURE TIME | CALORIMETRIC SAR | DIFFERENTIAL POWER SAR |
|---|---|---|---|---|
| TISSUE-EQUIV. MATERIAL #1 | 300 G | 10 MIN | 13.6 W/KG | 15.7 W/KG |
| TISSUE-EQUIV. MATERIAL #2 | 300 G | 6 MIN | 17.9 W/KG | 15.7 W/KG |
| TISSUE-EQUIV. MATERIAL #3 | 300 G | 6 MIN | 16.3 W/KG | 15.7 W/KG |
| | | | AV. 15.9 W/KG ($\pm$ 2.2 W/KG S.D.) | |
| CADAVER #1 | 335 G | 6 MIN | 15.9 W/KG | 15.5 W/KG |
| CADAVER #2 | 320 G | 6 MIN | 16.3 W/KG | 16.3 W/KG |
| CADAVER #3 | 348 G | 10 MIN | 14.2 W/KG | 15.1 W/KG |
| CADAVER #4 | 278 G | 6 MIN | 18.8 W/KG | 18.3 W/KG |

432

FRACTION INPUT POWER ABSORBED = 0.433 + 0.267(WEIGHT IN KG)
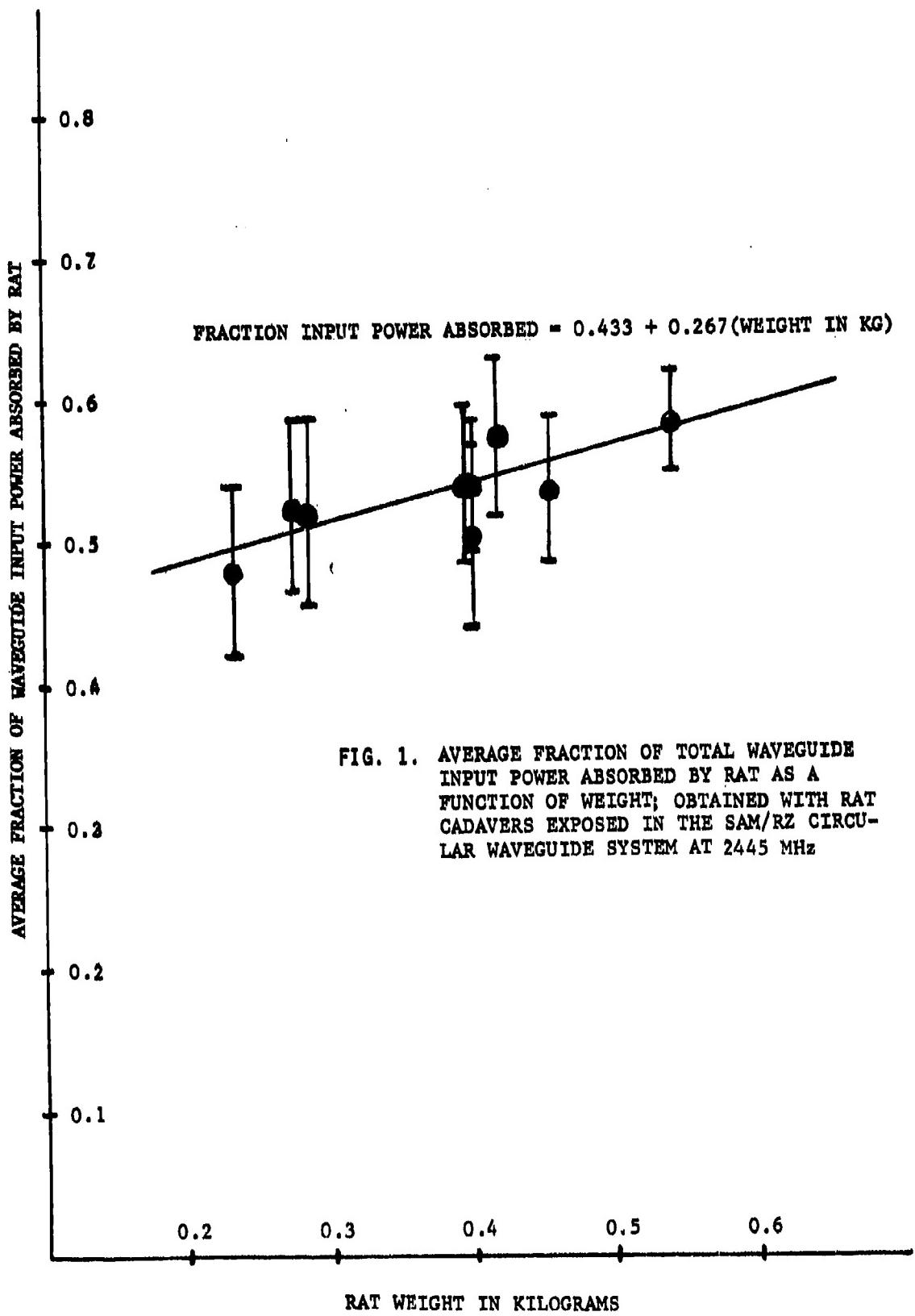
FIG. 1. AVERAGE FRACTION OF TOTAL WAVEGUIDE INPUT POWER ABSORBED BY RAT AS A FUNCTION OF WEIGHT; OBTAINED WITH RAT CADAVERS EXPOSED IN THE SAM/RZ CIRCULAR WAVEGUIDE SYSTEM AT 2445 MHz

FRACTION OF INPUT POWER ABSORBED = 0.362 + 0.350(WEIGHT IN KG)

FIG. 2.  AVERAGE FRACTION OF TOTAL WAVEGUIDE INPUT
POWER ABSORBED AS A FUNCTION OF WEIGHT;
MEASURED IN TISSUE-EQUIVALENT PHANTOMS
EXPOSED IN THE SAM/RZ CIRCULAR WAVEGUIDE
SYSTEM AT 2445 MHz

RAT WEIGHT IN KILOGRAMS

434
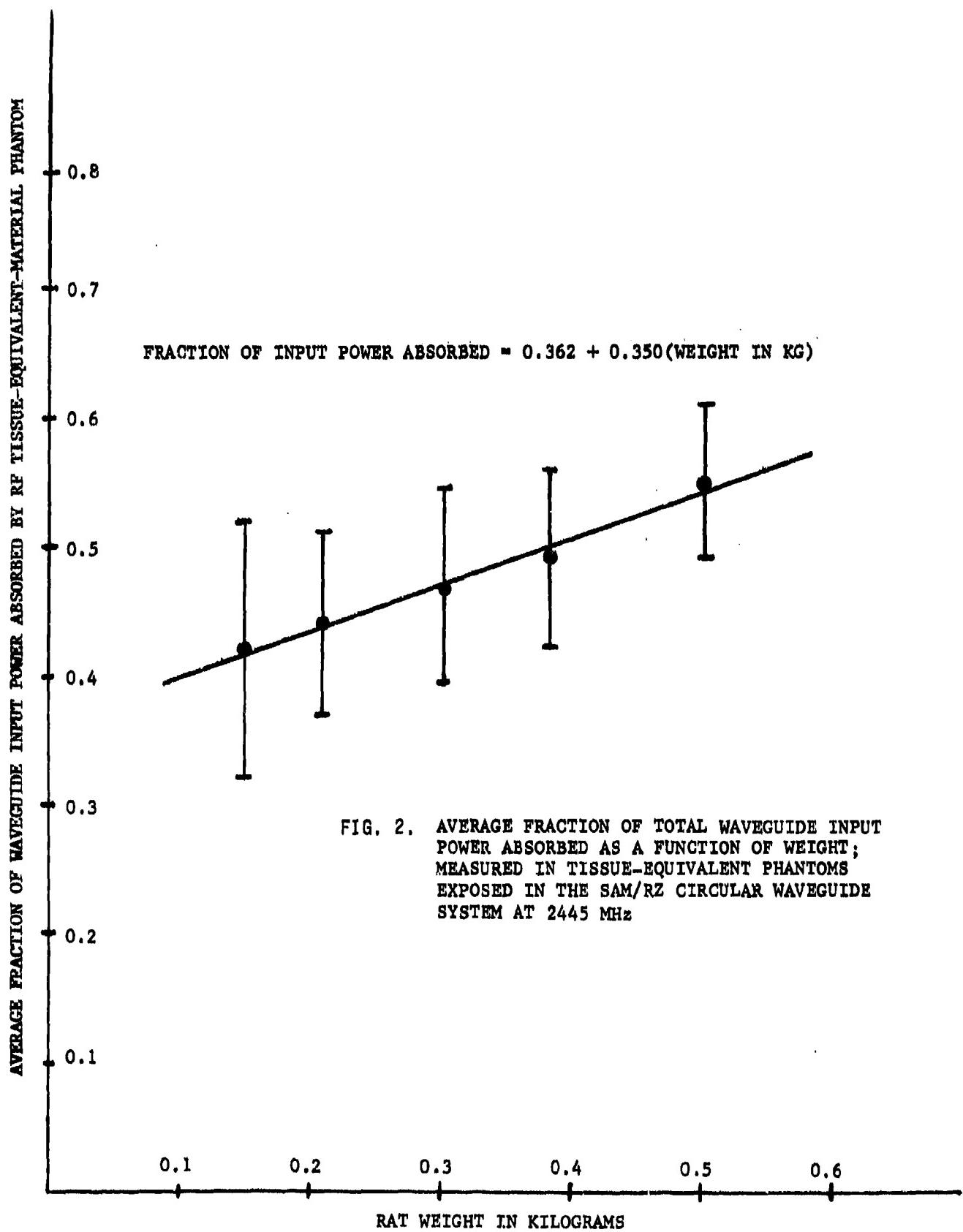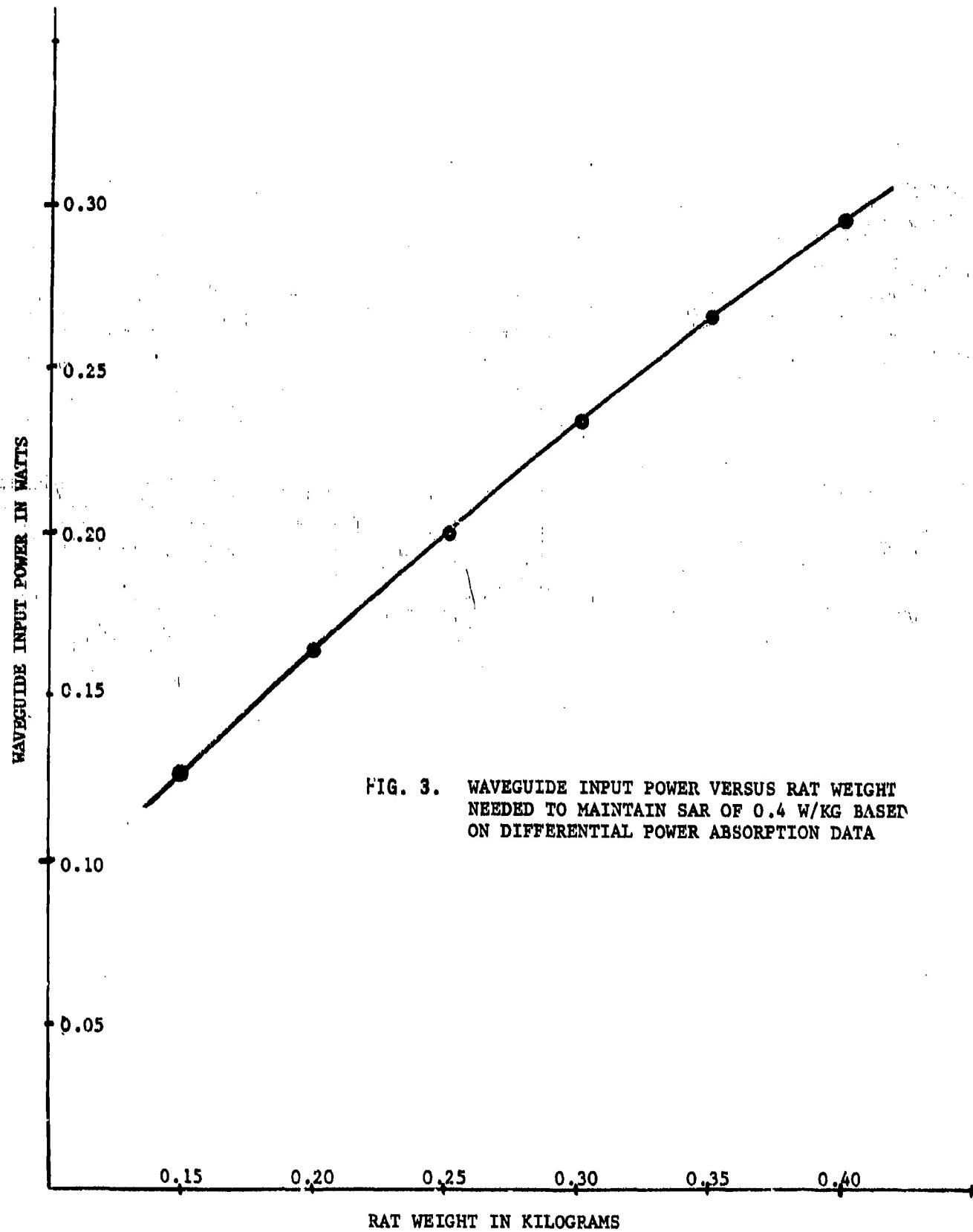
FIG. 3. WAVEGUIDE INPUT POWER VERSUS RAT WEIGHT NEEDED TO MAINTAIN SAR OF 0.4 W/KG BASED ON DIFFERENTIAL POWER ABSORPTION DATA

# LIST OF PARTICIPANTS

Stewart J. Allen
 Supervisory Physicist, Radiation Sciences Division, USAF School of Aero-
 space Medicine, Brooks AFB TX 78235

Eleanor A. Adair
 Senior Research Associate in Psychology, John B. Pierce Foundation,
 290 Congress Ave., New Haven CT 07519

Richard A. Albanese
 Biomathematical Modeling Branch, Data Sciences Division, USAF School of
 Aerospace Medicine, Brooks AFB TX 78235

William O. Berry
 Program Manager, AFOSR Life Sciences Directorate, Bolling AFB DC 20332

Richard J. Burgess
 Chief, Engineering Division, 1839th Engineering Installation Group,
 Keesler AFB MS 39534

Earl L. Bell
 Supervisory Mathematician, Data Sciences Division, USAF School of Aero-
 space Medicine, Brooks AFB TX 78235

Roger F. Brown
 Associate Professor, Life Sciences Department, University of Missouri-
 Rolla, Rolla MO 65401

George Croshaw, Capt, USAF, BSC
 Chief, Nonionizing Radiation Services, Occupational and Environmental
 Health Laboratory, Brooks AFB TX 78235

David K. Cohoon
 Biomathematical Modeling Branch, Data Sciences Division, USAF School of
 Aerospace Medicine, Brooks AFB TX 78235

Robert C. Downs, Jr., Capt, USAF
 United States Air Force Academy CO 80840

Carl H. Durney
 Professor and Chairman of Electrical Engineering, Research Professor of
 Bioengineering, University of Utah, Salt Lake City UT 84112

Joe A. Elder
 United States Environmental Protection Agency, Health Effects Research
 Laboratory, Research Triangle Park NC 27711

David N. Erwin
 Research Physiologist, Radiation Sciences Division, USAF School of Aero-
 space Medicine, Brooks AFB TX 78235

Charles S. Feldstone
    Manager, Behavioral Sciences, Southwest Research Institute, 6220 Culebra,
    San Antonio TX 78284

Melvin R. Frei
    Associate Professor of Biology, Trinity University, 715 Stadium Drive,
    San Antonio TX 78284

Om P. Gandhi
    Professor of Electrical Engineering, University of Utah, Salt Lake
    City UT 84112

Paul Greengard
    Professor of Pharmacology, Yale University School of Medicine,
    New Haven CT 06511

James D. Grissett
    Naval Aerospace Medical Research Laboratory, Pensacola FL 32508

Arthur W. Guy
    Director, Bioelectromagnetics Research Laboratory, University of
    Washington School of Medicine, Seattle WA 98195

Kenneth A. Hardy
    Physicist, Radiation Sciences Division, USAF School of Aerospace
    Medicine, Brooks AFB TX 78235

Rosaria P. Haugland
    Biochemist, Baylor University Medical Center, 3500 Gaston Ave.,
    Dallas TX 75246

Ferdinand Heinmets
    Research Scientist, Technology Incorporated, Life Sciences Division,
    511 West Rhapsody, San Antonio TX 78216

William D. Hurt
    Physicist, Radiation Sciences Division, USAF School of Aerospace
    Medicine, Brooks AFB TX 78235

P. F. Iampietro
    Director, Life Sciences Directorate, Bolling AFB DC 20332

Robert M. Ingle, Lt Col, USAF, MC
    Aerospace Medical Physician, Clinical Sciences Division, USAF School of
    Aerospace Medicine, Brooks AFB TX 78235

George R. James, Maj, USAF, BSC
    Directorate of Biotechnology, Office of Command Surgeon,
    Andrews AFB MD 20334

Johnathan L. Kiel, Capt, USAF, BSC
    Immunologist, Radiation Sciences Division, USAF School of Aerospace
    Medicine, Brooks AFB TX 78235

Robert Krueger
    Professor of Mathematics, University of Nebraska, Lincoln NE 68588

Jerome H. Krupp
    Veterinary Medical Officer, Radiation Sciences Division, USAF School of
    Aerospace Medicine, Brooks AFB TX 78235

Larry L. Kunz
    Associate Professor of Pathology, University of Washington School of
    Medicine, Seattle WA 98195

Stanley Marshall
    Professor, Department of Electrical Engineering, University of Missouri-
    Rolla, Rolla MO 65401

Martin L. Meltz
    Assistant Professor of Radiology, University of Texas Health Science
    Center, San Antonio TX 78284

James H. Merritt
    Research Chemist, Radiation Sciences Division, USAF School of Aerospace
    Medicine, Brooks AFB TX 78235

James K. Miller
    Chief, Electromagnetic Compatibility Branch, 1839th Engineering Installa-
    tion Group, Keesler AFB MS 39534

John C. Mitchell
    Chief, Radiation Physics Branch, Radiation Sciences Division, USAF School
    of Aerospace Medicine, Brooks AFB TX 78235

John C. Monahan
    Division of Biological Effects, Bureau of Radiological Health,
    12709 Twinbrook Parkway, Rocksville MD 20857

A. M. Muc
    Ontario Ministry of Labour, 400 University Ave., Toronto ON M7A1T7

Robert D. Myers
    Professor of Psychiatry and Pharmacology, University of North Carolina
    School of Medicine, Chapel Hill NC 27514

John M. Osepchuk
    Consulting Scientist, Raytheon Company, Research Division, 28 Seyon St.,
    Waltham MA 01254

Ronald C. Peterson
    Bell Laboratories, 600 Mountain Ave., Murray Hill NJ 07974

Peter Polson
    Research Engineer, National Aeronautics and Space Administration, Ames
    Research Center, Moffett Field CA 94035

Elliot Postow
    Electromagnetic Research Project Officer, Naval Medical R&D Command,
    National Naval Medical Center, Bethesda MD 20014

Earl W. Prohofsky
    Professor of Physics, Purdue University, West Lafayette IN 47907

Norbert Roberts
    Assistant Professor of Medicine, University of Rochester School of
    Medicine, Rochester NY 14642

Saul W. Rosenthal
    Polytechnic Institute of New York, Route 110, Farmingdale NY 11735

Sherwood W. Samn
    Mathematician, Data Sciences Division, USAF School of Aerospace Medicine,
    Brooks AFB TX 78235

Aaron P. Sanders
    Professor of Radiology, Duke University School of Medicine,
    Durham NC 27710

Ronald L. Seaman
    Research Engineer, Georgia Tech Engineering Experiment Station,
    Atlanta GA 30332

Mays L. Swicord
    Bureau of Radiological Health, 12721 Twinbrook Parkway, Rockville MD 20852

James Toler
    Biomedical Research Division, Georgia Tech Engineering Experiment Station,
    Atlanta GA 30332

Kathleen A. Walker
    Senior Research Assistant, University of Texas Health Science Center,
    San Antonio TX 78284

Steve E. Webber
    Associate Professor of Chemistry, University of Texas, Austin TX 78712

Gary W. West, Col, USAF, MC
    Deputy Chief, Radiation Sciences Division, USAF School of Aerospace
    Medicine, Brooks AFB TX 78235

David G. Wood, Maj, USAF, BSC
    Staff Bioenvironmental Engineer, Aerospace Medical Consultants Division,
    Directorate of Professional Services, Office of Surgeon General,
    Brooks AFB TX 78235